

Proceedings of the XVII International
Baldin Seminar on High Energy Physics Problems

RELATIVISTIC NUCLEAR PHYSICS AND QUANTUM CHROMODYNAMICS VOL. I



Editors: A. N. Sissakian, V. V. Burov, A. I. Malakhov

Dubna 2004
710513

Joint Institute for Nuclear Research

Relativistic Nuclear Physics and Quantum Chromodynamics

*Proceedings of the XVII International Baldin
Seminar on High Energy Physics Problems*

Dubna, September 27 – October 2, 2004

ISHEPP XVII

Volume I

Editors: A. N. Sissakian
V. V. Burov
A. I. Malakhov



УДК 539.17(042), 539.12.01(063)
ББК [22.382+22.315]я431
R41



Editors: *A. N. Sissakian, V. V. Burov, A. I. Malakhov*
Preparing proceedings to print: *S. G. Bondarenko, E. B. Plekhanov*
Photos by *Yu. A. Tumanov, E. B. Plekhanov, I. G. Zarubina*

The contributions are reproduced directly from the originals
presented by the Organizing Committee.

Relativistic Nuclear Physics and Quantum Chromodynamics:
R41 Proc. of the XVII Intern. Baldin Seminar on High Energy Physics Problems (Dubna, September 27 – October 2, 2004). — Dubna: JINR, 2005. — V. 1. — 390 p., photos.

ISBN 5-9530-0089-8

The Proceedings present the invited talks given by leading scientists in the field of relativistic nuclear physics at the traditional XVII International Baldin Seminar on High Energy Physics Problems «Relativistic Nuclear Physics and Quantum Chromodynamics» (Dubna, September 27 – October 2, 2004).

Релятивистская ядерная физика и квантовая хромодинамика:
Тр. XVII Междунар. Балдинского семинара по проблемам физики высоких энергий (Дубна, 27 сентября – 2 октября 2002 г.). — Дубна: ОИЯИ, 2005. — Т. 1. — 390 с., фото.

ISBN 5-9530-0089-8

В сборнике представлены доклады, которые были сделаны ведущими специалистами в области релятивистской ядерной физики на традиционном XVII Международном Балдинском семинаре по проблемам физики высоких энергий «Релятивистская ядерная физика и квантовая хромодинамика» (Дубна, 27 сентября – 2 октября 2004 г.).

УДК 539.17(042), 539.12.01(063)
ББК [22.382+22.315]я431



XVII International Baldin Seminar on High Energy Physics Problems

RELATIVISTIC NUCLEAR PHYSICS AND QUANTUM CHROMODYNAMICS

DUBNA, SEPTEMBER 27 - OCTOBER 2, 2004

International Advisory Committee:

A. Andrianov (St. Peterburg, Russia)
A. Antonov (Sofia, Bulgaria)
J. Bartke (Krakow, Poland)
C. Ciofi degli Atti (Perugia, Italy)
T. Donnelly (MIT, USA)
H. Gutbrod (GSI, Germany)
T. Hallman (BNL, USA)
W. Henning (GSI, Germany)
V. Kadyshevsky (JINR)
S. Kullander (Lund, Sweden)
J.-M. Laget (Saclay, France)
A. Lebedev (Moscow, Russia)
F. Lehar (Saclay, France)
G. Leksin (Moscow, Russia)
A. Logunov (Protvino, Russia)
H. Machner (Juelich, Germany)
V. Matveev (Moscow, Russia)
Sh. Nagamiya (KEK, Japan)
Yu. Novozhilov (St. Peterburg, Russia)
S. Nurushev (Protvino, Russia)
Ch. Perdrisat (JLAB, USA)
L. Pondrom (Madison, USA)
L. Schroeder (Berkeley, USA)
J. Schukraft (CERN)
A. Shebeko (Kharkov, Ukraine)
A. Slavnov (Moscow, Russia)
I. Tanihata (RIKEN, Japan)
A. Tavkhelidze (Tbilisi, Georgia)
A. Thomas (Adelaide, Australia)
H. Toki (Osaka, Japan)
E. Tomasi-Gustafsson (Saclay, France)
I. Tserruya (Rehovot, Israel)
B. Yuldashev (Tashkent, Uzbekistan)

Organizing Committee:

A.N. Sissakian (*Chairman*)
V.V. Burov (*Vice-Chairman*)
A.I. Malakhov (*Vice-Chairman*)
S.G. Bondarenko (*Sc. Secretary*)
E.B. Plekhanov (*Sc. Secretary*)
E.N. Russakovich (*Secretary*)
N.N. Agapov
A.A. Baldin
I.V. Boguslavsky
S.B. Gerasimov
A.D. Kovalenko
G.A. Kozlov
V.K. Lukyanov
V.A. Nikolaev
Yu.A. Panebratsev
N.M. Piskunov
M.G. Sapozhnikov
A.S. Vodopianov
S. Vokal
V.V. Voronov
P.I. Zarubin

WWW Page:

<http://relnp.jinr.ru/ishepp/>

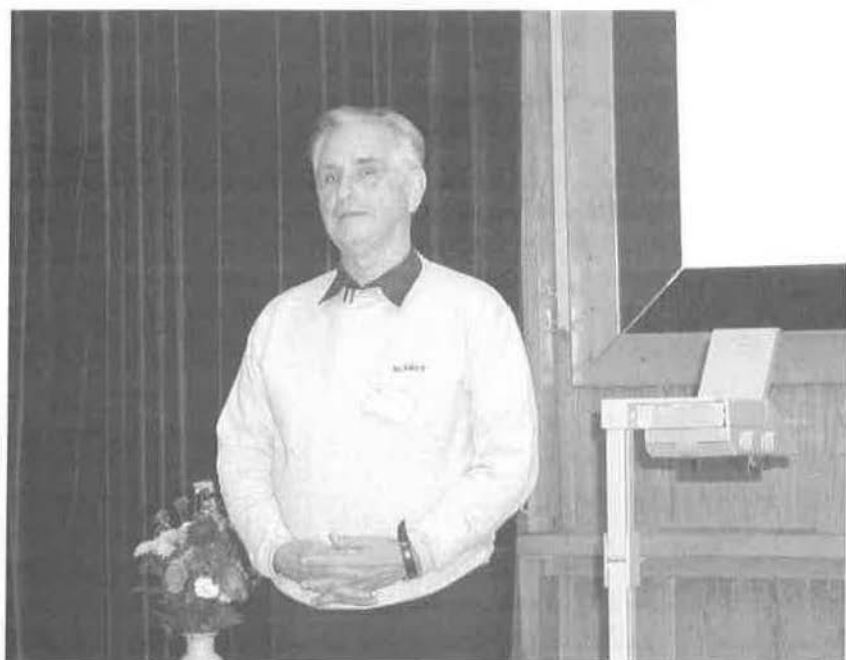
E-mail:

ishepp@thsun1.jinr.ru

Organizer

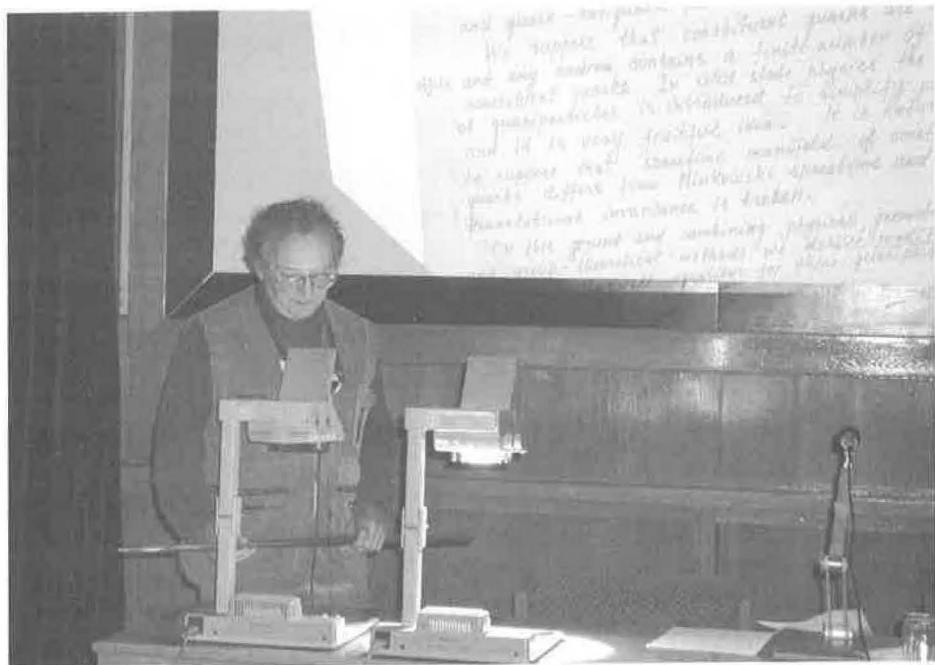
JOINT INSTITUTE FOR NUCLEAR RESEARCH

<http://www.jinr.ru/>



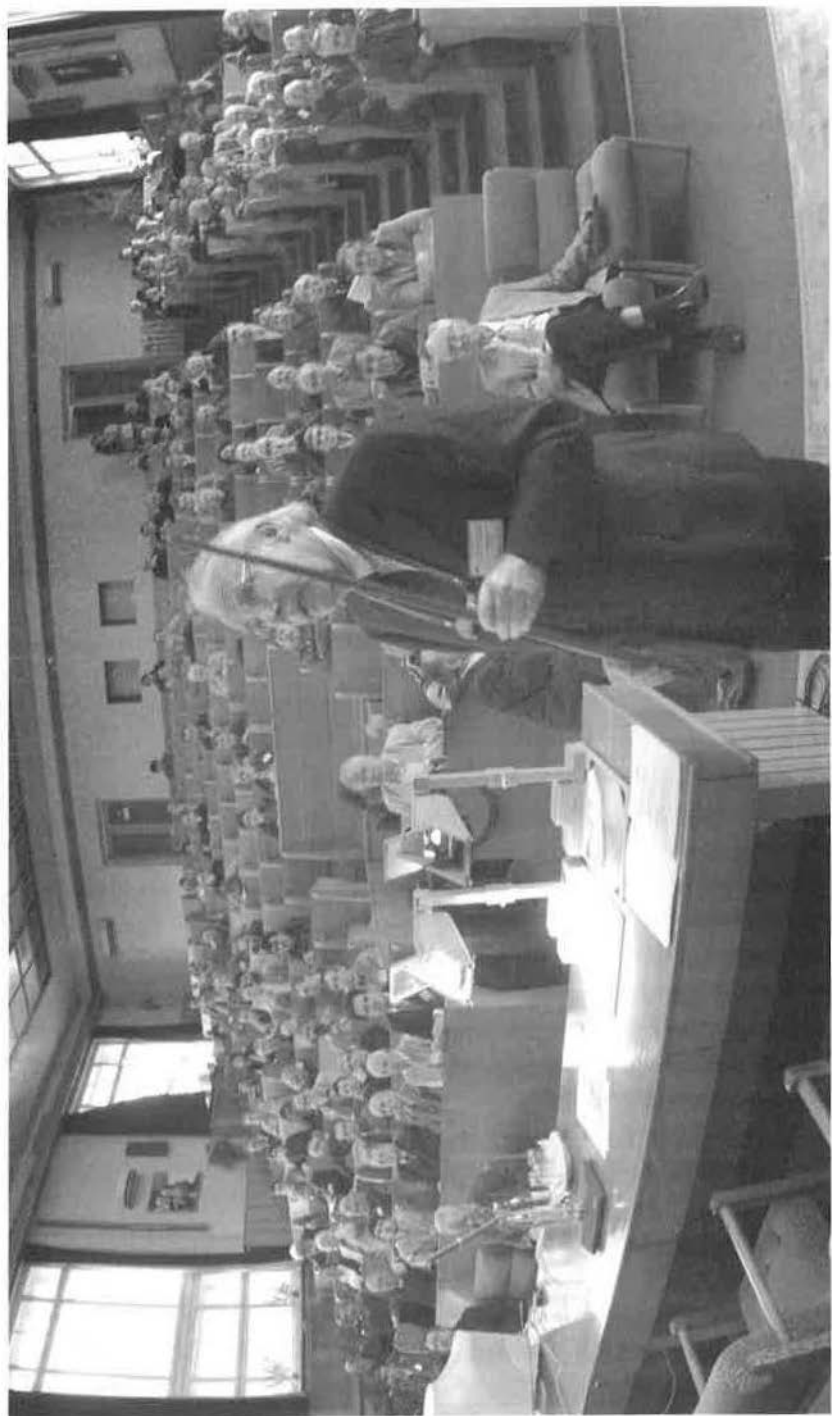














Contents

Volume I

Preface	13
---------------	----

I. QUANTUM CHROMODYNAMICS AT THE LARGE DISTANCES

PROTON FORM FACTOR MEASUREMENTS AT JEFFERSON LAB <i>C. Perdrisat, V. Punjabi (for the Jefferson Lab $G_{Ep}(III)$ Collaborations)</i>	17
---	----

MESONIC EXCHANGE CURRENTS IN THE DEUTERON. THE BRIDGE FROM NONRELATIVISTIC TO RELATIVISTIC NUCLEAR PHYSICS <i>S. G. Bondarenko et al.</i>	32
---	----

COULD LEPTONS BE COMPOSED FROM QUARKS OR ANTIQUARKS? <i>Y. E. Pokrovsky</i>	42
--	----

INSTANTON VACUUM BEYOND CHIRAL LIMIT <i>M. Musakhanov</i>	54
--	----

ON THE MOTION OF MATTER IN THE GEOMETRICAL GAUGE FIELD THEORY <i>N. P. Konopleva</i>	65
---	----

RANDOM LATTICE QCD AND CHIRAL BORN-INFELD THEORY <i>O. V. Pavlovsky</i>	70
--	----

THE NUCLEON-NUCLEON SCATTERING DESCRIPTION AT $E_{lab}=0.6$ GeV, THE DEUTERON PROPERTIES AND DEUTERON PHOTODISINTEGRATION IN THE RELATIVISTIC QUASIPOTENTIAL OPTICAL MODEL, BASED ON THE MOSCOW POTENTIAL <i>N. A. Khokhlov, V. A. Knyr, V. G. Neudatchin</i>	78
---	----

PRODUCTION OF CUMULATIVE PROTONS IN DIS OF NUCLEI, THE ROLE OF FLUCTONS, LPM EFFECT AND ALL THAT <i>S. M. Eliseev</i>	84
---	----

ON ELECTRODYNAMICS OF CONSTITUENT QUARKS AND QCD POTENTIAL <i>I. B. Pestov</i>	89
---	----

INSTANTONS AND STRUCTURE OF PENTAQUARK <i>H.-J. Lee</i>	96
--	----

ON THE RELATIONS BETWEEN TWO-PHOTON AND LEPTONIC WIDTHS OF LOW-LYING S-WAVE STATES OF CHARMONIUM <i>S. B. Gerasimov, M. Majewski</i>	102
CLOTHED PARTICLE REPRESENTATION IN QUANTUM FIELD THEORY: MASS RENORMALIZATION <i>V. Yu. Korda, A. V. Shebeko</i>	111
ELECTROPRODUCTION OF VECTOR MESONS AT SMALL x <i>S. V. Goloskokov</i>	120
THE INFLUENCE OF FRAGMENTATION MODELS IN PRODUCTION OF HADRON JETS IN ELECTRON-POSITRON ANNIHILATION <i>M. E. Zomorrodian</i>	126
PHYSICAL NATURE OF LOBACHEVSKY PARALLEL LINES AND A NEW INERTIAL FRAME TRANSFORMATION <i>N. G. Fadeev</i>	132
II. STRUCTURE FUNCTIONS OF HADRONS AND NUCLEI	
JET ENERGY DENSITY IN HADRON-HADRON COLLISIONS AT HIGH ENERGIES <i>J. V. Ilić, G. P. Škoro, M. V. Tokarev</i>	141
Z-SCALING AT RHIC <i>M. V. Tokarev</i>	151
ANISOTROPY IN RELATIVISTIC NUCLEAR COLLISIONS AND MICHELSON'S EXPERIMENTS WITH LIGHT <i>I. Zborovský</i>	167
Z-SCALING OF JET PRODUCTION AT TEVATRON <i>M. V. Tokarev, T. G. Dedovich</i>	173
SCALING IN INCLUSIVE ELECTRON SCATTERING FROM NUCLEI <i>M. K. Gaidarov et al.</i>	186
NEW ASPECTS IN THE ASYMPTOTICS OF THE DEUTERON ELECTROMAGNETIC FORM FACTORS <i>A. F. Krutov, V. E. Troitsky, N. A. Tsirova</i>	194
METHOD OF THE POLARIZED SEMI-INCLUSIVE DEEP INELASTIC SCATTERING DATA ANALYSIS IN THE NEXT-TO-LEADING QCD ORDER <i>A. N. Sissakian, O. Yu. Shevchenko, O. N. Ivanov</i>	200
MEASUREMENT OF HADRON PRODUCTION CROSS-SECTION IN COLLISIONS OF HIGHLY VIRTUAL PHOTONS <i>V. Pozdnyakov, Yu. Vertogradova</i>	206

III. RELATIVISTIC HEAVY ION COLLISIONS

MULTIPLICITY AND p_t CORRELATIONS IN RELATIVISTIC NUCLEAR COLLISIONS <i>R. S. Kolevatov, V. V. Vechernin</i>	213
LONG-RANGE CORRELATIONS IN Pb-Pb COLLISIONS AT 158 A*GeV <i>G. Feofilov (for NA49 Collaboration and SPbSU group)</i>	222
ON SPATIAL AND EVENT-BY-EVENT FLUCTUATIONS IN RELATIVISTIC HEAVY-ION COLLISIONS <i>Sh. Ahmad</i>	232
NEUTRINO OPACITY TO COLD NEUTRON MATTER <i>O. Benhar, A. Fabrocini, S. Fantoni, G. I. Lykasov</i>	238
SEARCH FOR SIGNAL ON PERCOLATION CLUSTER FORMATION IN NUCLEUS- NUCLEUS COLLISIONS AT RELATIVISTIC ENERGIES <i>O. B. Abidinov et al.</i>	246
INVESTIGATION OF CHARMONIUM STATES PRODUCTION IN p -A AND NUCLEUS- NUCLEUS COLLISIONS AT THE CERN SPS <i>N. S. Topilskaya (for the NA50 Collaboration)</i>	255
STRUCTURE FUNCTION F_L AT FIXED W IN THE K_T -FACTORIZATION APPROACH <i>A. V. Kotikov, A. V. Lipatov, N. P. Zotov</i>	263
MODEL FOR RESTORATION OF HEAVY-ION POTENTIALS AT INTERMEDIATE ENERGIES <i>K. M. Hanna et al.</i>	269
AZIMUTHAL STRUCTURES OF PRODUCED PARTICLES IN HEAVY-ION INTERACTIONS <i>S. Vokál et al.</i>	280
THE EXTRAORDINARY INTERACTION OF ^{14}N -NUCLEUS IN PHOTOEMULSION <i>G. Orlova</i>	288
ρ MESON PRODUCTION IN ULTRAPERIPHERAL $d\text{A}_{11}$ COLLISION <i>S. L. Timoshenko (for the STAR Collaboration)</i>	292
RANDOM MATRIX THEORY AND ANALYSIS OF NUCLEUS-NUCLEUS COLLISION AT HIGH ENERGIES <i>E. I. Shahaliev et al.</i>	296

IV. MULTIPARTICLE DYNAMICS

A AND K_s^0 PRODUCTION IN $p\bar{p}$ COLLISIONS AT 10 GeV/c <i>P. Zh. Aslanyan, V. N. Emelyanenko, G. G. Rikhkvitzkaya</i>	305
SEARCH FOR SCALING PROPERTIES IN MANY-PARTICLE STOCHASTIC PROCESSES <i>B. Słowiński</i>	314
STUDY OF MULTIPARTICLE PRODUCTION BY GLUON DOMINANCE MODEL (Part I) <i>E. S. Kokoulina, V. A. Nikitin</i>	319
STUDY OF MULTIPARTICLE PRODUCTION BY GLUON DOMINANCE MODEL (Part II) <i>P. F. Ermolov et al.</i>	327
THE LOBACHEVSKY SPACE IN RELATIVISTIC NUCLEAR PHYSICS <i>A. A. Baldin</i>	337
STRANGENESS CONSERVATION AND STRUCTURE OF PAIR CORRELATIONS OF NEUTRAL KAONS WITH LOW RELATIVE MOMENTA IN INCLUSIVE PROCESSES <i>V. L. Lyuboshitz, V. V. Lyuboshitz</i>	361

V. ACCELERATOR FACILITIES: STATUS AND PERSPECTIVES

BEAM-BASED MEASUREMENT OF DYNAMICAL CHARACTERISTICS IN NUCLOTRON <i>N. Blinnikov et al.</i>	369
SPIN AS AN ADDITIONAL TOOL FOR QGP INVESTIGATIONS <i>Yu. Karachuk, S. S. Shimanskiy</i>	375
TRANSMUTATION RESEARCH USING THE NUCLOTRON <i>W. Westmeier et al.</i>	379
ELECTRON-POSITRON PAIR CREATION IN THE FIELDS OF HIGH-INTENSITY OPTICAL LASERS <i>D. B. Blaschke, A. V. Prozorkevich, S. A. Smolyansky</i>	383

Volume II

VI. HADRON SPECTROSCOPY

BARYONIC RESONANCES WITH THE STRANGENESS $S = +1$ IN THE SYSTEM OF nK^+ FROM THE REACTION $np \rightarrow npK^+K^-$ AT THE MOMENTUM OF INCIDENT NEUTRONS $P_n=(5.20\pm 0.12)\text{GeV}/c$ <i>Yu. A. Troyan et al.</i>	13
OBSERVATION OF $S = +1$ NARROW RESONANCES IN THE SYSTEM K_s^0p FROM $p+C_3H_8$ COLLISION AT 10 GeV/c <i>P. Zh. Aslanyan, V. N. Emelyanenko, G. G. Rikhkvitzkaya</i>	26
WAVELET ANALYSIS OF DATA IN PHYSICS OF RESONANCES <i>V. I. Henner, T. S. Belozerova, P. G. Frick</i>	37
DIBARYONS IN HADRONIC PHYSICS AND NUCLEAR STRUCTURE <i>V. I. Kukulín, M. A. Shikhalev</i>	45
FURTHER EVIDENCE OF NARROW BARYONIC STRUCTURES WITH HADRONIC AS WELL AS LEPTONIC PROBES <i>B. Tatischeff, E. Tomasi-Gustafsson</i>	56
INSTANTONS IN HIGH ENERGY QCD PROCESSES: INSTANTONS AND THE SOFT POMERON FORMATION <i>A. E. Dorokhov, I. O. Cherednikov</i>	63
TWO-QUARK BOUND STATES: MESON SPECTRA AND REGGE TRAJECTORIES <i>G. G. Gorbunov, G. V. Efimov</i>	67
SOLVING THE INHOMOGENEOUS BETHE-SALPETER EQUATION <i>S. S. Semikh et al.</i>	75
DETERMINATION OF THE GLUEBALL MASS SPECTRUM WITH THE SPIN-ORBIT INTERACTION IN NONPERTURBATIVE QCD APPROACH <i>M. Dineykhán, S. A. Zhaugasheva, T. A. Kozhamkulov</i>	82

VII. APPLIED USE OF RELATIVISTIC BEAMS

INVESTIGATION OF TRANSMUTATION OF RADIOACTIVE WASTE OF ATOMIC REACTORS ^{129}I , ^{237}Np AND NEUTRONS GENERATION WITH 1.5 GEV PROTONS FROM THE NUCLOTRON AT THE SETUP "ENERGY PLUS TRANSMUTATION" (JINR, DUBNA) <i>M. I. Krivopustov et al.</i>	91
---	----

THOROUGH COMPARISON OF THE NEUTRON FLUXES GENERATED IN THE LEAD- URANIUM ASSEMBLY (INSTALLATION "ENERGY PLUS TRANSMUTATION") UNDER IRRADIATION WITH PROTONS AT ENERGY IN THE RANGE FROM 0.7 TO 2.0 GeV <i>A. N. Sosnin et al.</i>	110
EXPERIMENTAL STUDIES OF SPATIAL DISTRIBUTIONS OF NEUTRONS INSIDE AND AROUND THE SET-UP CONSISTED FROM A THICK LEAD TARGET AND A LARGE URANIUM BLANKET IRRADIATED BY RELATIVISTIC PROTONS <i>V. Wagner et al.</i>	111
EXPERIMENTAL AND THEORETICAL DETERMINATION OF ^{235}U , ^{238}U AND $^{\text{NAT}}\text{Pb}$ FISSION RATE DISTRIBUTIONS IN THE U/PB ASSEMBLY BOMBARDED WITH 1.5 GEV PROTONS <i>I. V. Zhuk et al.</i>	117
ON SOLUTION OF THE NUCLEAR PROBLEMS REDUCED TO A SYSTEM OF FIRST ORDER INTEGRAL FREDHOLM EQUATIONS <i>S. V. Korneev et al.</i>	124
ON THE EXPERIMENT OF NEUTRON SPECTRUM INVESTIGATION ON U/Pb- ASSEMBLY USING 0.7 GeV PROTON BEAM FROM THE JINR NUCLOTRON (DUBNA) <i>M. Bielewicz et al.</i>	125
INVESTIGATION OF TEMPERATURE FIELDS AND HEAT GENERATION IN THE LEAD BLOCK AND THE LEAD TARGET WITH THE URANIUM BLANKET OF THE INSTALLATION "ENERGY PLUS TRANSMUTATION" USING PROTON BEAMS FROM THE JINR SYNCHROPHASOTRON/NUCLOTRON <i>A. V. Voronkov et al.</i>	133
EXPERIMENTAL STUDIES OF TRANSMUTATION OF ^{129}I BY SPALLATION NEUTRONS USING JINR DUBNA PHASOTRON <i>M. Majerle (for Collaboration "Energy plus Transmutation")</i>	135
INVESTIGATION OF NEUTRON FIELDS ON THE SURFACE OF THE MASSIVE LEAD TARGET UNDER IRRADIATIONS WITH PROTONS AT ENERGIES OF 1.5 AND 5.0 GeV USING SYNCHROPHASOTRON (JINR, DUBNA) <i>M. K. Kievets et al.</i>	141
VIII. POLARIZATION PHENOMENA AND SPIN PHYSICS	
INVESTIGATION OF THE ANGULAR DEPENDENCE OF THE TENSOR ANALYZING POWER OF 9 GeV/c DEUTERON BREAKUP <i>L. S. Azhgirey et al.</i>	153

MEASUREMENTS OF ENERGY BEHAVIOURS OF SPIN-DEPENDENT np -OBSERVABLES OVER 1.2–3.7 GEV REGION <i>V. I. Sharov et al.</i>	161
SENSITIVITY OF THE POLARIZATION OBSERVABLES A_Y , A_{YY} , A_{XX} AND A_{XZ} OF THE $\vec{d}d \rightarrow p\ ^3H$ AND $\vec{d}d \rightarrow p\ X$ REACTIONS TO THE DEUTERON SPIN STRUCTURE AT 270 MEV <i>T. A. Vasiliev et al.</i>	178
SPIN AS A KINEMATICAL EFFECT OF THE RELATIVITY <i>O. S. Kosmachev</i>	185
THE POLARIZED CHARGE-EXCHANGE REACTION $\vec{d} + p \rightarrow (pp)_{1S_0} + n$ <i>V. Glagolev (for the ANKE Collaboration)</i>	192
SINGLE SPIN ASYMMETRY IN HIGH P_T CHARGED HADRON PRODUCTION OFF NUCLEI AT 40 GeV <i>V. V. Abramov et al.</i>	202
LONGITUDINAL POLARIZATION OF Λ AND $\bar{\Lambda}$ IN DEEP-INELASTIC SCATTERING AT COMPASS <i>M. G. Sapozhnikov (for the COMPASS Collaboration)</i>	208
DEUTERON-PROTON CHARGE EXCHANGE REACTION AT SMALL TRANSFER MOMENTUM <i>N. B. Ladygina, A. V. Shebeko</i>	214
NUCLEAR SPIN IN DIRECT DARK MATTER SEARCH <i>V. A. Bednyakov, F. Šimkovic, I. V. Titkova</i>	221
CHARM PRODUCTION IN NN AND γN COLLISIONS <i>E. Tomasi-Gustafsson</i>	231
TENSOR A_{yy} AND VECTOR A_y ANALYZING POWERS OF THE (d, p) AND (d, d) REACTIONS AT 5 GeV/c AND 178 MR <i>V. P. Ladygin et al.</i>	241
MEASUREMENTS OF THE TENSOR A_{xx} , A_{yy} , A_{zz} AND VECTOR A_y ANALYZING POWERS FOR THE $d + d \rightarrow\ ^3H + p$ AND $d + d \rightarrow\ ^3He + n$ REACTIONS AT 270 MeV <i>M. Janek et al.</i>	249
INCLUSIVE AND SEMI-INCLUSIVE ASYMMETRIES AT COMPASS <i>A. Yu. Korzenev (for the COMPASS Collaboration)</i>	255

IX. PROGRESS IN EXPERIMENTAL STUDIES AT THE HIGH ENERGY ACCELERATORS

FULL SIMULATION OF HIGGS BOSON DECAYS INTO FOUR LEPTONS FOR ATLAS AT THE LHC <i>A. Khodinov, M. Rijssenbeek, S. Padhi</i>	263
STUDY OF A POSSIBILITY TO DETECT Υ IN p -Pb AND Pb- p COLLISIONS AT THE LHC IN THE MUON SPECTROMETER OF ALICE <i>A. Morsch et al.</i>	268
PERFORMANCE OF THE SILICON DRIFT DETECTOR IN THE CASE OF PERPENDICULAR TRACKS AND INCLINED TRACKS <i>S. Kouchpil (for the ITS ALICE Collaboration)</i>	276
PRODUCTION AND IDENTIFICATION OF THE SUPERHEAVY HYDROGEN HYPERNUCLEUS ${}^6_{\Lambda}\text{H}$ <i>L. Majling et al.</i>	282
THE DIPOLE MAGNET IRON YOKE DESIGN FOR THE ALICE DIMUON ARM SPECTROMETER <i>V. Aréfiév et al.</i>	291
INCLUSIVE π^0 PRODUCTION BY PROTONS AND LIGHT NUCLEI ON C AND Cu TARGETS AT A MOMENTUM OF 4.5 GeV/c PER NUCLEON <i>Kh. U. Abraamyan et al.</i>	301
CLUSTER-FLUCTONS REVELATION IN NUCLEAR INTERACTIONS AT 4.2 (GeV/c)/N <i>V. N. Penev, A. I. Shklovskaya, E. N. Kladnitskaya</i>	311
INVESTIGATIONS IN VEKSLER AND BALDIN LABORATORY OF HIGH ENERGIES <i>A. I. Malakhov</i>	319
INVARIANT ANALYSIS OF THE FRAGMENTATION OF RELATIVISTIC NUCLEI IN EMULSION <i>P. I. Zarubin et al.</i>	339
PHYSICS AT COSY <i>H. Machner</i>	347
POLARIZED DEUTERONS AT THE NUCLOTRON <i>Yu. K. Pilipenko et al.</i>	353
Scientific Programme	358
List of Participants	370

Preface

The first 1969 Dubna Seminar of the series was devoted to vector mesons and included a considerable number of talks aimed to create gauge field theory, in particular, to solve the problems of quantization of the Yang Mills fields, their geometric interpretation, of the phenomenological applications of these theories to experiment. This was the first large-scale conference devoted to the main trend of fundamental interactions theory. Among the participants were professors N. N. Bogolubov, J. Bjorken, B. Zumino, M. A. Markov, S. Ting, L. D. Faddeev and others, who made the basic contribution to this field of physics. The subsequent seminars of this series were devoted to the physics of strong interactions, multiparticle production, relativistic nuclear physics, that is, to the problems which were, as it seemed at that time, rather far from the topics of the first Seminar.

Starting with the second half of the seventies the gauge field theory greatly affected the physics of fundamental interactions and this was naturally reflected in the program of the Seminars. The quantum chromodynamics as a theory of strong interactions based on the first principles and the possibility of its experimental check were the subject at the previous Seminars. The problems of relativistic nuclear physics, multiple production processes in nucleus-nucleus collisions, traditionally discussed at the Seminar, gained a large significance. Cumulative meson production, the laws governing the limiting fragmentation of nuclei and the nuclear reactions with large momentum transfers which were discovered in the early 1970s became the main trends in the program of investigations of relativistic nuclear collisions at the Synchrophasotron and were successfully interpreted in the language of quantum chromodynamics. The concept of the quark-parton structure functions of nuclei has been considerably developed. At the VI-th Seminar, the dependence of the structure functions normalized to the atomic weight that was later named the *EMC-effect*, was discussed. The results of the experiments on deep inelastic muon scattering on nuclei in the cumulative region were first reported there and gave convincing grounds for the conclusion about the properties of the quark-parton structure functions drawn on the basis of the study of the limiting fragmentation of nuclei.

At the VII-th Seminar attention was focused on the properties of the quark-parton structure functions of nuclei, and special sessions were devoted to this problem.

An essential part of the program of the previous Seminars was the phenomenological description of chromodynamics at large distances (bags, strings, multiquark systems, hidden colour, quark-gluon plasma, etc.).

In the past years the role of the colour degrees of freedom in nuclei has extensively been studied and discussed at special conferences devoted to it. The effect of the quark degrees of freedom on the properties of nuclei and nuclear reactions is undoubtedly the main perspective of the fundamental studies in nuclear physics. Multiquark interactions and the systems with a nonstandard number of quarks, especially dibaryons, multiquark configurations in nuclei, systems with hidden colour, etc. are of special interest. The problem of the spin content of the proton is the pressing problem of the day both for theory and experiment. All these problems are reflected in the suggested program.

After the VIII-th Seminar physics of relativistic nuclei has essentially been developed: beams of nuclei at energy 200 GeV/nucleon and new large detectors began to work. Scores of big collaborations joined the research of processes of multiple particle production in relativistic nuclear collisions and the problem of chromoplasma. The natural phenomena

in relativistic nuclear physics having an asymptotic character, have played the decisive role in a detailed design and estimation of cost of the accelerator complex and construction of installations on nuclear beams. The principles of symmetry and self-similarity can be used to predict inclusive cross sections of particle production, in the central rapidity region ($y = 0$). Recent analysis (see journal "*Physics of Particles and Nuclei*", 1996-2005) makes it possible to conclude that the hopes for obtaining dense and hot matter in heavy ultrarelativistic nuclear collisions were have not been realized yet. An overall idea about the investigation in the field of relativistic nuclear physics can be got from the Proceedings of the Dubna International Seminar of the present series. The interplay of hadronic structure and QCD interactions is one of the defining features of the *transition regime*.

Since XVI Seminar the meetings were devoted to memory of outstanding scientist Academician Alexander Michailovich Baldin (1926-2001). Academician A. M. Baldin's scientific and organizational activities were extremely versatile. He was the President of the *Council on Electromagnetic Interactions* and a member of the *Bureau of the Nuclear Physics Department of the Russian Academy of Sciences*, Editor-in-Chief of the journals "*Physics of Particles and Nuclei*" and "*Physics of Particles and Nuclei, Letters*" as well as a member of the Editorial Boards of many scientific publications. Among conferences that were organized by Alexander Michailovich of special importance is just this series of the *International Seminars on High-Energy Physics Problems* started in 1969 with M. A. Markov's support. They have been given an unofficial, somewhat witty, name "*Baldin autumn*".

The Proceedings of the XVII *International Baldin Seminars on High-Energy Physics Problems (Baldin ISHEPP)* include talks on hot problems of the relativistic nuclear physics and reports on status and perspectives of the important experiments which were devoted to investigations of the exotic properties and polarization phenomena of the relativistic nuclei. We would like to mention that the applied relativistic physics was intensively discussed and this fact found its reflection in the Proceedings. During the Seminar 117 reports of 205 participants from 17 countries were presented. We expect that the Proceedings will be interesting for scientists working in relativistic nuclear physics.

Editors

I.
QUANTUM
CHROMODYNAMICS
AT THE LARGE
DISTANCES

PROTON FORM FACTOR MEASUREMENTS AT JEFFERSON LAB

C.F. Perdrisat^{1†}, V. Punjabi² and the Jefferson Lab G_{Ep} (III) Collaborations³

(1) *the College of William and Mary, Williamsburg, VA 23187*

(2) *Norfolk State University, Norfolk, VA 23504*

(3) *12000 Jefferson Avenue, Newport News, VA 23666, USA*

† *E-mail: perdrisa@jlab.org*

Abstract

In two experiments at Jefferson Lab in Hall A, the first one in 1998 and the second in 2000, the ratio of the electromagnetic form factors of the proton was obtained by measuring P_t and P_ℓ , the transverse and longitudinal recoil proton polarization components, respectively, in $\vec{e}p \rightarrow e\vec{p}$; the ratio G_{Ep}/G_{Mp} is proportional to P_t/P_ℓ . Simultaneous measurement of P_t and P_ℓ provides good control of the systematic uncertainty. The first measurement of G_{Ep}/G_{Mp} ratio was made to $Q^2=3.5$ GeV² and the second measurement to $Q^2=5.6$ GeV². The results from these two experiments indicate that the ratio scales like $1/Q^2$, in stark contrast with cross section data analyzed by the Rosenbluth separation method which gives a constant value for this ratio. The incompatibility of the recoil polarization results with most of the Rosenbluth separation results appears now well established above Q^2 of about 3 GeV². The consensus at the present time is that the interference of the two-photon exchange with the Born term, which had been deemed negligible until recently, might explain the discrepancy between the results of the two techniques; the possibility that the discrepancy is due to incomplete radiative correction has also been recently discussed.

1. Introduction

The ratio of the elastic electromagnetic form factors of the proton, G_{Ep}/G_{Mp} , has been measured at Jefferson Lab (JLab) for Q^2 values ranging from 0.5 to 5.6 GeV². The technique used was the determination of the recoil proton polarization components in the $\vec{e}p \rightarrow e\vec{p}$ reaction, with both final state particles detected. The results of the two JLab experiments, the first one reaching to $Q^2=3.5$ GeV², and the second one to $Q^2=5.6$ GeV², are now published [1, 2] and well known. The ratio $\mu G_{Ep}/G_{Mp}$ was found to decrease linearly with Q^2 , from ≈ 1 at $Q^2=0.5$ GeV², down to 0.28 at $Q^2=5.6$ GeV²; in the dipole model this ratio would be 1.0 for all Q^2 values. These results demonstrated unambiguously for the first time that the Q^2 dependences of G_{Ep} and G_{Mp} are different from one another.

Double spin experiments [3, 4] measure the product $G_{Ep}G_{Mp}$ as well as G_{Mp}^2 , and hence determine the relative sign of the form factors. The combined results of the two JLab experiments were surprising as they appeared to contradict the consensus based on Rosenbluth separation results for G_{Ep}^2 and G_{Mp}^2 : the ratio $\mu_p G_{Ep}/G_{Mp}$ obtained with

the Rosenbluth method appear to be near 1 up to 5 GeV² [5]. This un-bridgeable difference between cross section and polarization experiments has been reinforced with two recent JLab Rosenbluth experiments [6, 7]; it appears increasingly difficult to explain the difference in the ratio by methodological or systematic errors.

Cross section data require very large radiative corrections, polarization data do not ([8]). It is still possible that the difference will be explained after reexamination of the standard radiative correction procedure [9]. Another possibility is that the single-photon exchange or Born approximation at the basis of form factor extraction, needs to be reexamined and the effect of two-photon exchange calculated [10]. The preliminary results of such calculations [11, 12] indicate that two-photon exchange, which enters as an interference between the one- and two-photon diagrams, can indeed affect the form factor extraction from cross section data significantly, but modifies the polarization results very little. The form factor extraction procedure is based on dominance of one-photon exchange; the consequences of a measurable two-photon exchange contribution for the extraction of form factors have been discussed by [13].

We are currently preparing a third measurement of the G_{Ep}/G_{Mp} -ratio at JLab, to extend the Q^2 -range to 9 GeV² [14]. This high priority experiment requires a new polarimeter to be installed in the focal plane of the high momentum spectrometer in Hall C, and a new large acceptance calorimeter to detect the electron. Both instruments are now in an advanced stage of construction. The experiment will be ready to go on the Hall C floor in the later part of 2005.

To resolve the problem of the incompatibility of the G_{Ep}/G_{Mp} -ratios obtained from cross section and polarization data, we have proposed [15] to measure the ratio G_{Ep}/G_{Mp} as a function of ϵ , the longitudinal polarization of the virtual photon, by the recoil polarization method. This study requires the same instrumentation as the G_{Ep} (III) experiment, and will hopefully occur immediately after it.

We will also review the results from several recent G_{Ep} experiments at JLab, and present the status of G_{En} [16, 17, 18, 19] and G_{Mn} [20] past and future measurements.

2. Polarization Method

In the One-Photon Exchange or Born approximation for elastic ep the observables of a recoil polarization experiment are the two components of the proton polarization in the reaction plane, P_t and P_ℓ , as follows:

$$\begin{aligned} I_0 P_t &= -2\sqrt{\tau(1+\tau)} G_{Ep} G_{Mp} \tan^2 \frac{\theta_e}{2} \\ I_0 P_\ell &= \frac{1}{M_p} (E_{beam} + E_e) \sqrt{\tau(1+\tau)} G_{Mp}^2 \tan^2 \frac{\theta_e}{2} \end{aligned}$$

I_0 is proportional to the unpolarized cross section and is given by:

$$I_0 = G_{Ep}^2 + \frac{\tau}{\epsilon} G_{Mp}^2 \quad (1)$$

where $\epsilon^{-1} = 1 + 2(1 + \tau) \tan^2(\frac{\theta_e}{2})$, and $\tau = Q^2/4M_p^2$.

An out-of-plane polarization component, P_n , can be the result of the interference between the Born term and 2-photon exchange. Such a component is independent of the beam helicity; it is expected to be at the level of 1-2 percent; it is hard to measure.

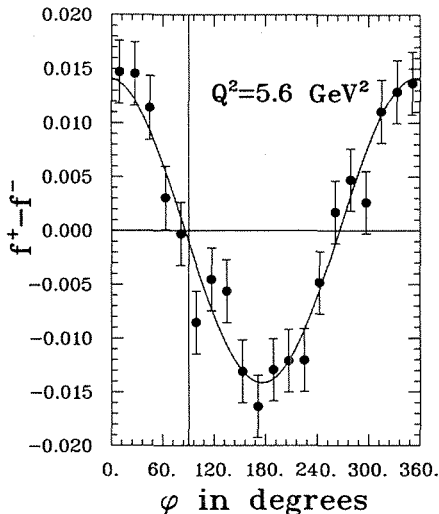


Figure 1: The azimuthal asymmetry distribution for $Q^2 = 5.6 \text{ GeV}^2$

In the two recoil polarization experiments at JLab the polarization of the recoil proton was measured in a polarimeter installed in the focal plane area of one of the large magnetic spectrometers of Hall A. A focal plane polarimeter consists of an analyzer block of C or CH_2 , preceded and followed by tracking wire chambers, in which the proton is scattered in a nuclear interaction; the normalized angular distribution of the protons scattered in the analyzer is given by:

$$f^\pm(\varphi) = \frac{1}{2\pi} (1 \pm A_y P_t^{fpp} \sin\varphi \mp A_y P_n^{fpp} \cos\varphi), \quad (2)$$

where P_n^{fpp} and P_t^{fpp} are the physical asymmetries at the focal plane polarimeter, and A_y is the analyzing power of the polarimeter; the \pm -sign denotes the two possible helicities of the polarized beam. In the data analysis f^\pm is approximated by the differential yield:

$$Y_i^\pm = \frac{1}{\Delta\varphi} \frac{N_i^\pm}{N_{in}^\pm \eta(\vartheta)}$$

where the index i refers to a bin in φ , $\Delta\varphi$ is the width of the bin, N_i^\pm is the number of events in bin i , N_{in}^\pm is the number of protons with specified helicity incident upon the FPP, and $\eta(\vartheta)$ is the differential efficiency of the analyzing reaction. Instrumental asymmetries

are cancelled by alternating the helicity denoted by \pm of the electron beam, and measuring Y^+ and Y^- . The difference $Y^+ - Y^-$ contains only the helicity dependent polarizations P_t^{fpp} and P_n^{fpp} , whereas the sum $Y^+ + Y^-$ contains a possible helicity independent part from two-photon exchange, and the instrumental asymmetries. Fig. 1 shows the azimuthal angular distribution of the asymmetry measured at the highest Q^2 reached so far, 5.6 GeV^2 .

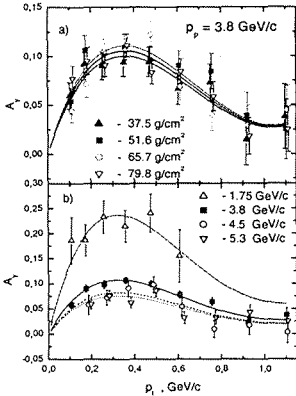


Figure 2: The Dubna calibration results for the analyzing power of CH_2 : top panel 4 analyzer thicknesses at $p_p = 3.8 \text{ GeV}/c$. Bottom panel fixed analyzer thickness of 51.6 gcm^{-2} and proton momenta $1.75, 3.8, 4.5$ and $5.3 \text{ GeV}/c$

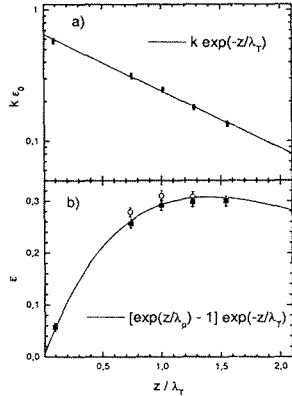


Figure 3: The Dubna calibration results: top panel attenuation of un-scattered beam versus analyzer thickness; bottom panel evolution of the efficiency integral with the analyzer thickness; note that in the text $\epsilon = \eta$

The polarimeter is characterized by the analyzing power, A_y , resulting from $\vec{L} \cdot \vec{S}$ coupling in the interaction of the proton with the analyzer nuclei, and the probability of interaction, $\eta(\vartheta)$, which is related to the inclusive differential pC or p(CH_2) yield; A_y depends only weakly upon the material of the analyzer, and $\eta(\vartheta)$ is determined by the total mean-free path in the material, λ_T , and the thickness of the analyzer. Hydrogen is best, CH_2 next best. Efficiency and analyzing power have been measured in Dubna in preparation for the third G_{Ep} JLab experiment [21] and are shown in Figs. 2 and 3.

In the JLab experiments the polarization of the recoil proton is measured in a polarimeter (FPP) located at the focal plane of one of the high resolution magnetic spectrometer. Vertical bending of the trajectories in the spectrometer rotates the polarization component P_t into a normal component at the analyzer, P_n^{fpp} , but does not change the polarization component P_t in first order.

In first approximation, at the target $P_t = P_n^{fpp} / \sin\chi$, and $P_t \sim P_t^{fpp}$, where χ is the spin precession angle in the dispersive plane of the magnetic spectrometer used to detect the recoil proton, given by

$$\chi = \gamma \Theta_B (\mu_p - 1),$$

where Θ_B is the bend angle of the trajectories in the dipole.

The desired ratio of form factors is then obtained from the target polarization components, P_t and P_ℓ , from the relation:

$$\frac{G_{Ep}}{G_{Mp}} = -\frac{P_t E_e + E'_e}{P_\ell} \tan \frac{\theta_e}{2}$$

3. Results of previous experiments

The JLab recoil polarization results are shown as the ratio $\mu_p G_{Ep}/G_{Mp}$, and compared with a selection of Rosenbluth results in Fig. 4. The Rosenbluth data included are those of the last SLAC measurement of Ref. [5], and the new JLab data of Refs. [6, 7].

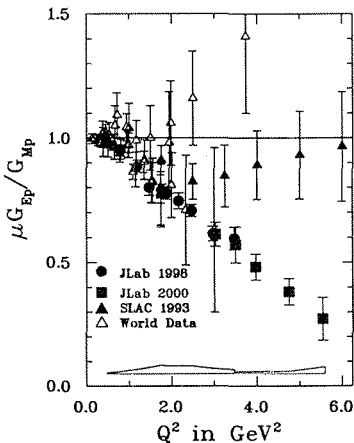


Figure 4: Ratio $\mu_p G_{Ep}/G_{Mp}$ from the JLab recoil polarization experiments, compared to a selection of ratios obtained by Rosenbluth separation method

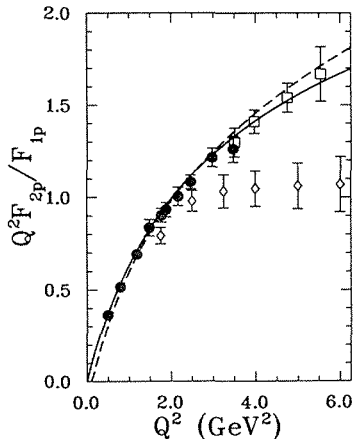


Figure 5: The ratio $Q^2 F_2/F_1$ from the JLab recoil polarization experiments, compared to recent pQCD predictions by Belitsky *et al* [22] and Brodsky [23].

The Sachs form factor ratio also determine the ratio of the Pauli and Dirac form factors F_2/F_1 ; the latter are shown in Fig. 5 where they are compared with two recent calculations based on perturbative QCD: the dashed curve is the modified pQCD prediction of Belitsky *et al* [22], which takes orbital angular momentum of the quarks into account; the solid line is an “empirical fit” from Brodsky [23], taking into account the logarithmic behavior of the F_2/F_1 - ratio inherent in pQCD.

4. Theoretical “Predictions”

Early attempts to understand the nucleon form factors were based on the vector meson dominance model or VMD. In 1972 Iachello [24] had predicted a zero crossing for G_{Ep}

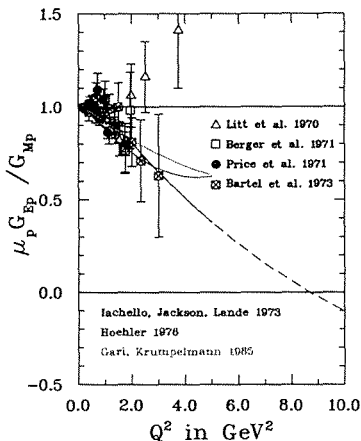


Figure 6: Form factor ratio compared to VMD calculations from the 1970's. Noticeable is Iachello's prediction of a zero crossing of the ratio; his model included a small hard core inside the proton

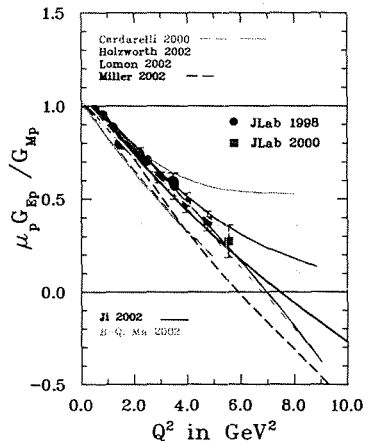


Figure 7: The ratio $Q^2 F_2 / F_1$ as determined in the recoil polarization experiments 93-027 and 99-007, compared to two recent pQCD predictions, by Belitsky *et al* [22] and Brodsky [23]

near 8 GeV², based on a modified VMD model including a small hard core inside the proton. This prediction is shown in Fig. 6, together with the other VMD fits and data of this period only [25, 26]. Two years before the first JLab measurement Holzwarth [27] had also predicted a zero crossing of G_{Ep} , based on the soliton model. This prediction and a number of current versions of the constituent quark [28, 29, 30], VMD [31] and di-quark model [32] predictions are shown in Fig. 7. All forms of the constituent quark model require a relativistic approach to reproduce the recoil polarization data. The relativistic di-quark model of Ma reproduces the right slope of decrease of the G_{Ep}/G_{Mp} ratio too. The revised pQCD prediction of Brodsky [23] as well as a form of pQCD including quark orbital angular momentum by Belitsky *et al* are also shown in this figure [22].

5. Possible origins of the discrepancy

Radiative corrections (RC) affect ep cross sections at the level of 30-40% and the data are corrected for it. The correction has to have an accuracy better than or of order 1% at $Q^2=5.6$ GeV² as the contribution of G_{Ep} to the cross section is smaller than 10%. The radiative correction to the cross section is ϵ dependent, and therefore affect the separation result directly; it is based on the seminal papers of Mo and Tsai [33] and Maximon and

Tjon [34], which do not include the inelastic contribution in the proton vertex correction. Radiative corrections affect the G_{Ep}/G_{Mp} -ratio from polarization data by less than 1% at a Q^2 of 5.6 GeV² when the proton defines the kinematics (see Afanasev [8]).

To explain the discrepancy between Rosenbluth and recoil polarization results, we have to also consider the two-photon exchange contribution; this was recently discussed by Guichon and Vanderhaegen [10], Blunden and Melnitchouk [11], Chen, Afanasev, Brodsky, Carlson and Vanderhaegen [12], and Rekaló and Tomasi-Gustafsson [13].

The possibility that the discrepancy is an experimental effect must of course also be examined. It appears that the discrepancy cannot be due to experimental systematics in the cross section measurement, as the recent ‘‘Super’’ Rosenbluth separation demonstrates (Segel et al [7]). This new JLab experiment was the first $^1H(e, p)$ measurement; all previous separations were based on $^1H(e, e')$; in this case radiative corrections are both smaller and different; yet the results are compatible with older Rosenbluth data. They are shown in Fig. 4 as red open triangles.

6. Two-Photon Exchange Contribution

Two-photon affects polarization observables and cross sections at the same level of a few %; but at large Q^2 the form factors from Rosenbluth separation are strongly affected by this small correction which is ϵ dependent and $G_{Ep}^2 \ll \tau G_{Mp}^2$, as we now know from the recoil polarization experiments.

The transverse polarization component, and therefore G_{Ep}/G_{Mp} , is affected only at the level of a few %; and this is the beauty of the method!

The calculations in Ref. [12] are based on generalized parton distributions which fit the proton form factor. The correction they calculate brings the Rosenbluth form factor results in approximative agreement with the recoil polarization results. Their prediction for the recoil polarization experiments is shown as a 3-dimensional plot in Fig. 8, as the absolute correction $\Delta(\mu R)$ to the form factor ratio $R = \mu_p G_{Ep}/G_{Mp}$, versus ϵ and Q^2 . It can be seen in this figure that at 9 GeV², the two-photon correction is smaller than the anticipated statistical uncertainty of 0.08 (see below) by a factor of 3-4.

Two-photon exchange affects form factor observables as an interference between the single- and two-photon processes. As a result the T-matrix depends on three complex amplitudes, \tilde{G}_M , \tilde{F}_2 and \tilde{F}_3 , instead of 2 real and relativistically invariant amplitudes, $G_M(Q^2)$ and $G_E(Q^2)$, which can be written as [10]:

$$T = \frac{e^2}{Q^2} \bar{u}(k') u(k) \bar{u}_p(p') \left(\tilde{G}_M \gamma^\mu - \tilde{F}_2 \frac{P^\mu}{M} + \tilde{F}_3 \frac{\gamma \cdot K P^\mu}{M^2} \right) u(p) \quad (3)$$

In Born approximation, the first two amplitudes are the usual G_M and F_2 (real) functions, and $\tilde{F}_3=0$. The polarization components are then given as [10]:

$$P_t = -\sqrt{\frac{2\epsilon(1-\epsilon)}{\tau}} \frac{C_B(\epsilon, Q^2) |\tilde{G}_M|^2}{d\sigma} \times \left\{ \frac{|\tilde{G}_M| - \cos \phi_{2M} |\tilde{F}_2| (1 + \tau)}{|\tilde{G}_M|} + \frac{\nu \cos \phi_{3M} |\tilde{F}_3|}{M^2 |\tilde{G}_M|} \right\}$$

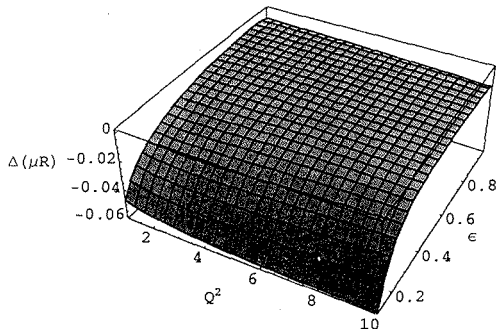


Figure 8: Calculated values of the correction $\Delta\mu_p G_{Ep}/G_{Mp}$ to the measured ratio versus Q^2 and ϵ

$$P_l = \sqrt{(1+\epsilon)(1-\epsilon)} \frac{C_B(\epsilon, Q^2) |\tilde{G}_M|^2}{d\sigma} \times \left\{ 1 + \frac{2\epsilon}{1+\epsilon} \cdot \frac{\nu \cos \phi_{3M} |\tilde{F}_3|}{M^2 |\tilde{G}_M|} \right\}$$

where C_B is a phase space factor.

One approach consists in connecting measured cross-sections and polarization component ratios at the same Q^2 and range of ϵ -values, and extract by a fitting procedure both the unknown "true" form-factor ratio R and the unknown two-photon contribution $Y_{2\gamma}$:

$$\frac{d\sigma_{red}(\epsilon)}{|\tilde{G}_M|^2} = 1 + \frac{\epsilon}{\tau} R^2 + 2\epsilon \left(1 + \frac{R}{\tau} \right) Y_{2\gamma}(\epsilon) \quad (4)$$

$$\frac{P_t}{P_l}(\epsilon_p) = -\sqrt{\frac{2\epsilon_p}{\tau(1+\epsilon_p)}} \frac{R + Y_{2\gamma}(\epsilon_p)}{1 + 2\epsilon_p Y_{2\gamma}(\epsilon_p)/(1+\epsilon_p)} \quad (5)$$

where ϵ and ϵ_p denote the ϵ -values at which we will have cross section and polarization data, respectively. The approved experiment in Hall C, 09-019, will measure G_{Ep}/G_{Mp} at fixed Q^2 of 2.6 GeV² with 1% statistics at 3 values of ϵ , 0.12, 0.60 and 0.78 [35].

7. The next Experiment

7.1. New Polarimeter

The experiment G_{Ep} (III) will extend the Q^2 -range to 9 GeV² and requires a better polarimeter than used in the two previous experiments. It is not possible to increase the analyzing power. Increasing the analyzer thickness does not work either; but increasing

the number of polarimeters in series does work. We have chosen a configuration for the new polarimeter with two identical FPPs in series, as shown in Fig. 9.

The forthcoming third phase of investigation of the proton form factors could not have

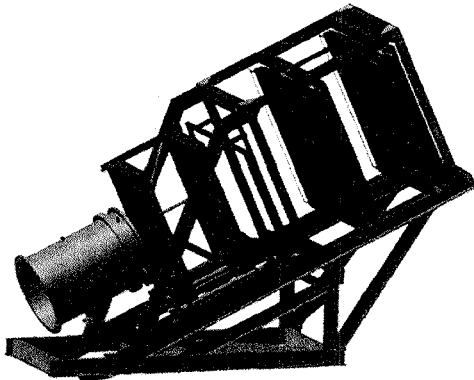


Figure 9: *Design drawing of the double polarimeter under construction for the third G_{EP} experiment in Hall C. The orange boxes are the permanent HMS focal plane drift chambers. The two magenta boxes represent the two pairs of drift chamber of the FPP; the two CH_2 analyzer blocks are not shown*

started without the A_y measurement in Dubna in 2001 [21], shown in Figs. 2 and 3 up to proton momentum of 5.3 GeV/c, with polarized proton beams obtained by breaking up polarized deuterons produced by the Synchrophasotron.

We have also tested the two polarimeter concept in Hall A by reconfiguring the FPP installed in the high resolution hadron spectrometer (HRSh). Data with a first CH_2 analyzer following the two focal plane drift chambers, followed by the two front chambers of the FPP, and then the permanent C analyzer followed by the two FPP back chambers have been taken during the real Compton scattering (RCS) and deuteron two-body photo-desintegration $\gamma d \rightarrow p(n)$. The results are shown in Fig. 10. The first analyzer was 44 cm of CH_2 and the second analyzer 50 cm of C. The data confirm that A_y is larger for CH_2 than for C and that A_y is the same for 44 and 100 cm of CH_2 from experiment JLab 99-007. Total efficiency for the double polarimeter was $\sim 50\%$, even though there were geometrical restrictions in the acceptance of the first polarimeter due to the improvised nature of the test.

The new polarimeter requires 4 large drift chambers; these chambers are currently being built in the Instrumentation group of the Laboratory for High Energy (LHE) at the Joint Institute for Nuclear Research (JINR) in Dubna, under the leadership of Prof. Yu. Zanevsky. A prototype fifth chamber has been received at JLab in November 2003, and is shown in Fig. 11. This is another fine example of the productive collaboration between LHE and our group in Virginia.

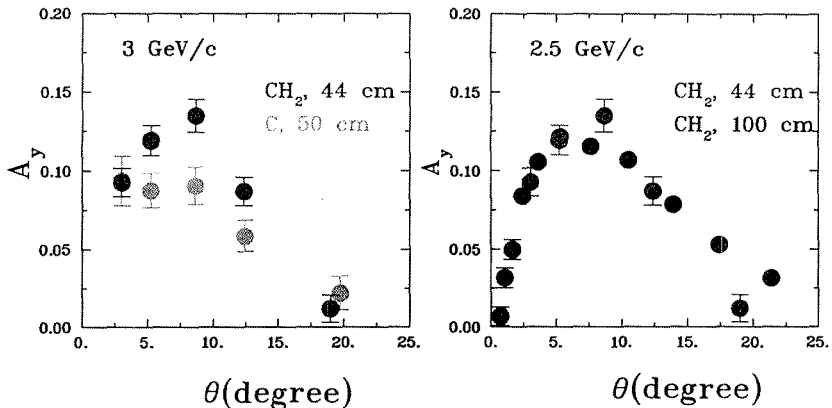


Figure 10: *Left panel: analyzing power in the CH₂ and C-sections of the double polarimeter clearly show the advantage of CH₂. Right panel: comparison of the result for 44 cm of CH₂, with those of ref. [2] for 100 cm of CH₂ confirming that no loss of analyzing power is visible with the thicker absorber*

7.2. Calorimeter BigCal

The continuation of the recoil polarization measurements of the G_{Ep}/G_{Mp} ratio to larger Q^2 is possible only if the electron detector solid angle matches the spectrometer solid angle, i.e. all electrons associated with a proton detected in the HMS FPP, are detected; the reason is that the cross section has become quite small, $\sim 10^{-37}$ cm². At $Q^2=9$ GeV² and with a beam energy of 6 GeV, this requires $\Delta\Omega_e=140$ msr (HMS has 7 msr). Such a solid angle matching can only be obtained with a large size calorimeter. We have constructed an electromagnetic calorimeter with 1744 bars of lead-glass, 1024 bars coming from Protvino and 720 bars from Yerevan; the individual bar size is 4x4 cm², length 45 and 40 cm, respectively. The status of the calorimeter in late 2003 can be seen in Fig. 12. The Čerenkov light produced by the showering of 1 to 2 GeV electrons is detected, making the calorimeter insensitive to non-showering particles like protons and pions. The frontal area of the calorimeter is 2.8 m².

8. Other form factor measurements at JLab

Two JLab experiments have measured the neutron electric form factor G_{En} in Hall C [16, 17], and one has measured the neutron magnetic form factor G_{Mn} in Hall B [20]. Two new experiments at JLab will measure the neutron electric form factor to larger Q^2 . The first will obtain the asymmetry in ${}^3\vec{H}e(\vec{e} \rightarrow en)^2H$ in Hall A to $Q^2=2.7$ GeV² [18], and in the second the neutron recoil polarization in ${}^2H(\vec{e} \rightarrow, e'\bar{n})p$ in Hall C to $Q^2=4.3$ GeV² [19] will be measured. With these two experiments we can expect that the characterization of the nucleon structure in elastic scattering will be much advanced in the near future.

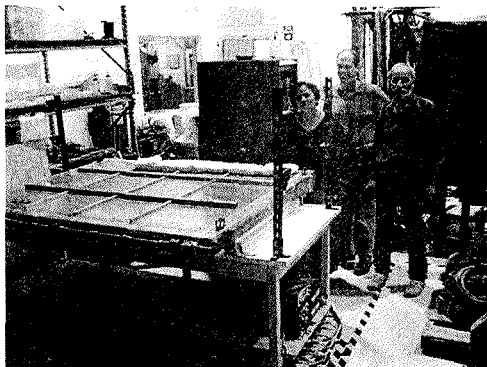


Figure 11: *The prototype drift chamber built at the LHE is inspected by Drs. Vina Punjabi, Mark K. Jones and Lev Smykov at JLab, Nov. 2003*

9. JLab upgrade to 12 GeV

The JLab upgrade to an energy of 12 GeV is now one of the top priorities for DOE. In the current scenario accelerator operation may be interrupted for 18 months sometimes in the time frame 2008-10, to install new arc magnets and new cavities. The 12 GeV should become available for experiments in 2012. The G_{Ep}/G_{Mp} -ratio can be measured as soon as an energy larger than 8.5 GeV becomes available in Hall C, to a Q^2 of 12 GeV^2 , using the new calorimeter and FPP being built for G_{Ep} (III) and the HMS. The recoil proton momentum will be 7.27 GeV/c. A planned superHMS spectrometer would allow the measurement of the G_{Ep}/G_{Mp} -ratio to 14 GeV^2 .

What will be A_y ? We hope to have the answer from the anticipated second Dubna calibration. The linear extrapolation of the A_y data from the first Dubna calibration [21], shown in Fig. 13 suggests that the analyzing power may be about 25% smaller than in the forthcoming 9 GeV^2 measurement; but we must check that nature behaves linearly with the planned next calibration at the Dubna Nuclotron.

10. Conclusions

We have presented the results of the two JLab recoil polarization experiments which measured the form factor ratio G_{Ep}/G_{Mp} using the recoil polarization technique from 0.5 to 5.6 GeV^2 . Above Q^2 of about 2 GeV^2 , these results are incompatible with ratios obtained using the traditional Rosenbluth separation method. This surprising finding has generated considerable work among theorists, but we do not have a definite explanation for the difference as of now; the two possibilities being discussed presently are the possibly incomplete radiate corrections and the previously neglected two-photon exchange contribution. Both affect the results of a Rosenbluth separation, but leave the recoil polarization essentially unchanged.



Figure 12: *Front view of the calorimeter taken in November, 2003: all lead-glass bars have been stacked. Currently the calorimeter is fully assembled and is being tested by taking cosmics data*

The history of proton form factor measurements, which started with the pioneering work of R. Hofstadter 50 years ago, illustrates the danger of using only one method to measure a given physical observable; the Rosenbluth separation method has been for a long time the only technique available to separate the form factors of elastic, quasi-elastic and inelastic electron scattering on the nucleon and nuclei, as in ep , $A(e, e'p)$ and $(e, e'\Delta)$ or $(e, e'N^*)$, respectively. A number of recent technological advances in accelerators and instrumentation, including high performing polarized beams and targets, and efficient polarimeters, have finally given us a second approach, and at the same time led to the discovery of a weakness of the older method, connected to the large radiative corrections required for cross section data.

The next measurement of the G_{Ep}/G_{Mp} ratio, $GE_p(\text{III})$, is currently being prepared. It will extend the Q^2 range to 9 GeV^2 . There are several theoretical calculation which anticipate that the ratio might change sign at a Q^2 smaller than 9 GeV^2 . The two new data points this next experiment will provide, and their anticipated statistical uncertainties, are shown in Fig. 14.

With another analyzing power measurement in Dubna, the Q^2 limit for G_{Ep}/G_{Mp} can be pushed to 12 GeV^2 once the energy upgrade at JLab is completed. Such an experiment has been proposed [36] and it potentially could be one of the early experiments with the upgraded JLab accelerator.

New neutron form factor measurements are very important, as the nucleon must be understood in its two isospin state forms. In view of a future measurements of G_{En} there is also a need for neutron analyzing power data; the NUCLOTRON at JINR is the only facility in the World, where such measurements could be made in the near future.

This work was supported in part by the U.S. National Science Foundation (NSF PHY-0140108) and the US Department of Energy (DEFG-02-89ER-40525).

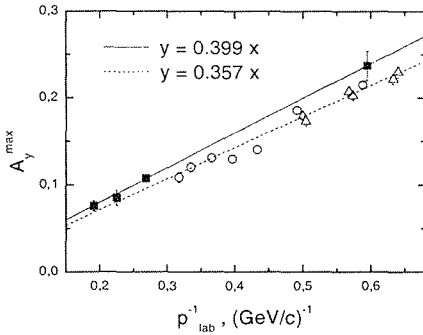


Figure 13: *The maximum value of the analyzing power A_y for carbon and CH_2 , versus the inverse of the proton momentum. The apparent linear behavior allows for a tentative extrapolation to larger momenta*

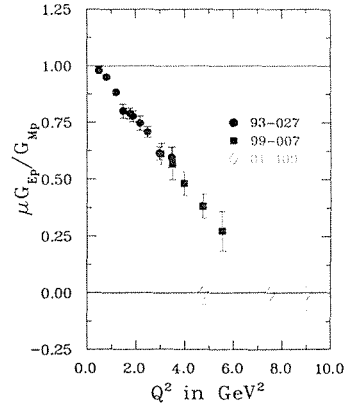


Figure 14: *Results of the two previous JLab recoil polarization experiments, and the two new data points approved for expt. 04-108*

References

- [1] M.K. Jones et al., Phys. Rev. Lett. **84**, 1398 (2000).
- [2] O. Gayou et al., Phys. Rev. Lett. **88**, 092301 (2002).
- [3] A.I. Akhiezer and M.P. Rekalo, Sov. Phys.-Doklady **13**, 572 (1968).
- [4] R. Arnold, C. Carlson and F. Gross, Phys. Rev. C**23**, 363 (1981).
- [5] L. Andivahis *et al.*, Phys. Rev. D **50**, 5491 (1994).
- [6] M.E. Christy *et al.*, nucl-e/0401030.
- [7] J. Arrington and R. Segel *et al.*, "New Measurements of G_E/G_M for the Proton", JLab experiment 01-001.
- [8] N. Merenkov, A. Afanasev and I. Akushevich, "Calculation of the QED correction to the recoil polarization by the electron structure function method", JLAB-THY-00-03, and A.V. Afanasev, I. Akushevich, A. Ilyichev and N. P. Merenkov, Phys. Lett. B **514**, 269 (2001).
- [9] E. Tomasi-Gustafsson and G.I. Gakh, hep-ph/0412137.
- [10] P.A.M. Guichon and M. Vanderhaeghen, Phys. Rev. Lett. **91**, 142303 (2003)
- [11] P.G. Blunden, W. Melnitchouk, J.A. Tjon, Phys. Rev. Lett. **91** 142304 (2003).
- [12] Y.-C. Chen, A. Afanasev, S.J. Brodsky, C.E. Carlson and M. Vanderhaeghen, submitted to P.R.L., also arXiv:hep-ph/0403058.

- [13] M.P. Rekaló and E. Tomasi-Gustafsson, Eur. Phys. J. A **22**, 331 (2004), and Nucl. Phys. A **740**, 271 (2004), and Nucl. Phys. A **742**, 322 (2004)
- [14] C.F. Perdrisat, V. Punjabi, M.K. Jones and E. Brash, "Measurement of G_{Ep}/G_{Mp} to $Q^2=9$ GeV² via recoil polarization" exp 04-108.
- [15] R. Gilman, L. Pentchev, C.F. Perdrisat and R. Suleiman, "Measurement of the Two-photon Exchange Contribution in ep Elastic Scattering using Recoil Polarization", exp.04-019.
- [16] H. Zhu *et al*, Phys. Rev. Lett. **87**, 081801 (2001).
- [17] R. Madey *et al* Phys. Rev. Lett. **91**, 122002 (2003).
- [18] B. Reitz, B. Wojtsekhowski, K. McCormick, "Measurement of the Neutron Electric Form Factor G_{En} at High Q^2 , exp. 02-013.
- [19] R. Madey, S. Kowalski, A. Yu. Semenov and B.D. Anderson, "The Neutron Electric Form Factor at $Q^2=4.3$ GeV² from the Reaction ${}^2H(\bar{e}, e'\bar{\nu}){}^1H$ via Recoil Polarimetry", exp. 04-110.
- [20] JLab proposal 94017, W. Brooks and M. Vineyard.
- [21] L.S. Azhgirey *et al*, AIP Conf. Proc. **675**, 826 (2003) and to be published in NIM (2005).
- [22] A.V. Belitsky, Xiandong Ji and Feng Yuan, hep-ph/0212351 v2 (2003).
- [23] S.J. Brodsky, hep-ph/0208158 v1 (2002).
- [24] F. Iachello, A.D. Jackson, and A. Landé, Phys. Lett. B **43**, 191 (1973).
- [25] G. Höhler *et al*, Nucl. Phys. B **114**, 505 (1976).
- [26] M.F. Gari and W. Kruempelmann, Z. Phys. A **322**, 689 (1985) 689; Phys. Lett. B **274**, 159 (1992); Phys. Lett. B **282**, 483(E) (1992).
- [27] G. Holzwarth, Zeitschr. Fuer Physik A **356**, 339 (1996); G. Holzwarth, hep-ph/0201138 v1 (2002).
- [28] M.R. Frank, B.K. Jennings and G.A. Miller, Phys. Rev. C **54**, 920 (1996).
- [29] F. Cardarelli and S. Simula Phys. Rev. C **62**, 65201 (2000); S. Simula, e-print nucl-th/0105024.
- [30] E. Pace, G. Salme, F. Cardarelli and S. Simula, Nucl. Phys. A **666&667**, 33c (2000).
- [31] E.L. Lomon, Phys.Rev. C **64**, 035204 (2001).
- [32] B.-Q. Ma, D. Quing and I. Schmidt, Phys. Rev C **65** 035205 (2002).
- [33] L.W. Mo and Y.S. Tsai, Rev. Mod. Phys. **41**, 205 (1969).

- [34] L.C. Maximon and J.A. Tjon, Phys. Rev. C **62**, 054320 (2000).
- [35] R. Suleiman, L. Pentchev, C.F. Perdrisat and R. Gilman, Jlab experiment 04-019.
- [36] “ G_{Ep}/G_{Mp} with an 11 GeV electron beam”; C.F. Perdrisat, V. Punjabi, M.K. Jones and E.J. Brash, letter of intent in 12 GeV proposal CD0, (2000), JLab.

MESONIC EXCHANGE CURRENTS IN THE DEUTERON. THE BRIDGE FROM NONRELATIVISTIC TO RELATIVISTIC NUCLEAR PHYSICS

S. G. Bondarenko², V. V. Burov^{2†}, N. Hamamoto^{1,2}, Y. Manabe^{1,2}, H. Toki¹

(1) *Research Center for Nuclear Physics, Osaka University*

(2) *Joint Institute for Nuclear Research*

† *E-mail: burov@theor.jinr.ru*

Abstract

Recent results obtained by the application of the Bethe-Salpeter approach to the analysis of elastic electron-deuteron scattering, with the separable NN kernel are presented. We analyze the role of the P waves (negative energy components) on the electromagnetic properties of the deuteron and compare it with the nonrelativistic results. It was shown that the contribution of the P waves must be taken into account to explain tensor polarization and charge form factor of the deuteron. The connection of the P waves with mesonic exchange currents (MEC) is demonstrated.

1. Introduction

The study of electromagnetic properties of the deuteron helps us to construct the theory of strong interactions and, in particular, the nucleon-nucleon interaction (see, for example, [1]). Theoretical research in this field is of topical interest which is reflected in recent review articles [2]-[8]. A large amount of available experimental data stimulate a further development of theoretical methods which are often restricted to qualitative predictions. The forthcoming experiments are expected to provide high-precision data, which will allow us to explore the region of large momentum transfer in elastic, inelastic and deep inelastic (DIS) electron-nucleus reactions.

The fact that nuclei consist of bound nucleons introduces a major problem for theoretical description of relativistic $l - A$ interactions. The deuteron is naturally the first object in the row of many other nuclei, and has received a vast number of treatments within many different approaches. One finds also that non-relativistic schemes of calculations are widely employed in the analysis, which can be justified for a few particular cases. On the other hand, the consistent consideration of the relativistic bound states is offered within the Bethe-Salpeter (BS) formalism (see, for example, review [8]), which allows qualitatively a new interpretation of the physics of the relativistic bound state and should not be regarded as an alternative scheme only.

We emphasize the covariant description of the BS formalism by taking the separable interaction, which is still a stage of infancy. In particular, the role of the abnormal parity states, is not yet confronted directly with experimental data, though the necessity is demonstrated in this paper.

2. Basic Formalism of the BS Approach

We start with the Bethe-Salpeter Equation (BSE) for NN T matrix:

$$T_{\alpha\beta,\delta\gamma}(P, p', p) = V_{\alpha\beta,\delta\gamma}(P, p', p) + i \int \frac{d^4 k}{(2\pi)^4} V_{\alpha\beta,\epsilon\lambda}(P, p', k) S_{\epsilon\eta}(P/2 + k) S_{\lambda\rho}(P/2 - k) T_{\eta\rho,\delta\gamma}(P, k, p), \quad (1)$$

where P is the total momentum, p and p' are the relative 4-momenta of the two nucleons before and after the interaction. They are connected with 4-momenta of first (q_1) and second (q_2) particles: $P = q_1 + q_2$, $p = (q_1 - q_2)/2$, $q_1 = P/2 + p$, $q_2 = P/2 - p$. $S_{\alpha\beta}(k)$ is one particle green function: $S_{\alpha\beta}(k) = [1/(k \cdot \gamma - m + i\epsilon)]_{\alpha\beta}$.

The bound state corresponds to a pole in T matrix at $P^2 = M_B^2$ (M_B is the mass of bound state) takes the form:

$$T_{\alpha\beta,\delta\gamma}(P, p', p) = \underbrace{\frac{\Gamma_{\alpha\beta}(P, p') \bar{\Gamma}_{\delta\gamma}(P, p)}{P^2 - M_B^2}}_{\text{bound state (mass=M}_B\text{)}} + \underbrace{R_{\alpha\beta,\delta\gamma}(P, p', p)}_{\text{other states}}, \quad (2)$$

where $\Gamma_{\alpha\beta}$ is the vertex function of BSE, and $R_{\alpha\beta,\delta\gamma}$ is regular at $P^2 = M_B^2$.

We can express the BS amplitude by the vertex function as:

$$\Phi_{\alpha\beta}(P, p) = S_{\alpha\gamma}\left(\frac{P}{2} + p\right) S_{\beta\delta}\left(\frac{P}{2} - p\right) \Gamma_{\gamma\delta}(P, p), \quad (3)$$

and we obtain the equation for the BS amplitude from Eq. (1-3):

$$\Phi_{\alpha\beta}(P, p) = i S_{\alpha\eta}\left(\frac{P}{2} + p\right) S_{\beta\rho}\left(\frac{P}{2} - p\right) \int \frac{d^4 k}{(2\pi)^4} V_{\eta\rho,\gamma\delta}(P, p, k) \Phi_{\gamma\delta}(P, k) \quad (4)$$

3. Partial-Wave Decomposition of the BS Amplitude

We determine two-particle spinor basis in c.m. frame as $U_{\mu_1}^{\rho_1(1)}(\mathbf{p}) \otimes U_{\mu_2}^{\rho_2(2)T}(-\mathbf{p})$, where μ is the spin projection, $\rho_{1,2}$ is so-called ρ -spin, which distinguish the positive and negative-energy states. Both of them are necessary to prepare the complete set for the two-particle bound state. The spinors $U_{\mu_1}^{\rho_1}(\mathbf{p})$ are connected with the Dirac free spinors $u_{\mu}(\mathbf{p})$ and $v_{\mu}(\mathbf{p})$ as

$$U_{\mu}^{\rho}(\mathbf{p}) = \begin{cases} u_{\mu}(\mathbf{p}), & \rho = +, \\ v_{-\mu}(-\mathbf{p}), & \rho = -. \end{cases} \quad (5)$$

The connections between the propagators and the spinors can be written as

$$\begin{aligned} [S(P/2 + p)]^{-1} U_{\mu}^{\rho(1)}(\mathbf{p}) &= \rho S_{\rho}^{(1)-1} U_{\mu}^{\rho(1)}(-\mathbf{p}), \\ [S(P/2 - p)]^{-1} U_{\mu}^{\rho(2)}(-\mathbf{p}) &= \rho S_{\rho}^{(2)-1} U_{\mu}^{\rho(2)}(\mathbf{p}), \end{aligned}$$

where $E_{\mathbf{p}} = \sqrt{\mathbf{p}^2 + m^2}$,

$$S_{\pm}^{(1)} = 1/(\sqrt{s}/2 + p_0 \mp E_{\mathbf{p}}), \quad S_{\pm}^{(2)} = 1/(\sqrt{s}/2 - p_0 \mp E_{\mathbf{p}}). \quad (6)$$

Here, we can write the partial wave expansion of the BS amplitude as

$$\begin{aligned}\Phi_{\alpha\beta}^{JM}(P, p) &= S_{\alpha\gamma}(P/2 + p)\Gamma_{\gamma\delta}^{JM}(P, p)S_{\delta\beta}^T(P/2 - p) \\ &= \sum_{LS\rho_1\rho_2} S_{\rho_1}^{(1)}S_{\rho_2}^{(2)}g_{JLS\rho_1\rho_2}(p_0, |\mathbf{p}|)\Gamma^{JLS\rho_1\rho_2}(\mathbf{p})U_c,\end{aligned}\quad (7)$$

where $U_c = i\gamma_2\gamma_0$, and $\Gamma^{JLS\rho_1\rho_2}(\mathbf{p})$ is the spin-angular function defined as

$$\begin{aligned}\Gamma^{JLS\rho_1\rho_2}(\mathbf{p})U_c &= i^L \sum_{\mu_1\mu_2m_Lm_S} (Lm_LSm_S|JM)(\frac{1}{2}\mu_1\frac{1}{2}\mu_2|Sm_S) \times \\ &\quad \times Y_{Lm_L}(\hat{\mathbf{p}})U_{\mu_1}^{\rho_1(1)}(\mathbf{p}) \otimes U_{\mu_2}^{\rho_2(2)T}(-\mathbf{p}).\end{aligned}\quad (8)$$

We introduce the symmetrical notation of ρ -spin for convenience, the radial part of the BS amplitude can be written as

$$\phi_{JLS\rho}(p_0, |\mathbf{p}|) = \sum_{\rho'} S_{\rho\rho'}(p_0, |\mathbf{p}|) g_{JLS\rho}(p_0, |\mathbf{p}|), \quad (9)$$

where $S_{\rho\rho'}$ is

$$\begin{aligned}S_+ &= S_{++} = (\sqrt{s}/2 + p_0 - E_{\mathbf{p}})^{-1}(\sqrt{s}/2 - p_0 - E_{\mathbf{p}})^{-1}, \\ S_- &= S_{--} = (\sqrt{s}/2 + p_0 + E_{\mathbf{p}})^{-1}(\sqrt{s}/2 - p_0 + E_{\mathbf{p}})^{-1}, \\ S_e &= S_{ee} = S_{oo} = (s/4 - p_0^2 - E_{\mathbf{p}}^2) \left((s/4 - p_0^2 - E_{\mathbf{p}}^2)^2 - 4p_0^2E_{\mathbf{p}}^2 \right)^{-1}, \\ S_o &= S_{eo} = S_{oe} = (2p_0E_{\mathbf{p}}) \left((s/4 - p_0^2 - E_{\mathbf{p}}^2)^2 - 4p_0^2E_{\mathbf{p}}^2 \right)^{-1}, \quad \text{others } s = 0.\end{aligned}\quad (10)$$

The BS amplitude for the deuteron has 8 states: ${}^3S_1^+, {}^3D_1^+, {}^1P_1^e, {}^1P_1^o, {}^3P_1^e, {}^3P_1^o, {}^3S_1^-, {}^3D_1^-$. ${}^3S_1^+, {}^3D_1^+$ are positive energy states and others include negative energy states.

4. Solution of the BSE

After the partial-wave decomposition, the BSE for T matrix has the following form:

$$\begin{aligned}T_{\alpha\beta}(p'_0, |\mathbf{p}'|, p_0, |\mathbf{p}|; s) &= V_{\alpha\beta}(p'_0, |\mathbf{p}'|, p_0, |\mathbf{p}|; s) + \\ &+ \frac{i}{2\pi^2} \int dk_0 \mathbf{k}^2 d|\mathbf{k}| \sum_{\gamma\delta} V_{\alpha\gamma}(p'_0, |\mathbf{p}'|, k_0, |\mathbf{k}|; s) S_{\gamma\gamma}(k_0, |\mathbf{k}|; s) T_{\gamma\beta}(k'_0, |\mathbf{k}'|, p_0, |\mathbf{p}|; s),\end{aligned}\quad (11)$$

here the indexes of Greece character correspond to the partial states ($\alpha : JLS\rho$).

We introduce separable *ansatz* to transform the BSE to a system of the linear equation in the following manner:

$$V_{\alpha\beta}(p'_0, |\mathbf{p}'|, p_0, |\mathbf{p}|; s) = \sum_{i,j=1}^N \lambda_{ij} g_i^{(\alpha)}(p'_0, |\mathbf{p}'|) g_j^{(\beta)}(p_0, |\mathbf{p}|), \quad \lambda_{ij} = \lambda_{ji}, \quad (12)$$

Then, the solution for the radial part of the BS amplitude can be written as

$$\phi_{JLS\rho}(p_0, |\mathbf{p}|) = \sum_{\rho'} \sum_{i,j=1}^N S_{\rho\rho'}(p_0, |\mathbf{p}|; s) \lambda_{ij} g_i^{(JLS\rho')} (p_0, |\mathbf{p}|) c_j(s), \quad (13)$$

Parameters of covariant Graz-II kernel of interaction

γ_1	28.69550 GeV ⁻²	λ_{11}	$2.718930 \cdot 10^{-4}$ GeV ⁶
γ_2	64.9803 GeV ⁻²	λ_{12}	$-7.16735 \cdot 10^{-2}$ GeV ⁴
β_{11}	$2.31384 \cdot 10^{-1}$ GeV	λ_{13}	$-1.51744 \cdot 10^{-3}$ GeV ⁶
β_{12}	$5.21705 \cdot 10^{-1}$ GeV	λ_{22}	16.52393 GeV ²
β_{21}	$7.94907 \cdot 10^{-1}$ GeV	λ_{23}	0.28606 GeV ⁴
β_{22}	$1.57512 \cdot 10^{-1}$ GeV	λ_{33}	$3.48589 \cdot 10^{-3}$ GeV ⁶

where $c_i(s)$ satisfy the following system of equations:

$$c_i(s) - \sum_{k,j=1}^N H_{ik}(s) \lambda_{kj} c_j(s) = 0, \quad (14)$$

$$H_{ij}(s) = \frac{i}{2\pi^2} \sum_{LS\rho\rho'} \int dk_0 \mathbf{k}^2 d|\mathbf{k}| S_{\rho\rho'}(k_0, |\mathbf{k}|; s) g_i^{(JLS\rho)}(k_0, |\mathbf{k}|) g_j^{(JLS\rho')}(k_0, |\mathbf{k}|). \quad (15)$$

5. Covariant Graz-II Interaction and P waves

To calculate various electromagnetic observables, we use the kernel which added P wave parts based on covariant Graz-II interaction. In above kernel (only positive states are taken into account: ${}^3S_1^+, {}^3D_1^+$), the functions g_i have the following form [9]:

$$\begin{aligned} g_1^{3S_1^+}(p_0, |\mathbf{p}|) &= \frac{1 - \gamma_1(p_0^2 - \mathbf{p}^2)}{(p_0^2 - \mathbf{p}^2 - \beta_{11}^2)^2}, \\ g_2^{3S_1^+}(p_0, |\mathbf{p}|) &= -\frac{(p_0^2 - \mathbf{p}^2)}{(p_0^2 - \mathbf{p}^2 - \beta_{12}^2)^2}, \\ g_3^{3D_1^+}(p_0, |\mathbf{p}|) &= \frac{(p_0^2 - \mathbf{p}^2)(1 - \gamma_2(p_0^2 - \mathbf{p}^2))}{(p_0^2 - \mathbf{p}^2 - \beta_{21}^2)(p_0^2 - \mathbf{p}^2 - \beta_{22}^2)^2}, \\ g_1^{3D_1^+}(p_0, |\mathbf{p}|) &= g_2^{3D_1^+}(p_0, |\mathbf{p}|) = g_3^{3S_1^+}(p_0, |\mathbf{p}|) \equiv 0. \end{aligned} \quad (16)$$

Parameters of covariant Graz-II are given in the Table.

In addition, we take into account the negative energy states: ${}^1P_1^c$ and ${}^1P_1^o$. The functions g_i of P waves have the following form:

$$\begin{aligned} g_4^{3S_1^+}(p_0, |\mathbf{p}|) &= g_4^{3D_1^+}(p_0, |\mathbf{p}|) = g_{1,2,3}^{1P_1^o}(p_0, |\mathbf{p}|) \equiv 0, \\ g_4^{1P_1^c}(p_0, |\mathbf{p}|) &= \frac{|\mathbf{p}|}{(p_0^2 - \mathbf{p}^2 - \beta_3^2)^2}, \\ g_4^{1P_1^o}(p_0, |\mathbf{p}|) &= \gamma_3 \frac{p_0}{m} \frac{|\mathbf{p}|}{(p_0^2 - \mathbf{p}^2 - \beta_3^2)^2}. \end{aligned} \quad (17)$$

The solution of the BSE can be written as

$$\phi_{3S_1^+}(p_0, |\mathbf{p}|) = (c_1 \lambda_{11} + c_2 \lambda_{12} + c_3 \lambda_{13} + c_4 \lambda_{14}) S_+ g_1^{3S_1^+}(p_0, |\mathbf{p}|) + \quad (18)$$

$$(c_1 \lambda_{12} + c_2 \lambda_{22} + c_3 \lambda_{23} + c_4 \lambda_{24}) S_+ g_2^{3S_1^+}(p_0, |\mathbf{p}|), \quad (19)$$

$$\begin{aligned}
\phi_{3D_1^+}(p_0, |\mathbf{p}|) &= (c_1\lambda_{13} + c_2\lambda_{23} + c_3\lambda_{33} + c_4\lambda_{34})S_+g_3^3D_1^+(p_0, |\mathbf{p}|), \\
\phi_{1P_1^e}(p_0, |\mathbf{p}|) &= (c_1\lambda_{14} + c_2\lambda_{24} + c_3\lambda_{34} + c_4\lambda_{44})(S_e g_4^1P_1^e(p_0, |\mathbf{p}|) + S_o g_4^1P_1^o(p_0, |\mathbf{p}|)), \\
\phi_{1P_1^o}(p_0, |\mathbf{p}|) &= (c_1\lambda_{14} + c_2\lambda_{24} + c_3\lambda_{34} + c_4\lambda_{44})(S_e g_4^1P_1^o(p_0, |\mathbf{p}|) + S_o g_4^1P_1^e(p_0, |\mathbf{p}|)).
\end{aligned}$$

$\phi_{1P_1^e}$ is even and $\phi_{1P_1^o}$ is odd under $p_0 \rightarrow -p_0$, which are decided by Eq. (7).

6. Elastic Electron-Deuteron Scattering

In the relativistic impulse approximation, the deuteron current matrix element can be written as

$$\begin{aligned}
\langle D'M' | J_\mu | D\mathcal{M} \rangle &= ie \int \frac{d^4p}{(2\pi)^4} \text{Tr} \left[\bar{\Phi}_{\mathcal{M}'}(P', p') \Gamma_\mu^{(p+n)}(q) \Phi_{\mathcal{M}}(P, p) (S^{(2)T}(q_2))^{-1} \right], \quad (20) \\
\Gamma_\mu^{(S)}(q) &= \gamma_\mu F_1^{(S)}(q^2) - \frac{\gamma_\mu \hat{q} - \hat{q} \gamma_\mu}{4m} F_2^{(S)}(q^2), \quad (21)
\end{aligned}$$

where $\Phi_{\mathcal{M}}(P, p)$ is BS amplitude of the deuteron, $P' = P + q$ and $p' = p + q/2$. q is the momentum transfer and $\eta = -q^2/4M^2 = Q^2/4M^2$ where M is the deuteron mass. The vertex of γNN interaction $\Gamma_\mu^{(S)}(q)$ is on-mass-shell form. The isoscalar form factors of the nucleon $F_{1,2}^{(S)}$ is the summation of two nucleons. To calculate the deuteron form factors, one should know at least three matrix elements with different total angular momentum projections and current component, for example, $\langle 0 | J_0 | 0 \rangle$, $\langle 1 | J_0 | 1 \rangle$ and $\langle 1 | J_1 | 0 \rangle$. The electric $F_C(q^2)$, quadrupole $F_Q(q^2)$ and magnetic $F_M(q^2)$ form factors are normalized as $F_C(0) = 1$, $F_Q(0) = M^2 Q_D$, $F_M(0) = \mu_D M/m$, where m is the nucleon mass, Q_D and μ_D are quadrupole and magnetic moments of the deuteron, respectively. The tensor polarization components of the final deuteron are expressed through the deuteron form factors as follows:

$$\begin{aligned}
T_{20} [A + B \tan^2 \frac{\theta_e}{2}] &= -\frac{1}{\sqrt{2}} \left[\frac{8}{3} \eta F_C F_Q + \frac{8}{9} \eta^2 F_Q^2 + \frac{1}{3} \eta (1 + 2(1 + \eta) \tan^2 \frac{\theta_e}{2}) F_M^2 \right], \\
T_{21} [A + B \tan^2 \frac{\theta_e}{2}] &= \frac{2}{\sqrt{3}} \eta (\eta + \eta^2 \sin^2 \frac{\theta_e}{2})^{1/2} F_M F_Q \sec \frac{\theta_e}{2}, \quad (22) \\
T_{22} [A + B \tan^2 \frac{\theta_e}{2}] &= -\frac{1}{2\sqrt{3}} \eta F_M^2,
\end{aligned}$$

where A and B are the deuteron structure functions.

7. Mesonic Exchange Currents

The nonrelativistic impulse approximation (NIA) for electron-deuteron scattering was investigated in many papers (see, for example, [11]). The calculations of the structure functions of the deuteron are made with different potentials:

- Hamada-Jonston (HJ), Reid Soft, Hard Core (RSC, RHC), Graz (Phenomenological);

- Paris, Nijmegen (Semi Phenomenological);
- Bonn (One Boson Exchange Potential (OBEP));
- Separable forms above NN potentials.

To improve the NIA one needs to take into account a number of corrections. The most important among them are: accounting of the electromagnetic vertex, relativistic corrections (RC), isobar currents (IC), quark admixture (QA) and mesonic exchange currents (MEC). RC can be taken into account by different methods, but the most important part of the RC is included in MEC, so one must be careful to avoid double counting. It was shown in paper [10] that IC do not play significant role in the region of considered transfer momenta. Thus, the MEC are the most important corrections to NIA which must be taken into account in elastic electron-deuteron scattering. The choice of the electromagnetic vertex, and MEC has been investigated in many papers (for details see, [11]). Here it would be opportune to mention that it was shown the connection between P waves and MEC pair currents in the papers [12] (see also review [8]).

8. Calculations and Results

To see the contribution of P waves, we use the Graz-II kernel parameters (see Table), and introduce the conditions to fix the freedom of the parameters for P waves:

$$\lambda_{14} = -\sqrt{\lambda_{11}}u_4, \quad \lambda_{24} = \sqrt{\lambda_{22}}u_4, \quad \lambda_{34} = \sqrt{\lambda_{33}}u_4, \quad \lambda_{44} = u_4^2, \quad (23)$$

$$H_{44}|_{s=M^2} = \frac{i}{2\pi^2} \int dk_0 \mathbf{k}^2 d|\mathbf{k}| [S_e (g_4^{1P_1^2} + g_4^{1P_1^2}) + S_o (g_4^{1P_1^2} g_4^{1P_1^2})] |_{s=M^2} = 0. \quad (24)$$

The deuteron binding energy E_d can be obtained under the condition of Eq. (24). Now we have two free parameters for P waves: u_4, γ_3 . For example, we calculate to fit the F_C node, the changing point of the sign, at $\gamma_3 = -15$. Then the parameter is decided as $u_4 \simeq -10$ or 9.75 . The result of calculations using the parameter set: $\gamma_3 = -15, u_4 = -10, \beta_3 = 0.4819$ GeV are given in Figs. (1-5). The experimental data in Figs. (1-3), (6-7) are taken from papers [13]-[15] and [16]; in Figs. (4-5) – from [17] and [18], respectively.

Curve denoted as "Graz-II only, Dipole" corresponds to the calculation for covariant Graz-II interaction kernel with only positive energy states: ${}^3S_1^+, {}^3D_1^+$ (see, [8]) and with the dipole type of nucleon form factors. Solid line, long and short dashes represent calculations taking into account P waves with the dipole type, vector meson dominance model (VMDM) [19] and relativistic harmonic oscillator model (RHOM) [20] nucleon form factors, respectively.

The calculations of the $A(q^2), T_{20}(q^2)$ in NIA, NIA+MEC with Paris and Bonn potentials and relativistic impulse approximation (accounting positive energy states only) are presented in Fig. (6) and (7), respectively. One see that NIA+MEC calculations with Paris potential gives good agreement with experimental data $A(q^2)$ in wide region of transfer momenta up to $4(\text{GeV}/c)^2$ and very good agreement with experimental data $T_{20}(q^2)$. Now comparing the Figs. (3) and (7) one see the P waves and MEC contributions give the same effect in description of the $T_{20}(q^2)$. This fact explains that in this region of the transfer momenta the main part of the MEC corresponds to the pair currents which are

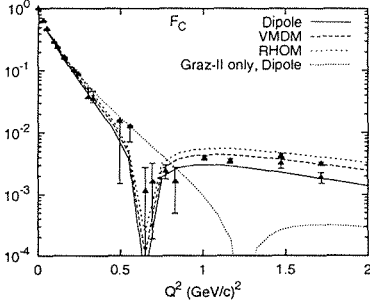


Figure 1: Charge form factor $F_C(q^2)$

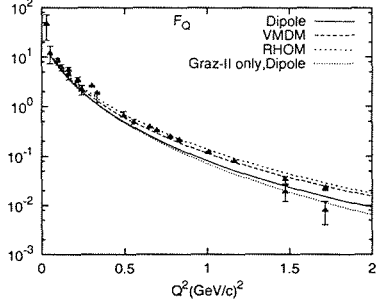


Figure 2: Quadrupole form factor $F_Q(q^2)$

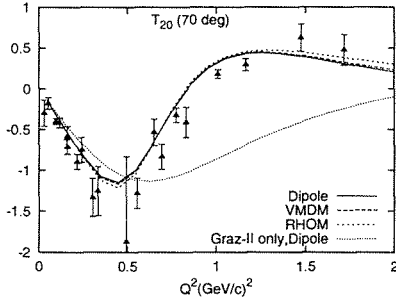


Figure 3: Tensor polarization $T_{20}(q^2)$ calculated at $\theta_e = 70^\circ$

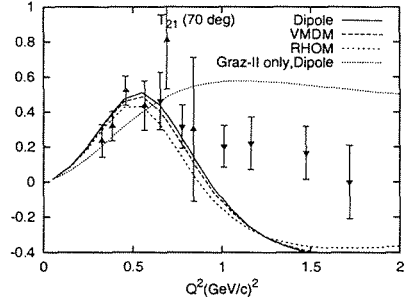


Figure 4: Tensor polarization $T_{21}(q^2)$ calculated at $\theta_e = 70^\circ$

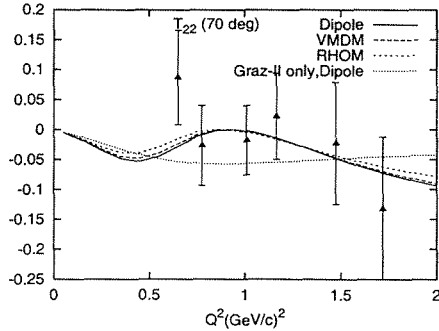


Figure 5: Tensor polarization $T_{22}(q^2)$ calculated at $\theta_e = 70^\circ$

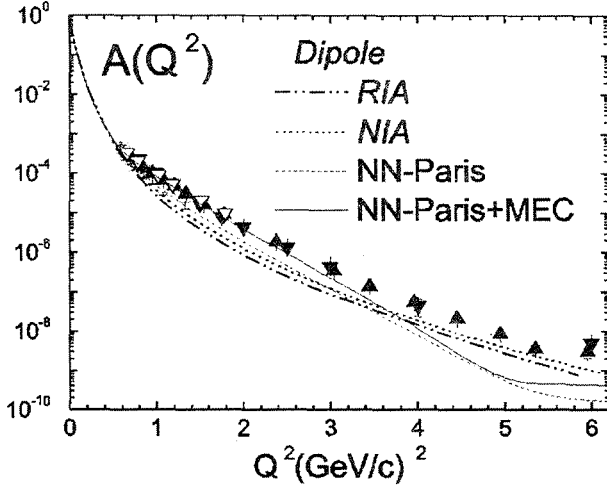


Figure 6: Structure function of the deuteron $A(q^2)$. The dash-dot-dot curve shows the relativistic impulse approximation (positive energy states) calculation. Short dashes (dots) line corresponds to the nonrelativistic impulse approximation (NIA) calculation with non-relativistic Graz-II (Paris) potential. Solid line corresponds to the nonrelativistic impulse approximation (NIA) calculation with Paris potential and MEC included. Experimental data are taken from [13]-[15], [16].

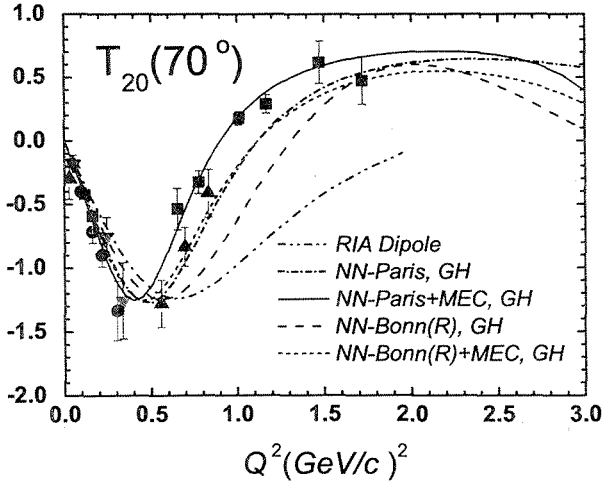


Figure 7: Tensor polarization $T_{20}(q^2)$ calculated at $\theta_e = 70^\circ$

approximately the same as it was mentioned above. But this is the limit of the possibility of applying NIA+MEC calculations to elastic electron deuteron scattering. To move far we must take into account RIA calculations.

9. Conclusion

We made an attempt to extract information about P waves by analyzing the charge form factor of the deuteron F_C . Why the F_C is appropriate characteristic of the deuteron? To receive answer on this question we can remember that in nonrelativistic approach one needs take into account mesonic exchange currents especially so-called pair currents to explain properties of the F_C . It was shown in papers [12], [8] the negative energy states in the deuteron have the direct connections with pair currents. We could see the contribution of the negative energy states ($^1P_1^e$, $^1P_1^o$) by fitting F_C , at a certain set of the parameters. We reproduced the F_C , F_Q and T_{20} at over $Q^2 = 2$ (GeV/c)² and T_{21} at $0 < Q^2 < 0.7$ (GeV/c)². And we show that MEC contributions to NIA approximations (main part at the Q^2 less then 2 (GeV/c)² is pair currents) are close connection with P waves in RIA calculations. Furthermore, we can calculate the form factors to fit F_M or B . Of course, this consideration has qualitative character only and the further investigation in this direction must be done.

ACKNOWLEDGMENTS

This work was partly supported by Sasakawa Scientific Research Grant from the Japan Science Society and Osaka University supporters' association and by Russian Foundation for Basic Research Grant No. 05-02-17698.

References

- [1] G. E. Brown, A. D. Jackson, *The Nucleon-nucleon interaction* (North-Holland Publ. Comp., 1976)
- [2] J. Carbonell *et al.*, *Phys. Rep.* 300 (1998) 215
- [3] R. Machleidt, I. Slaus, *J. Phys. G: Nucl. Phys.* 27 (2001) R69
- [4] M. Garçon, J. W. Van Orden, *Adv. Nucl. Phys.* 26 (2001) 203
- [5] R. Gilman, F. Gross, *preprint nucl-th/0111015*
- [6] G. Piller, W. Wise, *Phys. Rep.* 330 (2001) 1
- [7] V. V. Burov, A. V. Molochkov, G. I. Smirnov, *Phys. Part. Nucl.* 30 (1999) 579
- [8] S. G. Bondarenko, *et al.*, *Progr. Part. Nucl. Phys.* 48 (2002) 449
- [9] G. Rupp, J. A. Tjon, *Phys. Rev. C* 41 (1990) 472
- [10] H. Weber, *Phys. Rep.* 36 (1978) 277

- [11] V. V. Burov, V. N. Dostovalov, S. E. Suskov, *Particles and Nuclei* 23 (1992) 721
- [12] S. G. Bondarenko, V. V. Burov, M. Beyer, S. M. Dorkin. *Phys. Rev. C* 58 (1998) 3143; S. G. Bondarenko, V. V. Burov, M. Beyer, S. M. Dorkin. *Phys. of Atom. Nucl.* 62 (1999) 917
- [13] J.E. Elias *et al.*, *Phys. Rev.* 177 (1969) 2075 ;
- [14] S. Platchkov *et al.*, *Nucl. Phys. A* 510 (1990) 285
- [15] R.G. Arnold *et al.*, *Phys. Rev. Lett.* 35 (1975) 776
- [16] D. Abbott *et al.*, *Eur. Phys. J. A* 7 (2000) 421
- [17] D. M. Nikolenko *et al.*, *Phys. Rev. Lett.* 90 (2003) 072501
- [18] D. Abbott *et al.*, *Phys. Rev. Lett.* 84 (2000) 5053
- [19] F. Iachello, A. D. Jackson, A. Lande, *Phys. Lett. B* 43 (1973) 191
- [20] V. V. Burov *et al.*, *Europhys. Lett.* 24 (1993) 443

COULD LEPTONS BE COMPOSED FROM QUARKS OR ANTIQUARKS?

Y. E. Pokrovsky^{1†}

(1) *RRC "Kurchatov Institute", 123182, Kurchatov Sq.1, Moscow*

† *E-mail: pokr@mbslab.kiae.ru*

Abstract

It is shown that within QCD extended by a scalar field theory with spontaneously broken scale invariance, the leptons could be composite bound states from three quarks (qqq) or antiquarks ($\bar{q}\bar{q}\bar{q}$). The matter-antimatter asymmetry of Universe, and some new lepton and hadron properties predicted in this picture are discussed.

Key-words: QCD, scale invariance, quark, lepton, antimatter.

1. Introduction

The primary goals of elementary particle physics are the discovery of the ultimate building blocks of nature and understanding the relationship between their forces.

In the Standard Model (SM) all known leptons ($e, \nu_e, \mu, \nu_\mu, \tau, \nu_\tau$) and quarks (u, d, c, s, t, b) are grouped in three generations

$$\begin{pmatrix} e \\ \nu_e \end{pmatrix} \quad \begin{pmatrix} \mu \\ \nu_\mu \end{pmatrix} \quad \begin{pmatrix} \tau \\ \nu_\tau \end{pmatrix} - 6 \text{ leptons}$$

$$\begin{pmatrix} u \\ d \end{pmatrix} \quad \begin{pmatrix} c \\ s \end{pmatrix} \quad \begin{pmatrix} t \\ b \end{pmatrix} - 6 \text{ quarks}$$

and they are considered as fundamental (noncomposite) particles. Then all hadrons are composed from the quarks.

The remarkable agreement of the predictions of the SM with experimental observations shows the correctness of the spontaneously broken $SU(3)_C \otimes SU(2)_L \otimes U(1)_Y$ gauge theory at low energies. SM cannot, however, be an ultimate fundamental theory by itself because of some major shortcomings. For example, (i) excessive multiplication of elementary particles without a principle restricting their choice, and (ii) a large number (=22) of arbitrary parameters (3 gauge couplings + 6 masses of the quarks + 3 mass of charged leptons + 3 neutrino masses + 4 parameters in the KobayashiMaskawa matrix + 1 strong charge-parity (CP) violating parameter + 2 Higgs potential parameters = 22). Nevertheless, within SM there is no clear solution to the particle-antiparticle (baryon-antibaryon, electron-positron) asymmetry of Universe, and to some other fundamental problems.

A few basic ideas for the possible resolutions of the SM shortcomings have been suggested – grand-unification [1], supersymmetry [2], supergravity [3], and one of them is the idea of composite particles [4]. The most compelling arguments in favor of a substructure of leptons and quarks in terms of more fundamental subunits are that there exist so many leptons and quarks, and that they seemingly form the pattern of three "generations". Mainly, there are two types of composite models: technicolour and preonic models.

The idea of the technicolour [5] presumes that the Higgs bosons are composite, but quarks, leptons, and techniquarks are elementary. This idea encounters several difficulties and is mostly excluded, because of the constraints from the flavour changing neutral current processes and the electroweak (EW) oblique corrections [6].

Preonic ideas propose that not only the Higgs bosons, but also the quarks and leptons are composites of a common set of constituents, generically called preons. A particular class of preon models in which the flavour and the colour attributes of quarks and leptons are carried by separate preonic constituents, so that quarks and leptons in their simplest forms may be viewed as fermion-boson composites, are initiated by Pati and Salam [7]. A similar idea that treats only quarks but not leptons as composites is considered by Greenberg [8]. The Greenberg's idea has been subsequently considered by Pati and Salam in a set of papers, and by many authors¹. The approach developed in [19, 20, 21, 22, 23, 24] introduces a new phase in the preonic approach, when combined with local SUSY, provides a simple explanation for the protection of composite quark-lepton masses, the origin of diverse mass scales, family replication, and interfamily mass hierarchy. Nevertheless, the symmetry structure of the preon theory cannot strictly respect left-right, up-down and quark-lepton symmetries [25].

New idea suggested in this paper is that leptons could be composed from quarks (like the hadrons). This idea is based on the fact that there are more analogies between leptons and the lowest mass (spin^{Parity}, isospin - $J^P I = 1/2^+, 1/2$) baryons rather than between leptons and quarks: the leptons and baryons are colorless with entire electric charge in contrast to the color quarks with fractional electric charge. From this point of view quarks can be considered as fundamental particles for the leptons and hadrons: leptons, like hadrons in Quantum Chromodynamics (QCD), can be build from three quarks by an additional very short range Super Strong Dynamics (SSD).

$$\begin{array}{lcl}
 \text{SSD} \rightarrow & \begin{pmatrix} e^+ \\ \bar{\nu}_e \end{pmatrix} & \begin{pmatrix} \mu^+ \\ \bar{\nu}_\mu \end{pmatrix} & \begin{pmatrix} \tau^+ \\ \bar{\nu}_\tau \end{pmatrix} & - & 6 \text{ leptons} \\
 & \uparrow & \uparrow & \uparrow & & \\
 & \begin{pmatrix} u \\ d \end{pmatrix} & \begin{pmatrix} c \\ s \end{pmatrix} & \begin{pmatrix} t \\ b \end{pmatrix} & - & 6 \text{ quarks} \\
 \text{QCD} \rightarrow & \downarrow & \downarrow & \downarrow & & \\
 & \begin{pmatrix} uud \\ udd \end{pmatrix} & \begin{pmatrix} ccs \\ css \end{pmatrix} & \begin{pmatrix} ttb \\ tbb \end{pmatrix} & - & 6 \text{ lowest mass (JI=1/2,1/2) baryons} \\
 & \dots & \dots & \dots & - & 49 \text{ other ground states of baryons.}
 \end{array}$$

Another particular motivation for this idea is a possibility of clear explanation of electro-neutrality and baryon-electron (matter) dominance in Universe. Even if the total number of quarks is always exactly equal to the total number of antiquarks then after Big Bang and coalescence of the quarks and antiquarks to leptons and hadrons there are fluctuative differences in total numbers of leptons, antileptons, baryons and antibaryons. Then, after annihilation of all extra lepton and baryon pairs the remaining quarks in Universe are confined in protons, neutrons, and antineutrino², and, corresponding antiquarks are confined in electrons, and neutrinos.

There is an experimental test for this picture. Electroneutrality of Universe means the

¹With W bosons treated as composites in some of them e.g. [9, 10, 11]. Some other composite models assume that quarks and leptons can be made most economically as bound states of either a boson and a fermion [12] or three fermions [13, 14, 15]. The supersymmetric version is considered in [16, 17, 18].

²For simplicity small amounts of antinucleons, positrons, antineutrons, and unstable mesons generated in reactions with cosmic rays are not listed and discussed here

equal numbers of protons and electrons. Then for equal numbers of quarks and antiquarks in Universe (zero total baryon charge concerned with quarks), one can relate the difference between the total numbers of neutrino (N_ν) and antineutrino ($N_{\bar{\nu}}$) to the total number of neutrons (N_n)

$$N_\nu - N_{\bar{\nu}} = N_n. \quad (1)$$

Unfortunately, the known estimation $N_\nu \sim N_{\bar{\nu}} \sim (10^8 - 10^9)N_n$ signifies extreme difficulties in measuring N_ν and $N_{\bar{\nu}}$ with the accuracy high enough to verify (1).

Nevertheless, this quark picture of lepton structure seems attractive enough to explore some of its consequences, despite the fact that it is rather unconventional.

In this way we need to choose reasonable SSD taking into account at least the following three points: (i) a clear dynamical mechanisms for vanishing of $\bar{u}\bar{u}\bar{d}$, $\bar{c}\bar{c}\bar{s}$, $\bar{t}\bar{t}\bar{b}$ neutrino masses and small nonzero masses of charged leptons $\bar{u}\bar{u}\bar{d}$, $\bar{c}\bar{c}\bar{s}$, $\bar{t}\bar{t}\bar{b}$, (ii) clear dynamical explanation for the absence of almost massless $q\bar{q}$ (meson-like) states in the lepton sector (in contrast to 36 meson ground states in QCD), and (iii) clear dynamical reasons for the large difference between numbers of the lepton (= 6) and baryon (= 55) ground states. This means that SSD has to be very different from QCD.

Another important piont is that various experimental constraints request that the leptons have a size [26]

$$\Lambda_L^{-1} < 10^{-17} cm \sim (10 TeV)^{-1}. \quad (2)$$

Thus the bound-state dynamics of the quarks must be such that the masses of the qqq -leptons are extremely small compared to inverse sizes of the bound states. A possibility of keeping the masses of the tiny little size leptons small may be caused, in particular, by the scale invariance of the additional boson fields that critically strong interact with the quarks.

2. Spontaneously broken scale invariance and spinor-scalar solitons

Following the three points listed above lets introduce the additional (to QCD) self-interacting, color-singlet, odd G-parity scalar fields $\sigma_i(x)$ in the each generation i ($i = 1, 2, 3$) with a Lagrangian density of the most general renormalizable and scale invariant form, and with strong interaction between $\sigma_i(x)$ and color ($a = \tau, g, b$) quark fields $q_i^a(x)$ of the same generation³:

$$\mathcal{L}_{\sigma QCD} = \mathcal{L}_{QCD} + \sum_{i=1}^3 \left(\frac{1}{2} \partial_\mu \sigma_i \partial^\mu \sigma_i - g \sigma_i \bar{q}_i^a q_i^a - \frac{1}{4} \lambda \sigma_i^4 \right). \quad (3)$$

This model (lets call it σ QCD) contains seven parameters well known from QCD Lagrangian (\mathcal{L}_{QCD}) - Λ_{QCD} and quark masses⁴

$$\Lambda_{QCD}^{\overline{MS}} \approx 200 MeV, \quad (4)$$

³Without any interaction between $\sigma_i(x)$ and quarks of other generations $j \neq i$

⁴Quark masses are given at renormalization point $\mu_{QCD} = 2 GeV$

$$\left(\begin{array}{l} \hat{m}_u = (2 - 4)MeV \\ \hat{m}_d = (4 - 8)MeV \end{array} \right), \left(\begin{array}{l} \hat{m}_c = (1.15 - 1.35)GeV \\ \hat{m}_s = (0.08 - 0.13)GeV \end{array} \right), \left(\begin{array}{l} \hat{m}_t = (169 \pm 0.35)GeV \\ \hat{m}_b = (4.3 \pm 0.20)GeV \end{array} \right), \quad (5)$$

and two extra adjustable dimensionless parameters $g \sim 1$ and $\lambda \sim 1$. σ QCD is scale invariant in the limit of zero quark mass and zero QCD condensates, and admits stable dynamical solutions for $\lambda > 0$.

One of the central problems in σ QCD is understanding the nature of the vacuum part of the critically bounded solutions. In general, this vacuum can be characterized by simplest condensates – a σ -field condensate $\sigma_{vac}(x)$ and quark condensate $\langle vac|\bar{q}(x)q(x)|vac \rangle$.

Because of scale invariance the energy U as a function of the σ -field strength has one minimum instead of two minima in the Friedberg-Lee model [27] which is more complicated and explicitly violates the scale invariance.

In the absence of quarks, the potential

$$U(\sigma) = \frac{1}{4}\lambda\sigma^4, \quad (6)$$

and therefore σ is massless field with the normal vacuum state at zero.

In presence of quarks strongly interacting with σ -field a localized bounded state with scale invariant and nonzero quark condensate

$$\langle vac|\bar{q}(x)q(x)|vac \rangle = \frac{\gamma_{\bar{q}q}}{r^3} \quad (7)$$

may be formed, where the dimensionless constant $\gamma_{\bar{q}q}$ can be calculated self-consistently in σ QCD or estimated from bag model⁵.

For strongly bounded states the vacuum contribution (7) dominates on valence-quark contribution which vanishes when mass of the state tends to zero. In this case the potential U changes to

$$V(\sigma, r) = g\sigma \langle vac|\bar{q}(x)q(x)|vac \rangle + \frac{1}{4}\lambda\sigma^4. \quad (9)$$

Therefore near the center of the localized solution (let assume the center in the origin) the σ -field finds a new deeper minimum

$$\sigma_{vac}(\mathbf{r}) = - \left(\frac{\lambda}{g} \langle vac|\bar{q}(\mathbf{r})q(\mathbf{r})|vac \rangle \right)^{1/3} = - \left(\frac{\lambda}{g} \gamma_{\bar{q}q} \right)^{1/3} r^{-1} \quad (10)$$

at a large finite value $\sigma_{vac}(r)$ for every r (Fig.2): the interacting quarks form a nontopological spinor-scalar soliton.

In order to derive dynamical equations lets write for the scalar field

$$\sigma = \sigma_{vac} + \sigma_1, \quad (11)$$

⁵For MIT bag of radius R containing the fluctuating vacuum fields the quark condensate [28]

$$\langle vac|\bar{q}q|vac \rangle \approx - \frac{0.15 \cdot 3 \cdot 2}{R^3} < 0 \quad (8)$$

where factors 3 and 2 correspond to three colors and two flavors in each generation). Outside the bag $\langle vac|\bar{q}q|vac \rangle \rightarrow 0$.

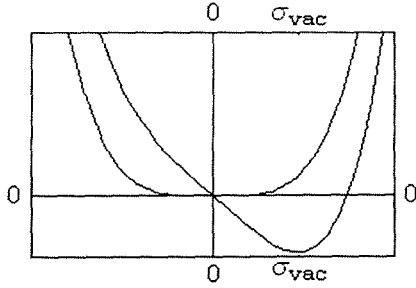


Figure 1: Typical form of the potential functions $U(\sigma)$, and $V(\sigma, r)$. Units on the vertical and horizontal axes are arbitrary

where σ_{vac} is a c-number field. It is convenient to work in the rest frame of the scalar field σ_{vac} . In this frame, $\sigma_{vac}(\mathbf{r})$ is time independent.

Then lets expand the operator $q(x)$ as follows:

$$q = \sum_k c_k q_k(r) \quad (12)$$

where $\{q_k\}$ is an arbitrary, complete orthonormal set of Dirac spinor functions and the c_k are fermion annihilation operators.

To lowest order in $\sigma_1(\mathbf{r})$ the $q_k(\mathbf{r})$ and $\sigma_{vac}(\mathbf{r})$ satisfy the coupled differential equations

$$(\vec{\alpha} \cdot \vec{p} + g\beta\sigma_{vac})q_k = \epsilon_k q_k \quad (13)$$

$$-\nabla^2 \sigma_{vac} + \lambda \sigma_{vac}^3 = -g \sum_k q_k^\dagger \beta q_k \quad (14)$$

The sum in (14) is over all occupied quark states. Not only the "valence" quark states are needed in solving these equations self-consistently, but also the sea quarks. Eq. (13) defines a complete set of basis states $\{q_k\}$ in which the quark field operator $q(x)$ is expanded. Therefore for a static localized solution to (13,14) the sum contain vacuum and valence quark contributions

$$\sum_k q_k^\dagger \beta q_k = \langle vac | \bar{q}(\mathbf{r}) q(\mathbf{r}) | vac \rangle + \langle val | \bar{q}(\mathbf{r}) q(\mathbf{r}) | val \rangle, \quad (15)$$

where the quark condensate can be used in form (7) with $\gamma_{\bar{q}q} = -0.15 \cdot 3 \cdot 2$ (see eq.(8)).

In deriving equations for the critically bounded states the contribution from the vacuum polarization dominates over the vanishing valence quark contribution $\langle val | \bar{q}(\mathbf{r}) q(\mathbf{r}) | val \rangle$. The last term in (15) can be omitted in calculations of $\sigma_{vac}(\mathbf{r})$. In this particular case equation (14) simplifies to

$$-\nabla^2 \sigma_{vac} + \lambda \sigma_{vac}^3 = -g \frac{\gamma_{\bar{q}q}}{r^3}, \quad (16)$$

and has pure Coulomb solution (10) in respect to the scale symmetry of σ QCD.

Inclusion of only σ_{vac} , the c-number part of the soliton field in (13) and (14), has led to what is essentially a mean-field approximation (MFA).

For the given $\sigma_{vac}(\mathbf{r})$ the total mass of the quark-scalar soliton can be calculated within MFA by use of the virial theorem [29]

$$\mathcal{E}_{soliton} = \int d^n x \left[\frac{n-3}{2} (\nabla \sigma_{vac})^2 + \frac{n+1}{4} \lambda \sigma_{vac}^4 + \left(\frac{m_q}{g} - \sigma_{vac} \right) \lambda \sigma_{vac}^3 \right], \quad (17)$$

The striking feature of Eq. (17) is the fact that for $n = 3$ (n is the number of spatial dimensions) the term with $\nabla \sigma_{vac} \sim r^{-4}$ vanishes, and the proportional to $\sigma_{vac}^4 \sim r^{-6}$ terms cancel out. This is an important feature, since σ_{vac}^4 is commonly held responsible for the stability of a theory with spontaneously broken scale symmetry. Thus in normal number of space dimensions ($n = 3$) the energy of the soliton diverges logarithmically

$$E_{soliton} = \sum_{quarks}^{valence} m_q \frac{\lambda}{g} \int d^3 x \sigma_{vac}^3 \approx -4\pi \sum_{quarks}^{valence} m_q \left(\frac{\lambda}{g} \right)^2 \gamma_{\bar{q}q} \ln \left(\frac{\Lambda_{\sigma QCD}}{\mu_{QCD}} \right). \quad (18)$$

The soliton energy (18) in MFA is proportional to sum of current masses of valence quarks (parameters of violation of scale symmetry), dimensionless constant $(\lambda/g)^2 \gamma_{\bar{q}q}$ ($\lambda \sim 1$ and $g \sim 1$, $\gamma_{\bar{q}q} \sim -1$), and a logarithmic factor. Therefore, taking into account (2) and (4) each valence quark contributes to the soliton mass

$$M_q \approx -4\pi m_q \left(\frac{\lambda}{g} \right)^2 \gamma_{\bar{q}q} \ln \left(\frac{\Lambda_{\sigma QCD}^2}{\Lambda_{QCD}^2} \right) > 116 \left(\frac{\lambda}{g} \right)^2 \gamma_{\bar{q}q} m_q \quad (19)$$

It should be noted that the spontaneous violation of scale symmetry in σ QCD is the reason for the exact cancellation of the large $\sim \Lambda_{\sigma QCD}$ contributions to the mass of the system. Nevertheless, for $(\lambda/g)^2 \gamma_{\bar{q}q}$ assumed to be 1 and for known estimations of current quark masses (5) the quark contributions (19) to the soliton mass are still much greater than the desired lepton (especially neutrino) masses.

A dynamical reason for taking into account renormalization of quark masses and coupling constants in (18), and for further reducing of the soliton mass from the large effective quark masses (M_q) to the neutrino masses, is the quantum corrections due to the fluctuating field σ_1 .

Although, the MFA already contains important nonlinear effects, deviations from this approximation are generated by σ_1 . If effects due to σ_1 are not too great, the separation will be a useful one. Lets utilize the MFA to generate a representation in terms of which the corrections can be calculated. The Hamiltonian (without the terms due to vector gluons, and counterterms) can be written

$$\begin{aligned} \mathcal{H} = & \mathcal{E}_{soliton} + \sum_k \epsilon_k (b_k^\dagger b_k + d_k^\dagger d_k) \\ & + \int d^3 x \left\{ \frac{1}{2} (\pi_1^2 + |\nabla \sigma_1|^2) + 3\lambda \sigma_{vac}^2 \sigma_1^2 + \frac{\lambda}{12} \sigma_{vac} \sigma_1^3 + \frac{\lambda}{24} \sigma_1^4 \right. \\ & \left. + g (\bar{q}q - \langle vac | \bar{q}q | vac \rangle) \sigma_1 \right\}, \quad (20) \end{aligned}$$

where π_1 is the momentum conjugated to σ_1 , $b_k = c_k$ are the particle operators for $\epsilon_k > 0$ and $d_k = c_k^\dagger$, where $k = (\kappa, m, \epsilon)$, $\bar{k} = (-\kappa, -m, -\epsilon)$ so that

$$q = \sum_{k (\epsilon_k > 0)} (b_k q_k + d_k^\dagger q_{\bar{k}}). \quad (21)$$

The b_k and d_k are particle and antiparticle annihilation operators.

Lets also expand σ_1 in terms of an arbitrary, complete set of functions, e.g., $\{s_j\}$, as

$$\sigma_1 = \sum_j (2\omega)^{-1/2} (a_j^\dagger + a_j) s_j \quad (22)$$

$$\pi_1 = i \sum_j (2\omega)^{1/2} (a_j^\dagger - a_j) s_j \quad (23)$$

where the a_j and a_j^\dagger are the usual Bose annihilation and creation operators. The index j is the collection of quantum numbers needed to describe the eigenstates s_j .

The s_j and ω_j can be fixed by requiring the s_j to satisfy the eigenvalue equation

$$(-\nabla^2 + 3\sigma_{vac}^2 - \omega_j^2) s_j(\mathbf{r}) = 0 \quad (24)$$

Now the Hamiltonian can be rewritten

$$\mathcal{H} = \mathcal{E}_{soliton} + \sum_k \epsilon_k (b_k^\dagger b_k + d_k^\dagger d_k) + \sum_j \omega_j (a_j^\dagger a_j + \frac{1}{2}) + \mathcal{H}', \quad (25)$$

where

$$\begin{aligned} \mathcal{H}' = & \int d^3x \left[g (\bar{q}q - \langle vac | \bar{q}q | vac \rangle) \sigma_1 \right. \\ & \left. + \frac{\lambda}{12} \sigma_{vac}^3 + \frac{\lambda}{24} \sigma_1^4 \right] \end{aligned} \quad (26)$$

The $\{q_k\}$ and $\{s_j\}$ define a basis in terms of which corrections due to H' can be calculated. This is very analogous to the weak particle-surface coupling representation of the Bohr-Mottelson unified model [30]. The representation states and spectra are relatively easy to solve for once the self-consistent $\sigma_{vac}(\mathbf{r})$ has been obtained. Numerous approximation methods are available for handling H' , such as perturbation theory or matrix diagonalization in a finite basis. Note that the nonlinear terms (σ_1^3 and σ_1^4) are not an essential complication. These terms additionally contribute to renormalization of quark masses m_q and coupling constants g and λ . In particular, due to quantum loop corrections, after the dimensional transmutation m_q , g , λ [31], and $\gamma_{\bar{q}q}$ [32] depend on the ratio of momentum transfer (p) to the characteristic scales Λ_{QCD} , and $\Lambda_{\sigma QCD}$:

$$m_q(p) = \hat{m}_q \left(\frac{\ln(\mu_{QCD}^2 / \Lambda_{QCD}^2)}{\ln(p^2 / \Lambda_{QCD}^2)} \right)^{16/11}, \quad (27)$$

$$g^2(p) \sim -\ln\left(\frac{p^2}{\Lambda_{\sigma QCD}^2}\right)^{-1}, \quad (28)$$

$$\lambda(p) \sim -\ln\left(\frac{p^2}{\Lambda_{\sigma QCD}^2}\right)^{-1}, \quad (29)$$

$$\gamma_{\bar{q}q}(p) \sim -\ln\left(\frac{p^2}{\Lambda_{\sigma QCD}^2}\right), \quad (30)$$

therefore the renormalized soliton energy

$$\mathcal{E}_{soliton} = \sum_{\substack{\text{valence} \\ \text{quarks}}} \mathcal{M}_q, \quad (31)$$

where

$$\begin{aligned} \mathcal{M}_q(\Lambda_{\sigma QCD}) = & -4\pi \left(\frac{\lambda}{g}\right)^2 \gamma_{\bar{q}q} \hat{m}_q \int_{\frac{\pi}{\Lambda_{\sigma QCD}}}^{\frac{\pi}{\mu_{QCD}}} \frac{dr}{r} \left(\frac{\ln(\mu_{QCD}^2/\Lambda_{QCD}^2)}{\ln(\pi^2/(r\Lambda_{QCD})^2)} \right)^{16/11} = \\ & -\frac{22}{5} \pi \gamma_{\bar{q}q} \left(\frac{\lambda}{g}\right)^2 \hat{m}_q \ln \left(\frac{\mu_{QCD}^2}{\Lambda_{QCD}^2} \right) \left(1 - \frac{\ln \left(\frac{\mu_{QCD}^2}{\Lambda_{QCD}^2} \right)^{5/11}}{\ln \left(\frac{\Lambda_{\sigma QCD}^2}{\Lambda_{QCD}^2} \right)^{5/11}} \right). \end{aligned} \quad (32)$$

It is ≈ 6 times smaller than (18) at $\Lambda_{\sigma QCD} = 10TeV$, and differs from (18) by the last logarithmic factor which is slightly decreasing with $\Lambda_{\sigma QCD}$.

These quantum corrections explicitly violate the scale invariance of σ QCD and form the characteristic large momentum scale of this theory $\Lambda_{\sigma QCD} > 10TeV$. Therefore σ QCD allows almost massless (relative to $\Lambda_{\sigma QCD}$) soliton solutions of very small radius $\sim \Lambda_{\sigma QCD}$. The scale symmetry of σ QCD leads to dynamical reduction of the characteristic energy scale of $\Lambda_{\sigma QCD}$ to sum of relatively small effective masses of valence quarks (32).

The further reduction of the soliton mass is possible by taking into account the remaining interactions between different quarks via exchanges of quanta of σ_1 with quantum numbers chosen to be $I^G J^P = 0^- 0^+$. Mass of $m_{\sigma_1} = \frac{\sqrt{3}}{2} \Lambda_{\sigma QCD}$ is large enough to appear as critically strong very short-range interaction between the moderately massive effective quarks. In particular, these values of masses allow to avoid undesirable lowlying excitations which are absent in the lepton's data.

The choice of the odd G -parity σ_1 -meson allows to avoid undesirable lowlying meson-like $q\bar{q}$ states. Because the source of this interaction is meson exchange it is related by crossing symmetry to the $q\bar{q}$ interaction which can be deduced directly by simply changing the sign of the odd G -parity exchange terms [33]. The most significant feature is that the short-range attraction in the qq system which is produced by the exchange of $I^G = 0^-$ σ_1 -meson becomes a strongly repulsive short-range force in $q\bar{q}$ systems. In addition, in $q\bar{q}$ system there is annihilation interaction which is always repulsive. Therefore in σ QCD lowlying $q\bar{q}$ mesons don't exist.

3. Critically bounded states

A specific feature for generation of the critically bounded (and therefore ultrarelativistic) states by the critically strong short-range interaction is that MFA is not enough even for rough estimations (because the strong two-particle or three-particle correlations play important role in such systems).

For example a relativistic three body approach for three equal fermions of mass m interacting via scalar zero-range forces [34] (in contrast to MFA) manifests the critically strong binding of three-particle system (zero total mass) when mass of the two-particle system $M_2 = M_c = 1.35m$ (Fig.3).

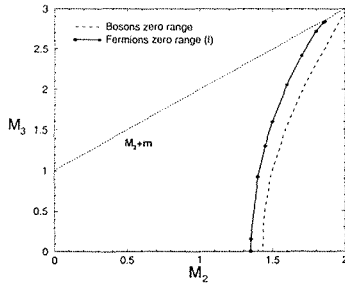


Figure 2: Three-fermion bound state mass M_3 versus two-fermion mass M_2 (solid line) in comparison to the three-boson bound state mass (dash line) calculated in the framework of the Light-Front Dynamics for zero-range scalar interaction [34]. The mass M_3 of the relativistic three-body bound state exists only when M_2 is greater than a critical value M_c ($\approx 1.43 m$ for bosons and $\approx 1.35 m$ for fermions, m is the constituent mass). For $M_2 = M_c$ the mass M_3 turns into zero

For $M_2 < M_c$ there are no three-particle solutions with real value of M_3 , what means from the physical point of view that three-body state no longer dominate in the system and configurations with quark-antiquark pairs became essential for the critically bounded states. This means that in σ QCD there is a critical value for coupling constant $g_{crit}(m_{q_1}, m_{q_2}, m_{q_3}, \lambda, \alpha_{QED}, Q) \approx 1$ so that for $g \geq g_{crit}$ masses of electrically neutral ($Q = 0$) states with tree valence quarks (udd, css, tbb) became extremely small and these states can be interpreted as antineutrinos⁶.

In order to estimate masses of the charged leptons lets assume

$$(\mathcal{M}_{q_1} + \mathcal{M}_{q_2} + \mathcal{M}_{q_3})\sqrt{1 - g^2/g_{crit}^2}$$

falloff of the 3-body mass versus g to the critical point $g_{crit} \approx 1.1$ (Fig.3).

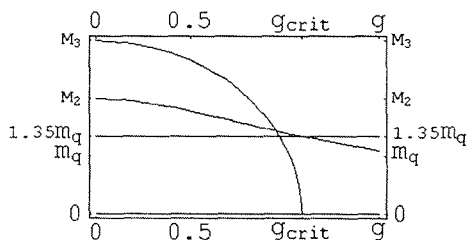


Figure 3: Typical behavior of a critically bounded $3q$, and strongly bounded $2q$ systems of quarks with equal masses (M_q) vs coupling constant g

Then small deviation from the critical point caused by difference in electromagnetic interactions of electrically neutral ($Q = 0$) qqq states (neutrinos) and charged ($Q = \pm 1$)

⁶Corresponding almost massless states with tree valence antiquarks ($\bar{u}\bar{d}\bar{d}, \bar{c}\bar{s}\bar{s}, \bar{t}\bar{b}\bar{b}$) can be interpreted as neutrinos.

states can be written in the following form⁷

$$m_{charged} = \sqrt{\frac{2\alpha_{QED}}{g_{crit}}} \left(2\mathcal{M}_q^{up}(\Lambda_{\sigma QCD}) + \mathcal{M}_q^{down}(\Lambda_{\sigma QCD}) \right), \quad (33)$$

where $\alpha_{QED} = 1/137$. Therefore, for a given value of still arbitrary $\Lambda_{\sigma QCD}$ and λ , σQCD allows estimate the masses of e , μ , τ leptons.

4. Proton mean life time and lepton scale

One of the most fundamental predictions of the quark structure of leptons is that proton is the first radial excitation of positron, and therefore proton must be unstable with decay, in particular, to $e^+\gamma$ via M1 transition. The proton mean life time

$$\tau(p \rightarrow e^+\gamma) \sim \left(\frac{4\alpha_{QED}}{9} \Lambda_{\sigma QCD} \left(\frac{m_p}{2\Lambda_{\sigma QCD}} \right)^3 \left(\frac{m_p}{4\Lambda_{\sigma QCD}} \right)^9 \right)^{-1} \quad (34)$$

must satisfy the experimental upper limit $\tau(p \rightarrow e^+\gamma) > 4.6 \cdot 10^{32}$ years. This take place if $\Lambda_{\sigma QCD} > 1.2 \cdot 10^6 GeV$.

5. Masses of charged leptons in σQCD

Taking into account that for $\Lambda_{\sigma QCD} > 1.2 \cdot 10^6 GeV$ \mathcal{M}_q is almost independent on $\Lambda_{\sigma QCD}$, and chosing $\lambda = 0.1$ σQCD predict the following values for masses of the charged leptons

$$m_e = 0.48(0.51)MeV, \quad m_\mu = 105(106)MeV, \quad m_\tau = 13.7(1.8)GeV, \quad (35)$$

where experimental values are given in parenthesis. The too large difference between the calculated masses and the data for m_τ may be caused by too large differences between masses of t and b quarks.

6. On EW properties of the composed leptons

In the simplest approach one expects parity to be conserved. Of course, this contradicts observation. Therefore one must attribute the observed parity violation to details of the σQCD dynamics which may be related to the fact that the observed fermions are much lighter than $\Lambda_{\sigma QCD}$. One way to accommodate the parity violation would be to assume the lepton structure only for the lefthanded fermions, and to construct the right-handed fermions differently (e.g. by interpreting them as elementary objects). Another way arises if there is additional force which is magnetic in origin. However, in this case one expects both P- and CP-violation, and it is not understood why the observed CP-violation is small. The problem of parity violation persists in all substructure models.

Nevertheless, some electroweak properties of the composed leptons (in particular, the axial coupling constant of the composed leptons $g_A = 1$ in contrast to $g_A \approx 1.25$ for nucleons) can be explained and estimated in σQCD .

⁷ $\sqrt{1 - (g_{crit} - \alpha)^2 / g_{crit}^2} \approx \sqrt{2\alpha / g_{crit}}$ for $\alpha \ll 1$

7. Conclusion

It is shown that leptons could be composite bound states from quarks or antiquarks ($e^- = |\bar{u}\bar{u}\bar{d}\rangle$, $\nu_e = |\bar{u}\bar{d}\bar{d}\rangle$, $e^+ = |uud\rangle$, $\bar{\nu}_e = |udd\rangle$, $\mu^- = |\bar{c}\bar{c}\bar{s}\rangle$, $\nu_\mu = |\bar{c}\bar{s}\bar{s}\rangle$, $\mu^+ = |ccs\rangle$, $\bar{\nu}_\mu = |css\rangle$, $\tau^- = |\bar{t}\bar{t}\bar{b}\rangle$, $\nu_\tau = |\bar{t}\bar{b}\bar{b}\rangle$, $\tau^+ = |ttb\rangle$, $\bar{\nu}_\tau = |tbb\rangle$) within QCD extended by additional scalar fields with sufficiently strong coupling constant and large renormalization scale $\Lambda_{\sigma QCD} > 10^6 GeV$: ground states of this theory are almost massless and localized at small radii $\sim \Lambda_{\sigma QCD}^{-1}$. They can be interpreted as the leptons. Baryons of $SU(3)$ multiplets in this picture are radial excitations of the leptons. At low energies, the small wave function overlap between the lepton and the hadron states then naturally leads to the large enough proton life time, the lepton number conservation, and do not affect the electroweak interactions. The lepton number symmetry is explicitly broken on the $\Lambda_{\sigma QCD}$ scale, but electrical charge and quark baryon number are exactly conserved. This theory leads to natural solution for the antimatter problem: the quarks are hidden in nucleons and $\bar{\nu}_e$, and the antiquarks are hidden in e^- and ν_e . In particular, this means that usual matter consists of equal numbers of quarks and antiquarks and can annihilate to photons and, correspondingly, can be created from photons in processes concerned with gravitational singularities.

8. Acknowledgments

The author is grateful to Organizing Committee of the International Seminar ISHEPP-2004 for invitation to participate in this Seminar, and for financial support. The work was supported in part by the Russian Foundation for Basic Research under grant SS-1885.2003.2.

References

- [1] H. Georgi and S. Glashow, *Phys. Rev. Lett.* **32**, 438 (1974).
- [2] P. Nath and R. Arnowitt, CERN-TH. Preprint 7227/94 Nub-TH-3089/94, CTP TAMU 28/94.
- [3] E. Witten, *Phys. Lett. B* **155**, 151 (1985).
- [4] L. Lyons, *Prog. In Part. and Nucl. Phys.* **10**, 227 (Pergamon Press, NY, 1983).
- [5] For a review, see E. Farhi and L. Susskind, *Phys. Rev.* **74** 277 (1981) and references therein.
- [6] D. C. Kennedy and B. W. Lynn, *Nucl. Phys. B* **322**, 1 (1989); D. C. Kennedy, *Nucl. Phys. B* **351**, 81 (1991); M. E. Peskin and T. Takeuchi, *Phys. Rev. Lett.* **65**, 964 (1990); G. Altarelli and R. Barbieri, *Phys. Lett. B* **253**, 161 (1991); G. Altarelli, R. Barbieri and S. Jadach, *Nucl. Phys. B* **369**, 3 (1992); and references therein.
- [7] J. C. Pati and A. Salam *Phys. Rev. D* **10** 275 1974 (footnote 7).
- [8] O. W. Greenberg, Private communication with J C Pati (1974).

- [9] H. Terezawa, *Prog. Theor. Phys.* **64**, 1763 (1980).
- [10] H. Fritzsch and G. Mandelbaum, *Phys. Lett. B* **102**, 113 (1981).
- [11] O. W. Greenberg and J. Sucher, *Phys. Lett. B* **99**, 339 (1981).
- [12] H. Fritzsch and G. Mandelbaum, *Phys. Lett. B* **102**, 319 (1981).
- [13] H. Harari and N. Seiberg, *Phys. Lett. B* **100**, 41 (1981).
- [14] H. Harari and N. Seiberg, *Phys. Lett. B* **98** 269 (1981).
- [15] H. Harari and N. Seiberg *Phys. Lett. B* **102**, 263 (1981).
- [16] J. C. Pati and A. Salam, *Nucl. Phys. B* **214**, 109 (1983).
- [17] J. C. Pati and A. Salam, *Nucl. Phys. B* **234**, 223 (1984).
- [18] R. Barbieri, *Phys. Lett. B* **121**, 43 (1983).
- [19] J. C. Pati, M. Cvetič and H. Sharachandra, *Phys. Rev. Lett.* **58**, 851 (1987).
- [20] J. C. Pati, *Phys. Lett. B* **228**, 228 (1989).
- [21] K. S. Babu, J. C. Pati and H. Stremnitzer, *Phys. Lett. B* **256**, 206 (1991).
- [22] K. S. Babu, J. C. Pati and H. Stremnitzer, *Phys. Rev. Lett.* **67**, 1688 (1991).
- [23] J. C. Pati, *Nucl. Phys. B Proc. Suppl. A* **22**, 115 (1991) and references therein.
- [24] K. S. Babu and J. C. Pati, *Phys. Rev. D* **48**, 1921 (1993).
- [25] J. Kimj, *J. Phys. G: Nucl. Part. Phys.* **24**, 1881 (1998).
- [26] O.W. Greenberg, and C.A. Nelson, *Phys. Rev. D* **10** 2567 (1974).
- [27] R. Friedberg and T. D. Lee, *Phys. Rev. D* **15**, 1694 (1977); **16**, 1096 (1977); **18**, 2623 (1978); T. D. Lee, *Particle Physics and Introduction to Field Theory* (Harwood Academic, New York, 1981); K. Huang and D. R. Stump, *Phys. Rev. D* **14**, 223 (1976).
- [28] K. A. Milton, *Phys. Lett. B* **104**, 49 (1981).
- [29] J. Rafelski, *Phys. Rev. D* **16**, 1890 (1977).
- [30] A. Bohr, and B. R. Mottelson, *Nuclear Structure* (Benjamin, New York, 1969, 1973), Vols. I and II.
- [31] A. Hasenfratz and P. Hasenfratz, *Nucl. Phys. B* **270**, 687 (1986).
- [32] C. Alexandrou, E. Follana, H. Panagopoulos, E. Vicari, *Nucl. Phys. B* **580**, 394 (2000).
- [33] J. S. Ball, A. Scotti, and D. Y. Wong, *Phys. Rev.* **142**, 1000 (1966).
- [34] V. A. Karmanov, and J. Carbonell, *Few-Body Systems*, **0**, 1 (2004)

INSTANTON VACUUM BEYOND CHIRAL LIMIT

M. Musakhanov

*Department of Physics, Pusan National University,
609-735 Pusan, Republic of Korea
& Theoretical Physics Dept, Uzbekistan National University,
Tashkent 700174, Uzbekistan
E-mail: musakhanov@pusan.ac.kr*

Abstract

In this talk it is discussed the derivation of low-frequencies part of quark determinant and partition function. As a first application, quark condensate is calculated beyond chiral limit with the account of $O(m)$, $O(\frac{1}{N_c})$, $O(\frac{1}{N_c}m)$ and $O(\frac{1}{N_c}m \ln m)$ corrections. It was demonstrated complete correspondence of the results to chiral perturbation theory.

Introduction

Instanton vacuum model assume that QCD vacuum is filled not only by perturbative but also very strong non-perturbative fluctuations – instantons. This model provides a natural mechanism for the spontaneous breaking of chiral symmetry (SBCS) due to the delocalization of single-instanton quark zero modes in the instanton medium. The model is described by two main parameters – the average instanton size $\rho \sim 0.3 fm$ and average inter-instanton distance $R \sim 1 fm$. These values was found phenomenologically [1] and theoretically [2] and was confirmed by lattice measurements [3, 4, 5, 6, 7]. On the base of this model was developed effective action approach [8, 9, 10], providing reliable method of the calculations of the observables in hadron physics at least in chiral limit.

On the other hand, chiral perturbation theory makes a theoretical framework incorporating the constraints on low-energy behavior of various observables based on the general principles of chiral symmetry and quantum field theory [11].

It is natural expect, that instanton vacuum model leads to the results compatible with chiral perturbation theory.

One of the most important quantities related with SBCS is the vacuum quark condensate $\langle \bar{q}q \rangle$, playing also important phenomenological role in various applications of QCD sum rule approach. Previous investigations [12] shows that beyond chiral limit and at small current quark mass $m \sim few MeV$ these quantity receive large so called chiral log contribution $\sim \frac{1}{N_c} m \ln m$ with fixed model independent coefficient. On the typical scale $1 GeV$ it become leading correction since $|\frac{1}{N_c} \ln m| \geq 1$. It was shown, that this correction is due to pion loop contribution [12, 11].

So, to be consistent we have to calculate simultaneously all of the corrections of order m , $\frac{1}{N_c}$, $\frac{1}{N_c} \ln m$ in order to find quark condensate beyond chiral limit.

In our previous papers [13, 14] on the base of low-frequencies part of light quark determinant Det_{low} , obtained in [15, 8, 16], was derived effective action. In this framework

was investigated current quark mass m dependence of the quark condensate, but without meson loop contribution [14].

In the present work we refine the derivation of the low-frequencies part of light quark determinant Det_{low} . The following averaging of Det_{low} over instanton collective coordinates is done independently over each instanton thanks to small packing parameter $\pi(\frac{\rho}{R})^4 \sim 0.1$ and also by introducing constituent quarks degree of freedoms ψ . This procedure leads to the light quarks partition function $Z[m]$. We apply bosonisation procedure to $Z[m]$, which is exact one for our case $N_f = 2$ and calculate partition function $Z[m]$ with account of meson loops. This one provide us the quark condensate with desired $O(m)$, $O(\frac{1}{N_c})$, $O(\frac{1}{N_c}m \ln m)$ corrections.

Low-frequencies part of light quark determinant

The main assumption of previous works [8, 9, 10] (see also review [16]) was that at very small m the quark propagator in the single instanton field A_i can be approximated as:

$$S_I(m \sim 0) \approx \frac{1}{i\hat{\partial}} + \frac{|\Phi_{0I}\rangle\langle\Phi_{0I}|}{im} \quad (1)$$

It gives proper value for the $\langle\Phi_{0I}|S_I(m \sim 0)|\Phi_{0I}\rangle = \frac{1}{im}$, but in $S_I(m \sim 0)|\Phi_{0I}\rangle = \frac{|\Phi_{0I}\rangle}{im} + \frac{1}{i\hat{\partial}}|\Phi_{0I}\rangle$ second extra term has a wrong chiral properties. We may neglect by this one only for the $m \sim 0$.

At the present case of non-small m we assume:

$$S_I \approx S_0 + S_0 i\hat{\partial} \frac{|\Phi_{0I}\rangle\langle\Phi_{0I}|}{c_I} i\hat{\partial} S_0, \quad S_0 = \frac{1}{i\hat{\partial} + im} \quad (2)$$

where

$$c_I = - \langle\Phi_{0I}|i\hat{\partial}S_0i\hat{\partial}|\Phi_{0I}\rangle = im \langle\Phi_{0I}|S_0i\hat{\partial}|\Phi_{0I}\rangle \quad (3)$$

The matrix element $\langle\Phi_{0I}|S_I|\Phi_{0I}\rangle = \frac{1}{im}$, more over

$$S_I|\Phi_{0I}\rangle = \frac{1}{im}|\Phi_{0I}\rangle, \quad \langle\Phi_{0I}|S_I = \langle\Phi_{0I}|\frac{1}{im} \quad (4)$$

as it must be.

In the field of instanton ensemble, represented by $A = \sum_I A_I$, full quark propagator, expanded with respect to a single instanton, and with account Eq. (2) is:

$$\begin{aligned} S &= S_0 + \sum_I (S_I - S_0) + \sum_{I \neq J} (S_I - S_0) S_0^{-1} (S_J - S_0) \\ &+ \sum_{I \neq J, J \neq K} (S_I - S_0) S_0^{-1} (S_J - S_0) S_0^{-1} (S_K - S_0) + \dots \\ &= S_0 + \sum_{I, J} S_0 i\hat{\partial} |\Phi_{0I}\rangle \left(\frac{1}{C} + \frac{1}{C} T \frac{1}{C} + \dots \right)_{IJ} \langle\Phi_{0J}| i\hat{\partial} S_0 \\ &= S_0 + \sum_{I, J} S_0 i\hat{\partial} |\Phi_{0I}\rangle \left(\frac{1}{C - T} \right)_{IJ} \langle\Phi_{0J}| i\hat{\partial} S_0 \end{aligned} \quad (5)$$

where

$$\begin{aligned} C_{IJ} &= \delta_{IJ} c_I = -\delta_{IJ} \langle \Phi_{0I} | i\hat{\partial} S_0 i\hat{\partial} | \Phi_{0I} \rangle, \\ (C - T)_{IJ} &= -\langle \Phi_{0I} | i\hat{\partial} S_0 i\hat{\partial} | \Phi_{0J} \rangle \end{aligned} \quad (6)$$

We are calculating Det_{low} using the formula:

$$\ln \text{Det}_{low} = \text{Tr} \int_{M_1}^m idm' (\bar{S}(m') - \bar{S}_0(m')) \quad (7)$$

Within zero-mode assumption (Eq. (2)) the trace is restricted to the subspace of instantons:

$$\text{Tr}(S - S_0) = -\sum_{I,J} \langle \Phi_{0,J} | i\hat{\partial} S_0^2 i\hat{\partial} | \Phi_{0,I} \rangle \langle \Phi_{0,I} | (\frac{1}{i\hat{\partial} S_0 i\hat{\partial}}) | \Phi_{0,J} \rangle \quad (8)$$

Introducing now the matrix

$$B(m)_{IJ} = \langle \Phi_{0,I} | i\hat{\partial} S_0 i\hat{\partial} | \Phi_{0,J} \rangle \quad (9)$$

it is easy to show that

$$\begin{aligned} \ln \text{Det}_{low} &= \text{Tr} \int_{M_1}^m idm' (S(m') - S_0(m')) = \sum_I \int_{B(M_1)}^{B(m)} (dB(m') \frac{1}{B(m')})_{II} \\ &= \text{Tr} \ln \frac{B(m)}{B(M_1)} = \ln \det B(m) - \ln \det B(M_1) \end{aligned} \quad (10)$$

which is desired answer. The determinant $\det B(m)$ from Eq. (10) is the extension of the Lee-Bardeen result [15] for the non-small values of current quark mass m .

Light quark effective action beyond chiral limit

Averaged Det_{low} leads to the partition function $Z[m]$, which for $N_f = 2$ has the form:

$$\begin{aligned} Z[m] &= \int d\lambda_+ d\lambda_- D\psi D\psi^\dagger \exp[\int d^4x \sum_{f=1}^2 \psi_f^\dagger (i\hat{\partial} + im_f) \psi_f \\ &\quad + \lambda_+ Y_2^+ + \lambda_- Y_2^- + N_+ \ln \frac{K}{\lambda_+} + N_- \ln \frac{K}{\lambda_-}], \end{aligned} \quad (11)$$

here λ_\pm are dynamical couplings (K is unessential constant, which provide under-logarithm expression dimensionless) [9, 13, 14]. Values of them are defined by saddle-point calculations. Y_2^\pm are t'Hooft type interaction terms [10]:

$$\begin{aligned} Y_2^\pm &= \frac{1}{N_c^2 - 1} \int d^4x [(1 - \frac{1}{2N_c}) \det iJ^\pm(\rho, x) + \frac{1}{8N_c} \det iJ_{\mu\nu}^\pm(x)] \\ J_{fg}^\pm(x) &= \int \frac{d^4k_f d^4l_g}{(2\pi)^8} \exp i(k_f - l_g) x q_f^+(k_f) \frac{1 \pm \gamma_5}{2} q_g(l_g) \\ J_{\mu\nu, fg}^\pm(x) &= \int \frac{d^4k_f d^4l_g}{(2\pi)^8} \exp i(k_f - l_g) x q_f^+(k_f) \frac{1 \pm \gamma_5}{2} \sigma_{\mu\nu} q_g(l_g) \end{aligned} \quad (12)$$

where $q(k) = 2\pi\rho F(k)\psi(k)$. The form-factor $F(k)$ is due to zero-modes and has explicit form $F(k) = -\frac{d}{dt}[I_0(t)K_0(t) - I_1(t)K_1(t)]_{t=\frac{|k|}{2}}$. In the following we will neglect by $J_{\mu\nu,fg}^\pm(x)$ interaction term, since it give a $O(\frac{1}{N_c^2})$ contribution to the quark condensate. Since $q(x) = \int \frac{d^4k}{(2\pi)^4} \exp(ikx) q(k)$, $J_{fg}^\pm(x) = q_f^\pm(x) \frac{1\pm\gamma_5}{2} q_g(x)$,

$$\begin{aligned} & \det \frac{iJ^+(x)}{g} + \det \frac{iJ^-(x)}{g} \\ &= \frac{1}{8g^2} (-(q^+(x)q(x))^2 - (q^+(x)i\gamma_5\vec{\tau}q(x))^2 + (q^+(x)\vec{\tau}q(x))^2 + (q^+(x)i\gamma_5q(x))^2). \end{aligned} \quad (13)$$

Here color factor $g^2 = \frac{(N_c^2-1)2N_c}{(2N_c-1)}$.

In the following we will take equal number of instantons and antiinstantons $N_+ = N_- = N/2$ and corresponding couplings $\lambda_\pm = \lambda$.

Now it is natural to bosonize quark-quark interaction terms (13) by introducing meson fields. For $N_f = 2$ case it is exact procedure. We have to take into account the changes of q and q^\dagger under the $SU(2)$ chiral transformations:

$$\delta q = i\gamma_5\vec{\tau}\vec{\alpha}q, \quad \delta q^\dagger = q^\dagger i\gamma_5\vec{\tau}\vec{\alpha}$$

to introduce appropriate meson fields, changing under $SU(2)$ chiral transformations as:

$$\delta\sigma = 2\vec{\alpha}\vec{\phi}, \quad \delta\vec{\phi} = -2\vec{\alpha}\sigma, \quad \delta\eta = -2\vec{\alpha}\vec{\sigma}, \quad \delta\vec{\sigma} = 2\eta\vec{\alpha}.$$

Then $\delta q^\dagger(\sigma + i\gamma_5\vec{\tau}\vec{\phi})q = 0$, $\delta q^\dagger(\vec{\tau}\vec{\sigma} + i\gamma_5\eta)q = 0$ means that these combinations of fields are chiral invariant¹. So, the interaction term has an exact bosonized representation:

$$\begin{aligned} & \int d^4x \exp[\lambda(\det \frac{iJ^+}{g} + \det \frac{iJ^-}{g})] \\ &= \int D\sigma D\vec{\phi} D\eta D\vec{\sigma} \exp \int d^4x [\frac{\lambda^{0.5}}{2g} q^\dagger(\sigma + i\gamma_5\vec{\tau}\vec{\phi} + i\vec{\tau}\vec{\sigma} + \gamma_5\eta)q - \frac{1}{2}(\sigma^2 + \vec{\phi}^2 + \vec{\sigma}^2 + \eta^2)] \end{aligned} \quad (14)$$

Then the partition function is

$$\begin{aligned} Z[m] &= \int d\lambda D\sigma D\vec{\phi} D\eta D\vec{\sigma} \exp[N \ln \frac{K}{\lambda} - N \\ &- \frac{1}{2} \int d^4x (\sigma^2 + \vec{\phi}^2 + \vec{\sigma}^2 + \eta^2) + \text{Tr} \ln \frac{\hat{p} + im + i\frac{\lambda^{0.5}}{2g} (2\pi\rho)^2 F(\sigma + i\gamma_5\vec{\tau}\vec{\phi} + i\vec{\tau}\vec{\sigma} + \gamma_5\eta) F}{\hat{p} + im}] \end{aligned} \quad (15)$$

(Tr(...)) means here $\text{tr}_{\gamma,c,f} \int d^4x \langle x | (...) | x \rangle$, where $\text{tr}_{\gamma,c,f}$ is the trace over Dirac, color, and flavor indexes.) In the following we assume $m_u = m_d = m$. Then common saddle point on λ , $\sigma (= \text{const})$ (*others* = 0) is defined by Eqs. $\frac{\partial V[m,\lambda,\sigma]}{\partial \lambda} = \frac{\partial V[m,\lambda,\sigma]}{\partial \sigma} = 0$, where the potential

$$V[m,\lambda,\sigma] = -N \ln \frac{K}{\lambda} + N + \frac{1}{2} V\sigma^2 - \text{Tr} \ln \frac{\hat{p} + i(m + M(\lambda,\sigma)F^2(p))}{\hat{p} + im} \quad (16)$$

¹Certainly, quark-quark interaction term Eq. (13) is non-invariant over $U(1)$ axial transformations, as it must be.

and we defined $M(\lambda, \sigma) = \frac{\lambda^{0.5}}{2g}(2\pi\rho)^2\sigma$. Then the common saddle-point on λ and σ is given by Eqs.:

$$N = \frac{1}{2}\text{Tr} \frac{iM(\lambda, \sigma)F^2(p)}{\hat{p} + i(m + M(\lambda, \sigma)F^2(p))} = \frac{1}{2}V\sigma^2. \quad (17)$$

The solutions of this Eqs. are λ_0 and $\sigma_0 = (2\frac{N}{V})^{1/2} = 2^{1/2}R^{-2}$. It is clear that $M_0 = M(\lambda_0, \sigma_0)$ has a meaning of dynamical quark mass, which is defined by this Eqs.. At typical values $R^{-1} = 200 \text{ MeV}$, $\rho^{-1} = 600 \text{ MeV}$ we have $\sigma_0^2 = 2(200 \text{ MeV})^4$, and in chiral limit $m = 0$ $M_0 \rightarrow M_{00} = 358 \text{ MeV}$, $\lambda_{00} \approx M_{00}^2$. It is clear that due to saddle-point equation (17) M_0 (and λ_0) become the function of the current mass m . This dependence was investigated in [14].

Vacuum with account of quantum corrections

The account of the quantum fluctuations around saddle-points σ_0, λ_0 will change the potential $V[m, \lambda, \sigma]$ to $V_{eff}[m, \lambda, \sigma]$ (it is clear that the difference between these two potentials is order of $1/N_c$). Then, the partition function is given by Eq.

$$Z[m] = \int d\lambda \exp(-V_{eff}[m, \lambda, \sigma]) \quad (18)$$

There is important difference between this instanton generated partition function $Z[m]$ and traditional NJL -type models – we have to integrate over the coupling λ here. As was mentioned before, this integration on λ by saddle-point method leads to exact answer. This saddle-point is defined by Eq.:

$$\frac{dV_{eff}[m, \lambda, \sigma]}{d\lambda} = 0 \quad (19)$$

which leads to the λ as a function of σ , i.e. $\lambda = \lambda(\sigma)$.

Then, the vacuum is the minimum of the effective potential $V_{eff}[m, \sigma]$, which is given by a solution of the equation

$$\frac{dV_{eff}[m, \sigma, \lambda(\sigma)]}{d\sigma} = \frac{\partial V_{eff}[m, \sigma, \lambda(\sigma)]}{\partial \sigma} = 0. \quad (20)$$

where it was used Eq. (19).

We denote a fluctuations as a primed fields Φ'_i . The action and corresponding V_{eff} now has a form:

$$S[m, \lambda, \sigma, \Phi'] = S_0[m, \lambda, \sigma] + S_V[m, \lambda, \sigma, \Phi'], \quad (21)$$

$$S_0[m, \lambda, \sigma] = V[m, \lambda, \sigma] = \frac{1}{2}V\sigma^2 - \text{Tr} \ln \frac{\hat{p} + i(m + M(\lambda, \sigma)F^2)}{\hat{p} + im} - N \ln \frac{K}{\lambda} + N$$

$$S_V[m, \lambda, \sigma, \Phi'] = \int d^4x \frac{1}{2}(\sigma'^2 + \vec{\phi}^2 + \vec{\sigma}'^2 + \eta'^2)$$

$$- \frac{1}{2\sigma^2} \text{Tr} \left[\frac{iM(\lambda, \sigma)F^2}{\hat{p} + i(m + M(\lambda, \sigma)F^2)} (\sigma' + i\gamma_5 \vec{\tau} \vec{\phi} + i\vec{\tau} \vec{\sigma}' + \gamma_5 \eta') \right]^2,$$

and

$$V_{eff}[m, \lambda, \sigma] = S_0[m, \lambda, \sigma] + V_{eff}^{mes}[m, \lambda, \sigma] \quad (22)$$

Here second term in Eq. (22) is explicitly represented by

$$V_{eff}^{mes}[m, \lambda, \sigma] = \frac{1}{2} \text{Tr} \ln \frac{\delta^2 S_V[m, \lambda, \sigma, \Phi']}{\delta \Phi'_i(x) \delta \Phi'_j(y)} = \frac{V}{2} \sum_i \int \frac{d^4 q}{(2\pi)^4} \ln \left[1 - \text{tr} \frac{1}{\sigma^2} \int \frac{d^4 p}{(2\pi)^4} \right. \\ \left. \times \frac{M(\lambda, \sigma) F^2(p)}{\hat{p} + i(m + M(\lambda, \sigma) F^2(p))} \Gamma_i \frac{M(\lambda, \sigma) F^2(p+q)}{\hat{p} + \hat{q} + i(m + M(\lambda, \sigma) F^2(p+q))} \Gamma_i \right], \quad (23)$$

where the factors $\Gamma_i = (1, i\gamma_5 \vec{\tau}, i\vec{\tau}, \gamma_5)$ and the sum on i is counted all corresponding meson fluctuations $\sigma', \phi', \vec{\sigma}', \eta'$. tr here means the trace over flavor, color and Dirac indexes. Integrals in Eq. (23) are completely convergent one due to the presence of the form-factors F .

Certainly the quantum fluctuations contribution will move the the coupling λ from λ_0 to $\lambda_0 + \lambda_1$ and σ as $\sigma_0 \rightarrow \sigma_0 + \sigma_1$, where $\frac{\lambda_1}{\lambda_0}$ and $\frac{\sigma_1}{\sigma_0}$ are of order $1/N_c$.

First, consider Eq. (19):

$$\lambda \frac{dV_{eff}[m, \lambda, \sigma]}{d\lambda} = N - \frac{1}{2} \text{Tr} \frac{iM(\lambda, \sigma) F^2}{\hat{p} + i(m + M(\lambda, \sigma) F^2)} + \frac{V}{2} \sum_i \int \frac{d^4 q}{(2\pi)^4} \quad (24) \\ \times [\sigma^2 - \text{tr} \int \frac{d^4 p}{(2\pi)^4} \frac{M(\lambda, \sigma) F^2(p)}{\hat{p} + i(m + M(\lambda, \sigma) F^2(p))} \Gamma_i \frac{M(\lambda, \sigma) F^2(p+q)}{\hat{p} + \hat{q} + i(m + M(\lambda, \sigma) F^2(p+q))} \Gamma_i]^{-1} \\ \times [-\text{tr} \int \frac{d^4 p}{(2\pi)^4} \frac{M(\lambda, \sigma) F^2(p)}{\hat{p} + i(m + M(\lambda, \sigma) F^2(p))} \Gamma_i \frac{M(\lambda, \sigma) F^2(p+q)}{\hat{p} + \hat{q} + i(m + M(\lambda, \sigma) F^2(p+q))} \Gamma_i \\ + i\text{tr} \int \frac{d^4 p}{(2\pi)^4} \left(\frac{M(\lambda, \sigma) F^2(p)}{\hat{p} + i(m + M(\lambda, \sigma) F^2(p))} \right)^2 \Gamma_i \frac{M(\lambda, \sigma) F^2(p+q)}{\hat{p} + \hat{q} + i(m + M(\lambda, \sigma) F^2(p+q))} \Gamma_i] = 0$$

From this saddle-point Eq. we get $\lambda = \lambda(\sigma)$.

From vacuum Eq. (20) we in similar manner arrive to:

$$\sigma \frac{\partial V_{eff}[m, \sigma, \lambda(\sigma)]}{\partial \sigma} = V \sigma^2 - \text{Tr} \frac{iM(\lambda(\sigma), \sigma) F^2}{\hat{p} + i(m + M(\lambda(\sigma), \sigma) F^2)} + \frac{V}{2} \sum_i \int \frac{d^4 q}{(2\pi)^4} \quad (25) \\ \times [\sigma^2 - \text{tr} \int \frac{d^4 p}{(2\pi)^4} \frac{M(\lambda(\sigma), \sigma) F^2(p)}{\hat{p} + i(m + M(\lambda(\sigma), \sigma) F^2(p))} \Gamma_i \\ \times \frac{M(\lambda(\sigma), \sigma) F^2(p+q)}{\hat{p} + \hat{q} + i(m + M(\lambda(\sigma), \sigma) F^2(p+q))} \Gamma_i]^{-1} \\ \times [2i\text{tr} \int \frac{d^4 p}{(2\pi)^4} \left(\frac{M(\lambda(\sigma), \sigma) F^2(p)}{\hat{p} + i(m + M(\lambda(\sigma), \sigma) F^2(p))} \right)^2 \Gamma_i \\ \times \frac{M(\lambda(\sigma), \sigma) F^2(p+q)}{\hat{p} + \hat{q} + i(m + M(\lambda(\sigma), \sigma) F^2(p+q))} \Gamma_i] = 0$$

Since we are believing to $1/N_c$ expansion, it is natural inside quantum fluctuations contribution (under the integrals over q) to take $\sigma = \sigma_0$, $M(\lambda(\sigma), \sigma) = M_0$.

To simplify the expressions introduce vertices $V_i^2(q)$, $V_i^3(q)$ and meson propagators $\Pi_i(q)$, which are defined as:

$$V_i^2(q) = \text{tr} \int \frac{d^4 p}{(2\pi)^4} \frac{M_0 F^2(p)}{\hat{p} + i\mu_0(p)} \Gamma_i \frac{M_0 F^2(p+q)}{\hat{p} + \hat{q} + i\mu_0(p+q)} \Gamma_i \quad (26)$$

$$V_i^3(q) = \text{tr} \int \frac{d^4 p}{(2\pi)^4} \left(\frac{M_0 F^2(p)}{\hat{p} + i\mu_0(p)} \right)^2 \Gamma_i \frac{M_0 F^2(p+q)}{\hat{p} + \hat{q} + i\mu_0(p+q)} \Gamma_i \quad (27)$$

$$\Pi_i^{-1}(q) = \frac{2}{R^4} - V_i^2(q). \quad (28)$$

Here $\mu_0(p) = m + M_0 F^2(p)$ and was taken into account that $\sigma_0^2 = 2R^{-4}$.

From Eqs. (24) and (25) we have

$$\frac{M_1}{M_0} \left[\frac{2}{R^4} + \frac{1}{V} \text{Tr} \left(\frac{M_0 F^2(p)}{\hat{p} + i\mu_0(p)} \right)^2 \right] = \sum_i \int \frac{d^4 q}{(2\pi)^4} (iV_i^3(q) - V_i^2(q)) \Pi_i(q) \quad (29)$$

$$\frac{\sigma_1}{\sigma_0} = -\frac{R^4}{4} \sum_i \int \frac{d^4 q}{(2\pi)^4} V_i^2(q) \Pi_i(q) \quad (30)$$

The vertices $V_i^2(q)$, $V_i^3(q)$ and the meson propagators $\Pi_i(q)$ are well defined functions, providing well convergence of the integrals in Eqs. (29), (30).

It is of special attention to **the contribution of pion fluctuations $\vec{\phi}'$ at small pion momentum q** . We shall demonstrate that this contribution leads to the famous chiral log term with model independent coefficient in the correspondence with previous calculations in NJL-model [18].

Pion inverse propagator of $\Pi_{\vec{\phi}'}^{-1}(q)$ at small $q \sim m_\pi$ is: $\Pi_{\vec{\phi}'}^{-1}(q) = f_{kin}^2(m_\pi^2 + q^2)$. At lowest order on m , $f_{kin,m=0} \approx f_\pi = 93 \text{ MeV}$, $m_\pi^2 \sim m$.

The vertices in the right side of Eq. (29) at $q = 0$ and in chiral limit are:

$$iV_{\vec{\phi}',m=0}^3(0) - V_{\vec{\phi}',m=0}^2(0) = 8N_c \int \frac{d^4 p}{(2\pi)^4} \frac{p^2 M_0^2(p)}{(p^2 + M_0^2(p))^2} \quad (31)$$

We see that the factor in the left side of Eq. (29) in the chiral limit is equal to:

$$\text{tr} \int \frac{d^4 p}{(2\pi)^4} \frac{i\hat{p} M_0(p)}{(\hat{p} + iM_0(p))^2} = -2(iV_{\vec{\phi}',m=0}^3(0) - V_{\vec{\phi}',m=0}^2(0)) \quad (32)$$

Collecting all the factors we get small $q \leq \kappa$ contribution of pion fluctuations $\vec{\phi}'$:

$$\begin{aligned} \frac{M_1}{M_0} \Big|_{\vec{\phi}', \text{small } q} &= -\frac{3}{2f_\pi^2} \int_0^\kappa \frac{d^4 q}{(2\pi)^4} \frac{1}{m_\pi^2 + q^2} \\ &= -\frac{3}{32\pi^2 f_\pi^2} \int_0^{\kappa^2} q^2 dq^2 \frac{1}{f_\pi^2(m_\pi^2 + q^2)} = -\frac{3}{32\pi^2 f_\pi^2} (\kappa^2 + m_\pi^2 \ln \frac{m_\pi^2}{\kappa^2 + m_\pi^2}) \end{aligned} \quad (33)$$

Here we put $m = 0$ everywhere except m_π . We see that the coefficient in the front of $m_\pi^2 \ln m_\pi^2$ is a model independent as it must be.

This one dictate the strategy of the following calculations of M_1 :

1. we have to extract analytically $\frac{1}{N_c} m \ln m$ term;
2. rest part of M_1 can be calculated numerically and expanded over m , keeping $\frac{1}{N_c}$ and $\frac{1}{N_c} m$ terms.

For actual numerical calculations we are using simplified version of the form-factor $F(p)$ from [17] (with corrected high momentum dependence):

$$F(p < 2\text{GeV}) = \frac{L^2}{L^2 + p^2}, \quad F(p > 2\text{GeV}) = \frac{1.414}{p^3} \quad (34)$$

where $L \approx \frac{\sqrt{2}}{\bar{\rho}} = 848 \text{ MeV}$.

At $N_c = 3$ semi-numerical calculations of M_1 and σ_1 lead to:

$$\frac{M_1}{M_0} = -0.662 - 4.64m - 4.01m \ln m \quad (35)$$

$$\frac{\sigma_1}{\sigma_0} = -0.523 - 4.26m - 4.00m \ln m \quad (36)$$

Here m is given in GeV . Certainly, in (35) the $m \ln m$ term is completely correspond to Eq. (33). $\frac{M_1}{M_0}$ is -66% in chiral limit and reach its maximum $\sim -20\%$ at $m \sim 0.115 GeV$.

The relative shift of the vacuum σ_1/σ_0 is -52% at the chiral limit and reach its maximum $\sim -2\%$ at $m \sim 0.125 GeV$.

The main contribution to both quantities $\frac{M_1}{M_0}$ and σ_1/σ_0 come from pion loops. Other mesons give the contribution $\sim 10\%$ to $O(\frac{1}{N_c})$ and $O(\frac{1}{N_c}m)$ terms.

Quark condensate

We have to calculate quark condensate beyond chiral limit taking into account $O(m)$, $O(\frac{1}{N_c})$, $O(\frac{1}{N_c}m)$ and $O(\frac{1}{N_c}m \ln m)$ terms. Quark condensate is extracted from the partition function:

$$\begin{aligned} \langle \bar{q}q \rangle &= \frac{1}{2V} \frac{dV_{eff}[m, \lambda, \sigma]}{dm} = \frac{1}{2V} \frac{\partial(V[m, \lambda, \sigma] + V_{eff}^{mes}[m, \lambda_0, \sigma_0])}{\partial m} \\ &= -\frac{1}{2V} \text{Tr} \left(\frac{i}{\hat{p} + i\mu(p)} - \frac{i}{\hat{p} + im} \right) + \frac{1}{2V} \frac{\partial V_{eff}^{mes}[m, \lambda_0, \sigma_0]}{\partial m} \end{aligned} \quad (37)$$

here $\lambda = \lambda_0 + \lambda_1$, $\sigma = \sigma_0 + \sigma_1$, $M = M_0 + M_1$, $\mu(p) = m + MF^2(p)$. First term of Eq. (37) is

$$\begin{aligned} &-\frac{1}{2V} \text{Tr} \left(\frac{i}{\hat{p} + i\mu_{min}(p)} - \frac{i}{\hat{p} + im} \right) \\ &= -4N_c \int \frac{d^4p}{(2\pi)^4} \left(\frac{\mu_0(p)}{p^2 + \mu_0^2(p)} - \frac{m}{p^2 + m^2} + \frac{M_1 M_0(p)(p^2 - \mu_0^2(p))}{M_0 (p^2 + \mu_0^2(p))^2} \right) \end{aligned} \quad (38)$$

Second term of Eq. (37) – meson loops contribution to the condensate is

$$\begin{aligned} &\frac{1}{2V} \frac{\partial V_{eff}^{mes}[m, \lambda_0, \sigma_0]}{\partial m} \\ &= \frac{i}{2} \sum_i \int \frac{d^4q}{(2\pi)^4} \left(\text{tr} \int \frac{d^4p}{(2\pi)^4} \frac{M_0(p)}{(\hat{p} + i\mu_0(p))^2} \Gamma_i \frac{M_0(p+q)}{\hat{p} + \hat{q} + i\mu_0(p+q)} \Gamma_i \right) \\ &\times \left(\frac{2N}{V} - \text{tr} \int \frac{d^4p}{(2\pi)^4} \frac{M_0(p)}{\hat{p} + i\mu_0(p)} \Gamma_i \frac{M_0(p+q)}{\hat{p} + \hat{q} + i\mu_0(p+q)} \Gamma_i \right)^{-1} \end{aligned} \quad (39)$$

At $m = 0$ and without meson loops the condensate is

$$\langle \bar{q}q \rangle_{00} = -4N_c \int \frac{d^4p}{(2\pi)^4} \frac{M_{00}(p)}{p^2 + M_{00}^2(p)} \quad (40)$$

Here $M_{00} = M_0[m = 0]$.

Let us to consider now the contribution of pion fluctuations $\vec{\phi}'$ to the quark condensate at small q . First we consider:

$$\frac{1}{2V} \frac{\partial V_{eff}^{\vec{\phi}', small q}[m, \lambda_0, \sigma_0]}{\partial m} = 12N_c \int \frac{d^4 q}{(2\pi)^4} \frac{M_0^2(p) \mu_0(p)}{(p^2 + \mu_0^2(p))^2} \int_0^\kappa \frac{d^4 q}{(2\pi)^4 f_{kin}^2 (m_\pi^2 + q^2)} \quad (41)$$

We keep m only in m_π^2 . Then at $m = 0$ $\mu_0(p) \Rightarrow M_0(p) \Rightarrow M_{00}(p)$, $f_{kin} \Rightarrow f_\pi$ and we have

$$\langle \bar{q}q \rangle = \langle \bar{q}q \rangle_{00} - \frac{M_1}{M_0} 4N_c \int \frac{d^4 p}{(2\pi)^4} \frac{M_{00}(p)(p^2 - M_{00}^2(p))}{(p^2 + M_{00}^2(p))^2} \quad (42)$$

$$+ 12N_c \int \frac{d^4 p}{(2\pi)^4} \frac{M_{00}^3(p)}{(p^2 + M_{00}^2(p))^2} \int_0^\kappa \frac{d^4 q}{(2\pi)^4} \frac{1}{f_\pi^2 (m_\pi^2 + q^2)} \\ = \langle \bar{q}q \rangle_{00} \left(1 - \frac{3}{2} \int_0^\kappa \frac{d^4 q}{(2\pi)^4} \frac{1}{f_\pi^2 (m_\pi^2 + q^2)} \right) \quad (43)$$

Eq. (33) for $\frac{M_1}{M_0}$ was applied here. We see that Eq. (43) is in the full correspondence with [11, 12].

Detailed numerical calculations lead to the semi-analytical formula for the quark condensate including all $O(m)$, $O(\frac{1}{N_c})$ and $O(\frac{1}{N_c} m \ln m)$ -corrections:

$$\langle \bar{q}q \rangle = \langle \bar{q}q \rangle_{m=0} (1 - 18.53 m - 7.72 m \ln m) \quad (44)$$

Here $\langle \bar{q}q \rangle_{m=0} = 0.52 \langle \bar{q}q \rangle_{00}$. Certainly, the $m \ln m$ term in Eq.(44) is in full correspondence with Eq. (43), as it must be. $\langle \bar{q}q \rangle / \langle \bar{q}q \rangle_{m=0}$ is a rising function of m until $m \sim 0.04 GeV$ and is a falling one in the region $m > 0.04 GeV$.

The main contribution to $O(\frac{1}{N_c})$, $O(\frac{1}{N_c} m)$ and $O(\frac{1}{N_c} m \ln m)$ terms in $\frac{\langle \bar{q}q \rangle}{\langle \bar{q}q \rangle_{00}}$ is due to pion loops. Other mesons give the contribution $\sim few\%$ to $O(\frac{1}{N_c})$ and $O(\frac{1}{N_c} m)$ terms.

$m_d - m_u$ effects in quark condensate

Current quark mass become diagonal 2×2 matrix with $m_1 = m_u, m_2 = m_d$, $m = m_1 \frac{1+\tau_3}{2} + m_2 \frac{1-\tau_3}{2} = m + \delta m \frac{\tau_3}{2}$. Here $m = \frac{m_1+m_2}{2}$, $\delta m = m_1 - m_2$. Let us introduce external field s_i . In our particular case it is $s_3 = i \frac{\delta m}{2}$, $s_1 = s_2 = 0$. Our aim is to find the asymmetry of the quark condensate $\frac{\langle \bar{u}u \rangle - \langle \bar{d}d \rangle}{\langle \bar{u}u \rangle}$, taking into account only $O(\delta m)$ terms and neglecting by $O(\frac{1}{N_c} \delta m)$, $O(\frac{1}{N_c} \delta m \ln m)$. It means that we neglect at all by meson loops contribution.

In the presence of the external field \vec{s} we expect also vacuum field $\vec{\sigma}$. Effective potential within requested accuracy is

$$V_{eff}[\sigma, \vec{\sigma}, m] \approx S_0[m, \lambda, \sigma, \vec{\sigma}] \quad (45) \\ = \frac{V}{2} (\sigma^2 + \vec{\sigma}^2) - \text{Tr} \ln \frac{\hat{p} + i\vec{\tau}\vec{s} + i(m + \bar{M}(\lambda, \sigma, \vec{\sigma})F^2)}{\hat{p} + im + i\vec{\tau}\vec{s}} - N \ln \frac{K}{\lambda} + N.$$

$\lambda, \sigma, \vec{\sigma}$ are defined by the vacuum equations:

$$\frac{\partial V_{eff}}{\partial \lambda} = 0, \quad \frac{\partial V_{eff}}{\partial \sigma} = 0, \quad \frac{\partial V_{eff}}{\partial \sigma_i} = 0. \quad (46)$$

They can be reduced to the following form:

$$\frac{1}{2} \text{Tr} \frac{F^2(p) M_i (m_i + M_i F^2(p))}{p^2 + (m_i + M_i F^2(p))^2} = N \quad (47)$$

where $M_i = \frac{\lambda^{0.5}}{2g} (2\pi\rho)^2 (\sigma \pm \sigma_3)$. Solution of these equations leads to $\lambda = \lambda[m, \vec{s}]$, $\sigma = \sigma[m, \vec{s}]$, $\sigma_i = \sigma_i[m, \vec{s}]$. We have to put them into V_{eff} and find $V_{eff} = V_{eff}[m, \vec{s}]$. Desired correlator is

$$\left. \frac{\partial V_{eff}[m, \vec{s}]}{\partial s_3} \right|_{s_3 = \frac{\delta m}{2}, s_{1,2}=0} \quad (48)$$

We calculate this correlator within requested accuracy, taking into account only $O(\delta m)$ terms. So, the difference of the vacuum quark condensates of u and d quarks is

$$\begin{aligned} & \langle \bar{u}u \rangle - \langle \bar{d}d \rangle \\ &= \frac{1}{V} \left[\text{Tr} \left(\frac{-i}{\hat{p} + i(m_u + M_u F^2)} - \frac{-i}{\hat{p} + im_u} \right) - \text{Tr} \left(\frac{-i}{\hat{p} + i(m_d + M_d F^2)} - \frac{-i}{\hat{p} + im_d} \right) \right] \end{aligned} \quad (49)$$

We expect that $\langle \bar{d}d \rangle < \langle \bar{u}u \rangle$ if $m_d > m_u$.

Typical values of light current quark masses [19] are $m_u = 5.1 \text{ MeV}$, $m_d = 9.3 \text{ MeV}$ on the scale 1 GeV (which is in fact close to our scale $\rho^{-1} = 0.6 \text{ GeV}$) leads to the asymmetry

$$\frac{\langle \bar{u}u \rangle - \langle \bar{d}d \rangle}{\langle \bar{u}u \rangle} = 0.026 \quad (50)$$

From this asymmetry and using sum-rules [20] we estimate strange quark condensate at $m_s = 120 \text{ MeV}$ as:

$$\frac{\langle \bar{s}s \rangle}{\langle \bar{u}u \rangle} = 0.43, \quad (51)$$

which is rather small. The reason that the asymmetry (50) is rather large.

Conclusion

In the framework of instanton vacuum model it was calculated simplest possible correlator – quark condensate with complete account of $O(m)$, $O(\frac{1}{N_c})$, $O(\frac{1}{N_c})$ and $O(\frac{1}{N_c} m \ln m)$ terms, demanding the calculation of meson loops contribution. Since initial instanton generated quark-quark interactions are nonlocal and contain corresponding form-factor induced by quark zero-mode, these loops correspond completely convergent integrals. The main loop corrections come from the pions, as it was expected. We found that $O(\frac{1}{N_c})$ corrections are very large $\sim 50\%$, which request the $\sim 10\%$ changing of the basic parameters – average inter-instanton distance R and average instanton size ρ to restore chiral limit value of the quark condensate $\langle \bar{q}q \rangle_{m=0}$ and other important quantities as f_π and m_π to their phenomenological values. This work in the progress.

In general, it was demonstrated, that instanton vacuum model is well working tool also beyond chiral limit and satisfy chiral perturbation theory.

Acknowledgement

I am very grateful to D. Diakonov for a useful discussions. This work was done in the collaboration with Hyun-Chul Kim and M. Siddikov and was partly supported by Republic of Korea "Brain Pool" Program.

References

- [1] E. V. Shuryak, Nucl. Phys. B **203** (1982) 93.
- [2] D. Diakonov and V. Y. Petrov, Nucl. Phys. B **245** (1984) 259.
- [3] M. C. Chu, J. M. Grandy, S. Huang and J. W. Negele, Phys. Rev. D **49** (1994) 6039.
- [4] J. W. Negele, Nucl. Phys. Proc. Suppl. **73** (1999) 92.
- [5] T. DeGrand, Phys. Rev. D **64** (2001) 094508.
- [6] P. Faccioli and T. A. DeGrand, Phys. Rev. Lett. **91** (2003) 182001.
- [7] P. O. Bowman, U. M. Heller, D. B. Leinweber, A. G. Williams and J. b. Zhang, Nucl. Phys. Proc. Suppl. **128** (2004) 23.
- [8] D. Diakonov and V. Y. Petrov, Nucl. Phys. B **272** (1986) 457.
- [9] D. Diakonov, V. Polyakov and C. Weiss, Nucl. Phys. B **461** (1996) 539.
- [10] D. Diakonov, Prog. Part. Nucl. Phys. **51**, 173 (2003), arXiv:hep-ph/9802298.
- [11] J. Gasser and H. Leutwyler, Annals Phys. **158** (1984) 142.
- [12] V. A. Novikov, M. A. Shifman, A. I. Vainshtein and V. I. Zakharov, Nucl. Phys. B **191**, 301 (1981).
- [13] M. Musakhanov, Eur. Phys. J. C **9** (1999) 235.
- [14] M. Musakhanov, Nucl. Phys. A **699** (2002) 340.
- [15] C. k. Lee and W. A. Bardeen, Nucl. Phys. B **153** (1979) 210.
- [16] T. Schafer and E. V. Shuryak, Rev. Mod. Phys. **70** (1998) 323.
- [17] V. Y. Petrov, V. Polyakov, R. Ruskov, C. Weiss and K. Goeke, Phys. Rev. D **59**(1999) 114018 (1999).
- [18] E. N. Nikolov, W. Broniowski, C. V. Christov, G. Ripka and K. Goeke, Nucl. Phys. A **608** (1996) 411.
- [19] H. Leutwyler, arXiv:hep-ph/9609467.
- [20] J. Gasser and H. Leutwyler, Nucl. Phys. B **250**, 465 (1985).

ON THE MOTION OF MATTER IN THE GEOMETRICAL GAUGE FIELD THEORY

N.P. Konopleva¹

*All-Russian Scientific Research Institute of Electromechanics,
Horomnyi tup. 4, Moscow 101000*

and

Bogoliubov Laboratory of Theoretical Physics, JINR, Dubna, 141980

Abstract

In the geometrical gauge field theory the motion equations of matter (elementary particles) are connected with the field equations. In the talk the problems arising from this connection are discussed. For the first time such problems arose in the Einstein's General Relativity. Einstein hoped for that solution of these problems will allow explanation of elementary particles nature without making use of quantum mechanics. But as it turned out the situation is more difficult. Here the corresponding problems are formulated for the connection of equations of particle motion and field equations in the geometrical gauge field theory. It is shown that appearance of the problems under discussion is inevitable effect of passage to relativism and local symmetries.

Key-words: gauge field theory, local symmetries, motion and field equations, relativistic vacuum.

Talk dedicated to the 125th jubilee of A.Einstein and to the centenary of D.Ivanenko, who was the first to riddle nucleous structure.

Two fundamental concepts are assumed by modern physics: matter and fields. The matter can exist both in discrete form (point particles, extensive bodies), and in the form of continuously distributed medium in space (liquids, gases, solid bodies). In the classic theory a field are always regarded as continuous something filling the whole space. But properties of this field are not mechanical.

Before GR creation it was supposed that all events being under physics consideration happen on vacuum background. The vacuum is the world state corresponding to absence of both fields, and particles. It is absolute, universal, and global, that is its properties are the same in every point of space and in every moment of time. The vacuum properties are not connected with matter motion and field properties. Just this vacuum is postulated in Newtonian mechanics, relativistic mechanics, and field theory without GR.

Such vacuum is a passive arena of events. But in reality we assume that *the vacuum state is only corresponding to particles absence (or other matter)*. In experiments a backing pump is often the tool for making of a real vacuum state. Therefore our assumption immediately leads us to relativism.

Even in Newtonian mechanics appearance of gravity is followed by loss of equal states of all space-time points. Particles behavior becomes depending on space-time point, and

¹*E-mail nelly@thsun1.jinr.ru; vniiem@orc.ru; fax: (095)2074962*

in this sense localization of particle motion laws arises. It can be said that in space without particles (or other matter) gravity induces localization of vacuum properties. Such vacuum is no longer global one. Similarly the local transformation of the vacuum for charged particles will arise if electromagnetic field will appear.

GR appearance changed our perception of gravitational field, space and time properties, and also of substance behavior in Universe. Moreover it necessitated to revise the vacuum properties. It was found that relativistic vacuum properties must be described by vacuum Einstein equations.

Usually in Maxwell's electrodynamics the law of charged particles motion is regarded as logically independent on the field equations. Therefore it must be added to them.

In GR the field equations with arbitrarily moving sources are absent. The motion of particles is determined by the same equation system that determines propagation of fields.

How is it possible to solve such equations which simultaneously determine field and motion of particles? Einstein with his collaborators went into this problem in 1927 (with Grommer) ([1]) and in 1938 (with Infeld and Hoffmann) ([2]).

They showed that the motion law of test particles (i.e. the motion along geodesic lines of Riemannian V_4) can be found as a corollary of the field equations. Therefore, it is not necessary to postulate the motion equations in addition to the field equations.

So, *for the first time it was shown that field theory can include a theory of mechanical motion of matter*. Einstein hoped to find an explanation of elementary particles nature (specifically electron) and quantum theory laws in this way.

But in the above Einstein's papers geodesic line equations were only obtained for the field singularities (gravitational field or gravity with electromagnetic field). Thus *electron was described as moving field singularity*. In proof approximate solutions were used.

These and of next years results were summarized in the L.Infeld and J.Plebansky monography "Motion and Relativity" of 1960 ([3]).

Thus, first solution of motion problem in GR was found by Einstein in 1938.

But in 1939 V.A.Fock proposed quite other way to solve the problem ([4], [5]). He showed that for massive extensive noninteracting bodies the motion equations can be obtained from Einstein equations as their corollary. They are also the geodesic lines equations. Moreover, he put a question of what kind of real objects and under which conditions can be the objects of application of GR? V.A.Fock found that such objects are cosmic bodies, as planets and stars being long distant from each other, but in no way it can be elementary particles. He took for granted that GR can not be applied to microworld objects. Fock's point of view is explained in his monography "Theory of space, time and gravitation" of 1955 ([6]).

By other method the same result was found by N.P.Konopleva in 1977. In paper "Gravitational experiments in space" ([7]) I discussed the conditions ensured realization to given precision of GR axioms in cosmic experiments. Distinctive feature of these experiments consists in existence of many factors exercising their influence on test bodies. It was found that under these conditions it is very difficult to make such object which will behave as pure gravitational test body of GR. It is complex technical problem for artificial objects. For natural objects I obtained a formula which arrived at a conclusion that the real massive bodies can appear as the test bodies, when their radii are enough large. Estimation shows that to within $10^{-8}g$ (g - acceleration due to gravity) planets and stars

can be regarded as GR test bodies, but elementary particles can not be regarded in this way. Even nuclei can only give precision of geodesic motion $\sim 10^{-5}g$. It is insufficiently for extraction of GR geodesic trajectories from all perturbed Newtonian one. Therefore elementary particles are poor test bodies. They can not precisely move along geodesic lines in real conditions.

But recently a new possibility of GR application to microworld was discovered. In the frame of geometrical theory of gauge fields it was shown by me that relativistic vacuum in classic theory of gauge fields is Einsteinian vacuum which is described by vacuum Einstein equations ([8], [9]). Hence, it is necessary to return to the question about connection between elementary particles and GR. This is the question of a connection between fields and matter both in microworld and macroworld.

Now Wheeler's results of 1955 become again very interesting ([10]). J.A.Wheeler and C.W.Misner demonstrated in 1957 third independent solution of motion problem in GR ([11]). At first it seems to be paradoxical. They shown that having only free electromagnetic and gravitational fields in vacuum without any singularities or massive bodies it can be constructed such solutions of Einstein-Maxwell equations which are everywhere regular and localized. These solutions describe objects which far from their centers look like massive neutral or charged particles in spite of neither mass nor charge is inside them. This effect results from nonlinearity of theory and nontrivial topology of Riemannian V_4 . Wheeler's point of view is explained in his book "Neutrinos, gravity and geometry" of 1960 ([12]).

It is necessary to note that in pure gravitational field without any matter or other fields regular solutions of vacuum Einstein equations are not exist. For example, presence of singularity, statics, and Schwarzschildian form of the solution arise from only its spherical symmetry. This fact is known as Birkhoff theorem ([13]). Schwarzschild's solution of 1916 ([14]) was strong, analytical, and had singularity in point $r = 0$, (r - radius). Single constant which defines this solution was interpreted as a mass of gravity source. Geodesic lines were considered trajectories of test bodies (or massless particles) moving in the field of this point source. But what kind of equations is guiding the motion of gravity source? It remained unknown. Schwarzschild's solution corresponds to null right side of Einstein equations, i.e. vacuum.

So, Einstein's equations permit to obtain as their corollary the motion equations of neutral particles and massive bodies, and also Lorentz equations describing charged particle motion in external electromagnetic and gravitational fields.

This indicates that in a sense Einstein equations contain mechanics and classical electrodynamics of moving particles and, hence *permit to overcome dualism of matter and fields*. Final answer will can be given after clarification of connection between Einstein equations and quantum physics laws.

The attempts to find this connection were launched by many scientists both in USSR, and in other countries. In USSR prof. D.Ivanenko was leading in this direction during many years ([15], [16]). His papers, books, and scientifically organizational activities promoted intensive development of science working in gravity and GR. Cited above books of Infeld and Plebanski, and also Wheeler were published in Russian thanks to prof. D.Ivanenko. At that time I was a student of third course of Moscow University and took part in translation of these books from English into Russian. They seemed to be very difficult to me, but attracted like a magnet, and until now I think about problems from

these books. They stimulated my interest in geometrical theory of interactions.

Creation of geometrical gauge field theory by the end of 60th ([17]) put again the same questions that were in GR. But now they concern more wide class of elementary particle interactions. Einstein equations are components of equation system of geometrical gauge field theory ([18]). All equations of this theory have clear geometrical meaning in terms of fibre bundle space geometry. Thus, not only gravity and electromagnetism, but also nuclear forces have a geometrical treatment.

Just as it is in GR, in geometrical gauge field theory the motion equations can be obtained as a corollary of the field equations. But it is necessary to note that theory nonlinearity is not cause of this effect.

When we go over from global space-time symmetries to the local one, which are defined by coordinate transformations $x^{\mu'} = f^{\mu}(x^{\nu})$, and f^{μ} - arbitrary continuous function, four identities arise according to the second Noether theorem ([17]). Just these identities reduce number of independent equations. Therefore four equations of motion turn into a corollary of the field equations. Covariant conservation law of energy-momentum tensor of the system of particles and fields corresponds to above local coordinate transformations and Noether's identities. Just it permit us to connect the equations of fields and particles with each other. Therefore, *the connection between fields and particles is direct result of localization of symmetries and relativism.*

NOW EINSTEINIAN PROGRAM IS OPENED AGAIN! We must to make a try at understanding of elementary particles nature through field equations.

Acknowledgments. It is a pleasure to thank the Organizers of the International Seminar ISHEPP XVII for their support of this investigation.

References

- [1] A.Einstein, J.Grommer, Sitzber. Preuss. Akad. Wiss., 1, S.2, 1927
- [2] A.Einstein, L.Infeld, B.Hoffinan, Ann. Math., **39**, p.65, 1938
- [3] L.Infeld, J.Plebanski, Motion and Relativity, Pergamon Press, N.Y., 1960
- [4] V.A.Fock, Journ. of Phys. (USSR), **1**, p.81, 1939
- [5] V.A.Fock, JETP, **9**, p.375, 1939
- [6] V.A.Fock, Theory of space, time and gravitation, GTTL, M., 1955; (Eng. iss.: Pergamon Press, London, 1959)
- [7] N.P.Konopleva, Usp. Fiz. Nauk, **123**, iss.4, p.537-563, 1977 (in English: Sov. Phys. Usp., **20**, p.973, 1977)
- [8] N.P.Konopleva, Gauge field vacuum structure in geometrical aspect, E2-2003-170, JINR, Dubna, 2003
- [9] N.P.Konopleva, in Proc. of XVI ISHEPP, 1 JINR, Dubna, 2004, p.31
- [10] J.A.Wheller, Phys. Rev., **97**, p.511, 1955

- [11] C.W.Misner, J.A.Wheeler, *Ann. of Phys.*, **2**, p.525, 1957
- [12] J.A.Wheeler, *Neutrinos, gravitation and geometry*, Bologna,1960
- [13] G.D.Birkhoff, *Relativity and Modern Physics*, Harward University Press, Cambridge, Mass., 1923
- [14] K.Schwarzschild, *Sitzungsber. d. Berl. Akad.*, S.189, 1916
- [15] *Gravitation and Cosmology*, Iss. dedicated to the centenary of Prof. D.D.Ivanenko, **10**, No. 1-2, (37-38), M., 2004
- [16] *Gravity, particles, and space-time*, Volume dedicated to the memory of Dimitri Ivanenko, ed. by P.Pronin and G.Sardanashvili, World Scientific, Singapore, 1996
- [17] N.P.Konopleva, V.N.Popov, *Gauge fields*, Chur-London-N.Y., 1981
- [18] N.P.Konopleva, "General Relativity and gauge gravity theories of higher order", in: *Proc. of "Int. Sem. on Math. Cosmology"*, 30.03-4.04 1998, Potsdam, World Scientific, Singapore, 1998, p.25

O.V. Pavlovsky[†]*Institute for Theoretical Problems of Microphysics, Moscow State University*[†] *E-mail: ovp@bog.msu.ru***Abstract**

In our work we extend the ideas of the derivation of the chiral effective theory from the lattice QCD [1] to the case of the random lattice regularization of QCD. Such procedure allows in principle to find contribution of any order into the chiral effective lagrangian. It is shown that an infinite subseries of the chiral perturbation can be summed up into the Born-Infeld term and the logarithmic correction to them.

1. Why do we need the Random Lattice QCD

Derivation of a chiral effective Lagrangian from lattice QCD has been attempted many times since long ago. The well-known Brezin & Gross trick [2] makes it possible to perform integration of the link matrix in the strong coupling regime and to obtain various first order chiral effective theories [3].

Although at first such approaches led to great success, they have not been very popular, because they do not allow to obtain any corrections to first order results. Lattice regularization breaks the rotational symmetry of the initial theory from the continuous rotation group down to a discrete group of rotations at fixed angles. Hence, lattice regularization approaches give correct results only for those tensors that are invariant with respect to such discrete groups. In particular, using the ordinary Hyper-Cubical (HC) lattice, one can obtain only a first order effective theory, while for corrections this method generates non-rotation invariant (non-Lorentz invariant) terms. Generation of high-order effective field theories requires a more symmetrical lattice.

The problem of breakdown of rotational symmetry on a lattice has been attracting important attention for a long time. It was shown [5] that in 4 dimensions the so-called Body Centered Hyper-Cubical (BCHC) or F4 lattice has the largest discrete symmetry group. (BCHC consists from the all sites of the HC lattice together with centers of its elementary cells.) This property of the BCHC lattice gives a possibility to obtain the next-to-leading (NL) correction to the first order of the chiral perturbation theory [1].

The results of the papers [1] are essential for our analysis, as they confirm the effectiveness of the idea of chiral effective lagrangian derivation from the lattice QCD. Moreover, these results are interesting from phenomenological point of view because, as is well known [4], the NL corrections violate the scale invariance of the prototype (first order) chiral theory that leads to generation of chiral topological solitons (Skyrmions). The Next-Leading order chiral effective theory that was implemented in [1] is in agreement with our phenomenological propositions [6], and in our work we will use methodological ideas from [1] in order to define the behaviour of chiral field near the confinement surface.

As one could see, in order to solve our problem, the Next-Leading order corrections are not enough. This theory has no solutions that look like chiral “bag”. Moreover, as

will be shown later, near the confinement surface (near the source of the chiral field), the influence of high order corrections became larger and larger. But the BCHC lattice method gives the NL corrections only and the further use of this method for the defining of the high order terms leads to generation of non-relativistic (non-rotational) invariant terms. It means that we need a more symmetric lattice than the BCHC lattice.

Unfortunately, a lattice which would be more symmetric than BCHC lattice cannot be constructed in 4 dimension. Moreover any method based on a lattice of a fixed geometry has artifacts coming from priority directions that correspond to basis vectors of the lattice. It is these artifacts that eventually lead to the problems with the rotational (relativistic) invariance rendering the use of the BCHC lattice to be only half measure. For solving our problem a modification of the initial concept of lattice regularization must be performed. We need to find a concept of lattice regularization that has no priority directions. Fortunately this concept is known for a long time and is called the Random Lattice approach [8].

The idea of Random Lattice was proposed originally by Voronoi and Delaunay: today this method is widely used in the modern science. For the quantum field theory the method was modified by Christ, Friedberg and Lee [8]. In these articles it has been shown that in order to restore the Lorentz (rotational) invariance, it is necessary to perform an average over an ensemble of random lattices. As a result one gets the averaging over all possible directions and it is intuitively clear that this procedure leads to the disappearance of the artifacts that cause the violation of the group of the space rotations.

But how to perform such random discretization? This procedure has the three steps:

- 1) Pick N sites x_i at random in the volume V .
- 2) Associate with each x_i a so-called Voronoi cell c_i

$$c_i = \{x \mid d(x, x_i) \leq d(x, x_j), \forall j \neq i\}$$

where $d(x, y)$ is a distance between points x and y . It means that the Voronoi cell c_i consists of all points x that are closer to the center site x_i than to any other site.

3) Constrict the dual Delaunay lattice by linking the center sites of all Voronoi cells which share a common face.

Now if one considers the the big ensemble of such Voronoi-Delaunay random lattices based on various distributions of sites x_i , it possible to prove that the original rotational symmetry is restored [8]. In our work we use this procedure to obtain an effective chiral lagrangian from lattice QCD. This methodological point of view it is a modification of the method proposed in [1] in the case of the Random Lattice approach.

2. From Lattice QCD to chiral lagrangians: step by step

Now let me briefly recall a general steps of the algorithm of derivation of the chiral lagrangian from the lattice QCD that was proposed in [1].

Step 1: Definitions

The starting point of our analysis is a standard lattice action with Willson fermions

$$Z = \int [DG][D\bar{\psi}][D\psi] \exp\{-S_{\text{pl}}(G) - S_q(G, \bar{\psi}, \psi) - S_J\}$$

where:

1) the plaquette gauge field term is defined by

$$S_{\text{pl}} = \frac{2N_c}{g^2} \sum_{\text{pl}} \left[1 - \frac{1}{N_c} \text{Re} G_{x,\mu} G_{x-\mu,\nu} G_{x+\nu,\mu}^+ G_{x,\nu}^+ \right], \quad G_{x,\mu} = \exp\left\{ ig \int_{\text{link}} dx'_\mu \mathcal{A}_\mu(x') \right\};$$

2) the link fermions term is defined by

$$S_q = \sum_{x,\mu} \text{tr}(\bar{A}_\mu(x) G_\mu(x) + G_\mu^+(x) A_\mu(x))$$

$$A_\mu(x)_b^a = \bar{\psi}_b(x + \mu) P_\mu^+ \psi^a(x), \quad \bar{A}_\mu(x)_b^a = \bar{\psi}_b(x) P_\mu^- \psi^a(x + \mu)$$

and $P_\mu^\pm = \frac{1}{2}(r \pm \gamma_\mu)$;

3) the source term is defined by

$$S_J = \sum_x J_\beta^\alpha(x) M_\alpha^\beta(x), \quad M_\alpha^\beta = \frac{1}{N_c} \psi^{\alpha,\beta}(x) \bar{\psi}_{\alpha,\beta}(x).$$

Step 2: Strong-coupling regime on the lattice and integration over the gauge field

In order to realize the strong-coupling regime on the lattice let us consider the limit of the large coupling constant g ($g \rightarrow \infty$). This limit was widely studied [3] and the main result is that in such limit integration over the gauge field can be performed. (Of course, the direct integration is difficult since there exists the plaquette term S_{pl} , but due to the strong-coupling limit on the first step plaquette contributions are negligible with respect to the contribution from the link integral S_q . The plaquette contributions could be considered in the systematic manner as perturbations in $1/g$ [3].)

Let us consider the leading order contribution in this strong-coupling expansion. The integrals over the gauge degrees of freedom can be calculated into the large N limit by using the standard procedure [3] and the result of these calculations is the following

$$Z = \int [D\bar{\psi}][D\psi] \exp\left\{ -N \sum_{x,\nu} \text{tr}[F(\lambda(x, \nu))] - S_J \right\}, \quad (1)$$

where $\lambda_\nu = -M(x) P_\nu^- M(x + \nu) P_\nu^+$ and

$$F(\lambda) = \text{tr}[(1 - \sqrt{1 - \lambda})] - \text{tr}[\log(1 - \frac{1}{2}\sqrt{1 - \lambda})].$$

Interestingly, the function $F(\lambda)$ has the typical form of the Born-Infeld action with a first logarithmic correction. This is no coincidence. In [7], it was shown by means of very similar technique that the low-energy theory of the IIB superstring has a Born-Infeld form. From the methodological point of view we perform a similar analysis for QCD on the lattice and it is important to note before starting our proof that our result will have a Born-Infeld form too.

Step 3: Integration over the fermion field and chiral limit

Our next step is the integration over the fermion degrees of freedom in (1). Using the source technique it was shown [1] that integral (1) can be re-written into the form of an integral over the unitary boson matrix M_x

$$Z = \int DM \exp S_{\text{eff}}(M). \quad (2)$$

As a matter of principle, we already performed the transformation from the color lattice degrees of freedom (G and ψ) to the boson lattice degrees of freedom (M). Now our task is to realize the continuum limit of expression (2).

This step of our analysis amounts to studying of the stationary points of the lattice action S_{eff} . Fortunately this is a very well studied task [9]. This problem is connected with well-known investigations of the critical behavior of the chiral field on the lattice and with the problem of the phase transformation on the lattice (for references see issue [10]). In [1], it was shown that for our task the stationary point is

$$\hat{M}_0 = u_0 \hat{I}, \quad u_0(m_q = 0, r = 1) = 1/4.$$

Now one can expressed $M(x)$ in terms of the pseudoscalar Goldstone bosons

$$M = u_0 \exp(i\pi_i \tau_i \gamma_5 / f_\pi) = u_0 [U(x) \frac{1 + \gamma_5}{2} + U^+(x) \frac{1 - \gamma_5}{2}]$$

and the effective action is given in the form of the Taylor expansion around this stationary point

$$S_{\text{eff}}(U) = -N \sum_{k=1}^{\infty} \frac{F^{(k)}(\lambda_0)}{k!} \sum_{x,\nu} \text{tr}[(\lambda_\nu(x) - \lambda_0)^k]. \quad (3)$$

Let us consider the expansion of the chiral field $U = \exp(i\pi_i \tau_i / f_\pi)$ on the lattice around the point x in power of the small step of the lattice a

$$U(x + \nu) = U(x) + a(\partial_\nu U(x)) + \frac{a^2}{2}(\partial_\nu^2 U(x)) + \dots$$

And for components of the Taylor expansion (3) one obtain

$$\begin{aligned} \text{tr}[(\lambda_\nu(x) - \lambda_0)] &= -2\lambda_0 \text{tr}(\alpha) \\ \text{tr}[(\lambda_\nu(x) - \lambda_0)^2] &= 2\lambda_0^2 \text{tr}(\alpha^2) - 4\lambda_0^2 \text{tr}(\alpha) \\ \text{tr}[(\lambda_\nu(x) - \lambda_0)^3] &= -2\lambda_0^3 \text{tr}(\alpha^3) + 6\lambda_0^3 \text{tr}(\alpha^2) \\ \text{tr}[(\lambda_\nu(x) - \lambda_0)^4] &= 2\lambda_0^4 \text{tr}(\alpha^4) - 8\lambda_0^4 \text{tr}(\alpha^3) + 4\lambda_0^4 \text{tr}(\alpha^2) \\ \text{tr}[(\lambda_\nu(x) - \lambda_0)^5] &= -2\lambda_0^5 \text{tr}(\alpha^5) \quad \dots \quad \dots \quad \dots \end{aligned}, \quad (4)$$

where $\alpha = a^2 \partial_\nu U \partial_\nu U^+ + O(a^4)$.

Step 4: Problem of rotational symmetry violation: examples of the Hyper-Cubical and Body Centered Hyper-Cubical lattices

Expressions (4) are very essential because these are a simplest illustration of all aspects of the violation of the rotational symmetry on the lattice. For this moment we assume nothing special about the structure of our lattice. We try to formulate our result as generally as possible and all information about the lattice contained in the vectors ν that correspond to the basic vectors of the lattice (for example, the vectors ν for the Hyper-Cubical lattice are the Cartesian basic vectors \vec{i} , \vec{j} , \vec{k} and \vec{i}). The leading order part can be calculated trivially. Indeed, using the simple Hyper-Cubical lattice where $\nu = i, j : i = (1 \dots 4)$ it is easy to show that the leading order contribution is the prototype chiral lagrangian

$$P_{O(p^2)} \sim \text{tr}[\partial_\mu U \partial^\mu U^+]. \quad (5)$$

As I said before the rotational symmetry violation argument does not allow to use the HC lattice calculation for the next-leading order contributions. For obtaining of these

contributions a more symmetrical lattice must be used. In [5] it was shown that this lattice is a Body Centered Hyper-Cubical (BCHC) or F4 lattice.

Unfortunately, this method can not be directly used for finding next contributions and the origin of this fact is again the violation of the rotation symmetry but now on the F4 lattice. Moreover, there are no any more symmetrical lattice with fixed positions of sites in 4-dimensional [5]. It means that we need an absolutely different lattice concept that guarantees the restoration of the initial symmetries. Fortunately this concept is known now. This is the Random Lattice concept (RL) [8].

3. Random Lattice in action

The basic idea of the RL is the averaging over the big ensemble of various lattices with random distributions of sites and it is possible to show that such averaging leads to the restoration of the rotational invariance. There are two methods of the realization of such scheme. A first one based on the Christ, Friedberg and Lee (CFL) technique [8].

Commonly CFL technique leads into complicated geometrical analysis. For our task it would be very useful to use the analogy between Random Lattice and Random Surface technique that was revealed recently [11, 13]. The idea is quit simple: for beginning let us consider a lattice with fixed positions (for simplicity it is possible to use the trivial HC lattice, where basis vectors are just $\vec{\nu} = \vec{i}, \vec{j} \dots$) in a flat space. For a simulation of the Random Lattice let us consider small deformations of the geometry of this space ($\gamma_{ij} \rightarrow g_{ij}$) so that one can rewrite the problem of the random lattice averaging in the terms of the random deformations of the geometry of this space [11]. This is a standard quantum gravity problem for which powerful methods of the Matrix Theory could be used.

In our problem we discuss the link integrals that depend on the basis vectors ν . All such integrals are considered separately for any lattice site x_i . It means that rotation invariance violation artifacts could be avoided by considering only rotation deformations of these basis vectors (translation and re-scaling deformation are left aside in our case).

Let $R \in SO(4)$ be a rotation operator of 4 dimensional vectors ν

$$\nu'_i = R_{ij}\nu_j.$$

It is essential to note that our task can be reformulated in the language of the standard Hermitian averaging because $SO(4) = SU(2) \times SU(2)$. For infinitesimal rotations we obviously have

$$R_{ij} = \delta_{ij} + H_{ij}, \quad (6)$$

where H_{ij} is a traceless antisymmetric matrix.

Consider the Gaussian Ensemble \mathfrak{H} of such arbitrary rotation. The matrix average of an arbitrary function f with respect to Gaussian measure is

$$\langle f \rangle_{\mathfrak{H}} = \frac{1}{N_0} \int dH e^{-\text{tr}(H^2)/2} f(H).$$

where dH is the standard Haar measure. The normalization factor N_0 is fixed by requiring that $\langle f = 1 \rangle_{\mathfrak{H}} = 1$.

Using of the Matrix integration technique one can prove the so-called Matrix Wick's theorem for traceless antisymmetric matrices [14, 11, 12, 13]

$$\begin{aligned} \langle H_{ij}H_{kl} \rangle_{\mathfrak{H}} &= \delta_{ij}\delta_{kl} - \delta_{il}\delta_{jk}, \\ \langle \prod_{(i,j)} H_{ij} \rangle_{\mathfrak{H}} &= \sum_{\text{pairings}} (-1)^{\kappa} \prod_{\text{pairs}} \langle H_{ij}H_{kl} \rangle_{\mathfrak{H}}, \end{aligned} \quad (7)$$

where the sum extends over all possible pairings and κ is the number of crossings in the pairing. The matrix average of any odd combination of H_{ij} equals zero due to the parity argument.

It is not hard to prove that the main contribution into the averaging sum over such infinitesimal rotations comes from the original non-deformable lattice (connected with the δ_{ij} part in (6)). In order to cancel non-deformable lattice artifacts let us consider the ensemble \mathfrak{H} without this non-deformable contribution: $\mathfrak{H}' = \mathfrak{H} - \mathfrak{o}$. Using such averaging, for leading order of chiral effective lagrangian one gets

$$\langle \text{tr}(\alpha) \rangle_{\mathfrak{H}'} = \langle \text{tr}(a^2 \partial_\nu U \partial_\nu U^+) \rangle_{\mathfrak{H}'} = \text{tr}(3a^2 \partial_i U \partial_i U^+) = \text{tr}(3a^2 (L_i L_i)),$$

where $L_i = U^+ \partial_i U$, and for the NL correction one obtains

$$\begin{aligned} \langle \text{tr}(\alpha^2) \rangle_{\mathfrak{H}'} &= \langle \text{tr}(a^4 \partial_\nu U \partial_\nu U^+ \partial_\nu U \partial_\nu U^+) \rangle_{\mathfrak{H}'} = \text{tr}(3^2 a^4 ((L_i L_i)^2 - \frac{1}{2} [L_i, L_j]^2)) = . \\ &= -3^2 a^4 \left(\frac{1}{2} \text{tr}^2(L_i L_i) + \text{tr}^2(L_i L_j) - 4 \text{tr}(L_i L_i L_j L_j) \right) = \end{aligned} \quad (8)$$

These results reproduce the HL and BCHL results and it is easy to see that this is just what we expected to receive because this contribution was obtained from many other approaches [6]. In such a way, we can apply this procedure to corrections of any orders from (4) and obtain the rotation invariant result due to the pairing. It means that the question about the derivation of the chiral effective lagrangian from Lattice QCD become just a combinatorial task.

It is interesting to point out that our $SU(2)$ -flavor result for coefficients in the NL order contribution of the Chiral Perturbation Theory (8)

$$L_1^r = \frac{L_2^r}{2} = -\frac{L_3^r}{4}$$

is in agreement with experiment data from $\pi\pi \rightarrow \pi\pi$ scattering [6] and these coefficients turn out to be closed to the model prediction of the V exchange [15].

In the last part of this section we show an application of our procedure. We will find that an infinite subseries of the chiral perturbation can be summed up into the Born-Infeld form.

If the expression (7) allows us to calculate all terms in expansion (4), let us consider just the first column there. It is easy to show that either of these is proportional to some power of the leading order contribution (5)

$$\begin{aligned} \text{tr}[\alpha] &\sim \text{tr}[L_\mu L^\mu] + \dots \\ \text{tr}[\alpha^2] &\sim \text{tr}[(L_\mu L^\mu)^2] + \dots \\ \text{tr}[\alpha^3] &\sim \text{tr}[(L_\mu L^\mu)^3] + \dots \\ \dots &\dots \dots \dots \dots \dots \\ \text{tr}[\alpha^n] &\sim \text{tr}[(L_\mu L^\mu)^n] + \dots \\ \dots &\dots \dots \dots \dots \dots \end{aligned} \quad (9)$$

Substituting (9) into (3) and collecting all terms which depend on the power of the prototype lagrangian one obtains the following expression for the effective chiral lagrangian

$$\mathcal{L}_{\text{eff}} \sim -\text{tr} \left[1 - \sqrt{1 - 1/\beta^2 L_\mu L^\mu} \right] - \text{tr} \left[\log \left(1 - \frac{1}{2} (1 - \sqrt{1 - 1/\beta^2 L_\mu L^\mu}) \right) \right] + \dots, \quad (10)$$

where \dots are all other terms (in particular the Skyrme term) and β is an effective coupling constant that depends on the value of our stationary point u_0 .

Now let us discuss the result (10). It was obtained that some part of chiral effective action has a Born-Infeld form plus a first logarithmic correction to it. In [16], it was shown that such form of the effective action plays a very essential role in the problem of the chiral bag formation because just these square-root terms generate the step-like distribution solutions that can be interpreted as internal phases in the two-phase model of the low-energy baryon states. Another terms play essential role only on large distances from the confinement surface and can be considered as corrections.

4. Conclusions

The aim of this paper is to derive the chiral effective lagrangian from QCD on the lattice at the strong coupling limit. We find that this theory looks like a Born-Infeld theory for the prototype chiral lagrangian. Such form of the effective lagrangian is expected. From the methodological point of view our consideration is very similar to the low-energy theorem in string theory that leads to the Born-Infeld action [7]. Moreover, in [16], it was shown that Chiral Born-Infeld Theory (without logarithmic corrections) has very interesting “bag”-like solutions for chiral fields. It was an additional motivation of our work.

The Chiral Born-Infeld theory is a good candidate for the role of the effective chiral theory and a model for a chiral cloud of baryons. In this model one can find not only spherical “bags”, it is possible also to study the “string”-like, toroidal or “Y-Sign”-like solutions, or some other geometry. The geometry of the confinement surface depends directly on the model of color confinement and it would be very interesting to use, for example, the Lattice QCD simulations for the color degrees of freedom in combination with our model for the external chiral field.

This work is partially supported by the Russian Federation President’s Grant 1450-2003-2. The hospitality and financial support of the ECT* in Trento is gratefully acknowledged.

References

- [1] S. Myint and C. Rebbi, Nucl. Phys. B **421**, 241 (1994) [arXiv:hep-lat/9401009]; S. Myint and C. Rebbi, arXiv:hep-lat/9401010; A. R. Levi, V. Lubicz and C. Rebbi, Phys. Rev. D **56**, 1101 (1997) [arXiv:hep-lat/9607022]; A. R. Levi, V. Lubicz and C. Rebbi, Nucl. Phys. Proc. Suppl. **53**, 275 (1997) [arXiv:hep-lat/9607025].

- [2] E. Brezin and D. J. Gross, Phys. Lett. B **97** (1980) 120; R. C. Brower and M. Nauenberg, Nucl. Phys. B **180** (1981) 221.
- [3] H. Kluberg-Stern, A. Morel, O. Napoly and B. Petersson, Nucl. Phys. B **190** (1981) 504; N. Kawamoto and J. Smit, Nucl. Phys. B **192**, 100 (1981); J. Hoek, N. Kawamoto and J. Smit, Nucl. Phys. B **199**, 495 (1982); I. Ichinose, Phys. Lett. B **135** (1984) 148; I. Ichinose, Nucl. Phys. B **249** (1985) 715; I. Ichinose, Phys. Lett. B **147** (1984) 449; I. Ichinose, Mod. Phys. Lett. A **17** (2002) 1355 [arXiv:cond-mat/0107447].
- [4] T. H. Skyrme, Proc. Roy. Soc. Lond. A **260** (1961) 127; **230** (1955) 277.
- [5] W. Celmaster, Phys. Rev. D **26**, 2955 (1982); W. Celmaster, Phys. Rev. D **28**, 2076 (1983); W. Celmaster, Phys. Rev. Lett. **52**, 403 (1984); H. Neuberger, Phys. Lett. B **199**, 536 (1987); G. Bhanot, K. Bitar, U. M. Heller and H. Neuberger, Nucl. Phys. B **343**, 467 (1990).
- [6] J. Gasser and H. Leutwyler, Nucl. Phys. B **250**, 465 (1985).
- [7] A. A. Tseytlin, Nucl. Phys. B **501** (1997) 41; A. A. Tseytlin, Nucl. Phys. B **501** (1997) 41. L. Chekhov and K. Zarembo, Mod. Phys. Lett. A **12**, 2331 (1997) [arXiv:hep-th/9705014]; J. Ambjorn and L. Chekhov, JHEP **9812**, 007 (1998) [arXiv:hep-th/9805212].
- [8] N. H. Christ, R. Friedberg and T. D. Lee, Nucl. Phys. B **202**, 89 (1982); N. H. Christ, R. Friedberg and T. D. Lee, Nucl. Phys. B **210**, 310 (1982); N. H. Christ, R. Friedberg and T. D. Lee, Nucl. Phys. B **210**, 337 (1982).
- [9] D. J. Gross and E. Witten, Phys. Rev. D **21**, 446 (1980); R. C. Brower, M. Campostrini, K. Orginos, P. Rossi, C. I. Tan and E. Vicari, Phys. Rev. D **53**, 3230 (1996) [arXiv:hep-th/9508015]; M. Campostrini, P. Rossi, A. Pelissetto and E. Vicari, Nucl. Phys. Proc. Suppl. **53**, 690 (1997) [arXiv:hep-lat/9607066].
- [10] P. Rossi, M. Campostrini and E. Vicari, Phys. Rept. **302**, 143 (1998) [arXiv:hep-lat/9609003].
- [11] F. David, "Simplicial quantum gravity and random lattices," arXiv:hep-th/9303127.
- [12] P. Di Francesco, arXiv:math-ph/9911002; P. Di Francesco, arXiv:cond-mat/0211591.
- [13] L. Bogacz, Z. Burda, J. Jurkiewicz, A. Krzywicki, C. Petersen and B. Petersson, Acta Phys. Polon. B **32**, 4121 (2001) [arXiv:hep-lat/0110063].
- [14] M. Mulase and A. Waldron, Commun. Math. Phys. **240**, 553 (2003) [arXiv:math-ph/0206011].
- [15] A. Pich, Rept. Prog. Phys. **58**, 563 (1995) [arXiv:hep-ph/9502366].
- [16] O. V. Pavlovsky, arXiv:hep-ph/0312349; O. V. Pavlovsky, arXiv:hep-ph/0312343; O. V. Pavlovsky, Phys. Lett. B **538** (2002) 202 [arXiv:hep-ph/0204313].

THE NUCLEON-NUCLEON SCATTERING DESCRIPTION AT $E_{lab} = 0 - 6$ GeV, THE DEUTERON PROPERTIES AND DEUTERON PHOTODISINTEGRATION IN THE RELATIVISTIC QUASIPOTENTIAL OPTICAL MODEL, BASED ON THE MOSCOW POTENTIAL

N.A. Khokhlov^{1†}, V.A. Knyr^{1††} and V.G. Neudatchin^{2†††}

(1) *Khabarovsk State University of Technology, 680035 Khabarovsk, Russia*

(2) *D.V. Skobel'syn Institute of Nuclear Physics, Moscow State University, 119899 Moscow, Russia*

† *E-mail: khokhlov@fizika.khstu.ru* ; †† *E-mail: knyr@fizika.khstu.ru* ;

††† *E-mail: neudat@nucl-th.sinp.msu.ru*

Abstract

The phase shift analysis data of nucleon-nucleon scattering up to $E_{lab} = 3$ GeV, NN scattering polarization at $E_{lab} = 5.13$ GeV and deuteron properties are described by the optical relativistic model based on deep attractive forbidden state quasipotentials. Angular distribution of the deuteron photodisintegration cross-section is calculated using these quasipotentials in relativistic point form dynamics.

Keywords: nucleon-nucleon interaction, Moscow potential, relativistic model

1. Introduction

There are a lot of various models of the nucleon-nucleon interaction. Nevertheless, we can distinguish only two principally different kinds of models. The first one is represented by the meson exchange potential (MEP) model and it goes conceptually back to the idea by Yukawa. These potentials are characterized by a repulsive core representing the exchange of vector mesons. Indeed, some quark model potentials are pragmatically close to these meson exchange potentials, though they are presently considered as a phenomenology [1].

The second kind of NN potentials corresponds to the Moscow potential model (MP), which is now represented by a family of potentials [2, 3, 4, 5]. The major characteristics of this model potentials are their strongly attractive behavior at short range and necessity of forbidden states for S and P partial waves. Microscopically, the MP corresponds to an excited quark configuration such as $s^4 p^2 [42]_x [42]_{CS}$ or $s^4 p^2 [42]_x [42]_{ST}$ in the nucleon-nucleon overlap region. Namely, it was stressed that $6q$ -configuration $s^4 p^2 [42]_x [2^3]_C [42]_{CS}$ offers a way to an enhanced virtual decay $N(2S)N \rightarrow D_C(0S)D_{\bar{C}}$ accompanied by a very strong attraction between the colored dipoles D_C and $D_{\bar{C}}$, $|D_C \rangle = |s^2 p [21]_x L = 1, [21]_C C = 1, [3]_{ST} \rangle$ (the terms $(0S)$ and $(2S)$ symbolize the mutual motion wave functions) [6]. The first preliminary RGM treatment of this kind has been made recently [7].

Furthermore, $s^4 p^2 [42]_x [42]_{ST}$ configuration may be predominant if a strong nonperturbative instanton-induced interaction between quarks does exist [8].

The excited quark configurations should be seen directly in a series of high-energy nuclear reactions involving the investigation of the baryon-baryon (BB) composition of the deuteron, viz. a quasielastic knockout such as ${}^2H(e, e'p)B$ [9] with energies of final

protons around 2 GeV, the polarization transfer in $d+p$ exclusive and inclusive high-energy backward scattering [10], etc.

In the present work, extending the line of investigations [2, 11, 3, 4], we show that the nucleon-nucleon scattering data (differential cross sections and polarizations), extended in energy up to $E_{lab} = 6$ GeV (for one to be able to judge the short-range NN interaction), seem just to reflect the desired quark effect and convincingly demonstrate the dominant role of the excited quark configurations $s^n p^m$ ($n = 4, m = 2$ for S waves; $n = m = 3$ for P waves). This is reflected by the efficiency of forbidden state potentials and by the corresponding very peculiar behavior of the scattering phase shifts, which is exhibited precisely in a wide energy interval of 0 – 6 GeV.

We present our new results developing approach proposed in [2]. We improve our previous results [2], where the qualitative description of the nucleon-nucleon scattering was obtained up to 6 GeV. The new nucleon-nucleon phase shift analysis data up to 3 GeV [12] are considered using the relativistic quasipotential optical model. It is shown that these data, NN scattering polarization at $E_{lab} = 5.13$ GeV and deuteron properties are described perfectly by the deep attractive forbidden state potentials. Angular distribution of the deuteron photodisintegration cross-section is calculated using these quasipotentials in relativistic point form dynamics.

2. The optical nucleon-nucleon potential

We rely in our potential relativistic optical model on the relativistic quantum mechanics of systems with a fixed number of particles (point form dynamics). The review of this approach can be found in [13].

This approach is based on the assumption that at not high energies we may consider the number of particles fixed, but the invariance group is the Poincare group. A system of two particles is described by the wave function, which is an eigenfunction of the mass operator or the mass squared operator. In this case we may represent this wave function as a product of the external and internal wave functions [14, 15]. The internal wave function is also an eigenfunction of the mass operator or the mass squared operator. It is known [16] that the mass squared method is consistent with conventional fitting of the Lorentz invariant cross section as a function of laboratory energy. We consider system of two particles (nucleons) with equal masses. Then the internal wave function $\chi(\mathbf{q})$ satisfies the following equation

$$\left[4(m^2 + \mathbf{q}^2) + V\right] \chi = M^2 \chi \quad (1)$$

or

$$\left(\frac{\mathbf{q}^2}{m} + \frac{V}{4m}\right) \chi = E \chi, \quad (2)$$

where

$$E = \frac{M^2 - 4m^2}{4m} = \frac{\kappa^2}{m}.$$

The eq. (2) formally coincides with the Schrödinger equation. In eqs. (1), (2) M^2 is the mass squared operator, m is the mass of the nucleon, V is the nucleon-nucleon potential, \mathbf{q} is the momentum operator of one of the nucleons in the center of masses system. We use system $\hbar = c = 1$. The quasicordinate representation corresponds to the realization

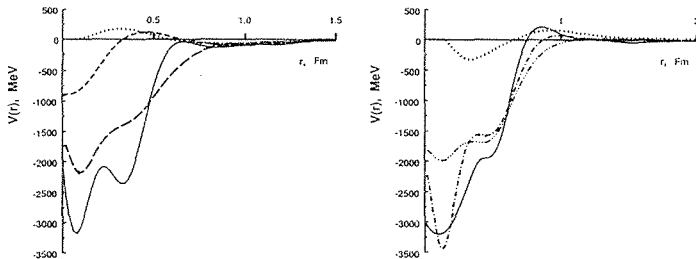


Figure 1: Quasipotentials. Left: solid line — 1S_0 potential; long dashed line — central 3S_1 potential; short dashed line — central 3D_1 potential; dotted line — tensor 3SD_1 potential. Right: solid line — 3P_0 potential; long dashed line — central 3P_2 potential; short dashed line — central 3P_2 potential; dotted line — tensor 3PP_2 potential. We extracted the tensor potential as a term multiplied by S_{12} operator only for the coupled-channels

$\mathbf{q} = -i\frac{\partial}{\partial r}$, $V = V(r)$. In [17] we showed that this formalism can be easily generalized to the case of inelastic channels, particularly it allows to take into account the isobar channels in NN scattering.

This formal coincidence allows us to apply our inversion algorithm, which is based on the Marchenko inversion and was presented in [18]. We applied this algorithm of inversion to reconstruction of the nucleon-nucleon MP. As input data for this reconstruction we used the modern phase shift analysis data up to 1200 MeV for isoscalar partial waves and up to 3 GeV for isovector partial waves of the nucleon-nucleon system [12]. The deuteron properties were taken from [19].

The real parts of the constructed partial potentials are presented in fig. 1. They may be downloaded from www.physics.khstu.ru in numerical form. Standard notation for central and tensor parts is used, so for 3S_1 — 3D_1

$$V_S(r) = V_1(r), \quad V_D(r) = V_2(r) + V_T(r)/2\sqrt{2}, \quad V_{tens}(r) = V_T(r)/\sqrt{2}$$

The imaginary parts of potentials are defined as in [18] and they can be easily calculated from the phase shift analysis data [12]. The phase shifts and mixing parameters are compared with the phase shift analysis data [12] in fig. 2. These and other our results can be downloaded from www.physics.khstu.ru. There the results of our deuteron properties calculations are presented and the higher partial wave potentials can be downloaded.

The constructed potential describes the phase shift analysis data up to 3 GeV and the deuteron properties. As an independent check of our MP model we calculated the pp and np scattering polarization $P(t)$ on the momentum-transfer value at the energy $E_{lab} = 5.13$ GeV. The results of this calculation are compared with the experiment data [20] in fig. 3. We calculated the angular distribution of the deuteron photodisintegration cross-section by means of the relativistic considerations (point form dynamics). This approach we have used successfully in our calculations of the hard bremsstrahlung accompanying the pp scattering [14]. The preliminary results of this calculation, which does not include some transition amplitudes, are presented in fig. 3.

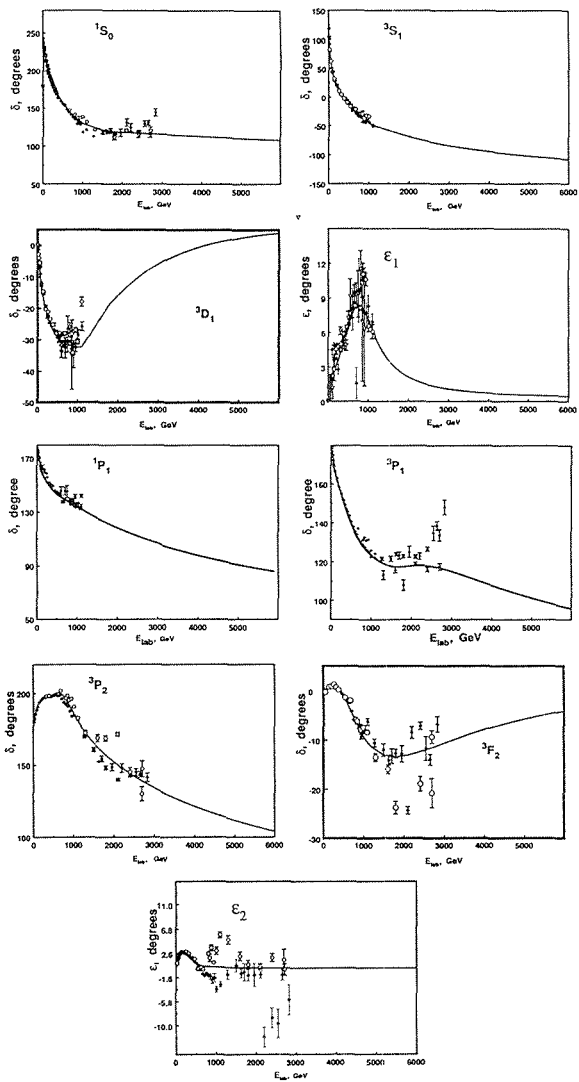


Figure 2: Phase shifts and mixing parameter

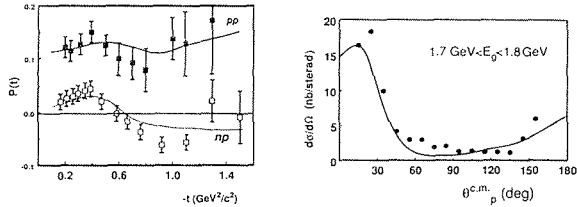


Figure 3: Left: Dependence of the pp and np scattering polarization $P(t)$ on the momentum transfer value at the energy $E_{lab} = 5.13$ GeV. Right: Angular distribution of the deuteron photodisintegration cross-section. Data are from [21]

3. Conclusion

From our results it follows that the all known NN scattering data and deuteron properties are described consistently by relativistic quasipotential optical model in point form dynamics with deep attractive forbidden state potential of the Moscow kind. We observe separation of the scattering phase shifts into two groups: the large S- and P-phase shifts which start from 2π or π at zero energy and the small shifts which include all the others. Our potential model is the first one that covers such a wide energy range. Unfortunately we cannot confirm the results of [5], that NN interaction may be described by a spin- and parity independent potential. This we believe is true only for low energies, but above approximately 500 MeV the dynamic structure of the underlying quark-quark interaction can be described only by more complex-dependent potential. The one of the reason for this is the dependence of the relativistic coordinate Wigner operator on the spin of a particle. The MP implies that close nucleons are relativistic so their interaction can be described by spin- and parity independent potential only approximately at low enough energies.

This model now may be used in various nuclear physics calculations. Object of our following research will be description of the reaction ${}^2H + \gamma \rightarrow n + p$ at moderately high energies of $E_\gamma \geq 2$ GeV [22] because unlike lower energies the meson exchange currents are strongly suppressed here (meson electroproduction data testify that e.g. the pion cut-off parameter Λ_π is 0.6 GeV [23, 24]). Hence, here the influence of the discussed radial short-range oscillations in S- and P-partial waves is expected to be seen (the pn final state interaction is important, as before). The applicability of our approach to this reaction is demonstrated by our preliminary results in fig. 3.

References

- [1] R. Machleidt, I. Slaus, J. Phys. G, V. 27, p. R69 (2001).
- [2] V.G. Neudatchin, N.P. Yudin, Yu.L. Dorodnykh, I.T. Obukhovskiy, Phys. Rev. **C43**, 2499 (1991).
- [3] V.I. Kukulin and V.N. Pomerantsev, Progr.Theor.Phys. **88**, 159 (1992)
- [4] S.B. Dubovichenko, Yad.Fiz. **60**, 499 (1997)
- [5] J.-M. Sparenberg, D. Baye, EUROPHYS. Lett., **59**(4), (2002).

- [6] V.G. Neudatchin and I.T. Obukhovskiy, in *Relativistic Nuclear Physics and QCD (Proc. XII Internat. Seminar, Dubna, 1994)* ed. by A.M. Baldin and V.V. Burov, JINR Pub. N E1,2-97-79 (JINR, Dubna 1997), vol.II, p.3
- [7] D. Bartz and Fl. Stancu, *Phys.Rev. C* **63**, 034001 (2001) and the private communication by Fl. Stancu
- [8] A.M. Kusainov, V.G. Neudatchin, I.T. Obukhovskiy, *Phys.Rev. C* **44**, 2343 (1991)
- [9] L.Ya. Glozman, V.G. Neudatchin, I.T. Obukhovskiy and A.A. Sakharuk, *Phys.Lett. B* **252**, 23 (1990); L.Ya. Glozman, V.G. Neudatchin and I.T. Obukhovskiy, *Phys.Rev. C* **48**,389 (1993); L.Ya. Glozman and A. Faessler, *Phys.Lett. B* **348**, 270 (1995)
- [10] M.P. Rekalov and I.M. Sitnik, *Phys.Lett. B* **356**, 434 (1995); B. Kuehn, Ch. Perdrisat and E.A. Strokovskiy, *Yad.Fiz.* **58**, 1873 (1995); L.S. Azhgirey and N.P. Yudin, *Yad.Fiz.* **63**, 2280 (2000)
- [11] V.G. Neudatchin, I.T. Obukhovskiy and Yu.F. Smirnov, *Phys.Lett. B* **43**, 12 (1973); V.G. Neudatchin, I.T. Obukhovskiy, V.I. Kukulkin and N.F. Golovanova, *Phys.Rev. C* **11**, 128 (1975)
- [12] R.A. Arndt, I.I. Strakovskiy and R.L. Workman, *Phys. Rev.* **C62**, 034005 (2000); R.A. Arndt, J.S. Hyslop and L.D. Roper, *Phys. Rev.* **D35**,128 (1987); J Bystricky, C. Lechanoine-Leluc, F. Lehar, *Eur. Phys. J.* **C4**, 607 (1998); J. Ball, J. Bystricky, J.-M. Fontaine et al, *Nuovo Cimento* **A111**, 13 (1988).
- [13] B.D. Keister and Polyzou, *Adv. Nucl. Phys.* **21** , 225 (1991).
- [14] N.A. Khokhlov, V.A. Knyr, V.G. Neudachin, *Phys. Rev.* **C68**, 054002 (2003).
- [15] F.M. Lev , *nucl-th/9403222*.
- [16] T.W. Allen, G.L. Payne, Wayne N. Polyzou, *nucl-th/0005062*.
- [17] V.A. Knyr, N.A. Khokhlov, *Phys. of At. Nucl.*, **V. 67**, N5, 937 (2004).
- [18] N.A. Khokhlov, V.A. Knyr, *nucl-th/04110092*.
- [19] T. Ericson, W Weise, *Pion and nuclei*. Clarendon press. Oxford. (1988); R. Machleidt. *Adv. In Nucl. Phys.* **V. 19**, 189 (1989).
- [20] R. Diebold, D. S. Ayres, S. L. Kramer, A. J. Pawlicki, and A. B. Wicklund *Phys. Rev. Lett.* **35**, 632-635 (1975); P. R. Robrish *et al.*, *Phys. Lett. B* **31**, 617 (1970); M. Borghini et al., *ibid.* **B31**, 405 (1970).
- [21] M. Mirazita et al, *Phys. Rev.* **C70**, 014005 (2004).
- [22] J.E. Belz, *Phys.Rev.Lett.* **74**, 646 (1995); C. Bochna, *Phys.Rev.Lett.* **81**, 4576 (1998); L.L. Frankfurt, G.A. Miller, M.M. Sargsian and M.I. Strikman, *Phys.Rev.Lett.* **84**, 3045 (2000)
- [23] R.R. Loucks, V.R. Pandharipande and R. Shrivastava, *Phys.Rev. C* **49**, 342 (1994)
- [24] V.G. Neudatchin, N.P. Yudin and L.L. Sviridova, *Yad.Fiz.* **60**, 2020 (1997); *Yad.Fiz.* **64**, 1680 (2001)

PRODUCTION OF CUMULATIVE PROTONS IN DIS OF NUCLEI, THE ROLE OF FLUCTONS, LPM EFFECT AND ALL THAT

S.M. Eliseev

*Bogoliubov Laboratory of Theoretical Physics ,
Joint Institute for Nuclear Research, 141980 Dubna, Russia,
E-mail: selis@thsun1.jinr.ru*

Abstract

In this contribution a model for the quark-parton propagating from nuclear medium will be presented. Landau-Pomeranchuk-Migdal (LPM) effect was introduced. All calculations were performed by Monte Carlo method. The chance of the observing of Blokhintsev's fluctons from the generation of more energetic cumulative nucleons along with the implication of LPM effect for other physical problem will be discussed. Also, the new data from NOMAD detector will be presented.

1. Introduction

At present, the semi-inclusive hadron production in Deep Inelastic Scattering (SIDIS) of nuclear targets has become a focal point of investigations at the intersection of QCD and relativistic heavy ion physics. Its purpose is at least twofold: this reaction should help us to understand how a given QCD medium have effect on the non-perturbative hadronization mechanisms. In the second place, such a trial also can help to observe the attenuation effect or quenching of jets of partons and its formation time in nuclear medium. This is evidently a suggestive issue in the physics of high energy heavy ion collisions where the quark-gluon plasma is expected to be produced. In order to investigate the possible emergence of quark-gluon plasma, it is necessary to understand the properties of ordinary multiparticle productions mechanisms in more simple conditions than in the relativistic collisions of heavy ions.

In addition, the question of fundamental importance in QCD is the fragmentation and hadronization-mechanism which converts quark and gluon quanta into integrally-charged final state hadrons. Hadronization is a *large distance* process for which we only have models at present. According to the parton model, a high energy lepton interacts with a nucleon transferred a considerable amount of the momentum to one of the quarks of the nucleon. As a result, lepton-nucleon scattering allows us to investigate the hadronization of quark-diquark jets (or strings) in vacuum. For lepton-nucleus scattering these jets may interact with spectator nucleons. In other words lepton-nucleus scattering provides a nontrivial possibility to analyze space-time evolution of jets inside a nuclear matter. In contrast with hadroproduction, intranuclear cascading can be studied without complicate effects of projectile rescattering or interactions of projectile constituent. Another feature of the lepton-nucleus interaction is the fact that, due to the extraordinary small lepton-nucleon cross-section, the interaction can practically take place anywhere in the nucleus. As a consequence all the nucleons participate in the scattering. The last few years have

witnessed a great revival of interest in SIDIS (see, e.g., recent HERMES, NOMAD, and other studies [1-7]).

2. The model

We developed a cascade model of multiproduction of neutrino-nuclei interaction. The model describes a branching process of the evolution of parton's jet (up to hadronization) in the atomic nucleus. We assume that the interaction between incident an lepton and a target nucleus takes place in a lepton-nucleon interaction. The nucleus is excited by a series of collisions between secondaries (produced in the first lepton-nucleon interaction) and the intranuclear nucleons. This process continues until all secondaries escape target nucleus. A part of the energy is spread through the nucleus to produce a fully-equilibrated nucleus which then decays statistically. The process of generation of particles is simulated by the Monte Carlo (MC) method. The characteristics of the partons from neutrino-nucleon interaction and of the produced particles with nucleons in nucleus are taken from experiments with free nucleons. (The parton spectra is assumed to be the same as hadronic one. That approach is based on the concept of "Local Parton Hadron Duality".)

The space-time characteristics of lepton-nucleon interactions inside the target nucleus were taken into consideration. The space-time characteristics of lepton-nucleon interactions inside the target nucleus were taken into consideration. The cross section for the next collision of a secondary particle with a nucleon inside the nucleus is given by

$$\sigma_{hN} = \sigma_{hN}^{exp}(1 - e^{-\tau/\tau_0}), \quad (1)$$

where τ is the time from the moment of production of this particle in the previous collision and σ_{hN}^{exp} is the experimentally determined total interaction cross section of a hadron with a nucleon in nucleus at the energy of the secondary particle produced. Thus, only after a time τ does the cross section of intranuclear interaction reach the value σ_{hN}^{exp} -hadronic LPM effect [8-12]. The parameter τ_0 is a certain characteristic corresponding to the formation time of the secondary generated hadron.

During the evolution to physical hadrons the produced particle will dissipate with reduced cross sections. For a collision inside nuclear medium this means that during their formation time the produced hadrons travel with a lower scattering probability. Therefore, the formation time plays an suggestive role in the dynamics of nuclear multiproduction: relativistic heavy ion collisions, hadron induced reactions etc. From the analysis of SIDIS, the formation length parameter L_f (in the system of a moving parton) was found to be $\approx 0.5 fm$ [6]. So, at a finite value of L_f , secondary particles-pions-are formed in nucleus not instantly but after a time. For the probability of Blokhintsev's fluctons in a nucleus we adopt original expression

$$\beta_k^A \sim \binom{A}{k} \left(\frac{V_\xi}{V_0} \right)^{k-1} A^{1-k} \quad (2)$$

obtained in the framework of simple idea of nucleons clustering in nuclei (see, e.g., [6] and references therein).

Here $V_\xi \sim \frac{4}{3}\pi r_\xi^3$, $V_0 \sim \frac{4}{3}\pi r_0^3$ and parameters $r_\xi = 0.75 fm$, $r_0 = 1.2 fm$.

3. Results

Figure demonstrates the spectrum of protons emitted backwards, with respect to the beam direction, which have energies not allowed by the kinematics of collisions on a free and stationary nucleon. The dashed curve (with *big slope*) manifests the of proton with $P^2 \leq 0.2(\text{GeV}/c)^2$. The mechanism of such slow proton production is a process of the evaporation of the residual nuclei excited in the stage of the propagation of jets in the nuclei. It is worth to remark that in our approach the evolution of quark-gluon jets in nuclei in the framework of our model is accompanied by a nucleon emission at backward angles and momentum ≥ 300 MeV/c (cumulative nucleons).

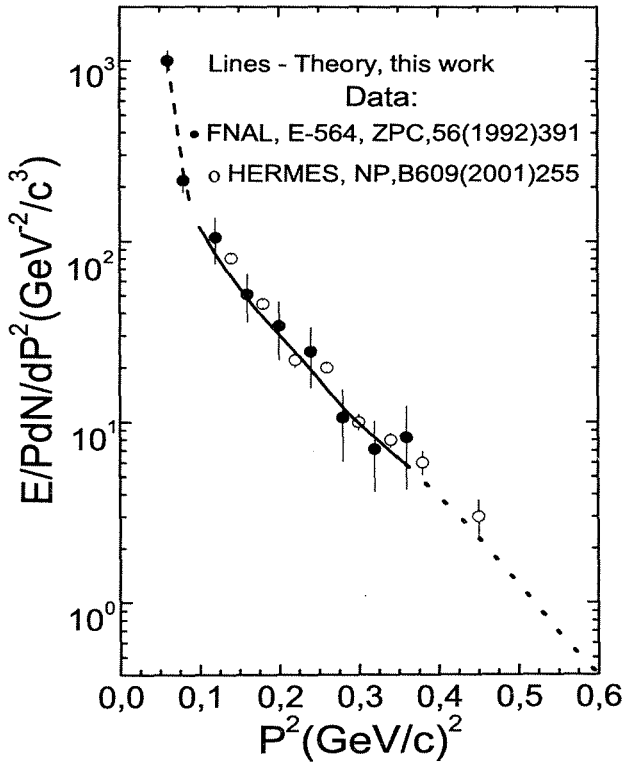


Figure 1: Backward protons momentum distribution

The spectrum of such protons is depicted by the right part of the dash curve on Figure (with smaller slope than the left one). In our model the underlying mechanism responsible for energetic protons production was the ordinary *quasideuteron* intranuclear absorption process. Such Cumulative Protons(CP) were observed in deep inelastic charged-current neutrino-emulsion interactions [12-18]. The experimental multiplicity of CP 0.33 ± 0.07

are in good agreement with the calculated one equal to 0.29 [6]. The effect of intranuclear absorption of particles (pions) by intranuclear ‘deuterons’ is well known in the theory of nuclear reactions at intermediate energy. This process is essential only for the slow pions (of energy $\leq 1\text{GeV}$). At high energy beams this effect makes all only some percents. As a result, the *existing* experimental data on CP from SIDIS of neutrino on nuclei can be interpreted, see solid line on Figure.

Further more, we insert the four nucleons fluctuations in our model, through formula (2) to explore the chance to catch more energetic nucleons (that it is observed in the recent experiment [2,3]). In such a way, we predicted the production of more energetic nucleons (see dot line on Figure). This forecast can be tested in the new class of experiment with much more statistics. In addition, our estimation of zone formation is in agreement with the other finding for different particle–nucleus reactions (see [19] and references therein). In conclusion, effect of the formation of particle is essential in many high energy phenomenon, e.g., in the study of signatures for QGP formation: “jet quenching”, the structure of anomalous J/ψ suppression in nuclear collisions, etc [20,21].

References

- [1] F. Arleo *et al.*, Phys. Rev. C **61**, 054906-1 (2000).
- [2] NOMAD, P. Astier *et al.*, Nucl. Phys. **B609**, 255, (2001).
- [3] HERMES, A. Airapetian *et al.*, Eur. Phys. J. **C20**, 479, (2001).
- [4] O. Benhar, S. Fantoni, G.I. Lykasov, U. Sukhatme, V.V. Uzhinsky, Eur.Phys.J. **A19**, 147, (2004).
- [5] O. Benhar, S. Fantoni, G.I. Lykasov, U. Sukhatme, Phys.Lett. **B527**, 73, (2002).
- [6] S.M. Eliseev, Eur.Phys.J. **A18**, 147, (2003).
- [7] Alberto Accardi, Valeria Muccifora, Hans-Juergen Pirner, Nucl.Phys. **A720**, 131, (2003).
- [8] L.D. Landau *et al.*, Dok. Akad. Nauk SSSR **92**, 535 (1953).
- [9] E.L. Feinberg, in *Problems of theoretical physics, Moscow: Science, 1972, pp. 248.*
- [10] N.N. Nikolaev, Usp. Fiz. Nauk **134**, 369 (1980).
- [11] S.M. Eliseev *et al.*, Sov. J. Nucl. Phys. **40**, 601 (1984).
- [12] A. El-Naghy *et al.*, J. Phys. G: Nucl. Part. Phys. **16**, 39 (1990).
- [13] M. Derrick *et al.*, Phys. Rev. D **24**, 1071 (1981).
- [14] H. Deden *et al.*, Nucl.Phys. **B198**, 365 (1982).
- [15] S. Barlag *et al.*, Z. Phys. C **11**, 283 (1982).
- [16] D. Baranov *et al.*, Z.Phys. C **21**, 189 (1984).

- [17] N. Baker *et al.*, Phys.Rev. D **34**, 1251 (1986).
- [18] R. Ammar *et al.*, ZhETF Let. **49**, 189 (1989).
- [19] T. Falter, W. Cassing, K. Gallmeister, U. Mosel, Phys.Lett. B**594**, 61, (2004).
- [20] Jörg Hüfner, Pengfei Zhuang, in Proc. of XIIth International Conference on Selected Problems of Modern Physics *Dedicated to the 95th anniversary of the birth of D.I. Blokhintsev (1908-1979), Dubna, June 8 - 11, 2003*, D1,2-2003-219, p.282.
- [21] Xin-Nian Wang Nucl.Phys. A**715**, 775, (2003).

ON ELECTRODYNAMICS OF CONSTITUENT QUARKS AND QCD POTENTIAL

Ivanhoe B. Pestov [†]

Bogoliubov Laboratory of Theoretical Physics, Joint Institute for Nuclear Research, 141980

Dubna, Moscow Region, Russia

[†] *E-mail: pestov@thsun1.jinr.ru*

Abstract

It is supposed that constituent quarks are confined objects. We derive Dirac and Maxwell equations for these quasiparticles from the condition that translation invariance is broken. It is found that the modified electrostatic potential has exactly a form of the well-known strong (QCD) potential. Thus, it is shown that confinement may cause modification of physical laws and the QCD potential can be considered as a new evidence of constituent quarks inside the proton.

1. Introduction

The discovery of hadron mass spectra has led to the introduction of fruitful concept of quarks [1] which are currently referred to as constituent quarks. A rigorous derivation of the constituent quarks from QCD is lacking, but constituent quarks are commonly believed to be quasiparticles emerging from the dressing valence quarks with gluons and quark-antiquark pairs. The idea to use constituent quarks as an intermediate step between the current quarks (i.e. fundamental degrees of freedom of the QCD Lagrangian) and hadrons was put forward and developed in [2]. In this model any hadron contains a finite number of constituent quarks. Here we formulate electrodynamics of the constituent quarks under conjecture that they are confined inside hadron and hence the translation invariance is broken. On this ground we derive Dirac and Maxwell equations for constituent quarks combining physical, geometrical, and group theoretical methods. We found that the modified electrostatic potential actually coincides with the well-known strong (QCD) potential. Because there is direct evidence supporting the strong potential [3], one can conclude that experiments at the CERN $p\bar{p}$ collider can be interpreted in the framework of the model in question as evidence of constituent quarks inside the proton.

To break translation invariance, we use the Kaluza-Klein idea about additional dimension of space and introduce the five-dimensional Minkowski spacetime $M_{1,4}^5$ with Cartesian coordinates x^i ($i = 0, 1, 2, 3, 4$) and metrics

$$ds^2 = \eta_{ij} dx^i dx^j = (dx^0)^2 - (dx^1)^2 - (dx^2)^2 - (dx^3)^2 - (dx^4)^2,$$

where as usually $x^0 = ct$, $x^1 = x$, $x^2 = y$, $x^3 = z$, $x^4 = u$. Note that the four-dimensional Minkowski spacetime $M_{1,3}^4$ may be considered as a plane $x^4 = 0$ in $M_{1,4}^5$. The translation invariance is broken by the relativistic invariant constraint

$$\eta_{ij} x^i x^j = (x^0)^2 - (x^1)^2 - (x^2)^2 - (x^3)^2 - (x^4)^2 = -a^2, \quad (1)$$

where a is the constant of the model which can be considered as some characteristic length connected with confinement and constituent quarks. Thus, the spacetime manifold for constituent quarks is outlined. The paper is organized as follows. The Dirac equation for the wave function of the constituent quark is derived and eigenvalues of the Dirac Hamiltonian are found in Sec.2. The Maxwell equations are formulated and Coulomb law is established in Sec.3. Our conclusions are summarized in Sec.4.

2. The Dirac equation of constituent quark

We will use the scalar product $(X, Y) = \eta_{ij}U^iV^j$ for any vector fields $X = U^i\partial_i$ and $Y = V^i\partial_i$ in the five-dimensional Minkowski spacetime. The vector fields

$$P_i = \delta_i^k \partial_k, \quad M_{ij} = (x_i \delta_j^k - x_j \delta_i^k) \partial_k,$$

where $x_i = \eta_{ij}x^j$, are generators of the Poincare group of the five-dimensional Minkowski spacetime. All vector fields M_{ij} are orthogonal to the radius-vector $R = x^k \partial_k$, but this is not the case for the vector fields P_i (translations). Representing P_i as the sum of the component aligned with the direction of the radius vector R and the component orthogonal to this direction, we obtain the vector fields

$$M_i = aP_i + \frac{1}{a}(R, P_i)R = (a\delta_i^k + \frac{1}{a}x_i x^k) \partial_k,$$

which are tangent to surface (1), because from (1) it follows that $(R, M_i) = 0$ at each point. The vector fields M_i and M_{ij} are generators of the group of spacetime symmetry of the model because we have

$$[M_i, M_j] = -M_{ij}, \quad [M_i, M_{jk}] = \eta_{ij}M_k - \eta_{ik}M_j \quad (2)$$

and constraint (1) is invariant with respect to the action of these operators. Let us now introduce the operators (vector fields)

$$X_0 = M_0, \quad X_1 = M_{14} + M_{23}, \quad X_2 = M_{24} + M_{31}, \quad X_3 = M_{34} + M_{12}. \quad (3)$$

It is straightforward to see that the vector fields X_0 , X_1 , X_2 , and X_3 are continuous and do not vanish at any point of the spacetime manifold. Because $(X_a, X_b) = 0$ for $a \neq b$, $a, b = 0, 1, 2, 3$ and

$$(X_0, X_0) = -(X_1, X_1) = -(X_2, X_2) = -(X_3, X_3) = a^2 + x_0^2,$$

the vector fields X_0 , X_1 , X_2 , and X_3 are linearly independent at each point of the spacetime manifold. Thus, it is shown that the spacetime background of the model has a spinor structure. It should be noted that this is the feature of constraint (1) only and hence the spacetime sector of the model actually is unique.

From (2), it follows that

$$[X_0, X_\mu] = 0, \quad [X_\mu, X_\nu] = 2e_{\mu\nu\lambda}X_\lambda, \quad \mu, \nu, \lambda = 1, 2, 3,$$

where $e_{\mu\nu\lambda}$ is the completely antisymmetric Levi-Civita symbol specified by the equality $e_{123} = 1$. In this way, we have proven that the our model admits a simply transitive group

of transformations whose generators are given by (3) and which has only the following nonzero structure constants:

$$f_{23}^1 = f_{31}^2 = f_{12}^3 = 2. \quad (4)$$

In our case, this group plays the role of the group of translation in familiar Minkowski spacetime.

In accordance with the original Dirac equation and consideration given above, we write the Dirac equation for the constituent quarks in the following form:

$$\gamma^c P_c \psi = \mu \psi, \quad (5)$$

where

$$\gamma^a \gamma^b + \gamma^b \gamma^a = 2\eta^{ab}, \quad P_c = X_c + \frac{iqa}{\hbar c} A_c, \quad \eta^{ab} = (1, -1, -1, -1).$$

Here q is the charge of a particle, and A_c are the components of the vector potential of the electromagnetic field in the basis X_a . In equation (5)

$$\mu = mca/\hbar,$$

since operators (3) are dimensionless.

In general, $[X_a, X_b] = f_{ab}^c X_c$ and hence

$$[P_a, P_b] = f_{ab}^c P_c + \frac{iqa}{\hbar c} F_{ab},$$

where

$$F_{ab} = X_a A_b - X_b A_a - f_{ab}^c A_c \quad (6)$$

are the components of the strength tensor of the electromagnetic field in the basis X_a , whereas f_{bc}^a are given by (4).

To have a more concrete representation about quantum mechanics of constituent quarks, it is important to derive eigenvalues E of the Dirac Hamiltonian of the free particle. Squaring equation (5) and using (4), we obtain the following equation for E :

$$E^2 \psi = m^2 c^4 \psi - \frac{c^2 \hbar^2}{a^2} (\Delta + P) \psi,$$

where $P = \Sigma_1 \nabla_1 + \Sigma_2 \nabla_2 + \Sigma_3 \nabla_3$ and $\Sigma_\mu = \frac{1}{2} \epsilon_{\mu\nu\lambda} \gamma^\nu \gamma^\lambda$. Since $\Delta + P = -P(P+1)$, where Δ is the Laplacian on a three-dimensional sphere, then

$$E^2 = m^2 c^4 + p(p+1) \frac{c^2 \hbar^2}{a^2},$$

where p is an eigenvalues of the operator P . It can be shown that $p = \pm 3, \pm 4, \dots$. For the energy, we then have

$$E^2 = m^2 c^4 + n(n+1) \frac{c^2 \hbar^2}{a^2} = m^2 c^4 (1 + n(n+1) \frac{\lambda^2}{a^2}), \quad (7)$$

where $n = 2, 3, \dots$ and $\lambda = \hbar/mc$. Formula (7) gives the quantum-mechanical value of the energy of the free constituent quark. Consider it in more detail. At large a , the moment of inertia $I = ma^2$ is also large, so that the angular velocity is small. Therefore,

the nonrelativistic limit can be found from the condition $a \gg \lambda$. In this limit it follows from (7) that $E = mc^2 + L^2/2I$, where $L^2 = n(n+1)\hbar^2$ and $I = ma^2$. The last relation corresponds to the formula $E = mc^2 + P^2/2m$ for the kinetic energy of the free particles in the limit $v \gg c$. We can also see that in the model, separation of the energy of a particle into the internal and kinetic parts has no strict meaning as it is evident from relation (7), $E \rightarrow mc^2$ only when $a \rightarrow \infty$ or $I \rightarrow \infty$.

3. On the Coulomb law for the constituent quarks

When the wave equation is established it is not difficult to derive the equations of electromagnetic field and then to find electrostatic potential as a solution of the Maxwell equations.

The Jacobi identity $[P_a[P_b, P_c]] + [P_b[P_c, P_a]] + [P_c[P_a, P_b]] = 0$ results in the first four Maxwell equations

$$X_a \bar{F}^{ab} + \frac{1}{2} f_{ad}^b \bar{F}^{ad} = 0. \quad (8)$$

where f_{bc}^a take the values (4) and $\bar{F}^{ab} = \frac{1}{2} e^{abcd} F_{cd}$, where e^{abcd} are components of the anti-symmetric Levi-Civita unit tensor in the basis X_a . In view of the known dual symmetry of the Maxwell equations, from (8) it follows that the remaining Maxwell equations are of the form

$$X_a F^{ab} + \frac{1}{2} f_{ad}^b F^{ad} = \frac{4\pi a}{c} j^b, \quad (9)$$

where j^b are components of the current vector in the basis X_a .

Now we write the Maxwell equations for the constituent quarks in the three-dimensional vector form. Before doing so it is useful to introduce an intrinsic coordinate system in the spacetime manifold of the model in question, which is defined by the vector field X_0 . In accordance with the definition of X_0 , we have the following system of ordinary differential equations for integral curvatures of this vector field:

$$\frac{dx^0}{cd\tau} = 1 + (x^0)^2/a^2, \quad \frac{dx^m}{cd\tau} = x^0 x^m / a^2, \quad m = 1, 2, 3, 4.$$

Under the condition $x^0(0) = 0$, we have the solution in the following form:

$$x^0 = a \tan \frac{c\tau}{a}, \quad x^m = \frac{au^m}{\cos(c\tau/a)},$$

where u^m , $m = 1, 2, 3, 4$ are constants of integration. It is easy to see that the intrinsic time variable τ and parameters u^m define the intrinsic coordinate system of the model. In this coordinate system we have for the operator X_0

$$X_0 = \frac{a}{c} \frac{\partial}{\partial \tau}.$$

To write the Maxwell equations for \vec{E} and \vec{H} , we put as usual

$$j^a = (c\rho, \vec{j}), \quad A_a = (\varphi, -\vec{A}),$$

$$E_\mu = F_{0\mu}, \quad H_\mu = \frac{1}{2}e_{\mu\nu\lambda}F^{\nu\lambda}, \quad \mu, \nu, \lambda = 1, 2, 3.$$

Then from (6) we obtain

$$\vec{E} = -\frac{a}{c} \frac{\partial}{\partial \tau} \vec{A} - \nabla \varphi, \quad \vec{H} = \text{rot} \vec{A} = \nabla \times \vec{A} - 2\vec{A}, \quad (10)$$

where $\nabla = (\nabla_1, \nabla_2, \nabla_3)$, $\nabla_\mu = X_\mu$, $\mu = 1, 2, 3$.

Considering that $\text{div} \vec{A} = \sum_{\mu=1}^3 \nabla_\mu A_\mu$, we can recast the Maxwell equations (8) and (9) into the familiar vector form

$$-\frac{a}{c} \frac{\partial}{\partial \tau} \vec{H} = \text{rot} \vec{E}, \quad \text{div} \vec{H} = 0, \quad \text{rot} \vec{H} = \frac{a}{c} \frac{\partial}{\partial \tau} \vec{E} + \frac{4\pi a}{c} \vec{j}, \quad \text{div} \vec{E} = 4\pi a \rho. \quad (11)$$

Let us now consider the Coulomb law for the particles in question. The electrostatic potential can be derived as a solution of the equations of electrostatics, which is invariant under the group of Euclidean motions, including rotations and translations. In the case being considered, we seek a Coulomb potential in an analogous manner. From (10) and (11), it follows that for an electrostatic field $\text{div} \vec{E} = 4\pi a \rho$, $\vec{E} = -\nabla \varphi$, and consequently, φ obeys the Poisson equation

$$\Delta \varphi = -4\pi a^2 \rho. \quad (12)$$

As it is well known, the electron Coulomb potential

$$\phi_e(r) = \frac{e}{r}$$

is the fundamental solution to the Laplace equation $\Delta \phi = \text{div grad} \phi = 0$. In the framework of our consideration the Coulomb potential for the charge particle can be derived as follows. Consider the stereographic projection S^3 from point $(0,0,0,-a)$ onto the ball $r^2 = x^2 + y^2 + z^2 \leq a^2$:

$$x^1 = fx, \quad x^2 = fy, \quad x^3 = fz, \quad x^4 = a(1-f),$$

where $f = 2a^2/(a^2 + r^2)$. Then, it follows that the element of length on the three-dimensional sphere can be represented in the form

$$ds^2 = f^2(dx^2 + dy^2 + dz^2)$$

and hence the Laplace equation on S^3 can be written as follows:

$$\Delta \phi = f^{-3} \text{div}(f \text{grad} \phi) = 0.$$

We seek the solution to this equation that is invariant under the transformation of the group $SO(3)$. This subgroup of the $SO(4)$ group is determined by fixing the point $(0,0,0,-a)$. Let us put

$$\psi = f \frac{1}{r} \frac{d\phi}{dr}.$$

Since

$$\Delta \phi = f^{-3} \left(r \frac{d\psi}{dr} + 3\psi \right) = r^{-2} f^{-3} \frac{d}{dr} (r^3 \psi),$$

then $r^3\psi = c_1 = \text{constant}$. Thus, we have

$$\frac{d\phi}{dr} = c_1 \frac{a^2 + r^2}{2a^2r^2} = c_1 \left(\frac{1}{2r^2} + \frac{1}{2a^2} \right)$$

and hence

$$\phi_q = c_1 \left(-\frac{1}{2r} + \frac{r}{2a^2} \right) + c_2. \quad (13)$$

Now we have the electrostatic potentials ϕ_e outside the ball $r^2 = x^2 + y^2 + z^2 \leq a^2$ and electrostatic potential (13) inside the ball. We should demand that the electrostatic potential is a continuous function and hence put $\phi_e(a) = \phi_q(a)$, so that $c_2 = e/a$ and the Coulomb potential for constituent quarks can be represented as follows:

$$\phi_q(r) = q \left(\frac{1}{2r} - \frac{r}{2a^2} \right) + \frac{e}{a}, \quad (14)$$

where q is the charge of particle.

It should be noted that our expression (14) coincides with the so called strong potential [3]

$$V_s = -\frac{4}{3} \frac{\alpha_s}{r} + kr$$

(which is in agreement with experiment) and hence exhibits clearly its electrodynamic nature. We also see that the boundary condition $\phi_e(a) = \phi_q(a)$ does not fix the charge q of constituent quark (leaving it as a free parameter) and hence our model does not contradict the standard QCD nomenclature.

For possible applications it is useful to put together the Hamiltonian for the electron and for the constituent quark. The electron Hamiltonian has as usual the following form:

$$\mathbf{H}_e = c(\alpha, \mathbf{P}_e) + \rho_3 m_e c^2,$$

where $\mathbf{P}_e = i\hbar\nabla$. For the constituent quark we have

$$\mathbf{H}_q = c(\alpha, \mathbf{P}_q) + \rho_3 m_q c^2,$$

where

$$\mathbf{P}_q = \frac{i\hbar}{a} (\mathbf{r} \times \nabla + \frac{a^2 - r^2}{2a} \nabla + \frac{\mathbf{r}}{a} (\mathbf{r}, \nabla)).$$

Here,

$$\mathbf{P}_q = \frac{i\hbar}{a} \mathbf{X}, \quad \mathbf{X} = (X_1, X_2, X_3)$$

and X_1, X_2, X_3 are expressed through the stereographic coordinates.

4. Conclusion

If the model of quarks is consistent with QCD, then we need to recognize that constituent quarks exist inside hadron, which is especially emphasized in the two-stage model of hadron structure [3]. In these frameworks the electrodynamics of constituent quarks can be formulated both naturally and uniquely. Then it can be shown that the modified Coulomb potential coincides with the QCD potential. Hence the so-called strong potential

has an electrodynamic nature and it is not reason for confinement but it is a consequence. The reason for confinement may be connected with the derivation from QCD Lagrangian of interactions that are expressed in a geometrical form by the constraint (1). Here the method of background field in a gauge theory may be very important [4] (monopole solution as background). Since it is shown that confinement leads to the modification of the physical laws in the region of confinement, a new possibility opens in the problem of confinement.

References

- [1] M. Gell-Mann, Phys. Lett. **8**, 214 (1964); G.Zweig, CERN Report No. TH401, 1964.
- [2] R.Petronzio, S.Simula and G.Ricco, Phys. Rev. D **67**, 094004 (2003); N. Cabibbo and R. Petronzio, Nucl.Phys. B **137**, 395 (1978).
- [3] D.H. Perkins, Introduction to High Energy Physics, Cambridge University Press,(2000).
- [4] B.S.De Witt, Phys.Rev. **162**, 1195 (1967).

INSTANTONS AND STRUCTURE OF PENTAQUARK

Hee-Jung Lee[†]

*Departament de Física Teòrica and Institut de Física Corpuscular,
Universitat de València-CSIC, E-46100 Burjassot (Valencia), Spain*

† E-mail: Heejung.Lee@uv.es

Abstract

We are discussing the influence of the complex structure of the QCD vacuum on the properties of the exotic multiquark states, specially the possibility for the existence of a deeply bound pentaquark. We show that the specific spin-flavor properties of the instanton induced interaction between the quarks leads to the existence of light tri- and di-quark clusters inside the pentaquark. This strong quark correlations might be behind the anomalous properties of the pentaquark.

1. Introduction

The status of the exotic Θ^+ baryon still very controversial both in theory and experiment (see reviews [1] and [2]). The instantons, strong fluctuations of gluon fields in the vacuum, play a crucial role in the realization of spontaneous chiral symmetry breaking in Quantum Chromodynamics and in the effective description of the spectroscopy for conventional hadrons. The instantons induce the 't Hooft interaction between the quarks which has strong flavor and spin dependence, a behavior which explains many features observed in the hadron spectrum and in hadronic reactions (see reviews [3, 4, 5] and references therein).

In a recent papers [6], we have suggested a triquark-diquark model for the pentaquark based on instanton induced interaction. This interaction produces a strong attraction in flavor antisymmetric states. As a result of this dynamics quasi-bound light ud and $ud\bar{s}$ -states can be formed. Furthermore the instanton induced interaction governs the dynamics between quarks at intermediate distances, i.e. $r \approx \rho_c \approx 0.3$ fm, where ρ_c is the average instanton size in the QCD vacuum. This scale is much smaller than the confinement size $R \approx 1$ fm and therefore it favors that the clusters inside the large confinement region exist.

2. Pentaquark structure in a constituent quark model with an instanton induced interaction

The most important instanton induced interaction in quark systems is the multi-quark 't Hooft interaction, which arises from the quark zero modes in the instanton field (see Fig. 1).

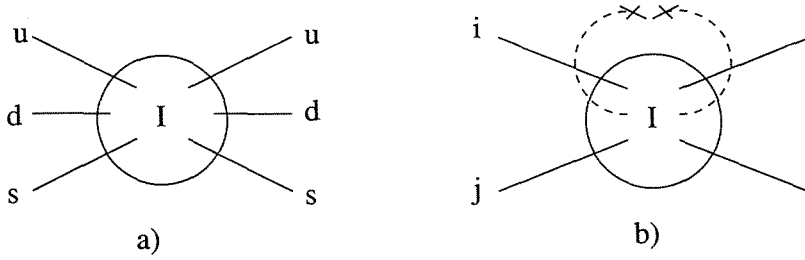


Figure 1: The instanton induced a) three-quark uds interaction and b) two-quark ud , us , ds interactions. In the figure I denotes the instanton, $i, j = u, d, s, i \neq j$

For $N_f = 3$ (Fig. 1a) and $N_c = 3$ this interaction is given by [7]:

$$\begin{aligned}
 \mathcal{L}_{eff}^{(3)} = & \int d\rho n(\rho) \left\{ \prod_{i=u,d,s} \left(m_i^{cur} \rho - \frac{4\pi}{3} \rho^3 \bar{q}_{iR} q_{iL} \right) \right. \\
 & + \frac{3}{32} \left(\frac{4}{3} \pi^2 \rho^3 \right)^2 \left[\left(j_u^a j_d^a - \frac{3}{4} j_{u\mu\nu}^a j_{d\mu\nu}^a \right) \left(m_s^{cur} \rho - \frac{4}{3} \pi^2 \rho^3 \bar{q}_{sR} q_{sL} \right) \right. \\
 & + \frac{9}{40} \left(\frac{4}{3} \pi^2 \rho^3 \right)^2 d^{abc} j_{u\mu\nu}^a j_{d\mu\nu}^b j_s^c + \text{perm.} \left. \right] + \frac{9}{320} \left(\frac{4}{3} \pi^2 \rho^3 \right)^3 d^{abc} j_u^a j_d^b j_s^c \\
 & \left. + \frac{if^{abc}}{256} \left(\frac{4}{3} \pi^2 \rho^3 \right)^3 j_{u\mu\nu}^a j_{d\nu\lambda}^b j_{s\lambda\mu}^c + (R \longleftrightarrow L) \right\}, \quad (1)
 \end{aligned}$$

where, m_i^{cur} is the quark current mass, $q_{R,L} = (1 \pm \gamma_5)q(x)/2$, $j_i^a = \bar{q}_{iR} \lambda^a q_{iL}$, $j_{i\mu\nu}^a = \bar{q}_{iR} \sigma_{\mu\nu} \lambda^a q_{iL}$, ρ is the instanton size and $n(\rho)$ is the density of instantons.

One can obtain an effective two-quark interaction induced by instantons from the three-quark interaction (1) by connecting two quark legs through the quark condensate (Fig. 1b). In the limit of small instanton size one obtains simpler formulas for effective two- and three-body point-like interactions [8, 9, 10]:

$$\begin{aligned}
 \mathcal{H}_{eff}^{(2)}(r) = & -V_2 \sum_{i \neq j} \frac{1}{m_i m_j} \bar{q}_{iR}(r) q_{iL}(r) \bar{q}_{jR}(r) q_{jL}(r) \left[1 + \frac{3}{32} (\lambda_u^a \lambda_d^a + \text{perm.}) \right. \\
 & \left. + \frac{9}{32} (\vec{\sigma}_u \cdot \vec{\sigma}_d \lambda_u^a \lambda_d^a + \text{perm.}) \right] + (R \longleftrightarrow L), \quad (2)
 \end{aligned}$$

and

$$\begin{aligned}
 \mathcal{H}_{eff}^{(3)}(r) = & -V_3 \prod_{i=u,d,s} \bar{q}_{iR}(r) q_{iL}(r) \left[1 + \frac{3}{32} (\lambda_u^a \lambda_d^a + \text{perm.}) \right. \\
 & + \frac{9}{32} (\vec{\sigma}_u \cdot \vec{\sigma}_d \lambda_u^a \lambda_d^a + \text{perm.}) - \frac{9}{320} d^{abc} \lambda^a \lambda^b \lambda^c (1 - 3(\vec{\sigma}_u \cdot \vec{\sigma}_d + \text{perm.})) \\
 & \left. - \frac{9f^{abc}}{64} \lambda^a \lambda^b \lambda^c (\vec{\sigma}_u \times \vec{\sigma}_d) \cdot \vec{\sigma}_s \right] + (R \longleftrightarrow L), \quad (3)
 \end{aligned}$$

where $m_i = m_i^{cur} + m^*$ is the effective quark mass in the instanton liquid. These forms are suitable for calculating the instanton induced contributions within a constituent quark picture.

In addition to the instanton interaction, we will take into account the perturbative one-gluon hyperfine interaction

$$V_{OGE}^{qq} = - \sum_{i>j} \frac{b}{m_i m_j} \vec{\sigma}_i \cdot \vec{\sigma}_j \lambda_i^a \lambda_j^a, \quad (4)$$

between quarks.

We use the following mass formula for the colorless ground hadronic states and color triquark and diquark states

$$M_h = E_0^{B,M} + \sum_i N_i m_i + E_{I2} + E_{I3} + E_{OGE}, \quad (5)$$

where N_i is number of the quarks with flavor i in the state. In Eq. (5)

$$\begin{aligned} E_{OGE} &= \langle h | V_{OGE} | h \rangle = - \sum_{i>j} \frac{b}{m_i m_j} M_{i,j}^{OGE}, \\ E_{I2} &= \langle h | V_{I2} | h \rangle = - \sum_{i \neq j} \frac{a}{m_i m_j} M_{i,j}^{I2}, \end{aligned} \quad (6)$$

and E_{I3} are the matrix elements of the OGE and two- and three-body instanton interactions, respectively.

After fit of the baryon and vector meson masses we have got the following values for the parameters [6]

$$\begin{aligned} m_0 &= 263 \text{ MeV}, \quad m_s = 407 \text{ MeV}, \quad E_0^M = 214 \text{ MeV}, \\ E_0^B &= 429 \text{ MeV}, \quad a = 0.0039 \text{ GeV}^3, \quad b = 0.00025 \text{ GeV}^3. \end{aligned} \quad (7)$$

Now we estimate the mass of $\Theta^+ udud\bar{s}$ in the model with instanton induced correlations between the quarks. One of the peculiarities of the instanton induced interaction is its strong flavor dependence, i.e., it is not vanishing only for the interaction among quarks of different flavor. For the ud diquark system the strong instanton attraction is possible only in the isospin $I = 0$ channel. Thus, preferably the configuration in the $udud$ subsystem will be two separated isoscalar ud diquarks. The remaining antiquark \bar{s} can join one of the diquarks to create a triquark $ud\bar{s}$ configuration in the instanton field. In this triquark state all quarks have different flavors, therefore the instanton interaction is expected to be maximal. Another peculiarity of the instanton interaction is that it is maximal in the system with the minimal spin. Thus, a pentaquark configuration with $S = 1/2$ $ud\bar{s}$ triquark and ud $S = 0$ diquark should be preferable. Therefore our final triquark–diquark picture for the pentaquark with instanton forces between quarks arises as shown in Fig. 2a, where the triquark is a quasi-bound state in the field of the instanton (anti-instanton) and the diquark is a quasi-bound state in the anti-instanton (instanton) field. To avoid the coalescence of the triquark–diquark state into single $udud\bar{s}$ cluster configuration, where the instanton interaction is expected to be much weaker, due to the Pauli principle for the same flavor quarks in instanton field, we assume a non-zero orbital momentum $L = 1$ in the triquark–diquark system. The centrifugal barrier protects the clusters from getting close and prohibits the formation of the much less bound five quark cluster.

It should be mentioned, that, from our point of view, the possibility of a pentaquark configuration formed by two ud -diquark clusters and a single antiquark \bar{s} , shown in (Fig. 2b), as implied by the Jaffe–Wilczek [11] and the Shuryak–Zahed [12] models, is suppressed by extra powers of the instanton density, $f = n_{eff}\pi^2\rho_c^4 \approx 1/10$ in the instanton model as compared with the triquark–diquark configuration of Fig. 2a.

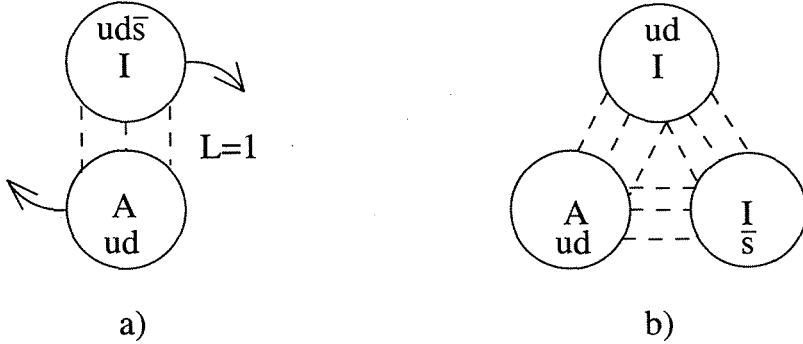


Figure 2: (a) Our instanton model for the pentaquark, (b) is the instanton picture for JW and SZ models. I (A) denotes instanton (anti-instanton) configurations. Dashed lines indicate gluon lines.

According to the Pauli statistics in the $ud\bar{s}$ $I = 0$ triquark state the ud diquark can be in $S = 0$ spin and $\bar{3}_c$ color state (A state) or in $S = 1$, 6_c color state (B state). In KL [13] only B has been considered. In fact, there is a strong mixing between the two states due to both the one-gluon and the instanton interactions, and one cannot neglect either.

Finally we have for the ud -diquark and the $ud\bar{s}$ -triquark states the following masses (see for details [6])

- diquark : $M_{di} = 442$ MeV, $M_{0di} = 740$ MeV,
 $\Delta M_{OGE} = -24$ MeV, $\Delta M_{I_2} = -274$ MeV;
- triquark A : $M_{tri} = 955$ MeV, $M_{0tri} = 1362$ MeV,
 $\Delta M_{OGE} = -40$ MeV, $\Delta M_{I_2} = -407$ MeV, $\Delta M_{I_3} = 40$ MeV;
- triquark B : $M_{tri} = 859$ MeV, $M_{0tri} = 1362$ MeV,
 $\Delta M_{OGE} = -50$ MeV, $\Delta M_{I_2} = -513$ MeV, $\Delta M_{I_3} = 60$ MeV;
- off - diagonal AB : $\Delta M_{OGE} = 32$ MeV, $\Delta M_{I_2} = 164$ MeV,
 $\Delta M_{I_3} = -49$ MeV, (8)

where M_0 is the mass of the state without the one-gluon and instanton contributions. From (8) it follows that the two-body instanton interaction gives a very large and negative contribution to the masses for all diquark and triquark states. At the same time, the one-gluon contribution is rather small. After diagonalization of the mass matrix for the A and B states, we obtain for the two mixed triquark states

$$M_{light}^{tri} = 753 \text{ MeV and } M_{heavy}^{tri} = 1061 \text{ MeV.} \quad (9)$$

The mass of light triquark cluster is smaller than the sum of the masses of the K meson and the constituent u and d quarks. Therefore, the pentaquark cannot dissociate to the $Ku(d)$ system. Thus, the Θ^+ , as a system of light triquark and diquark clusters, can decay only by rearrangement of the quarks between these clusters. However, this rearrangement is suppressed by the orbital momentum $L = 1$ barrier between the clusters. As a consequence, the centrifugal barrier, provides the mechanism for a very small width in the case of the Θ^+ .

Let us estimate the total mass of Θ^+ if built as a system of a triquark cluster with mass 753 MeV, a diquark cluster with mass 442 MeV bound together in relative $L = 1$ orbital momentum state. The reduced mass for such triquark–diquark system is $M_{red}^{tri-di} = 279$ MeV. This mass is approximately equal to the “effective” reduced mass of the strange quarks in the Φ meson, $M_{red}^\Phi \approx M_\Phi/4 = 255$ MeV. For two strange quarks, the $L = 1$ energy of orbital excitation, can be estimated from the experimental mass shift between Φ meson and the $L = 1$ $f_1(1420)$ state

$$\Delta E(L = 1) \approx M_{f_1(1420)} - M_\Phi = 400 \text{ MeV}. \quad (10)$$

By neglecting the small difference between the reduced mass in the strange–anti–strange quark system and the triquark–diquark system, we estimate the mass of the light pentaquark in our model as

$$M_{\Theta^+} = M_{light}^{tri} + M_{di} + \Delta E(L = 1) \approx 1595 \text{ MeV}, \quad (11)$$

which is close to the data.

3. Conclusion

We have suggested in papers [6], as reported here, a triquark–diquark model for the pentaquark based on instanton induced interaction. It is shown, within the constituent quark model, that this strong interaction leads to the very light uds triquark and ud diquark color states. In order to check our suggestion we have done a sum rule calculation which incorporates the direct instanton effects [16]. We have shown that instantons lead to a large stability for the correlator of the color triquark current as a function of the Borel parameter. We observe the formation of two negative parity uds states with spin one-half and isospin zero. These triquark states might be behind of the unusual properties of the observed pentaquark state presented here as in [6].

References

- [1] R.L. Jaffe, hep-ph/0409065; hep-ph/0409362; K. Maltman, hep-ph/0408144, M.Oka, hep-ph/0406211.
- [2] K. Hicks, hep-ph/0408001; Q. Zhao and F.E. Close, hep-ph/0404075.
- [3] T. Schäfer and E.V. Shuryak, Rev. Mod. Phys. **70** (1998) 1323.
- [4] D. Diakonov, Prog. Par. Nucl. Phys. **51** (2003) 173.

- [5] A.E.Dorokhov, N.I.Kochelev and Yu.A. Zubov, *Int. J. Mod. Phys.* **8A** (1993) 603.
- [6] N.I. Kochelev, H.-J. Lee, V. Vento, *Phys. Lett.* **B594** (2004) 87.
- [7] M.A.Shifman, A.I.Vainshtein, A.I.Zakharov, *Nucl. Phys.* **B163**, 43 (1980).
- [8] A.E. Dorokhov and N.I.Kochelev, Preprint JINR-E2-86-847 (1986), hep-ph/0411362.
- [9] A.E. Dorokhov, N.I.Kochelev, Yu.A. Zubov, *Yad. Fiz.* **50** (1989) 1717 (*Sov. J. Nucl. Phys.* **50** (1989) 1065), *Z. Phys.* **C65** (1995) 667; N.I. Kochelev, *JETP Lett.* **70** (1999) 491.
- [10] S. Takeuchi and M. Oka, *Phys. Rev. Lett.* **66** (1991) 1271.
- [11] R.L. Jaffe and F. Wilczek, *Phys.Rev.Lett.* **91** (2003) 232003.
- [12] E. Shuryak and I. Zahed, hep-ph/0310270.
- [13] M. Karliner and H.J. Lipkin, *Phys. Lett.* bf B575 (2003) 249, hep-ph/0307243.
- [14] A.E. Dorokhov and N.I. Kochelev, *Z. Phys.* **C46** (1990) 281.
- [15] E.V. Shuryak, *Nucl. Phys.* **B203**, 93; 116; 140 (1982).
- [16] H.-J. Lee, N.I. Kochelev, V. Vento, hep-ph/0412127.

ON THE RELATIONS BETWEEN TWO-PHOTON AND LEPTONIC WIDTHS OF LOW-LYING S-WAVE STATES OF CHARMONIUM

S.B.Gerasimov^{1†} and M.Majewski²

(1) *Bogoliubov Laboratory of Theoretical Physics, JINR, Dubna*

(2) *University of Lodz, Department of Theoretical Physics, Lodz, Poland*

† *E-mail: gerasb@thsun1.jinr.ru*

Abstract

The relation between the ratio $\Gamma_{ee}(\psi')/\Gamma_{ee}(J/\psi)$ and $\Gamma_{2\gamma}(\eta'_c)/\Gamma_{2\gamma}(\eta_c)$, expressed in terms of the configuration mixing amplitudes, induced by the contact spin-spin interaction of quarks in the ground and radial excitation states, is shown to give, after inclusion of the newly derived relativistic corrections, the radiative η'_c - and η_c -width ratio in fair accord with recent experiments. The dynamical model is also proposed to derive the ratio of relative probability of the ground ($\eta_c(2980)$)- and first radial excitation ($\eta'_c(3640)$)-state formation in $\gamma\gamma$ -collisions followed by their decay into the $\bar{K}K\pi$ and $p\bar{p}$ channels.

1. Two-photon decays of heavy quarkonia provide valuable information on heavy quark dynamics and have been under consideration in recent experimental [1, 2, 3, 4, 5, 6, 7, 8, 9] and theoretical [12, 13, 14, 15, 16, 17, 18] studies. It seems reasonable to assume, at least as a first approximation, that there is no mixing between light and heavy quark sectors, and that one can consider the needed transition amplitudes separately for mesons constructed of the u-, d-, s-, and heavy c- and b-quarks.

In this work, we concentrate on the charmed quark sector and our main concern in this problem will be the question of the degree of model (in)dependence of the S -wave $Q\bar{Q}$ annihilation rates, or their ratios, with respect to the role of short-range spin-dependent forces. This is an important theoretical question because in many approximate relativistic approaches to description of the annihilation of bound antiquark-quark S -wave states that are subjected to strong short-range interactions one needs to introduce the cut-off procedures to get rid of singular behaviour of matrix elements considered, the cut-off parameters or the "smearing" procedures being introduced basically on the phenomenological grounds.

2. We start with just postulating for mass operator of the heavy quark ($Q = c, b$), S -wave systems the simplest spin-dependent matrix

$$\langle n' | \hat{M} | n \rangle = M_n \delta_{nn'} + C \cdot \psi_{nS}(0) \psi_{n'S}(0) \cdot \langle \vec{\sigma}_Q \cdot \vec{\sigma}_{\bar{Q}} \rangle \quad (1)$$

and write down a simple perturbation theory expressions to have the estimation for the mutual change of the ground and first radial excited states due to switching on the contact spin-spin potential

$$\Psi_n(0) = \psi_n(0) + \sum_m \langle m | \hat{V} | n \rangle / (E_n^{(0)} - E_m^{(0)}), \quad (2)$$

where $|i\rangle \equiv \psi_i$ and $E_i^{(0)}$ are the wave functions and energies of the unperturbed hamiltonian and \hat{V} is the perturbation potential that we identify with the contact spin-spin interaction of quarks.

Applying Eq.(2) successively to $\psi_{nS}(J)$, where $n = 1, 2$ - the quantum numbers of the S-wave radial excitations of the $\bar{c}c$ - quarkonia with the spin $J = 0, 1$, using the specific (*i.e.* proportional the δ -function) form of the perturbation potential) and keeping everywhere the terms of the first order in $\mathcal{O}(\hat{V})$ we get the relations

$$\begin{aligned} R_{2S/1S}^J|_{hfs} &\simeq \frac{\Psi_{2S}^J(0)^2}{\Psi_{1S}^J(0)^2}|_{hfs} \\ &\simeq \frac{\psi_{2S}(0)^2}{\psi_{1S}(0)^2} \cdot \frac{[(1 + V_{11}^J(m_2^0 - m_1^0)^{-1} + V_{33}^J(m_2^0 - m_3^0)^{-1} + \dots)]^2}{[(1 + V_{22}^J(m_1^0 - m_2^0)^{-1} + V_{33}^J(m_1^0 - m_3^0)^{-1} + \dots)]^2} \\ &\simeq \frac{\psi_{2S}(0)^2}{\psi_{1S}(0)^2} \cdot [1 + 2(s_2^J - s_1^J)], \end{aligned} \quad (3)$$

where s_n^J ; $J = 0, 1$ is the sum of terms of the order $\mathcal{O}(\hat{V})$ entering the denominator and numerator of (3). Using the evident relation $V^{J=0} = -3V^{J=1}$ we obtain

$$R_{2S/1S}^{J=0}|_{hfs} + 3 \cdot R_{2S/1S}^{J=1}|_{hfs} \simeq 4 \cdot \frac{\psi_{2S}(0)^2}{\psi_{1S}(0)^2}, \quad (4)$$

We make an estimation for the ratio $\Gamma(\eta_c' \rightarrow \gamma\gamma)/\Gamma(\eta_c \rightarrow \gamma\gamma)$ on the basis of experimental data of leptonic charmonium decays, approximate validity of lowest order perturbation theory for the color-hyperfine splitting interaction as well as on newly obtained form of the relativistic corrections to the considered decays.

We remind first the known results [10, 11] for lowest order QCD corrections:

$$\frac{m_{\eta_c}^2 \Gamma(\eta_c \rightarrow \gamma\gamma)}{m_{J/\psi}^2 \Gamma(J/\psi \rightarrow e^+e^-)} = \frac{4}{3} \left(1 + 1.96 \frac{\alpha_s}{\pi}\right) \frac{|\Psi_{\eta_c}(0)|^2}{|\Psi_{J/\psi}(0)|^2}, \quad (5)$$

where α_s should be evaluated at the charm scale [16].

In certain chosen ratios, such as

$$\frac{\Gamma_{\gamma\gamma}^{\eta_c'} \Gamma_{ee}^{J/\psi}}{\Gamma_{\gamma\gamma}^{\eta_c} \Gamma_{ee}^{\psi'}} = \left(\frac{m_{\eta_c} m_{\psi'}}{m_{\eta_c'} m_{J/\psi}}\right)^2 \frac{R_{2S/1S}^{J=0}}{R_{2S/1S}^{J=1}} \quad (6)$$

the ratios of $\psi_{nS}(0)$'s are cancelled and also the QCD radiative corrections are assumed to be mutually compensated not only in the next-to-leading order (NLO), but also in the higher orders of the perturbation theory, which, as seen from refs.[15, 19, 20], are not negligible. We assume further on, that each type of studied corrections can be approximately represented in factorized form

$$\begin{aligned} \Psi_{nS}^J(0) &\equiv |\psi_{nS}(0)|^2 (1 + \delta^J(rad) + \delta_{nS}^J(rel) + \delta_{nS}^J(hfs)) \simeq \\ &\simeq |\psi_{nS}(0)|^2 (1 + \delta^J(rad))(1 + \delta_{nS}^J(rel))(1 + \delta_{nS}^J(hfs)) \end{aligned} \quad (7)$$

That means that $1 + \delta^J(rad)$ factor coincides, in the lowest order radiative correction with $1 + (a^J/\pi)\alpha_s(m_c)$ where $(a^{J=1} = -5.34)$ and $(a^{J=0} = -3.38)$, and it is seen to be cancelled,

together with higher order terms, also in both the leptonic ($R_{2S/1S}^{J=1}$) and 2-photon ($R_{2S/1S}^{J=0}$) "single ratios".

The notation $\delta_{nS}^J(hfs)$ refers to the correction factor due to the spin-spin potential-induced factors in (4) and this type of corrections is not cancelled in the double ratio (6) unlike the mentioned linear combination of the "single ratios" (4).

The relativistic correction factor $1 + \delta_{nS}^J(rel)$ is defined in the following manner. The static approximation for both Γ_{ee} and $\Gamma_{\gamma\gamma}$, resulting in their proportionality to the respective wave function value "at origin", $\psi_{nS}(0)$, follows from neglecting of the dependence of the bound quark annihilation amplitudes on their internal motion momenta

$$|\int d\vec{p} A(c\bar{c}(\vec{p}) \rightarrow ee(\gamma\gamma)) \phi_{nS}(\vec{p})|^2 \sim |\psi_{nS}(0)|^2 |A_{thr}(c\bar{c} \rightarrow ee(\gamma\gamma))|^2. \quad (8)$$

We have found that the adequacy of appearance the $\psi_{nS}(0)$ with the relativistic correction factor $1 + \delta_{nS}^J(rel)$ in the non-static annihilation amplitudes with their dependence on the internal quark momenta taken into account can be inferred from the explicit form of newly defined averages

$$2\sqrt{1 + \delta_{nS}^{J=0}(rel)} \simeq \frac{m_c^2}{\epsilon_{nS}^2} \int \frac{d^3p}{(2\pi)^3} \phi_{nS}(p) \frac{\epsilon_{nS}}{p} \log\left(\frac{\epsilon_{nS} + p}{\epsilon_{nS} - p}\right) / \int \frac{d^3p}{(2\pi)^3} \phi_{nS}(p), \quad (9)$$

$$\sqrt{1 + \delta_{nS}^{J=1}(rel)} \simeq \left(\int \frac{d^3p}{(2\pi)^3} \phi_{nS}(p) \left(1 - \frac{\epsilon_{nS} - m_c}{3\epsilon_{nS}}\right) \right) / \int \frac{d^3p}{(2\pi)^3} \phi_{nS}(p), \quad (10)$$

where $\phi_{nS}(p)$ is the nS -state wave function in the momentum representation, and ϵ_{nS} is the quark energy in the nS -state. The momentum-dependent factors of the $(c\bar{c})_{nS} \rightarrow e^+e^-(\gamma\gamma)$ amplitudes are given, *e.g.*, in [17], but instead of taking $\epsilon(p) = (m_c^2 + p^2)^{1/2}$ we prefer to define the continuation of the $c\bar{c}$ -annihilation amplitudes to the bound state kinematics following the so-called "on-energy-shell / off-mass-shell" prescription when $\epsilon(p) \rightarrow \epsilon_{nS} = m_{nS}/2$ is now remains independent of the internal motion momentum $|\vec{p}|$ while being averaged with wave functions $\phi_{nS}(\vec{p})$ in (10). This picture of a bound state dynamics underlies the appearance of the relativistic Schrödinger-type wave equations, such as the quasipotential equation suggested by Todorov [23] or different variants thereof, *e.g.*, [24]. In this prescription, the relativistic correction factor for the electron-positron annihilation of vector charmonia is especially simple because there is no additional momentum-dependent factors in the integrand, while the $\delta_{nS}^{J=0}(rel)$ is derived directly from the relation

$$2[1 + \delta_{nS}^{J=0}(rel)]^{1/2} = \frac{m_c^2}{\epsilon_{nS}^2} \left(\int \frac{d^3p}{(2\pi)^3} \phi_{nS}(p) \frac{\epsilon_{nS}}{p} \log\left(\frac{\epsilon_{nS} + p}{\epsilon_{nS} - p}\right) / \left(\int \frac{d^3p}{(2\pi)^3} \phi_{nS}(p) \right) \right) \\ = 2 \frac{m_c^2}{\epsilon_{nS}^2} \int_0^\infty dr \psi_{nS}(r) \sin(\epsilon_{nS} r) / \psi_{nS}(0) \quad (11)$$

$$\simeq 2 \frac{m_c^2}{\epsilon_{nS}^2} \cdot [\psi_{nS}(0) - \frac{1}{\epsilon_{nS}^2} \psi_{nS}''(0) + \dots] / \psi_{nS}(0), \quad (12)$$

where masses m_{nS} correspond to masses calculated without spin-dependent corrections: $m_{1S} \simeq (3m_{J/\psi} + m_{\eta_c})/4$, $m_{2S} \simeq (3m_{\psi'} + m_{\eta_c'})/4$.

Keeping only the first term in asymptotic series for the Fourier integral (12), we obtain, in the accord with the Riemann-Lebesgue lemma, the simple approximate relation

$$[1 + \delta_{nS}^{J=0}(rel)]^{1/2} \simeq \frac{m_c^2}{\epsilon_{nS}^2} \quad (13)$$

demonstrating more strong dependence on the relativistic corrections of the two-photon decay amplitude as compared with the leptonic one

$$[1 + \delta_{nS}^{J=1}(rel)]^{1/2} = 1 - \frac{\epsilon_{nS} - m_c}{3\epsilon_{nS}}. \quad (14)$$

Besides the relativistic corrections to be taken explicitly, we have observed a significant contribution to our relation for ratios (6) due to inclusion of the short-ranged spin-dependent interaction which modifies the vector and pseudoscalar wave functions "at zero" quite asymmetrically. However, for the linear combination (4) of two ratios the "hyperfine" corrections are compensated up to terms of the order $\mathcal{O}(\hat{V}^2)$.

Collecting now all found corrections we get the resulting relation between the widths of the lowest lying states of charmonia

$$\frac{\Gamma_{\gamma\gamma}^{\eta_c'} (m_{\eta_c'} m_{2S}^2)}{\Gamma_{\gamma\gamma}^{\eta_c} (m_{\eta_c} m_{1S}^2)} + 3 \frac{\Gamma_{ee}^{\psi'} (m_{\psi'} m_{2S} (m_{1S} + m_c))}{\Gamma_{ee}^{J/\psi} (m_{J/\psi} m_{1S} (m_{2S} + m_c))} = 4 \left(\frac{\psi_{2S}(0)}{\psi_{1S}(0)} \right)^2, \quad (15)$$

from where it follows

$$\frac{\Gamma_{\gamma\gamma}^{\eta_c'}}{\Gamma_{\gamma\gamma}^{\eta_c}} = 0.21 \pm 0.06, \quad (16)$$

if we take $(\psi_{2S}(0)/\psi_{1S}(0))^2 = 0.653$ and $m_c = 1.48$ GeV according to [21, 22], $\Gamma_{\gamma\gamma}^{\eta_c}$, masses and leptonic widths from [1]. A rather large uncertainty of the ratio obtained is largely due to experimental errors of the measured leptonic widths. It should be noted, that unlike the very $\psi_{nS}(0)$'s their calculated ratios are much less model-dependent. In particular, the ratio entering (15) calculated with the Cornell (*i.e.*, the "linear+Coulomb") type potential is close to ratio calculated with the "running" $\alpha_s(r)$, that make the one-gluon-exchange potential softer at small distances, although the very $\psi_{1S}(0)$'s are differing about two times from each other [22]. We believe that mild smearing or regularization of the short-ranged quark interactions providing formal finiteness of the $\psi_{nS}(0)$'s, following from the relativistic equations, will also leave their ratios relatively intact. Besides the relativistic corrections to the $c\bar{c}$ -quark annihilation amplitudes, one should take in view the relativistic corrections to the $\psi_{nS}(0)$ themselves. We have already took into account the relativistic corrections due to the short-ranged spin-spin interactions of charm quarks. There are, surely, certain spin independent corrections. We approach to their estimation on the basis of the relativistic Schrödinger - type equation [24] which was introduced and employed to use maximally and directly the experience of the nonrelativistic formalism. Due to more complex dependence of the wave equation on the full energy of the two-quark system $W_{nS} = 2\epsilon_{nS}$ it is convenient to introduce the "renormalized" wave function $\tilde{\psi}_{nS}$: $\psi_{nS} = \tilde{\psi}_{nS}/\sqrt{2W_{nS}}$. For $\tilde{\psi}_{nS}$ that is now normalized to unity, the familiar scaling behaviour can be foreseen $|\tilde{\psi}_{nS}(0)|^2 \propto \epsilon_{red}^{3/(n+2)}$, where instead of the reduced mass $m_{red} = m_c$ we should use the "reduced energy" $\epsilon_{red} = \epsilon_{nS}$. Hence, the scaling behaviour $|\psi_{nS}^2(0)|^2 \propto \epsilon_{nS}^{(3/(n+2)-1)}$ follows for the squared "relativized" wave function at zero interquark distance. The exponent n of the effective power-behaved potential lies in the interval $-1 \leq n \leq 1$, presumably, closer to $n = 1$ especially for the radial excited states, where $n = 1$ represents the linear behaviour of the confinement potential. So, one can expect substantial compensation of these type correction in the ratios entering (15) and the

exact compensation takes place in the double ratio (6). For these reasons more detailed and quantitative discussion of this correction is not developed in the present work.

As has been mentioned, the ratios of $\psi_{nS}(0)$ are dropped in (6) and one can obtain a kind of the lower bound for the double width's ratio leaving only one, beyond and next to unity, term in every infinite sum of the perturbation corrections to $\Psi_{nS}^J(0)$ due to the contact spin-spin potential of charmed quarks treated as a first order term of perturbation theory. Including then already fixed relativistic corrections and assuming, as earlier, the cancellation of the (static!) radiative corrections, we obtain

$$\frac{\Gamma_{\gamma\gamma}^{\eta_c'} \Gamma_{ee}^{J/\psi}}{\Gamma_{\gamma\gamma}^{\eta_c} \Gamma_{ee}^{\psi'}} \left(\frac{m_{\eta_c'} m_{2S} m_{J/\psi} (m_{2S} + m_c)}{m_{\eta_c} m_{1S} m_{\psi'} (m_{1S} + m_c)} \right)^2 \geq \left(1 + \frac{V_{11}^{J=0} + V_{22}^{J=0}}{m_{2S} - m_{1S}} \right)^2 / \left(1 + \frac{V_{11}^{J=1} + V_{22}^{J=1}}{m_{2S} - m_{1S}} \right)^2 \simeq 1 - 8 \frac{V_{11}^{J=1} + V_{22}^{J=1}}{m_{2S} - m_{1S}}, \quad (17)$$

from where a new constraint follows

$$\frac{\Gamma_{\gamma\gamma}^{\eta_c'}}{\Gamma_{\gamma\gamma}^{\eta_c}} \geq 0.1. \quad (18)$$

and where the numerical values [1] for $m_{1S}^{J=1}$, $m_{2S}^{J=1}$, defined earlier, and $V_{11}^{J=1} = (m_{J/\psi} - m_{\eta_c})/4$, $V_{22}^{J=1} = (m_{\psi'} - m_{\eta_c'})/4$, were used. The comparison of (16) and (18) tells about a significant role of sums $\langle nS | \hat{V}^J | nS \rangle$ over $n \geq 1, 2$ in the definition of the individual ratios of $\Gamma_{ee}^{J/\psi} / \Gamma_{ee}^{\psi'}$ and especially of $\Gamma_{\gamma\gamma}^{\eta_c'} / \Gamma_{\gamma\gamma}^{\eta_c}$.

To make contact with the available experimental data for radiative widths of charmonia it is necessary to estimate also their relative branchings referring to the studied hadronic decay channels.

The main assumptions underlying our estimations of branching ratios $\mathcal{B}_h^{\eta_c'}$ and $\mathcal{B}_h^{\eta_c}$ entering the experimentally measured processes of the two-photon fusion producing η_c and η_c' and subsequent hadronic decays $\eta_c (\eta_c') \rightarrow h$, where $h \equiv K\bar{K}\pi$ [3] or $h \equiv p\bar{p}$ [6], are the following. We assume a simple kinematic structure of the respective decay amplitudes and approximate dynamical assumption for the ratio of relevant couplings or, rather, complex form-factors in the considered vertices

$$A(\eta_c(\eta_c') \rightarrow K\bar{K}\pi) = g(\eta_c(\eta_c') \rightarrow K\bar{K}\pi) \frac{1}{2} \varphi_K^\dagger \vec{\tau} \varphi_K \vec{\varphi}_\pi, \quad (19)$$

$$A(\eta_c(\eta_c') \rightarrow p\bar{p}) = g(\eta_c(\eta_c') \rightarrow p\bar{p}) F_c(m_{c\bar{c}}^2) \bar{u}(P_p) \gamma_5 v(P_{\bar{p}}), \quad (20)$$

$$A(\eta_c(\eta_c') \rightarrow G_m G_m) = g(\eta_c(\eta_c') \rightarrow G_m G_m) \varepsilon_{\mu\nu\rho\sigma} e_1^\mu e_2^\nu e_2^\rho e_1^\sigma, \quad (21)$$

$$\frac{|g(\eta_c \rightarrow h)|^2}{|g(\eta_c \rightarrow G_m G_m)|^2} \simeq \frac{|g(\eta_c' \rightarrow h)|^2}{|g(\eta_c' \rightarrow G_m G_m)|^2}, \quad (22)$$

where only isospin structure of the $K\bar{K}\pi$ decay channel is indicated in the first line and the generalization to the $SU(3)$ -symmetry can easily be written down. We include the form-factor $F_c(Q^2)$ in (20) to mention about its possible variation depending on the time-like momentum transferred in the interval $m_{\eta_c}^2 \leq Q^2 \leq m_{\eta_c'}^2$. We note that unlike the vector charmonia J/ψ - and ψ' -decays, the pseudoscalar decay channel branchings

$\mathcal{B}(\eta_c'(\eta_c) \rightarrow (h, \gamma)(c\bar{c}))$ containing the charmed quarks, *e.g.*, the decay $\eta_c' \rightarrow 2\pi\eta_c$, are much less significant, due to smallness of the coupling constant $\alpha_s(m_c) \simeq 0.3$, as compared to the branching ratios of $\mathcal{B}(\eta_c'(\eta_c) \rightarrow h)$ decays, where h denotes hadron states composed of the light (u, d, s) quarks. Following usual practice (or, alternatively, the quark-hadron duality hypothesis for inclusive processes), we identify the total width of these processes with the width of the bound $c\bar{c}$ -quark annihilation to pair of "free" gluons $\Gamma(\eta_c(\eta_c') \rightarrow G_m G_m)$. Further, we attribute to gluons finite "effective" (or dynamical) mass m_G of order 0.7 GeV which was advocated in ref. [25] and in some earlier works cited therein, on the basis of the detailed study of the experimental photon spectrum in the inclusive reaction $J/\psi \rightarrow \gamma G_m G_m \rightarrow \gamma X$. The evaluation of the important transition probabilities $\eta_c(\eta_c') \rightarrow K\bar{K}\pi$, studied in several experiments, see, *e.g.* [3] and further references therein, have been performed with the help of the integral relation for invariant 3-body phase space [26]

$$\rho(m_0 \rightarrow m_1 + m_2 + m_3) = \frac{1}{128\pi^3 m_0^2} \int_{s_2}^{s_3} \frac{ds}{s} F(s, s_1, s_2, s_3, s_4),$$

$$F(s, s_1, s_2, s_3, s_4) = [(s - s_1)(s - s_2)(s_3 - s)(s_4 - s)]^{0.5} \quad (23)$$

where $s_{2,1} = (m_1 \pm m_2)^2$, $s_{4,3} = (m_0 \pm m_3)^2$ and we choose $m_0 = m_{\eta_c(\eta_c')}$, $m_1 = m_2 = m_K$, $m_3 = m_\pi$. After that, the integral which is essential part of the ratio $\mathcal{B}_{K\bar{K}\pi}^{\eta_c'}/\mathcal{B}_{K\bar{K}\pi}^{\eta_c}$ can easily be calculated numerically.

Including standard relativistic normalization factors of the initial states, summing and averaging over spin degrees of freedom of the listed amplitudes squared and using the assumed relation (22), we obtain

$$\frac{\mathcal{B}_h^{\eta_c'}}{\mathcal{B}_h^{\eta_c}} = \begin{cases} 0.83, & \text{for } h = K\bar{K}\pi, \\ 0.65 \cdot (F_c(m_{\eta_c'}^2)/F_c(m_{\eta_c}^2))^2, & \text{for } h = p\bar{p}, \end{cases} \quad (24)$$

hence, our results follow in Table 1, where the upper bound for the $p\bar{p}$ -decay channel refers to the ratio of the form-factors put equal unity and where we present also some recent theoretical predictions and experimental results for widths of the $\eta_c(\eta_c')$ -to- $\gamma\gamma$ decays and their ratios.

The behaviour of the unitary-singlet, pseudoscalar form-factors in the hadronic transition vertexes is of considerable interest for the understanding of mechanisms of sequential processes $\eta_c(\eta_c') \rightarrow G_m G_m \rightarrow \text{light hadrons}$. The closeness of our estimated $R(\eta_c'/\eta_c)$ decay-ratio in the $K\bar{K}\pi$ channel, with no additional form-factors included, to the CLEO data looks intriguing and needs more investigation to be understood. At any rate, in the $p\bar{p}$ channel one should expect more strong dependence of the result on the $(m_{\eta_c}^2/m_{\eta_c'}^2)^n$ ratio, where the effective power n is expected to be two units larger in the decay amplitude for two-baryon final state as compared with amplitudes for two-meson states, according the quark-counting rules. The two-gluon state mediating the $c\bar{c}$ - and $q^n\bar{q}^n$ - states, where $q = u, d, s$, would provide a new testing ground for the checking the generalized parton approach or the diquark model which were successful in the description of the two-photon annihilation processes, like $\gamma\gamma \rightarrow p\bar{p}$, etc. Therefore, the further study of the reactions $p\bar{p} \rightarrow \eta_c(\eta_c') \rightarrow \gamma\gamma$ (or $K\bar{K}\pi$) with better statistics and accuracy is of interest, *e.g.*, at a planned antiproton storage ring at GSI.

Table 1: Recent theoretical and experimental results of the η_c and η_c' two-photon decay width (the notations: $h \equiv \bar{K}K\pi$ for ref.[3] and $h \equiv \bar{p}p$ for ref.[7, 6] , the entry with superscript (x) is our estimate using other works)

	$\Gamma_{2\gamma}^{\eta_c}$ KeV	$\Gamma_{2\gamma}^{\eta_c'}$ KeV	$\Gamma_{2\gamma}^{\eta_c}/\Gamma_{2\gamma}^{\eta_c'}$	$\Gamma_{2\gamma}^{\eta_c} \mathcal{B}_h^{\eta_c}/\Gamma_{2\gamma}^{\eta_c} \mathcal{B}_h^{\eta_c'}$
PDG [1]	7.5 ± 0.8			
CLEO [2, 3]	$7.6(0.8)(2.3)$			$0.18(0.05)(0.02)$
E760/E835 [7, 6]	$6.7_{-1.7}^{+2.4}(2.3)$			≤ 0.16
L3 [8]	$6.9(1.7)(2.1)$	≤ 2		
DELPHI [9]			≤ 0.34	
Gupta[12]	10.94			
Münz[13]	3.50 ± 0.40	1.38 ± 0.30	$0.39 \pm 0.10^{(x)}$	
Chao [14]	6-7	2	$0.28 - 0.33^{(x)}$	
Fabiano [16]	$8.18(0.57)(0.04)$			
Ebert [17]	5.5	1.8	$0.33^{(x)}$	
Kim[18]	7.14 ± 0.95	4.44 ± 0.48	$0.62 \pm 0.10^{(x)}$	
This work		$1.6 \pm 0.5^{(x)}$	0.21 ± 0.06	$0.18, h \equiv K\bar{K}\pi$ $\leq 0.15, h \equiv p\bar{p}$

3. Finally, we note that the relation (15) can be applied to any pairs of the "hyperfine-split" radial-excited states. In particular, using it for pairs of ratios $R_{3S/1S}$ and $R_{3S/2S}$ with the needed input values $m_{\psi^*} = 4039$ MeV, $\Gamma_{ee}^{\psi^*} = .89 \pm .08$ keV [27, 28], $|\psi_{3S}(0)/\psi_{1S(2S)}(0)|^2 = .56(.86)$ [22] we obtain an estimation $m_{\eta_c} \simeq 4003$ MeV and $\Gamma_{\gamma\gamma}^{\eta_c}/\Gamma_{\gamma\gamma}^{\eta_c'} \simeq .22$ of the "naked" (i.e., without possible hadronic corrections due to virtual, open-charm intermediate ($D\bar{D}^* + \bar{D}D^*$) - states) parameters of still to be observed η_c -resonance.

Our main results, the relation (15) and the numerical entries in Table 1, demonstrate a considerable suppressing effect of the relativistic and "hyperfine" spin-dependent corrections on the recently observed two-photon decay of the $\eta_c'(3640)$ -resonance. If it is true, this effect should display itself also in the total width $\Gamma_{tot}^{\eta_c}$, represented by the decay into two gluons, either massless or effectively massive, in which case, using the average value $\Gamma_{tot}^{\eta_c} = 32.3 \pm 2.2$ MeV of the CLEO [3] and BaBar [4] results, we have got the estimate of the total width of the $\eta_c'(3640)$ - resonance

$$\Gamma_{tot}^{\eta_c'} = \begin{aligned} & (32.3 \pm 2.2) \cdot (.21 \pm .06) \simeq 6.8 \pm 2.0 \text{ MeV, for } m_G = 0, \\ & (32.3 \pm 2.2) \cdot (.21 \pm .06) \cdot ((1 - 4m_G^2/m_{\eta_c}^2)/(1 - 4m_G^2/m_{\eta_c}^2))^{3/2} \\ & \simeq 7.8 \pm 2.3 \text{ MeV, for } m_G \simeq .7 \text{ GeV.} \end{aligned}$$

More precise measurement of this important parameter, as compared with the published [3] result $\Gamma_{tot}^{J_c} = 6.3_{-4.0}^{+12.4}$ MeV, would be very desirable.

Acknowledgements

S.G. thanks Prof.J.Rembielinski and the staff of the Department of Theoretical Physics for warm hospitality and partial support during his visits to University of Lodz.

The partial support of this work by the Bogoliubov-Infeld foundation is gratefully acknowledged.

References

- [1] K. Hagiwara, et al., Particle Data Group Collaboration, Phys. Rev. **D66**, (2002) 010001.
- [2] The CLEO Collaboration, G. Brandenburg et al., Phys.Rev. Lett. **85**, 3095 (2000), hep-ex/0006026.
- [3] The CLEO Collaboration, D.M.Asner, et al., Phys.Rev.Lett., 92, (2004) 142001, hep-ex/0312058.
- [4] The BABAR Collaboration, B. Aubert et al., Phys.Rev.Lett. 92 (2004) 142002, hep-ex/0311038.
- [5] The BELLE Collaboration, S. K. Choi et al., Phys. Rev. Lett. **89**, (2002) 02001, hep-ex/0206002.
- [6] The E835 Collaboration, M. Ambrogiani et al.,Phys. Rev.**D64** (2001) 052003.
- [7] The E760 Collaboration, T. A. Armstrong et al., Phys. Rev. **D52** (1995) 4839.
- [8] The L3 Collaboration, M. Acciarri et al., Phys. Lett. **B 461** (1999) 155, hep-ex/9909008.
- [9] The DELPHI Collaboration, P. Abreu et al., Phys. Lett. **B 441** (1998) 479.
- [10] R. Barbieri, R Gatto, R. Kogerler, Phys. Lett., **B60**, 183 (1976).
- [11] W. Y. Keung, I. J. Muzinich, Phys. Rev. **D27** (1983) 1518.
- [12] S.N. Gupta, J. M. Johnson, W. W. Repko, Phys.Rev. **D54** (1996) 2075, hep-ph/9606349.
- [13] C. Münz, Nucl. Phys. **A 609** (1996) 364, hep-ph/9601206.
- [14] Kuang-Ta Chao, Han-Wen Huang, Jing-Hua Liu and Jian Tang, Phys. Rev. **D56**, 368 (1997), hep-ph/9601381.
- [15] A. Czarnecki, K. Melnikov, Phys. Lett. **B 519** (2001) 212, hep-ph/0109054.

- [16] N. Fabiano, G. Pancheri, Eur. Phys. J. C **25** (2002) 421, hep-ph/0204214.
- [17] D. Ebert, R. N. Faustov, V. O. Galkin, Mod. Phys. Lett. A **18** (2003) 601, hep-ph/0302044.
- [18] C.S.Kim, T. Lee,G.-L. Wang, hep-ph/0411075.
- [19] M. Beneke, A. Signer, V.A. Smirnov, Phys. Rev. Lett., **80** (1998) 2535, hep-ph/9712302.
- [20] A. Czarnecki, K. Melnikov, Phys. Rev. Lett., **80** (1998) 2531, hep-ph/9712222.
- [21] W.Buchmüller, S.H.H.Tye, Phys.Rev. **D24** (1981) 132.
- [22] E.J. Eichten, C. Quigg, Phys. Rev. **D 52** (1995) 1726, hep-ph/9503356.
- [23] I.T. Todorov, Phys. Rev. **D 3**, (1971) 2352.
- [24] S.B.Gerasimov, Prog.Part.Nucl.Phys.**8**, (1982) 207; Ed. Sir D. Wilkinson, Pergamon Press, 1982.
- [25] J.H. Field, Phys. Rev. **D 66** (2002) 013013, hep-ph/0101158.
- [26] A.I. Davydychev, R. Delbourgo, hep-th/0209233.
- [27] K.K.Seth, hep-ex/0405007
- [28] The BES Collaboration, J.Z. Bai, et al.,Phys. Rev. Lett. **88** (2002) 101802, hep-ex/0102003.

CLOTHED PARTICLE REPRESENTATION IN QUANTUM FIELD THEORY: MASS RENORMALIZATION

V.Yu. Korda^{1†} and A.V. Shebeko^{2*}

(1) *Institute of Electrophysics & Radiation Technologies, NAS of Ukraine, Kharkov, Ukraine*

(2) *NSC Kharkov Institute of Physics & Technology, NAS of Ukraine, Kharkov, Ukraine*

† *E-mail: kvyu@kipt.kharkov.ua*

* *E-mail: shebeko@kipt.kharkov.ua*

Abstract

We consider the neutral pion and nucleon fields interacting via the pseudoscalar Yukawa-type coupling. The method of unitary clothing transformations is used to handle the so-called clothed particle representation, where the total field Hamiltonian H and the three boost operators in the instant form of relativistic dynamics take on the same sparse structure in the Hilbert space of hadronic states. In this approach the mass counterterms are cancelled (at least, partly) by commutators of the generators of clothing transformations and the field interaction operator. This allows the pion and nucleon mass shifts to be expressed through the corresponding three-dimensional integrals whose integrands depend on certain covariant combinations of the relevant three-momenta. The property provides the momentum independence of mass renormalization. The present results prove to be equivalent to the results obtained by Feynman techniques.

1. Recollections

Recently [1, 2] the so-called unitary clothing transformation approach has been employed for an approximate treatment of simplest eigenstates of total field Hamiltonian H . We mean the physical vacuum Ω (the lowest-energy H eigenstate) and the observable one-particle states $|\mathbf{p}\rangle$ with the momentum \mathbf{p} . By definition, the vector $|\mathbf{p}\rangle$ belongs to the H eigenvalue $E_{\mathbf{p}} = \sqrt{\mathbf{p}^2 + m^2}$, where m is the mass of a free particle (e.g., fermion). We call it the physical mass. Thus, m appears here in a natural way via the relativistic dispersion law vs m as a pole of the full particle propagator. In this context, we note the paper [3] where the one-particle energies have been calculated for a nonlocal model of interacting charged and neutral mesons using stationary perturbation theory.

Normally, the mass shifts are expressed through the particle self-energy functions evaluated in nontrivial field theories as expansions in the coupling constants. Miscellaneous self-energy contributions give rise to undesirable divergences. Their removal requires considerable intellectual efforts associated with a consequent regularization of the divergent integrals involved. In the S-matrix calculations they are encountered as early as in the first nonvanishing approximation in the coupling constants. In this connection, note a possible way [4, 5] to express the S -matrix directly in terms of renormalized masses and interactions between clothed particles, these quasiparticles within the approach under consideration (cf. [6]).

Regarding the mass renormalization problem we recall one more realization of the unitary transformation method [7, 8], where the Hamiltonian for interacting fields was blockdiagonalized using Okubo's idea. While in [7] the π , ρ , ω and σ mesons were coupled with nucleons via the Yukawa-type interactions, the authors of [8] dealt with scalar "nucleons" and mesons with a simpler coupling. This enabled not only to derive the effective (Hermitian and energy independent) interactions ("quasipotentials") between nucleons, as done in [7], but also to separate the one-nucleon contribution to the Hamiltonian with the renormalized nucleon mass. The authors of [8] have shown that their expression for the second-order nucleon mass shift coincides with the corresponding expression found by Feynman technique. In particular, this shift is independent of the nucleon momentum.

What follows is an extension of the approach [2] to the mass renormalization problem in the clothed particle representation (CPR).

2. Underlying formalism

We proceed with a total Hamiltonian H ,

$$H \equiv H(\alpha) = H_F(\alpha) + H_I(\alpha), \quad H_I(\alpha) = V(\alpha) + M_{ren}(\alpha), \quad (1)$$

where the unperturbed (free) Hamiltonian $H_F(\alpha)$ and the interaction term $H_I(\alpha)$ depend on the destruction(creation) operators α (α^\dagger) of the "bare particles with physical masses" (cf., [2]). $V(\alpha)$ is the primary interaction between these particles and $M_{ren}(\alpha)$ are necessary mass counterterms.

The clothing procedure is aimed at rewriting H in a new form

$$H \equiv K(\alpha_c) = K_F(\alpha_c) + K_I(\alpha_c), \quad (2)$$

where the free part $K_F(\alpha_c)$ and the interaction $K_I(\alpha_c)$ are expressed through the new destruction(creation) operators α_c (α_c^\dagger) such that

$$\alpha_c(\mathbf{k}, r)\Omega = 0, \quad H\alpha_c^\dagger(\mathbf{k}, r)\Omega = k_0\alpha_c^\dagger(\mathbf{k}, r)\Omega, \quad \forall k = (k_0, \mathbf{k}), r. \quad (3)$$

Here Ω denotes the state without physical particles, \mathbf{k} the particle momentum, $k_0 = \sqrt{\mathbf{k}^2 + \mu^2}$, μ the physical mass of the particle and r the polarization index, if any. The "clothed" operators α_c obey the same algebra as the "bare" operators α do. One should note that $K_F(\alpha_c) \neq H_F(\alpha)$ but coincides with $H_F(\alpha_c)$,

$$K_F(\alpha_c) = H_F(\alpha_c) = \int d\mathbf{k} k_0 \sum_r \alpha_c^\dagger(\mathbf{k}, r) \alpha_c(\mathbf{k}, r). \quad (4)$$

The operator $K_I(\alpha_c)$ contains the interactions responsible for processes with physical particles. The property of the clothed one-particle states $\alpha_c^\dagger\Omega$ to be the H eigenstates is provided if

$$K_I\alpha_c^\dagger\Omega = 0. \quad (5)$$

The clothing itself is implemented via the relation

$$\alpha(\mathbf{k}, r) = W(\alpha_c) \alpha_c(\mathbf{k}, r) W^\dagger(\alpha_c), \quad \forall \mathbf{k}, r, \quad (6)$$

where the unitary transformation (UT)

$$W(\alpha_c) = W(\alpha) = \exp R(\alpha_c), \quad R^\dagger = -R, \quad (7)$$

removes from H the so-called 'bad' terms (see [2]).

With the help of (6) we rewrite the total Hamiltonian as

$$\begin{aligned} H &= H(\alpha) = H(W(\alpha_c)\alpha_c W^\dagger(\alpha_c)) = W(\alpha_c)H(\alpha_c)W^\dagger(\alpha_c) = K(\alpha_c) \\ &= H_F(\alpha_c) + H_I(\alpha_c) + [R, H_F] + [R, H_I] + \frac{1}{2}[R, [R, H_F]] + \frac{1}{2}[R, [R, H_I]] + \dots \end{aligned} \quad (8)$$

The operator $K(\alpha_c)$ is the same Hamiltonian as $H(\alpha)$ but it has another dependence on its argument α_c compared to $H(\alpha)$.

In the Yukawa-type model considered here at the first stage of the clothing procedure to meet the requirement (5) one needs to require (details in [2]):

$$V = [H_F, R_1], \quad (9)$$

where R_1 is the generator of the first clothing UT $W_1 = \exp R_1$. Doing so, we find

$$K(\alpha_c) = H_F(\alpha_c) + M_{ren}(\alpha_c) + \frac{1}{2}[R_1, V] + [R_1, M_{ren}] + \frac{1}{3}[R_1, [R_1, V]] + \dots \quad (10)$$

The four-operator (g^2 -order) interactions between clothed particles stem from $\frac{1}{2}[R_1, V]$ (see, e.g., [9, 10]). The two-operator contributions to it can be compensated by $M_{ren}(\alpha_c)$, bringing the definition of the particle mass shifts in the g^2 -order. The r.h.s. of Eq. (10) embodies other bad terms of the g^2 - and higher orders, which can be eliminated in the same way via the subsequent UT's.

3. Clothing procedure in action. Cancellation of mass counterparts

In the following model, where a neutral spinor (fermion) field ψ interacts with a neutral pseudoscalar meson field ϕ by means of the Yukawa coupling, H can be expressed through bare destruction (creation) operators $a(\mathbf{k})$ ($a^\dagger(\mathbf{k})$), $b(\mathbf{p}, r)$ ($b^\dagger(\mathbf{p}, r)$) and $d(\mathbf{p}, r)$ ($d^\dagger(\mathbf{p}, r)$) for the meson, the fermion and the antifermion, respectively. Here \mathbf{k} and \mathbf{p} are the particle momenta. In fact, we have its free part

$$H_F \equiv H_F(\alpha) = \int d\mathbf{k} \omega_{\mathbf{k}} a^\dagger(\mathbf{k}) a(\mathbf{k}) + \int d\mathbf{p} E_{\mathbf{p}} [b^\dagger(\mathbf{p}, r) b(\mathbf{p}, r) + d^\dagger(\mathbf{p}, r) d(\mathbf{p}, r)], \quad (11)$$

and the primary interaction

$$V(\alpha) = \int d\mathbf{k} \hat{V}^{\mathbf{k}} a(\mathbf{k}) + H.c., \quad \hat{V}^{\mathbf{k}} = \int d\mathbf{p}' d\mathbf{p} \sum_{r, r'} F^\dagger(\mathbf{p}', r') V^{\mathbf{k}}(\mathbf{p}', r'; \mathbf{p}, r) F(\mathbf{p}, r), \quad (12)$$

where operator column F and row F^\dagger are composed of the bare nucleon and antinucleon operators (e.g., $F^\dagger(\mathbf{p}, r) \equiv [b^\dagger(\mathbf{p}, r), d(-\mathbf{p}, r)]$), and we have introduced the c-number matrices

$$V^{\mathbf{k}}(\mathbf{p}', r'; \mathbf{p}, r) = \begin{bmatrix} V_{11}^{\mathbf{k}}(\mathbf{p}', r'; \mathbf{p}, r) & V_{12}^{\mathbf{k}}(\mathbf{p}', r'; \mathbf{p}, r) \\ V_{21}^{\mathbf{k}}(\mathbf{p}', r'; \mathbf{p}, r) & V_{22}^{\mathbf{k}}(\mathbf{p}', r'; \mathbf{p}, r) \end{bmatrix}$$

$$= \frac{ig}{(2\pi)^{3/2}} \frac{m}{\sqrt{2\omega_{\mathbf{k}} E_{\mathbf{p}} E_{\mathbf{p}'}}} \delta(\mathbf{p} + \mathbf{k} - \mathbf{p}') \left[\begin{array}{cc} \bar{u}(\mathbf{p}', r') \gamma_5 u(\mathbf{p}, r) & \bar{u}(\mathbf{p}', r') \gamma_5 v(-\mathbf{p}, r) \\ \bar{v}(-\mathbf{p}', r') \gamma_5 u(\mathbf{p}, r) & \bar{v}(-\mathbf{p}', r') \gamma_5 v(-\mathbf{p}, r) \end{array} \right].$$

Here $u(\mathbf{p}, r)$ and $v(\mathbf{p}, r)$ are the Dirac spinors, which satisfy the equations $(\hat{p} - m)u(\mathbf{p}, r) = 0$ and $(\hat{p} + m)v(\mathbf{p}, r) = 0$ with $\hat{p} = E_{\mathbf{p}}\gamma^0 - \mathbf{p}\gamma$, $E_{\mathbf{p}} = \sqrt{\mathbf{p}^2 + m^2}$ and $\omega_{\mathbf{k}} = \sqrt{\mathbf{k}^2 + \mu^2}$.

According to [2], the corresponding generator $R = R_1(\alpha_c) = \mathcal{R} - \mathcal{R}^\dagger$ that meets the condition (9) repeats the operator structure of V , viz.,

$$\mathcal{R} = \int d\mathbf{k} \hat{R}_c^{\mathbf{k}} a_c(\mathbf{k}), \quad \hat{R}_c^{\mathbf{k}} = \int d\mathbf{p}' d\mathbf{p} \sum_{r, r'} F_c^\dagger(\mathbf{p}', r') R^{\mathbf{k}}(\mathbf{p}', r'; \mathbf{p}, r) F_c(\mathbf{p}, r), \quad (13)$$

Here, unlike the fermion operators F and F^\dagger in Eq. (12) the operator column F_c and row F_c^\dagger are composed of the clothed nucleon and antinucleon operators. As shown in [2], the c-number 2×2 matrix $R^{\mathbf{k}}$ is determined by

$$R_{i,j}^{\mathbf{k}}(\mathbf{p}', r'; \mathbf{p}, r) = V_{i,j}^{\mathbf{k}}(\mathbf{p}', r'; \mathbf{p}, r) / [(-1)^{i-1} E_{\mathbf{p}'} - (-1)^{j-1} E_{\mathbf{p}} - \omega_{\mathbf{k}}], \quad (i, j = 1, 2). \quad (14)$$

We will focus upon those contributions in the r.h.s. of the equation

$$\begin{aligned} [R, V] &= \int d\mathbf{k}_1 d\mathbf{k}_2 \left\{ [\hat{R}_c^{\mathbf{k}_2}, \hat{V}_c^{\mathbf{k}_1}] a_c(\mathbf{k}_2) a_c(\mathbf{k}_1) \right. \\ &\quad \left. - [\hat{R}_c^{\mathbf{k}_2 \dagger}, \hat{V}_c^{\mathbf{k}_1}] a_c^\dagger(\mathbf{k}_2) a_c(\mathbf{k}_1) + \hat{V}_c^{\mathbf{k}_1} \hat{R}_c^{\mathbf{k}_2 \dagger} \delta(\mathbf{k}_1 - \mathbf{k}_2) \right\} + H.c., \quad (15) \end{aligned}$$

which are bilinear either in the meson or fermion operators.

As mentioned, they may be cancelled by respective counterparts from the operator $M_{ren}(a_c) = M_{ren,mes}(\alpha_c) + M_{ren,ferm}(\alpha_c)$ with

$$M_{ren,mes}(\alpha_c) = \frac{\delta\mu^2}{4} \int \frac{d\mathbf{k}}{\omega_{\mathbf{k}}} \left[2a_c^\dagger(\mathbf{k}) a_c(\mathbf{k}) + a_c(\mathbf{k}) a_c(-\mathbf{k}) + a_c^\dagger(\mathbf{k}) a_c^\dagger(-\mathbf{k}) \right], \quad (16)$$

and

$$M_{ren,ferm}(\alpha_c) = m\delta m \int \frac{d\mathbf{p}}{E_{\mathbf{p}}} \sum_{r, r'} F_c^\dagger(\mathbf{p}, r') M(\mathbf{p}, r'; \mathbf{p}, r) F_c(\mathbf{p}, r), \quad (17)$$

where the matrix M is given by

$$\begin{aligned} M(\mathbf{p}, r'; \mathbf{p}, r) &= \begin{bmatrix} M_{11}(\mathbf{p}, r'; \mathbf{p}, r) & M_{12}(\mathbf{p}, r'; \mathbf{p}, r) \\ M_{21}(\mathbf{p}, r'; \mathbf{p}, r) & M_{22}(\mathbf{p}, r'; \mathbf{p}, r) \end{bmatrix} \\ &= \frac{\delta(\mathbf{p}' - \mathbf{p})}{E_{\mathbf{p}}} \begin{bmatrix} \delta_{r'r} & \bar{u}(\mathbf{p}', r') v(-\mathbf{p}, r) \\ \bar{v}(-\mathbf{p}', r') u(\mathbf{p}, r) & -\delta_{r'r} \end{bmatrix}. \end{aligned}$$

We use the standard notation $\delta m = m_0 - m$ and $\delta\mu^2 = \mu_0^2 - \mu^2$.

As shown in [2] meson mass shift of the g^2 -order is

$$\delta\mu^2 = \frac{2g^2}{(2\pi)^3} \int \frac{d\mathbf{p}}{E_{\mathbf{p}}} \left\{ \frac{p_- k}{\mu^2 + 2p_- k} - \frac{pk}{\mu^2 - 2pk} \right\} = \frac{2g^2}{(2\pi)^3} \int \frac{d\mathbf{p}}{E_{\mathbf{p}}} \left\{ 1 + \frac{\mu^4}{4(pk)^2 - \mu^4} \right\}, \quad (18)$$

i.e., it is independent of the meson momentum \mathbf{k} . Here we have introduced the 4-vectors $p = (E_{\mathbf{p}}, \mathbf{p})$, $p_- = (E_{\mathbf{p}}, -\mathbf{p})$ and $k = (\omega_{\mathbf{k}}, \mathbf{k})$.

In the course of our consideration, the second-order contributions to the fermion mass counterterm are cancelled by the following two-operator combination,

$$\frac{1}{2} [R, V]_{2ferm} = \int dk F_c^\dagger X^k F_c = \int dk \{ b_c^\dagger X_{11}^k b_c + b_c^\dagger X_{12}^k d_c^\dagger + d_c X_{21}^k b_c + d_c X_{22}^k d_c^\dagger \}. \quad (19)$$

Explicit expressions for the c-number matrix elements X_{ij}^k in terms of V_{ij}^k and R_{ij}^k can be found in [11]

First of all, we are interested in cancellation of the $b_c^\dagger b_c$ and $d_c d_c^\dagger$ to get a prescription in determining the fermion (nucleon) mass renormalization (of course, in the g^2 -order). To this end, we assume

$$m\delta m^{(2)} M_{11} + \int dk X_{11}^k = 0, \quad m\delta m^{(2)} M_{22} + \int dk X_{22}^k = 0, \quad (20)$$

or in spinor space,

$$\begin{aligned} m\delta m^{(2)} \frac{\delta(\mathbf{p}' - \mathbf{p})}{E_{\mathbf{p}}} \delta_{r'r} &= - \int dk X_{11}^k(\mathbf{p}', r'; \mathbf{p}, r), \\ m\delta m^{(2)} \frac{\delta(\mathbf{p}' - \mathbf{p})}{E_{\mathbf{p}}} \delta_{r'r} &= \int dk X_{22}^k(\mathbf{p}', r'; \mathbf{p}, r). \end{aligned} \quad (21)$$

After this all we need is to prove that each of these integrals depend on fermion momentum and spin as $C(p) \delta(\mathbf{p}' - \mathbf{p}) \delta_{r'r} / E_{\mathbf{p}}$ and show that $C(p)$ is a constant. As shown in [11],

$$\int dk X_{11}^k(\mathbf{p}', r'; \mathbf{p}, r) = - \frac{g^2}{4(2\pi)^3} \frac{\delta(\mathbf{p}' - \mathbf{p})}{E_{\mathbf{p}}} \delta_{r'r} I(p), \quad (22)$$

where

$$I(p) = \int \frac{dk}{E_{\mathbf{p}-\mathbf{k}} \omega_{\mathbf{k}}} \left\{ \frac{m^2 - E_{\mathbf{p}} E_{\mathbf{p}-\mathbf{k}} + \mathbf{p}(\mathbf{p}-\mathbf{k})}{E_{\mathbf{p}} - E_{\mathbf{p}-\mathbf{k}} - \omega_{\mathbf{k}}} - \frac{m^2 + E_{\mathbf{p}} E_{\mathbf{p}-\mathbf{k}} + \mathbf{p}(\mathbf{p}-\mathbf{k})}{E_{\mathbf{p}} + E_{\mathbf{p}-\mathbf{k}} + \omega_{\mathbf{k}}} \right\}. \quad (23)$$

After some transformations we find,

$$I(p) = I_1(p) + I_2(p),$$

$$\begin{aligned} I_1(p) &= \int \frac{dk}{\omega_{\mathbf{k}}} p k \left\{ \frac{1}{\mu^2 - 2pk} - \frac{1}{\mu^2 + 2pk} \right\}, \\ I_2(p) &= \int \frac{dq}{E_{\mathbf{q}}} \left\{ \frac{m^2 - pq}{2[m^2 - pq] - \mu^2} + \frac{m^2 + pq}{2[m^2 + pq] - \mu^2} \right\}. \end{aligned}$$

Thus, mass shift of interest is

$$\delta m^{(2)} = \frac{g^2}{4m(2\pi)^3} I(p) = \frac{g^2}{4m(2\pi)^3} [I_1(m, 0, 0, 0) + I_2(m, 0, 0, 0)]. \quad (24)$$

The second relation (21) leads to the same result since $X_{22}^k = -X_{11}^k$. The integrals involved in Eq. (24) can be reduced to the elementary ones. Remaining crossed $b_c^\dagger d_c^\dagger$ and $d_c b_c$ terms in Eq. (19) are bad having nonvanishing matrix elements between the vacuum Ω and two-fermion states. It turns out that they are not covariant and should be removed by means of a consequent UT linear in them. Thus, unlike the meson mass renormalization only the particle-conserving part of the nucleon mass counterterm (responsible for one fermion \rightarrow one fermion transition) may be cancelled via one and the same clothing UT.

4. Comparison with an explicitly covariant calculation. Elimination of divergences in the S -matrix

The considered procedure enables us to remove from the Hamiltonian in CPR not only "bad" terms. Simultaneously, "good" two-particle terms are eliminated too being compensated with corresponding mass counterterms. Along the guideline some ultraviolet divergences inherent in the conventional form of H cannot appear in the S -matrix. In the context, let us recall Dyson expansion for the S operator,

$$S = 1 - i \int_{-\infty}^{\infty} dt_1 H_I(t_1) + (-i)^2 \frac{1}{2!} \int_{-\infty}^{\infty} dt_1 \int_{-\infty}^{\infty} dt_2 P [H_I(t_1) H_I(t_2)] + \dots, \quad (25)$$

where, as usually, $H_I(t) = \exp[iH_F t] H_I(a) \exp[-iH_F t]$ is an interaction in Dirac (D) picture. To be definite, we consider the interacting neutral pion and nucleon fields with the operator $H_I(\alpha) = V(\alpha) + M_{ren}(\alpha)$ (see Eqs.(12) and (17)) and matrix elements $\langle f | S^{(2)} | i \rangle$ of the S operator in g^2 -order, sandwiched between initial and final $\pi^0 N$ states,

$$|i\rangle = a^\dagger(\mathbf{k}) b^\dagger(\mathbf{p}, r) \Omega_0, \quad |f\rangle = a^\dagger(\mathbf{k}') b^\dagger(\mathbf{p}', r') \Omega_0. \quad (26)$$

We are interested in competition between fermion mass renormalization contribution to $S^{(2)}$ and the so-called fermion self-energy diagram contribution:

$$\langle f | S_{SE}^{(2)} | i \rangle = -\frac{g^2}{(2\pi)^3} m^2 I_F(p) \frac{\delta(\mathbf{p}' - \mathbf{p})}{E_p} \delta(\mathbf{k}' - \mathbf{k}) \delta(E_{p'} + \omega_{k'} - E_p - \omega_k) \delta_{r'r}, \quad (27)$$

$$I_F(p) = \int \frac{d^4 q}{q^2 - \mu^2 + i0} \left\{ 1 - \frac{p(p-q)}{m^2} \right\} \frac{1}{(p-q)^2 - m^2 + i0},$$

or

$$I_F(p) = \int d\mathbf{q} \int_{-\infty}^{\infty} dq_0 \frac{1}{q_0^2 - \omega_q^2 + i0} \left\{ 1 - \frac{p_0(p_0 - q_0) - \mathbf{p}(\mathbf{p} - \mathbf{q})}{m^2} \right\} \frac{1}{(p_0 - q_0)^2 - E_{\mathbf{p}-\mathbf{q}}^2 + i0}.$$

The "forward-scattering" process associated with this diagram would be responsible for appearance of certain infinity in $\pi^0 N$ scattering amplitude $\langle f | T | i \rangle$. Following a common practice, the divergence should be compensated by $\langle f | M_{ferm}^{(2)}(\alpha) | i \rangle$ piece, viz., it is required that

$$2\pi i \langle f | M_{ferm}^{(2)}(\alpha) | i \rangle \delta(E_f - E_i) = \langle f | S_{SE}^{(2)} | i \rangle. \quad (28)$$

At this point, one should emphasize that similar well-known steps become unnecessary if from the beginning we operate with clothed particle representation $K(\alpha_c)$ of Hamiltonian $H(\alpha)$. This new form of H does not contain ultraviolet divergences and, being constructed via sequential unitary transformations, gives new unitarily equivalent forms of the S operator (see [4, 5]). It is important that the approach enables us to evaluate one and the same S matrix with nonperturbative methods.

Now, by taking into account pole disposition for propagators involved and carrying out q_0 -integration, one can get,

$$\langle f | S_{SE}^{(2)} | i \rangle = \frac{\pi i}{2} \frac{g^2}{(2\pi)^3} \frac{\delta(\mathbf{p}' - \mathbf{p})}{E_p} \delta(\mathbf{k}' - \mathbf{k}) \delta(E_{p'} + \omega_{k'} - E_p - \omega_k) \delta_{r'r}$$

$$\times \int \frac{d\mathbf{q}}{E_{\mathbf{p}-\mathbf{q}}\omega_{\mathbf{q}}} \left\{ \frac{m^2 - E_{\mathbf{p}}E_{\mathbf{p}-\mathbf{q}} + \mathbf{p}(\mathbf{p}-\mathbf{q})}{E_{\mathbf{p}} - E_{\mathbf{p}-\mathbf{q}} - \omega_{\mathbf{q}}} - \frac{m^2 + E_{\mathbf{p}}E_{\mathbf{p}-\mathbf{q}} + \mathbf{p}(\mathbf{p}-\mathbf{q})}{E_{\mathbf{p}} + E_{\mathbf{p}-\mathbf{q}} + \omega_{\mathbf{q}}} \right\}. \quad (29)$$

The three-dimensional integral in (29) coincides with integral $I(p)$ defined by Eq. (23). Hence, one can write

$$\langle f | S_{SE}^{(2)} | i \rangle = \frac{\pi i}{2} \frac{g^2}{(2\pi)^3} I(p) \frac{\delta(\mathbf{p}' - \mathbf{p})}{E_{\mathbf{p}}} \delta(\mathbf{k}' - \mathbf{k}) \delta(E_{\mathbf{p}'} + \omega_{\mathbf{k}'} - E_{\mathbf{p}} - \omega_{\mathbf{k}}) \delta_{r'r}. \quad (30)$$

It follows from (27) and (30) that

$$I_F(p) = -\frac{\pi i}{2m^2} I(p), \quad (31)$$

i.e., we have found another proof of the p -independence of $I(p)$ since $I_F(p)$ is an explicitly covariant quantity. Besides, we have expressed the Feynman one-loop integral $I_F(p)$ through other covariant integrals $I_1(p)$ and $I_2(p)$.

5. Some general links

Let us consider the momentum independence in question from a general point of view, viz., for the one-particle matrix elements

$$\langle \mathbf{k}' | S | \mathbf{k} \rangle = \langle \mathbf{k}' | [1 + S^{(1)} + S^{(2)} + \dots] | \mathbf{k} \rangle$$

to be definite between the spinless (pion) states $|\mathbf{k}\rangle = a^\dagger(\mathbf{k}) |\Omega_0\rangle$. We are interested in

$$\langle \mathbf{k}' | S^{(2)} | \mathbf{k} \rangle = -2\pi i \delta(\omega_{\mathbf{k}'} - \omega_{\mathbf{k}}) \langle \mathbf{k}' | T^{(2)}(\omega_{\mathbf{k}}) | \mathbf{k} \rangle$$

with the second order T -operator

$$T^{(2)}(\omega_{\mathbf{k}}) = V(\omega_{\mathbf{k}} + i0 - H_F)^{-1} V$$

To set links with previous results it is sufficient to note that

$$\frac{1}{2} \langle \mathbf{k}' | [R_1, V] | \mathbf{k} \rangle = \langle \mathbf{k}' | V(\omega_{\mathbf{k}} + i0 - H_F)^{-1} V | \mathbf{k} \rangle \quad (32)$$

if pion mass $\mu < 2m$. In particular, it means that within the considered model for V the propagator with intermediate nucleon-antinucleon states in Eq. (32) is not singular. Then, according to [2], the generator R_1 is

$$R_1 = -i \lim_{\varepsilon \rightarrow 0+} \int_0^{\infty} dt V_D(t) e^{-\varepsilon t},$$

and proof of Eq. (32) is trivial. Here, as usually, $V_D(t) = \exp[iH_F t] V \exp[-iH_F t]$.

Using translational invariance of V , one can show that

$$\langle \mathbf{k}' | V(\omega_{\mathbf{k}} + i0 - H_F)^{-1} V | \mathbf{k} \rangle = \frac{\delta(\mathbf{k}' - \mathbf{k})}{\omega_{\mathbf{k}}} G(k),$$

where $G(k)$ is a function of the four-momentum $k = (\omega_{\mathbf{k}}, \mathbf{k})$. Indeed, putting $V = \int dx V(\mathbf{x})$ with the interaction density $V(\mathbf{x})$ in the D picture being the Lorentz scalar

$$U(\Lambda) V_D(x) U^{-1}(\Lambda) = V_D(\Lambda x), \quad (33)$$

and using

$$(\omega_{\mathbf{k}} + i0 - H_F)^{-1} = -i \lim_{\epsilon \rightarrow 0^+} \int_0^{\infty} dt e^{i(\omega_{\mathbf{k}} + i\epsilon - H_F)t},$$

we arrive at

$$G(k) = -i (2\pi)^3 \frac{1}{2} \lim_{\epsilon \rightarrow 0^+} \int_{-\infty}^{\infty} dt e^{-\epsilon|t|} \int d\rho \langle \Omega_0 | a(k) V_D\left(\frac{1}{2}\rho\right) V_D\left(-\frac{1}{2}\rho\right) a^\dagger(k) | \Omega_0 \rangle.$$

Here, as in [2], we are addressing operators $a(k) = \sqrt{\omega_{\mathbf{k}}} a(\mathbf{k})$ that meet the covariant commutation rules

$$[a(k), a^\dagger(k')] = \omega_{\mathbf{k}} \delta(\mathbf{k}' - \mathbf{k}).$$

It results in appearance of a typical combination

$$-2\pi i \frac{\delta(\omega_{\mathbf{k}'} - \omega_{\mathbf{k}}) \delta(\mathbf{k}' - \mathbf{k})}{\omega_{\mathbf{k}}} G(k)$$

in the correspondent S -matrix element. Thus, $G(k)$ is independent on k . At this point, let us recall the relativistic invariance property

$$\frac{\langle k' | S | k \rangle}{\sqrt{\omega_{\mathbf{k}'} \omega_{\mathbf{k}}}} = \frac{\langle \Lambda k' | S | \Lambda k \rangle}{\sqrt{\omega_{\mathbf{k}'_\Lambda} \omega_{\mathbf{k}_\Lambda}}}.$$

In its turn, the meson mass shift can be connected with the c -number $G(k) = G(\mu, 0, 0, 0)$ in evaluating the one-meson matrix elements in the l.h.s. of Eq. (32).

This consideration gives us a possible (probably, general) way when finding the momentum independence of mass shifts within this three-dimensional formalism, at least, in the first nonvanishing order in coupling constant.

6. Summary

We have demonstrated here how the mass shifts in the system of interacting pion and nucleon fields can be calculated by the use of the clothed particle representation. The respective mass counterterms are compensated and determined directly in the Hamiltonian.

The procedure described above has an important feature, viz., the mass renormalization is made simultaneously with the construction of a new family of quasipotentials (Hermitian and energy independent) between the physical particles (the quasiparticles of the method). Explicit expressions for the quasipotentials can be found in [2, 9].

By using a comparatively simple analytical means, we could show that the three-dimensional integrals, which determine the pion and nucleon renormalizations in the second order in the coupling constant g , can be written in terms of the Lorentz invariants

composed of the particle three-momenta. In other words, these integrals are independent of the particle momentum.

The experience acquired has allowed us, on the one hand, to reproduce the manifestly covariant result by Feynman techniques and, on the other hand, to derive a new representation for the Feynman integral that corresponds to the fermion self-energy diagram. Of course, here we are dealing with the coincidence of the two divergent quantities: one of them is determined by the nucleon mass renormalization one-loop integral, while the other stems from the commutator $[R, V]$. We are trying to overcome this drawback by means of the introduction of the cutoff functions in momentum space. Such functions have certain properties to do the theory to be satisfied the basic symmetry requirements.

References

- [1] A.V. Shebeko and M.I. Shirokov, *Prog. Part. Nucl. Phys.* **44**, 75 (2000).
- [2] A.V. Shebeko and M.I. Shirokov, *Phys. Part. Nucl.* **32**, 31 (2001).
- [3] M.I. Shirokov, Preprint P2-2000-277, Dubna, 2000.
- [4] A.V. Shebeko, In: Proc. the 16th International Baldin Seminar on High Energy Physics Problems (10-15 June 2002, Dubna, Russia).
- [5] A.V. Shebeko, *Nucl. Phys.* **A737**, 252 (2004).
- [6] E. Stefanovich, *Ann. Phys.* **292**, 139 (2001).
- [7] A.Yu. Korchin and A.V. Shebeko, *Phys. At. Nucl.* **56**, 1663 (1993).
- [8] A. Krüger and W. Glöckle, *Phys. Rev.* **C60**, 024004 (1999).
- [9] A.V. Shebeko and V.Yu. Korda, Contribution to the 16th International Baldin Seminar on High Energy Physics Problems (10-15 June 2002, Dubna, Russia). Book of abstracts, p. 42.
- [10] V.Yu. Korda, L. Canton and A.V. Shebeko. Contribution to 17th International IU-PAP Conference on Few-Body Problems in Physics (5-10 June 2003, TUNL, Durham, NC, USA). Book of abstracts, p. 113.
- [11] V.Yu. Korda and A.V. Shebeko, *Phys. Rev.* **D70**, 085011 (2004).

ELECTROPRODUCTION OF VECTOR MESONS AT SMALL x

S.V. Goloskokov[†]

*BLTP, Joint Institute for Nuclear Research
Dubna 141980, Moscow region, Russia*

† E-mail: goloskko@thsun1.jinr.ru

Abstract

Vector meson electroproduction is analyzed within the two-gluon (2G) model and the generalized parton distribution (GPD) approach at small x -Bjorken. We demonstrate that 2G and GPD models are not completely equivalent. At the same time, both models are in reasonable agreement with available experimental data on light vector meson electroproduction.

1. Vector meson production in 2G and GPD models

This report is devoted to investigation of vector meson electroproduction at small Bjorken x and large photon virtuality. In the low - x region the predominant contribution to the process is determined by the 2G exchange and the vector meson is produced via the photon-two-gluon fusion. At large Q^2 the cross section for the vector meson production is dominated by the $\gamma_L^* \rightarrow V_L$ amplitude which factorizes [1] into a hard meson photoproduction off gluons, and GPD. The amplitudes of $\gamma_\perp^* \rightarrow V_\perp$ and the $\gamma_\perp \rightarrow V_L$ transitions which are important in polarized observables are suppressed as a power of $1/Q$ and exhibit infrared singularities [2]. Similar properties of vector meson production amplitudes were found within the 2G model by several authors [3]. Calculation of these higher twist amplitudes requires a regularization scheme which depends on a model. The modified perturbative approach (MPA) [4] which includes the transverse quark motion gives possible ways of regularizing these end-point singularities. In this report, the MPA is used to study amplitudes of vector meson electroproduction for longitudinally and transversely polarized photons within the 2G and GPD models. Singularities in the amplitudes occurring in collinear approximation are regularized by the transverse quark momentum.

The leading twist term of the wave function gives a vanishing contribution to the amplitudes with a transversally polarized vector meson in the massless limit. To calculate these amplitudes, it is necessary to include in consideration the higher twist terms in the wave function. In this report, we use the k -dependent wave function [5]

$$\hat{\Psi}_V = g[(\not{V} + M_V)\not{E}_V + \frac{2}{M_V}\not{V}\not{E}_V\not{K} - \frac{2}{M_V}(\not{V} - M_V)(E_V \cdot K)]\phi_V(k_\perp^2, \tau). \quad (1)$$

Here V is a momentum and M_V is a mass of a vector meson, E_V is its polarization, τ is a fraction of momentum V carried by the quark, and K is its transverse momentum: $K^2 = -k_\perp^2$. The first term in (1) represents the standard wave function of the vector meson. The leading twist contribution to the longitudinal vector meson polarization is determined by the $M_V\not{E}_V$ term in (1). The k -dependent terms of the wave function are essential for the amplitude with transversely polarized light mesons.

Let us consider vector meson production in MPA within the 2G model. The leading over s term of the $\gamma^* \rightarrow V$ amplitude is mainly imaginary. The imaginary part of the amplitude can be written as an integral over τ and k_\perp and has the form [6, 7]

$$T_{\lambda_V, \lambda_\gamma}^V = N \int d\tau \int dk_\perp^2 \frac{H^g(\xi, \xi, t) \phi_V(k_\perp^2, \tau) A_{\lambda_V, \lambda_\gamma}(\tau, k_\perp^2)}{(k_\perp^2 + \bar{Q}^2)^3}, \quad (2)$$

where N is the normalization constant, $\bar{Q}^2 = \tau\bar{\tau}Q^2$, $\bar{\tau} = 1 - \tau$. Positive proton helicities are omitted here for simplicity. In calculation of (2) the Feynman gauge is used and t -channel gluons are polarized longitudinally. The function $H^g(\xi, \xi, t)$ is connected to the gluon GPD at $x = \xi$ point [7], where skewness ξ is related to Bjorken- x by $\xi \simeq x/2$. The meson wave function ϕ_V is used in a simple Gaussian form [8]

$$\phi_V(k_\perp^2, \tau) = 8\pi^2 \sqrt{2N_c} a_V^2 \exp \left[-a_V^2 \frac{\mathbf{k}_\perp^2}{\tau\bar{\tau}} \right]. \quad (3)$$

Transverse momentum integration of (3) leads to the asymptotic form of a meson distribution amplitude $\phi_V^{AS} = 6\tau\bar{\tau}$.

The hard amplitudes $A_{\lambda_V, \lambda_\gamma}$ in (2) are calculated perturbatively. The $\gamma_L^* \rightarrow V_L$ amplitude has the form [7]

$$A_{L,L} = 4 \frac{s}{\sqrt{\bar{Q}^2}} \left[\bar{Q}^2 + k_\perp^2 (1 - 4\tau\bar{\tau}) \right] \left(\bar{Q}^2 + k_\perp^2 \right). \quad (4)$$

For the amplitude with transversely polarized photons and vector mesons we find

$$A_{T,T} \sim \frac{2s}{M_V} \bar{Q}^2 \left[k_\perp^2 (1 + 4\tau\bar{\tau}) + 2M_V^2 \tau\bar{\tau} \right] (E_\perp^\gamma E_\perp^V). \quad (5)$$

For the light meson production the resulting amplitude is proportional to k_\perp^2 . The term proportional to M_V^2 appears in the amplitude for heavy mesons too.

The $\gamma_T^* \rightarrow V_L$ transition amplitude is determined by the function

$$A_{L,T} \sim \frac{2s}{M_V} \bar{Q}^2 \left[2M_V^2 \tau\bar{\tau} - k_\perp^2 (1 - 2\tau) \right] \frac{(E_\perp^\gamma r_\perp)}{M_V}. \quad (6)$$

It can be found that if we omit the k^2 terms in the denominator of (2), the $T_{T,T}$ and $T_{L,T}$ amplitudes will have the end-point singularities at $\tau(\bar{\tau}) = 0$ [7]. All amplitudes in the 2G model are mainly imaginary. The real part of the amplitude can be obtained from the imaginary part using the derivative rule

$$\text{Re } T \sim -\frac{\pi}{2} \frac{d}{d \ln x} \text{Im } T. \quad (7)$$

The real parts of the amplitudes are small, about 30% with respect to its imaginary part.

The vector meson electroproduction can be studied within the GPD approach at large photon virtuality Q^2 . At small Bjorken- x we shall consider as before the predominated gluon contribution. The $\gamma_L^* \rightarrow V_L$, $\gamma_T^* \rightarrow V_T$, $\gamma_T^* \rightarrow V_L$ amplitudes are calculated within the MPA. In the GPD model we consider the Sudakov suppression of large quark-antiquark separations. These effects provide additional suppression of contributions from

the end-point regions, in which one of the quarks entering into the meson wave function becomes soft and factorization breaks down. As previously, including the transverse quark momenta regularizes singularities and gives a possibility of calculating the transition amplitudes at large Q^2 which are important for polarized observables. The amplitudes $\gamma_{\mu}^* p \rightarrow V_{\mu} p$ can be represented in the form [9]:

$$T_{\mu',\mu} = \frac{e}{2} C_V \int_0^1 \frac{d\bar{x}}{(\bar{x} + \xi)(\bar{x} - \xi + i\epsilon)} \times \left\{ \left[\mathcal{H}_{\mu'+,\mu+}^{(g)} + (-1)^{\mu'+\mu} \mathcal{H}_{-\mu'+,-\mu+}^{(g)} \right] H^g(\bar{x}, \xi, t) \right\}, \quad (8)$$

The flavor factor for ρ -meson production is $C_{\rho} = 1/\sqrt{2}$.

The hard scattering amplitudes \mathcal{H} in (8) are written for the positive transverse gluon polarization and can be represented as a convolution of the hard part $A_{\mu',\mu}^{(g)}$, which is calculated perturbatively, and the wave function (3)

$$\mathcal{H}_{\mu'+,\mu+}^{V(g)} = \frac{2\pi\alpha_s(\mu_R) f_V}{N_c} \int_0^1 d\tau \int \frac{d^2\mathbf{k}_{\perp}}{16\pi^3} \phi_V(k_{\perp}^2, \tau) A_{\mu',\mu}^{(g)}(x, \xi, \mathbf{k}_{\perp}, Q^2). \quad (9)$$

Here the scale μ_R is determined by the largest mass scale appearing in the hard scattering amplitude: $\mu_R = \max\{\tau Q, \bar{\tau} Q, \dots\}$.

2. Amplitude structure and description of experiment

The GPD model leads to the following form of helicity amplitudes

$$T_{LL} \propto 1; \quad T_{TT}^{V(g)} \propto \frac{|\mathbf{k}_{\perp}|}{Q}; \quad T_{TL}^{V(g)} \propto \frac{\sqrt{-t}}{Q}. \quad (10)$$

This behavior is similar to those obtained in the 2G model.

The 2G and GPD approaches are hoped to be equivalent at small x . Unfortunately, the amplitude structure in the models are not equivalent. As mentioned before, in the 2G model all amplitudes are mainly imaginary. In the GPD approach the integration over x occurs in (8)

$$\begin{aligned} T^{V(g)} &\sim \int_0^1 \frac{d\bar{x} H(\bar{x})}{(\bar{x} + \xi)(\bar{x} - \xi + i\epsilon)} = I(\bar{x} < \xi) + I(\bar{x} > \xi) \\ &= \int_0^{\xi} \frac{d\bar{x} H(\bar{x})}{(\bar{x} + \xi)(\bar{x} - \xi + i\epsilon)} + \int_{\xi}^1 \frac{d\bar{x} H(\bar{x})}{(\bar{x} + \xi)(\bar{x} - \xi + i\epsilon)} \end{aligned} \quad (11)$$

For the nonflip T_{LL} and T_{TT} amplitudes we have no singularities in integrated functions $H(\bar{x})$, and both $I(\bar{x} < \xi)$ and $I(\bar{x} > \xi)$ contribute to the Re part of amplitude. These integrals are not small, have different signs and compensate each other mainly. As a result, the real part of the LL and TT amplitudes is quite small and is consistent with the one obtained from (7). In the case of the T_{LT} amplitude we have quite a different result. In this case, we find an additional coefficient $1/\sqrt{s u} \propto 1/\sqrt{\bar{x}^2 - \xi^2}$ in the hard amplitude H in (11) which becomes imaginary in the $\bar{x} < \xi$ integration region. Consequently, the real

part of the T_{LT} amplitude is determined only by $I(\bar{x} > \xi)$ integral. This contribution is not small and we find that $\text{Re } T_{LT} > \text{Im } T_{LT}$ for this amplitude. Thus, properties of the T_{LT} amplitude in the 2G and GPD models are quite different. It is difficult to imagine that these amplitudes might be equivalent at small x .

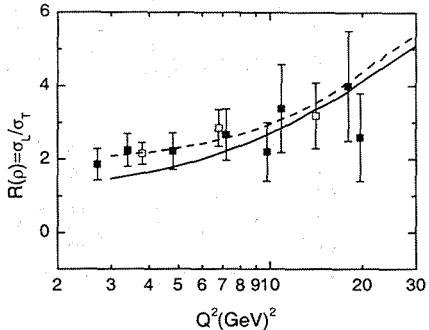
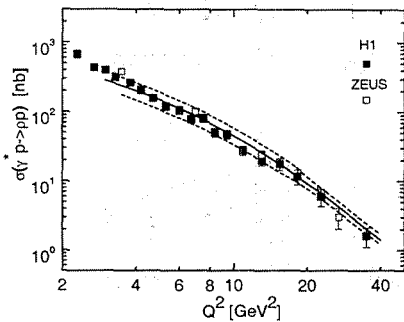


Figure 1: Left: The cross section for $\gamma^* p \rightarrow \rho^0 p$ vs. Q^2 for fixed values of $\langle W \rangle = 75$ GeV. Full line- GPG model results. Dashed lines show the μ_R sensitivity. Data are from [10, 11]

Figure 2: Right: Q^2 dependence R of ρ production at $\langle W \rangle = 75$ GeV. Full curve -2G model, dashed curve -GPD results. Data are from [10, 11]

Let us consider the description of experimental data in the 2G and GPD models. In both the cases we have the a_v parameter in the wave function which determines the average value of $\langle k_1^2 \rangle$ in hard subprocess. In the numerical evaluation of meson electroproduction a reasonable description of experimental data is obtained for $a_\rho = 0.8$ GeV $^{-1}$ in the 2G model and for $a_\rho = 0.52$ GeV $^{-1}$ in the GPD model. The parameter f_v is determined by the standard value and for ρ meson production we use $f_\rho = 0.216$ GeV. Estimations of the amplitudes are carried out using the $\Lambda_{QCD} = 0.22$ GeV. The cross section for $\gamma^* p \rightarrow \rho p$ production integrated over t is shown in Fig. 1 (full line). Good agreement with experiment is to be observed. The results for ϕ production can be found in [9]. It is important to analyse the dependence of cross section on the scale μ_R . The results for cross section for $\bar{\mu}_R = \{\sqrt{2}\mu_R, \mu_R/\sqrt{2}\}$ are shown in Fig.1 by dashed lines. It can be seen that the $\bar{\mu}_R$ sensitivity of the cross section is of the order of experimental errors.

Using the calculated amplitudes we can determine contributions to the cross section with longitudinal and transverse photon polarization and its ratio as

$$N_L = |T_{LL}^V|^2, \quad N_T = |T_{TT}^V|^2 + |T_{LT}^V|^2, \quad R = \frac{N_L}{N_T}. \quad (12)$$

Note that in (12) summation over proton helicities is assumed. We omit here the T_{TL} and T_{-TT} amplitudes which are small in the models. In terms these quantities the spin-density matrix elements (SDME) can be defined, e.g.

$$r_{00}^{04} = \frac{1}{N_T + \varepsilon N_L} (|T_{LT}^V|^2 + \varepsilon |T_{LL}^V|^2). \quad (13)$$

The model results for the ratio of cross section R are shown in Fig. 2. For both the

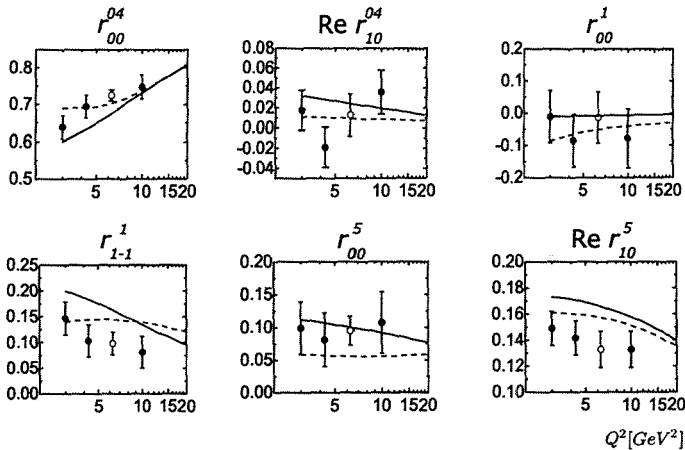


Figure 3: Q^2 dependence SDME of ρ production at $\langle -t \rangle = 0.15 \text{ GeV}^2$ and $\langle W \rangle = 75 \text{ GeV}$. Full curve -2G model, dashed curve -GPD results. Data are taken from [10, 11]

models this ratio is growing with Q^2 and is consistent with experiment. In Fig.3, we show six essential SDME. In the approximation, when we put the T_{TL} and T_{TT} amplitudes to be zero, the other SDME are connected with the matrix elements from Fig. 3 or equal to zero. The description of experimental data in both the models is reasonable.

We would like to note that from the data on $d\sigma/dt$ the diffraction peak slope $B \sim 6 \text{ GeV}^{-2}$ at $Q^2 \sim 5 \text{ GeV}^2$ can be determined [10, 11]. This value is connected with the diffraction peak slope of the T_{LL} amplitude because its contribution to the cross section is most essential. The diffraction peak slopes of the T_{TL} and T_{TT} amplitudes are not well defined. In calculation of spin observables we suppose that the diffraction peak slope $B_{LT} \sim B_{LL}$ and B_{TT} might be different. The slope $B_{TT} \sim B_{LL}$ in the 2G model and $B_{TT} \sim B_{LL}/3$ in the GPD model is used. Predictions of both the models are in agreement with the known t -dependence of experimental data at small momentum transfer [10]. The results found in [3] are very close to estimations obtained here within the 2G model (Fig.3).

3. Conclusion

Light vector meson electroproduction at small x was analyzed in this report within the 2G and GPD models. In both the models the amplitudes were calculated using MPA and the wave function (1) which consider the transverse quark momentum. By including the higher twist effects k_{\perp}^2/Q^2 in the denominators of $T_{\lambda_V, \lambda_\gamma}^V$ in (2) we regularize the end-point singularities in the amplitudes with transversally polarized photons. It was found that the 2G and GPD models, which are expected to be equivalent at small x , lead to similar results for the leading twist T_{LL} amplitude. At the same time, properties of the amplitudes suppressed as a power of $1/Q$ are different in the models. This was demonstrated here for the T_{LT} amplitude. Thus, the 2G and GPD models are not completely equivalent at small x . It was shown that the diffraction peak slopes of the T_{TT} and T_{LT} amplitudes are not

well defined. The knowledge of these slopes is essential in analyses of SDME. Information about B_{TT} and B_{LT} can be obtained from t -dependence of SDME.

At the same time, both approaches lead to an accurate description of the cross section for the light meson production. We found a reasonable results for SDME and R ratio in the 2G and GPD models. This means that at the present time we have two solutions for the scattering amplitudes which are in agreement with existing experimental data. Unfortunately, all data on spin observables have now large experimental errors. This does not permit one to determine which model is relevant to experiment. To clarify the situation, an additional theoretical study of the T_{TT} and T_{LT} amplitudes is needed. An experimental investigation to reduce errors in SDME is extremely important. Study of t dependence of SDME can give important information on either diffraction peak slopes in helicity amplitudes are of the same order of magnitude or different.

This work is supported in part by the Russian Foundation for Basic Research, Grant 03-02-16816 and by the Heisenberg-Landau program.

References

- [1] X. Ji, Phys. Rev. **D55**, 7114 (1997); A.V. Radyushkin, Phys. Lett. **B380**, 417 (1996); J.C. Collins *et al.*, Phys. Rev. **D56**, 2982 (1997).
- [2] L. Mankiewicz and G. Piller, Phys. Rev. **D61**, 074013 (2000); I.V. Anikin and O.V. Teryaev, Phys. Lett. **B554**, 51 (2003).
- [3] D.Yu. Ivanov and R. Kirschner, Phys.Rev. D **59**, 114026 (1998); E.V. Kuraev, N.N. Nikolaev and B.G. Zakharov, JETP Lett. **68**, 696 (1998); I.P. Ivanov and N.N. Nikolaev, JETP Lett. **69**, 294 (1999); I. Royen and J.-R. Cudell, Nucl. Phys. B **545**, 505 (1999).
- [4] J. Botts and G. Sterman, Nucl. Phys. **B325**, 62 (1989).
- [5] J. Bolz, J.G. Körner and P. Kroll, Z. Phys. **A350**, 145 (1994).
- [6] A.D. Martin, M.G. Ryskyn and T. Teubner, Phys. Rev. **D60**, 014022 (2000);
- [7] S.V. Goloskokov, Proc of X-th Workshop On High Energy Spin Physics, Dubna, September 2003, hep-ph/0312353.
- [8] R. Jakob and P. Kroll, Phys. Lett. **B315**, 463 (1993); Err-ibid. **B319**, 545 (1993).
- [9] S.V. Goloskokov, P. Kroll, and B. Postler, Proc of DIS03 workshop, St. Petersburg, April 2003, p. 243; hep-ph/0308140; S.V. Goloskokov, P. Kroll, to appear in Proc of Spin 2004 Symposium, October 2004, Trieste, Italy; hep-ph/0411251; S.V. Goloskokov, P. Kroll, hep-ph/0501242;
- [10] C. Adloff *et al.* [H1 Collaboration], Eur. Phys. J. **C13**, 371 (2000).
- [11] J. Breitweg *et al.* [ZEUS Collaboration], Eur. Phys. J. **C6** 603, (1999); *ibid.* **C12**, 393 (2000).

THE INFLUENCE OF FRAGMENTATION MODELS IN PRODUCTION OF HADRON JETS IN ELECTRON-POSITRON ANNIHILATION

M.E. Zomorrodian

*Department of physics, School of Sciences, Ferdowsi university, Mashhad,
Islamic Republic of Iran, 91775-1436
E-mail: Zomorrod@Ferdowsi.um.ac.ir*

Abstract

The analysis of electron positron annihilations to hadrons in the range of energies below 60 GeV shows that apart from two jet events, there are also signs of three jet events which are interpreted according to the QCD, as a gluon radiating by a quark. However, the higher order diagrams lead to four jet events. In this paper, we investigate the fragmentation of quarks and gluons into hadron jets. Acoplanarity is a parameter for our analysis to four jet events. We expect that the Acoplanarity to be a nonzero value for our four jet events. This result is consistent with the results obtained by the Monte-Carlo and also by the results obtained at the other experiments as well as at the lower energies.

Keywords: hadron jets, Acoplanarity.

1. Introduction

Quantum Chromodynamics (QCD) successfully accounts for many features observed in high energy e^+e^- annihilation data, examples of which include violation of scaling in inclusive particle distributions, jet broadening, and multi-jet events. In the world of QCD, the sources of the experimentally observed jets are quarks and gluons. Jets initiated by quarks or antiquarks have been studied in great detail in various experiments. However little is known about jets which originate from high energy gluons. Bartel et al., [1] have presented evidences that particle distribution in three jet events originate from hard gluon bremsstrahlung ($e^+e^- \rightarrow q\bar{q}g$) are only described by models in which gluon jets of the same energy. In this paper we study the quark and gluon jet fragmentation properties, by using the most well known algorithm, JADE and DURHAM[2,3]. In section two we describe briefly the experimental procedure. In section 3 we define observable, followed by physics results in section 4. Section 5 includes our conclusions.

2. Experimental procedure

The AMY detector (Fig1) consists of a tracking detector and shower counter inside a 3-T solenoid magnetic coil which is surrounded by a steel flux return yoke followed by a muon detection system. The charged - particle tracking detector consists of a 4 layer

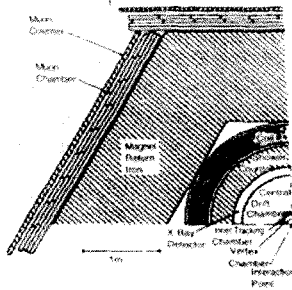


Figure 1:

cylindrical array of drift tubes (inner tracking chamber, or ITC) and a 40 - layer cylindrical drift chamber (central drift chamber, or CDC) with 25 axial layers of wires and 15 stereo layers. Charged particles are detected efficiently over the polar angle region $\cos\theta$ with a momentum resolution $\frac{\Delta P_T}{P_T} = 0.7\% \times [P_T(\text{GeV}/c)]$. Radially, outside of the CDC is a 15-radiation-length cylindrical electromagnetic calorimeter (barrel shower counter, or SHC) which serves as a photon detector. The detector fully covers the angular region $\cos\theta < 0.73$. Selection of multi-hadron final states from e^+e^- annihilation was based on the charged particle momenta measured in the CDC and on the neutral-particle energy measured in SHC. Further details may be found in Ref.[11].

3. Definition of observables

Jets are defined by means of JADE clustering algorithm. For each pair of i and j , the quantity y_{ij} is calculated as

$$y_{ij} = \frac{2E_i E_j (1 - \cos\theta_{ij})}{E_{vis}^2} \quad (1)$$

where E_i and E_j are the particles energies, θ_{ij} is the angle between the momentum directions and E_{vis} is the total visible energy in the event. The pair with the smallest value of y_{ij} is found, and if this is below a given resolution parameter y_{cut} the pair is replaced by a pseudo-particle with four momentum $P^\mu = P_i^\mu + P_j^\mu$. The procedure is then repeated using the new set of particles and pseudo particles. When all the values of y_{ij} are greater than y_{cut} , the clustering procedure stops. Each particle in the event is uniquely associated with a cluster (jet).

As is well known, the number of jets separated in this way, in a given event may be different, in certain conditions, for different values of the test variable y_{cut} and the relative rate of multi-jet events is a strong function of y_{cut} . Nevertheless, as far as the jet finding conditions fulfil the requirement of being infrared and collinear safe and are simple enough for implementation in the experimental analysis and theoretical calculations, a reliable comparison of the data with the fixed order perturbative QCD calculations can be used. Another story is that within the class of jet finding algorithm some test variables and

recombination procedures can be implemented more naturally into the QCD calculations, especially for small y_{cut} values, when the logarithmic terms need to be identified and resumed to all orders of α_s before a reliable prediction can be made. It is for this reason that a new jet finding algorithm called the DURHAM algorithm has been proposed[3]. In this algorithm, relative transverse momentum replaces the invariant mass of the original JADE algorithm as the jet resolution variable, which is defined as

$$y_{ij} = \frac{2 \min\{E_i^2, E_j^2\}(1 - \cos \theta_{ij})}{E_{vis}^2} \quad (2)$$

the results obtained with this algorithm and especially the fraction of 3-jet events selected by them, depend on the value of y_{cut} .

However, qualitatively our conclusions presented below are valid for all reasonable values of y_{cut} . Therefore, only results obtained with the fixed values of $y_{cut}(\text{JADE})=0.02$ and $y_{cut}(\text{DURHAM})=0.008$ will be presented.

For a meaningful comparison of two algorithms the values of y_{cut} for them should be different because of their different definitions (1) and (2). The value of $y_{cut}(\text{DURHAM})=0.008$ has been determined by the requirement that the fraction of 3 jet events reconstructed by the two algorithms should be the same.

Finally we briefly describe the future of four jet events predicted by second order QCD. For this purpose we define the event shape parameter Acoplanarity[5] as

$$A = 4 \min(\sum_i |p_i^\perp| / \sum_i |p_i|)^2 \quad (3)$$

where the p_i are the particle or parton momenta and the p_i^\perp are their components perpendicular to a plane which is oriented such that the quantity in brackets is minimized. Whereas, before hadronization, two and three jet events have zero Acoplanarity, four-jet events in general are non-planar and give nonzero values for this parameter.

4. Physics Results

The difference between quark and gluon jets manifest themselves in the fragmentation function, defined as

$$x_E = \frac{E_{part}}{E_{jet}} \quad (4)$$

Figure 2 shows x_E distribution for quark and gluon jets. For both types of jets, fragmentation parameter decreases with the energy, but the difference between them implies a softer particle energy spectrum within the gluon jet.

Our results are also consistent with the results obtained at LEP energies[10].

Further, we show in figures 3 and 4 the multiplicity distribution for quark and gluon jets separately. By taking into account the statistical errors on the average values, the figures indicate that within a few standard deviations, the particles in the gluon jet have a higher multiplicity than the particles in the quark jet.

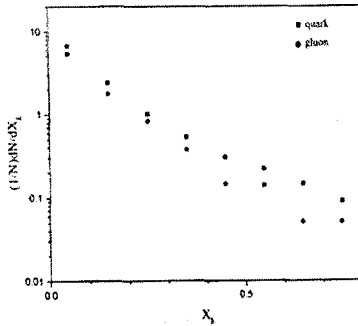


Figure 2: Fragmentation distribution for quark and gluon jets

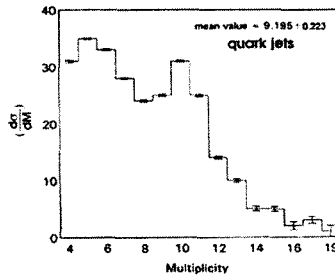


Figure 3: Multiplicity distribution for quark jets

Furthermore, the ratio of the two multiplicities is 1.304 ± 0.031 . This numerical value is in a good agreement with the OPAL results[8]. Our results are also consistent with the QCD theory[6,7].

Next, we study the properties of four jet events predicted by second order QCD. To achieve this, figure 5 shows the Acoplanarity distribution separately for two and three jet events (L23) and also for two, three, and inclusion of four jet events (L234). Both L23 and L234 are normalized to the total number of events. As the figure indicates, both distributions show a peaking at low Acoplanarity values, with a falling off distribution towards the higher values of the parameter. However we observe that L234 does not fall as fast as L23 by increasing Acoplanarity. This indicates that a small proportion of events is subject to two hard gluon radiations at wide angle by the quarks, which is predicted by second order QCD. We conclude that there is a possibility for radiation of two hard gluons in 60 GeV e^+e^- annihilations. This result is also consistent with the QCD theory.

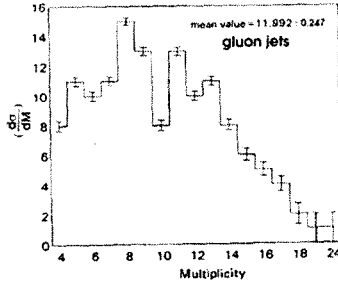


Figure 4: Multiplicity distribution for gluon jets

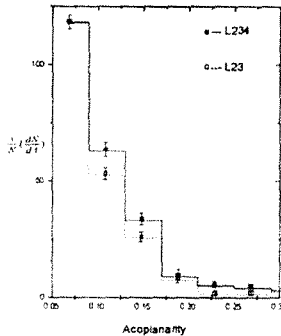


Figure 5: Acoplanarity distribution for two and three jet events (L23) as well as for two, three and four jet events (L234)

5. conclusions

In this paper we investigate fragmentation of charged particles in e^+e^- annihilation at 60 GeV center of mass energy in terms of the fragmentation parameter x_E and also in terms of multiplicity distributions.

In QCD, one expects quark and gluon jets to differ because of greater colour charge carried by the gluon. Quantitatively, therefore, one anticipates that gluon jets would have higher multiplicity, softer fragmentation and broader in angle. Our results are consistent with QCD theory.

We also report the experimental distribution in the parameter Acoplanarity which is sensitive to four jet structure, according to the second order QCD theory. The results we obtain for this parameter is also consistent with the results obtained for other experiments and also with the four jet events predicted by second order QCD[7,9].

Acknowledgments

I would like to acknowledge the KEK staff and the AMY collaboration for giving us the opportunity of using the AMY data for this analysis.

References

- [1] JADE Collab, W. Bartel et al., Phys.Lett., 123B, 460(1983), Z.Phys, C21, 37(1983).
- [2] JADE Collab, W. Bartel et al., Z.Phys , C33, 23(1986), S. Bethke et al., phys.Lett., B213, 235(1988).
- [3] S. Catani et al., Phys.Lett., B264, 432(1991).
- [4] Y. K. Kim et al., Phys.Rev.Lett., 63, 1772(1989).
- [5] B. Anderson et al., Phys. Lett., 94B, 211(1980).
- [6] P. Nason and B. R. Webber, Nucl.Phys., B421, 473(1995).
- [7] P. J. Rijken and W. L. Van Neerven, Phys.Lett., B386, 422(1996).
- [8] OPAL Collab, P. D. Acton et al., Z.Phys., C58, 387(1993).
- [9] JADE Collab, W. Bartel et al., Phys.Lett., B115, 338(1982).
- [10] JADE Collab, M. B. Lumenstengel et al., Phys.Lett., B517, 37(2001).
- [11] AMY Collab, T. umita et al., Phys.Rev., D42,1339(1990).

PHYSICAL NATURE OF LOBACHEVSKY PARALLEL LINES AND A NEW INERTIAL FRAME TRANSFORMATION

N.G. Fadeev

Joint Institute for Nuclear Research, Dubna, Russia

E-mail: fadeev@sunse.jinr.ru

Abstract

The synchronous process of particle motion and light beams propagation has been found to reveal a new physical equivalent for Lobachevsky parallel lines in the velocity space. The process revealed also its fruitfulness in solving in a new way the main problem in relativity - the problem of time synchronization for different space points [1]. The first obvious consequences of the new solution - such as simultaneity, proper time, inertial frame coordinate transformation and relativistic velocity summation law - are also presented in this paper.

1. Introduction

The Lobachevsky velocity space being adequate to the relativistic mechanics is widely used to study particle interaction processes in modern high energy physics [2]. The main Lobachevsky axiom, violating the Euclidean V-th postulate, is known as the geometrical equivalent of the experimental fact of the two photons pion decay $\pi^0 \rightarrow \gamma\gamma$ [3]. Due to the requirement of the constant light velocity principle its kinematics gives arise the Lobachevsky parallel lines (LPL) in the velocity space. But the dynamics of this decay mode is still not known and its kinematics gives nothing new for the relativistic mechanics except the demonstration of its properties.

As it has turned out there exists a new more fruitful physical equivalent for the LPL. Further developments of the approach published earlier in [4] have been described in this paper. We consider light propagation according to the Huygens principle and the independency of the light beams. So, the phenomena of light diffraction and interference are not considered. It is assumed that the time counting for a space point starts when a light front comes to that point. This is also the moment of a secondary light hemisphere emission, according to the Huygens principle. We accept the constant light velocity principle and we use the same plane light fronts as widely used to explain the light reflection and refraction phenomena. The basic knowledge of Lobachevsky geometry [2, 3, 5] is assuming.

2. Physical nature of Lobachevsky parallel lines

Let us consider two inertial frames K and K_s . Each of the frames may be associated with a particle. The space axes of both frames are parallel and K_s is moving with constant velocity V along the X -axis of frame K . It is assumed that their origins, O and O_s , coincide when the plane light front directed at the parallel angle θ_L reaches the point O

(a lateral beam is moving from bottom to top in XY -plane as shown in Fig.1a). At this initial moment a light sphere (hemisphere to the falling front) starts to spread out from O . The parallel angle θ_L is defined as

$$\cos \theta_L \equiv \cos \Pi(\rho/k) = th(\rho/k) = V/c \equiv \beta, \quad (k = c) \quad (1)$$

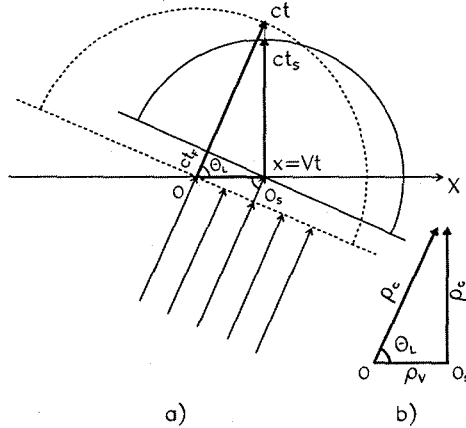


Figure 1: a) Synchronization of the K_s -motion (Vt) and the light rays (ct and ct_s) propagation by the side light beam. b) Lobachevsky parallel lines in the velocity space plane corresponding to synchronous motions of ct , ct_s and Vt in Euclidean plane ($c = 1$ is used for rapidities)

here β is the velocity V in units of c , ρ/k is a value of rapidity ρ in units of $k = c$, $\Pi(\rho/k) \equiv \theta_L$ is a parallel angle, k is the Lobachevsky constant, c is the velocity of light. The second equality $\beta = th(\rho/c)$ in (1) is known from the Beltrami model [2] and used to define a particle rapidity:

$$\rho/c = 1/2 \ln ((1 + \beta)/(1 - \beta)). \quad (2)$$

The first equality in (1) can be rewritten as

$$\theta_L \equiv \Pi(\rho/k) = 2 \operatorname{arctg} e^{-\rho/c}, \quad (3)$$

known as the Lobachevsky function. It is seen from (1) that for any rapidity (and its velocity) there is a definite angle θ_L . For the negative argument of the Lobachevsky function the parallel angle θ_L changes to $\pi - \theta_L$ [2], which corresponds to the same velocity but for the opposite direction.

Let us consider a space-time point $(x = Vt, t)$ in frame K . The light ray from the origin O will get to this point in time x/c (Einstein's signal) but the lateral beam's ray will come there first with some delay (relatively to O) in the moment of time t_F as

$$ct_F = x \cos \theta_L = Vt \cos \theta_L = ct \cos^2 \theta_L, \quad (4)$$

and then a new light sphere starts to spread out from the x -point. By the given moment of time t a new sphere will spread out to the radius

$$ct_s = ct - ct_F = ct - x \cos \theta_L = ct - xV/c, \quad t_s = t - xV/c^2, \quad (5)$$

and for $x = Vt$:

$$ct_s = ct - ct \cos^2 \theta_L = ct \sin^2 \theta_L = ct (1 - V^2/c^2), \quad (6)$$

where ct is the light sphere radius from origin O , so that $ct_s < ct$.

Let us choose two light rays from these two spheres: one, ct , emitted from O under the angle θ_L to the X -axis in some plane, and the other, ct_s , emitted from O_s (located at x) perpendicular to the X -axis in the same plane (see Fig.1a). Three segments ct, Vt and ct_s form a rectangular triangle. But two sides of triangle, ct and ct_s , have no common (intersection) point at no moment of time t , so they are parallel in any chosen Euclidean plane. As rapidity (2) for the light velocity is the infinity, then the obtained triangle transforms into the LPL or, more precisely, into the parallel lines in one side on the Lobachevsky plane in the velocity space as it is illustrated in Fig.1b.

Thus, the LPL in a velocity space corresponds to the light rays ct and ct_s emitted (according to the Huygens principle) from different points and different times and synchronized with particle motion Vt by the side light beam. The physical reason for the lack of intersection point in Euclidean space is the time delay t_F (see (4)). As the value of time delay t_F for given x and V is defined by c (with changing V the θ_L changes but not the c) then one can conclude that the basic reason for the V -th postulate violation in the velocity space is the constant light velocity principle.

To find out light rays corresponding to LPL in another side, one can consider a lateral beam to another direction (from top to bottom) in the same plane (as shown in Fig.2a and Fig.2b).

For light rays corresponding to the LPL (in both sides) for negative argument of Lobachevsky function (for $V < 0$), one should use a pair of lateral beams directed opposite to X -axis, i.e. from right to left (for $V > 0$ the beams were directed from left to right), as shown in Fig.2c and Fig.2d.

Thus, the moving reference frame (for $V > 0$ and/or $V < 0$) can be associated with the definite lateral light beams. The rest frame ($V = 0$) is associated with the direct beams at $\theta_L = \pi/2$ (as shown in Fig.2). Lobachevsky function has the same form for the rest frame and for the moving ones, i.e. it follows the principle of relativity. So, Lobachevsky function expresses the constant light velocity principle at $k = c$.

The synchronization method used to reveal the new physical nature of Lobachevsky parallel lines is also fruitful in solving the main problem of relativity - the problem of time synchronization for different space points.

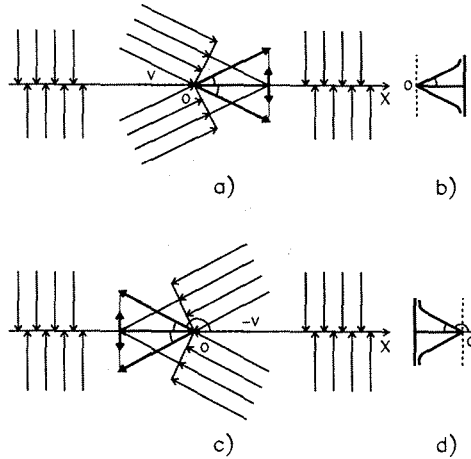


Figure 2: a) Two lateral light beams (for $V > 0$) give two pairs of light rays ct and ct_s for both sides of the plane (top and bottom), synchronous with K_s -motion Vt . b) Parallel lines in both sides on Lobachevsky plane, corresponding to synchronous motions in a). The plots for $V < 0$ are shown in c) and d)

3. x and t - coordinate transformation and light ether concept

Let us continue with the inertial frames K and K_s for $V > 0$. One can assume that a pair of direct beams (from top and bottom) reaches X -axis at the same moment of time as a pair of lateral beams (from left to right) reaches the point where both origins coincide. All x -points (including O) are "exited" simultaneously, and this moment of time is usually chosen as the initial one for K frame (the same for all coordinates). The initial moment of time for any x -point is delayed by t_F relative to the lateral beams (see (4)) so that time t_s at a given moment of time t (in K) is defined by (5). Thus, due to the synchronization of K and K_s frames (by the corresponding pairs of direct and lateral fronts) two moments of time, t and t_s , can be defined at any x point. For the chosen event (x, t) time t_s depends only on the velocity of the moving frame K_s .

Let us define the time t in the fixed frame via the distance ct passed by the light ray emitted from the point O at the parallel angle θ_L to X -axis in some plane. It is seen from Fig.1-Fig.3 that for any event (x, t) the delay time ct_F is just a projection of the given x -point on the chosen light ray ct .

Obviously, the displacement of K_s origin $Vt = ct \cos\theta_L$ is just a projection of the light ray ct on the X -axis. So, for any given coordinate x at a given time t a value x_s relative

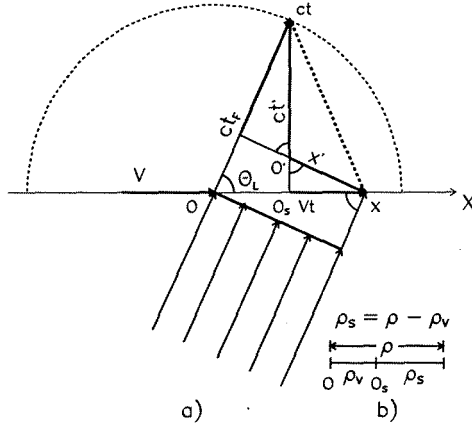


Figure 3: a) An illustration of the inertial frame x and t coordinate transformation (including Lorentz transformation). b) A velocity space diagram corresponding to x and t shifts. The x -coordinate is the x -position of a particle, moving with a velocity of $v = x/t$ in K frame by the moment of time t

to the origin O_s is

$$x_s = x - Vt = x - ct \cos \theta_L. \quad (7)$$

For any event ($x = Vt$, t) a relative coordinate is $x_s = 0$. It means that time t_s (see (5) and (6)) is the proper time of K_s , i.e. the time "measured" by means of a "moving clock", when one spectator observes the light sphere with the radius ct in K and in the same time t a moving spectator observes another light sphere with the radius ct_s (both spheres are triggered off by the lateral light beams). For the event (x, t) the corresponding moment of time t_s is the time "measured" by means of the "moving clock" located at the point x_s of K_s . Unlike of t in K , the time t_s defined for O_s is not all the same for the points on X_s -axis.

Indeed, from (4) one can see that the initial moment of time (provoked by the lateral light front) propagates along X -axis with the velocity v_F :

$$v_F \equiv x/t_F = c/\cos \theta_L = c^2/V = c/\beta > c. \quad (8)$$

So, for $0 < V < c$ any two events (x_1, t) and (x_2, t) have different time t_s in K_s . For $V \rightarrow 0$ ($\theta_L \rightarrow \pi/2$ for side beams) the velocity $v_F \rightarrow \infty$ and one comes to the Newton time $t_s \rightarrow t$, and for $V = c$ ($\theta_L = 0$) the proper time $t_s = 0$.

Thus, for any event (x, t) in K the corresponding coordinates in K_s are simple shifts (see (5) and (7)). To obtain the values of shifts, one should make symmetrical projections as described above.

We have used this symmetry to find out the Lorentz coordinates x' and t' for a moving frame. To get them, one has to find the crossing point O' of two perpendiculars producing the projections for any (x, t) event (see Fig.3). Then the length of the interval from O' to x corresponds to x' :

$$x' = (x - ct \cos \theta_L) / \sin \theta_L = (x - Vt) / \sqrt{1 - V^2/c^2}, \quad x_s = x' \sin \theta_L, \quad (9)$$

and the distance from O' to the ct corresponds to ct' :

$$ct' = (ct - x \cos \theta_L) / \sin \theta_L = (ct - xV/c) / \sqrt{1 - V^2/c^2}, \quad ct_s = ct' \sin \theta_L. \quad (10)$$

It is seen from (9) and (10) that primed and shifted coordinates are related as the corresponding projections. But the point O' , which is always considered as the origin of the moving frame, does not coincide in space with O_s . It is also seen that the line $O'x'$ is not parallel to the X -axis. So, it seems obvious that the primed values can not be regarded as the coordinates in a moving frame.

The distance between the given points x and ct (dashed line in Fig.3) can be defined via the primed and unprimed values:

$$l^2 \equiv c^2 t^2 + x^2 - 2ctx \cos \theta_L = c^2 t'^2 + x'^2 + 2ct'x' \cos \theta_L \equiv l'^2, \quad (11)$$

or as a sum of two terms, either as $l^2 = s_1^2 + s_2^2$ (to get it one should add $\pm x^2$ to the left part of (11) and $\pm x'^2$ to its right part), or as $l^2 = -s_1^2 + s_3^2$ (add $\pm c^2 t^2$ to the left part of (11) and $\pm c^2 t'^2$ to the right part), where:

$$s_1^2 = c^2 t^2 - x^2 = c^2 t'^2 - x'^2 = \gamma^2 (c^2 t_s^2 - x_s^2), \quad \gamma = 1/\sin \theta_L = 1/\sqrt{1 - V^2/c^2}, \quad (12)$$

$$s_2^2 = 2x(x - ct \cos \theta_L) = 2x'(x' \pm ct' \cos \theta_L), \quad s_3^2 = 2ct(ct - x \cos \theta_L) = 2ct'(ct' \pm x' \cos \theta_L). \quad (13)$$

Term s_1^2 is known as an invariant interval. Obviously, it is only a part of the full distance l^2 and is a result of cancelling of two equal values, either s_2^2 , or s_3^2 in the expressions for $l^2 = l'^2$. Terms s_2^2 and s_3^2 may differ by sign: (+)/(-) corresponds to the point O' located inside/outside the cone defined by the angle θ_L . For an event $(x = Vt, t)$ term s_2^2 is equal to zero (as $x_s = x' = 0$) and $s_3^2 = 2s_1^2$, so $l^2 \equiv s_1^2 \equiv l'^2$. The Lorentz coordinate transformations for this particular case have been usually presented in the manuals (e.g. [6]).

From (13) one can find (using the second formulae in (9, 10))

$$x = (x_s + ct_s \cos \theta_L) / \sin^2 \theta_L = (x_s + Vt_s) / (1 - V^2/c^2), \quad (14)$$

and

$$ct = (ct_s + x_s \cos \theta_L) / \sin^2 \theta_L = (ct_s + Vx_s/c) / (1 - V^2/c^2), \quad (15)$$

which are the reverse transformation from the moving frame to the rest frame. To check that, one can solve (5) and (7) for x and ct (once the factor $1/\sin \theta_L$ is inserted into the brackets then the terms in brackets became the lengths of perpendiculars corresponding to the mentioned projection symmetry).

It is seen from (5),(7) and (14-15) that the direct and reverse transformations are different: the latter could not be obtained by changing V to $-V$. This means that one

$y \sin \theta_L / c$ (since the secondary sphere starts to spread out from the first point). So, the light way difference is

$$c\Delta t \equiv \Delta y = y - y \sin \theta_L. \quad (16)$$

To compensate for this difference and make the initial moment of time counting caused by the lateral beam to be the same for x_s and y_s , the origin of K_s frame should be shifted along the Y -axis by the value of Δy (16). Then the y -coordinate in K_s frame is

$$y_s = y - \Delta y = y \sin \theta_L = y \sqrt{1 - V^2/c^2} \quad (17)$$

and the transverse coordinate

$$z_s = z - \Delta z = z \sin \theta_L = z \sqrt{1 - V^2/c^2}. \quad (18)$$

The reverse transformation is also obvious:

$$y = y_s / \sin \theta_L = y_s / \sqrt{1 - V^2/c^2}, \quad z = z_s / \sin \theta_L = z_s / \sqrt{1 - V^2/c^2}. \quad (19)$$

Then for the non-invariant interval (see(12)) one can get

$$c^2 t^2 - x^2 - y^2 - z^2 = \gamma^2 (c^2 t_s^2 - x_s^2 - y_s^2 - z_s^2). \quad (20)$$

So, for any event (x, y, z, t) in K there is the "parallel" event (x_s, y_s, z_s, t_s) corresponding to the moving K_s frame shifted in space and time in an appropriate way. These two sets of coordinates are related by the equation (20).

The obtained coordinate transformation leads to the contracted interval but this does not contradict to the relativistic velocity summation law. Since the energy-momentum transformation is a direct consequence of the velocity summation law, then the Lorentz energy-momentum transformation is valid in this approach [7]. Also in [7] relativistic effects considered in detail, and the four elements complex fraction invariant and a new wave equation in framework of this approach were proposed.

5. Conclusions

- A complete correspondence has been established between Lobachevsky parallel lines in the velocity space and the synchronous process of particle and light beams propagation in the Euclidean space.
- The constant light velocity principle and a time delay in the emission of two light rays has been found as the physical reason for absence of their intersection point in the Euclidean space and for the violation of the V-th postulate in the Lobachevsky velocity space.
- Lobachevsky function has been found as a tool to express the constant light velocity principle.
- A new method of time synchronization for different space points have been found and a new contents of the simultaneity conception, common time and proper time, have been formulated.
- A new inertial frame coordinate transformation, as the simple shifts, has been found. It leads to the known relativistic velocity summation law and requires the existence of the light (moving) "ether".

- It has been shown, that the initial moment of time counting for the moving frame propagates in space in the same direction with a finite velocity greater than the velocity of light.
- The relativistic effects have been shown to take place due to the coordinate and time shifts of the origin point. One can find the values of space or time intervals to be the same in the moving and the rest frames by changing the measurement way.
- It has been shown, that Lorentz energy-momentum transformation is a straightforward consequence of the relativistic velocity summation law.
- The four elements complex fraction invariant and a possible wave equation have been presented.

The author is grateful to A.P. Cheplakov and O.V. Rogachevsky for useful discussions.

References

- [1] A. Einstein, in paper collection: Principle of relativity, M.:Atomizdat, 1973, page 97;
- [2] N.A. Chernikov, Lobachevsky geometry and relativistic mechanics, in Particles and Nucleus, 1973, v.4, part.3, page 733;
- [3] Ja.A. Smorodinsky, Lobachevsky geometry and Einstein kinematics, in "Einstein collection 1971" M.:Nauka, 1972, page 272;
- [4] N.G. Fadeev, The inertia system coordinate transformation based on the Lobachevsky function, in Proceedings of the Int. Conf. on "New Trends in High-Energy Physics", Yalta (Crimea), September 22-29, 2001, Kiev-2001, page 282;
- [5] N.V. Efimov, Advanced geometry, M.: Nauka, 1978, pages 90,107,304,343,393;
- [6] L.D. Landau and E.M. Lifshitz, Theory of field, M: Fizmatgiz, 1962, page 20;
- [7] N.G. Fadeev, Physical nature of Lobachevsky parallel lines and a new inertia system coordinate transformation, JINR preprint E2-2003-181, Dubna, 2003 (english) and JINR preprint P2-2004-048, Dubna, 2004 (russian).

II.
STRUCTURE
FUNCTIONS
OF HADRONS
AND NUCLEI

JET ENERGY DENSITY IN HADRON-HADRON COLLISIONS AT HIGH ENERGIES

J.V. Ilić¹, G.P. Škoro^{2†} and M.V. Tokarev³

(1) *Institute of Nuclear Sciences "Vinča", Belgrade, Serbia and Montenegro*

(2) *Faculty of Physics, University of Belgrade, Belgrade, Serbia and Montenegro*

(3) *Veksler and Baldin Laboratory of High Energies, Joint Institute for Nuclear Research,
Dubna, Russia*

† *E-mail: goran@ff.bg.ac.yu*

Abstract

The average particle multiplicity density $dN/d\eta$ is the dynamical quantity which reflects some regularities of particle production in low- p_T range. The quantity is an important ingredient of z -scaling. Experimental results on charged particle density are available for pp , pA and AA collisions while experimental properties of the jet density are still an open question. The goal of this work is to find the variable which will reflect the main features of the jet production in low transverse energy range and play the role of the scale factor for the scaling function $\psi(z)$ and variable z in data z -presentation. The appropriate candidate is the variable we called "scaled jet energy density". Scaled jet energy density is the probability to have a jet with defined E_T in defined x_T and pseudorapidity regions. The PYTHIA6.2 Monte Carlo generator is used for calculation of scaled jet energy density in proton-proton collisions over a high energy range ($\sqrt{s} = 200 - 14000$ GeV) and at $\eta = 0$. The properties of the new variable are discussed and sensitivity to "physical scenarios" applied in the standard Monte Carlo generator is noted. The results of scaled jet energy density at LHC energies are presented and compared with predictions based on z -scaling.

1. Introduction

For the description of particle production in high- p_T pp , $\bar{p}p$ and pA collisions at high energies, the z -scaling concept is proposed in [1]. In the framework of z -scaling, such experimental observables as inclusive cross-section $Ed^3\sigma/dp^3$ and the average charged particle multiplicity density $\rho \equiv dN/d\eta$ are used to construct the scaling function $\psi(z)$ and variable z . The scaling, known as z -scaling, reveals interesting properties. There are the independence of the scaling function, $\psi(z)$, on collision energy and an angle of produced objects (hadron, photon). A general concept of the scaling is based on such fundamental principles as self-similarity, locality, fractality and scale-relativity [2, 3]. Because the scaling function $\psi(z)$ is well defined in hadron-hadron collisions and expressed via two experimental observables, it is clear that the quantity can be used to study the properties of jet production, too.

In z -scaling concept, the average charged particle multiplicity density plays the role of the scale factor, $z \sim 1/\rho(s)$, and $\psi(z) \sim 1/\rho(s, \eta)$. Experimental results on charged particle density are available for pp , pA and AA collisions while experimental properties of the jet density are still an open question. In the case of jets, there are a lot of

uncertainties (knowledge of parton distribution and fragmentation functions, knowledge of factorization, renormalization and fragmentation scales, uncertainties in the parton shower modelling etc.) causing the problems in understanding of jet behavior at very high energies. The goal of this work is to find the variable which will reflect the main features of the jet production in low transverse energy range at a given energy and play the role of the scale factor.

The paper is organized as follows. A basic description of a scale factor in z -scaling concept as well as results of Monte Carlo simulations on a scale factor in the case of charged particles production are given in Sec.2. New results on a scale factor for jet production based on the analysis of the experimental data and Monte Carlo simulations are described in Sec.3. Discussion of the obtained results at the LHC energies is presented in Sec.4. Conclusions are summarized in Sec.5.

2. Scale factor in z -scaling concept

One of the most interesting problems in the modern particle physics is a search for general properties of quark and gluon interactions in collisions of leptons, hadrons and nuclei. Universal approach to description of the processes allows us detail understanding of the physical phenomena underlying the secondary particle production. Up to date, the investigation of hadron properties in the high energy collisions has revealed widely known scaling regularities. Some of the most popular and famous are the Feynman scaling [4] for inclusive hadron production, the Bjorken scaling observed in deep inelastic scattering (DIS) [5], y -scaling valid in DIS on nuclei [6], limiting fragmentation established for nuclei fragmentation [7], scaling behaviour of the cumulative particle production [8, 9, 10], KNO scaling [11] and others. However, detailed experimental study of the established scaling laws has shown certain violations of these. The domains in which the observed regularities are violated is of great interest. These can be relevant in searching for new physical phenomena - quark compositeness, new interactions, quark-gluon plasma and others.

The concept of the z -scaling is introduced in [1] for the description of inclusive production cross sections in $pp/\bar{p}p$ interactions at high energies and high p_T values of secondary particles. The scaling function $\psi(z)$ is expressed via the invariant inclusive cross section $E d^3\sigma/dp^3$ and the average charged particle multiplicity density $\rho(s, \eta)$. The function $\psi(z)$ is found to be independent of collision energy \sqrt{s} and an angle θ of the inclusive particle. The scaling was also applied for the analysis of the inclusive particle productions in pA collisions [2], jet productions [12], etc. The scaling function of direct photon production was found to reveal the power behavior of $\psi(z) \sim z^{-\beta}$ [13]. The properties of the scaling are assumed to reflect the fundamental properties of particle structure, interaction and production. The scaling function describes the probability to form the produced particle with formation length z . The existence of the scaling itself means that the hadronization mechanism of particle production reveals such fundamental properties as self-similarity, locality, fractality and scale-relativity.

But, it was also found that there is a strong sensitivity of the scaling behavior on the energy dependence of the scale factor $\rho(s)$ at $\eta = 0$. The experimental results show that scale factor $\rho(s)$ (the average charged particle multiplicity density) is well defined quantity (at least up to Tevatron energies) and that simulation results of standard Monte Carlo generators (as PYTHIA) are in nice agreement with available experimental data. But, it is clear that this scale factor cannot be used for description of processes in the

case of jet production at high energies and that corresponding variable for jets must be found. This variable should represent the main properties of jet production at low E_T and must be, as much as possible, independent of jet energy E_T . It should be noted that the scale factor $\rho(s, \eta)$ in the case of particle production has such properties. Because of that and for the sake of completeness, we start the story about the jet scale factor with short description of the properties of charged particle multiplicity density based on the results of Monte Carlo simulations.

The PYTHIA Monte Carlo generator [14] is used for calculations of charged particle multiplicity density in hadron-hadron (pp , πp) collisions in high energy range and at pseudorapidity $\eta = 0$. In both the cases, the dependence of density ρ on energy, \sqrt{s} , at $\eta = 0$ was fitted by the function: $\rho(s) = a \cdot s^b$, where a and b are free parameters. Choice of the fitting function reflects the experimentally observed power law dependence of charged particle density on energy. On the other hand, the properties of this power law should be a consequence of the Pomeron trajectory with intercept $\Delta = \alpha_P - 1$. Based on analysis of available experimental data the value of the quantity was found to be 0.105. Charged particle density $\rho(s)$ in pp interactions was simulated in the energy range $\sqrt{s} = 50 \div 14000$ GeV. The value of $d\sigma^{ch}/d\eta$ for every energy was normalized to the corresponding value of the inelastic cross-section σ_{inel} . The results of simulations are shown in Figure 1(a). As can be seen, the fit is satisfactory, with parameters equal to $a = 0.74(12)$ and $b = 0.105(11)$. This result fully agrees with theoretical predictions and available experimental results. It is expected that multiplicity density of charged particles at $\sqrt{s} = 14$ TeV will follow the same energy dependence but it is, in principle, still an open question. The Monte Carlo simulations of charged particle density at LHC which are in progress (see, for example, ATLAS TDR, p.480 [15]) give results for multiplicity density at $\eta = 0$ in the range from 4.5 up to 10. Charged particle density $dN^{ch}/d\eta$ in πp collisions was simulated in the energy range $\sqrt{s} = 10 \div 200$ GeV. The chosen energy range is relatively narrow, but it is, at the moment, experimentally available. The results of simulations are presented in Figure 1(b). The parameter values were found to be $a = 0.59(8)$ and $b = 0.126(17)$. For pp and πp collisions, we have obtained practically the same value for parameter b (within the errors). Also, in the energy region from 50 to 200 GeV there is no difference between densities in pp and πp collisions.

The power law dependence of charged particle density on energy \sqrt{s} is valid for pA too. In the case of pA collisions, the densities of charged particles can be parameterized [2] by the formula: $dN^{ch}/d\eta \simeq 0.67 \cdot A^{0.18} \cdot s^{0.105}$, where A is the atomic weight of the corresponding nucleus.

3. Jet energy density

In the case of jets, the situation is much more complicated. For example, in [12], the average jet multiplicity density dependence on energy $\rho(s)$, resulted from requirements of z-scaling, is used for analysis of jet production at high energies. The authors used different experimental results on jet cross-sections to produce semi-empirical energy dependence of jet scale factor. The result of that analysis is reproduced in Table 1. Also, the authors give the prediction of jet multiplicity density at LHC energies but emphasized that high accuracy measurements of absolute cross section normalization and the jet density are very important to verify the energy independence of the scaling function $\psi(z)$. On the other hand, the search for the "universal" jet scale factor is complicated because the cross

sections for jet production have non-trivial behavior. The cross sections for production of jets with a fixed transverse energy E_T rise with \sqrt{s} . This is because the important x values decrease and there are more partons at smaller x . But, cross sections for jets with transverse momentum that is a fixed fraction of \sqrt{s} fall with \sqrt{s} . This is mostly because the partonic cross sections fall with E_T like E_T^{-2} .

Table 1. The average jet multiplicity density $\rho(s)$ normalized to the value at $\sqrt{s} = 1800$ GeV in $\bar{p}p$ and pp collisions over the central pseudorapidity range as a function of collision energy [12]

\sqrt{s} [GeV]	63	200	630	1000	1800	7000	14000
Average jet density (normalized)	0.35	0.5	0.67	0.84	1	1.57	1.95

Keeping all that in mind, we performed Monte Carlo analysis of jet production and found the variable that satisfied all the criteria. The detailed description is given below and started with definitions of variables used in jet production analysis.

3.1. Main definitions

Jets are experimentally defined as the amount of energy deposited in the cone of radius $R = \sqrt{(\Delta\eta)^2 + (\Delta\phi)^2}$ in the space (η, ϕ) , where $\Delta\eta$ and $\Delta\phi$ specify the extent of the cone in the pseudorapidity and azimuth. The pseudorapidity η is determined via the center mass angle θ by the formula $\eta = -\ln(\tan(\theta/2))$. In this work, the value of cone radius was taken to be $R = 0.7$.

The inclusive jet cross section measures the probability of observing a hadronic jet with a given E_T and η in a hadron-hadron collision. The inclusive jet cross section is usually expressed in terms of the invariant cross section

$$E \frac{d^3\sigma}{dp^3}. \quad (1)$$

In the experiments [16, 17], the measured variables are the transverse energy (E_T) and pseudorapidity (η). In terms of these variables, the cross section is expressed as follows

$$\frac{d^2\sigma}{dE_T d\eta}. \quad (2)$$

The quantities (1) and (2) are related by

$$E \frac{d^3\sigma}{dp^3} = \frac{1}{2\pi E_T} \frac{d^2\sigma}{dE_T d\eta}. \quad (3)$$

The expression (3) follows if the jets are assumed to be massless. For most measurements, the cross section is averaged over some range of pseudorapidity. In this paper as in [16, 17], we analyzed jets in central pseudorapidity region $|\eta| < 0.5$.

3.2. Results

The PYTHIA6.2 Monte Carlo generator [14] is used for calculation of inclusive jet cross sections in hadron-hadron (pp , $\bar{p}p$) collisions in high energy range and for pseudorapidity

$\eta = 0$. As a first step, we simulated the inclusive jet cross sections at Tevatron energies $\sqrt{s} = 1800$ and 630 GeV. The comparison between the Monte Carlo simulations and experimental data [17] is shown in Figure 2. Black points denote experimental data while red crosses denote Monte Carlo results. The agreement is very good. But, this agreement can be obtained only if the higher-order effects are included in PYTHIA code. This can be done in PYTHIA 6.2 by including the so-called K-factor. K-factor is the ratio of NLO cross section and LO cross section. In this case, we used the model with separate factors for ordinary and colour annihilation graphs. As expected, we can see very strong dependence on the jet transverse energy E_T .

In order to compare jets cross sections at two different colliding energies the so-called "scaled dimensionless cross section" (SDCS) is used. This variable reads

$$SDCS = E_T^4 \cdot E \frac{d^3\sigma}{dp^3}. \quad (4)$$

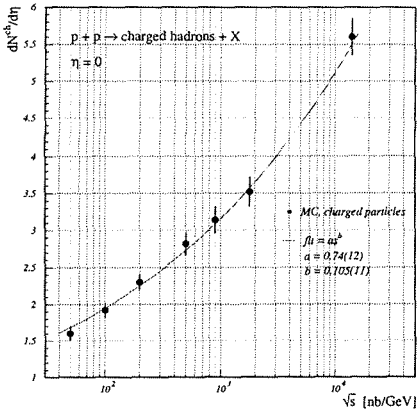
The scaling hypothesis, which is motivated by the Quark-Parton Model, predicts that this variable plotted against $x_T = (2E_T/\sqrt{s})$ will be independent of the collision energy \sqrt{s} . However, QCD leads to scaling violation through the running coupling constant α_s and the evolution of the PDF's [17]. Theoretically, the scaled dimensionless cross sections at different collision energies should be nearly exponential and close to one another [17], or in other words, the ratio of SDCS's for different energies should be a constant when plotted as a function of x_T . Figure 3(a) shows the ratio of dimensionless inclusive jet cross sections at $\sqrt{s} = 630$ and 1800 GeV and for $|\eta| < 0.5$ as well as corresponding results of Monte Carlo simulations¹.

This variable was our starting point, because it practically does not depend on x_T . It can be seen in Figure 3(a) that $SDCS(630)/SDCS(1800) > 1$. It means that the SDCS decreases with increasing colliding energy. On the other hand, the scale factor for jets ρ_{jet} should take into account the rise of the jet E_T with increasing \sqrt{s} (for the same x_T bin) and the behavior of σ_{jet} for minijets production which increase with energy approximately as $s^\delta \ln(s)$, where δ value is between 0 and 0.4 (from QCD expectations and HERA results).

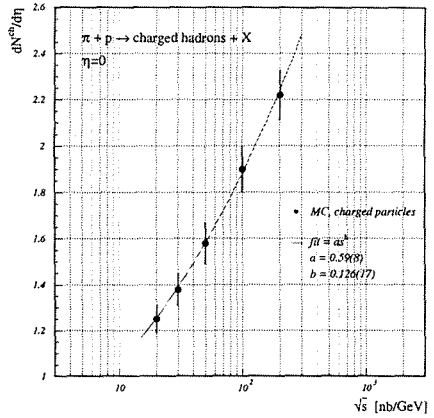
So, the next step was to find the variable similar to the SDCS with taking into account above requirements. The natural choice was to multiply the SDCS value with corresponding jet E_T and to divide with number of jets in η region. The variable, we called "scaled jet energy density", then has the form:

$$Scaled \text{ jet energy density} = SDCS \cdot \frac{E_T}{N_{jet}}. \quad (5)$$

¹J. Womersley wrote about these results: "Both CDF and DO have measured the ratio of jet cross sections, exploiting a short period of data taking at the latter center of mass energy at the end of Run I. This ratio is expected to be a rather straightforward quantity to measure and to calculate. Unfortunately, the two experiments are not obviously consistent with each other (especially at low x_T) or with the NLO QCD expectation for the ratio. At least two explanations have been suggested for the discrepancy. It seems that more work, both theoretical and experimental, is needed before this question can be resolved."

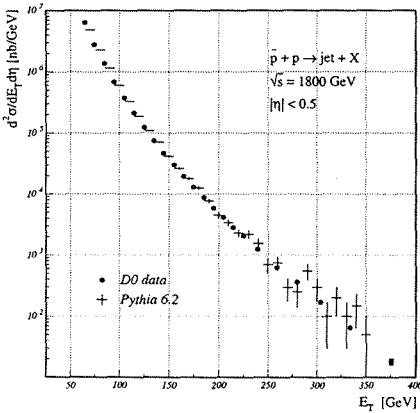


(a)

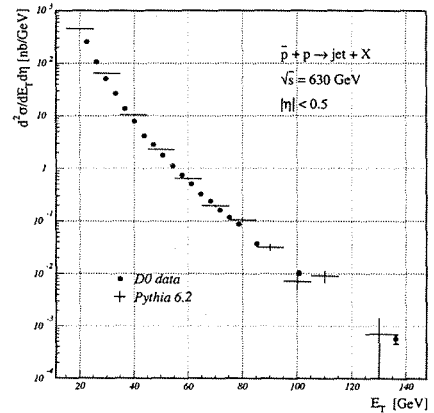


(b)

Figure 1. (a) Charged particle multiplicity density $dN^{ch}/d\eta$ at $\eta = 0$ as a function of energy \sqrt{s} in pp collisions. (b) Charged particle multiplicity density $dN^{ch}/d\eta$ at $\eta = 0$ as a function of energy \sqrt{s} in πp collisions

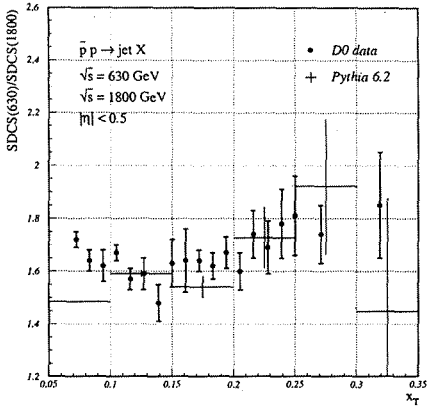


(a)

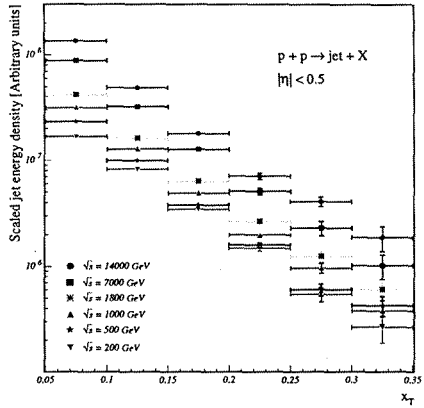


(b)

Figure 2. The comparison between the MC simulations and experimental data on inclusive jet cross sections for $|\eta| < 0.5$ in pp collisions at Tevatron energies $\sqrt{s} = 1800$ and 630 GeV [17]. Black points - experiment, red crosses - Monte Carlo results

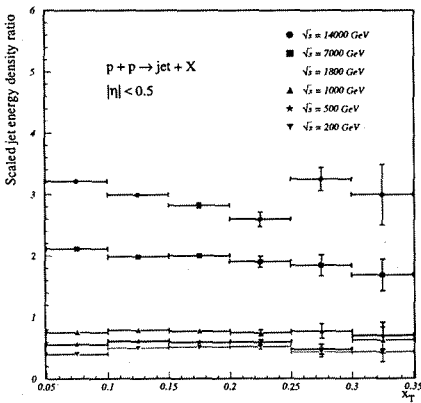


(a)

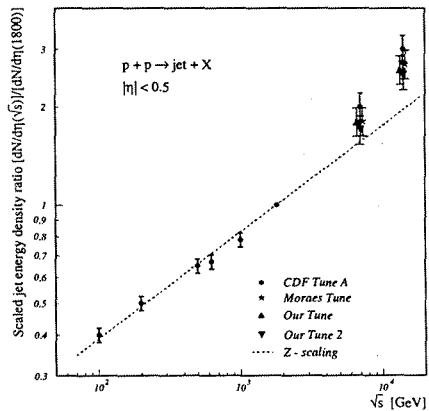


(b)

Figure 3. (a) The ratio of dimensionless inclusive jet cross sections at $\sqrt{s} = 630$ and 1800 GeV and for $|\eta| < 0.5$ in comparison with corresponding results of Monte Carlo simulations. (b) The scaled jet energy density in central pseudorapidity region for different collision energies (from 200 to 14000 GeV) as a function of x_T



(a)



(b)

Figure 4. The scaled jet energy density ratio (see text) in central pseudorapidity region for different collision energies (from 200 to 14000 GeV) as a function of x_T (a) and \sqrt{s} (b)

The shape of this variable for different colliding energies is x_T independent. It increases with energy \sqrt{s} (from 200 to 14000 GeV). The results are shown in Figure 3(b). This variable has the straightforward interpretation - it reflects the probability to have a jets with defined E_T in defined x_T and pseudorapidity region (in this case we talk about central region). The x_T independence of scaled jet energy density is clearly seen when the values are normalized. Following the procedure described in [12] we applied the normalization by dividing the scaled jet energy density values for different \sqrt{s} with corresponding value for $\sqrt{s} = 1800$ GeV. The results are given in Figure 4(a). These ratios show one interesting property: they do not depend on the value of cone radius R in jet finder algorithm. This is important feature because there is a indication that jets at LHC will be broader than expected [15]. So, on the basis of these variable properties, we conclude that this variable can be a good candidate for the role of scale factor (ρ_{jet}) for jet analysis in the framework of z -presentation.

Thus, Figure 4(b) shows the ratio $\rho_{jet}(\sqrt{s})/\rho_{jet}(1800)$ as a function of \sqrt{s} compared with predictions of z -scaling. The first impression is that corresponding values agree very well up to Tevatron energies. In other words, introduction of new variable fully confirms z -scaling predictions for jets for available energies.

4. Discussion

However, we should be very careful with results of Monte Carlo simulations at LHC energy. Extrapolations to LHC energies, based on measurements at the Tevatron show the importance of taking into account the processes when (relatively) small transverse momenta are involved. The description of this problem is given in [18]: "Most of the time the protons will pass through each other with low amount of momentum (low- p_T) being transferred between the interacting partons. Occasionally there will be a hard parton-parton collision, resulting in large transverse momentum outgoing particles. Perturbative QCD is highly successful when applied to hard processes (large- p_T) but cannot be applied to soft interactions (low- p_T). Alternative approaches to describe soft processes are therefore required. PYTHIA's model for hadron-hadron collisions attempts to extend perturbative (high- p_T) picture down to low- p_T region considering the possibility that multiple parton scattering takes place in hadron-hadron collisions". These "soft" processes can violate expected distribution even in hard processes. For example, the violation of KNO scaling is also attributed to secondary processes taking place in the hadron scattering.

The problem of accounting low- p_T processes is present at the Tevatron energies, too. It was found that the default PYTHIA settings does not describe the minimum bias and underlying event data at CDF and D0 experiments. But, with appropriate tunings for PYTHIA [18, 19] those minimum bias and underlying event data can be described. So-called CDF - tune A is the best model describing experimental data from the Tevatron. However, it fails to reproduce several minimum bias distributions at lower energies. On the other hand, tune from [18] gives reasonable description of underlying event data and nice description of minimum bias distributions. The relevant PYTHIA6.2 parameters values in different tuning [18, 19] are shown in Table 2.

This problem is interesting also in the case of jet production. It should be noted that the results for jet energy density shown in Figures 2-4 are obtained with CDF Tune A parameters with fixed p_T cut for multiple interactions at different collision energies. The changes in results compared with default PYTHIA values are small at energies up to 1800 GeV, but situation could be quite different at the LHC.

Table 2. The relevant PYTHIA6.2 parameters values in different tuning [18, 19].

Parameter	Deafult	CDF - Tune A	Moraes Tune	Our Tune
PARP(67)	1.0	4.0	1.0	1.0
MSTP(82)	1	4	4	4
PARP(82)	1.9	2.0	1.8	1.8
PARP(84)	0.2	0.4	0.5	0.6
PARP(85)	0.33	0.9	0.33	0.66
PARP(86)	0.66	0.95	0.66	0.66
PARP(89)	1000	1800	1000	1000
PARP(90)	0.16	0.25	0.16	0.16

At the LHC the important topic will be multiple parton scattering i.e. the simultaneous occurrence of two independent hard (semihard, soft) scattering in the same interaction. On the other hand, in a hard scattering process, the underlying event has a hard component (initial + final-state radiation and particles from the outgoing hard scattered partons) and a soft component (beam-beam remnants). In case of such extreme colliding energies the small differences in "physical scenarios" can produce sizeable differences in scaled jet energy density. Analyzing the parameters values in Table 2, all the tunes assume smooth transition between high and low- p_T regions ($MSTP(82) = 4$) instead of cut on p_T ($MSTP(82) = 1$). It can be seen that main changes are for values of parameters PARP(84), PARP(85) and PARP(86). PARP(84) regulates the size of the hadron core if the double Gaussian matter distribution in hadrons is assumed. PARP(85) and PARP(86) describe the probability that multiple parton scattering produces two gluons with color connections to the nearest neighbors or as a closed gluon loop. We also applied our tune by increasing the probability of producing two gluons with color connections to the nearest neighbors in multiple interactions and by increasing the size of of the hadrons core (right column in Table 2). This results in decrease of scaled jet energy density ratio at the LHC energies and corresponding values are very close to prediction of Z-scaling. Comparing the values of jet energy density at the LHC energy (Figure 4(b)) simulated with different tuning [18, 19] and our tune, it can be concluded that this variable is sensitive (at the level of $10 \div 20\%$) to the changes of these parameters.

5. Conclusions

In this work we tried to find the variable which will reflect the main features of the jet production in low transverse energy range at a given energy and play the role of the scale factor for description of jets in the framework of z -scaling. The PYTHIA6.2 Monte Carlo generator was used for calculation of jet production in proton-proton collisions over a high energy range ($\sqrt{s} = 100 \div 14$ TeV) and for pseudorapidity $\eta = 0$. We introduced the variable we called the "scaled jet energy density". The scaled jet energy density is the probability to have a jet with defined E_T in defined x_T and pseudorapidity regions. Its definition is related to the "scaled dimensionless cross section" and its features (for example, x_T independence) show that this variable can be used in the studies of jet production at high energies. The important result is that properties of new variable fully

confirms z -scaling predictions for jets production at available energies. Detailed analysis of the variable behavior at the LHC energies show that it is sensitive to relatively small differences in applied "physical scenarios" in standard Monte Carlo generators. The fact is that there are sizeable uncertainties in LHC predictions generated by different models so the alternative approach as z -scaling is very important for understanding of inclusive processes of jet production at high energies.

Acknowledgments. One of the authors (M.T.) would like to thank I.Zborovský for numerous fruitful and stimulating discussions of the obtained results.

References

- [1] I. Zborovsky, Yu. Panebratsev, M. Tokarev, G. Škoro, *Phys. Rev.* **D54**, 5548 (1996).
- [2] I. Zborovsky, M. Tokarev, Yu. Panebratsev, G. Škoro, *Phys. Rev.* **C59**, 2227 (1999).
- [3] L. Nottale, *Fractal SpaceTime and Microphysics*, World Scientific, Singapore, 1993.
- [4] R.P. Feynman, *Phys. Rev. Lett.* **23**, 1415 (1969).
- [5] J.D. Bjorken, *Phys. Rev.* **179**, 1547 (1969);
J.D. Bjorken and E.A. Paschos, *Phys. Rev.* **185**, 1975 (1969).
- [6] P. Bosted *et al.*, *Phys. Rev. Lett.* **49**, 1380 (1982).
- [7] J. Benecke *et al.*, *Phys. Rev.* **188**, 2159 (1969).
- [8] A.M. Baldin, *Particles and Nuclei* **8**, 429 (1977).
- [9] V.S. Stavinsky, *Particles and Nuclei* **10**, 949 (1979).
- [10] G.A. Leksin, Preprint ITEP-147, Moscow 1976, 12p.; In: Proc. of the XVIII International Conference on High Energy Physics, Tbilisi, 1976, JINR D1,2-10400, Dubna, 1977, A6-3.
- [11] Z. Koba, H.B. Nielsen, and P. Olesen, *Nucl. Phys.* **B40**, 317 (1972).
- [12] M. Tokarev, T. Dedovich, *Int. Jour. of Mod. Phys.* **A15**, 3495 (2000).
- [13] M. V. Tokarev and E. V. Potrebenikova, *Comput. Phys. Commun.* **117**, 229 (1999).
- [14] T. Sjostrand *et al.*, *Computer Physics Commun.* **135**, 238 (2001).
- [15] ATLAS TDR 15, CERN/LHCC/99-15, Volume II.
- [16] F. Abe *et al.* [CDF Collaboration], *Phys. Rev. Lett.* **77**, 438 (1996).
- [17] B. Abbott *et al.* [D0 Collaboration], *Phys. Rev. Lett.* **82**, 2451 (1999); *Phys. Rev.* **D64**, 032003 (2001); FERMILAB-PUB-00/216-E (DEC 2000).
- [18] A. Moraes, C. Buttar and I. Dawson, Talk given at the Meeting "HERA and the LHC", CERN, 26th March 2004.
- [19] A. Korytov, "Soft QCD Phenomena in High-ET Jet Events at CDF", Talk given at the EPS 2003 Meeting, July 17-23, 2003, Aachen.

Z-SCALING AT RHIC

M.V. Tokarev

*Veksler and Baldin Laboratory of High Energies,
Joint Institute for Nuclear Research,
141980, Dubna, Moscow region, Russia
E-mail: tokarev@sunhe.jinr.ru*

Abstract

The concept of z -scaling reflecting the general regularities of high- p_T particle production is reviewed. Properties of data z -presentation are discussed. New data on high- p_T particle spectra obtained at the RHIC are analyzed in the framework of z -presentation. It was shown that these experimental data confirm z -scaling. Predictions of strange particle spectra are considered to be useful for understanding of strangeness origin in mesons and baryons and search for new physics phenomena at the RHIC.

1. Introduction

Search for scaling regularities in high energy particle collisions is always to be a subject of intense investigations [1]-[10]. Commissioning of the Relativistic Heavy Ion Collider (RHIC) at the Brookhaven National Laboratory (BNL) gives new possibilities to perform experimental investigations in a new physics domain. The RHIC is a next generation of a proton-proton colliders after ISR designed to accelerate protons at center of mass energy range $\sqrt{s} = 50 - 500$ GeV aimed to clarify origin of proton's spin and discover a new state of nuclear matter, Quark Gluon Plasma.

High energy of colliding particles and high transverse momentum of produced particles are most suitable for precise QCD test of production processes with hard probes like high- p_T hadrons, direct photons and jets. Therefore, search for general regularities of high- p_T single inclusive particle spectra of hadron-hadron and hadron-nucleus collisions are of interest to establish complementary restrictions for theory.

The universal phenomenological description (z -scaling) of high- p_T particle production cross sections in inclusive reactions is developed in [11, 12]. The approach is based on properties of particle structure, their constituent interaction and particle formation such as locality, self-similarity and fractality. The scaling function ψ and scaling variable z are expressed via experimental quantities such as the inclusive cross section $E d^3\sigma/dp^3$ and the multiplicity density of charged particles $dN/d\eta$. Data z -presentation is found to reveal symmetry properties (energy and angular independence, A- and F-dependence, power law). The properties of ψ at high z are assumed to be relevant to the structure of space-time at small scales [13, 14, 15]. The function $\psi(z)$ is interpreted as the probability density to produce a particle with a formation length z .

In the report we present the results of analysis of new data on high- p_T particle spectra obtained at the RHIC. The obtained results are compared with other ones based on the data obtained at lower collision energy \sqrt{s} . The results are considered as a new confirmation of z -scaling at the RHIC.

2. Z-scaling

The idea of z -scaling is based on the assumptions [6] that gross feature of inclusive particle distribution of the process (1) at high energies can be described in terms of the corresponding kinematic characteristics

$$M_1 + M_2 \rightarrow m_1 + X \quad (1)$$

of the constituent subprocess written in the symbolic form (2)

$$(x_1 M_1) + (x_2 M_2) \rightarrow m_1 + (x_1 M_1 + x_2 M_2 + m_2) \quad (2)$$

satisfying the condition

$$(x_1 P_1 + x_2 P_2 - p)^2 = (x_1 M_1 + x_2 M_2 + m_2)^2. \quad (3)$$

The equation is the expression of locality of hadron interaction at constituent level. The x_1 and x_2 are fractions of the incoming momenta P_1 and P_2 of the colliding objects with the masses M_1 and M_2 . They determine the minimum energy, which is necessary for production of the secondary particle with the mass m_1 and the four-momentum p . The parameter m_2 is introduced to satisfy the internal conservation laws (for baryon number, isospin, strangeness, and so on).

The equation (3) reflects minimum recoil mass hypothesis in the elementary subprocess. To connect kinematic and structural characteristics of the interaction, the quantity Ω is introduced. It is chosen in the form

$$\Omega(x_1, x_2) = m(1 - x_1)^{\delta_1} (1 - x_2)^{\delta_2}, \quad (4)$$

where m is a mass constant and δ_1 and δ_2 are factors relating to the anomalous fractal dimensions of the colliding objects. The fractions x_1 and x_2 are determined to maximize the value of $\Omega(x_1, x_2)$, simultaneously fulfilling the condition (3)

$$d\Omega(x_1, x_2)/dx_1|_{x_2=x_2(x_1)} = 0. \quad (5)$$

The fractions x_1 and x_2 are equal to unity along the phase space limit and cover the full phase space accessible at any energy.

Self-similarity is a scale-invariant property connected with dropping of certain dimensional quantities out of physical picture of the interactions. It means that dimensionless quantities for the description of physical processes are used. The scaling function $\psi(z)$ depends in a self-similar manner on the single dimensionless variable z . It is expressed via the invariant cross section $Ed^3\sigma/dp^3$ as follows

$$\psi(z) = -\frac{\pi s}{(dN/d\eta)\sigma_{in}} J^{-1} E \frac{d^3\sigma}{dp^3} \quad (6)$$

Here, s is the center-of-mass collision energy squared, σ_{in} is the inelastic cross section, J is the corresponding Jacobian. The factor J is the known function of the kinematic variables, the momenta and masses of the colliding and produced particles.

The function $\psi(z)$ is normalized as follows

$$\int_0^\infty \psi(z) dz = 1. \quad (7)$$

The relation allows us to interpret the function $\psi(z)$ as a probability density to produce a particle with the corresponding value of the variable z .

Principle of fractality states that variables used in the description of the process diverge in terms of the resolution. This property is characteristic for the scaling variable

$$z = z_0 \Omega^{-1}, \quad (8)$$

where

$$z_0 = \sqrt{\hat{s}_\perp} / (dN/d\eta). \quad (9)$$

The variable z has character of a fractal measure. For the given production process (1), its finite part z_0 is the ratio of the transverse energy released in the binary collision of constituents (2) and the average multiplicity density $dN/d\eta|_{\eta=0}$. The divergent part Ω^{-1} describes the resolution at which the collision of the constituents can be singled out of this process. The $\Omega(x_1, x_2)$ represents relative number of all initial configurations containing the constituents which carry fractions x_1 and x_2 of the incoming momenta. The δ_1 and δ_2 are the anomalous fractal dimensions of the colliding objects (hadrons or nuclei). The momentum fractions x_1 and x_2 are determined in a way to minimize the resolution $\Omega^{-1}(x_1, x_2)$ of the fractal measure z with respect to all possible sub-processes (2) subjected to the condition (3). The variable z was interpreted as a particle formation length.

The scaling function of high- p_T particle production, as shown below, is described by the power law, $\psi(z) \sim z^{-\beta}$. Both quantities, ψ and z , are scale dependent. Therefore we consider the high energy hadron-hadron interactions as interactions of fractals. In the asymptotic region the internal structure of particles, interactions of their constituents and mechanism of real particle formation manifest self-similarity over a wide scale range.

3. Z-scaling before RHIC

It was established [11, 12] that of data z -presentation reveals the properties such as the energy and angular scaling, the power law, A - and F -dependencies of the scaling function $\psi(z)$. Numerous experimental data on high- p_T particle spectra obtained at U70, ISR, SpS and Tevatron used in the analysis [11, 12] are compatible each others in z -presentation and give us a good reference frame for future analysis of RHIC data.

Let us remind some properties of p_T -presentation. The first one is the strong dependence of the cross section on energy \sqrt{s} . The second feature is a tendency that the difference between particle yields increases with the transverse momentum p_T and the energy \sqrt{s} . The third one is a non-exponential behavior of the spectra at $p_T > 4$ GeV/c. The energy independence of data z -presentation means that the scaling function $\psi(z)$ has the same shape for different \sqrt{s} over a wide p_T range.

Figure 1(a) shows the dependence of the cross section of π^+ -meson production in $p-p$ interactions on transverse momentum p_T at $\sqrt{s} = 11.5 - 53$ GeV in a central rapidity range. The data cover a wide transverse momentum range, $p_T = 0.2 - 10$ GeV/c.

Figure 1(b) demonstrates z -presentation of the same data sets. One can see that the scaling function $\psi(z)$ demonstrates independence on collision energy \sqrt{s} over a wide energy and transverse momentum range at $\theta_{cms} \simeq 90^\circ$.

As seen from Figure 1(b) the scaling function reveals a linear z -dependence on the log-log scale at high- z . It corresponds to the power law, $\psi(z) \sim z^{-\beta}$. The value of the slope parameter β is independent of the energy \sqrt{s} over a wide range of high transverse

momentum. This is considered as indication that the mechanism of particle formation reveals self-similar and fractal properties.

The p_T -presentation demonstrates a strong angular dependence as well. Figure 1(c) shows the dependence of the cross section of π^0 -meson production in $p-p$ collisions on transverse momentum at $\sqrt{s} = 53$ GeV and the center of mass angle $\theta_{cms} = (5 - 90)^\circ$.

The angular independence of data z -presentation means that the scaling function $\psi(z)$ has the same shape for different values of an angle θ_{cms} of produced particle over a wide p_T and \sqrt{s} range. Figure 1(b) demonstrates z -presentation of the same data sets and experimental confirmation of the angular scaling of $\psi(z)$.

The z -presentation of data gives indication on F -independence of the scaling function [16]. The property means that the scaling function $\psi(z)$ for different species of produced hadrons ($\pi^{\pm,0}, K^\pm, \bar{p}$) at high- z is described by the power law, $\psi(z) \sim z^{-\beta}$, and the slope parameter β is independent of flavor content of produced hadrons. Figure 1(e) illustrates the F -independence of $\psi(z)$ at high- z for hadron production in $p-Be$ collisions. For comparison of different data sets the transformation $z \rightarrow (\alpha_A \alpha_F) \cdot z$, $\psi \rightarrow (\alpha_A \alpha_F)^{-1} \cdot \psi$ of the scaling variable z and the scaling function ψ have been used. The parameters α_A and α_F are independent of energy \sqrt{s} and momentum p_T . The property is considered as universality of particle formation mechanism over a wide range of small scales. We assume that it relates to a structure of space-time itself.

4. Z-scaling at RHIC

Recently the STAR and PHENIX Collaborations presented new data on inclusive high- p_T particle spectra measured at the RHIC in $p-p$ collisions at $\sqrt{s} = 200$ GeV. In the section the data are compared with other ones and used as the experimental test of z -scaling.

4.1. Charged hadrons

The high- p_T spectra of charged hadrons produced in $p-p$ and $Au-Au$ collisions at energy $\sqrt{s} = 200$ GeV within $|\eta| < 0.5$ were measured by the STAR Collaboration [17]. The results are presented in Figure 2(a). The p_T -distribution of charged hadrons produced in $Au-Au$ collisions were measured at different centralities. The shape of the cross section drastically changes as centrality increases. The spectrum for $p-p$ collisions is similar to the spectrum observed in the peripheral $Au-Au$ collisions. The STAR data [17] for $p-p$ collisions correspond to non-single diffraction cross section. Other experimental data correspond to inelastic cross section. Therefore in the analysis the multiplicity particle density $dN/d\eta$ for non-single diffraction interaction for STAR data were used. The RHIC data and other ones for $p-p$ collisions obtained at the U70 [18], Tevatron [19, 20] and ISR [21] are shown in Figure 2(b). The charged hadron spectra were measured over a wide kinematic range $\sqrt{s} = 11.5 - 200$ GeV and $p_T = 0.5 - 9.5$ GeV/c. The strong energy dependence and the power behavior of particle p_T -spectrum are found to be clearly. The energy independence of data z -presentation shown in Figure 3(c) is confirmed. Verification of the asymptotic behavior of ψ at $\sqrt{s} = 200$ GeV and reach of value of z up to 30 and more are of interest.

4.2. π^0 -mesons

The PHENIX Collaboration published the new data [25] on the inclusive spectrum of π^0 -mesons produced in $p-p$ collisions in the central rapidity range at RHIC energy $\sqrt{s} =$

200 GeV. The transverse momenta of π^0 -mesons were measured up to 13 GeV/c. The p_T - and z -presentations of data for π^0 -meson spectra obtained at ISR [26, 27, 28, 29, 30] and RHIC [25] are shown in Figures 3(a) and 3(b). One can see that p_T -spectra of π^0 -meson production reveal the properties similar to that found for charged hadrons. The new data [25] on π^0 -meson inclusive cross sections obtained at the RHIC as seen from Figure 3(b) are in a good agreement with our earlier results [11]. Thus we can conclude that the available experimental data on high- p_T π^0 -meson production in $p-p$ collisions confirm the property of the energy independence of $\psi(z)$ in z -presentation.

4.3. η -mesons

New data on η -meson spectra in $p-p$ collisions at $\sqrt{s} = 200$ GeV in the range $p_T = 1.2 - 8.5$ GeV/c are presented by the PHENIX Collaboration in [23]. The η/π^0 ratio is found to be 0.54 ± 0.05 in the range $p_T = 3.5 - 9$ GeV/c. The value is in agreement with existing data. We compare the data with other ones obtained at $\sqrt{s} = 30., 31.6, 38.8, 53.$ and $63.$ GeV [24, 37]. Data p_T - and z -presentations are shown in Figures 4(a) and 4(b). As seen from Figure 4(b) the results of our new analysis confirm the energy independence of the scaling function for η -meson production in $p-p$ collisions over a wide \sqrt{s} and p_T range. Note that new result on the η/π^0 ratio indicates on flavour independence of the scaling function at high- z .

4.4. Λ and $\bar{\Lambda}$ hyperons

Here we analyze the new data obtained by the STAR Collaboration [31] on p_T -spectra of neutral strange particles ($K_S^0, \Lambda, \bar{\Lambda}$) produced in $p-p$ collisions at $\sqrt{s} = 200$ GeV. The transverse momentum spectra are shown in Figure 5(a). We have not any other data to compare with the STAR data and construct the scaling function. Therefore the F -dependence of z -presentation was used to determine the scaling function for Λ and $\bar{\Lambda}$. The experimental data (see Figure 3) on inclusive cross section of π^0 -mesons produced in $p-p$ collisions at $\sqrt{s} = 23 - 200$ GeV are used to construct the asymptotics of $\psi(z)$. The dashed line shown in Figure 5(b) is the fit of the data. As seen from Figure 3(b) and Figure 5(b) the scaling function is described by the power law, $\psi(z) \sim z^{-\beta}$, on the log-log scale at high- z . The transformation of the variable z and the scaling function ψ for Λ (Fig.5(b)) and $\bar{\Lambda}$ in the form $z \rightarrow \alpha_F \cdot z, \quad \psi \rightarrow \alpha_F^{-1} \cdot \psi$ was used for coincidence of the asymptotics for $\Lambda, \bar{\Lambda}$ and π^0 . Note that the scaling function $\psi(z)$ for Λ reveals different behavior at low- and high- z ranges. It is valid for $\bar{\Lambda}$ as well. The parameterizations of $\psi(z)$ for Λ and $\bar{\Lambda}$ were used to predict particle spectra (see Figures 5(c) and 5(d)) at $\sqrt{s} = 63, 200$ and 500 GeV at high- p_T .

4.5. ϕ -mesons

Recently the STAR Collaboration presented the new data [32] on spectra of ϕ -mesons produced in $Au-Au$ and non-singly-diffractive $p-p$ collisions at energy $\sqrt{s} = 200$ GeV. The decay mode $\phi \rightarrow K^+K^-$ was used to reconstruct ϕ -mesons up to $p_T = 3.7$ GeV/c

The cross sections as a function of the difference of the transverse mass m_t and the mass of ϕ -meson m_ϕ are shown in Figure 6(a). The data can be used to test z -scaling and verify models of strange particle formation. The p_T -distribution of ϕ -mesons produced in $Au-Au$ collisions measured at different centralities reveals exponential behavior. The slope of spectra changes with the centrality. The spectrum for $p-p$ collisions at high- p_T indicates on power behavior. The scaling functions for ϕ and the asymptotics for π^0 are shown in Figure 6(b). The F -dependence of data z -presentation was used to predict ϕ -meson spectra

at $\sqrt{s} = 41.6, 63, 200$ and 630 GeV and $\theta_{cms} = 90^\circ$ at high- p_T . Note also that $p - p$ spectra of ϕ -mesons is important to study the nuclear modification factor R_{AA} over a wide p_T -range and obtain direct information about the dense nuclear matter at hadron formation.

4.6. Ξ^- and Ξ^+ hyperons

The STAR Time Projection Chamber (TPC) provides excellent tracking of charged particles with good momentum resolution [33]. Present statistics are sufficient to reconstruct Ξ^- and Ξ^+ hyperons over a wide p_T -range [34]. The decay mode $\Xi^- \rightarrow \Lambda\pi^-$ was used to reconstruct Ξ^- up to $p_T = 4$. GeV/c. Mid-rapidity transverse momentum spectra for Ξ^- and Ξ^+ from $p - p$ at energy $\sqrt{s} = 200$ GeV and $|y| < 0.75$ are shown in Figure 7(a).

The flavor independence of ψ at high- z for different pieces allows us to construct the scaling function of Ξ^- (see Fig. 7(b)) and Ξ^+ over a wide z -range using the asymptotics for π^0 -mesons and to predict inclusive cross sections of Ξ^- and Ξ^+ hyperon production at high- p_T . The transverse momentum spectra for Ξ^- and Ξ^+ are shown in Figure 7(c) and Figure 7(d), respectively.

As shown in [35] the PYTHIA simulation of Ξ^- spectrum in $p - p$ collisions at $\sqrt{s} = 200$ GeV does not reproduce the STAR data. Therefore our predictions can be used to tune various PYTHIA parameters. To study azimuthal correlation of strange and charged particles and strange tagging jet production in $p - p$ collisions statistics should be gained. Moreover sophisticated algorithms [36] could essentially decrease background and increase efficiency of strange particles reconstruction as well.

4.7. K_S^0 -mesons

Here we compare the STAR data [31] for K_S^0 -meson cross sections with data for K^+ -mesons obtained at the U70 [18], Tevatron [19, 20] and ISR [21] at lower energies 11.5, 19.4, 23.8, 27.4, 38.8 and 53 GeV. The data p_T - and z -presentations are shown in Figures 8(a) and 8(b), respectively. As seen from Figure 8(a) the energy dependence of the cross section enhances with p_T . The shape of the scaling function for K_S^0 -mesons coincides with similar one for K^+ -mesons in the range $z = 0.2 - 3.0$. It gives evidence that mechanism of neutral and charged strange K -meson formation is the same one and it reveals property of self-similarity.

4.8. π^+ -mesons

The PHENIX Collaboration presented in [22] the new data on inclusive cross section of identified hadrons ($\pi^\pm, K^\pm, p, \bar{p}$) produced in $p - p$ collisions at $\sqrt{s} = 200$ GeV in the central rapidity range. Transverse momentum of particles is measured up to 2.2 GeV/c. Data p_T - and z -presentations for π^+ -mesons are shown in Figure 9. We compare the data with another ones obtained at the U70 [18], Tevatron [19, 20] and ISR [21] at lower energies $\sqrt{s} = 11.5 - 53$ GeV. As seen from Figure 9(b) the scaling function corresponding to data [22] is in good agreement with our results obtained previously [11].

5. Conclusion

Analysis of new experimental data on high- p_T hadrons ($h^\pm, \pi^0, \eta, \Lambda, \bar{\Lambda}, \phi, \Xi^-, \Xi^+, K_S^0, \pi^+$) produced in $p - p$ collisions at the RHIC in the framework of data z -presentation was performed.

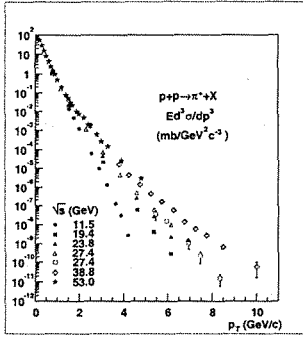
The scaling function $\psi(z)$ and scaling variable z are expressed via the experimental quantities, the invariant inclusive cross section $Ed^3\sigma/dp^3$ and the multiplicity density of

charged particles $\rho(s, \eta)$. The scaling function ψ is interpreted as a probability density to produce a particle with the formation length z .

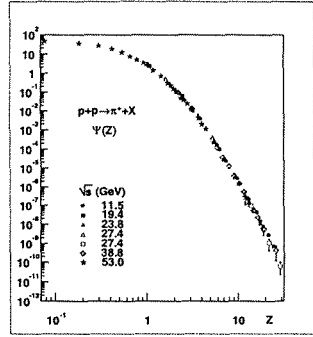
The general regularities of high- p_T particle production described by z -scaling were found to be valid in the new kinematical range accessible at the RHIC. Using the properties of z -scaling predictions of spectra of strange particles ($\Lambda, \bar{\Lambda}, \phi, \Xi^-, \bar{\Xi}^+$) produced in $p-p$ collisions at RHIC energies in high- p_T range were made. The obtained results are considered to be useful for understanding of strangeness origin in meson and baryons. New evidence that mechanism of particle formation reveals self-similar and fractal properties at high- p_T range was obtained.

Thus we conclude that new data obtained at RHIC confirm the general concept of z -scaling. The further inquiry and search of violation of the scaling can give information on new physics phenomena in high energy hadron collisions and determine domain of applicability of the strong interaction theory.

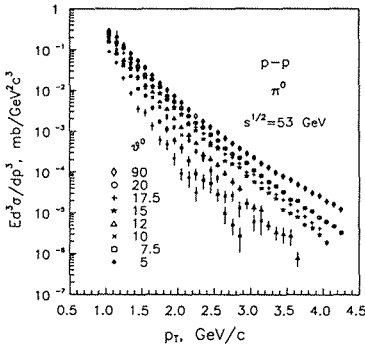
Acknowledgments. The author would like to thank I.Zborovský, Yu.Panebratsev, O.Rogachevski and A.Kechechyan for collaboration and numerous fruitful and stimulating discussions of the problem.



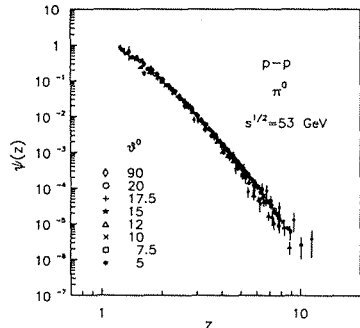
a)



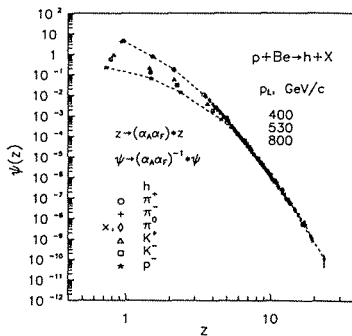
b)



c)

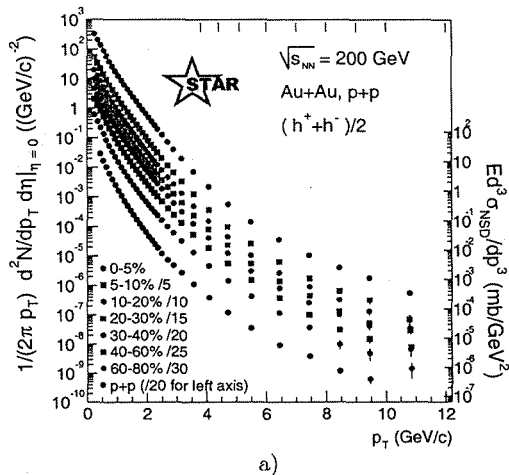


d)

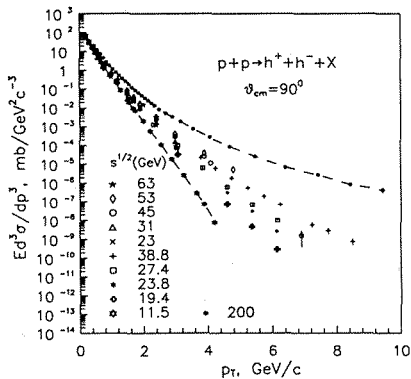


e)

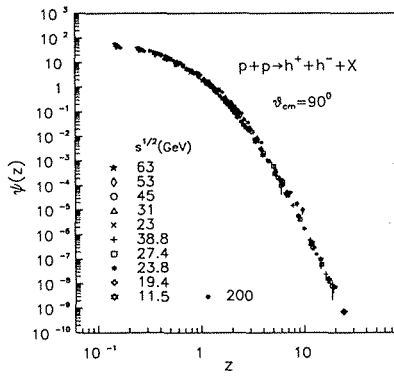
Figure 1. The p_T -(a,c) and z -presentations of experimental data on inclusive cross section of particles produced in $p-p$ collisions. The energy (b), angular (d) scaling and F^2 -dependence (e) of the function $\psi(z)$. Experimental data are taken from [17, 18, 19, 20, 21]



a)

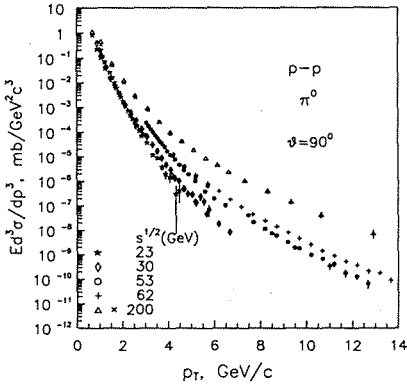


b)

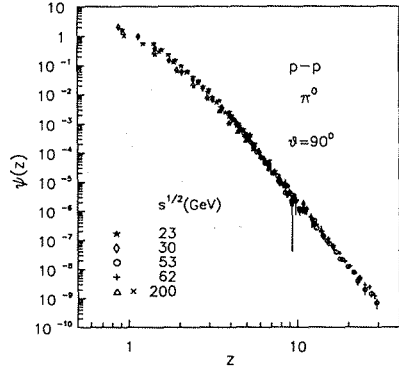


c)

Figure 2. (a) Experimental data [17] on the inclusive cross sections of charged hadrons produced in $Au - Au$ and $p - p$ collisions at $\sqrt{s_{NN}} = 200$ GeV and $\theta_{cms} \simeq 90^\circ$ as a functions of the transverse momentum p_T . Data (b) p_T - and (c) z -presentations of data taken from [18, 19, 20, 21] and [17].

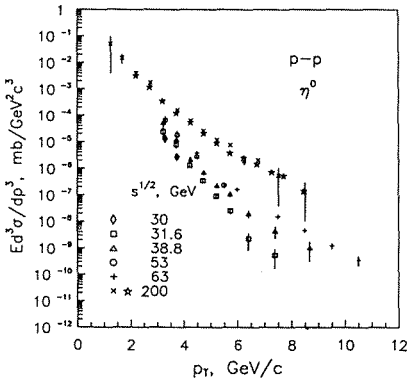


a)

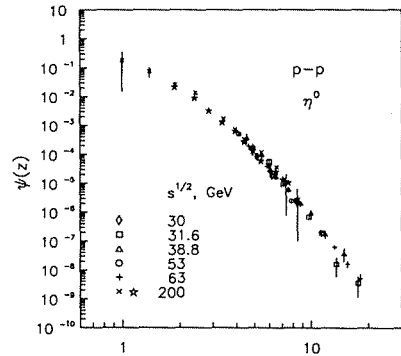


b)

Figure 3. The dependence of the inclusive cross section of π^0 -meson production on the transverse momentum p_T in $p-p$ collisions at $\sqrt{s} = 30, 53, 62$ and 200 GeV and the angle θ_{cm} of 90° . The experimental data are taken from [26, 27, 28, 29, 30] and [25]. (b) The corresponding scaling function $\psi(z)$

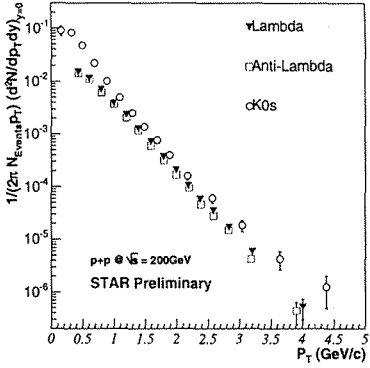


a)

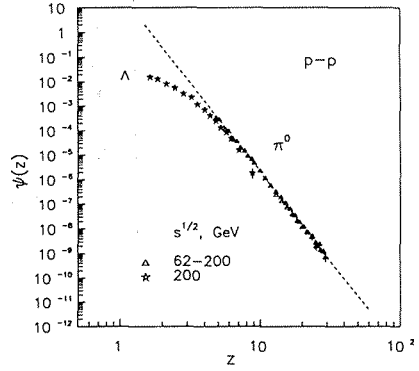


b)

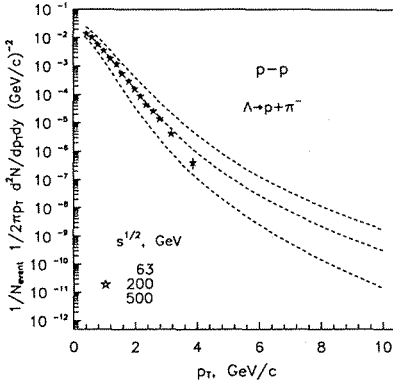
Figure 4. (a) The inclusive cross section of η -mesons produced in $p-p$ collisions in the central rapidity range as a function of the transverse momentum p_T at $\sqrt{s} = 30 - 63$ GeV and 200 GeV. Experimental data are taken from [24, 37] and [23]. (b) The corresponding scaling function $\psi(z)$



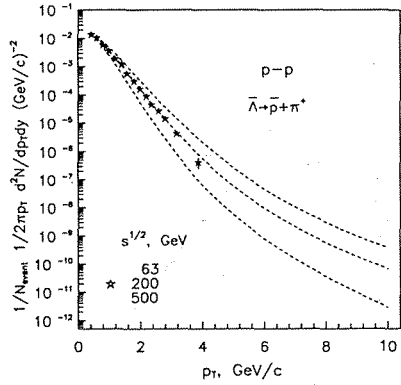
a)



b)

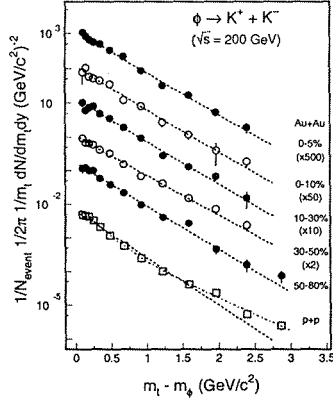


c)

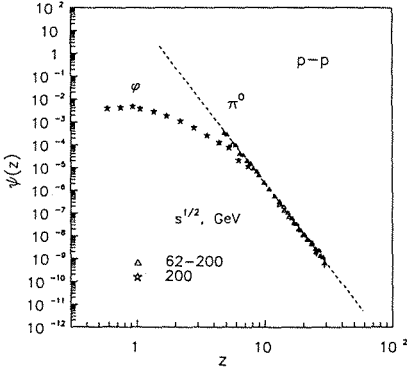


d)

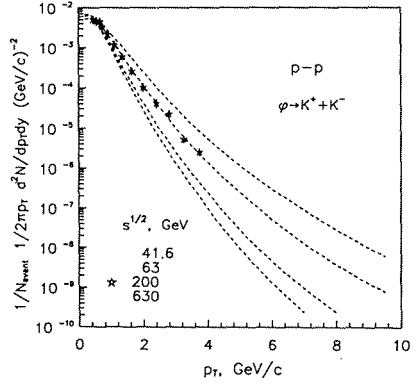
Figure 5. (a) The inclusive cross sections of hadrons K_S^0 , Λ , $\bar{\Lambda}$ produced in $p-p$ collisions at $\sqrt{s} = 200$ GeV in central rapidity range as a functions of the transverse momentum p_T . Experimental data are taken from [31]. (b) Z -presentation of Λ and π^0 experimental data on cross sections. Predictions of the inclusive spectra for Λ (c) and $\bar{\Lambda}$ (d) production in $p-p$ collisions at $\sqrt{s} = 63, 200, 500$ GeV and $\theta_{cms} \simeq 90^\circ$



a)

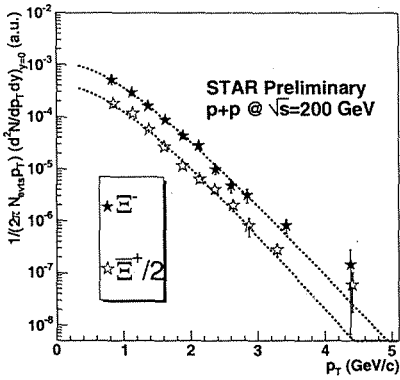


b)

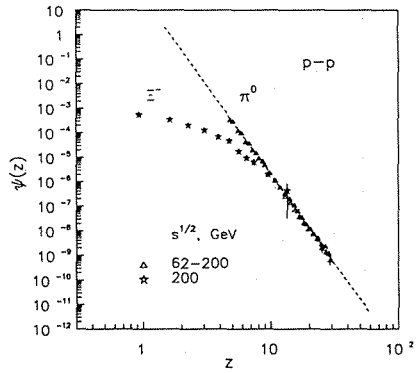


c)

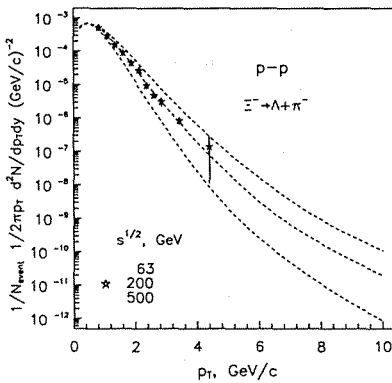
Figure 6. (a) The inclusive cross sections of ϕ -mesons produced in $Au - Au$ and $p - p$ collisions at $\sqrt{s_{cm}} = 200$ GeV in central rapidity range as a functions of $m_t - m_\phi$. Experimental data are taken from [32]. (b) Z -presentation of ϕ and π^0 experimental data on cross sections. (c) Predictions of the inclusive spectra for ϕ -meson production in $p - p$ collisions at $\sqrt{s} = 41.6, 63, 200, 500$ GeV and $\theta_{cms} \simeq 90^\circ$.



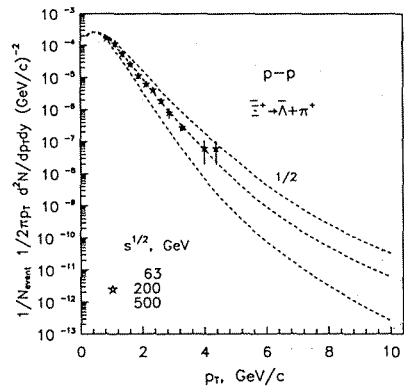
a)



b)

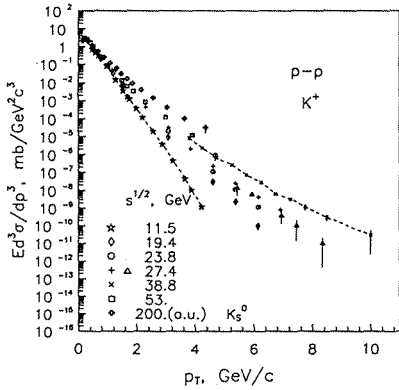


c)

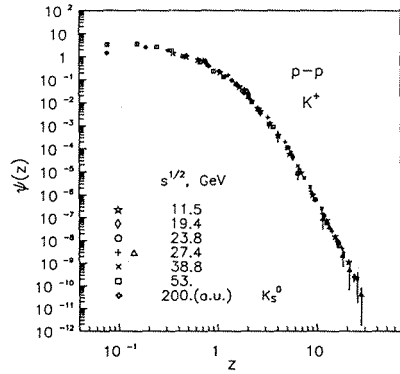


d)

Figure 7. (a) The inclusive cross sections of Ξ^- and Ξ^+ hyperons produced in $p-p$ at $\sqrt{s} = 200$ GeV in central rapidity range as a functions of the transverse momentum p_T . Experimental data are taken from [34]. (b) Z -presentation of Ξ^- and π^0 experimental data on cross sections. Predictions of the inclusive spectra for Ξ^- (c) and Ξ^+ (d) production in $p-p$ collisions at $\sqrt{s} = 63, 200, 500$ GeV and $\theta_{\text{cms}} \simeq 90^\circ$

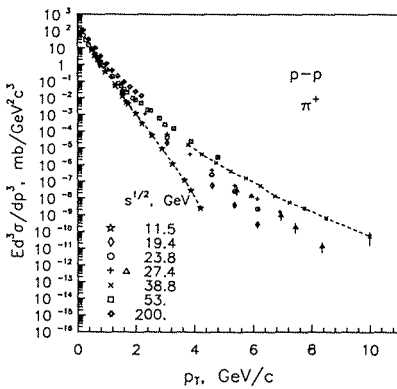


a)

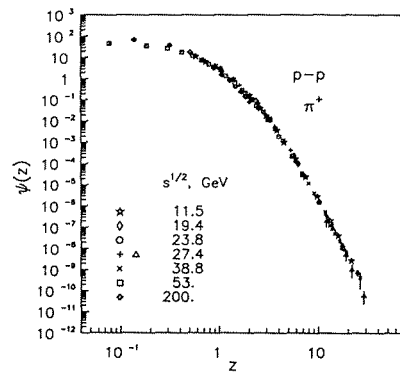


b)

Figure 8. (a) The inclusive cross sections of K^+ - and K_S^0 -mesons produced in $p-p$ collisions in the central rapidity range as a function of the transverse momentum at $\sqrt{s} = 11.5 - 53$ GeV and 200 GeV. Experimental data are taken from [18, 19, 20, 21] and [31]. (b) The corresponding scaling function $\psi(z)$



a)



b)

Figure 9. (a) The inclusive cross section of π^+ -mesons produced in $p-p$ collisions in the central rapidity range as a function of the transverse momentum p_T at $\sqrt{s} = 11.5 - 53$ GeV and 200 GeV. Experimental data are taken from [18, 19, 20, 21] and [22]. (b) The corresponding scaling function $\psi(z)$

References

- [1] R.P. Feynman, Phys. Rev. Lett. **23**, 1415 (1969).
- [2] J.D. Bjorken, Phys. Rev. **179**, 1547 (1969); J.D. Bjorken, and E.A. Paschos, Phys. Rev. **185**, 1975 (1969).
- [3] P. Bosted *et al.*, Phys. Rev. Lett. **49**, 1380 (1972).
- [4] J. Benecke *et al.*, Phys. Rev. **188**, 2159 (1969).
- [5] A.M. Baldin, Sov. J. Part. Nucl. **8**, 429 (1977).
- [6] V.S. Stavinsky, Sov. J. Part. Nucl. **10**, 949 (1979).
- [7] G.A. Leksin: Report No. ITEF-147, 1976; G.A. Leksin: in *Proceedings of the XVIII International Conference on High Energy Physics*, Tbilisi, Georgia, 1976, edited by N.N. Bogolubov *et al.*, (JINR Report No. D1,2-10400, Tbilisi, 1977), p. A6-3.
- [8] Z. Koba, H.B. Nielsen, and P. Olesen, Nucl. Phys. **B 40**, 317 (1972).
- [9] V.A. Matveev, R.M. Muradyan, and A.N. Tavkhelidze, Part. Nuclei **2 7** (1971); Lett. Nuovo Cim. **5**, 907 (1972); Lett. Nuovo Cim. **7**, 719 (1973).
- [10] S. Brodsky, and G. Farrar, Phys. Rev. Lett. **31**, 1153 (1973); Phys. Rev. **D 11**, 1309 (1975).
- [11] I.Zborovský, Yu.A.Panebratsev, M.V.Tokarev, and G.P.Škoro, Phys. Rev. **D 54**, 5548 (1996); I.Zborovský, M.V.Tokarev, Yu.A.Panebratsev, and G.P.Škoro, Phys. Rev. **C59**, 2227 (1999); M.V.Tokarev, T.G.Dedovich, Int. J. Mod. Phys. **A15**, 3495 (2000); M.V.Tokarev, O.V.Rogachevski, T.G.Dedovich, J. Phys. G: Nucl. Part. Phys. **26**, 1671 (2000); M.V.Tokarev, O.V.Rogachevski, and T.G.Dedovich, Preprint No. E2-2000-90, JINR (Dubna, 2000); M.Tokarev, I.Zborovský, Yu.Panebratsev, and G.Skoro, Int. J. Mod. Phys. **A16**, 1281 (2001); M.Tokarev, hep-ph/0111202; M.Tokarev, D.Toivonen, hep-ph/0209069; G.P.Skoro, M.V.Tokarev, Yu.A.Panebratsev, and I.Zborovský, hep-ph/0209071; M.V.Tokarev, G.L.Efimov, and D.E.Toivonen, Physics of Atomic Nuclei, **67**, 564 (2004). M.Tokarev, Acta Physica Slovaca, **54**, 321 (2004).
- [12] M.V.Tokarev, JINR Preprint E2-98-92, Dubna, 1998; JINR Preprint E2-98-161, Dubna, 1998; M.V.Tokarev, E.V.Potrebenikova, Computer Physics Communications **117**, 229 (1999); M.Tokarev, G.Efimov, hep-ph/0209013.
- [13] L.Nottale, *Fractal Space-Time and Microphysics* (World Sci., Singapore, 1993).
- [14] B.Mandelbrot, *The Fractal Geometry of Nature* (Freeman, San Francisco, 1982).
- [15] I.Zborovský, hep-ph/0311306.
- [16] M.Tokarev, In *Proceedings of the International Workshop "Relativistic Nuclear Physics: From Hundreds of MeV to TeV"*, Varna, Bulgaria, September 10-16, 2001, p.280-300; JINR E1,2-2001-290.

- [17] J.Adams *et al.*, (STAR Collaboration) Phys. Rev. Lett. **91**, 172302 (2003).
- [18] V.V.Abramov *et al.*, Sov. J. Nucl. Phys. **41** (1985) 700; Pis'ma v ZhETF **33** (1981) 304; Sov. J. Nucl. Phys. **31** (1980) 937.
- [19] J.W.Cronin *et al.*, Phys. Rev. **D 11**, 3105 (1975);
D.Antreasyan *et al.*, Phys. Rev. **D 19**, 764 (1979).
- [20] D.Jaffe *et al.*, Phys. Rev. **D 40**, 2777 (1989).
- [21] B.Alper *et al.*, Nucl. Phys. **B 87**, 19 (1975).
- [22] M.Harvey *et al.*, (PHENIX Collaboration) In *Proceedings of the Quark Matter 2004, January 11-17,2004, Oakland, California, USA*; <http://qm2004.lbl.gov/>.
- [23] H.Hiejima *et al.*, (PHENIX Collaboration) In *Proceedings of the Quark Matter 2004, January 11-17,2004, Oakland, California, USA*; <http://qm2004.lbl.gov/>.
- [24] C.Kourkouvelis *et al.*, Phys. Lett. **B 84**, 277 (1979).
- [25] S.S.Adler *et al.*, (PHENIX Collaboration) Phys. Rev. Lett. **91**, 241803 (2003).
- [26] A.L.S. Angelis *et al.*, Phys. Lett. **B79**, 505 (1978).
- [27] C. Kourkouvelis *et al.*, Phys. Lett. **B83**, 257 (1979).
- [28] C. Kourkouvelis *et al.*, Z. Phys. **5**, 95 (1980).
- [29] D. Lloyd Owen *et al.*, Phys. Rev. Lett. **45**, 89 (1980).
- [30] K. Eggert *et al.*, Nucl. Phys. **B98**, 49 (1975).
- [31] J.Adams & M.Heinz *et al.*,(STAR Collaboration) In *Proceedings of the Quark Matter 2004, January 11-17,2004, Oakland, California, USA*; <http://qm2004.lbl.gov/>; nucl-ex/0403020.
- [32] J.Adams *et al.*, (STAR Collaboration) nucl-ex/0406003.
- [33] M.Anderson *et al.*, (STAR Collaboration) Nucl. Instrum. Meth. **A499**, 659 (2003).
- [34] R.Witt *et al.*, (STAR Collaboration) nucl-ex/0403021.
- [35] B.Bezverkhy *et al.*, (STAR Collaboration) Workshop "Hot Quark 2004", July 18-24, 2004, Taos Valley, New Mexico, USA.
- [36] A.Kechechyan, Private communication.
- [37] G.Alverson *et al.*, Phys. Rev. **D 48**, 5 (1993); L.Apanasevich *et al.*, Phys. Rev. Lett. **81**, 2642 (1998); hep-ex/9711017; M.Begel *et al.*, Workshop "High p_T Phenomena at RHIC", BNL, November 1-2, 2001.

ANISOTROPY IN RELATIVISTIC NUCLEAR COLLISIONS AND MICHELSON'S EXPERIMENTS WITH LIGHT

I. Zborovský

*Nuclear Physics Institute, Academy of Sciences of the Czech Republic, Řež, Czech Republic
E-mail: zborovsky@ujf.cas.cz*

Abstract

Considering ultra-relativistic nuclear collisions as interactions of parton fractals, effective structural space-time anisotropy can be induced in the interaction region. We argue that uni-directional violation of the reflection invariance implied by the anisotropy does not contradict with the Michelson-Morley type experiments searching for anisotropy of light propagation in space-time.

1. Self-similarity and fractality in inclusive reactions

Production of particles from high energy collisions of hadrons and nuclei reflects symmetries underlying their interactions at constituent level. Elementary sub-processes of the constituents are similar. This involves structure of the constituents at various scales which possess typical fractal character. One of the expressions aiming to account for the self-similarity and fractality as general property of hadronic interactions is z -scaling observed in inclusive reactions at high energies [1]. The scaling variable

$$z = z_0 \Omega^{-1}, \quad (1)$$

$$\Omega(x_1, x_2) = (1 - x_1)^{\delta_1} (1 - x_2)^{\delta_2} \quad (2)$$

is self-similarity parameter which has character of a fractal measure. For given inclusive reaction, its finite part, z_0 , is proportional to the transverse energy released in the underlying collision of constituents. The divergent part, Ω^{-1} , describes resolution at which the collision of the constituents can be singled out of this reaction. The $\Omega(x_1, x_2)$ is relative number of all initial configurations containing the constituents which carry fractions x_1 and x_2 of the incoming momenta. The δ_1 and δ_2 are related to the anomalous fractal dimensions of the colliding objects (hadrons or nuclei) and characterize fractal sub-structure of their constituents. The variable z contains internal symmetry - the space-time relativity with respect to structural degrees of freedom [2]. Such realization of the relativity principle corresponds to minimal resolution of the fractal measure z at which the underlying constituent sub-processes can be singled out of the inclusive reaction. Using the minimal value of Ω^{-1} , one can introduce "the structural velocity u ",

$$u = \frac{U}{\sqrt{1+U^2}}, \quad U = \frac{\alpha - 1}{2\sqrt{\alpha}} \xi, \quad \alpha = \delta_2 / \delta_1. \quad (3)$$

Here ξ is scale dependent kinematical factor connected with spatial resolution. The factor ξ is Lorentz invariant with respect to motion. Beside fractal structure of hadrons and

nuclei we consider structural properties of space-time vacuum which is not an empty space. Its intimate structure is governed by the same processes which influence the very structure of hadrons and nuclei at small scales. The way through which space-time properties are related to matter properties is instructive. It consists in attributing to space-time those properties of matter which are universal. It was suggested by many authors [3] that one of such universal property is fractality, the never ending self-similar content of matter forming its intimate structure at small scales.

In particular, this can be tested in ultra-relativistic collisions of hadrons and nuclei. If the colliding objects possess mutually different anomalous fractal dimensions ($\delta_1 \neq \delta_2$), it is natural to imagine that, due to fractality, vacuum structure becomes polarized (or acquires anisotropy) along the collision axis. Exploiting such connections, the structural velocity u can be visualized as effective anisotropy of space-time induced by the interaction. Scale dependence of the fractal polarization of space-time is given by the factor ξ . One of the attributes of scale dependent fractal space-time is the fundamental consequence, namely breaking of the reflection invariance with regard to real motion. If insisting simultaneously that breaking of the reflection invariance does not disturb spatial isotropy, one arrives at the space-time metrics [2]

$$\eta(\vec{u}) = \begin{pmatrix} -\delta_{ij} + u_i u_j & -u_i \\ -u_j & 1 \end{pmatrix}. \quad (4)$$

This corresponds to the invariant

$$t^2 - r^2 - 2t\vec{u} \cdot \vec{r} + (\vec{u} \cdot \vec{r})^2 = \tau^2. \quad (5)$$

The structural velocity $\vec{u} = (0, 0, u)$ is induced characteristic of space-time which does not change with motion. It depends on the fractal dimensions and on the scale resolution in the Lorentz invariant way. Contrary to this, the motion velocity $\vec{v} = d\vec{r}/dt$ characterizes motion and depends on the reference system. Its transformation properties are given by $r'' = \Delta(\vec{v}, \vec{u})r'$ where $r \equiv (\vec{r}, t)$. The transformation matrix has the form

$$\Delta(\vec{v}, \vec{u}) = \begin{pmatrix} \delta_{ij} + G v_i v_j + \Gamma v_i u_j & -\Gamma v_i \\ -G_- v_j - \Gamma_- u_j & 1 + \Gamma_- \end{pmatrix} \quad (6)$$

where

$$\Gamma = \frac{1}{\sqrt{(1 - \vec{u} \cdot \vec{v})^2 - v^2}}, \quad G = \frac{(1 - \vec{u} \cdot \vec{v})\Gamma - 1}{v^2} \quad (7)$$

and

$$\Gamma_- = Gv^2 - \Gamma\vec{u} \cdot \vec{v}, \quad G_- = \Gamma - G\vec{u} \cdot \vec{v}. \quad (8)$$

The factor Γ is generalization of the Lorentz factor for non-zero space-time anisotropy \vec{u} . It determines range of the accessible values of the motion velocities which becomes a rotational ellipsoid

$$(v_{\parallel} + e)^2 + \gamma^2 v_{\perp}^2 = \gamma^4, \quad \gamma = (1 - u^2)^{-1/2}. \quad (9)$$

Here v_{\parallel} and v_{\perp} denote the velocity components which are parallel and perpendicular to the space-time structural anisotropy \vec{u} , respectively. The ellipsoid is given by the major semi-axis $a = \gamma^2$ and by the minor semi-axis $b = \gamma$. Its eccentricity is $e = \gamma\sqrt{\gamma^2 - 1}$. One focus of the ellipsoid is in the point $\vec{v} = 0$.

2. Michelson-Morley type experiments

The important question in our approach is if, in principle, the light velocity value can be anisotropic in whatever inertial reference system. Standard interpretation of the Michelson-Morley type experiments including optical interferometer experiments [4] seems to be negative with this respect. The experiments steadily reproduce "no fringe shift" and, therefore, do not support any deviation which would point to even tiny portion of the anisotropic spread of light. We show below that the Michelson-Morley type experiments do not imply absolute absence of anisotropy in light propagation. The argumentation includes arbitrary accuracy of relativistic effects.

2.1. Two mirror set-up

In the original Michelson-Morley experiment the interferometer with two perpendicular arms of the length d_I and d_{II} has been used (Fig.1a). A signal from a light source was divided into two rays, I and II, traveling perpendicular to each other along the arms. The mirrors placed on the ends of the spectrometer arms reflected the light back to the telescope where the rays interfered with each other. Interference fringes between the two rays are due to phase difference $\Delta t = t_{II} - t_I$. When the apparatus is rotated through an angle of 90° , the orientation of the spectrometer arms is interchanged. According to standard interpretation, such rotation of the apparatus should cause a shift of the interference fringes between the two rays, if the light propagation would be anisotropic. In this contribution we show that this must not be the case for the metrics (4) for any value of the space-time anisotropy \vec{u} up to the arbitrary order of accuracy.

Suppose there exists a space-time anisotropy \vec{u} induced by some reasons. Let us assume that the anisotropy results in the metric changes (4) associated with deformation of the spherical light front. In this case, the light front becomes an ellipsoid (9) with one focus in the point where the light was emitted. Consider the ellipse (Fig.1b) which forms intersection of the ellipsoid with a plane passing through this focus. The focus is common for the ellipse and the ellipsoid as well. Moreover, for any orientation of this plane

$$\frac{A}{B^2} = \frac{a}{b^2}, \quad (10)$$

where A and B or a and b are major and minor semi-axes of the ellipse or the ellipsoid, respectively. Suppose the spectrometer arms define the considered plane and therefore determine such ellipse in this plane. The velocities of the two rays I and II mark out four different points on the ellipse. We denote the sections connecting the focus of the ellipse with these points by $v_1(\phi)$ or $\bar{v}_1(\phi)$ and $v_2(\phi)$ or $\bar{v}_2(\phi)$, respectively. The difference $\Delta t = t_{II} - t_I$ between times which the light rays take to travel in spectrometer arms II and I can be expressed as follows

$$\Delta t = d_{II} \left(\frac{1}{v_2(\phi)} + \frac{1}{\bar{v}_2(\phi)} \right) - d_I \left(\frac{1}{v_1(\phi)} + \frac{1}{\bar{v}_1(\phi)} \right). \quad (11)$$

The angle ϕ describes orientation of the arms in the spectrometer plane. Because of the anisotropy, the velocities of light propagation in different directions, $v_i(\phi)$, are not equal and depend on the orientation of the spectrometer arms. On the other hand, the spatial

distances (lengths of arms d_I, d_{II}) do not depend on the orientation of the spectrometer in the metrics (4). This follows from the known fact [5] that the spatial geometry is not simply given by the spatial part η_{ij} of the four dimensional metric $\eta_{\mu\nu}(\vec{u})$. In the considered case, the spatial metric η_{ij}^* is isotropic

$$\eta_{ij}^* = -\eta_{ij} + \eta_i^* \eta_j^* = \delta_{ij}, \quad \eta_i^* = \frac{\eta_{i0}}{\sqrt{\eta_{00}}}. \quad (12)$$

Therefore, lengths d_I and d_{II} are invariant under space rotations and do not depend on the angle ϕ .

Now we exploit the following geometrical property of the ellipse. While the sections $v_i(\phi)$ and $\bar{v}_i(\phi)$ connecting points of the ellipse with its focus depend on their orientation ϕ , the combinations

$$\frac{1}{v_i(\phi)} + \frac{1}{\bar{v}_i(\phi)} = \frac{2A}{B^2}, \quad i = 1, 2 \quad (13)$$

are invariant with respect to the angle ϕ . Using the relations (9)-(13), we get

$$\Delta t = t_{II} - t_I = 2(d_{II} - d_I). \quad (14)$$

This relation means that difference between times the light rays II and I take to travel in the spectrometer arms with the lengths d_{II} and d_I does not depend on the spectrometer orientation ϕ . Therefore, rotation of the spectrometer apparatus can not cause any shift of the interference fringes even for $\vec{u} \neq 0$.

2.2. Three mirror set-up

In this part we demonstrate that the invariant property with respect to rotation of a more complicated spectrometer is also valid. Consider the spectrometer with three mirrors which reflect the rays of light along the sides of a triangle KLM (Fig.2a). A light signal is emitted in the point K and then travels along the path d_1 , d_2 , and d_3 . The corresponding time interval

$$t_{KLM} = \frac{d_1}{v_1(\phi)} + \frac{d_2}{v_2(\phi)} + \frac{d_3}{v_3(\phi)} \quad (15)$$

is function of the velocities $v_1(\phi)$, $v_2(\phi)$, and $v_3(\phi)$. The velocities are depicted on the velocity diagram in Fig.2b. They depend on the orientation ϕ of the triangle KLM in the spectrometer plane. We show that if the three mirror set-up rotates, the time t_{KLM} remains invariant, though values of the velocities $v_i(\phi)$ change during such rotation. Let us start with the elementary relation

$$\frac{d_1}{\sin \alpha_1} = \frac{d_2}{\sin \alpha_2} = \frac{d_3}{\sin \alpha_3} \equiv d_{KLM} \quad (16)$$

in the triangle KLM . When exploiting the relations $\beta_i = \pi - \alpha_i$ between the angles in Figs. 2a and 2b, one can write

$$t_{KLM} = d_{KLM} \left(\frac{\sin \beta_1}{v_1(\phi)} + \frac{\sin \beta_2}{v_2(\phi)} + \frac{\sin \beta_3}{v_3(\phi)} \right). \quad (17)$$

Because of spatial rotational invariance (12), the angles α_i , β_i and the distances d_i do not depend on the angle ϕ , i.e they do not depend on the rotation of the apparatus as the

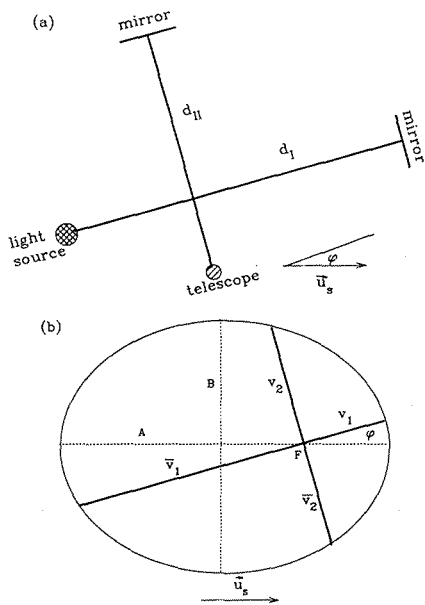


Figure 1: (a) Sketch of the Michelson-Morley experiment. (b) Corresponding velocity diagram. The \vec{u}_s is projection of the space-time anisotropy \vec{u} into the spectrometer plane

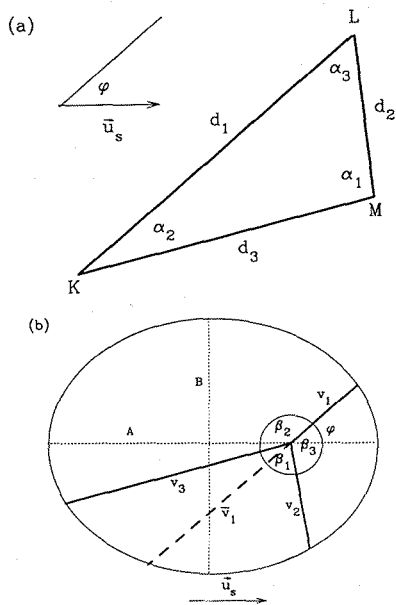


Figure 2: (a) Space diagram of a three mirror set-up. (b) Corresponding velocity diagram

whole. The ϕ invariance of the expression (17) is consequence of the following geometrical property of any ellipse. While the magnitudes of the sections $v_i(\phi)$ are functions of the angle ϕ , the combination

$$\frac{\sin \beta_1}{v_1(\phi)} + \frac{\sin \beta_2}{v_2(\phi)} + \frac{\sin \beta_3}{v_3(\phi)} = \frac{A}{B^2} (\sin \beta_1 + \sin \beta_2 + \sin \beta_3) \quad (18)$$

is invariant with respect to ϕ . The invariance (13) is special case of this relation. Using Eqs. (16)-(18), one gets the expression $t_{KLM} = d_1 + d_2 + d_3$ which does not depend on the orientation ϕ . Therefore, time t_{KLM} the light rays take to travel along the triangle KLM does not depend on the rotation of three mirror set-up in the spectrometer plane.

Imagine now a light signal emitted in the point L divides into two rays which interfere in the point K. Suppose the first ray travels the distance d_1 and the second ray advances along $d_{II} = d_2 + d_3$. The difference $\Delta t = t_{II} - t_I$ between times which the light rays take to travel from L into K can be expressed as follows

$$\Delta t = \frac{d_2}{v_2(\phi)} + \frac{d_3}{v_3(\phi)} - \frac{d_1}{\bar{v}_1(\phi)}. \quad (19)$$

Adding the zero value of $d_1/v_1(\phi) - d_1/v_1(\phi)$ to the right hand side of (19) and exploiting Eqs. (13) and (18), one arrives at the expression

$$\Delta t = d_2 + d_3 - d_1 \quad (20)$$

which does not depend on ϕ . As a consequence, arbitrary rotation of the three mirror set-up will not cause any shift of the interference fringes measured in the point K.

The "null result" of the interference fringe shifts with rotations holds for any multi mirror set-up and for any value of the space-time anisotropy \vec{u} . We do not advocate the anisotropic spread of light in general. We point only to the fact that Michelson-Morley type experiments do not contradict with particular situations in which the anisotropy of light propagation could not be a priori excluded. In particular this can be true in ultra-relativistic collisions of hadrons and nuclei where idea of an effective structural space-time anisotropy induced by the interaction comes from the z-scaling. We have shown that, in principle, this idea does not contradict to our experience observed at larger scales.

References

- [1] I. Zborovský, M.V. Tokarev, Yu.A. Panebratsev, and G.P. Škoro, Phys. Rev. C **59**, 2227 (1999); M.V. Tokarev, Yu.A. Panebratsev, I. Zborovský, and G.P. Škoro, Int. J. Mod. Phys. A **16**, 1281 (2001).
- [2] I. Zborovský, hep-ph/0311306.
- [3] G.N. Ord. J. Phys. A: Math. Gen. **16**, 1869 (1983); L. Nottale, *Fractal Space-Time and Microphysics: Towards a Theory of Scale Relativity* (World Scientific, Singapore, 1993).
- [4] A.A. Michelson, Amer. Journ. of Science (3), **22**, 20 (1881); A.A. Michelson and E.W. Morley, ibd, **34**, 333 (1887);
- [5] C. Moller, *The Theory of Relativity* (Oxford, 1952).

Z-SCALING OF JET PRODUCTION AT TEVATRON

M.V. Tokarev* and T.G. Dedovich

*Veksler and Baldin Laboratory of High Energies,
Joint Institute for Nuclear Research,
141980, Dubna, Moscow region, Russia*

**E-mail: tokarev@sunhe.jinr.ru*

Abstract

New data on jet production obtained by the CDF and D0 Collaborations at the Tevatron in Run II are analyzed in the framework of z -scaling. Properties of data z -presentation are discussed. Physics interpretation of the scaling function $\psi(z)$ as a probability density to produce a particle with the formation length z is argued. It was shown that these experimental data confirm z -scaling.

1. Introduction

The production of very large transverse momentum hadron jets in hadron-hadron collision at high energies at SpS in CERN observed by UA2 and UA1 Collaborations confirming the hints of jet production in the experiment of AFS Collaboration at ISR was an convincing experimental proof of quarks and gluons existence confirming the theory of strong interaction - Quantum ChromoDynamics (QCD). The wide study of the phenomena is performed in $\bar{p} - p$ collisions at highest energy at the Tevatron [1, 2].

Jets are experimentally observed as a strong correlated group of particles in space-time which are copiously produced at hadron colliders. They are result of hard scattering of quarks and gluons and their subsequent transformation into real particles.

New era of QCD precision measurements is starting at hadron colliders RHIC, Tevatron and LHC. The study of the energy and angular dependencies of jet and dijet cross sections, invariant mass distribution of jets, structure and content of jets and their fragmentation properties is considered to give enough information both for verification of the theory (QCD and SM) and search for new physics phenomena in new kinematical domain.

Fragmentation of partons into hadrons is one of the least understanding feature of QCD. Even though the primary scattering process is described in term of perturbative QCD the hadronization chain contains very low, respective to the parent parton, p_{\perp} hadrons. Therefore the whole process is clearly a non-perturbative phenomena involving final state interactions which have to conserve color and baryon number. The quarks and gluons carry color charge and are essentially massless in the theoretical calculations. A hadron jet has no color charge and often large invariant mass. Thus jets are ambiguous objects and should be treated in such a way that these unavoidable ambiguities do not play an important role [3].

A search for general properties of jet production in hadron-hadron collisions is of great interest, especially in connection with commissioning such large accelerators of nuclei and proton as the RHIC at BNL and the LHC at CERN. The main physical goals of the investigations at these colliders are to search for and study Quark Gluon Plasma (QGP) - the hot and extremely dense phase of the nuclear matter, Higgs boson and particles

of new generation predicted by supersymmetry theories, and to understand origin of the proton spin.

Jets are traditionally considered to be one of the good probes for study the hard interaction between quarks and gluons in the surrounding nuclear matter and search for indication on phase transition. Jet production in collisions of polarized protons at the RHIC give a new tool for study of enigmatical Nature of particle spin as well.

In the report we present the results of our analysis of new data on jet production obtained by the CDF and D0 Collaborations at the Tevatron in Run II in the framework of z -scaling concept. The concept is based on the fundamental principles such as self-similarity, locality and fractality of structure of colliding objects, interaction of their constituents and mechanism of particle formation.

The scaling function $\psi(z)$ and scaling variable z used for presentation of experimental data are expressed via the observable quantities, such as an inclusive cross section and multiplicity density. The function ψ has simple physical interpretation as the probability density to form a jet with formation length z .

We would like to emphasize that the properties of z -presentation for jet production give evidence on fractality of jet formation mechanism at very small scale up to 10^{-4} Fm. This is the region where the geometry of space-time itself could play an important role for search for general regularities of all fundamental interactions.

The results of our new analysis are found to be in good agreement with previous ones [5] and are considered as a new confirmation of z -scaling at the Tevatron.

2. Z-scaling

In the section we would like to remind some basic ideas and definitions of z -scaling. As shown in [4, 5, 6] self-similarity of high- p_T particle formation reveals itself as possibility to describe physical process in terms of the scaling function $\psi(z)$ and scaling variable z . The function is expressed via the invariant cross section $Ed^3\sigma/dp^3$ and the multiplicity density $dN/d\eta$ as follows

$$\psi(z) = -\frac{\pi s}{(dN/d\eta)\sigma_{in}} J^{-1} E \frac{d^3\sigma}{dp^3} \quad (1)$$

Here, s is the center-of-mass collision energy squared, σ_{in} is the inelastic cross section, J is the corresponding Jacobian. The factor J is the known function of the kinematic variables, the momenta and masses of the colliding and produced particles.

The normalization equation

$$\int_0^\infty \psi(z) dz = 1 \quad (2)$$

allows us to interpret the function $\psi(z)$ as a probability density to produce a particle with the corresponding value of the variable z .

The variable z as established in [4, 5, 6] reveals property of fractal measure. It can be written in the form

$$z = z_0 \Omega^{-1}. \quad (3)$$

The finite part z_0 is the ratio of the transverse energy released in the binary collision of constituents and the average multiplicity density $dN/d\eta|_{\eta=0}$. The divergent part Ω^{-1}

describes the resolution at which the collision of the constituents can be singled out of this process. The quantity $\Omega(x_1, x_2) = m(1 - x_1)^{\delta_1}(1 - x_2)^{\delta_2}$ represents relative number of all initial configurations containing the constituents which carry fractions x_1 and x_2 of the incoming momenta. The δ_1 and δ_2 are the anomalous fractal dimensions of the colliding objects (hadrons or nuclei). The momentum fractions x_1 and x_2 are determined in a way to minimize the resolution $\Omega^{-1}(x_1, x_2)$ of the fractal measure z with respect to all possible sub-processes satisfying the momentum conservation law. The variable z is interpreted as a particle formation length.

The general regularities of z -scaling for jet production in $p - p$ and $\bar{p} - p$ collisions at the ISR, SpS and Tevatron were established in [5]. In the present report the regularities are verified by using new experimental data obtained by the D0 and CDF Collaboration at the Tevatron in Run II.

3. Jets at hadron colliders

A jet is experimentally observed as a strong correlated group of particles in space-time. At low collision energies high- p_T hadrons were only observed and considered as result of hard scattering of elementary hadron constituents. At high collision energy \sqrt{s} jets are copiously produced at hadron colliders such as SpS and Tevatron. They are considered as an experimental signature of quarks and gluons interactions.

Figure 1 demonstrates the high- p_T spectra of π^0 -mesons produced at the ISR and azimuthal correlations of jets produced in $\bar{p} - p$ collisions at the SpS and Tevatron and in $p - p$ collisions at the RHIC.

3.1. Jet definition

In interaction of colliding hadrons two (or more) highly collimated collection of particles having approximately equal transverse momentum are observed. These collimated beams of particles in space-time are called jets. The strong correlation of high- p_T particles from the jets in the azimuthal plane is one of main features of jet production. The high- p_T hadrons are considered to be produced by hadronization of quarks and gluons. A typical dijet event is assumed to consist of hard interaction and underlying event. The last one includes initial and final gluon and quark radiation, secondary semi-hard interactions, interaction between remnants, hadronization and jet formation. Thus the procedure for extraction information on hard constituent interactions and comparison with theoretical calculation in the framework of QCD is an indirect one and sophisticated algorithms of data analysis are required.

3.2. Cone algorithm

A standard definition of a jet to facilitate comparisons of measurements from different experiments and with theoretical predictions was accepted in the Snowmass Accord [11].

The Snowmass Jet Algorithm defines a jet as a collection of partons, particles or calorimeter cells contained within a cone of an open angle R . All objects in an event have a distance from the jet center $\Delta R_i = \sqrt{(\phi_i - \phi_{jet})^2 + (\eta_i - \eta_{jet})^2}$, where (ϕ_{jet}, η_{jet}) define direction of the jet and (ϕ_i, η_i) are the coordinates of the parton, particle or center of the

calorimeter cell. If $\Delta R_i \leq R$ then the object is a part of jet. The transverse energy E_T and direction of jet are defined by formulas

$$E_T = \sum_{i \in R_i \leq R} E_T^i$$

$$\eta_{jet} = (1/E_T) \cdot \sum_{i \in R_i \leq R} \eta^i \cdot E_T^i \quad (4)$$

$$\phi_{jet} = (1/E_T) \cdot \sum_{i \in R_i \leq R} \phi^i \cdot E_T^i$$

An iterative procedure for finding the jets given by the Snowmass algorithm includes determination of jet seeds, jet cone formation, determination of the transverse energy and direction of jet. The definition of jet seed is not given by the algorithm. The Snowmass Accord does not deal with jet overlap.

At the parton level seeds could be partons, points lying between pairs of partons, a set of points randomly located in the $\eta - \phi$ space. Experimentally the seed could be defined as any cell in calorimeter or clusters of calorimeter cells. Therefore there are different treatment of jets at the parton and calorimeter level. To accommodate the difference between the jet definitions at the parton and calorimeter level in the modified Snowmass algorithm a purely phenomenological parameter R_{sep} has been suggested [12]. At the parton level R_{sep} is the distance between two partons when the clustering algorithm switches from a one jet to a two jet final state, even though both partons are contained within the jet defining cone. The maximum allowed distance ΔR between two partons in a parton jet divided by the cone size used: $R_{sep} = \Delta R/R$. The value of R_{sep} depends on details of the jet algorithm used and the experimental jet splitting and merging scheme.

3.3. Clustering k_T -algorithm

Clustering algorithms in contrast to cone algorithms, which globally find the jet direction, successively merge pairs of nearby vectors. The order in which vectors are recombined into jets defines the algorithm. The k_T -algorithm combines vectors based on their relative transverse momentum.

Several variants of the clustering k_T -algorithm for hadron collisions have been proposed [13]. It is designed to be independent of the order in which the seeds are processed. It is infrared and collinear safe. The initial seeds are all charged particles with $k_{T,i}$ in a given η -range. Each seed is labeled as prejet. Measure or closeness criterion in phase space is defined for each prejet and pair of prejets as follows

$$d_i = k_{T,i}^2 \quad (5)$$

$$d_{i,j} = \min\{k_{T,i}^2, k_{T,j}^2\} \cdot \Delta R_{i,j}^2 / R^2 \quad (6)$$

Here R is a jet cone size, $\Delta R_{i,j}$ is the distance between two prejets (i and j) in (η, ϕ) space. The procedure of jet finding includes the next steps: computation of the measure of all prejets and all pairs of prejets; finding of the prejet or pair of prejets with the smallest measure d_{min} ; promotion it to a jet and remove its particles from considerations if d_{min} arises from a single prejet; combination the pair into a new prejet and recompute measure

for all prejets and pairs of prejets if d_{min} arises from a pair of prejets; continuation previous steps until all prejets have been promoted to jet.

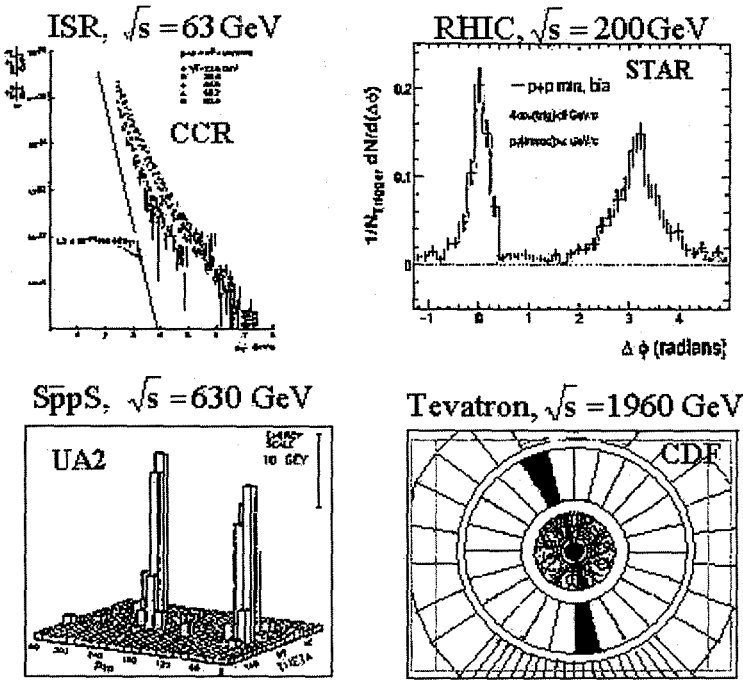


Figure 1. Jets at the ISR, RHIC, SpS and Tevatron colliders

Here we would like to note that different modifications of cone and clustering algorithms have been used in analysis of experimental and theoretical jet data to obtain their compatibility [11, 13, 14, 15]. It is especially important for study of soft and hard processes contribute to jet formation [16]. Transformation of quarks and gluons into real particles is considered to include evolution of constituent structure and their interactions at different scales. It corresponds to different scheme used for evolution of parton distribution functions [17, 18, 19]. Therefore general regularities which can be extracted from experimental data could give complementary constraints on theoretical models of jet formation and new insight on origin of particle mass as well.

4. Z -scaling and jet production at Tevatron in Run II

In this section we analyze new data on inclusive cross section of jet production in $\bar{p}-p$ collisions at $\sqrt{s} = 1960$ GeV obtained by the D0[20, 22] and CDF [21, 23] Collaborations at the Tevatron in Run II and compare them with our previous results [5].

4.1. Energy independence of ψ

The production hadron jets at the Tevatron probes the highest momentum transfer region currently accessible and thus potentially sensitive to a wide variety of new physics. The information on inclusive jet cross section at high transverse momentum range is the basis to test QCD, in particular to extract the strong coupling constant $\alpha_S(Q^2)$, the parton distribution functions and to constrain uncertainties for gluon distribution in the high- x range. In Run II, as mention in [23], the measurement of jet production and the sensitivity to new physics will profit from the large integrated luminosity and the higher cross section, which is associated with the increase in the center-of-mass energy from 1800 to 1960 GeV. Therefore the test of z -scaling for jet production in $\bar{p} - p$ collisions in new kinematic range is of great interest to verify scaling features established in our previous analysis [5].

The D0 and CDF Collaborations have carried out the measurements [20, 21] of transverse spectra of single inclusive cross sections of jet production at $\sqrt{s} = 1960$ GeV. In the D0 [20] and CDF [21] experiments single jets were registered in the $0.0 < |\eta| < 0.5$ and $0.1 < |\eta| < 0.7$ ranges, respectively. The data were used in present analysis.

New data on inclusive cross sections of jet production in $\bar{p} - p$ collisions obtained by the D0 Collaboration at the Tevatron in Run II are presented in Figure 2(a) [20]. Spectrum of jet production is measured at $\sqrt{s} = 1960$ GeV in the pseudorapidity and transverse momentum ranges $|\eta| < 0.5$ and $p_T = 60 - 560$ GeV/c, respectively. Data p_T - and z -presentations are shown in Figure 2(b) and 2(c), respectively. Note that results of present analysis of new D0 data are in a good agreement with our results [4] based on the data [14] obtained by the same Collaboration in Run I. The energy independence and the power law (the dashed line in Figure 2(c)) of the scaling function $\psi(z)$ are found to be as well.

The dependence of single jet cross section on transverse momentum of jet in $\bar{p} - p$ collisions at $\sqrt{s} = 630, 1800$ and 1960 GeV is shown in Figure 3(a). The data [15, 21] covers momentum range $p_T = 10 - 560$ GeV/c. The energy dependence of jet cross section is observed to be strong from $\sqrt{s} = 630$ to 1800 GeV. and weak from 1800 to 1960 GeV. Data p_T and z -presentation is shown in Figure 3(b) and 3(c), respectively. As seen from Figure 3(c) new data [21] are in agreement with other ones obtained in Run I. The energy independence of $\psi(z)$ is observed up to $z \simeq 4000$. Asymptotic behavior of scaling function is described by the power law, $\psi(z) \sim z^{-\beta}$ (the dashed line in Figure 3(c)). The slope parameter β is energy independent over a wide p_T -range.

4.2. Angular independence of ψ

Let us consider the angular dependence of p_T - and z -presentations new of D0 [22] and CDF [23] data. The D0 and CDF collaborations have carried out the measurements [22, 23] of the angular dependence of the single inclusive cross sections of jet production at $\sqrt{s} = 1960$ GeV. In the D0 experiment [22] a single jet was registered in the range $0.0 < |\eta| < 2.4$. In the CDF experiment [23] jets were registered in the ranges $0.1 < |\eta_1| < 2.8$.

We would like to note that the strong dependence of the cross sections on the angle of produced jet was experimentally found at the SpS and the Tevatron in Run I.

Figures 4(a) and 5(a) show the dependence of the cross sections of the $\bar{p} + p \rightarrow jet + X$

process on the transverse momentum p_{\perp} at $\sqrt{s} = 1960$ GeV for different rapidity intervals, $0.5 < |\eta| < 2.4$ and $0.1 < |\eta| < 2.8$, measured by the D0 and CDF Collaborations, respectively. The p_T -presentation of new data [22, 23] demonstrates the strong angular dependence as well. The qualitative regularities of jet spectra at $\sqrt{s} = 1960$ GeV are similar to ones at $\sqrt{s} = 630$ GeV and 1800 GeV.

We verify the hypothesis of the angular scaling for z -presentation of the data for jet production in $\bar{p} - p$ collisions. The angular scaling of data z -presentation means that the scaling function $\psi(z)$ at given energy \sqrt{s} has the same shape over a wide p_T and pseudorapidity range of produced jets.

Figure 4(b,c) and 5(b,c) demonstrate p_T and z -presentation of the D0 [22] and CDF [23] data sets, respectively. Taking into account errors of the experimental data we can conclude that the data confirm the angular scaling of $\psi(z)$. Nevertheless it is necessary to note that some points (last five and seven points corresponding to the (1.4,2.1) and (2.1,2.8) pseudorapidity ranges of the data [23] and two last points corresponding to the (1.5,2.0) and (2.0,2.4) pseudorapidity ranges of the data [22]) deviate from the power law. This is not real indication of z -scaling violation. The reason of the deviation is impossibility to take correctly into account the kinematical conditions of constituent subprocess due to large pseudorapidity bins for reconstructed jets. The smaller angular binning and more higher statistics of data are necessary to resolve the problem.

4.3. Jet multiplicity density $dN/d\eta$

The important ingredient of z -scaling is the multiplicity density $\rho(s, \eta) \equiv dN/d\eta$. The quantity is well determined in analysis of high- p_T particle production. The energy dependence of $\rho(s)$ for charged hadrons produced in $p - p$ and $\bar{p} - p$ collisions at $\eta = 0$ is measured up to $\sqrt{s} = 1800$ GeV. The dependence is used to construct z and ψ for different pieces of particles.

In the case of jet production the quantity is not well determined. It is connected with the experimental and theoretical determination of jets. In the analysis [5] the normalized jet multiplicity density $\rho(s)/\rho_0$ has been used. The value of $\rho(s)/\rho_0$ at the normalization point $\sqrt{s} = 1800$ GeV is equal to 1.

Figure 6 shows the dependence of $\rho(s)/\rho_0$ on the collision energy \sqrt{s} . At the accessible energy range the dependence is well described by the power law shown in Figure 6 by the dashed line.

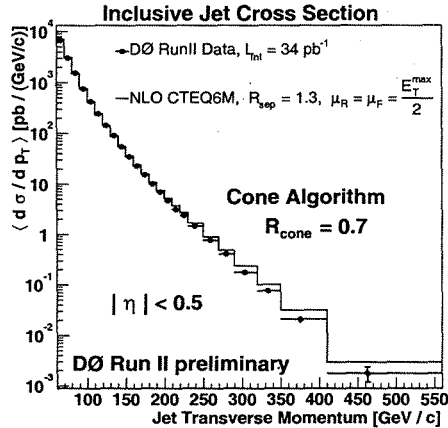
5. Conclusion

Analysis of new experimental data on jet production in $\bar{p} - p$ collisions obtained at the Tevatron in Run II by the CDF and D0 collaborations in the framework of data z -presentation was performed.

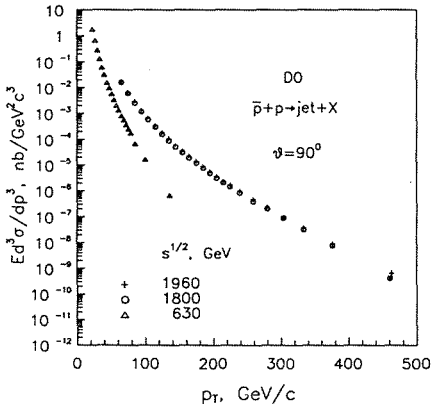
The scaling function $\psi(z)$ and scaling variable z expressed via the experimental quantities, the invariant inclusive cross section $Ed^3\sigma/dp^3$ and the jet multiplicity density $\rho(s, \eta)$ are constructed. The scaling function ψ is interpreted as a probability density to produce a jet with the formation length z .

The general regularities of jet production (the energy and angular independence of ψ , and the power law) found at the ISR, SpS and Tevatron in Run I are confirmed in new

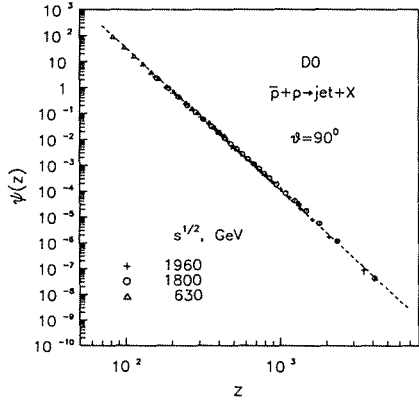
kinematical range ($\sqrt{s} = 1960$ GeV and $p_T = 10 - 550$ GeV/c). Results of our analysis of new experimental data are found to be in good agreement with results obtained by the D0 and CDF Collaboration in Run I. The obtained results are new evidence that mechanism of jet formation reveals self-similar and fractal properties over a wide transverse momentum range.



a)

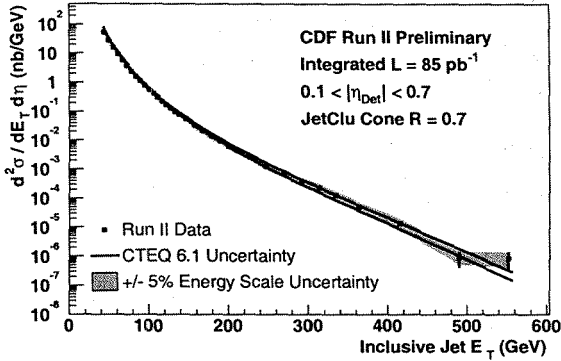


b)

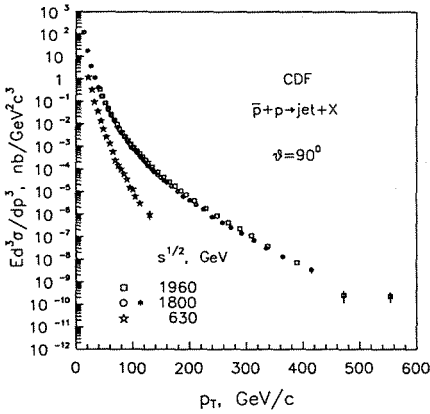


c)

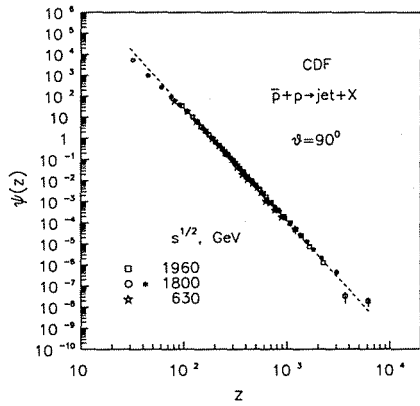
Figure 2. (a) The preliminary D0 data [20] on inclusive spectrum $d\sigma/dp_T$ of one jets produced in $\bar{p} - p$ collisions at $\sqrt{s} = 1960$ GeV in the central pseudorapidity range $|\eta| < 0.5$ as a function of the transverse momentum. (b) The D0 data on invariant cross section $E d^3\sigma/dp^3$ of jet production at $\sqrt{s} = 630, 1800$ GeV [14] and 1960 GeV [20] in p_T - and (c) z -presentations. The dashed line represents the power fit to the data



a)



b)

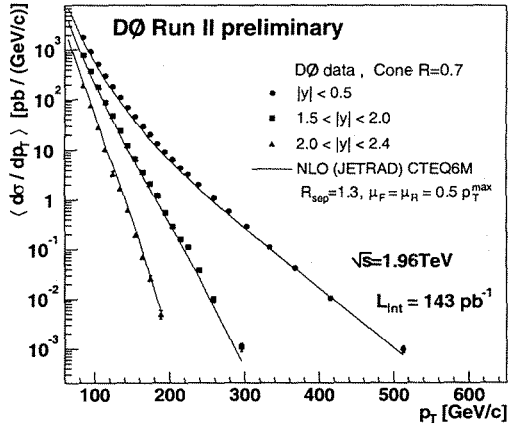


c)

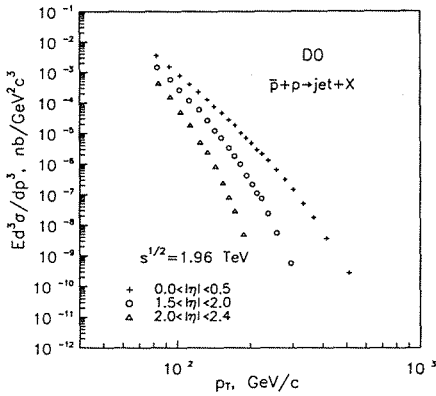
Figure 3. a) The preliminary CDF data [21] on inclusive spectrum $d^2\sigma/dE_T d\eta$ of one jets produced in $\bar{p}-p$ collisions at $\sqrt{s} = 1960$ GeV in the central pseudorapidity range $0.1 < |\eta| < 0.7$ as a function of the transverse momentum. (b) The CDF data on invariant cross section $E d^3\sigma/dp^3$ of jet production at $\sqrt{s} = 630, 1800$ GeV [15] and 1960 GeV [21] in p_T - and (c) z -presentations. The dashed line represents the power fit to the data

Thus we conclude that new data obtained at the Tevatron confirm the general concept of z -scaling. The further inquiry and search for violation of the scaling could give information on new physics phenomena in high energy hadron collisions and determine domain of validity of the strong interaction theory and the Standard Model itself.

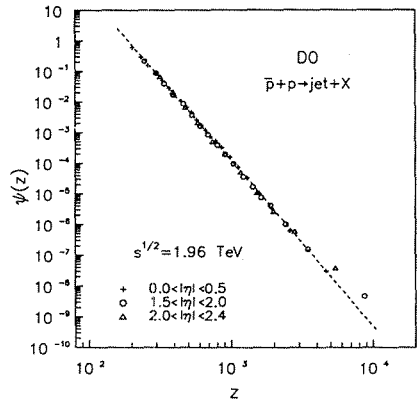
Acknowledgments. The authors would like to thank I. Zborovský, Yu. Pabrattsev, and O. Rogachevski for collaboration and numerous fruitful and stimulating discussions of the problem.



a)

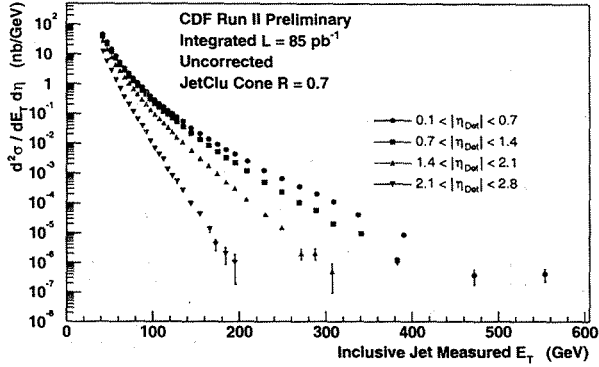


b)

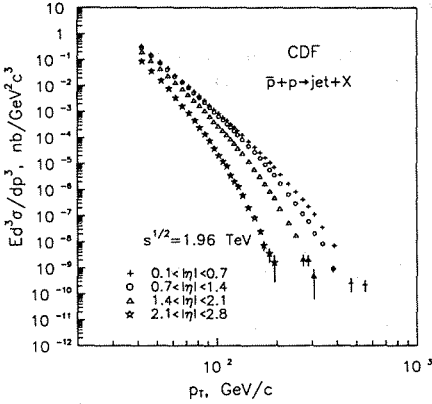


c)

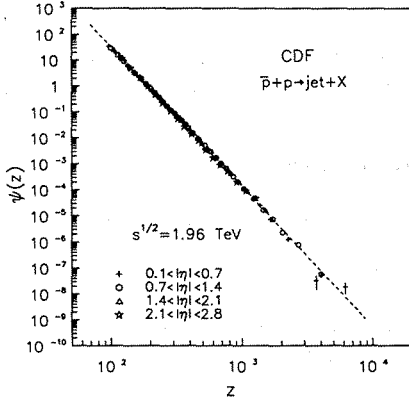
Figure 4. a) The preliminary D0 data [22] on inclusive spectrum $d\sigma/dp_T$ of one jets produced in $\bar{p}-p$ collisions at $\sqrt{s} = 1960$ GeV in the different pseudorapidity ranges $0. < |\eta| < 0.5$, $2.5 < |\eta| < 2.0$ and $2.0 < |\eta| < 2.4$ as a function of the transverse momentum p_T . (b) The D0 data on invariant cross section $Ed^3\sigma/dp^3$ of jet production at $\sqrt{s} = 1960$ GeV [22] in p_T - and (c) z -presentations. The dashed line represents the power fit to the data



a)



b)



c)

Figure 5. a) The preliminary CDF data [23] on inclusive spectrum $d^2\sigma/dE_T d\eta$ of one jets produced in $\bar{p}-p$ collisions at $\sqrt{s} = 1960$ GeV in the different pseudorapidity ranges $0.1 < |\eta| < 0.7$, $0.7 < |\eta| < 1.4$, $1.4 < |\eta| < 2.1$, and $2.1 < |\eta| < 2.8$ as a function of the transverse momentum p_T . (b) The CDF data on invariant cross section $E d^3\sigma/dp^3$ of jet production at $\sqrt{s} = 1960$ GeV [23] in p_T - and (c) z -presentations. The dashed line represents the power fit to the data

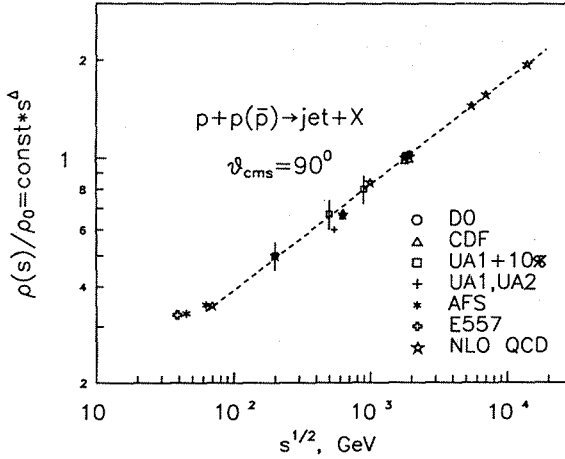


Figure 6. The dependence of the normalized jet multiplicity density $\rho(s)/\rho_0$ in $\bar{p}-p$ collisions on energy \sqrt{s} . The dashed line represents the power fit to the data

References

- [1] A.Korytov, *Sov. J. Nucl. Phys.* **67**, 51 (2004).
- [2] F.Rimondi *et al.*, (CDF Collaboration) *Sov. J. Nucl. Phys.* **67**, 128 (2004).
- [3] S.D. Ellis, *Talk presented at the XXVIII Rencontres de Moriond (1999)*; *hep-ph/9306280*.
- [4] I.Zborovský, Yu.A.Panebratsev, M.V.Tokarev, G.P.Škoro, *Phys. Rev. D* **54**, 5548 (1996); I.Zborovský, M.V.Tokarev, Yu.A.Panebratsev, G.P.Škoro, *Phys. Rev. C* **59**, 2227 (1999); M.V.Tokarev, O.V.Rogachevski, T.G.Dedovich, *J. Phys. G: Nucl. Part. Phys.* **26**, 1671 (2000); M.V.Tokarev, O.V.Rogachevski, and T.G.Dedovich, Preprint No. E2-2000-90, JINR (Dubna, 2000); M.Tokarev, I.Zborovský, Yu.Panebratsev, G.Skoro, *Int. J. Mod. Phys. A* **16**, 1281 (2001); M.Tokarev, *hep-ph/0111202*; M.Tokarev, D.Toivonen, *hep-ph/0209069*; G.P.Skoro, M.V.Tokarev, Yu.A.Panebratsev, I.Zborovský, *hep-ph/0209071*; M.V.Tokarev, G.L.Efimov, D.E.Toivonen, *Physics of Atomic Nuclei*, **67**, 564 (2004). M.Tokarev, *Acta Physica Slovaca*, **54** (2004) 321.
- [5] M.V.Tokarev, T.G.Dedovich, *Int. J. Mod. Phys. A* **15**, 3495 (2000).
- [6] M.V.Tokarev, JINR Preprint E2-98-92, Dubna, 1998; JINR Preprint E2-98-161, Dubna, 1998; M.V.Tokarev, E.V.Potrebenikova, *Computer Physics Communications* **117**, 229 (1999); M.Tokarev, G.Efimov, *hep-ph/0209013*.
- [7] L.Nottale, *Fractal Space-Time and Microphysics* (World Sci., Singapore, 1993).
- [8] B.Mandelbrot, *The Fractal Geometry of Nature* (Freeman, San Francisco, 1982).

- [9] I.Zborovský, hep-ph/0311306.
- [10] M.Tokarev, In *Proceedings of the International Workshop "Relativistic Nuclear Physics: From Hundreds of MeV to TeV"*, Varna, Bulgaria, September 10-16, 2001, p.280-300; JINR E1,2-2001-290.
- [11] J.Huth *et al.*, In *Proceedings of Research Directions for the Decade, Snowmass, 1990*, edited by E.L. Berger (World Scientific, Singapore, 1992).
- [12] S.D.Ellis, Z.Kunszt, D.Soper, Phys. Rev. Lett. **69**, 3615 (1992).
- [13] S.Catani, Yu.L.Dokshitzer, B.R.Webber, Phys. Lett. **B285**, 191 (1992); S.Catani, Yu.L.Dokshitzer, M.H.Seymour, B.R.Webber, Nucl. Phys. **B406**, 187 (1993); S.D.Ellis, D.E.Soper, Phys. Rev. **D48**, 3160 (1993).
- [14] B.Abbott *et al.*, (D0 Collaboration) Phys. Rev. **D64**, 032003 (2001).
- [15] F.Abe *et al.*, (CDF Collaboration) Phys. Rev. Lett. **62**, 613 (1989); **68**, 1104 (1992); **70**, 1376 (1993); **74**, 3439 (1995); **77**, 438 (1996); **80**, 3461 (1998).
- [16] R.Field, D.Stuart, In *Run II Jet Physics: Proceedings of the Run II QCD and Weak Boson Physics Workshop, Fermilab, February 1, 2000*.
G.C. Blazey *et al.*, In *Run II Jet Physics: Proceedings of the Run II QCD and Weak Boson Physics Workshop, Fermilab, February 1, 2000*; hep-ex/0005012.
- [17] V.N.Gribov, L.N.Lipatov, Sov. J. Nucl. Phys. **15**, 438 (1972); **15**, 675 (1972).
L.N.Lipatov, Sov. J. Nucl. Phys. **20**, 93 (1975).
G.Altarelli, G.Parisi, Nucl.Phys. **B26**, 298 (1977).
Yu.I.Dokshitzer, Sov.Phys. JETP **46**, 641 (1977).
- [18] L.N.Lipatov, Sov. J. Nucl. Phys. **23**, 642 (1976).
V.S.Fadin, E.A.Kuraev, L.N.Lipatov, Phys. Lett. **B60**, 50 (1975).
E.A.Kuraev, L.N.Lipatov, V.S.Fadin, Sov. Phys. JETP **44**, 45 (1976); **45**, 199 (1977).
Ya.Ya.Balitsky, L.N.Lipatov, Sov. J. Nucl. Phys. **28**, 822 (1978).
- [19] M.Ciafaloni, Nucl. Phys. **B296**, 49 (1988).
S.Catani, F.Fiorani, G.Marchesini, Phys. Lett. **B234**, 339 (1990); Nucl. Phys. **B336**, 18 (1990). M. Marchesini, Nucl. Phys. **B445**, 49 (1995).
- [20] M.Begel *et al.*, (D0 Collaboration) hep-ex/0305072.
- [21] A.Meyer *et al.*, (CDF Collaboration) Mod. Phys. Lett. **A18**, 1643 (2003).
- [22] F.Chlebana *et al.*, (D0 & CDF Collaboration) In *Proceedings of XXXII International Conference on High Energy Physics, August 16-22, 2004, Beijing, China*.
- [23] M.Tönnemann *et al.*, (CDF Collaboration) hep-ex/0310055; M.Gallinaro, In *Proceedings of XXXVIII Rencontres de Moriond session "QCD and High Energy Hadronic Interactions"*, Les Arcs, France, March 22-29, 2003.

SCALING IN INCLUSIVE ELECTRON SCATTERING FROM NUCLEI

M.K. Gaidarov^{1†}, A.N. Antonov¹, M.V. Ivanov¹, D.N. Kadrev¹, E. Moya de Guerra² and J.M. Udias³

(1) *Institute of Nuclear Research and Nuclear Energy, Bulgarian Academy of Sciences, Sofia 1784, Bulgaria*

(2) *Instituto de Estructura de la Materia, CSIC, Serrano 123, 28006 Madrid, Spain*

(3) *Departamento de Física Atómica, Molecular y Nuclear, Facultad de Ciencias Físicas, Universidad Complutense de Madrid, Madrid E-28040, Spain*

† *E-mail: gaidarov@inrne.bas.bg*

Abstract

A concept of relativistic y -scaling and an approach of superscaling going beyond the relativistic Fermi gas model are applied to describe the most recent data on inclusive electron scattering from nuclei. We calculate the asymptotic scaling function $f(y)$ of the deuteron using nucleon momentum distribution obtained in the framework of the relativistic light-front dynamics (LFD) method. The LFD $f(y)$ reproduces well the experimental data even at very large negative y recently reached at TJLAB. Scaling functions $f(\psi')$ for different nuclei and for different transfer momenta are constructed within the coherent density fluctuation model (CDFM). The results for $f(\psi')$ agree with the available experimental data at different transfer momenta and energies below the quasielastic peak position, showing superscaling for negative values of ψ' including also those smaller than -1 . It is shown that the superscaling in nuclei can be explained quantitatively on the basis of the similar behavior of the high-momentum components of the nucleon momentum distribution in the CDFM in light, medium, and heavy nuclei which is known to be due to the short-range and tensor correlations in nuclei.

1. Introduction

High-energy electron scattering from nuclei can provide important information on the wave function of nucleons in the nucleus. In particular, using simple assumptions about the reaction mechanism, scaling functions can be deduced that, if shown to scale (i.e., if they are independent of the momentum transfer), can provide information about the momentum and energy distribution of the nucleons. Several theoretical studies [1, 2, 3] motivated by West's pioneer work on y -scaling [4] have indicated that such measurements may provide direct access to studies of short-range nucleon-nucleon (NN) correlation effects. This scaling is usually called scaling of the first kind. The comparison of the scaling functions of various nuclei with mass number $A \geq 4$ led to the conclusion that these functions are the same [5, 6]. This behaviour is called scaling of the second kind which, together with scaling of the first kind, leads to superscaling.

Recently inclusive electron scattering has been studied at the Thomas Jefferson National Accelerator Facility (TJNAF) with 4.045 GeV incident beam energy from C, Fe and Au targets [7] to $Q^2 \approx 7$ (GeV/c)². Data were also taken using liquid targets of hydrogen

and deuterium [8]. The data presented in [7, 8] represent a significant increase of the Q^2 range compared to previous SLAC measurement [9], in which an approach to the scaling limit for heavy nuclei is suggested but for low values of $|y| < 0.3$ GeV at momentum transfers up to 3 (GeV/c)², and, moreover, a scaling behaviour is observed for the first time at very large negative y ($y = -0.5$ GeV/c). Obviously, a complete understanding of this electron-nucleus scattering requires a relativistic approach to the quantities related to the y -scaling analysis for a detailed comparison with the experimental data.

A relativistic y -scaling has been considered in [10] by generalizing the nonrelativistic scaling function to the relativistic case. Realistic solutions of the spinor-spinor Bethe-Salpeter (BS) equation for the deuteron with realistic interaction kernel were used for systematic investigation of the relativistic effects in inclusive quasielastic electron-deuteron scattering. It has been demonstrated in [10] that, if the effects from the negative energy P -states are disregarded, the concept of covariant momentum distribution can be introduced. Recently a successful relativistic description of the nucleon momentum distribution in deuteron has been done [11] within the light-front dynamics method [12, 13]. The most important result from the calculations in [11] is the possibility of the LFD method to describe simultaneously both deuteron charge form factors (that has been shown in [14]) and the momentum distribution.

In the analyses [5, 6] the Fermi momentum for the relativistic Fermi gas (RFG) was used as a physical scale to define the proper scaling variable ψ' for each nucleus. As emphasized in [6], the actual dynamical physics content of the superscaling phenomenon considered is more complex than that provided by the RFG framework. In particular, as noticed there, the extension of the superscaling property to large negative values of ψ' ($\psi' < -1$) is not predicted by the RFG model. Thus, it is worth considering the superscaling in theoretical approaches which go beyond the RFG model. One of them is the coherent density fluctuation model (e.g. [15, 16, 17, 18]) which gives a natural extension of the Fermi-gas case to realistic finite nuclear systems.

The aim of our work is twofold. First, using the nucleon momentum distribution $n(k)$ obtained with the LFD method to calculate the deuteron scaling function and to compare it with the recent TJNAF data and with the BS result. Second, to see to what extent superscaling can be explained using the CDFM.

The paper is organized as follows. In Section II the y -scaling analysis of the deuteron within the LFD method is considered. The superscaling in nuclei beyond the relativistic Fermi gas model is presented in Section III. The summary of the present work is given in Section IV. More details of the explanation and results can be found in Refs. [19, 20].

2. y -scaling analysis of the deuteron within the light-front dynamics method

The scaling function is defined as the ratio of the measured cross section to the off-shell electron-nucleon cross section multiplied by a kinematic factor:

$$F(q, y) = \frac{d^2\sigma}{d\Omega d\nu} (Z\sigma_p + N\sigma_n)^{-1} \frac{q}{[M^2 + (y+q)^2]^{1/2}}, \quad (1)$$

where Z and N are the number of protons and neutrons in the target nucleus, respectively, σ_p and σ_n are the off-shell cross sections, and M is the mass of the proton. In analysing

quasielastic scattering in terms of the y -scaling a new variable $y = y(q, \nu)$ is introduced [21]. Then the nuclear structure function which is determined using the spectral function $P(k, E)$ as

$$F(q, \nu) = 2\pi \int_{E_{min}}^{E_{max}(q, \nu)} dE \int_{k_{min}(q, \nu, E)}^{k_{max}(q, \nu, E)} k dk P(k, E), \quad (2)$$

can be expressed in terms of q , and y rather than q and ν (see Eq. (1)). In Eq. (2) $E = E_{min} + E_{A-1}^*$ is the nucleon removal energy with E_{A-1}^* being the excitation energy of the final $A - 1$ nucleon system.

At high values of q a pure scaling regime is achieved, where $k_{min} \approx |y - (E - E_{min})|$ and Eq. (2) becomes

$$F(q, y) \rightarrow f(y) = 2\pi \int_{E_{min}}^{\infty} dE \int_{|y - (E - E_{min})|}^{\infty} k dk P(k, E). \quad (3)$$

In Eq. (3) the particular behavior of $P(k, E)$ at large k and E is used in order to extend the upper limits of integration to infinity [2].

In the deuteron one always has $E_{A-1}^* = 0$, so that the spectral function is entirely determined by the nucleon momentum distribution $n(k)$, i.e. $P(k, E) = n(k)\delta(E - E_{min})$, and, consequently, $k_{min} = |y|$ for any value of q . The scaling function (3) reduces to the longitudinal momentum distribution

$$f(y) = 2\pi \int_{|y|}^{\infty} k dk n(k). \quad (4)$$

The scaling function for deuteron calculated within the LFD method is shown in Fig. 1. It is compared with the TJNAF experimental data [8] for all measured angles. The Q^2 values are given for Bjorken $x = Q^2/2M\nu = 1$ and correspond to elastic scattering from a free nucleon. It is seen from Fig. 1 that the relativistic LFD scaling function is in good agreement with the data in the whole region of negative y available. As known, the scaling breaks down for values of $y > 0$ due to the dominance of other inelastic processes beyond the quasielastic scattering. Our LFD deuteron scaling function is also compared in Fig. 1 with the scaling function obtained within the BS formalism [10]. A small difference between the two results is observed for $y < -400$ MeV/c but, at the same time, the theoretical LFD scaling function is closer to the experimental data in the same region of y . The fact that both LFD and BS functions reveal similar behavior is a strong indication in favor of the consistency of the two relativistic covariant approaches in case of the y -scaling.

3. Superscaling in nuclei beyond the relativistic Fermi gas model

The scaling function in the RFG model expressed by the variable ψ' has the form [6]

$$f_{RFG}(\psi') = \frac{3}{4}(1 - \psi'^2)\Theta(1 - \psi'^2)\frac{1}{\eta_F^2} \left\{ \eta_F^2 + \psi'^2 \left[2 + \eta_F^2 - 2\sqrt{1 + \eta_F^2} \right] \right\}, \quad (5)$$

where $\eta_F = k_F/m_N$, m_N being the nucleon mass.

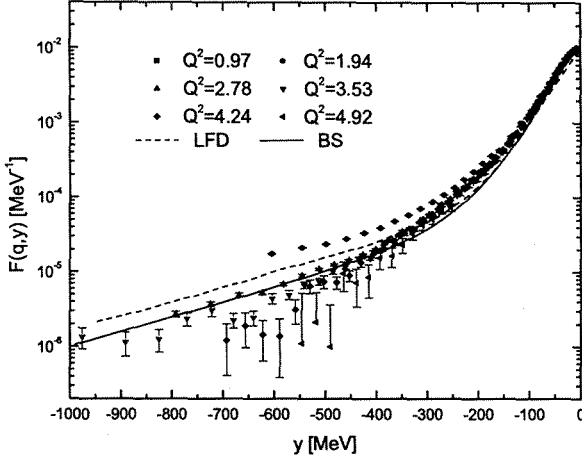


Figure 1: The scaling function of deuteron. The experimental data for different Q^2 values are from [8]. The solid and dashed curves represent the LFD calculations of this work and BS result of Ref. [10]

As shown in [6], the relationship between ψ' and the usual y -variable, in the approximation for the mass of the residual nucleus $M_{A-1}^0 \rightarrow \infty$, is given by the expression

$$\psi' = \frac{y}{k_F} \left[1 + \sqrt{1 + \frac{1}{4\kappa^2} \frac{1}{2} \eta_F \left(\frac{y}{k_F} \right)} + \mathcal{O}[\eta_F^2] \right], \quad (6)$$

where $\kappa = q/2m_N$.

Our basic assumptions within the CDFM is that the scaling function for a finite nucleus $f(\psi')$ can be defined by means of the weight function $|F(x)|^2$, weighting the scaling function for the RFG at given generator coordinate x (i.e. for a given density

$$\rho_0(x) = \frac{3A}{4\pi x^3} \quad (7)$$

and Fermi momentum

$$k_F(x) = \left(\frac{3\pi^2}{2} \rho_0(x) \right)^{1/3} \equiv \frac{\alpha}{x} \quad \text{with} \quad \alpha = \left(\frac{9\pi A}{8} \right)^{1/3} \simeq 1.52A^{1/3}. \quad (8)$$

Thus the scaling function $f(\psi')$ in the CDFM will be an infinite superposition of the RFG scaling functions $f(\psi'(x))$.

Let us introduce the notation

$$c \equiv \frac{1}{2m_N} \sqrt{1 + \frac{1}{4\kappa^2}}. \quad (9)$$

Then one can write from Eqs. (6) and (9), neglecting $\mathcal{O}[\eta_F^2]$, the scaling variable $\psi'_x(y)$ corresponding to the relativistic Fermi gas with the density $\rho_0(x)$ (7) and Fermi momentum $k_F(x)$ (8) in the form:

$$\psi'_x(y) = \frac{p(y)}{k_F(x)} = \frac{p(y)x}{\alpha}, \quad (10)$$

where for the cases of interest

$$p(y) = \begin{cases} y(1+cy), & y \geq 0 \\ -|y|(1-c|y|), & y \leq 0, |y| \leq 1/(2c). \end{cases} \quad (11)$$

For further use it is more convenient to introduce the notation

$$\psi'_x(y) = \frac{k_F}{k_F(x)} \frac{p(y)}{k_F} = \frac{k_F}{k_F(x)} \psi'. \quad (12)$$

Using the Θ -function in Eq. (5), the weighted scaling function for a finite nucleus can be presented by the integral

$$f(\psi') = \int_0^{\alpha/(k_F|\psi'|)} dx |F(x)|^2 \frac{3}{4} \left[1 - \left(\frac{k_F x \psi'}{\alpha} \right)^2 \right] \times \left\{ 1 + \left(\frac{x m_N}{\alpha} \right)^2 \left(\frac{k_F x \psi'}{\alpha} \right)^2 \left[2 + \left(\frac{\alpha}{x m_N} \right)^2 - 2 \sqrt{1 + \left(\frac{\alpha}{x m_N} \right)^2} \right] \right\}, \quad (13)$$

where the Fermi momentum k_F will not be a fitting parameter (as it is in the RFG model) for the different nuclei, but will be also calculated consistently in the CDFM,

$$k_F = \int_0^\infty dx k_F(x) |F(x)|^2 = \alpha \int_0^\infty dx \frac{1}{x} |F(x)|^2 \quad (14)$$

for each nucleus, with α given by Eq. (8). As can be seen from Eqs. (13), (12) and (11) in our approach the scaling function $f(\psi')$ is symmetric at the change of ψ' to $-\psi'$.

The scaling function $f(\psi')$ has been calculated using Eq. (13) by means of the weight function $|F(x)|^2$ determined from its relationship to the density distribution $\rho(r)$:

$$|F(x)|^2 = - \frac{1}{\rho_0(x)} \left. \frac{d\rho(r)}{dr} \right|_{r=x}, \quad (\text{at } d\rho(r)/dr \leq 0). \quad (15)$$

For the latter we used those obtained from experimental data on electron scattering from nuclei and muonic atoms.

We calculated the scaling function $f(\psi')$ (13) for various nuclei and transfer momenta. A symmetrized diffused Fermi density distribution has been used for ^4He and ^{12}C [22] and a diffused Fermi distribution for the heavier nuclei. The values of the half-radius R and diffuseness parameter b are given in Table 1 together with the results for the CDFM Fermi momentum k_F (14).

Table 1: Values of the parameters R and b (in fm) used in the calculations and the results for k_F (in fm $^{-1}$) obtained in the CDFM.

Nuclei	R	b	k_F
^4He	1.710	0.290	1.201
^{12}C	2.470	0.420	1.200
^{27}Al [23]	3.070	0.519	1.267
^{56}Fe [23]	4.111	0.558	1.270
^{197}Au [24]	6.419	0.449	1.335

In Fig. 2 are presented the results for the scaling function in the CDFM for $q=1000$ MeV/c and for ^4He , ^{12}C , ^{27}Al and ^{197}Au . The values of the parameters R and b for ^4He and ^{12}C (given in Table 1) lead to charge rms radii 1.71 fm and 2.47 fm, respectively, which coincide with the experimental ones [23]. The values of R and b for ^{27}Al are taken from [23]. The results of the CDFM scaling function (solid lines) are compared with the RFG predictions (dotted lines). In the RGF model, due to the Θ -function in Eq. (5), $f(\psi') = 0$ for $\psi' \leq -1$. As can be seen, the CDFM results give a good agreement with the data for the interval for ψ' from 0 till $\psi' < -1$ for all nuclei (including ^{56}Fe which is not shown). The only exception was observed for ^{197}Au using the values of the parameters $R = 6.419$ fm and $b = 0.449$ fm given in [24], for which the result is shown in Fig. 2 by dashed line.

4. Conclusion

The results of the present work can be summarized as follows:

i) The concept of relativistic y -scaling can be introduced in the light-front dynamics relativistic description of inclusive quasielastic eD scattering, in the same way as it is done in the conventional nonrelativistic approach. It has been pointed out that for $|y| > 400$ MeV/c the differences between the LFD and the nonrelativistic scaling functions are very large.

ii) The effective inclusion of the relativistic nucleon dynamics and of short-range NN correlations can be better seen when analyzing electron scattering at high momentum transfer from complex nuclei, for which a proper theoretical y -scaling analysis is still lacking. Such an investigation is in progress.

iii) We propose an extension of the RFG model to calculate the scaling function $f(\psi')$ in finite nuclei within the coherent density fluctuation model. In this model $f(\psi')$ is a weighted superposition of scaling functions for relativistic Fermi gases with different densities. The weight function is calculated using the known charge density distributions in nuclei.

iv) We calculate the scaling function $f(\psi')$ for inclusive electron scattering for ^4He , ^{12}C , ^{27}Al , ^{56}Fe and ^{197}Au nuclei and for various values of the transfer momentum $|\mathbf{q}|=1650$, 1560, 1000 and 500 MeV/c. The results agree with the available experimental data at different transferred momenta, and energies below the quasielastic peak position, showing superscaling for negative values of ψ' including also those smaller than -1. This is an improvement over the RFG model predictions where the scaling function becomes abruptly zero beyond $\psi' = -1$.

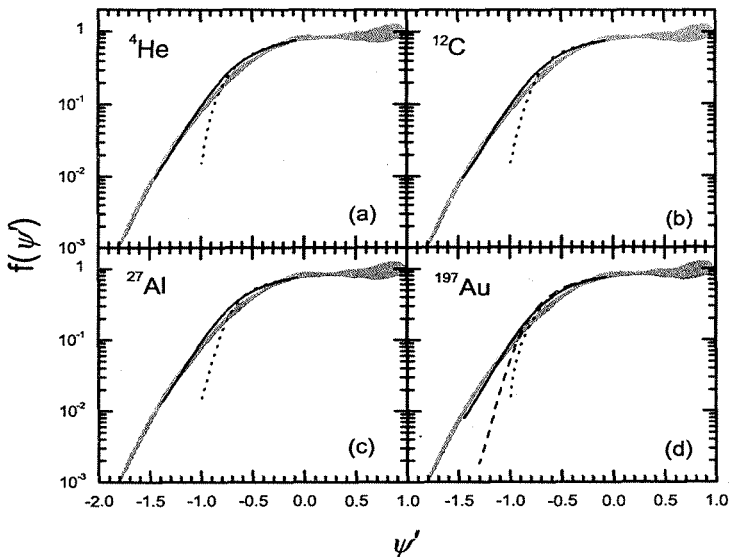


Figure 2: Results for the scaling function in the CDFM (solid line) calculated using Eqs. (13) and (14) at $q = 1000$ MeV/c and for ${}^4\text{He}$, ${}^{12}\text{C}$, ${}^{27}\text{Al}$ and ${}^{197}\text{Au}$ (with $b = 1.0$ fm for the latter) compared with the data (grey area) from [6]. The dotted line is the RFG result using Eq. (5). The dashed line in the case of ${}^{197}\text{Au}$ corresponds to the CDFM result with $b = 0.449$ fm

Four of the authors (A.N.A., M.K.G., D.N.K. and M.V.I.) are thankful to the Bulgarian National Science Foundation for partial support under the Contract No. Φ -1416. This work was partly supported by funds provided by DGI of MCyT (Spain) under Contracts BFM 2002-03562, BFM 2000-0600 and BFM 2003-04147-C02-01 and by the Agreement (2004 BG2004) between the CSIC (Spain) and the Bulgarian Academy of Sciences.

References

- [1] Xiangdong Ji and J. Engel, Phys. Rev. C **40**, R497 (1989).
- [2] C. Ciofi degli Atti, E. Pace, and G. Salmè, Phys. Rev. C **43**, 1155 (1991).
- [3] M.K. Gaidarov, A.N. Antonov, S.S. Dimitrova, and M.V. Stoitsov, Int. J. Mod. Phys. E **4**, 801 (1995).
- [4] G.B. West, Phys. Rep. **18**, 263 (1975).

- [5] T. W. Donnelly and I. Sick, *Phys.Rev. Lett.* **82**, 3212 (1999).
- [6] T. W. Donnelly and I. Sick, *Phys. Rev. C* **60**, 065502 (1999).
- [7] J. Arrington *et al.*, *Phys. Rev. Lett.* **82**, 2056 (1999).
- [8] J. Arrington, PhD Thesis (1998).
- [9] D.B. Day *et al.*, *Phys. Rev. Lett.* **59**, 427 (1987).
- [10] C. Ciofi degli Atti, D. Faralli, A.Yu. Umnikov, and L.P. Kaptari, *Phys. Rev. C* **60**, 034003 (1999).
- [11] A.N. Antonov, M.K. Gaidarov, M.V. Ivanov, D.N. Kadrev, G.Z. Krumova, P.E. Hodgson, and H.V. von Geramb, *Phys. Rev. C* **65**, 024306 (2002).
- [12] J. Carbonell and V.A. Karmanov, *Nucl. Phys A* **581**, 625 (1995).
- [13] J. Carbonell, B. Desplanques, V.A. Karmanov, and J.-F. Mathiot, *Phys. Rep.* **300**, 215 (1998) (and references therein).
- [14] D. Abbott *et al.*, Jefferson Lab. t_{20} Collaboration, *Phys. Rev. Lett.* **84**, 5053 (2000).
- [15] A.N. Antonov, V.A. Nikolaev, and I.Zh. Petkov, *Bulg. J. Phys.* **6**, 151 (1979); *Z.Phys. A* **297**, 257 (1980); *ibid.* **A304**, 239 (1982).
- [16] A.N. Antonov, V.A. Nikolaev, and I.Zh. Petkov, *Nuovo Cimento A* **86**, 23 (1985).
- [17] A.N. Antonov, P.E. Hodgson, and I. Zh. Petkov, *Nucleon Momentum and Density Distributions in Nuclei* (Clarendon Press, Oxford, 1988).
- [18] A.N. Antonov, P.E. Hodgson, and I. Zh. Petkov, *Nucleon Correlations in Nuclei* (Springer-Verlag, Berlin-Heidelberg-New York, 1993).
- [19] M.K. Gaidarov, M.V. Ivanov, and A.N. Antonov, in *Nuclear Theory'21: Proceedings of 21st International Workshop on Nuclear Theory*, Rila, Bulgaria, 2002, edited by V. Nikolaev (Heron Press, Sofia, 2002), p.193; nucl-th/0207081
- [20] A.N. Antonov, M.K. Gaidarov, D.N. Kadrev, M.V. Ivanov, E. Moya de Guerra, and J.M. Udias, *Phys. Rev. C* **69**, 044321 (2004).
- [21] E. Pace and G. Salmè, *Phys. Lett. B* **110**, 411 (1982).
- [22] V.V. Burov, D.N. Kadrev, V.K. Lukyanov, and Yu.S. Pol', *Phys. At. Nucl.* **61**, 525 (1998).
- [23] H. De Vries, C.W. De Jager, C. De Vries, *At.Data Nucl.Data Tables* **36**, 495 (1987).
- [24] J.D. Patterson and R.J. Peterson, *Nucl. Phys. A* **717**, 235 (2003).

NEW ASPECTS IN THE ASYMPTOTICS OF THE DEUTERON ELECTROMAGNETIC FORM FACTORS

A.F. Krutov^{1†}, V.E. Troitsky^{2‡} and N.A. Tsirova^{1§}

(1) Samara State University, Ac. Pavlov St. 1, 443011 Samara, Russia

(2) D.V. Skobeltsyn Institute of Nuclear Physics, Moscow State University, Vorobjevy Gory,
119992 Moscow, Russia

† E-mail: krutov@ssu.samara.ru

‡ E-mail: troitsky@theory.sinp.msu.ru

§ E-mail: ntsirova@ssu.samara.ru

1. Introduction

The deuteron is in focus of theoretical and experimental researches on an extent of several decades. The reasons of attention to this nuclear system are well known. First, this is the unique stable two-particles model. So it can be investigated with a great precision. Second, there is a plenty of the reliable experimental information about this system. That's why the deuteron is the first test of every model of NN interaction. Third, studying the deuteron structure in reactions of ed-scattering at very high momentum transfer it is possible to receive the information on a role of quark degrees of freedom in nuclear systems. Fourth, the deuteron-bounding energy is small. So the deuteron is a source of the information about a structure of its components.

The deuteron electromagnetic form factors allow us to describe quantifiable an interaction between the deuteron and electromagnetic field. Form factors can be calculated in terms of information about electron elastic scattering by deuteron.

The electron elastic scattering cross-section by deuteron is calculating by this formula [1], [2], [3]:

$$\frac{d\sigma}{d\Omega} = \left(\frac{d\sigma}{d\Omega} \right)_{Mott} \left[1 + \frac{2E_i}{M_d} \sin^{-2} \frac{\theta}{2} \right]^{-1} [G_C^2 + G_Q^2 + (1 + 2(1 + \eta_D) \tan^2 \frac{\theta}{2}) G_M^2], \quad (1)$$

with

$$\eta_D = -\frac{q^2}{4M_d^2}, \quad \left(\frac{d\sigma}{d\Omega} \right)_{Mott} = \frac{\alpha^2}{4E_i^2} \cos^2 \frac{\theta}{2} \csc^4 \frac{\theta}{2}. \quad (2)$$

The expression $\left(\frac{d\sigma}{d\Omega} \right)_{Mott}$ is a scattering cross-section by non-structure spin-free particle derived by Mott. 3 terms (G_C , G_Q , G_M) are the form factors making contribution to the full cross-section. They are due to charge, quadrupole moment and magnetic moment of the deuteron.

In the case of low momentum transfer we can describe an elastic ed-scattering by a nonrelativistic model. But there is a discrepancy between the theory and experiments in the case of high momentum transfer. But the modern development of elastic ed-scattering experiments is due to the advent of exactly high-intensity electron beam. For example,

scientists of Jefferson Laboratory carry out experiments of ed-scattering at very high momentum transfer (12 GeV^2).

In the Ref. [4] formulas defining form factors were derived by means of relativistic Hamiltonian dynamics. In this paper we find asymptotic properties of these expressions in the case of high momentum transfer. We also find asymptotics of the nonrelativistic form factors to estimate relativistic corrections. Last, we establish connection between asymptotic form factors behavior and the behavior of wave functions at small distances.

2. Nonrelativistic deuteron form factors at $Q^2 \rightarrow \infty$

In the case of nonrelativistic impulse approximation we present the next expressions for standart electromagnetic form factors: charge, quadrupole and magnetic dipole [5]:

$$\begin{aligned} G_C^{NR}(Q^2) &= \sum_{l,l'} \int k^2 dk k'^2 dk' u^l(k) \tilde{g}_{0C}^{ll'}(k, Q^2, k') u^{l'}(k'), \\ G_Q^{NR}(Q^2) &= \frac{2M_d^2}{Q^2} \sum_{l,l'} \int k^2 dk k'^2 dk' u^l(k) \tilde{g}_{0Q}^{ll'}(k, Q^2, k') u^{l'}(k'), \\ G_M^{NR}(Q^2) &= -M_d \sum_{l,l'} \int k^2 dk k'^2 dk' u^l(k) \tilde{g}_{0M}^{ll'}(k, Q^2, k') u^{l'}(k'). \end{aligned} \quad (3)$$

In these formulas $\tilde{g}_{0i}^{ll'}(k, Q^2, k')$, $i = C, Q, M$ are nonrelativistic free two-particle charge, quadrupole and magnetic dipole form factors. They describe electromagnetic properties of the non-interacting two nucleon system. $u_l(k)$ are the wave functions, $l, l' = 0, 2$ are orbital moments. Formulas for nonrelativistic free two-particle form factors are given in the Ref. [5].

In the modern models of nucleon-nucleon interaction the deuteron wave functions are represented by the next fits:

$$u_0(k) = \sqrt{\frac{2}{\pi}} \sum_j \frac{C_j}{(k^2 + m_j^2)}, \quad u_2(k) = \sqrt{\frac{2}{\pi}} \sum_j \frac{D_j}{(k^2 + m_j^2)}. \quad (4)$$

C_j and D_j are the numerical coefficients.

Corresponding expressions in coordinate are following:

$$\begin{aligned} u_0(r) &= \sum_j C_j \exp(-m_j r), \\ u_2(r) &= \sum_j D_j \exp(-m_j r) \left[1 + \frac{3}{m_j r} + \frac{3}{(m_j r)^2} \right]. \end{aligned}$$

Coefficients C_j and D_j are fitted for used wave functions to behave right at origin. Conditions for these coefficients are represented by formulas:

$$\sum_j C_j = 0, \quad \sum_j D_j = \sum_j D_j m_j^2 = \sum_j \frac{D_j}{m_j^2} = 0.$$

These conditions gives us the next standard behavior at small distances:

$$u_0(r) \sim r, \quad u_2(r) \sim r^3.$$

Let $F_d(Q^2) = \sqrt{A(Q^2)}$. In this expression $A(Q^2)$ is elastic structure function, which enters the differential cross-section. This function could be expressed in terms of the electromagnetic deuteron form factors: charge, quadrupole and magnetic dipole:

$$A(Q^2) = G_C^2(Q^2) + \frac{8}{9} \eta^2 G_Q^2(Q^2) + \frac{2}{3} \eta G_M^2(Q^2), \quad \eta = \frac{Q^2}{4M_d^2}. \quad (5)$$

We find asymptotic properties of integrals (3) by a modified Laplas method with Q^2 as a large positive parameter. Calculating these integrals we obtain the next deuteron form factors asymptotics:

$$F_d^{NR}(Q^2) \sim \frac{1}{(Q^2)^3}. \quad (6)$$

3. Relativistic deuteron form factors at $Q^2 \rightarrow \infty$

In the case that $Q^2 > 1 \text{ GeV}^2$ it is necessary to take into account relativistic corrections in the electromagnetic deuteron structure. Relativistic description of the deuteron is constructed by means of relativistic Hamiltonian dynamics. This approach was elucidate in the Ref. [4]. In this approach we present electromagnetic deuteron form factors by analogy with nonrelativistic case [5]:

$$\begin{aligned} G_C(Q^2) &= \sum_{i,i'} \int d\sqrt{s} d\sqrt{s'} \varphi^i(s) g_{0C}^{i'}(s, Q^2, s') \varphi^{i'}(s'), \\ G_Q(Q^2) &= \frac{2M_d^2}{Q^2} \sum_{i,i'} \int d\sqrt{s} d\sqrt{s'} \varphi^i(s) g_{0Q}^{i'}(s, Q^2, s') \varphi^{i'}(s'), \\ G_M(Q^2) &= -M_d \sum_{i,i'} \int d\sqrt{s} d\sqrt{s'} \varphi^i(s) g_{0M}^{i'}(s, Q^2, s') \varphi^{i'}(s'). \end{aligned} \quad (7)$$

In these formulas $g_{0i}^{i'}(s, Q^2, s'), i = C, Q, M$ are relativistic free two-particle charge, quadrupole and magnetic dipole form factors. Formulas for relativistic free two-particles form factors are given in the Ref. [5]. $\varphi^i(s)$ are the deuteron wave functions in sense of Relativistic Hamiltonian Dynamics. These functions are solutions of eigenvalue problem for a mass squared operator for the deuteron:

$$\hat{M}_d^2 |\psi\rangle = M_d^2 |\psi\rangle.$$

The mass operator is constructed in the following way:

$$\hat{M}_d^2 = \hat{M}_0^2 + \hat{V}.$$

In this expression M_0 is a mass operator of the two-nucleon system without interaction, and V is an interaction operator.

An eigenvalue problem for a mass squared operator is a nonrelativistic Schrödinger equation within a second order on deuteron binding energy. So the deuteron wave functions in sense of relativistic Hamiltonian dynamics differ from nonrelativistic wave functions in fact by conditions of normalization with relativistic density of states only:

$$\sum_{l=0,2} \int_0^\infty \varphi_l^2(k) \frac{dk}{2\sqrt{k^2 + M^2}} = 1,$$

$$\varphi_l(k) = \sqrt[4]{4(k^2 + M^2)} k u_l(k).$$

Calculating integrals (7) we obtain relativistic form factors asymptotics by analogy with (6).

$$F_d(Q^2) \sim \frac{1}{(Q^2)^{13/4}}. \quad (8)$$

We compare obtained function with experimentally measured (see [6]). An area of asymptotic behavior is not achieved in the case of momentum transfer from [6]. Using deuteron $A(Q^2)$ results from JLab we obtain the next behavior of this function in experimentally accessible area:

$$F_d^{exp}(Q^2) \sim \frac{1}{(Q^2)^{3.8}}. \quad (9)$$

1. Quark dynamics

At distances much less than the nucleon size, the underlying quark substructure of the nucleons cannot be ignored. At sufficiently "large" momentum transfers, the few-body form factors are expected to be calculable in terms of only quarks and gluons. The first attempt at a quark-gluon description of the few-body elastic form factors was based on the dimensional-scaling quark model. It was made in Refs. [7], [8]. The underlying dynamical mechanism during elastic scattering is the hard rescattering of the constituent quarks via exchange of hard gluons. In this approach asymptotics of the deuteron form factors should follow the power law:

$$F_h(Q^2) \sim \frac{1}{(Q^2)^{n_h-1}},$$

n_h - number of constituent quarks in hadrons. For the deuteron case:

$$F_h(Q^2) \sim \frac{1}{(Q^2)^5}.$$

Fig. 1 shows the recent JLab Hall A and older SLAC and Saclay data on the deuteron form factor, multiplied by $(Q^2)^5$. This is predicted data, but it is evident that the data tends to asymptotics of quark counting rules.

So an inverse problem can be set. Theoretically, asymptotics of the quark dynamics allow us to obtain information on the wave functions behaviour at origin. The deuteron wave function can be presented in the following way:

$$u_0(k) = \sqrt{\frac{2}{\pi}} \sum_j \frac{C_j}{(k^2 + m_j^2)^\alpha}.$$

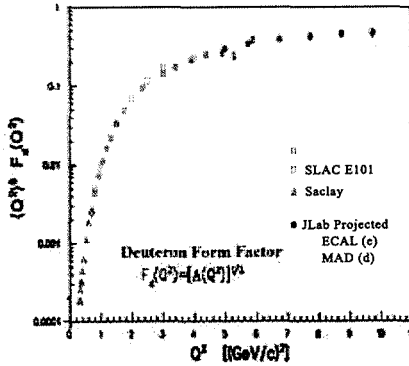


Figure 1: Projected data for the deuteron form factor $F_d(Q^2)$ with an 11 GeV JLab beam. Also shown are existing JLab, SLAC, and Saclay data [9]

Here α is a some additional parameter. In standard representation (4) $\alpha = 1$ and it doesn't result in quark asymptotics. It was obtained that quark asymptotics is achieved with $\alpha = 11/4$.

In coordinate representation we obtain the next expression for the deuteron wave function:

$$u_0(r) = \frac{32}{21 \sqrt{\pi} \Gamma\left(\frac{3}{4}\right)} \sum_j C_j m_j \left(\frac{r}{2m_j}\right)^{9/4} K_{\frac{5}{4}}(r m_j).$$

It has the following behaviour in small and large distances in this representation:

$$r \rightarrow 0, \quad u_0(r) \sim r \frac{2 \Gamma\left(\frac{1}{4}\right)}{21 \sqrt{\pi} \Gamma\left(\frac{3}{4}\right)} \sum_j \frac{C_j}{m_j^{5/2}},$$

$$r \rightarrow \infty, \quad u_0(r) \sim r^{7/4} \frac{2^{9/4}}{21 \Gamma\left(\frac{3}{4}\right)} \sum_j \frac{C_j}{m_j^{7/4}} e^{-r m_j}.$$

As we can see, it is linear in small distances and the wave function diminishes exponentially in large distances, that is right.

5. Conclusions

In summary we obtained an asymptotics of the deuteron electromagnetic form factors in the nonrelativistic impulse approximation. We also estimated the relativistic correction to the asymptotics. Finally, we have obtained the expressions for the wave functions which give the asymptotic of the electromagnetic form factors coinciding with quark counting rules.

This work was supported in part by the program "The development of the high school scientific potential" (grant 75358), and The Dynasty Foundation.

References

- [1] Glendenning N. K., Kramer G., Phys. Rev., **126** 2152 (1962).
- [2] Gourdin M., Nuovo Cimento, **28**, 533 (1963).
- [3] T.A. Griffi, L.I. Schiff, High Energy Physics, vol.1, New York, 1967, p.341.
- [4] A.F. Krutov, V.E. Troitsky, Phys.Rev.C **65**, 045501 (2002).
- [5] A.F. Krutov, V.E. Troitsky, Phys.Rev.C. **68**, 044307 (2003).
- [6] L.C. Alexa et al., Phys.Rev.Let. **82**, 1374 (1999).
- [7] S. J. Brodsky and G. R. Farrar, Phys. Rev. Lett. **31**, 1153 (1973).
- [8] V. A. Matveev, R. M. Muradyan and A. N. Tavkhelidze, Lett. Nuovo Cimento **7**, 719 (1973).
- [9] pCDR for The 12 GeV Upgrade of CEBAF. Jefferson Lab. Report of June, 2004.

METHOD OF THE POLARIZED SEMI-INCLUSIVE DEEP INELASTIC SCATTERING DATA ANALYSIS IN THE NEXT-TO-LEADING QCD ORDER

A.N. Sissakian, O.Yu. Shevchenko[†] and O.N. Ivanov[‡]

Joint Institute for Nuclear Research, Dubna, Russia

[†] *E-mail: Oleg.Chevchenko@cern.ch*

[‡] *E-mail: ivon@jinr.ru*

Abstract

The semi-inclusive deep inelastic scattering (SIDIS) process is considered. It is proposed a method allowing the direct extraction from the SIDIS data of the first moments of the polarized quark distributions in the next to leading (NLO) QCD order. The validity of the procedure is confirmed by the respective simulations. To this end both broken and symmetric sea scenarios are considered. Especial attention is paid to the application of the proposed procedure to such important questions as the symmetry of the light quark polarized sea and the polarized strangeness content in nucleon. In this connection the kinematic conditions of the HERMES and COMPASS experiments are studied.

The main points of interests for the modern semi-inclusive deep inelastic scattering (SIDIS) experiments with longitudinally polarized beam and target are the strange quark, light sea quark and gluon contributions to the nucleon spin (see, for example [1] and references therein). Of special importance is also still open question whether the polarized light quark sea symmetric or not, i.e., if the quantity¹ $\Delta_1\bar{u} - \Delta_1\bar{d}$ is equal to zero or not. At the same time it was shown[2, 3] that to get the reliable results on such the tiny quantities as Δs and $\Delta_1\bar{u} - \Delta_1\bar{d}$ from the data obtained at the relatively small average Q^2 available to modern SIDIS experiments (such as HERMES and COMPASS), one should apply next-to-leading order (NLO) QCD analysis. The respective procedure of Δ_1q extraction in NLO QCD order have been proposed in ref [4]. In ref. [4] it was shown that the proposed procedure could be successfully applied for the *direct* extraction from the SIDIS data of the quantities Δ_1u_V , Δ_1d_V and, eventually, of the quantity $\Delta_1\bar{u} - \Delta_1\bar{d}$. The respective equations for these quantities look as

$$\Delta_1u_V = \frac{1}{5} \frac{A_p^{exp} + A_d^{exp}}{L_1 - L_2}; \quad \Delta_1d_V = \frac{1}{5} \frac{4A_d^{exp} - A_p^{exp}}{L_1 - L_2}, \quad (1)$$

for valence distributions and

$$\Delta_1\bar{u} - \Delta_1\bar{d} = \frac{1}{2} \left| \frac{g_A}{g_V} \right| - \frac{2A_p^{exp} - 3A_d^{exp}}{10(L_1 - L_2)} \quad (2)$$

¹From now on the notation $\Delta_1q \equiv \int_0^1 dx \Delta q$ will be used to distinguish the local in Bjorken x polarized quark densities $\Delta q(x)$ and their first moments.

or the $\Delta_1\bar{u} - \Delta_1\bar{d}$. All the quantities in the r.h.s of these equations contain only already measured unpolarized quark distributions and pion fragmentation functions (favored and unfavored, entering the coefficients L_1 and L_2 , respectively), known NLO Wilson coefficients and the so-called “difference asymmetries” (see, for example, [1, 4, 5]) for the pion production on the proton and deuteron targets, $A_p^{\pi^+ - \pi^-}$ and $A_d^{\pi^+ - \pi^-}$, entering the quantities A_p^{exp} and A_d^{exp} . Thus, these difference asymmetries are the only unknown input which should be measured to find the quantities $\Delta_1 u_V$, $\Delta_1 d_V$ and $\Delta_1\bar{u} - \Delta_1\bar{d}$ using Eqs. (1) and (2).

In the paper [4] it was performed the detailed analysis on the possibility to correctly extract in NLO QCD order of the quantities $\Delta_1 u_V$, $\Delta_1 d_V$ and $\Delta_1\bar{u} - \Delta_1\bar{d}$ in the real conditions of the HERMES and COMPASS experiments. Special attention was paid to the such important questions as the statistical errors on the difference asymmetries² and to the uncertainties caused by the low x_B regions unavailable to HERMES and COMPASS. First of all, the performed in [4] analysis confirms that the proposed NLO QCD extraction procedure meets the main requirement: to reconstruct the quark moments in the accessible to measurement x_B region. On the other hand, it was shown that even with the rather overestimated low x_B uncertainties given in [4], one can conclude that the question is $\Delta_1\bar{u} - \Delta_1\bar{d}$ equal to zero or not could be answered even with the HERMES kinematics in the case of strongly asymmetric polarized sea. In any case, the situation is much better with the available to COMPASS x_B region.

At present COMPASS experiment uses only the polarized deuteron target in the muon part of its program. Besides, it is obvious that the statistic of semi-inclusive events with pion production is much higher than the respective statistics of kaon production (one identify about 90% pions among all semi-inclusive events). So, it is of interest to see could we extract so important quantity as polarized strangeness in nucleon using only pion production on the deuteron target. To this end we will use so-called “sum asymmetries” (see, for example, [5] and references therein) $A_d^{h+\bar{h}}(x, Q^2) = \int_{0.2}^1 dz_h (g_1^{d/h} + g_1^{\bar{d}/\bar{h}}) / \int_{0.2}^1 dz_h (F_1^{d/h} + F_1^{\bar{d}/\bar{h}})$ and also the $SU_f(3)$ sum rule $a_8 = F + D$. Then, operating quite analogously to the case of difference asymmetries [4], after some simple algebra one obtains the following NLO QCD equation for the quantity $\Delta_1 s + \Delta_1\bar{s}$ we are interesting in:

$$(\Delta_1 s + \Delta_1\bar{s})_{NLO} = \frac{A_{exp(d)}^{\pi^+ + \pi^-} - 5(3F - D) (L_1^{[qq]} + L_2^{[qq]} + 2L_g^{[qq]})}{10(L_1^{[qq]} + L_2^{[qq]}) + 4L_s^{[qq]} + 24L_g^{[qq]}}, \quad (3)$$

$$A_{exp(d)}^{\pi^+ + \pi^-} \equiv \int_0^1 dx A_d^{\pi^+ + \pi^-} \int_{0.2}^1 dz_h (F_{1d}^{\pi^+} + F_{1d}^{\pi^-}),$$

$$L_q^{[qq]h}(Q^2) \equiv \int_{0.2}^1 dz_h \left[D_q^h(z_h, Q^2) + \frac{\alpha_s}{2\pi} \int_{z_h}^1 \frac{dz'}{z'} \Delta_1 C_{qq}(z') D_q^h\left(\frac{z_h}{z'}, Q^2\right) \right], \quad (4)$$

$$L_g^{[qq]h}(Q^2) \equiv \frac{\alpha_s}{2\pi} \int_{0.2}^1 dz_h \frac{dz'}{z'} \Delta_1 C_{gq}(z') D_g^h\left(\frac{z_h}{z'}, Q^2\right), \quad (5)$$

²At first sight it could seem that the difference asymmetries suffer from the much larger errors in comparison with the usual asymmetries because of the difference of π^+ and π^- counting rates presents in denominator. However, fortunately, for the proton and deuteron target it is not the case because on these targets (on the contrary to the neutron target) π^+ production essentially exceeds π^- production. As a consequence, the statistical errors occur quite acceptable [4].

Table 1: The upper part presents the results on $\Delta_1 s + \Delta_1 \bar{s}$ obtained from integration of GRSV2000NLO parametrization (symmetric sea I and broken sea II scenario). The lower part presents results on $\Delta_1 s + \Delta_1 \bar{s}$ extracted from the simulated sum asymmetry.

x_B	Q^2	$[\Delta_1 s + \Delta_1 \bar{s}]_I$	$[\Delta_1 s + \Delta_1 \bar{s}]_{II}$
$0.0001 < x_B < 0.99$	7.45 GeV^2	-0.119	0.002
$0.003 < x_B < 0.7$	7.45 GeV^2	-0.088	0.008
x_B	Q_{mean}^2	$[\Delta_1 s + \Delta_1 \bar{s}]_I$	$[\Delta_1 s + \Delta_1 \bar{s}]_{II}$
$0.003 < x_B < 0.7$	7.45 GeV^2	-0.10 ± 0.01	0.01 ± 0.01

where $\Delta_1 C(z)_{qq,qq} \equiv \int_0^1 dx \delta C_{qq,qq}(x, z)$ are the first moments of the NLO Wilson coefficients which can be found in [10] and the fragmentation functions $D_1 \equiv D_u^{\pi^+} = D_u^{\pi^-} = D_d^{\pi^+} = D_d^{\pi^-}$ (favored), $D_2 \equiv D_d^{\pi^+} = D_d^{\pi^-} = D_u^{\pi^-} = D_u^{\pi^+}$ (unfavored), $D_s \equiv D_s^{\pi^+} = D_s^{\pi^-} = D_s^{\pi^+} = D_s^{\pi^-}$ (unfavored) can be found in ref. [7]. To understand is it possible to correctly extract the quantity $\Delta_1 s + \Delta_1 \bar{s}$ using proposed NLO QCD procedure, we, just as before [4], perform the simulations using the polarized event generator PEPSI. The all simulation conditions exactly correspond to the COMPASS kinematics (see [4] for details). Let us analyze the results from Table 1. One can see that for both symmetric I and broken II scenarios, the results of reconstruction of the quantity $\Delta_1 s + \Delta_1 \bar{s}$ in the accessible x_F region are in good agreement with the respective input parametrizations. So, just performed analysis confirms that the proposed NLO extraction procedure is applicable for $\Delta_1 s + \Delta_1 \bar{s}$ extraction.

It is of importance to have a possibility to extract in NLO QCD not only the sum $\Delta_1 s + \Delta_1 \bar{s}$ but also the difference³ $\Delta_1 s - \Delta_1 \bar{s}$. To this end we will apply the difference asymmetries

$$A_N^{h-\bar{h}}(x, Q^2) = \int_{0.2}^1 dz_h (g_1^{N/h} - g_1^{N/\bar{h}}) / \int_{0.2}^1 dz_h (F_1^{N/h} - F_1^{N/\bar{h}})$$

for the K^\pm production on the deuteron target. Operating quite analogously to the case of pion difference asymmetries (see derivation of Eqs. (20) for $\Delta_1 u_V, \Delta_1 d_V$ in [4]) one gets the simple equation for the quantity $\Delta_1 s - \Delta_1 \bar{s}$ we are interesting in:

$$\frac{1}{2}(\Delta_1 s - \Delta_1 \bar{s}) = \Delta_1 u_V + \Delta_1 d_V - \frac{A_{exp(d)}^{K^+ - K^-}}{\bar{L}_1 - \bar{L}_2} \quad (6)$$

where

$$\begin{aligned} \bar{L}_1 &\equiv L_u^{[qq]K^+} = L_u^{[qq]K^-} = L_s^{[qq]K^+} = L_s^{[qq]K^-}, \\ \bar{L}_2 &\equiv L_u^{[qq]K^-} = L_u^{[qq]K^+} = L_s^{[qq]K^+} = L_s^{[qq]K^-}, \end{aligned}$$

with $L_q^{[qq]K^+(K^-)}$ given by Eq. (4), and

$$\begin{aligned} A_{exp(d)}^{K^+ - K^-} &\equiv \int_0^1 dx A_d^{K^+ - K^-} \Big|_Z [u_V + d_V] \\ &\times \int_Z^1 dz_h [1 + \otimes \frac{\alpha_s}{2\pi} \tilde{C}_{qq} \otimes] (\bar{D}_1 - \bar{D}_2). \end{aligned} \quad (7)$$

³Let us recall that on the contrary to the sum $\Delta_1 s + \Delta_1 \bar{s}$ (which in principle could be extracted using only the inclusive DIS data) the quantity $\Delta_1 s - \Delta_1 \bar{s}$ could be extracted only from the semi-inclusive DIS data.

Table 2: The upper part presents the results on $\Delta_1 u$, $\Delta_1 d$ and $\Delta_1 \bar{q}$ obtained from integration of GRSV2000NLO parametrization (symmetric sea scenario). The lower part presents the respective results extracted from the simulated asymmetries applying the proposed NLO procedure with GRSV2000NLO parametrization entering the generator as an input.

x_B region	$\Delta_1 u$	$\Delta_1 d$	$\Delta_1 \bar{q}$
$0.023 < x_B < 0.6$	0.724	-0.302	-0.026
$0.023 < x_B < 0.6$	0.702 ± 0.020	-0.274 ± 0.025	-0.027 ± 0.013

It is seen that all dependence on the fragmentation functions in the r.h.s of Eq. (6) reduces to the only “effective” fragmentation function $D' = \bar{D}_1 - \bar{D}_2$. At the same time, the favored and unfavored kaon fragmentation functions \bar{D}_1 and \bar{D}_2 are still poorly known. Thus, to obtain $\Delta_1 s - \Delta_1 \bar{s}$ using Eq. (6) one should first obtain D' using unpolarized data and (probably⁴) the existing unpolarized event generators (LEPTO and PYTHIA) properly tuned to the conditions of the respective SIDIS experiments such as HERMES and COMPASS.

Let us now apply the proposed procedure to the real data⁵ of HERMES[6] on asymmetries $A_{p,d}, A_{p,d}^{\pm}$. The proposed procedure in this case allows to obtain the simple expressions for the NLO quantities $\Delta_1 u$, $\Delta_1 d$ and $\Delta_1 \bar{q} \equiv \Delta_1 \bar{u} = \Delta_1 \bar{d} = \Delta_1 s = \Delta_1 \bar{s}$ via the quantities $A_{(exp)p,d}, A_{(exp)p,d}^{\pm}$. The later, just as the quantities A_p^{exp}, A_d^{exp} in the case of difference asymmetries[4], contain only already measured unpolarized quark distributions, fragmentation functions⁶, known NLO Wilson coefficients and the measured asymmetries $A_{p,d}, A_{p,d}^{\pm}$. Certainly, one could choose only three equations (containing any three of six measured asymmetries) to obtain the minimal non-degenerate system which can be directly solved with respect to NLO quantities $\Delta_1 u$, $\Delta_1 d$ and $\Delta_1 \bar{q}$. However, to increase the precision of extraction, we, as usual, use the fitting procedure where we include all six available quantities $A_{(exp)p,d}, A_{(exp)p,d}^{\pm}$ entering the constructed χ^2 .

We again perform the testing of our method using the GRSV2000(NLO)[8] parametrization as an input. Comparing the upper and lower parts of the Table 2, one can see that the results of $\Delta_1 u$, $\Delta_1 d$ and $\Delta_1 \bar{q}$ reconstruction are in a good agreement with the input parametrization. Thus, the performed testing shows that our procedure can be applied to $\Delta_1 u$, $\Delta_1 d$ and $\Delta_1 \bar{q}$ reconstruction.

Let us now perform NLO extraction of $\Delta_1 u$, $\Delta_1 d$ and $\Delta_1 \bar{q}$ from the real HERMES data[6] on $A_{p,d}, A_{p,d}^{\pm}$. It is of importance that the unpolarized quark densities entering the quantities $A_{(exp)p,d}, A_{(exp)p,d}^{\pm}$ are obtained from the structure functions F_2 . Thus, dealing with the real data one should first express SIDIS structure function F_1^h (entering the quantities $A_{(exp)}$) via F_2^h : $F_2^h = 2xF_1^h(1 + R)$ and then use pQCD NLO expressions for F_2^h through the respective unpolarized quark densities and Wilson coefficients[10]. The

⁴For example, HERMES[6] used properly event generator LEPTO to extract the purities (which are just the combination of the respective fragmentation function and unpolarized quark distributions)

⁵Since the kaon fragmentation functions are still poorly known, while here we mainly would like to check the validity of the method itself (irrespective to this problem), we will consider here the most simple case of the pion production with the assumption $\Delta_1 \bar{u} = \Delta_1 \bar{d} = \Delta_1 s = \Delta_1 \bar{s} \equiv \Delta_1 \bar{q}$. The application of the method to the kaon asymmetries is now in preparation.

⁶The parametrization for the fragmentation functions from ref. [7] is used for both testing with PEPSI[9] and reconstruction from the real HERMES data

Table 3: The results on NLO extracted $\Delta_1 u$, $\Delta_1 d$ and $\Delta_1 \bar{q}$ from the HERMES data on asymmetries $A_{p,d}$, $A_{p,d}^{\pi^\pm}$.

$\Delta_1 u$	$\Delta_1 d$	$\Delta_1 \bar{q}$
0.624 ± 0.063	-0.355 ± 0.070	0.016 ± 0.038

Table 4: The results on $\Delta_1 u$, $\Delta_1 d$ and $\Delta_1 \bar{q}$ obtained from the respective integrals of parametrizations AAC2003 and BB over the accessible to HERMES x_B region.

Parametrization	$\Delta_1 u$	$\Delta_1 d$	$\Delta_1 \bar{q}$
AAC2003	0.691	-0.293	-0.034
BB	0.667	-0.274	-0.024

respective results are presented in the Table 3.

It is instructive to compare the results of Table 3 with the respective integrals of two latest NLO parametrizations[11]; see Table 4. It is seen that the results are in a good agreement within the errors.

Thus, the performed analysis argues that the proposed procedure is acceptable for extraction of $\Delta_1 q$ in the next-to-leading QCD order.

The authors are grateful to R. Bertini, M. P. Bussa, O. Denisov, O. Gorchakov, A. Efremov, N. Kochelev, A. Korzenev, A. Kotzinian, V. Krivokhizhin, E. Kuraev, A. Maggiora, A. Nagaytsev, A. Olshevsky, G. Piragino, G. Pontecorvo, J. Pretz, I. Savin, A. Sidorov and O. Teryaev, for fruitful discussions.

References

- [1] COMPASS collaboration (G. Baum et al.), "COMPASS: A proposal for a common muon and proton apparatus for structure and spectroscopy", CERN-SPSLC-96-14 (1996).
- [2] E. Leader, D.B. Stamenov, Phys. Rev. **D67** (2003) 037503
- [3] A.N. Sissakian, O.Yu. Shevchenko and O.N. Ivanov, Phys. Rev. **D 68** (2003) 031502(R).
- [4] A.N. Sissakian, O.Yu. Shevchenko and O.N. Ivanov, Phys. Rev. **D 70** (2004) 074032.
- [5] E. Christova and E. Leader, Nucl. Phys **B 607** (2001) 369.
- [6] HERMES collaboration (A. Airapetian et al.), DESY-04-107, Jul 2004, hep-ex/0407032.
- [7] S. Kretzer, Phys.Rev. **D 62** (2000) 054001.
- [8] M. Gluck, E. Reya, M. Stratmann, W. Vogelsang, Phys.Rev. **D 63** (2001) 094005.
- [9] L. Mankiewicz, A. Schafer, M. Veltri, Comput. Phys. Commun.**71** (1992) 305-318.

- [10] D. de Florian and R. Sassot, Phys. Rev. **D 62** (2000) 094025.
- [11] Asymmetry Analysis Collaboration (M. Hirai et al), Phys. Rev. **D 69** (2004) 054021 (AAC2003);
J. Blumlein, H. Bottcher Nucl.Phys. **B636** (2002) 225.

MEASUREMENT OF HADRON PRODUCTION CROSS-SECTION IN COLLISIONS OF HIGHLY VIRTUAL PHOTONS

V. Pozdnyakov, Yu. Vertogradova

Joint Institute for Nuclear Research (JINR), Dubna, Russia

Abstract

Double-tagged interactions of photons with virtualities Q^2 between 10 GeV^2 and 200 GeV^2 are analyzed with the data collected by DELPHI detector from 1998 to 2000, corresponding to an integrated luminosity of 550 pb^{-1} . The cross section of the reaction $\gamma^*\gamma^* \rightarrow \text{hadrons}$ is measured and compared to the LO and NLO BFKL calculations.

1. Introduction

Double-tagged two-photon interactions $e^+e^- \rightarrow e^+e^-\gamma^*\gamma^* \rightarrow e^+e^- + \text{hadrons}$ are studied with the DELPHI detector [1] at the CERN LEP II collider. Both scattered electrons¹ are detected by the Small angle Tile Calorimeter (STIC). If the virtualities of the photons are large enough, the LO process like the Born-box $\gamma^*\gamma^* \rightarrow q\bar{q}$ is expected to be comparable to the processes with (multi)gluon exchange between the $q\bar{q}$ dipole [2], which is described by the BFKL equation [3].

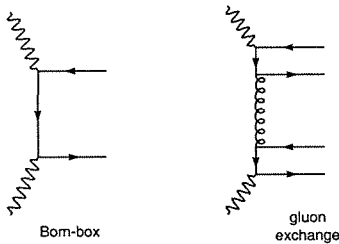


Figure 1: Main diagrams corresponding to the $\gamma^*\gamma^* \rightarrow \text{hadrons}$ process

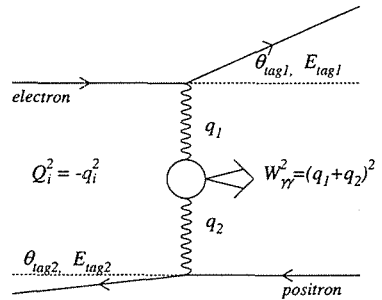


Figure 2: Kinematics of $\gamma^*\gamma^*$ interactions

¹Throughout this paper, electron stands both for electron and positron.

Two-photon interactions are therefore a suitable process to investigate BFKL dynamics. Figure 1 shows the main diagrams relevant to the analysis.

Figure 2 illustrates the kinematics of the process. We use the following notations: p_i ($i=1,2$) are the four-momenta of the beam electrons, \sqrt{s} is the e^+e^- centre-of-mass energy, E_{beam} is the beam energy; the scattered electrons' four-momenta, polar angles and energies are p'_i , θ_i and E_i respectively.

The variables relevant to this study are the virtualities of the photons, Q_i^2 , the invariant mass of the two photons $W_{\gamma^*\gamma^*}$ and a dimensionless variable Y :

- $Q_i^2 = -(p_i - p'_i)^2 = 4E_i E_{beam} \sin^2(\theta_i/2)$
- $W_{\gamma^*\gamma^*}^2 = -(q_1 + q_2)^2 \simeq s y_1 y_2$ with $y_i = 1 - (E_i/E_{beam}) \cos^2(\theta_i/2)$;
- $Y = \ln(W_{\gamma^*\gamma^*}^2 / \sqrt{Q_1^2 Q_2^2})$

The Y variable is used to compare the multihadron data with the BFKL predicted cross section within the approximations $W_{\gamma^*\gamma^*}^2 \gg Q_i^2$ and $|\ln(Q_1^2/Q_2^2)| < 1$, where the second condition is needed to select virtualities of the photons of the same order.

2. Data analysis

A detailed description of the DELPHI detector and of its performance is presented in Ref. [1]: here only the components relevant to the present analysis will be briefly mentioned.

The scattered electrons are detected in the luminosity monitor STIC, which covers the region from 29 mrad to 185 mrad in the polar angle θ . Given the energy and angular resolution of the STIC calorimeter, the Q^2 resolution varies between 1 GeV² and 2.5 GeV² in the Q^2 domain of the present analysis.

Charged particles are detected in the barrel and endcap tracking systems. The combined momentum resolution provided by the tracking system is a few per-mill in the momentum range of this study.

The study is done with the DELPHI data taken during 1998-2000 runs at e^+e^- centre-of-mass energies from 189 GeV to 209 GeV, corresponding to an integrated luminosity of 550 pb⁻¹.

The following criteria are used in order to select $\gamma^*\gamma^* \rightarrow hadrons$ events and to suppress the background contamination:

- There are two clusters with energy deposition E_i greater than 30 GeV, one in each arm of the STIC and the polar angle θ_i exceeds 2.2° for each cluster.
- Q_i^2 is between 10 GeV² and 200 GeV² for both tagged particles.
- The acollinearity of the scattered electrons is below 179.8 degrees (removes the superimposition between Bhabha events and untagged two-photon events).
- Each event contains at least 3 charged particles with the invariant mass calculated from the particles' 4-momenta, W_{had} , larger than 2 GeV. Particles are considered if

their momentum is greater than 400 MeV/c, their polar angle is within the interval $20^\circ - 160^\circ$ and their impact parameters are smaller than 4 cm in $R\phi$ and 10 cm in z .

- The cluster energy in the STIC, normalized to the beam energy, is larger than 0.85 if the energy of another cluster is below 0.5. (suppress the contamination coming from $e^+e^- \rightarrow hadrons$ events).
- The thrust value of the charged particles, calculated in their centre-of-mass system, is less than 0.98 for the events with charged multiplicity below 5 (removes most of the $\gamma^*\gamma^* \rightarrow \tau^+\tau^-$ events).

After these requirements 434 events have been selected. The trigger efficiency [4] is estimated from the redundancy of the trigger and from a parameterization of the single track efficiency, and turns out to be close to the unit.

The event generators used to simulate the $\gamma^*\gamma^*$ events and the non-negligible background processes are listed below as well as the respective expected contributions.

- TWOGAM (version 2.02) [5] and PYTHIA (version 6.205) [6] event generators are used to simulate $\gamma^*\gamma^*$ interactions. The expectations are (331 ± 8) and (330 ± 8) events, respectively. The Monte Carlo generators include the quark-parton model (QPM) part and also the leading-order predictions for the resolved photon contribution.
- The background coming from the process $e^+e^- \rightarrow hadrons$ is simulated with KK2f generator (version 4.14) [7] and its contribution is estimated as (27 ± 3) events.
- The contamination of τ pairs produced in the two-photon interactions is evaluated as (26 ± 3) events by using the TWOGAM program.
- The coincidence of an off-momentum electron with a $\gamma^*\gamma \rightarrow hadrons$ single-tagged event is evaluated as (5 ± 2) events.

3. Results

The background subtracted data are corrected for detector acceptance and averaged efficiency using two models. The total cross section σ_{ee} of the $e^+e^- \rightarrow e^+e^- + hadrons$ interactions, within the phase space limited by the criteria Q_i^2 between 10 GeV² and 200 GeV², and W_{had} above 2 GeV/c², is measured to be (2.09 ± 0.17) pb using the corrections for detector effects based on TWOGAM and (1.86 ± 0.14) pb for the corrections based on PYTHIA. The statistical and systematic uncertainties are added in quadrature. The expectation of the quark-parton model is (1.81 ± 0.02) pb as obtained with TWOGAM.

The $\gamma^*\gamma^* \rightarrow hadrons$ interactions are expected to be sensitive to (multi)gluon exchange (fig.1). The multigluon ladder is described by BFKL equation [3], which predicts a growth of the cross section at large Y . Note that the BFKL calculations are valid within the approximations $W_{\gamma^*\gamma^*}^2 \gg Q_i^2$ (the variable Y should be larger than 2) and $|\ln(Q_1^2/Q_2^2)| < 1$ (to maintain the photon virtualities approximately equal).

The experimental conditions of the present study ($Q_i^2 \gg m_e^2$ and the symmetry for tagged particle detection) permit to simplify the relation between σ_{ee} and $\sigma_{\gamma^*\gamma^*}$, which initially reads [8] (the interference terms are omitted)

$$\sigma_{ee} = \sum_{i,j=T,L} L_{ij}\sigma_{ij},$$

to a relation involving an effective cross section $\sigma_{\gamma^*\gamma^*}$,

$$\sigma_{ee} = L_{TT}\sigma_{\gamma^*\gamma^*} \text{ with } \sigma_{\gamma^*\gamma^*} = \sigma_{TT} + 2\epsilon\sigma_{LT} + \epsilon^2\sigma_{LL},$$

where L_{TT} is the flux of the transversely polarized photons calculable in QED, ϵ is around 0.94, $\sigma_{LT} \simeq 0.2\sigma_{TT}$ and $\sigma_{LL} \simeq 0.05\sigma_{TT}$ [9]. The TWOGAM event generator including QED radiative corrections has been used to calculate L_{TT} : it uses the decomposition of the cross section for different photon helicities [8].

The measured cross-section of the hadron production in collisions of two highly virtual photons is presented in figure 3.

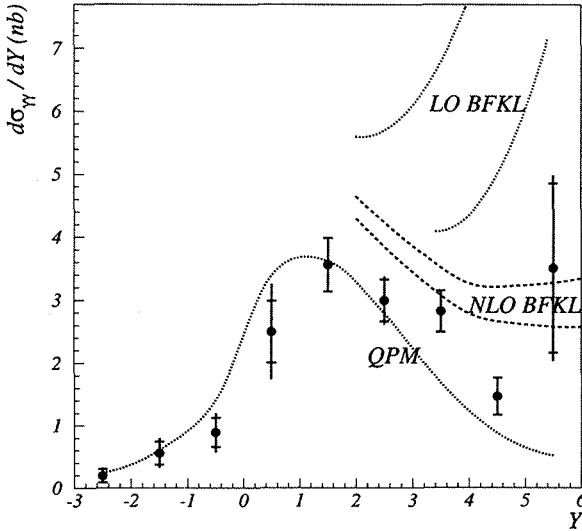


Figure 3: The differential cross section for the reaction $\gamma^*\gamma^* \rightarrow \text{hadrons}$. The total error bars indicate the sum in quadrature of the statistical (inner error bars) and of the systematic uncertainties. The lowest dotted curve corresponds to the expectation of the quark-parton model (QPM, quark-box diagram, figure 1). The two upper dotted lines represent the BFKL calculations in the leading order [10]. The next-to-leading calculations [11] are shown by the two dashed curves in the middle. The two curves for the BFKL calculations correspond to the Regge scale parameter changing between Q^2 (upper line) and $4Q^2$ (lower one). The QPM contribution is added to both the LO and the NLO BFKL expectations

In conclusion, the differential cross section $d\sigma_{\gamma^*\gamma^*}/dY$ of the $\gamma^*\gamma^* \rightarrow \text{hadrons}$ interactions is measured and is compared with the predictions based on LO and NLO BFKL calculations. The leading order calculations clearly disagree with the data while the next-to-leading order predictions are found to be more consistent with the data, although the LEP energy is not sufficient to see a sizable effect due to the BFKL type contribution.

References

- [1] DELPHI Collab., P. Aarnio *et al.*, Nucl. Instr.& Meth. **A303** (1991) 233;
DELPHI Collab., P. Abreu *et al.*, Nucl. Instr.& Meth. **A378** (1996) 57.
- [2] H.G. Dosch, T. Gousset and H.J. Pirner, Phys. Rev. **D57** (1998) 1666.
- [3] E.A. Kuraev, L.N. Lipatov and V.S. Fadin, Sov. Phys. JETP **45** (1977) 199;
Ya.Ya. Balitski and L.N. Lipatov, Sov. J. Nucl. Phys. **28** (1978) 822.
- [4] DELPHI Collab., A. Augustinus *et al.*, Nucl. Instr. & Meth. **A515** (2003) 782.
- [5] TWOGAM event generator, L. Lönnblad *et al.*, "γγ event generators" in "Physics at LEP2", ed. G. Altarelli, T. Sjöstrand and F. Zwirner, CERN 96-01 (1996), volume 2, 224.
- [6] T. Sjöstrand, Comput. Phys. Commun. **82** (1994) 74.
- [7] S. Jadach, B. Ward and Z. Was, Comput. Phys. Commun. **130** (2000) 260.
- [8] V.M. Budnev, I.F. Ginzburg, G.V. Meledin and V.G. Serbo, Phys. Rep. **15** (1975) 181.
- [9] S.J. Brodsky, F. Hautmann and D.E. Sopper, Phys. Rev. **D56** (1997) 6957.
- [10] J. Bartels, C. Ewerz and R. Staritzbichler, Phys. Lett. **B492** (2000) 56;
C. Ewerz, private communication.
- [11] V.T. Kim, L.N. Lipatov and G.B. Pivovarov, "The next-to-leading BFKL pomeron with optimal renormalization", Proceeding of the International Conference on elastic and diffractive scattering 1999, Protvino, Russia, ed. V.A. Petrov and A.V. Prokudin, World Sci., Singapore (2000) 237;
V. Kim, private communication.

III.

RELATIVISTIC HEAVY ION COLLISIONS

MULTIPLICITY AND p_t CORRELATIONS IN RELATIVISTIC NUCLEAR COLLISIONS

R.S. Kolevatov and V.V. Vechernin[†]

V.A.Fock Institute of Physics, St.Petersburg State University

[†] *E-mail: vecherni@pink.phys.spbu.ru*

Abstract

The theoretical description of the correlations between observables in two separated rapidity intervals for AA-interactions at high energies is presented. In the case with the real nucleon distribution density of colliding nuclei the MC calculations of the long-range correlation functions at different values of impact parameter are done.

For n - n and p_t - n correlations it is shown that the impact parameter fluctuations at a level of a few fermi, unavoidable in the experiment, significantly change the magnitude of correlation coefficients. The rise of p_t - n and especially p_t - p_t correlation coefficients is found when one passes from SPS to RHIC and LHC energies.

1. String fusion model (SFM)

The colour string model [1, 2] originating from Gribov-Regge approach is being widely applied for the description of the soft part of the multiparticle production in hadronic and nuclear interactions at high energies. In this model at first stage of hadronic interaction the formation of the extended objects - the quark-gluon strings - takes place. At second stage the hadronization of these strings produces the observed hadrons. In the original version the strings evolve independently and the observed spectra are just the sum of individual string spectra. However in the case of nuclear collision, with growing energy and atomic number of colliding nuclei, the number of strings grows and one has to take into account the interaction between them.

One of possible approaches to the problem is the colour string fusion model [3]. The model is based on a simple observation that due to final transverse dimensions of strings they inevitably have to start to overlap with the rise of their density in transverse plane. At that the interaction of string colour fields takes place, which changes the process of their fragmentation into hadrons as compared with the fragmentation of independent strings. So we have one more interesting nonlinear phenomenon in nuclear interactions at high energies - the field of physics the investigations in which were initiated by pioneer works of academician A.M. Baldin [4].

It was shown [3, 5, 6] that the string fusion phenomenon considerably damps the charged particle multiplicity and simultaneously increase their mean p_t value as compared with the case of independent strings. In accordance with a general Schwinger idea [7] and the following papers [8, 9] (colour ropes model) two possible versions of string fusion mechanism were suggested.

The first version [5] of the model assumes that the colour fields are summing up only locally in the area of overlaps of strings in the transverse plane. So we will refer to this

case as a *local* fusion or *overlaps*. In this case one has

$$\langle n \rangle_k = \mu_0 \frac{S_k}{\sigma_0} \sqrt{k} \quad \langle p_i^2 \rangle_k = p^2 \sqrt{k} \quad (1)$$

Here $\langle n \rangle_k$ is the average multiplicity of charged particles originated from the area S_k , where k strings are overlapping, and $\langle p_i^2 \rangle_k$ is the same for their squared transverse momentum. The μ_0 and p^2 are the average multiplicity and squared transverse momentum of charged particles produced from a decay of one single string, and σ_0 is its transverse area.

In the second version [10] of the model one assumes that the colour fields are summing up globally - over total area of each cluster in the transverse plane - into one average colour field. This case corresponds to the summing of the source colour charges. We will refer to this case as a *global* fusion or *clusters*. In this case we have

$$\langle n \rangle_{cl} = \mu_0 \frac{S_{cl}}{\sigma_0} \sqrt{k_{cl}} \quad \langle p_i^2 \rangle_{cl} = p^2 \sqrt{k_{cl}} \quad k_{cl} = \frac{N_{cl}^{str} \sigma_0}{S_{cl}} \quad (2)$$

Here $\langle n \rangle_{cl}$ is the average multiplicity of charged particles originated from the cluster of the area S_{cl} and $\langle p_i^2 \rangle_{cl}$ is the same for their squared transverse momentum. The N_{cl}^{str} is the number of strings forming the cluster.

Note that in two limit cases both versions give the same results.

For N non-overlapping strings we have in the *local* version: $k = 1$, $S_1 = N\sigma_0$, $\langle n \rangle = \langle n \rangle_1 = N\mu_0$ and $\langle p_i^2 \rangle = \langle p_i^2 \rangle_1 = p^2$. In the *global* version in this case we have N clusters each formed by only one string, so $k_{cl} = 1$, $\langle n \rangle = N\langle n \rangle_{cl} = N\mu_0$ and $\langle p_i^2 \rangle = \langle p_i^2 \rangle_{cl} = p^2$.

For N totally overlapped strings we have in the *local* version: $k = N$, $S_N = \sigma_0$, $\langle n \rangle = \langle n \rangle_N = \sqrt{N}\mu_0$ and $\langle p_i^2 \rangle = \langle p_i^2 \rangle_N = \sqrt{N}p^2$. In the *global* version in this case we have one cluster of the area $S_{cl} = \sigma_0$ formed by N string, so $k_{cl} = N$, $\langle n \rangle = \langle n \rangle_{cl} = \sqrt{N}\mu_0$ and $\langle p_i^2 \rangle = \langle p_i^2 \rangle_{cl} = \sqrt{N}p^2$.

So in both versions of the model when we pass from N non-overlapping strings to N totally overlapped strings the average multiplicity decreases from $\langle n \rangle = N\mu_0$ to $\langle n \rangle = \sqrt{N}\mu_0$ and the mean p_i^2 increases from $\langle p_i^2 \rangle = p^2$ to $\langle p_i^2 \rangle = \sqrt{N}p^2$.

2. Cellular analog of SFM

To simplify calculations in the case of real nucleus-nucleus collisions a simple cellular model originating from the string fusion model was proposed [11]. In the framework of the cellular analog along with the calculation simplifications the asymptotics of correlation coefficients at large and small string densities can be found analytically in the idealized case with the homogeneous string distribution, which enables to use these asymptotics later for the control of the Monte-Carlo (MC) algorithms.

Two versions of the cellular model as the original SFM can be formulated - with local and global string fusion. In this model we divide all transverse (impact parameter) plane into cells of order of the transverse string size σ_0 .

In the version with *local* fusion the assumption of the model is that if the number of strings belonging to the ij -th cell is k_{ij} , then they form higher colour string, which emits in average $\mu_0 \sqrt{k_{ij}}$ particles with mean p_i^2 equal to $p^2 \sqrt{k_{ij}}$ (compare with (1)). Note that zero "occupation numbers" $k_{ij} = 0$ are also admitted.

In the version with *global* fusion at first we define the neighbour cells as the cells with a common link. Then we define the cluster as the set of neighbour cells with non zero occupation numbers $k_{ij} \neq 0$. After that we can apply the same formulae of the global fusion (2) as in the original SFM, where N_{cl}^{str} is the number of strings in the cluster and S_{cl}/σ_0 is the number of cells in the cluster.

From event to event the number of strings k_{ij} in the ij -th cell will fluctuate around some average value - \bar{k}_{ij} . Clear that in the case of real nuclear collisions these average values \bar{k}_{ij} will be different for different cells. They will depend on the position (s_{ij}) of the ij -th cell in the impact parameter plane (s is two dimensional vector in the transverse plane). In the case of nucleus-nucleus AB -collision at some fixed value of impact parameter \mathbf{b} one can find this *average* local density of primary strings \bar{k}_{ij} in the point s_{ij} using nuclear profile functions $T_A(s_{ij} + \mathbf{b}/2)$ and $T_B(s_{ij} - \mathbf{b}/2)$.

In MC approach knowing the \bar{k}_{ij} one can generate some configuration $C \equiv \{k_{ij}\}$. To get the physical answer for one given event (configuration C) we have to sum the contributions from different cells in accordance with *local* or *global* algorithm (see above), which corresponds to the integration over s in transverse plane. Then we have to sum over events (over different configurations C). Note that as the event-by-event fluctuations of the impact parameter at a level of a few fermi are inevitable in the experiment one has to include the impact parameter b into definition of configuration $C \equiv \{b, k_{ij}\}$.

3. Long-range correlations

The idea [5, 6, 12] to use the study of long-range correlations in nuclear collisions for observation of the colour string fusion phenomenon based on the consideration that the quark-gluon string is an extended object which fragmentation gives the contribution to wide rapidity range. This can be an origin of the long-range correlations in rapidity space between observables in two different and separated rapidity intervals. Usually in an experiment they choose these two separated rapidity intervals in different hemispheres of the emission of secondary particles one in the forward and another in the backward in the center mass system. So sometimes these long-range rapidity correlations are referred as the forward-backward correlations (FBC).

In principle one can study three types of such long-range correlations:

n - n - the correlation between multiplicities of charged particles in these rapidity intervals,

p_t - p_t - the correlation between transverse momenta in these intervals and

p_t - n - the correlation between the transverse momentum in one rapidity interval and the multiplicity of charged particles in another interval.

Usually to describe these correlations numerically one studies the average value $\langle B \rangle_F$ of one dynamical variable B in the backward rapidity window Δy_B , as a function of another dynamical variable F in the forward rapidity window Δy_F . Here $\langle \dots \rangle_F$ denotes averaging over events having a fixed value of the variable F in the forward rapidity window. The $\langle \dots \rangle$ denotes averaging over all events. So we find the correlation function $\langle B \rangle_F = f(F)$.

It's naturally then to define the correlation coefficient as the response of $\langle B \rangle_F$ on the variations of the variable F in the vicinity of its average value $\langle F \rangle$. At that useful also to

go to the relative variables, i.e. to measure a deviation of F from its average value $\langle F \rangle$ in units of $\langle F \rangle$, and the same for B . So it's reasonable to define a correlation coefficient b_{B-F} for correlation between observables B and F in backward and forward rapidity windows in the following way:

$$b_{B-F} \equiv \frac{\langle F \rangle}{\langle B \rangle} \left. \frac{d\langle B \rangle_F}{dF} \right|_{F=\langle F \rangle} \quad (3)$$

As the dynamical variables we use the multiplicity of charged particles (n), produced in the given event in the given rapidity window, and the *event(!)* mean value of their transverse momentum (p_t), i.e. the sum of the transverse momentum magnitudes of all charged particles, produced in the given event in the given rapidity window (Δy), divided by the number of these particles (n):

$$p_t \equiv \frac{1}{n} \sum_{i=1}^n |p_{ti}|, \quad \text{where} \quad y_i \in \Delta y; \quad i = 1, \dots, n. \quad (4)$$

So we can define three correlation coefficients:

$$b_{n-n} \equiv \frac{\langle n_F \rangle}{\langle n_B \rangle} \left. \frac{d\langle n_B \rangle_{n_F}}{dn_F} \right|_{n_F=\langle n_F \rangle} \quad b_{p_t-p_t} \equiv \frac{\langle p_{tF} \rangle}{\langle p_{tB} \rangle} \left. \frac{d\langle p_{tB} \rangle_{p_{tF}}}{dp_{tF}} \right|_{p_{tF}=\langle p_{tF} \rangle}$$

$$b_{p_t-n} \equiv \frac{\langle n_F \rangle}{\langle p_{tB} \rangle} \left. \frac{d\langle p_{tB} \rangle_{n_F}}{dn_F} \right|_{n_F=\langle n_F \rangle} \quad (5)$$

Here n_B , n_F are the multiplicities and p_{tB} , p_{tF} are the *event* (4) mean transverse momentum of the charged particles, produced in the given event correspondingly in the backward (Δy_B) and forward (Δy_F) rapidity windows.

4. Results of the calculations

In Figs.1-3 the results of the MC calculations of these correlation coefficients are presented for nucleus-nucleus collisions at different values of the centrality. In all figures (\circ) and (\bullet) denote the results of calculations in the framework of the original SFM (with the taking into account the real geometry of merging strings) for its *local (overlaps)* and *global (clusters)* versions correspondingly. The (\square) and (\blacksquare) denote the results of calculations in the framework of the cellular analog of SFM for its *local* and *global (clusters)* versions. All presented results are for the forward rapidity window of 2 unit length ($\Delta y_F = 2$). The lines are only to guide the eye.

In Fig.1 we present the b_{n-n} correlation coefficient for AuAu collisions at RHIC energy and in Fig.2 we present the b_{p_t-n} correlation coefficient for PbPb collisions at LHC energy. In both figures the calculations are fulfilled three times:

- 1) at fixed values of impact parameter ($db = 0$),
- 2) with impact parameter fluctuations within 1 fm window ($db = 1$),
- 3) with impact parameter fluctuations within the whole class of centrality ($db = \text{class}$) (for LHC by convention this value is taken to be equal 3 fm, $db = 3$) We see that the impact parameter fluctuations at a level of a few fermi significantly change the magnitude of correlation coefficients. Note also that all results obtained in the framework of the

original SFM and its cellular analog for their local and global versions practically coincide, except for the p_t - n correlation at fixed value of impact parameter at LHC energy, where the correlation coefficient b_{p_t-n} is very small.

In Fig.3 the energy dependence of the $b_{p_t-p_t}$ correlation coefficient is presented. The calculations are made for the 1 fm impact parameter window ($db = 1$). In this case we see the considerable rise of p_t - p_t correlation coefficient from SPS to LHC energies.

5. Conclusion

In the case with the real nucleon distribution density of colliding nuclei the MC calculations of the long-range correlation functions at different values of impact parameter are done. For n - n and p_t - n correlations it is shown that the impact parameter fluctuations at a level of a few fermi, unavoidable in the experiment, significantly change the magnitude of correlation coefficients for all centrality classes as compared to ones calculated earlier at the fixed values of impact parameter [13].

It is shown also, that for the p_t - p_t correlation the event-by-event correlation between event mean values of transverse momenta of the particles emitted in two different rapidity intervals does not decrease to zero with the increase of the number of strings in contrast with the correlation between the transverse momenta of single particles produced in these two rapidity windows which was studied earlier [13].

The rise of p_t - n and especially p_t - p_t correlation coefficients is found when one passes from SPS to RHIC and LHC energies.

Acknowledgments

The authors would like to thank M.A. Braun and G.A. Feofilov for numerous valuable encouraging discussions. The work has been partially supported by the Russian Foundation for Fundamental Research under Grant No. 05-02-17399-a.

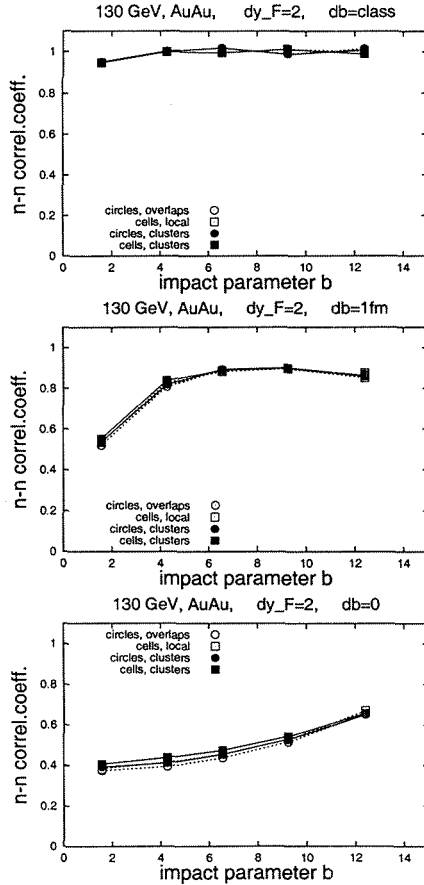


Figure 1: The b_{n-n} correlation coefficient for AuAu collisions at $\sqrt{s} = 130$ GeV as a function of the impact parameter b for tree choices of impact parameter window db (see text)

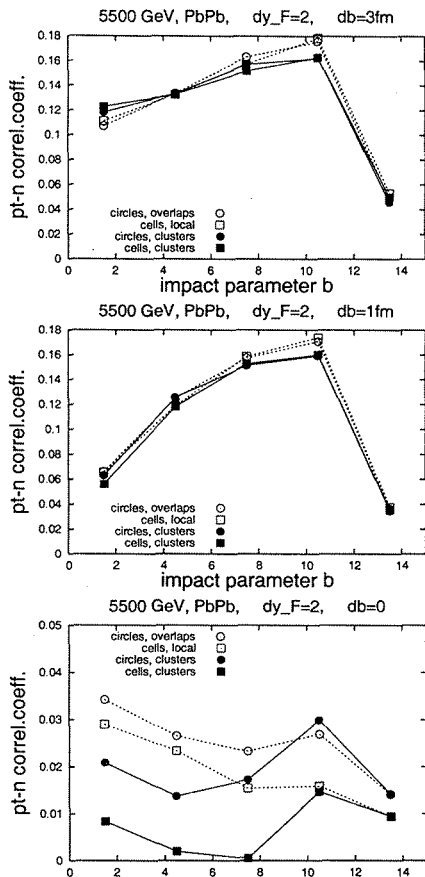


Figure 2: The same as in Fig.1 but for the b_{p_t-n} correlation coefficient for PbPb collisions at $\sqrt{s} = 5500$ GeV

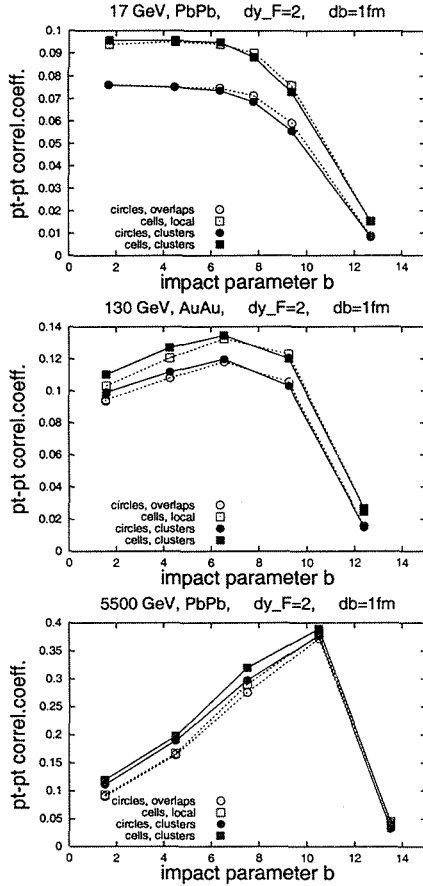


Figure 3: The $b_{p_t-p_t}$ correlation coefficient as a function of the impact parameter b (at $db = 1$ fm) for tree choices of the initial energy: $\sqrt{s} = 17$; 130 and 5500 GeV

References

- [1] A. Capella, U.P. Sukhatme, C.-I. Tan and J. Tran Thanh Van, Phys. Lett. **B81**, 68 (1979); Phys. Rep. **236**, 225 (1994).
- [2] A.B. Kaidalov, Phys. Lett. **116B**, 459 (1982);
A.B. Kaidalov and K.A. Ter-Martirosyan, Phys. Lett. **117B**, 247 (1982).
- [3] M.A. Braun and C. Pajares, Phys. Lett. **B287**, 154 (1992);
Nucl. Phys. **B390**, 542, 549 (1993).
- [4] A.M. Baldin et al., Preprint JINR P9-5442, Dubna, 1970;
A.M. Baldin et al., Preprint JINR P1-5819, Dubna, 1971;
A.M. Baldin, Investigations with relativistic nuclei, MIFI, Moscow, 1975.
- [5] M.A. Braun and C. Pajares, Eur. Phys. J. **C16**, 349 (2000).
- [6] M.A. Braun and C. Pajares, Phys. Rev. Lett. **85**, 4864 (2000).
- [7] J. Schwinger, Phys. Rev. **82**, 664 (1951).
- [8] T.S.Biro, H.B.Nielsen and J.Knoll, Nucl. Phys. **B245**, 449 (1984).
- [9] A.Bialas and W.Czyz, Nucl. Phys. **B267**, 242 (1986).
- [10] M.A. Braun F. del Moral and C. Pajares, Phys. Rev. **C65**, 024907 (2002).
- [11] V.V. Vechernin and R.S. Kolevatov, hep-ph/0304295; hep-ph/0305136 (Russian versions will appear in the journal "Vestnik SPbU").
- [12] N.S. Amelin, N. Armesto, M.A. Braun, E.G. Ferreira and C. Pajares, Phys. Rev. Lett. **73**, 2813 (1994).
- [13] M.A. Braun, R.S. Kolevatov, C. Pajares and V.V. Vechernin, Eur. Phys. J. **32**, 535 (2004).

LONG-RANGE CORRELATIONS IN PbPb COLLISIONS AT 158 A*GeV

C. Alt⁹, T. Anticic²¹, B. Baatar⁸, D. Barna⁴, J. Bartke⁶, L. Betev^{9,10}, H. Bialkowska¹⁹, C. Blume⁹, B. Boimska¹⁹, M. Botje¹, J. Bracinik³, R. Bramm⁹, R. Brun¹⁰, P. Bunčić^{9,10}, V. Cerny³, P. Christakoglou², O. Chvala¹⁵, J.G. Cramer¹⁷, P. Csató⁴, N. Darmanov¹⁸, A. Dimitrov¹⁸, P. Dinkelaker⁹, V. Eckardt¹⁴, G. Farantatos², D. Flierl⁹, Z. Fodor⁴, P. Foka⁷, P. Freund¹⁴, V. Friese⁷, J. Gál⁴, M. Gaździcki^{9,12}, G. Georgopoulos², E. Gładysz⁶, K. Grebieszko²⁰, S. Hegyi⁴, C. Höhne¹³, K. Kadija²¹, A. Karev¹⁴, M. Kliemant⁹, S. Kniese⁹, V.I. Kolesnikov⁸, T. Kollegger⁹, E. Kornas⁶, R. Korus¹², M. Kowalski⁶, I. Kraus⁷, M. Kreps³, M. van Leeuwen¹, P. Lévai⁴, L. Litov¹⁸, B. Lungwitz⁹, M. Makariev¹⁸, A.I. Malakhov⁸, M. Mateev¹⁸, B.W. Mayes¹¹, G.L. Melkumov⁸, C. Meurer⁹, A. Mischke⁷, M. Mitrovski⁹, J. Molnár⁴, S. Mrówczyński¹², G. Palla⁴, A.D. Panagiotou², D. Panayotov¹⁸, A. Petridis², M. Pikna³, L. Pinsky¹¹, F. Pühlhofer¹³, R. Renfordt⁹, A. Richard⁹, C. Roland⁵, G. Roland⁵, M. Rybczyński¹², A. Rybicki^{6,10}, A. Sandoval⁷, N. Schmitz¹⁴, P. Seyboth¹⁴, F. Siklér⁴, B. Sitar³, E. Skrzypczak²⁰, G. Stefanek¹², R. Stock⁹, H. Ströbele⁹, T. Susa²¹, I. Szentpétery⁴, J. Sziklaj⁴, V. Trubnikov²⁰, D. Varga⁴, M. Vassiliou², G.I. Veres^{4,5}, G. Vesztegombi⁴, D. Vranić⁷, A. Wetzler⁹, Z. Włodarczyk¹², I.K. Yoo¹⁶, J. Zaranek⁹, J. Zimányi⁴

¹*NIKHEF, Amsterdam, Netherlands.*

²*Department of Physics, University of Athens, Athens, Greece.*

³*Comenius University, Bratislava, Slovakia.*

⁴*KFKI Research Institute for Particle and Nuclear Physics, Budapest, Hungary.*

⁵*MIT, Cambridge, USA.*

⁶*Institute of Nuclear Physics, Cracow, Poland.*

⁷*Gesellschaft für Schwerionenforschung (GSI), Darmstadt, Germany.*

⁸*Joint Institute for Nuclear Research, Dubna, Russia.*

⁹*Fachbereich Physik der Universität, Frankfurt, Germany.*

¹⁰*CERN, Geneva, Switzerland.*

¹¹*University of Houston, Houston, TX, USA.*

¹²*Institute of Physics Świętokrzyska Academy, Kielce, Poland.*

¹³*Fachbereich Physik der Universität, Marburg, Germany.*

¹⁴*Max-Planck-Institut für Physik, Munich, Germany.*

¹⁵*Institute of Particle and Nuclear Physics, Charles University, Prague, Czech Republic.*

¹⁶*Department of Physics, Pusan National University, Pusan, Republic of Korea.*

¹⁷*Nuclear Physics Laboratory, University of Washington, Seattle, WA, USA.*

¹⁸*Atomic Physics Department, Sofia University St. Kliment Ohridski, Sofia, Bulgaria.*

¹⁹*Institute for Nuclear Studies, Warsaw, Poland.*

²⁰*Institute for Experimental Physics, University of Warsaw, Warsaw, Poland.*

²¹*Rudjer Boskovic Institute, Zagreb, Croatia.*

and

G. Feofilov, R. Kolevatov, V. Kondratiev, P. Naumenko, V. Vechernin
V. Fock Institute for Physics of Saint-Petersburg State University, St. Petersburg, Russia

Reported by G. Feofilov (for NA49 collaboration and SPbSU group)

Abstract

We present the 1st results of the event-by-event study of long-range correlations between event mean p_t and charged particle multiplicity using NA49 experimental data in two separated rapidity intervals in 158 A*GeV PbPb collisions at the CERN SPS. Noticeable long range correlations are found. The most striking feature is the negative p_t - n correlation observed for the central PbPb collisions. Results are compared to the predictions of the HIJING event generator and of the String Fusion Model favoring a string fusion hypothesis.

Key-words: experiment, relativistic heavy ions, color strings fusion, long-range correlations.

1. Introduction

These investigations are motivated by the predictions of the string fusion model [1] pointing to the possibility of observation of long-range correlations as a signature of a string fusion phenomenon. Such a phenomenon is expected to occur at the large string density values reached in high energy nucleus-nucleus collisions [2]. So they were proposed for studies in ALICE at the LHC [3], and now a careful choice of the observables is in progress (see [6], [7]).

Meanwhile it is extremely interesting to apply these ideas to the existing experimental data obtained at the SPS and RHIC energies.

Up to now the experimental study of long-range correlations in nucleus-nucleus interactions was performed only for multiplicities in [5] (SS collisions at 200A-GeV).

The large acceptance detector NA49 at the SPS at CERN provides the opportunity for studies of various types of correlations. So, in this work we present the 1st results of the event-by-event study of long-range correlations between event mean p_t and charged particle multiplicity using NA49 experimental data obtained in two separated rapidity intervals in 158 A*GeV PbPb collisions at the CERN SPS.

The following types of correlations were investigated:

1) n_B - n_F - the correlations between the charged particle multiplicities in backward and forward rapidity intervals,

2) p_{tB} - p_{tF} - the correlations between the event mean transverse momentum obtained in the backward window and the event mean transverse momentum in the forward rapidity window,

3) p_{tB} - n_F and n_B - p_{tF} - the correlations between the event mean transverse momentum in one rapidity interval and the charged particle multiplicity in another interval.

Experimental results are compared to the predictions of the HIJING event generator and of the String Fusion Model (SFM).

2. Long Range correlations. Experimental method

The data were collected by the NA49 large acceptance detector [8] in 1996 at the CERN SPS in collisions of a Pb beam at 158 A GeV/c energy ($\sqrt{s}=17.3$ GeV per nucleon) with a Pb target foil.

The details on the NA49 installation and standard raw data treatment procedure (track reconstruction, event centrality definition, trigger efficiency etc), can be found elsewhere [8], [9]. These details were taken into account both in our data treatment procedures and in the theoretical (SFM) analysis.

A total of about 129000 minimum bias events were considered. Additionally we used also high statistics samples of 161000 events for the 1st centrality class and 194000 events for the 2nd centrality class obtained with a central trigger.

Two windows in rapidity were chosen to be named "backward" ($y_B \in (-0.29, 0.33)$) and "forward" ($y_F \in (0.91, 2.0)$) for the event-by-event studies.

We define for each event the following observables: the number of charged particles n registered in a given "backward" or "forward" window (n_B or n_F) and the relevant event mean transverse momenta p_{tB} or p_{tF} of these particles (see [3]).

Then the following 2D distributions were accumulated event-by-event: (n_B, n_F) , (p_{tB}, n_F) and (p_{tB}, p_{tF}) . After that we define for each plot the average value of the variable in the "backward" window at the fixed value of the variable in the "forward" window. So we obtain the following plots: $\langle n_B \rangle_{n_F}$ and $\langle p_{tB} \rangle_{n_F}$ vs. n_F and $\langle p_{tB} \rangle_{p_{tF}}$ vs. p_{tF} (in a way similar to [3]).

One of the main features of the results is the linear dependence observed for the majority of these correlation functions. So we applied linear parameterizations, an example for the n - n correlations is:

$$\langle n_B \rangle_{n_F} = a + \beta_{nn} \cdot n_F$$

here the strength of the correlation is measured by the coefficient β_{nn} . In case of p_t - p_t and p_t - n correlations the coefficients $\beta_{p_t p_t}$ and $\beta_{p_t n}$ were defined in a similar manner.

Various long-range correlations between these observables were studied for minimum bias events as well as for several classes of collision centrality defined in Table.1 and Fig.1.

Table 1: Fraction in % of inelastic cross-section for centrality event classes

	class-1	class-2	class-3
%	< 5	5-12.5	12.5-23.5
Nch	800 - 1500	700 - 1300	400 - 1200
Ev	0-9250	9250-14670	14670-21190
	class-4	class-5	class-6
%	23.5-33.5	33.5-43.5	> 43.5
Nch	200 -900	100 - 700	10 - 500
Ev	21190-26080	26080-29340	29340-36000

Here Nch denotes the region of event multiplicity, Ev (GeV/c) the region of energy Eveto recorded by the zero-degree calorimeter for a given class.

The Eveto energy window size (Δ Eveto) was varied around the relevant central values inside Ev for a given centrality class in order to study the effect of its influence on n - n , p_t - p_t and p_t - n correlation coefficients. A kind of plateau in the correlation coefficients was reached at the values of Δ Eveto windows that are comparable with the intrinsic resolution

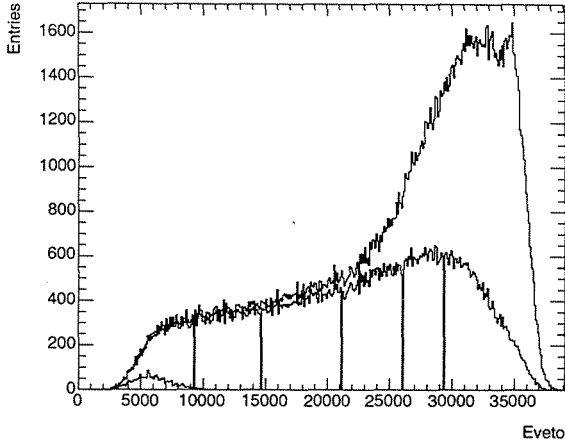


Figure 1: NA49 Eveto calorimeter spectra (Eveto values are in GeV) before and after all cuts applied. Positions of the Eveto intervals selected for centrality analysis of long-range correlations are indicated by the vertical bars. The Eveto data sample defined by the events forming the "plateau" region of the correlation plots is also shown separately inside the 1st class (see text)

(about 2900GeV) of the zero-degree calorimeter. Thus the influence of the class width could be excluded, keeping only the unavoidable finite Eveto resolution influence on the final results.

The final values of correlation coefficients extracted by the variation of Δ Eveto are shown vs. collision centrality class in Fig.2, 3 (Black squares are the experimental data. Only statistical errors are shown. Straight lines are to guide the eye.)

The following picture is found:

1) Strong n - n long range correlations are obtained for all centrality classes. A monotonous decrease of the n - n correlation coefficient is observed from peripheral towards central collisions (from 0.35 to about 0.1), see Fig.2.

2) The p_t - p_t correlations are noticeable (about one error bar at present level of statistics) only in the peripheral region (the 5th and 6th centrality classes), therefore they are not shown here.

3) The p_t - n correlations demonstrate a tendency to move from *positive* values in the peripheral collisions region to *negative* for the central collisions, see Fig.3. Negative correlation values are obtained for the 1st ($\beta_{p_t, n} = -0.00008 \pm 0.00001$ (GeV/c)) and the 2nd ($\beta_{p_t, n} = -0.00003 \pm 0.00001$ (GeV/c)) centrality classes.

Minimum bias event data were also analysed. Plots of the long range forward-backward correlations of charged particles obtained for minimum bias PbPb collisions at $\sqrt{s}=17.3$ GeV are presented below in Figs.4,5,6.

A number of intriguing features was observed:

1) A linear dependence of $\langle n_B \rangle_{n_F}$ on n_F is seen in the region of forward multiplicities up to the values of n_F about 210. A "plateau" is observed at higher values of n_F (see Fig.4).

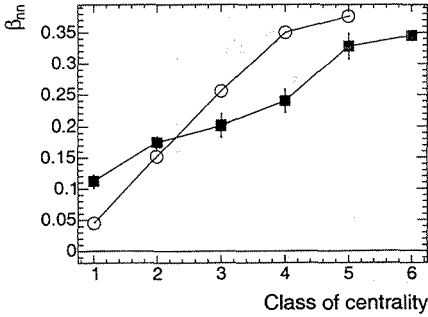


Figure 2: Long range forward-backward n - n correlation coefficients (squares) vs. centrality class for PbPb collisions at $\sqrt{s}=17.3$ GeV. Open circles: String Fusion Model. Horizontal line: the absence of correlations as described by the SFM "without fusion"

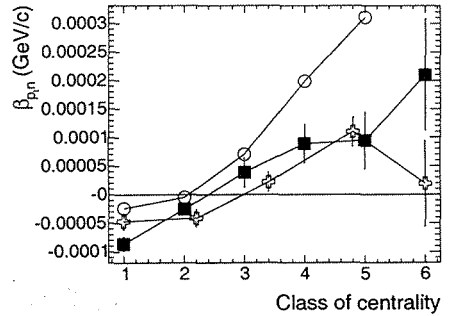


Figure 3: Long range forward-backward p_t - n correlation coefficients (squares) vs. centrality class for PbPb collisions at $\sqrt{s}=17.3$ GeV. Open crosses: HIJING; Open circles: String Fusion Model. Horizontal line: SFM "without fusion"

2) The dependence of $\langle p_{tB} \rangle_{n_F}$ on n_F is very close to linear in the interval n_F between 50-210. "A plateau", or p_{tB} "saturation" at the level of about 0.36 GeV/c is also observed at values of forward multiplicities n_F higher than 210 (see Fig.5). The picture is qualitatively similar to the one for pp-collisions at 31GeV and 63 GeV [10].

3) The events with multiplicities higher than 210 that are forming the "plateau" region of the correlation plots (about 2000 events out of 129000 total) represent a fraction of the 1st centrality class (see the Fig.1).

4) A complicated non-linear behavior of $\langle p_{tB} \rangle_{p_{tF}}$ vs. p_{tF} is discovered (see Fig.6). This non-linear dependence of $\langle p_{tB} \rangle_{p_{tF}}$ on p_{tF} has a "bump" that reaches about 0.35 GeV/c at values of p_{tF} of about 0.35 GeV/c.

3. Analysis of Long Range correlations for PbPb at 158 A*GeV

There could be at least two reasons for the experimentally observed *negative values* of the p_t - n long-range correlation coefficients obtained in the present work for the very central PbPb collisions at 158 A*GeV under the condition of the narrow Eveto window:

- (i) String Fusion effects for *fixed* number of participants;
- (ii) Kinematical constraints due to the energy conservation in string production and decay.

We first compared the observed long-range correlations with the standard event generator HIJING [11].

Normalization factors were applied for the HIJING multiplicity values (0.7 for the forward and 0.42 for the backward rapidity window.) Another factor = 0.9 was also appliced

for the HIJING mean p_t values in order to take into account the experimental acceptance cuts. In case of HIJING we did not use the detailed acceptance parametrization or trigger event cuts, because the main goal was to obtain a general trend.

These normalizations enable us to reproduce the data both for the centrality dependence of correlation coefficients (see Fig.3) and for the minimum bias events (see Fig.4,5,6).

The reason for this is, first of all, that a collectivity phenomenon is included in the HIJING model phenomenologically in the form of the Cronin effect that accounts for the growth of the mean p_t with the multiplicity.

Secondly, the observed *negative* correlations are reproduced by HIJING for the 1st centrality class under the condition of a narrow Eveto window. This means that the kinematical constraints on the string decay play an important role at the given energies.

One has to keep in mind, that the observation of these "*negative correlations*" could be damped by such nuclear density effects as fluctuations in the number of participants leading to "*positive correlations*". So, the observed transition from *negative* to *positive* long range correlations (reproduced in HIJING) is simply related to the relative increase of the fluctuations in the number of nucleon-nucleon collisions for the peripheral events.

A microscopic explanation of these phenomena was obtained in the framework of a simplified MC String Fusion Model[12], [13].

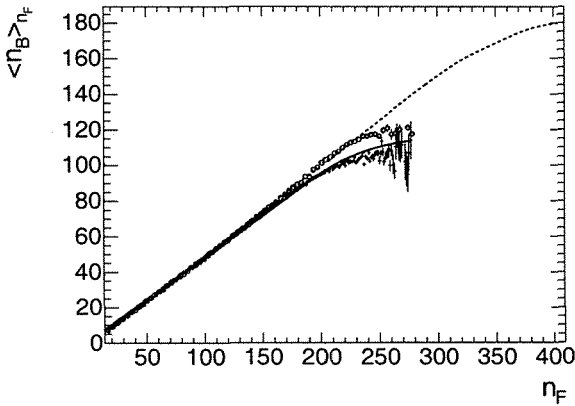


Figure 4: The average backward multiplicity $\langle n_B \rangle$ at fixed n_F vs. values of n_F . Crosses: experimental data. Solid curve: SFM. Open circles: HIJING (normalized, see text). Dotted curve: SFM calculations without string fusion

The model is based on the assumption of the interaction of overlapping strings (quark-gluon string fusion) and it takes into account the changes of the mean values of the observables in the case of overlap. The increase of the tension in the area of K overlapping strings gives rise to an increase of the mean p_t^2 and the mean number of particles, emitted from this area, proportional to \sqrt{K} . At the same time, in case of the non-overlapping strings (non-interacting strings) the multiplicity of charged particles is just proportional to the total number of strings, while the mean p_t stays constant.

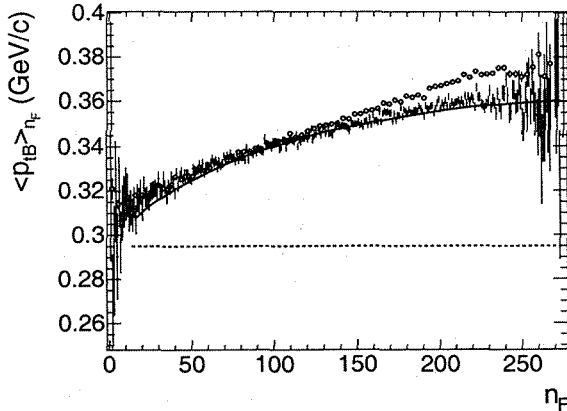


Figure 5: The average transverse momentum $\langle p_{tB} \rangle$ at fixed n_F vs. values of n_F . HIJING predictions are normalized both for p_t and multiplicity. Crosses: experimental data. Solid curve: SFM. Open circles: HIJING (normalized, see text). Dotted curve: SFM calculations without fusion

As to the long range $p_t - n$ and $p_t - p_t$ correlations, they imply the presence of at least two types of particle sources extended in the rapidity space and characterized by different values of mean p_t . So in the case of “no string interaction” the model shows zero forward-backward $p_t - n$ and $p_t - p_t$ correlations. As an example see the results of the SFM calculations without string fusion in Fig.3. SFM Monte-Carlo calculations of the correlations were done both at fixed values of the impact parameter and taking into account its inevitable fluctuations (e.g. due to the finite zero-degree calorimeter resolution). The real nucleon density distribution for the colliding nuclei was used. The specific experimental trigger conditions including the event selection (see Fig.1) were also taken into account in the SFM calculations.

The general growth of the n - n long-range correlation coefficients towards the peripheral collisions observed in case of narrow Eveto windows is well understood in the framework of the SFM (See Fig.2).

The *negative values* of the p_t - n long-range correlation coefficients obtained for the very central collisions in case of narrow Eveto windows and the increase of positive correlations for more peripheral classes were reproduced in the SFM calculations (see Fig.3). It was also confirmed that the observed transition from *the negative to the positive* p_t - n long range correlations is related to the trivial relative increase of the fluctuations in the number of nucleon-nucleon collisions in case of the peripheral events.

The results of the Monte-Carlo SFM calculations for the minimum bias PbPb events at $\sqrt{s} = 17.3$ GeV using the SFM approach are presented in Fig.4,5,6. One can see that a rather detailed description of minimum bias data is achieved in the framework of the SFM.

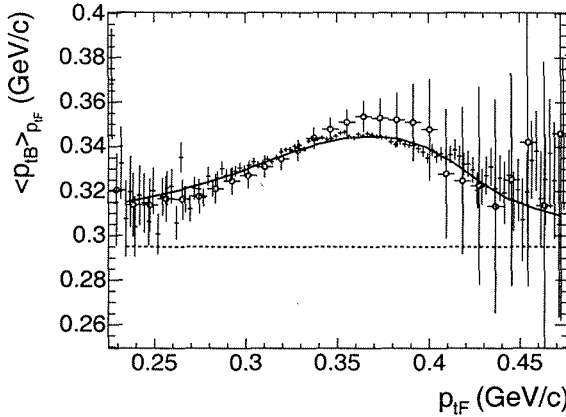


Figure 6: The average backward transverse momentum $\langle p_{tB} \rangle$ at fixed p_{tF} vs. values of p_{tF} . Crosses: experimental data. Solid curve: SFM. Open circles: HIJING (normalized, see text). Dotted curve: SFM calculations without string fusion

4. Conclusions

1. Experimental evidence for long-range correlations in multi particle production measured in two separated rapidity intervals in PbPb collisions at 158 A*GeV is found.
2. A complicated non-linear dependence of $\langle n_B \rangle_{n_F}$ and $\langle p_{tB} \rangle_{n_F}$ on n_F and of $\langle p_{tB} \rangle_{p_{tF}}$ on p_{tF} is observed for the minimum bias events.
3. The centrality dependence of the correlation coefficients shows the following features:

- 1) Strong n - n long range correlations are obtained for all centrality classes. A monotonous decrease of n - n correlation coefficients is observed from peripheral towards central collisions (from 0.35 to about 0.1).
- 2) The p_t - p_t correlations are noticeable (about one error bar at present level of statistics) only in the peripheral region (the 5th and 6th centrality classes).
- 3) The p_t - n correlations demonstrate a tendency to move from *positive* values in peripheral collision region to *negative* values for the central collisions.

Negative correlation coefficients $\beta p_t n$ are obtained for the 1st and the 2nd centrality classes, the values are -0.00008 ± 0.00001 GeV/c and -0.00003 ± 0.00001 GeV/c.

- 4) The observed transition from *negative* to *positive* long range correlations is described both in HIJING and SFM due to the relative increase of the fluctuations in the number of nucleon-nucleon collisions for the peripheral events.
4. The analysis in the framework of HIJING and SFM indicates that both models are providing a quantitative description of the observed long-range correlations in minimum bias events as well as of their centrality dependence. HIJING does this by

a phenomenological increase of the mean p_t for the multiple nucleon-nucleon collisions, while the SFM provides a microscopic explanation of the observed collectivity effects. So, we conclude that the results are favouring the string fusion hypothesis.

5. Further checks of the string fusion hypothesis at higher energies (RHIC and LHC) are very desirable.

Acknowledgements: This work was supported by the US Department of Energy Grant DE-FG03-97ER41020/A000, the Bundesministerium für Bildung und Forschung, Germany, the Polish State Committee for Scientific Research (2 P03B 130 23, SPB/CERN/P-03/Dz 446/2002-2004, 2 P03B 04123), the Hungarian Scientific Research Foundation (T032648, T032293, T043514), the Hungarian National Science Foundation, OTKA, (F034707), the Polish-German Foundation, and the Korea Research Foundation Grant (KRF-2003-070-C00015).

St.Petersburg State University group acknowledges with thanks the kind financial support of GSI and Frankfurt University at the early stage of this work that helped to start the data analysis. We also express our deep gratitude to M.Braun for the permanent support and interest in this investigation and to N.Armeστο for useful discussions. This job was also partially covered by the grants No.1649 and A13157 of the Ministry of Education of Russian Federation.

References

- [1] M.A.Braun and C.Pajares, Phys. Lett. **B287**,154 (1992); Nucl. Phys. **B390**, 542 (1993).
- [2] N.S.Amelin, N.Armeστο, M.A.Braun, E.G.Ferreiro and C.Pajares, Phys. Rev. Lett. **73**, 2813 (1994); M.A.Braun,C.Pajares, Phys.Rev.Let, **85**,4864-4867 (2000); M.A.Braun,R.S.Kolevatov,C.Pajares.V.V.Vechernin, Eur.Phys.J.**C32**, 535-546 (2004).
- [3] P.A.Bolokhov, M.A.Braun, G.A.Feofilov, V.P.Kondratiev, V.V.Vechernin, Internal Note/PHY.ALICE-INT-2002-20, 16p (2002).
- [4] P.A.Bolokhov, M.A.Braun, G.A.Feofilov, V.P.Kondratiev and V.V.Vechernin, Abstracts of the XVI International Baldin Seminar on High Energy Physics Problems, JINR, Dubna, p.115 and p.116 (2002).
- [5] J.Bachler et.al, Z.Phys.**C56**, 347-354 (1992).
- [6] ALICE Physics Performance Report, chapter 6 ("Event-by-event studies"), to be published.
- [7] NA49 Collaboration at CERN and G.Feofilov, R.Kolevatov, V.Kondratiev, P.Naumenko, V.Vechernin, Abstracts of the XVII International Baldin Seminar on High Energy Physics Problems, Dubna, Russia, September 27-October 2, p.59, (2004) (to be published).
- [8] S.Afanasiev et al.,NIM **A430**, 216-244 (1990).

- [9] T. Anticic *et al.* (NA49 Collaboration), arXiv:hep-ex/0311009.
- [10] G. Arnison *et al.*, Phys.Lett.**B118**, 167 (1982).
- [11] M. Gyulassy and X-N Wang, Preprint **LBL-34246**, February 4, (1997).
- [12] R.S.Kolevatov, V.V.Vechernin, "Multiplicity and p_t correlations in AA-interactions at high energies", report submitted to the QFTHEP'2004, St.Petersburg, (2004), to be published.
- [13] V.V.Vechernin, R.S.Kolevatov, arXiv:hep-ph/0304295; 0305136.

ON SPATIAL AND EVENT-BY-EVENT FLUCTUATIONS IN RELATIVISTIC HEAVY-ION COLLISIONS

Shakeel Ahmad

Department of Physics, Aligarh Muslim University, Aligarh, India

† *E-mail: Shakeel.Ahmad@cern.ch*

Abstract

Erraticity analysis of the experimental data on 14.5A GeV/c $^{28}\text{Si-AgBr}$ collisions is carried out. It is demonstrated that like multifractal spectral through G_q moments, erraticity spectrum may also be constructed which help extract maximum information on self similar fluctuations. Comparison of the findings with the Monte Carlo models reveals that the observed erratic fluctuations are not only because of the statistical reasons but may have some dynamical contents too.

1. Introduction

Power law behaviour of the scaled factorial moments, F_q , referred to as the intermittency[1] has been extensively used to investigate fluctuations and chaos in multiparticle production in high energy hadronic and heavy-ion(AA) collisions[2 and references therein]. These investigations reveal that the presence of large fluctuations in small phase space bins may be rare but not impossible. It has, however, been pointed out[3] that F_q estimated by taking the vertical or the horizontal average can not fully account for all the fluctuations that a system may exhibit because of the averaging procedures adopted. The values of $F_q^{(e)}$, if calculated on e-by-e basis, exhibit large fluctuations and therefore, a distinct distribution of $F_q^{(e)}$ for a given q and M may be observed for a sample of events; q is the order of moment and M is the number of equally spaced bins in the pseudorapidity (η) space. Such a distribution is envisaged to help disentangle some useful and interesting information about chaotic behaviour of multiparticle production. A few moments of $F_q^{(e)}$ distribution, for example, the normalized moments $C_{p,q}$ are likely to serve the purpose. If $C_{p,q}$ exhibit a power law behaviour then such a behaviour is referred to as erraticity[3]. It may be stressed that erraticity analysis would take into account simultaneously the spatial as well as the e-by-e fluctuations beyond intermittency. Studies involving erratic fluctuations in hadronic and heavy-ion collisions, carried out so far[4-6] are not conclusive. It was, therefore, considered worthwhile to examine erraticity behaviour in relativistic AA collisions. Attention is focussed on the behaviour of erraticity exponents and erraticity spectrum which are likely to provide maximum information on self-similar fluctuations[3]. Hence analysis of the experimental data on 14.5A GeV/c $^{28}\text{Si-AgBr}$ collisions is carried out for this purpose. The findings are compared with the predictions of QCD inspired models.

2. Experimental Details

A stack of ILLFORD-G5 emulsion exposed to 14.5AGeV/c silicon-ions from AGS, BNL, has been used in the present study. The events due to the AgBr group of targets were selected by using the criterion that the number of heavily ionizing tracks, n_h , in an interaction must be ≥ 8 . By applying this criterion, 274 interactions from a random sample of 505 events characterized by $n_h \geq 0$ produced in the interactions of ^{28}Si nuclei with emulsion nuclei were considered. The other relevant details regarding scanning procedure, criteria of event selection, classification of tracks, methods of measurements, etc., may be found elsewhere[7].

3. Method of analysis

A detailed description about the method of erraticity analysis may be found in refs.3-6. However, a brief description is considered necessary and is, therefore, presented here. In order to reduce the effect of non-flatness of the single particle distribution in pseudorapidity (η) space, the η values are transformed into the cumulative variable, $X(\eta)$, defined as[8];

$$X(\eta) = \frac{\int_{\eta_{\min}}^{\eta} \rho(\eta) d(\eta)}{\int_{\eta_{\min}}^{\eta_{\max}} \rho(\eta) d(\eta)} \quad (1)$$

the event factorial moment describing the spatial pattern of an event is calculated from:

$$F_q^{(e)} = \frac{\langle n(n-1)\dots(n-q+1) \rangle_e}{\langle n \rangle_e^q} \quad (2)$$

where n is the charged particle multiplicity in a particular bin. To quantify e-by-e fluctuations in $F_q^{(e)}$, the normalized moments, $C_{p,q}$ are calculated using

$$C_{p,q} = \langle \Phi_p(q) \rangle^p \quad ; \quad \Phi_p(q) = \frac{F_q^{(e)}}{\langle F_q^{(e)} \rangle} \quad (3)$$

The order q is an integer while p takes on any value > 0 . If $C_{p,q}$ exhibit a power law behaviour of the type, $C_{p,q} \propto M^{(\psi_p(q))}$ for a given q , then such a behaviour is referred to as erraticity[3]; ψ_p is the erraticity exponent. The normalized moments $C_{p,q}$ are sensitive to the e-by-e fluctuations and its derivative around $p = 1$,

$$\mu_q = \left. \frac{d}{dp} \psi_p(q) \right|_{p=1} \quad (4)$$

describes the degree of e-by-e fluctuations, and is referred to as entropy index[6]. Another entropy like quantity Σ_q is defined as:

$$\Sigma_q = \langle \Phi_q \ln \Phi_q \rangle \quad (5)$$

and the entropy index μ_q may also be calculated from Σ_q using:

$$\mu_q = \frac{\delta \Sigma_q}{\delta \ln M} \quad (6)$$

Although, the scaling behaviour exhibited by $C_{p,q}$ moments is opposite to that observed in the case of G_q moments[3], yet, like multifractal spectrum, erraticity spectrum $e(\alpha_p)$ may be defined for a given q as:

$$e(\alpha_p) = p\alpha_p - \psi_p \quad (7)$$

where $\alpha_p = \frac{d\psi_p}{dp}$. The function $e(\alpha_p)$ describes certain properties of erraticity more directly than ψ_p . It is clear from these definitions that $\alpha_1(q) = \mu_q$ and for this value of $p(=1)$, $e(\alpha_p) = \alpha_p$. On the other hand, for all other values of p , $e(\alpha_p)$ will be greater than α_p .

4. Results and Discussion

4.1. Experimental Results

Pseudorapidity values of the relativistic charged particles produced in each interaction in the η -range, $\eta_0 \pm 3.0$ are transformed into cumulative variable $X(\eta)$, where η_0 is the centre-of-mass hadron-nucleon rapidity. Values of $C_{p,q}$ are calculated for different values of M , p and q and the variations of $\ln C_{p,q=2}$ with $\ln M$ are shown in Fig.1; the error bars are shown for the alternate sets of data to avoid overlapping. In the same figure, dependence of dependence of Σ_q on $\ln M$ are shown. The asymptotic power law behaviour of

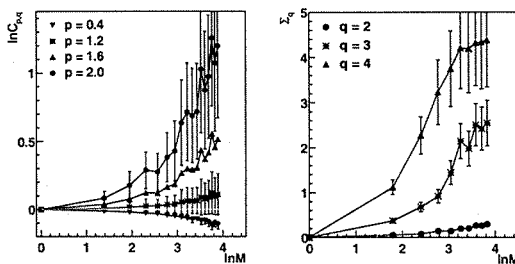


Figure 1: Variations of $\ln C_{p,2}$ and Σ_2 with $\ln M$

$C_{p,2}$ and Σ_q with decreasing bin-width indicates the presence of erraticity in 14.5A GeV/c $^{28}\text{Si-AgBr}$ collisions. Values of entropy index, $\mu_q (= \frac{d}{dp} \psi_p(q) \Big|_{p=1})$ are calculated for $q = 2, 3$ and 4. These values are determined by evaluating ψ_p at $p = 0.9$ and 1.1 and are presented in Table 1.

Table 1

q	μ_q				
	Expt.	HIJING	IEH	QCD	QCD
				q-jet	g-jet
2	0.15 ± 0.02	0.10 ± 0.01	0.01 ± 0.01	0.11	0.02
3	0.33 ± 0.05	0.28 ± 0.01	0.04 ± 0.01	0.42	0.03
4	0.89 ± 0.03	0.78 ± 0.02	0.15 ± 0.01	0.98	0.16

In order to disentangle further information about the spatial and e-by-e fluctuations, the values of erraticity exponents, ψ_p , are determined by plotting $\ln C_{p,q}$ against $\ln M$ and doing the fits in the linear region ($M = 5-20$). Using these values of ψ_p , the values of $\alpha_p (= \frac{d\psi_p}{dp})$ are estimated and the erraticity spectra, $e(\alpha_p)$, thus obtained for $q = 2$ and 4 are displayed in Fig.2. The straight lines in the figure correspond to $e(\alpha_p) = \alpha_p$. It is

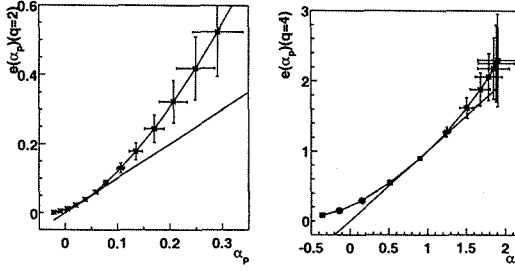


Figure 2: Erraticity spectra, $e(\alpha_p)$ for $q = 2, 4$

interesting to notice in the figure that the line is tangent to the curve at the point for $p = 1$. At this point the parameter $e(\alpha_p)$ acquires a minimum value equal to α_p . This would, therefore, make entropy index, μ_q to satisfy $\mu_q = \alpha_1(q)$. However, for other values of p , $e(\alpha_p)$ is comparatively higher than α_p . The experimental data used in the present study, therefore, indicate that like the multifractal spectrum, erraticity spectrum may also be constructed, if scaling behaviour exists. This, in turn, would help disentangle maximum information relating to the horizontal and vartical fluctuations of the data that exhibit self similar properties.

4.2. Comparison with Monte Carlo Models

It has been pointed out[4-6] that the observed erratic fluctuations in high energy hadronic and heavy-ion collisions are mostly due to the statistical reasons. For investigating the dominance of statistical fluctuations over the erraticity behaviour, therefore, correlation-free MC events are simulated in the framework of independent emission hypothesis(IEH) model, which is based on the following assumptions:

- i. Multiplicity distribution of the simulated data sample should be similar to the experimental one,
- ii. for an event with multiplicity n_s , $X(\eta)$ values of its n_s particles should be uniformly distributed in the range 0-1 and
- iii. there should be no correlation amongst the emitted particles.

By adopting these criteria, a sample of 16440 events (IEH events) are generated and analysed. Furthermore, in order to compare the experimental findings with the predictions of QCD inspired models, a sample of 14025 events similar to the experimental ones are

generated using the MC code, HIJING-1.33. These events are generated according to the percentage of interactions of the incident beam with different targets in emulsion[9]. Variations of the erraticity moments $\ln C_{2,3}$ and Σ_3 with $\ln M$ obtained for the experimental and simulated data are exhibited in Fig.3. It is noted that the HIJING MC findings are

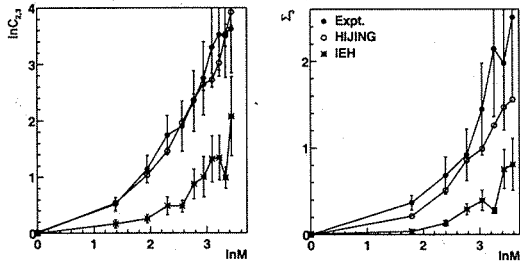


Figure 3: Variations of $\ln C_{p,2}$ and Σ_2 with $\ln M$

close to the experimental ones while the IEH MC data give significantly smaller values of the two moments. In Fig.4 erraticity spectra corresponding to the different data sets are compared. It is evident that the straight line ($\epsilon(\alpha_p) = \alpha_p$) is the common tangent. It is noted too that the spectra corresponding to the experimental and HIJING data almost overlap but a significant departure of the spectrum due to the IEH data from that due to the experimental one is noted. These findings, therefore, clearly indicate that the erratic fluctuations observed in the present study are not only due to the statistical reasons but may have some contributions because of the dynamical reasons too.

The values of entropy index, μ_q are evaluated for the MC data sets too and are presented

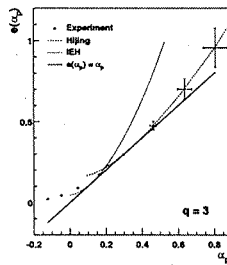


Figure 4: Erraticity spectrum for the experimental and MC data

in Table 1 along with those obtained in MC simulations performed in the framework of perturbative QCD for quark jets and for gluon jets[10]. It is observed that the values of μ_q corresponding to the experimental and HIJING data are close to those predicted by the perturbative QCD for quark jets. Since higher values of μ_q correspond to smaller entropy and more chaoticity[10], it may be concluded that our data clearly exhibits the chaotic nature of multiparticle production in relativistic AA collisions.

5. Conclusions

Based on the present investigations, following conclusions may be arrived at:

1. The observed power law behaviour of the normalized moments, $C_{p,q}$, indicates that erratic fluctuations exhibited by the experimental data are much larger as compared to those obtained from the MC simulations.
2. The values of μ_q agree fairly well with the predictions of perturbative QCD for quark-jets and indicates that the particle production in AA collisions is more chaotic than that expected from the correlation-free MC events.
3. Similar to the multifractal spectrum, erraticity spectrum may also be obtained which may help disentangling useful information regarding the entropy and(or) chaoticity in particle production phenomenon.
4. Comparison of various findings based on the experimental, HIJING and IEH-MC data suggests that the observed fluctuations in the case of experimental events might have some dynamical origin.

References

- [1] A. Bialas and R. Peschanski, Nucl. Phys. **B273** 703(1986).
- [2] E. A. De. Wolf et al Rep. **270**, 48(1996).
- [3] R.C. Hwa, Acta Phy. Pol. B27, 1789(1996).
- [4] L.Fuming et al Phys. Lett **B576**, 293 2001.
- [5] F. Jinghua et al Phy. Lett. **B472**,161,2000.
- [6] M.R. Atayan et al (EHS/NA22 Collaboration) Phys. Lett. **B558**, 22(2003).
- [7] Shakeel Ahmad et al Acta.Phys.Pol. **35**, 809, 2004: J.Phys.**G30**, 1145, 2004.
- [8] A. Bialas and M. Gazdzicki, Phys. Lett. **B252**, 483(1990).
- [9] M. I. Adamoich et. al. (EMU01 Collaboration), Phys. Lett. **B201**, 397(1988).
- [0] Z. Cao and R.C. Hwa Phys. Rev. Lett. **75**, 1268(1995): Phys. Rev. **D53**, 6608(1996).

NEUTRINO OPACITY TO COLD NEUTRON MATTER

O.Benhar¹, A.Fabrocini², S.Fantoni³, G.I.Lykasov⁴

- (1) *INFN, Sezione Roma 1, I-00185, Roma, Italy*
- (2) *Dipartimento di Fisica "E.Fermi", Università di Pisa, and INFN, Sezione di Pisa, I-56100, Pisa, Italy*
- (3) *International School for Advanced Studies (SISSA) and INFN, Sezione di Trieste, I-30014, Trieste, Italy*
- (4) *JINR, Dubna, Moscow region, 141980, Russia*

Abstract

The weak dynamic form factors of cold neutron matter have been calculated within correlated basis function (CBF) theory using a realistic hamiltonian. The results show that the effect of nucleon-nucleon correlations on the density and spin-density responses are different. The role of long range correlations has been investigated comparing the CBF responses to those resulting from Landau theory of Fermi liquids. The neutrino mean free path have been obtained combining the two approaches.

PACS numbers:13.15.+g.26.60.+c.97.60.Jd

1. Introduction

Neutrino processes in a nuclear medium play an important role in astrophysics. For instance, neutrino propagation in dense neutron or protonneutron matter gives relevant information about the stellar evolution and the stars structure [1, 2] and [3, 4]. The key ingredient in neutrino transport calculation is the neutrino opacity. Its theoretical evaluation, however, involves several approximations in the calculation of the neutrino cross sections.

In this paper we focus on the analysis of the density-density and spin-density dynamic form factors (FF) constructed within the different approaches and apply them to the calculation of the elastic and quasi-elastic neutrino cross section and its mean free path. An approach which takes some care of the nucleon-nucleon interaction and of the consequent nucleon properties modifications based on the CBF is suggested. This effect results to be sizable, with respect to calculations performed within the Fermi gas approximation. Comparing the calculated FF with the corresponding results obtained within the Landau Fermi liquid theory (LT) we find some difference between them. Therefore we are matching these two approaches LT and CBF to calculate the elastic neutrino mean free path due to the neutral weak current.

2. Weak neutrino response

The description of nuclear responses in the quasi-elastic region is based upon the approach developed in Ref.[6] The basic ansatz consists in assuming that the nuclear excited state can be described as a product of a Slater determinant and a many-body correlation

function which is the same correlation function describing the ground state:

$$|\Psi_f \rangle = F|\Phi_f \rangle \quad (1)$$

where the many-body correlation function F is the product of the two-body correlation functions [6, 7], Φ_f includes a Slater determinant which differs from Φ_0 by the fact that a certain number of hole single particle states have been substituted with particle wave functions. Here Φ_0 is a Slater determinant formed by a set of orthonormal single particle wave functions. The many-body nuclear response depending on the energy transfer ω and the three-momentum transfer \mathbf{q} to an external field $Q(\mathbf{q})$ is written in the form [7]

$$\chi_{CBF}(\omega, \mathbf{q}) = \sum_f \frac{\langle \Psi_0 | Q^+(\mathbf{q}) | \Psi_f \rangle \langle \Psi_f | Q(\mathbf{q}) | \Psi_0 \rangle}{\langle \Psi_f | \Psi_f \rangle \langle \Psi_0 | \Psi_0 \rangle} \delta(E_f - E_0 - \omega) \quad (2)$$

The weak dynamic form factors $S_V(\mathbf{q}, \omega)$ and $S_A(\mathbf{q}, \omega)$ are related to the corresponding response functions $\chi_{V,A}(\mathbf{q}, \omega)$ [19]

$$S_{V,A}(\mathbf{q}, \omega) = \frac{1}{2\pi n} \frac{1}{1 - \exp(-\beta\omega)} \text{Im}(\chi_{V,A}(\mathbf{q}, \omega)) \quad (3)$$

where $\beta = 1/k_B T$, k_B is the Boltzman constant, T is the temperature, n is the density of neutron matter. They can be calculated, for example within the Landau Fermi liquid theory [15, 1]. The response functions χ_V and χ_A are related to the density and spin-density fluctuations of quasiparticles δn_p^s and δn_p^a respectively, here p is the quasiparticle momentum, see Ref.[1]

$$\chi_{V,A} = \frac{\sum_p \text{Tr}[\sigma \delta n_p^{s,a}(\mathbf{q}, \omega)]}{g \mu_B H(\mathbf{q}, \omega)} \quad (4)$$

where g is the Lande' g factor, μ_B is the Bohr magneton H is the perturbing magnetic field chosen in the z direction.

Solving the Landau transport equation for density and spin-density fluctuations of quasiparticles in a medium one can find the following forms for $\chi_{V,A}(\mathbf{q}, \omega)$ presented in Ref.[1]:

$$\chi_{V,A}(\mathbf{q}, \omega) = \frac{N(0)}{V} \frac{g(\lambda)}{1 + [F_0^{V,A} + \lambda^2 F_1^{V,A} / (1 + F_1^{V,A} / 3)] g(\lambda)} \quad (5)$$

where $N(0)/V = m^* p_F(n) / \pi^2$, $\lambda = \omega / q v_F$, $v_F = p_F / m$, $F_0^{V,A}$, $F_1^{V,A}$ are the Landau parameters corresponding to the interaction of two quasiparticles with the relative orbital moments $l = 0$ and $l = 1$ respectively,

$$g(\lambda) = 1 - \frac{\lambda}{2} \ln \left| \frac{\lambda + 1}{\lambda - 1} \right| + i \frac{\pi}{2} \lambda \theta(1 - |\lambda|) \quad (6)$$

Here p_F , m , m^* are the Fermi momentum, the bare and the effective nucleon masses respectively. According to the conventional notations for the Landau parameters $F_0^V = F_0$, $F_1^V = F_1$ and $F_0^A = G_0$, $F_1^A = G_1$ [17, 18].

3. Application to the neutrino scattering in a medium

Let us apply the response function to the analysis of the neutrino propagation in a cold pure neutron matter at low energies. Actually the weak responses in symmetric nuclear matter have been calculated recently in Ref.[8] within the CBF theory using the Tamm-Dankoff approximation. We will compare our calculations with the results presented in Ref.[8] and find some difference. The weak response of nuclei has been studied also in Ref.[9] and a difference between the electromagnetic and weak FF has been shown.

The elastic or quasi-elastic neutrino-neutron scattering is due by the weak neutral current. According to the Weinberg-Salam model, the Lagrangian of such interaction has the form [10, 11] and [12, 1]

$$\mathcal{L}_I(x) = \frac{G_F}{\sqrt{2}} l_\mu(x) j_z^\mu(x) \quad (7)$$

where $G_F = 1.166 \text{GeV}^{-2} \times 10^{-5} = 1.436 \times 10^{-49} \text{erg.cm}^3$ is the Fermi weak coupling constant,

$$l_\mu(x) = \bar{\psi}_\nu \gamma_\mu (1 - \gamma_5) \psi_\nu \quad (8)$$

is the lepton weak neutral current,

$$j_z^\mu(x) = \frac{1}{2} \bar{\psi}_n \gamma^\mu (C_V - C_A \gamma_5) \psi_n \quad (9)$$

is the third component of the isospin current, $C_V = 1$, $C_A = 1.25$ are the vector and axial coupling constant. At low neutrino energies we may use the following approximation for the hadronic current [1]

$$\bar{\psi}_n \gamma^\mu (C_V - C_A \gamma_5) \psi_n \rightarrow C_V \psi_n^+ \psi_n \delta_0^\mu - C_A \psi_n^+ \sigma_i \psi_n \delta_i^\mu \quad (10)$$

Applying the weak response given by the eq.(2) we have two response functions: the vector response χ_{CBF}^V and the axial vector one χ_{CBF}^A .

Using these forms for the leptonic and hadronic currents one can get the equation for the rate of neutrino-neutron elastic scattering in a pure neutron matter at low energies, see for example Refs.[1, 5] and Ref.[4].

$$W_{fi} = \frac{G^2 n}{4V} [C_V^2 (1 + \cos(\theta)) \mathcal{S}_V(\mathbf{q}, \omega) + C_A^2 (3 - \cos(\theta)) \mathcal{S}_A(\mathbf{q}, \omega)] \quad (11)$$

However, the hadronic vector $\bar{\psi}_n \psi_n \delta_0^\mu$ current and the axial $\bar{\psi}_n \sigma_i \psi_n \delta_i^\mu$ current can be modified in a medium. The vector and axial constants C_V , C_A are renormalized, however they can be changed in a medium about 10-15% according to [13, 14]. Therefore we neglect this effect. We also neglect the antisymmetric part $\mathcal{L}^a(\mathbf{q}, \omega)$ of the spin-spin dynamic form factor and use only its symmetric part $\mathcal{L}_{ij}^s(\mathbf{q}, \omega) \equiv \delta_{ij} \mathcal{S}_A(\mathbf{q}, \omega)$ because one can show that it is proportional to \mathbf{q}^2/m^2 .

4. Neutrino mean free path

Let us apply the obtained form for the density and spin-density FF to compute the mean free path l at the zero temperature $T = 0$, for the nondegenerate neutrino case. In this case, according to Ref.[1]

$$1/l = V \int \frac{d^3q}{(2\pi)^3} W_{fi} \quad (12)$$

At $T = 0$ the integral in eq.(12) is splitted into two parts [1]

$$\int_0^{2P_\nu/(1+v_F)} dq \int_0^{qv_F} d\omega + \int_{2P_\nu/(1+v_F)}^{2P_\nu} dq \int_0^{c(2P_\nu-q)} d\omega \quad (13)$$

where P_ν is the magnitude of the initial neutrino momentum. The Gamow-Teller part $1/l_{GT}$ of $1/l$ is related to W_{fi}^{GT} with help of the eq.(12), where

$$W_{fi}^{GT} = \frac{G^2 n}{4V} C_A^2 (3 - \cos(\theta)) S_A(\mathbf{q}, \omega) \quad (14)$$

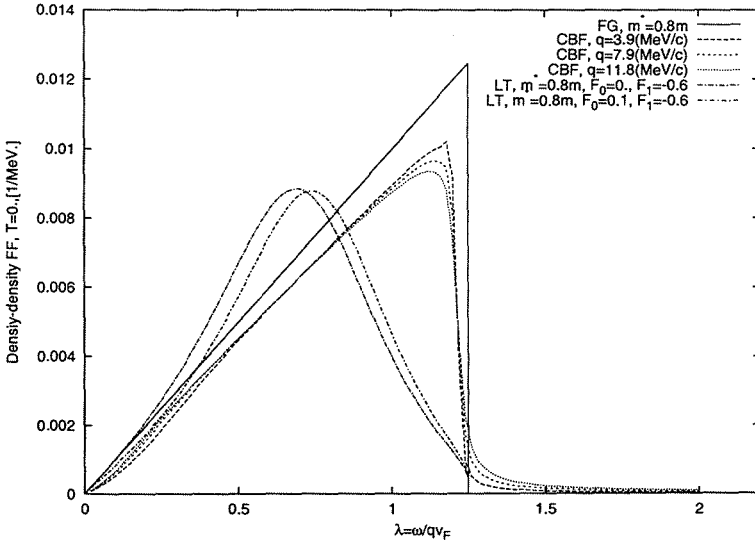


Figure 1: The density dynamic FF S_V obtained within the Landau theory, the CBF approach and FG approximation at different q and $T = 0$ as a function of λ

Results and discussion

Fig. 1 we compare the density dynamic FF's obtained from CBF theory, Landau theory of Fermi liquids (LT) [1] and the FG model. The values of the Landau parameters

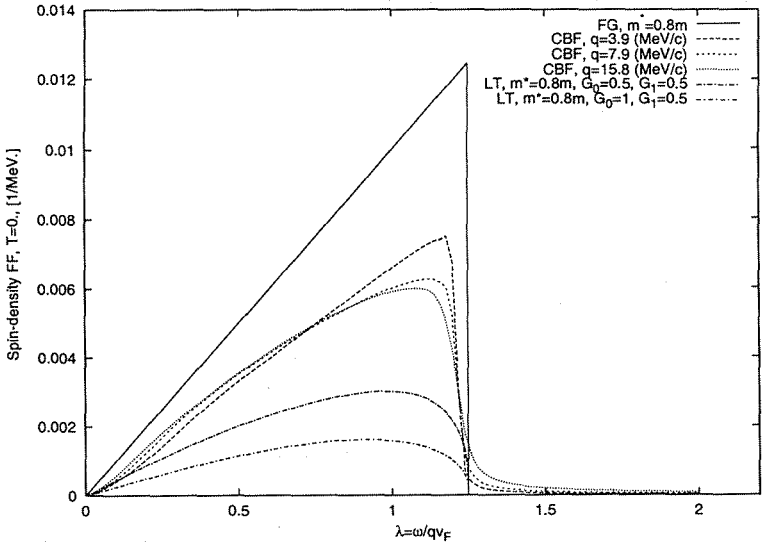


Figure 2: Same as in Fig.1 for the spin-density FF \mathcal{S}_A

employed in the LT calculation are $F_0 = .09$ [1] and $F_1 = -.6$, chosen so as to reproduce the effective mass $m^* \sim 0.8 m$ resulting from CBF calculations [16]. It has to be pointed out that while the LT and FG FF in the limit of low q and ω only depend upon the ratio $\lambda = \omega/qv_F$ [1], the CBF FF depends upon both q and ω .

It appears that the main effect of short range correlations included in the CBF calculation can be described by introducing an effective mass m^* . Replacing the bare nucleon mass m with $m^* \sim 0.8 m$ in the FG response leads in fact to a quenching of the peak and a redistribution of the strength towards larger values of λ . The resulting FG response is very similar to the CBF one.

The different behavior of the CBF and LT responses is a consequence of the fact that the CBF calculation does not include long range correlation, which are known to be important at low momentum transfer.

The spin-density FF's $\mathcal{S}_A(\mathbf{q}, \omega)$ are shown in Fig. 2 as a function of λ . In this case the difference between the FG and CBF results is a factor ~ 2 , that cannot be accounted for by the effective mass. This feature is likely to be ascribed to the spin dependence of the correlation operator employed to construct the correlated states. Two lines of the LT calculation correspond to $G_1 = 0.5$ [1] and $G_0 = 1, G_1 = 0.5$ [17, 18]. In contrast to the case of the density responses shown in Fig. 1, the difference between LT and CBF, due to the effect of long range correlations, is larger. It has to be pointed out that this difference cannot be resolved by adjusting the Landau parameters within the range corresponding to reasonable values of the spin susceptibility [20].

We were matching two different calculations valid at low values of q and moderate momentum transfers respectively and calculated the elastic neutrino mean free path l . In Fig.3 (left panel) the Gamow-Teller part l_{GT} of l calculated within the suggested hybrid

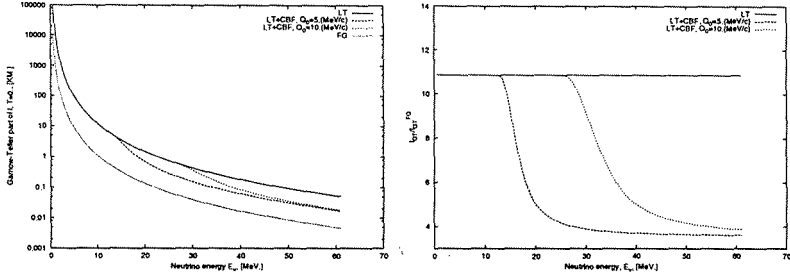


Figure 3: The Gamow-Teller part of the elastic neutrino mean free path at $T = 0$ for the equilibrium density of neutron matter $n = 0.16(fm)^{-3}$ as a function of the initial neutrino energy E_ν at the different matching points Q_0 (left panel). The ratio of our calculations to the ones obtained within the FG approximation at different values of Q_0 (right panel)

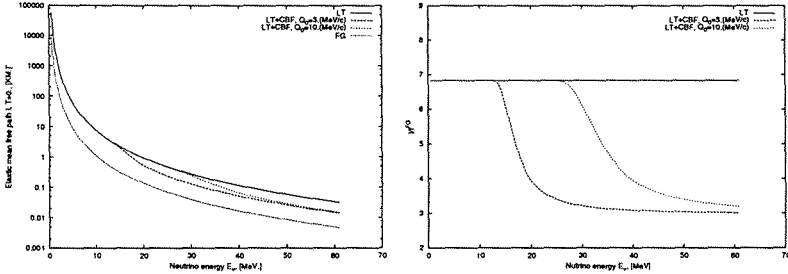


Figure 4: Same as in Fig.3 for the elastic neutrino mean free path

approach as a function of the neutrino energy E_ν is presented and compared with calculation of performed within the Fermi gas approximation (FG) at the saturation nuclear density $n = 0.16(fm)^{-1}$. One can see a big difference between these two calculations at low neutrino energies, see Fig.3 (right panel). Here Q_0 is the transferred momentum value at which we are matching the LT and the CBF approaches. In Fig.4 (left panel) the total neutrino mean free path l for neutron matter at $n = 0.16(fm)^{-1}$ including both dynamic FF calculated within the suggested approach and the FG approximation are presented. The difference between two calculations is presented in Fig.4 (right panel). Let us note that the neutrino mean free path in neutron stars and symmetric nuclear matter have been analyzed recently in Refs.([21, 22]) within the Brueckner-Hartree-Fock approximation at finite temperatures and Ref.([8]) for a cold symmetric nuclear matter.. Actually, there is not a contradiction between our results and the ones presented in these Refs. at moderate neutrino energies, $E_\nu > 20.(MeV)$. However at low E_ν one can find this difference about a few times. It could be due to the fact that the application of the LT including effectively the long-range correlations at low q and ω is different from the approaches used in Refs.[8, 21] and Ref.[22]. Let us also stress that at low neutrino

energies, for example $E_\nu < 20.(MeV)$ the LT results in a main contribution to the elastic neutrino mean free path.

6. Conclusion

The presented analysis of the neutrino propagation in a neutron matter at the normal density and zero temperature has shown the following. The spin-density FF $\mathcal{S}_A(\mathbf{q}, \omega)$ calculated within the CBF approach is less than the one obtained within the FG approximation at moderate values of $q(4, MeV/c < q < 20.MeV/c)$ and $\omega(0 \leq \omega \leq qv_F)$ about 2 times. It leads to the difference between the mean free paths calculated within the CBF and FG approximation about 3 times like in Ref.[8]. Whereas the application of LT to the construction of $\mathcal{S}_A(\mathbf{q}, \omega)$ at low $q(q < 4.MeV/c)$ leads to a larger difference, about 4-5 times. As its consequence the neutrino mean free path at $E_\nu < 4. - 5.(MeV)$ calculated with these two approaches has a difference about 5-6 times. The density dynamic FF $\mathcal{S}_V(\mathbf{q}, \omega)$ calculated within both LT and CBF differs from the one obtained within the FG approximation much less than $\mathcal{S}_A(\mathbf{q}, \omega)$. It results in much larger values (about 10 times) for the Gamow-Teller part l_{GT} of the neutrino mean free path l in comparison to the FG model at $E_\nu < 4. - 5.(MeV)$. Therefore one can conclude that the contribution of the spin effects for a neutrino opacity at low E_ν is sizable.

Acknowledgements

The authors are very grateful to prof. C.J.Pethick and prof. I.Bombaci for useful discussions and comments.

References

- [1] Naoki Iwamoto and C.J.Pethick, Phys Rev. D**25** 313 (1982)
- [2] M.Prakash, I. Bombaci, M.Prakash, P.J.Ellis, J.M.Lattiner, R.Knorren, Phys.Rep.280 (1997) 1,
- [3] M.Prakash, Phys.Rep. 242 (1994) 297.
- [4] S.Reddy, M.Prakash J.M.Lattiner and J.A.Pons, Phys.Rev. D**59** 28888 (1999).
- [5] G.Raffelt, D.Seckel, Phys.Rev. D**52** 1780 (1995).
- [6] S.Fantoni, V.R.Pandharipande, Nucl.Phys. A**473** 234 (1987)
- [7] J.E.Amaro, F.Arias de Saaveda, A.M.Lallena, G.Co, A.Fabocini and S.Rashad, nucl-th/9910024
- [8] S.Cowel and V.R.Pandharipande, Phys.Rev. C**70** 035801 (2004)
- [9] A.Botrugno and G.Co, nucl-th/0409041
- [10] S.Weinberg, Phys.Rev.Lett. **19** (1967) 1264.
- [11] A.Salam, in *Elementary particle Theory: Relativistic Groups and Analyticity (Nobel Symposium N8)* edited by N.Svartholm (Almqvist and Wiksell, Stockholm, 1968).

- [12] S.L.Glashow, Nucl.Phys. **22** (1961) 579.
- [13] W.Bentz, A.Arima and H.Baier, Ann.Phys., 200 (1990)127.
- [14] L.E.Marcucci, et al., Phys.Rev. C63(2000)015801.
- [15] L.D.Landau, Zh.Eksp.Teor.Fiz.,v.32,N59(1957 [Sov.Phys.JETP, v.5,101(1957)].
- [16] reference on CBF calculations of effective mass
- [17] S.O.Backman and O.Sjobeng and A.D.Jackson, Nucl.Phys. A**321** 10 (1979).
- [18] A.Schwenk, G.E.Brown and B.Friman, Nucl.Phys. A**703** 745 (2002).
- [19] Philippe Nozie'res, David Pines, "The Theory of Quantum Liquids", Perseus Books, Cambridge, Massachusets.
- [20] S.Fantoni, A.Sarsa, K.E.Schmidt, Phys.Rv.Lett. **87** 181101 (2001).
- [21] Caiwan Shen, U.Lombardo, N.Van Giai and W.Zue, Phys.Rev. C**68**, 055802 (2003).
- [22] J.Marguren, I.Vidaia and I.Bombaci, Phys.Rev. C**68** 055806 (2003).

SEARCH FOR SIGNAL ON PERCOLATION CLUSTER FORMATION IN NUCLEUS-NUCLEUS COLLISIONS AT RELATIVISTIC ENERGIES

O.B. Abdinov¹, A. Kravcakova², A.A. Kuznetsov³, M.K. Suleymanov^{1,2†},
A. S. Vodopianov³, S. Vokal^{2,3}

- (1) *Physics Institute of AS Baku, Azerbaijan*
(2) *University of P.J. Safarik, Kosice, Slovakia*
(3) *BVHEL, JINR, Dubna, Russia*
† *E-mail: mais@sunhe.jinr.ru*

Abstract

For qualitative understanding of the regime change existence in the behavior of some centrality depending characteristics of events has been suggested to consider the appearance of the strongly interacting matter mixed phase (MP). The MP has been predicted by QCD for the temperatures around the critical temperature T_c and could be formed as a result of nucleon percolation in density nuclear matter. Our main goal is to get a new experimental confirmation of the percolation cluster formation as an accompanying effect of the MP formation. To reach the goal, the experimental data on $Kr + Em$ - reaction at 0.95 GeV/nuc and $Au + Em$ - reaction at 10.6 GeV/nucl. with a number of target fragments $N_h > 8$ have been analyzed. The behavior of the distributions of the target and the projectile fragments have been studied. The experimental data have been compared with these coming from the cascade-evaporation model. We can conclude that:

- the centrality of collision could be define of as a number of the target g-fragments in $Kr + Em$ reactions at energies 0.95 A GeV/nucl and as a number of projectile F -fragments with $Z \geq 1$ in $Au + Em$ reactions at energies 10.6 A GeV/nucl;
- the formation of the percolation cluster sufficiently influences the characteristics of nuclear fragments;
- there are points of the regime changes in the behavior of some characteristics of s -particles as a function of centrality which could be qualitatively understood as a result of the big percolation cluster formation.

1. Introduction

Mixed Phase: Studying of the behavior of the hadron-nuclear and nuclear-nuclear interactions characteristics as a function of collision centrality Q is an important experimental method to get information about changes of the nuclear matter phase, because the increasing Q could lead to the growth of the nuclear matter baryon density. In other words, the regime change in the behavior of some centrality depending characteristics of events is expected by varying of Q to be a signal on phase transition. This method is considered to be the best tool for reaching the quark-gluon plasma phase of strongly interacting matter. Some experimental results have already demonstrate the existence of the regime changes in the event characteristics behavior as a function of collision centrality [1]-[8].

The regularity is observed for hadron-nuclear [1]-[2], heavy [3]-[7] and light nuclear [8] interactions in a large domain of nuclear masses and initial energies. It has been also observed for the behavior of some centrality characteristics of π -mesons, nucleons, fragments, strange particles, and even for the ones of J/ψ . So, the regime changes under consideration could not be related with the existence of the predicted QCD point for the hadronic matter quark-gluon phase transition and therefore has been suggested [9] to consider the appearance of the strongly interacting matter mixed phase (MP) for qualitative understanding of the regularity. MP has been predicted by QCD for the temperatures around the critical temperature T_c and could be formed as a result of nucleon percolation in density nuclear matter. The last is related with the following.

Percolation cluster: It is well known that the statistical and percolation theories can describe critical phenomena best of all and in other hand the regime changes under consideration have also been observed for small density and temperature at which the conditions to apply statistical theories are practically absent. So, one could say that the percolation approach is practically the only one to describe the results. Paper [10] discussed that percolation clusters much larger than hadrons, within which color is not confined; deconfinement is thus related to percolation cluster formation. This is the central topic of the percolation theory, and hence, the connection between percolation and deconfinement seems very likely [11]. So the experimental information on the particular conditions of the MP formation could be very important to fix the onset stage of deconfinement for its future identification. To extract the signals on the accompanied effects of MP could be one of the ways to get the experimental information on the MP formation. The percolation cluster formation could be one of these effects where the MP formation could start at high energies.

Physical picture: We can consider the following physical picture to understand qualitatively the mentioned above.

At low energies: At some critical values of centrality Q_c the compressed compound nuclear system could appear. In this system the thermal equilibrium could be established as a result of Fermi motion and the percolation occur that would result in big percolation cluster formation one will then be fragment on the nuclear fragments. So the process of the percolation cluster could influence the nuclear fragments characteristics. This idea was experimentally tested in [12] for high energy interactions. In section 2 we shall show the experimental results for the heavy nuclear interaction at the low energies.

At middle and high energies. First we have to note that in comparison with the low energy interaction at middle and high energies the contributions of multiparticle collisions have to increase strongly (particularly in the region of central collisions near Q_c) and the quark-gluon degree of freedom of matter could appear. In paper [13] it is discussed that the hadron-chemical-equilibrium could be established as a result of multiparticle collisions during the heavy nuclear interactions. In this system the percolation could occur and the big percolation cluster might be formed. But in comparison with the low energy picture in this case the percolation cluster could consist of hadrons and quarks representing a mixed phase. One more issue to be considered in section 2 is a possibility to get the signal on percolation cluster formation in high energy heavy nuclear interactions.

As we have mentioned above, the idea that the process of the percolation cluster could influence the nuclear fragments characteristics was experimentally tested in [12]. It will be the main idea to get the information on the percolation cluster formation. To reach

this goal, two ways of Q determination were used in paper [12]. In one way the values of Q were determined as a number of protons emitted in one event and in the second one – as a number of protons and fragments emitted in one event. The events of ^{12}CC -interaction at the momentum of 4.2 A GeV/c were used [14]. The experimental data were compared with the simulation data coming from the quark-gluon string model (QGSM) without the nuclear fragments [15]. They was supposed that the behavior of the events' number dependent of Q determined the both ways have to be similar if there are no clusters as a source of fragments and they would differ if the cluster exists as one. It was obtained that the form of the distribution strongly differs for the distribution with different Q determination ways. In the second case the two steps structure was indicated in the behaviour of the distribution which could not be described by the model. This result has demonstrated that the influence of nuclear fragmentation processes on the behaviour of the events number dependent of Q has a critical character. But it is clear that the light nuclear interaction is not a good object to study the fragmentation processes. The main properties of the nuclear fragmentation were obtained at low and middle energy collisions of heavy nuclei [16]. So, we turn to the low and high energies collisions of heavy nuclei and our main goal is to get a new experimental confirmation of the percolation cluster formation as an accompanying effect of the MP formation.

Centrality of the collisions: Before discussing the experimental results we would like to touch upon one more question which is more important for the centrality experiments. It is clear that the centrality of collisions Q not be experimentally defined directly. In different experiments the values of Q are defined as a number of identified protons, projectiles' and targets' fragments, slow particles, all particles, as the energy flow of the particles with emission angles $\theta \simeq 0^\circ$ or with $\theta \simeq 90^\circ$. Apparently, it is not simple to compare quantitatively the results on Q -dependencies obtained in different papers and in other hand the definition of Q could significantly influence the final results. So we believe it is necessary to understand what centrality Q is? Usually for a chosen variable to fix Q it is supposed that its values have to increase linearly with a number of colliding nucleons or baryon density of the nuclear matter. The simplest mechanism that could give this dependence is cascade approach. So we have used one of the versions of the cascade-evaporation model CEM [17] to choose the variable to fix Q for studying the centrality dependence of the event characteristics.

2. Experiment

Distribution of the fragments. To reach the goal, we have analyzed the experimental data on $Kr + Em$ - reaction at 0.95 GeV/nucleon [18] and $Au + Em$ - reaction at 10.6 GeV/nucleon [19]. We have considered the events with a number of $N_h > 8$ to select the heavy nuclear collisions (in papers [18]- [19] this condition was not used). According to the mentioned above idea on the centrality event selection, we have studied the behavior of the distributions of the target fragments (g - and h - fragments) and the projectile fragments with charge $Z \geq 1$ (F -fragments). The experimental data have been compared with these coming from the CEM [17].

The $Kr + Em$ reactions at 0.95 GeV/nucleon. Fig 1a-f shows the yields of g -, h - and F -fragments in the $Kr + Em$ (at 0.95 GeV/nucleon, Fig. 1 a-c.) and in $Au + Em$ (at 10.6 GeV/nucleon, Fig. 1d-f.) reactions. The results coming from the CEM are also drawn. We can see that:

The g -fragments experimental multiplicity distribution (N_g) for the $Kr+Em$ reactions is well described by the model (Fig. 1a). We would remind that in the framework of CEM g -fragments are considered as the results of cascading collisions in the target spectator and participant. So N_g could be used to fix the centrality of collisions (result I).

The target h -fragments multiplicity (N_h) distribution shape for the $Kr+Em$ reactions (Fig. 1b) cannot be described by the CEM in the region of N_h values $15 < N_h < 32$. If we remember that the N_h is the number of the final state target fragments in the event which is the sum of the target black fragments (N_b) and N_g , we would say that the CEM can't describe the multiplicity distributions of b -particles which are the slowest target fragments and so they have to get much more information on the state of the nuclear target. In recent paper [20] one of the authors of the using CEM has shown that to describe fully the b -particles yields, it is necessary to take into account the percolation mechanism and formation of big percolation cluster. So, we could assert that this observed difference between the behavior of the experimental and model N_h - distributions is related with the formation of big percolation cluster (result II);

The behavior of the experimental distribution of projectile fragments with $Z \geq 1$ produced in $Kr+Em$ collisions (Fig. 1c) is not in agreement with the result coming from the CEM in full area of the N_F definition either. At the point $N_F = 2$ the model gives the result more than one order higher in comparison with the experiment. Two other N_F regions are observed (at $7 < N_F < 14$ and $30 < N_F < 40$) where the obtained by the model and the the experimental data do not agree with each other and we can see that the difference has a critical character because it appears only at some values of N_F (result III). The formation of the big percolation cluster could give this critical behavior, for example, as the result of appearance of the physical picture described above (for low energy interactions).

The Au+Em reactions at 10.6 GeV/nuc. The experimental distribution of g -particles from $Au-Em$ reactions (Fig. 1d) can not be described by the model in full region of the N_g definition. We can separate some region in the relative between the behaviors of the experimental and the model distributions. In the region of $N_g < 5$ the model can describe the experimental distribution. In the region of $N_g > 15$ the experimental values of N_i decrease with N_g while the values coming from the model are constant in the region $5 < N_g < 40$. The model could not describe the distribution of h -particles in full region of the N_h -definition either that is seen from Fig. 1e. The model could only describe the experimental distribution of N_h in the region of $22 < N_h < 32$. So, we can say that for the reaction under consideration the N_g as well as the N_h could not be used to fix the centrality of collisions (result IV). We believe that the result could also be understood qualitatively in the framework of the above-mentioned physical picture (for high energy interactions). In recent paper [21] the bond percolation model is used to interpret 10.2 GeV/c $p+Au$ multifragmentation data. The critical value of the percolation parameter $p_c = 0.65$ was found from the analysis of the intermediate mass fragments charge distribution.

The distribution of projectile fragments with $Z \geq 1$ produced in $Au+Em$ collisions is in good agreement with the result coming from the CEM. So, we can see that the projectile fragments are produced by the mechanism similar to the cascade-evaporation one and N_F could be used to fix the centrality for these reactions (result V).

Correlation. It is clear that the obtained results are not sufficient to confirm fully the

percolation cluster formation especially at high energy collisions for which the contributions of multiparticle collisions have to increase strongly, and particularly in the region of central collisions near the critical values of centrality. As it has been mentioned at such high energies the hadron-chemical equilibrium were established and the percolation could occur. But in comparison with the low energy physical picture, in this case the percolation cluster could consist of hadrons and quarks represents a mixed phase.

Thus, one needs to get additional information in future to confirm the percolation cluster formation.

A number of the final-state-relativistic single charged particles (s) in the emulsion experiments (it is called the multiplicity of the shower particles and is denoted by $\langle n_s \rangle$) might be most sensitive to the dynamics of the interaction at high energies (as well as the values of pseudorapidity η of s -particles). So, we have studied the correlation between the characteristics of s -particles and the values of centrality. As we have mentioned above, to fix the centrality, one might use the variable N_g for $Kr + Em$ reactions and N_F for $Au + Em$ ones. Here we discuss the results of our study.

Fig. 2a-c presents the average values of multiplicity $\langle n_s \rangle$ for s -particles produced in $Kr + Em$ and $Au + Em$ reactions and the average values of pseudorapidity for s -particles produced in $Au + Em$ reactions. We can say that there are two regions in the behavior of the values of $\langle N_s \rangle$ as a function of N_g for the $Kr + Em$ reaction (Fig. 2a). In the region of: $N_g < 40$ the values of $\langle N_s \rangle$ increase linearly with N_g , here the CEM also gives the linear dependence but with the slope less than the experimental one; $N_g > 40$ the CEM gives the values for N_s greater than the experimental observed ones, the last saturates in this region, the effect could not be described by the CEM. It has been previously observed in emulsion experiments [16]. It is clear that there to be some effects which could stop (or sufficiently moderate) the increase of N_s . The effect of the percolation cluster formation could be one of that effects. The moderation of the values of N_s as a function of N_F is also observed for the $Au + Em$ reaction at 10.6 GeV/nucl. (Fig. 2c) near the point of the $N_F \simeq 40 - 50$ seems to be a point of the regime change which is absent for the distribution coming from the CEM.

Thus, we can say that the effects which could stop (or sufficiently moderate) the dependence of $\langle N_s \rangle$ as a function of centrality appear at some values of N_g and N_F . It strengthens the result VII because the process of percolation cluster formation is a critical effect which appears at some critical values of centrality. If we compare the behavior of the experimental and theoretical distributions for the values of η of s -particles produced in the $Au + Em$ reaction as a function of N_F (Fig. 1c), we would get one more confirmation on the existence of the point $N_F \simeq 40 - 50$, behind which the values of η are systematically less than the CEM expectation. But in the region of $N_F > 40 - 50$ the model describes the experimental distribution rather well.

So, we can say that the points of regime change are observed in the behavior of the characteristics of s -particles as a function of centrality. In the central collisions region the increase of the average values of multiplicities are sufficiently moderate (or stopped) and the average values of η decrease and could not be described by the CEM. It could be qualitatively understood within the formation of the big percolation cluster.

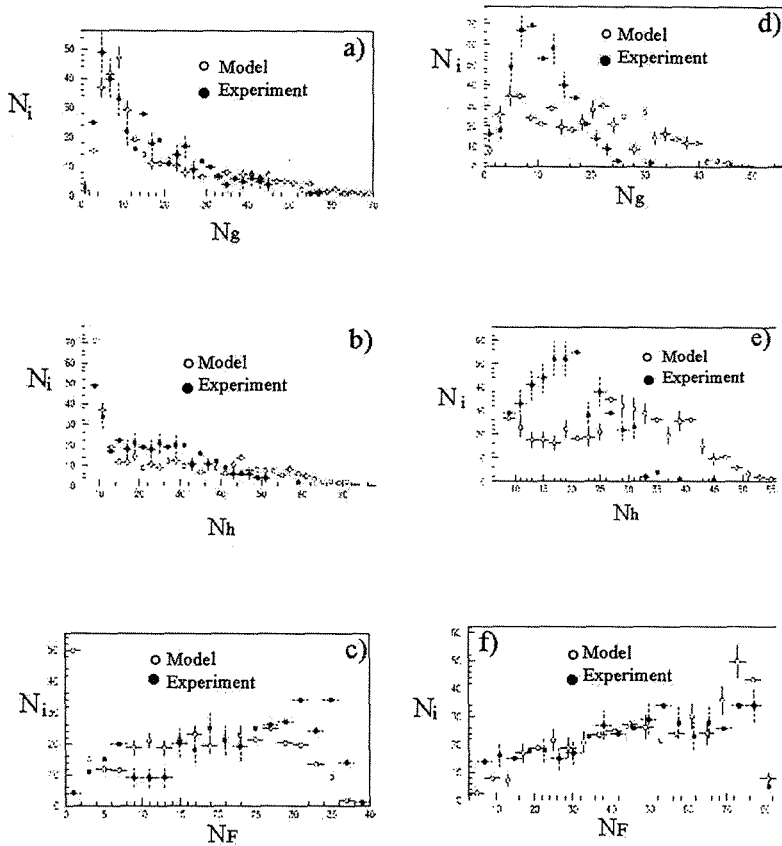


Figure 1: Distribution of the target a) g -fragments; b) h -fragments; projectiles' c) F -fragments produced in the $Kr + Em$ reactions at 0.95 GeV/nucleon and target d) g -fragments; e) h -fragments; projectile f) F -fragments produced in the $Au + Em$ reactions at 10.6 GeV/nucleon. It also gives the results coming from the CEM calculation.

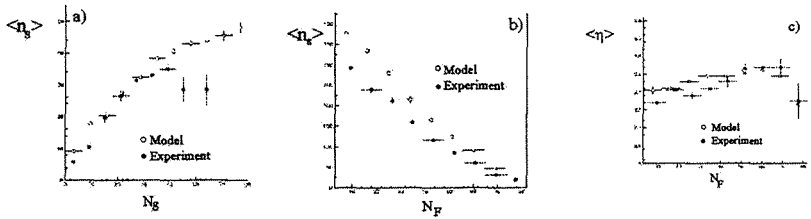


Figure 2: a) average values of s -particle multiplicity produced in the $Kr + Em$ reactions at 0.95 GeV/nucleon as a function of N_g ; average values of the b) multiplicity; c) pseudo-rapidity of s -particles produced in $Au + Em$ reactions at 10.6 GeV/nucleon as a function of N_F . It also shows the result coming from the CEM

3. Conclusion

We can conclude that:

- the centrality of collision could be define as a number of the target g -fragments in $Kr+Em$ reactions at energies 0.95 A GeV/nucleon and as a number of projectile F -fragments with $Z \geq 1$ in $Au + Em$ reactions at energies 10.6 A GeV/nucleon;
- the formation of the percolation cluster sufficiently influences the characteristics of nuclear fragments;
- there are points of the regime changes in the behavior of some characteristics of s -particles as a function of centrality which could be qualitatively understood as a result of the big percolation cluster formation.

References

- [1] I. Chemakin et al. The BNL E910 Collaboration, E-print:nucl-ex/9902009, (1999).
- [2] Ron Soltz for the E910 Collaboration. J. Phys. G: Nucl. Part. Phys. **27**, (2001) 319-326
- [3] Fu-Hu Liu et al. Phys. Rev. C **67**, 047603 (2003)
- [4] A. Abduzhamilov et al., Z. Phys. C **40**, 223 (1988)
- [5] F.H. Liu, Chin. J. Phys. (Taipei) **40**, 159 (2002)
- [6] A.L.S. Angelis et al. The HELIOS/3 Collaboration, Eur. Phys. J. **C13**, 433-452 (2000).
- [7] M.C. Abreu et al. Phys.Let. **B450**,456 (1999); M.C. Abreu et al. Phys.Let. **B410**, 337,(1997); M.C. Abreu et al. Phys.Let. **B410**,327, (1997); M.C. Abreu et al. By NA50 Collaboration : Phys.Lett.**B499**,85-96, (2001).
- [8] M.K. Suleimanov et al., Phys.Rev. C **58**, 351, (1998).
- [9] A.N. Sissakian et al. Selected Transactions of the University "DUBNA". Collected Articles., 44-68 (2004)
- [10] H Satz. Rept.Prog.Phys. **63**,1511,(2000)
- [11] H. Satz, Nucl. Phys. **A 642** , 130, (1998); G. Baym, Physica **96A** , 131 (1979); T. Celik, F. Karsch and H. Satz, Phys. Lett. **97 B**,128, (1980).
- [12] M.K. Suleymanov et al. Nucl.Phys.A **734S**, E104-E107, (2004); M.K. Suleymanov et al. Proceedings of the Conference: Bologna2000, Bologna, Italy, 375,(2000).
- [13] P. Braun-Munzinger , J. Stachel, Christof Wetterich. Phys.Lett. **B596**,61-69 (2004).
- [14] N. Akhbabian et al.- JINR Preprint 1-12114, Dubna (1979); N.S. Angelov et al.- JINR Preprint 1- 12424, Dubna (1989) ; A.I. Bondorenko et al., JINR Communication, P1-98-292, Dubna (1998).

- [15] N.S. Amelin, L.V. Bravina, Sov. J. Nucl. Phys. **51**, 211 (1990) ; N.S. Amelin et al., Sov. J. Nucl. Phys. **50**, 272 (1990).
- [16] W. Resisdorf, E-print: nucl-ex/0004008 (2000).
- [17] G.J. Musulmanbekov, Proc. of the 11th EMU01 Collaboration Meeting, Dubna, Russia, (1992); Proc. 11th Int. Symp. on High Energy Spin Phys., Bloomington, (1994); AIP Conf. Proc. **343**, 428 (1995).
- [18] S.A. Krasnov et al., Czech. J. Phys. **46**, No.6 , 531 (1996).
- [19] M.I. Adamovich et al., Phys. Lett. **B 352** (1995).
- [20] G. Musulmanbekov, A. Al-Haidary. Russian Journal of Nucl. Phys., **66**, 1-9 (2003).
- [21] M. Kleine Berkenbusch et al., Phys. Rev. Lett. **88**, 022701 (2002)

INVESTIGATION OF CHARMONIUM STATES PRODUCTION IN p -A
AND NUCLEUS-NUCLEUS COLLISIONS AT THE CERN SPS

N.S.Topilskaya for the NA50 Collaboration:

INR, Moscow, Russia

e-mail: topilaska@inr.ru

B.Alessandro¹², C.Alexa⁴, R.Arnaldi¹², M.Atayan¹⁴, S.Beolè¹², V.Boldea⁴,
P.Bordalo^{7,a}, G.Borges⁷, C.Castanier³, J.Castor³, B.Chaurand¹⁰, B.Cheyne¹³,
E.Chiavassa¹², C.Cicalo⁵, M.P.Comets⁹, S.Constantinescu⁴, P.Cortese¹, A.De Falco⁵,
G.Dellacasa¹, N.De Marco¹², A.Devaux³, S.Dita⁴, J.Fargeix³, P.Force³, M.Gallo¹²,
C.Gerschel⁹, P.Giubellino^{12,b}, M.B.Golubeva⁸, A.A.Grigorian¹⁴, S.Grigorian¹⁴,
F.F.Guber⁸, A.Guichard¹³, H.Gulkanyan¹⁴, R.Haroutunian¹³, M.Idzik^{12,c}, D.Jouan⁹,
T.L.Karavitcheva⁸, L.Kluberg¹⁰, A.B.Kurepin⁸, Y.Le Bornec⁹, C.Lourenço⁶, M.Mac
Cormick⁹, A.Marzari-Chiesa¹², M.Masera^{12,b}, A.Masoni⁵, M.Monteno¹², A.Musso¹¹,
P.Petiau¹⁰, A.Piccotti¹², J.R.Pizzi¹³, F.Prino¹², G.Puddu⁵, C.Quintans⁷, L.Ramello¹,
S.Ramos^{7,a}, L.Riccati¹², H.Santos⁷, P.Saturnini³, E.Scomparin¹², S.Serci⁵,
R.Shahoyan^{7,e}, F.Sigaudou¹², M.Sitta¹, P.Sonderegger^{6,a}, X.Tarrago⁹, N.S.Topilskaya⁸,
G.L.Usai^{5,b}, E.Vercellin¹², L.Villatte⁹, N.Willis⁹, T.Wu⁹

¹Univ. del Piemonte Orientale, Alessandria and INFN-Torino, Italy.

²LAPP, CNRS-IN2P3, Annecy-le-Vieux, France.

³LPC, Univ. Blaise Pascal and CNRS-IN2P3, Aubière, France.

⁴IFA, Bucharest, Romania.

⁵Univ. di Cagliari/INFN, Cagliari, Italy.

⁶CERN, Geneva, Switzerland.

⁷LIP, Lisbon, Portugal.

⁸INR, Moscow, Russia.

⁹IPNO, Univ. de Paris-Sud, CNRS-IN2P3, Orsay, France.

¹⁰LLR, Ecole Polytechnique, CNRS-IN2P3, Palaiseau, France.

¹¹IRS, CNRS-IN2P3, Univ. Louis Pasteur, Strasbourg, France.

¹²Univ. di Torino/INFN, Torino, Italy.

¹³IPN, Univ. Claude Bernard, CNRS-IN2P3, Villeurbanne, France.

¹⁴YerPhI, Yerevan, Armenia.

^aAlso at IST, Univ. Técnica de Lisboa, Lisbon, Portugal.

^bAlso at CERN, Geneva, Switzerland.

^cAlso at FPNT, Univ. of Mining and Metallurgy, Cracow, Poland.

^dNow at UERJ, Rio de Janeiro, Brazil.

^eOn leave of absence from YerPhI, Yerevan, Armenia.

^fOn leave of absence from York Collège, CUNY, New York, USA.

Abstract

Charmonium production in Pb-Pb collisions at 158 GeV/c per nucleon is investigated from the data, collected in year 2000, under improved experimental conditions with the target system placed in vacuum. The study of the transverse momentum distributions of J/ψ as a function of the centrality of the collision shows that the observed J/ψ suppression in Pb-Pb interactions is particularly significant mainly at low transverse momentum where it strongly depends on centrality. For peripheral Pb-Pb collisions, the transverse momentum dependence of the J/ψ suppression is qualitatively similar to the dependence observed in p-A and S-U collisions. Comparing peripheral and central Pb-Pb collisions, the data show a relative suppression in the whole p_T range although its amplitude significantly decreases with increasing transverse momentum.

Key-words: heavy ions collisions, charmonium suppression, transverse momentum dependence.

1. Introduction

Charmonium production has been measured by the NA50 Collaboration in Pb-Pb collisions at 158 GeV/c per nucleon and in proton-nucleus collisions at 400 and 450 GeV/c [1, 2]. The suppression of the J/ψ yield in ultrarelativistic heavy ion collisions is considered as a potential signature of the phase transition from normal nuclear matter to a deconfined state of quarks and gluons.

Normal nuclear absorption of J/ψ has been measured in proton-induced reactions. The corresponding cross-section, deduced in the frame of a Glauber calculation, amounts to 4.18 ± 0.35 mb [3]. It provides thereby the J/ψ normal nuclear absorption reference as a function of the path in nuclear matter that the produced $c\bar{c}$ pair has to go through the matter, a quantity which is directly related to the centrality of the collision. The main result of the NA50 experiment in the study of Pb-Pb collisions is that whereas peripheral Pb-Pb collisions approximately follow the normal nuclear absorption pattern, a departure from this normal behaviour is observed for semi-central reactions which increases in amplitude with increasing centrality. The Drell-Yan cross section is used as a reference one, since it exhibits linear scaling with $A \cdot B$, the product of the target and projectile mass numbers, like the number of nucleon-nucleon collisions in the interaction. Besides, most of the systematic errors cancel out in the ratio of cross sections which is insensitive, in particular, to the absolute incident flux uncertainty.

Preliminary results obtained from our latest data samples collected under improved experimental conditions can be found in [4, 5]. In this article we extend our analysis of J/ψ production and study the suppression as a function of the transverse momentum of the charmonium state.

2. Transverse momentum distribution of charmonium

To investigate in more detail the features of the reaction mechanism, we study the transverse momentum and transverse mass distributions of the J/ψ yield. In particular, the dependence, as a function of the centrality of the collision, of the mean square transverse momentum and of the slope of the M_T spectra were obtained and can be found in [6].

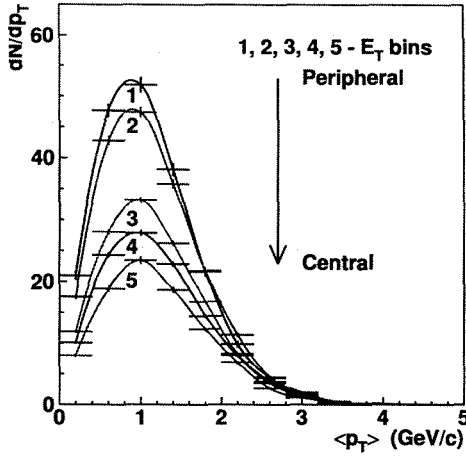


Figure 1: Ratio F of the J/ψ production cross section for Pb-Pb collisions at 158 GeV/c per nucleon as a function of the transverse momentum in GeV/c to the DY cross section or 5 E_T bins

When rescaled to the same energy and as a function of the mean length path of J/ψ in nuclear matter, the mean square transverse momentum of J/ψ exhibits the same behaviour for p-A, S-U and Pb-Pb collisions [7], which could be related to initial parton scattering. The data also show a change of the slope of the T dependence on the energy density near the value where the J/ψ production cross section starts to deviate from the normal absorption curve [8].

The data collected in year 2000 are of the high quality what allows a more detailed study of the J/ψ suppression as a function of the transverse momentum. We study the ratio of the J/ψ cross section to the Drell-Yan cross section (we consider here the Drell-Yan with invariant mass higher than $4.2 \text{ GeV}/c^2$), which is proportional to the J/ψ yield per nucleon-nucleon collision. Events are binned according to the neutral transverse energy E_T which is experimentally measured, on an event by event basis, by an electromagnetic calorimeter with laboratory pseudorapidity coverage in the range [1.1-2.3]. E_T is connected with the centrality of the collision in which dimuons are produced.

We plot on Fig.1 and Fig.2 the ratio F of the J/ψ to the DY cross section in the corresponding E_T bin as a function of the transverse momentum p_T for 5 transverse energy bins (Fig.1) and as a function of the transverse energy E_T for 11 transverse momentum bins up to $p_T = 5.0 \text{ GeV}/c$ (Fig.2). The figures show that, whereas for low values of p_T there is a significant J/ψ suppression which strongly increases with centrality, when p_T increases, the dependence of the J/ψ normalized yield on centrality becomes weaker and weaker. In other words, the suppression observed on the integrated p_T yield from peripheral to central collisions originates mainly from the suppression of J/ψ with low p_T values. In order to better investigate this dependence we consider the ratio R_i of each p_T distribution corresponding to a given E_T bin i with respect to the first and most

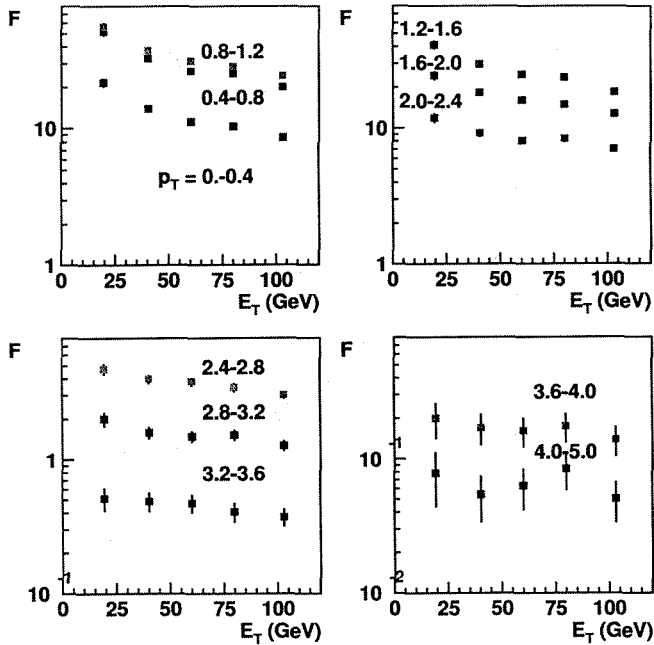


Figure 2: Ratio F of the J/ψ production cross section for Pb-Pb collisions at 158 GeV/c per nucleon in the p_T bins shown on the plots (in GeV/c) to the DY cross section, as a function of the measured neutral transverse energy in GeV

peripheral bin, namely:

$$R_i = (J/\psi_i / DY_i) / (J/\psi_1 / DY_1)$$

Fig.3 displays the four ratios R_i as a function of p_T . It shows that with respect to the most peripheral collisions, J/ψ becomes more and more suppressed, with increasing centrality but also with decreasing p_T values. For high p_T values, above 3.5 GeV/c, the suppression although still increasing with centrality, exhibits no significant p_T dependence for the central collisions.

We compare Pb-Pb collisions with p-A reactions where the J/ψ survival probability is affected by normal nuclear absorption only. In this case, when the J/ψ yield is parametrized according to A^α , nuclear absorption leads to a value of α lower than unity reflecting the absorption of the $c\bar{c}$ pair within the target. Now we perform more complex study when the survival probability as a function of p_T is considered. Within the frame of the same NA50 experiment, we have therefore made a study of the J/ψ yield p_T dependence for 400 GeV p-induced reactions on 6 different target nuclei: Be, Al, Cu, Ag, W and Pb. We have considered the same 11 p_T bins and have measured the ratio F in each of them for the six different targets. We have used the above A^α parametrization of the J/ψ cross section separately in each of the 11 p_T bins in order to perform a p_T dependent analysis. The results are shown in Fig.4.

The results of the J/ψ production study in p-A reactions are illustrated in Fig.5. They

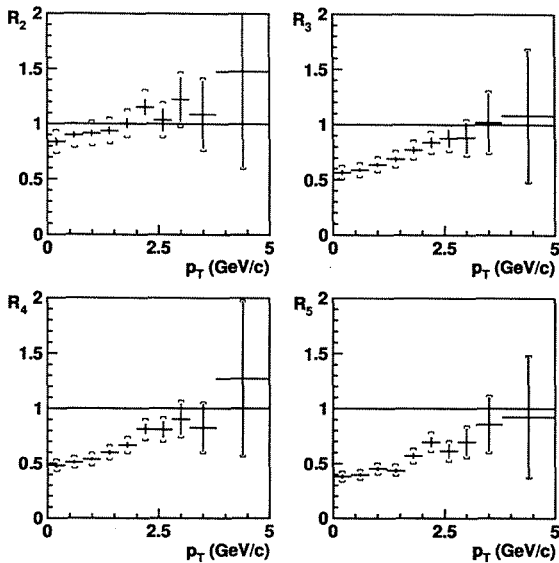


Figure 3: Ratios R_i of the J/ψ transverse momentum distribution normalized to the DY cross section in the E_i bin $2 < i < 5$ to the first E_1 bin. The solid error bars on each data point are the statistical errors of the J/ψ yield ratios. The error bars with systematic errors from the DY cross section ratios are given as brackets

show that whereas for low values of p_T J/ψ production as a function of the atomic mass number A increases less than proportionally to A (Drell-Yan is proportional to A and both are proportional to the number of nucleus-nucleus collisions) leading to a value of α lower than unity, for high p_T values J/ψ production increases faster than A so that the corresponding value of α is higher than 1. There is a kind of normal nuclear absorption for the lower p_T values but the magnitude of this absorption decreases with increasing p_T then vanishes and turns to overproduction for high p_T already above 2 GeV/c. This is, in fact, a wellknown behaviour observed since long in the production of hadrons and known as the Cronin effect.

For comparison we show in Fig.6 the data for S-U collisions as obtained from the NA38 experiment, where the effect of absorption is seen for low p_T ($R < 1$), together with some hints of enhancement for high p_T ($R > 1$) suggesting, within errors, a behaviour similar to the Cronin effect observed in p-A collisions. The Pb-Pb data can be rebinned using only 3 bins of transverse energy in order to minimize statistical fluctuations. Fig.7 shows that for the most central Pb-Pb collisions and with respect to the most peripheral bin, the suppression exists for all values of p_T . The centrality dependence decreases with increasing p_T . For the highest p_T values, no overproduction is observed: there is always an absorption which increases with centrality, although less pronounced than for small p_T and which, moreover, does not exhibit any significant p_T dependence.

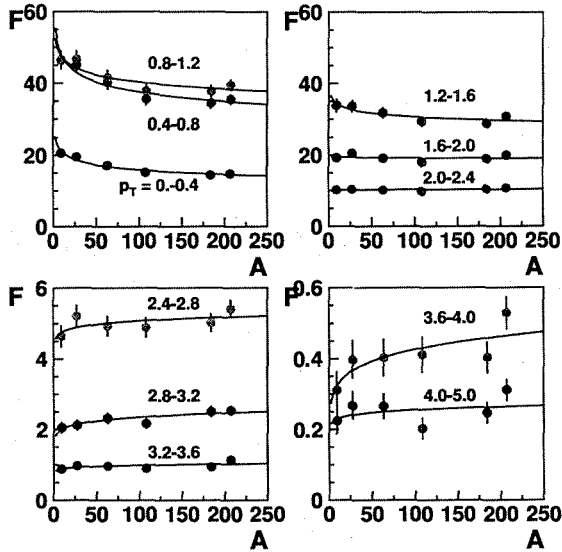


Figure 4: Ratio F of the J/ψ production cross section for proton-nucleus collisions at 400 GeV/c in the p_T bins shown on the plots (in GeV/c) to the DY cross section, as a function of the atomic number of the target nucleus. The J/ψ yield is parametrized according to A^α

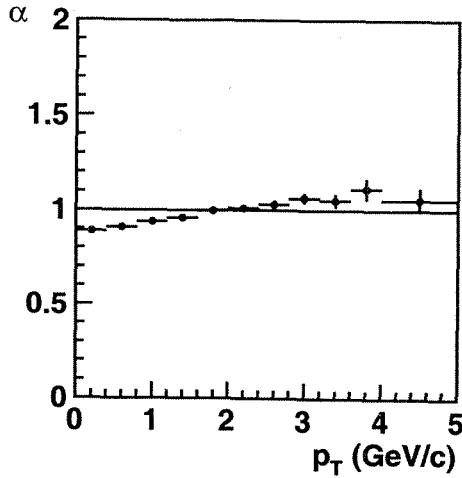


Figure 5: Parameter α obtained from the fit of the proton-nucleus J/ψ production cross sections as a function of the transverse momentum (GeV/c).

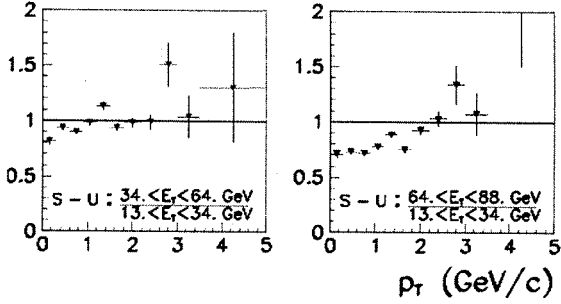


Figure 6: Ratios R_i of the J/ψ transverse momentum distribution normalized to the DY cross section for S-U collisions from the NA38 experiment for the case of three E_T intervals

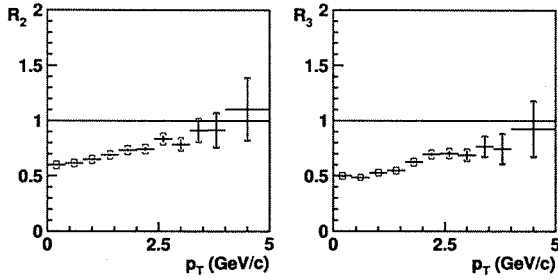


Figure 7: Ratios R_2 and R_3 of the J/ψ transverse momentum distribution normalized to the DY cross section for the second and third centrality bins with respect to the first and most peripheral one, in the case of three E_T intervals, for Pb-Pb collisions. The error bars have the same meaning as on Figure 3

3. Conclusions

The dependence of the J/ψ suppression pattern on p_T for Pb-Pb collisions is somewhat different from what is observed in the case of normal nuclear J/ψ absorption from p-induced reactions. In the latter case we see the change from absorption to enhancement with the increase of transverse momentum. For Pb-Pb collisions and for the whole p_T range, only absorption is observed with increasing centrality. Moreover, the data show that absorption is significantly stronger for low p_T and almost p_T independent for the most central collisions and for the highest values of the transverse momentum.

References

- [1] M.C.Abreu et al.(NA50 Collaboration), Phys.Lett. B477 (2000) 28 and references therein.
- [2] B.Alessandro et al. (NA50 Collaboration), Eur.Phys.J. C33 (2004) 33;
P.Cortese et al. (NA50 Collaboration), Nucl.Phys. A715 (2003) 679.
- [3] B.Alessandro et al. (NA50 Collaboration), CERN-PH-EP/2004-052, submitted to Eur. Phys. J.C.
- [4] G. Borges et al. (NA50 Collaboration), J. Phys. G: Nucl. Part. Phys. **30** (2004) S1351.
- [5] H.Santos et al.(NA50 Collaboration), J. Phys. G: Nucl.Part.Phys. **30** (2004) S1175.
- [6] M.Abreu et al. (NA50 Collaboration), Phys.Lett. B499 (2001) 85.
- [7] A.B.Kurepin et al. (NA50 Collaboration), Nucl.Phys. A721 (2003) 249.
- [8] N.S.Topilskaya et al. (NA50 Collaboration), Nucl.Phys. A715 (2003) 675.

STRUCTURE FUNCTION F_L AT FIXED W IN THE k_T -FACTORIZATION APPROACH

A.V. Kotikov¹, A.V. Lipatov² and N.P. Zotov^{2†}

- (1) *BLThPh, Joint Institute for Nuclear Research, 141980 Dubna, Russia*
(2) *Skobeltsyn Institute of Nuclear Physics, Lomonosov Moscow State University
119992 Moscow, Russia*

† *E-mail: zotov@theory.sinp.msu*

Abstract

The results for structure function F_L , obtained in the k_T -factorization and collinear approaches, are compared with recent H1 experimental data at fixed W values.

1. Introduction

The longitudinal structure function (SF) $F_L(x, Q^2)$ is a very sensitive QCD characteristic and is directly connected to the gluon content of the proton. It is equal to zero in the parton model with spin-1/2 partons and has got nonzero values in the framework of perturbative Quantum Chromodynamics. The perturbative QCD, however, leads to a quite controversial results. At the leading order (LO) approximation F_L amounts to about 10 ÷ 20% of the corresponding F_2 values at large Q^2 range and, thus, it has got quite large contributions at low x range. The next-to-leading order (NLO) corrections to the longitudinal coefficient function are large and negative at small x [1]-[3] and can lead to negative F_L values at low x and low Q^2 values (see [3, 4]). Negative F_L values demonstrate a limitations of the applicability of perturbation theory and the necessity of a resummation procedure, that leads to coupling constant scale higher than Q^2 (see [3], [5]-[7]).

The experimental extraction of F_L data requires a rather cumbersome procedure, especially at small values of x . Recently, however, there have been presented new precise preliminary H1 data [8] on the longitudinal SF F_L , which have probed the small- x region $10^{-5} \leq x \leq 10^{-2}$.

In Ref. [9] the standard perturbative QCD formulas and also the so called k_T -factorization approach [10] based on Balitsky-Fadin-Kuraev-Lipatov (BFKL) dynamics [11] are used for the analysis of the above data. Here we present the main results of our analysis.

In the framework of the k_T -factorization approach a study of the longitudinal SF F_L has been done firstly in Ref. [12]. We follow a more phenomenological approach [13](see also [14, 15]), where we analyzed F_L data in a broader range at small x , using the different parameterizations of the unintegrated gluon distribution function $\Phi_g(x, k_{\perp}^2)$ (see Ref. [16]).

2. Theoretical framework

The unintegrated gluon distribution $\Phi_g(x, k_\perp^2)$ (f_g is the (integrated) gluon distribution in the proton multiplied by x and k_\perp is the transverse part of the gluon 4-momentum k^μ)

$$f_g(x, Q^2) = \int^{Q^2} dk_\perp^2 \Phi_g(x, k_\perp^2) \quad (\text{hereafter } k^2 = -k_\perp^2) \quad (1)$$

is the basic dynamical quantity in the k_T -factorization approach. It satisfies the BFKL equation [11].

Then, in the k_T -factorization the SF $F_{2,L}(x, Q^2)$ are driven at small x primarily by gluons and are related in the following way to $\Phi_g(x, k_\perp^2)$:

$$F_{2,L}(x, Q^2) = \int_x^1 \frac{dz}{z} \int^{Q^2} dk_\perp^2 \sum_{i=u,d,s,c} e_i^2 \cdot \hat{C}_{2,L}^g(x/z, Q^2, m_i^2, k_\perp^2) \Phi_g(z, k_\perp^2), \quad (2)$$

where e_i^2 are charge squares of active quarks.

The functions $\hat{C}_{2,L}^g(x, Q^2, m_i^2, k_\perp^2)$ can be regarded as SF of the off-shell gluons with virtuality k_\perp^2 (hereafter we call them *hard structure functions* by analogy with similar relations between cross-sections and hard cross-sections). They are described by the sum of the quark box (and crossed box) diagram contribution to the photon-gluon interaction (see, for example, Fig. 1 in [13]).

Notice that the k_\perp^2 -integral in Eqs. (1) and (2) can be divergent at lower limit, at least for some parameterizations of $\Phi_g(x, k_\perp^2)$. To overcome the problem we change the low Q^2 asymptotics of the QCD coupling constant within hard structure functions. We applied the ‘‘freezing’’ procedure [17], which contains the shift $Q^2 \rightarrow Q^2 + M^2$, where M is an additional scale, which strongly modifies the infrared α_s properties. For massless produced quarks, ρ -meson mass m_ρ is usually taken as the M value, i.e. $M = m_\rho$. In the case of massive quarks with mass m_i , the $M = 2m_i$ value is usually used. For the unintegrated gluon distribution $\Phi(x, k_\perp^2, Q_0^2)$ we use the so-called Blumlein’s parameterization (JB) [18]. Note that there are also several other popular parameterizations, which give quite similar results excepting, perhaps, the contributions from the small k_\perp^2 -range: $k_\perp^2 \leq 1 \text{ GeV}^2$ (see Ref. [16]).

The JB parameterization depends strongly on the Pomeron intercept value. In different models the Pomeron intercept has different values. So, in our calculations we apply the H1 parameterization [19], which are in good agreement with perturbative QCD.

We calculate the SF F_L as the sum of two types of contributions - the charm quark one F_L^c and the light quark one F_L^l :

$$F_L = F_L^l + F_L^c. \quad (3)$$

For the F_L^l part we use the massless limit of hard SF (see [13]). We always use $f = 4$ in our fits, because our results depend very weakly on the exact f value.

3. Numerical results

In Fig. 1 we show the SF F_L with ‘‘frozen’’ coupling constant as a function of Q^2 for fixed W in comparison with H1 experimental data [8]. The k_T -factorization results lie

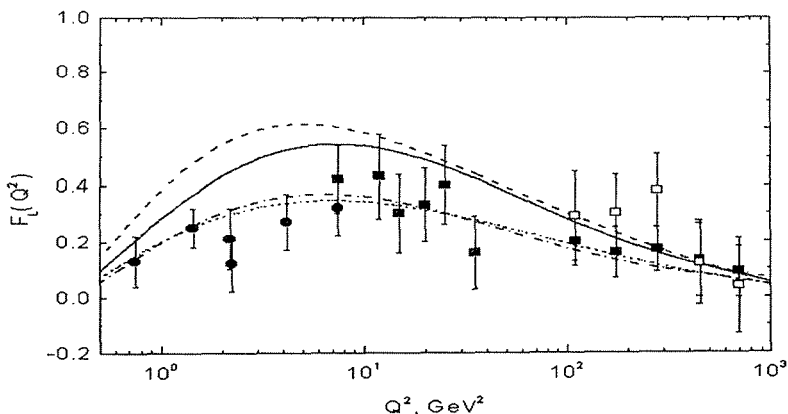


Figure 1: Q^2 dependence of $F_L(x, Q^2)$ (at fixed $W = 276$ GeV). The experimental points are from [8]. Solid curve is the result of the k_T -factorization approach, dashed, dash-dotted and dotted curves - the results of the collinear LO, NLO and LO with $\mu^2 = 127Q^2$ calculations, respectively

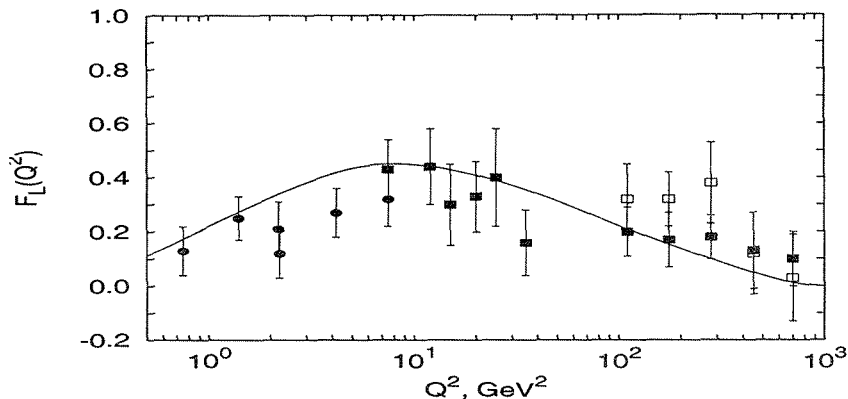


Figure 2: Q^2 dependence of $F_L(x, Q^2)$ (at fixed $W = 276$ GeV). The experimental points are as in Fig. 1. Solid curve is the result of the k_T -factorization approach with the 3LLM unintegrated gluon distribution from [23]

between the collinear ones, that demonstrates clearly the particular resummation of high-order collinear contributions at small x values in the k_T -factorization approach. We also see excellent agreement between the experimental data and collinear approach with GRV parton densities [20] at NLO approximation (the corresponding coefficient functions were taken from the papers [1]). The NLO corrections are large and negative and decrease the F_L value by an approximate factor of 2 at $Q^2 < 10$ GeV². Our k_T -factorization results

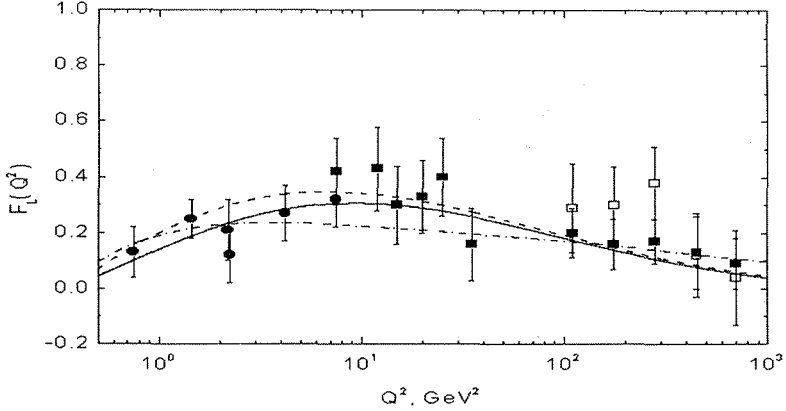


Figure 3: Q^2 dependence of $F_L(x, Q^2)$ (at fixed $W = 276$ GeV). The experimental points are as in Fig. 1. Solid curve is the result of the k_T -factorization approach at $\mu^2 = 127Q^2$, dashed curve - the collinear LO calculations at $\mu^2 = 127Q^2$, dash-dotted curve - from the R_{world} -parametrization

are in good agreement with the data for large and small parts of the Q^2 range. We have, however, some disagreement between the data and theoretical predictions at $Q^2 \sim 3$ GeV². The disagreement exists in both cases: for collinear QCD approach at the LO approximation and for k_T -factorization. It is possible to assume, that the disagreement comes from two reasons: additional higher-twist contributions, which are important at low Q^2 values¹, or/and NLO QCD corrections.

It was shown that the saturation (non-linear QCD) approaches contain information of all orders in $1/Q^2$, they resum higher-twist contributions [21]. The analysis of the behaviour of the longitudinal structure function $F_L(x, Q^2)$ in the saturation models was done in Ref. [22]². In Fig. 2 we demonstrate our k_T -factorization description of $F_L(Q^2)$, at fixed W with the unintegrated gluon distribution proposed in Ref. [23] which takes into account non-linear (saturation) effects.

Concerning the NLO corrections in the k_T -factorization approach a rough estimation of that can be done in the following way. Consider firstly the BFKL approach. A popular resummation of the NLO corrections is done in [6], which demonstrates that the basic effect of the NLO corrections is the strong rise of the α_s argument from Q^2 to $Q_{eff}^2 = K \cdot Q^2$ where $K = 127$, i.e. $K \gg 1$.

The use of the effective argument Q_{eff}^2 in the DGLAP approach at LO approximation leads to results which are very close to the ones obtained in the case of NLO approximation: see the dot-dashed and dotted curves in Fig. 1. Thus, we hope that the effective argument represents the basic effect of the NLO corrections also in the framework of the k_T -factorization, which in some sense lies between the DGLAP and BFKL approaches.

¹Some part of higher-twist contributions was took into account by the "freezing" procedure.

²N.Z. thanks M.V.T. Machado for useful discussion of this problem.

The results obtained in the k_T -factorization and collinear approaches based on Q_{eff}^2 argument are presented in Fig. 3. There is very good agreement between the experimental data and both theoretical approaches.

Moreover, we also present in Fig. 3 the F_L results based on the R_{world} -parameterization for the $R = \sigma_L/\sigma_T$ ratio (see [24]) (because $F_L^i = F_2 R/(1 + R)$), and the F_2 parameterization from our previous paper [13]. The results are in good agreement with other theoretical predictions as well as with experimental data.

4. Conclusion

In the framework of k_T -factorization and perturbative QCD at LO and NLO approximations we have analyzed recent H1 preliminary data [8].

We have found very good agreement between the experimental data and collinear NLO results. The LO collinear and k_T -factorization results show a disagreement with the H1 data in the range $2 < Q^2 < 10 \text{ GeV}^2$ values. It was assumed that the disagreement comes from the absence of additional higher-twist or/and NLO corrections. We shown that the account of higher-twist contributions in the form of saturation effects results in better description of the experimental data. The NLO corrections were modeled by choosing large effective scale in the QCD coupling constant. The effective corrections significantly improve also the agreement with the H1 data under consideration.

Acknowledgements

One of the authors (A.V.K.) is supported in part by Alexander von Humboldt fellowship. A.V.L. is supported in part by INTAS YSF-2002 grant N° 399 and "Dinastiya" Foundation. N.P.Z. thanks the Organizing Committee for financial support and L. Jönsson for discussion of the H1 data [8].

References

- [1] W.L. van Neerven and E.B. Zijlstra, Phys. Lett. **B272**, 127 (1991); E.B. Zijlstra and W.L. van Neerven, Phys. Lett. **B273**, 476 (1991), Nucl. Phys. **B383**, 525 (1992).
- [2] D.I. Kazakov and A.V. Kotikov, Theor.Math.Phys. **73**, 1264 (1987); Nucl.Phys. **B307**, 721 (1988); E. **B345**, 299 (1990). Phys.Lett. **B291**, 171 (1992); D.I. Kazakov, A.V. Kotikov, G. Parente, O.A. Sampayo, and J. Sanchez Guillen, Phys. Rev. Lett. **65**, 1535 (1990).
- [3] A.V. Kotikov, JETP Lett. **59**, 1 (1994); Phys. Lett. **B338**, 349 (1994).
- [4] A.D. Martin, R.G. Roberts, W.J. Stirling and R.S. Thorne, Phys. Lett. **B531**, 216 (2002) Eur. Phys. J. C **23**, 73 (2002); J. Pumplin, D. R. Stump, J. Huston, H.L. Lai, P. Nadolsky and W.K. Tung, JHEP **0207**, 012 (2002).
- [5] Yu.L. Dokshitzer and D.V. Shirkov, Z. Phys. **C67**, 449 (1995); W.K. Wong, Phys. Rev. **D54**, 1094 (1996).

- [6] S.J. Brodsky, V.S. Fadin, V.T. Kim, L.N. Lipatov and G.B. Pivovarov, JETP. Lett. **70**, 155 (1999).
- [7] M. Ciafaloni, D. Colferai and G.P. Salam, Phys. Rev. **D60**, 114036 (1999); JHEP **07**, 054 (2000); R.S. Thorne, Phys. Lett. **B474**, 372 (2000); Phys. Rev. **D60**, 054031 (1999); **D64**, 074005 (2001); G. Altarelli, R.D. Ball and S. Forte, Nucl. Phys. **B621**, 359 (2002).
- [8] E.M. Lobodzinska, Acta Phys. Polon. **B35**, 223 (2004); P. Newman, hep-ex/0312018.
- [9] A.V. Kotikov, A.V. Lipatov and N.P. Zotov, hep-ph/0403135.
- [10] S. Catani, M. Ciafaloni and F. Hautmann, Nucl. Phys. **B366**, 135 (1991); J.C. Collins and R.K. Ellis, Nucl. Phys. **B360**, 3 (1991); E.M. Levin, M.G. Ryskin, Yu.M. Shabelskii and A.G. Shuvaev, Sov. J. Nucl. Phys. **53**, 657 (1991).
- [11] L.N. Lipatov, Sov. J. Nucl. Phys. **23**, 338 (1976); E.A. Kuraev, L.N. Lipatov and V.S. Fadin, Sov. Phys. JETP **44**, 443 (1976), **45**, 199 (1977); Ya.Ya. Balitzki and L.N. Lipatov, Sov. J. Nucl. Phys. **28**, 822 (1978); L.N. Lipatov, Sov. Phys. JETP **63**, 904 (1986).
- [12] S. Catani and F. Hautmann, Nucl. Phys. **B427**, 475 (1994); S. Catani, Preprint DFF 254-7-96 (hep-ph/9608310).
- [13] A.V. Kotikov, A. V. Lipatov, G. Parente and N.P. Zotov, Eur. Phys. J. C **26**, 51 (2002); A.V. Kotikov, A.V. Lipatov and N.P. Zotov, Eur. Phys. J. C **27**, 219 (2003).
- [14] J. Blumlein, J. Phys. **G19**, 1623 (1993).
- [15] B. Badelek, J. Kwieciniski and A. Stasto, Z. Phys. **C74**, 297 (1997).
- [16] Bo Andersson et al. (Small x Collaboration), Eur. Phys. J. **C25**, 77 (2002).
- [17] N. Nikolaev and B.M. Zakharov, Z. Phys. **C49**, 607 (1991); **C53**, 331 (1992).
- [18] J. Blumlein, Preprints DESY 95-121 (hep-ph/9506403).
- [19] H1 Collab.: C. Adloff et al., Phys. Lett. **B520**, 183 (2001).
- [20] M. Gluck, E. Reya and A. Vogt, Z. Phys. **C67**, 433 (1995).
- [21] J. Bartels, K. Golec-Biernat, K. Peters, Eur. Phys. J. **C17**, 121 (2001); E. Gotsman, E. Levin, U. Maor, L.D. McLerran, K. Tuchin, Nucl. Phys. **A683**, 383 (2001).
- [22] V.P. Goncalves, M.V.T. Machado, Eur. Phys. J. **C37**, 299 (2004).
- [23] E. Gotsman, E. Levin, M. Lublinsky and U. Maor, Eur. Phys. J. **C27**, 411 (2003).
- [24] SLAC Collab., L.W. Whitlow, Phys. Lett. **B250**, 193 (1990).

MODEL FOR RESTORATION OF HEAVY-ION POTENTIALS AT INTERMEDIATE ENERGIES

K.M. Hanna^{1,2}, K.V. Lukyanov², V.K. Lukyanov², B. Słowiński^{3,4}, E.V. Zemlyanaya²

(1) *Math. and Theor. Phys. Dept., NRC, Atomic Energy Authority, Cairo, Egypt*

(2) *Joint Institute for Nuclear Research, Dubna, Russia*

(3) *Faculty of Physics, Warsaw University of Technology, Warsaw, Poland*

(4) *Institute of Atomic Energy, Otwock-Swierk, Poland*

Abstract

Three types of microscopic nucleus-nucleus optical potentials are constructed using three patterns for their real and imaginary parts. Two of these patterns are the real V^H and imaginary W^H parts of the potential which reproduces the high-energy amplitude of scattering in the microscopic Glauber-Sitenko theory. Another template V^{DF} is calculated within the standard double-folding model with the exchange term included. For either of the three tested potentials, the contribution of real and imaginary patterns is adjusted by introducing two fitted factors. An acceptable agreement with the experimental data on elastic differential cross-sections was obtained for scattering the $^{16,17}\text{O}$ heavy-ions at about hundred Mev/nucleon on different target-nuclei. The relativization effect is also studied and found that, to somewhat, it improves the agreement with experimental data.

Keywords: heavy-ion optical potential, microscopic scattering theory, double-folding model, high-energy approximation.

1. Introduction

One of the main goals of studying heavy-ion scattering remains to obtain the nucleus-nucleus optical (complex) potential. Such a potential is required not only for physical interpretation of experimental data in elastic channel but also to get the optical-model wave functions used in the DWBA calculations of direct inelastic processes and of the nucleons removal reactions. Unfortunately, when fitting data with the help of phenomenological optical potentials one cannot obtain their parameters unambiguously. The other problem is that the parameters of phenomenological potentials depend on the collision energy, atomic numbers and isospins of nuclei. These dependencies present many difficulties in composing appropriate formulae for the global heavy-ion potentials of scattering.

Therefore one ought to follow the more justified way for searching the nucleus-nucleus potentials, namely, to develop the respective microscopic models. In this connection, the attractive and commonly used models are based on the double-folding (DF) procedure, where one calculates integrals with overlapping the density distribution functions of colliding nuclei and the effective nucleon-nucleon potentials (see, e.g., [1, 2, 3]). Moreover, the microscopic models arose considerable interest because they can supply us with underlying effective NN-forces at normal and higher nuclear densities (see, e.g., [4]). This in-medium dependence of NN-potentials is of the great importance in both nuclear- and astro-physics where deeper understanding of e.g. neutron stars and super novae phenomena is needed.

In nucleus-nucleus scattering at energies near and higher the Coulomb barrier, most applications were made by using the optical potential where the real part is calculated within the microscopic model with the direct and exchange terms included, while the imaginary part of the potential is taken in a phenomenological Woods-Saxon form with a three or more adjustable parameters. In this model, say, semi-microscopic model [1, 2, 3], one further free parameter is usually introduced to renormalize the real DF-part of the optical potential. Thus, the general problem still remains when one parametrizes the global dependence of the imaginary part on the potential energy, atomic numbers,... etc.

In the present work, we suggest the method where the pattern potentials are used to compose the microscopic nucleus-nucleus optical potential. As a basis we take the complex potential which fully corresponds to the microscopic high-energy approximation of Glauber and Sitenko [5, 6], being later developed in [7, 8] for deriving the nucleus-nucleus scattering amplitude. This potential (composed of both the real and imaginary parts) depends on energy and uses density distributions of nuclei and the nucleon-nucleon amplitude of scattering with the in-medium effects included. Besides, we take into consideration the microscopic DF-potential, the real one, and use it as a pattern for constructing the full nucleus-nucleus potential. We hope that this regular procedure for obtaining the complex potentials can protect one against the possible non-physical forms of phenomenological potentials obtained in the standard fitting procedure.

In Section 2 the microscopical formulation is presented while Section 3 is devoted to results, discussions, and some conclusions.

2. Microscopic Optical Potentials

To formulate the very complicated many-body scattering problem in terms of an equivalent optical potential one should to appeal not only to its theoretical elegance but also to develop the reliable methods which provide its reasonably simple relation to experimental data. In principle, the optical potential in its general form as is done, e.g., in [9], has a very complicated and nonlocal form. However, one believes that it can be presented in the equivalent local form by using a realistic localized expression for the density matrix. So, below we will test the microscopic nucleus-nucleus energy- and density-dependent optical potential in a compact form as follows:

$$U_{opt}(r) = N_r V(r) + i N_{im} W(r). \quad (1)$$

Here the three patterns for both of the real $V(r)$ and imaginary $W(r)$ parts are calculated by using the appropriate microscopic models while the normalizing factors N_r and N_{im} are considered as free parameters to be fitted to the experimental data.

The matter of fact is that, for nucleus-nucleus scattering, the surface region of optical potentials plays a decisive role in predictions of differential and total cross-sections. Consequently, the usually ensured microscopic models are substantiated namely in this outer region of the collision. Indeed, in a preceding paper [10] a method was developed for the restoration of nucleus-nucleus optical potentials derived on the basis of Glauber-Sitenko microscopic scattering theory where, in the so called optical limit, the microscopic phase was given in the form

$$\Phi_N(b) = \frac{\bar{\sigma}_{NN}}{2} (i + \bar{\alpha}_{NN}) \int d^2 s_p d^2 s_t \rho_p^\circ(s_p) \rho_t^\circ(s_t) f_N(|\xi = \mathbf{b} + \mathbf{s}_p - \mathbf{s}_t|). \quad (2)$$

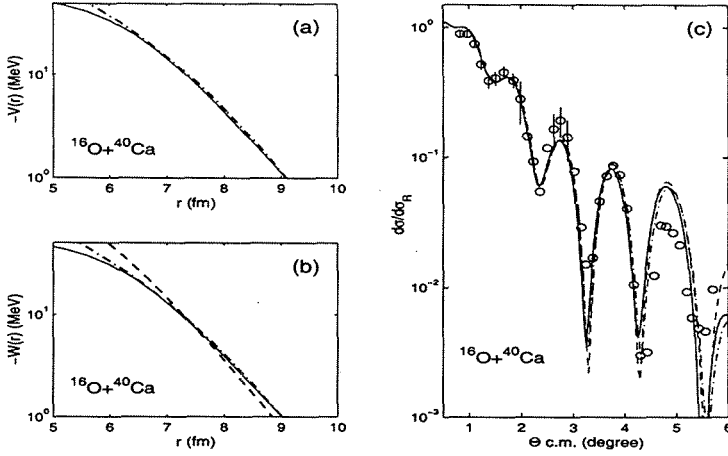


Figure 1: The optical potentials U_{opt}^B and V_{opt}^C obtained basing on the HEA- and DF-patterns with the fitted N_r and N_{im} coefficients (see Table 1A), and the respective ratios of the elastic differential cross-sections to the Rutherford one, for $^{16}\text{O}+^{40}\text{Ca}$ at $E_{lab} = 1503$ MeV. Panels (a) and (b) are designed for the real and imaginary parts of potentials, where dashed curves are the real and imaginary parts of potentials with the patterns V^H (or W^H), while dash-dotted curves are for those with the patterns V^{DF} ; the fitted parts of WS-potential from [17] are shown by solid lines. In panel (c), solid curve is calculations with WS-potential, dashed - with U_{opt}^B , and dash-dotted - with U_{opt}^C . Open circles - experimental data from [17]

Here $\rho_p^o(r)$ and $\rho_t^o(r)$ are the point nucleon density distributions of the projectile and target nuclei, respectively, and $\rho^o(s) = \int_{-\infty}^{\infty} \rho^o(\sqrt{s^2 + z^2}) dz$ is the profile function of $\rho^o(r)$. Also, the function $f_N(\xi) = (2\pi)^{-2} \int d^2q \exp(-iq\xi) \tilde{f}_N(q)$ is expressed through the form factor $\tilde{f}_N(q)$ of the NN-scattering amplitude, taken in the form $\tilde{f}_N(q) = \exp(-q^2 r_{N rms}^2 / 6)$ with $r_{N rms}$, the NN-interaction *rms* radius. Here $\bar{\sigma}_{NN}$ is the total cross section of the NN-scattering while $\bar{\alpha}_{NN}$ is the ratio of the real-to-imaginary part of the forward NN-scattering amplitude, and both of these quantities depend on energy. We denote that the "bar" means averaging on isotopic spins of colliding nuclei. In [10], this phase (2) was compared with another phenomenological one defined through the optical potential $U(r) = V(r) + iW(r)$ as follows,

$$\Phi(b) = -\frac{1}{\hbar v} \int_{-\infty}^{\infty} U(\sqrt{b^2 + z^2}) dz, \quad (3)$$

where v is the relative motion velocity. An analytic expression was used for the phase $\Phi(b)$ of (3), obtained in [11] for the symmetrized Woods-Saxon (SWS) potential, which is the most realistic phenomenological potential often applied in many calculations. The parameters of the SWS-potential were adjusted such that to fit the shape of the phenomenological phase (3) to the microscopic one (2) in the outer region of space $b \sim R_p + R_t$. As

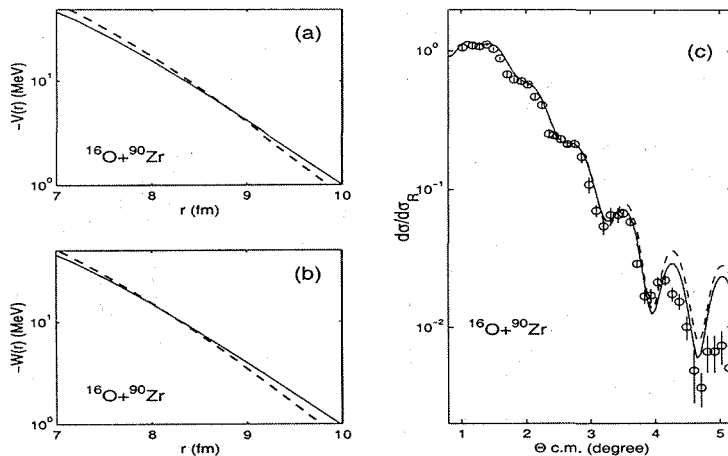


Figure 2: The same as in Fig.1 but for scattering $^{16}\text{O}+^{90}\text{Zr}$ with optical potential U_{opt}^A .

a result of this procedure it was obtained a set of SWS-potentials which coincide in their tails but have different interiors, and all of them were in a reasonable agreement with elastic scattering differential cross-sections at small angles. Although this method gave surface-equivalent realistic WS-type potentials which means the exclusion of ambiguities in the peripheral region of the interaction, it puts us in face of the traditional old standing ambiguity problem of the optical potentials especially in their internal region.

In such situation, we intend in this work to suggest another approach to restore an optical potential. Towards this aim we believe that the use of microscopic potential models is more reliable in search of a realistic optical potential than fitting a phenomenological one. As a first candidate in this search we suggest to use unambiguous potential that corresponds to the HEA microscopic phase (2). This potential has been obtained independently in [12], by applying the inverse Fourier transform to the HEA-phase (2), and in [13], by substituting the standard expression for the direct DF-potential in the definition of the phase (3). As a result, the so-called HEA-optical potential is as follows:

$$U_{opt}^H(r) = V^H(r) + iW^H(r), \quad (4)$$

where

$$V^H(r) = -\frac{2E}{k(2\pi)^2} \bar{\sigma}_{NN} \bar{\alpha}_{NN} \int dq q^2 j_0(qr) \bar{\rho}_p^\circ(q) \bar{\rho}_t^\circ(q) \bar{f}_N(q), \quad (5)$$

$$W^H(r) = -\frac{2E}{k(2\pi)^2} \bar{\sigma}_{NN} \int dq q^2 j_0(qr) \bar{\rho}_p^\circ(q) \bar{\rho}_t^\circ(q) \bar{f}_N(q). \quad (6)$$

Here $\bar{\rho}_{p(t)}^\circ(q)$ are form factors of the corresponding point densities $\rho_{p(t)}^\circ(r)$ of the projectile and target nuclei, where the latter functions can be obtained by unfolding the nuclear densities $\rho_{p(t)}(r)$ (see, e.g., [14]), which are usually given in tabulated forms. Thus, the suggested model is free from parameters when calculating the real V^H and the imaginary W^H parts of the potential. The important and novel point of this method is that it

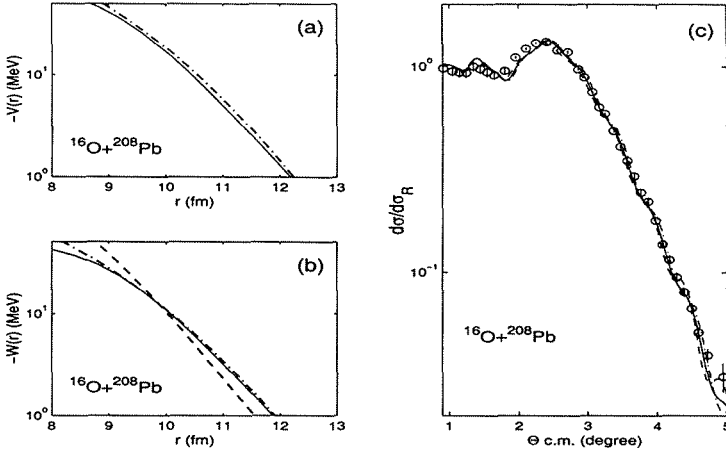


Figure 3: The same as in Fig.1 but for scattering $^{16}\text{O}+^{208}\text{Pb}$ with optical potentials U_{opt}^B and U_{opt}^C

provides to calculate the imaginary part of the potential (6) in a microscopic way. We remind, that in the standard semi-microscopic model one estimates only the real part of the potential using DF-procedure, while the imaginary part is usually taken in a phenomenological WS-form with three or sometimes more fitted parameters. In the present work, in addition to the HEA-potential, we also apply a DF-procedure to estimate the real part of the optical potential, which includes both the direct and exchange terms (see, e.g., [2, 3]):

$$V^{DF} = V^D + V^{EX} \quad (7)$$

where

$$V^D(r) = \int d^3r_p d^3r_t \rho_p(\mathbf{r}_p) \rho_t(\mathbf{r}_t) v_{NN}^D(\mathbf{r}_{pt}), \quad \mathbf{r}_{pt} = \mathbf{r} + \mathbf{r}_t - \mathbf{r}_p, \quad (7a)$$

$$V^{EX}(r) = \int d^3r_p d^3r_t \rho_p(\mathbf{r}_p, \mathbf{r}_p + \mathbf{r}_{pt}) \rho_t(\mathbf{r}_t, \mathbf{r}_t - \mathbf{r}_{pt}) \times v_{NN}^{EX}(\mathbf{r}_{pt}) \exp\left[\frac{i\mathbf{K}(r)\mathbf{r}_{pt}}{M}\right]. \quad (7b)$$

The dependence on energy in the potential comes from the local relative momentum notion defined as $K(r) \simeq \{2Mm/\hbar^2[E - V_N(r) - V_C(r)]\}^{1/2}$ where $Mm = A_p A_t m / (A_p + A_t)$ is the reduced mass, E is the relative energy in the center-of-mass frame, and $V_C(r)$, the responsible part of the interaction due to the Coulomb potential. We adopt here an energy- and density-dependent version for the effective interaction as given in [3] where the effective interaction v_{NN} is expressed in the form of M3Y force multiplied by the factor $F(\rho) = C[1 + \alpha \exp(-\beta\rho) - \gamma\rho]$ which depends on the densities $\rho = \rho_p + \rho_t$, and also the additional factor $(1 - 0.003 E/A_p)$ is introduced to correct the dependence upon the incident laboratory energy per nucleon.

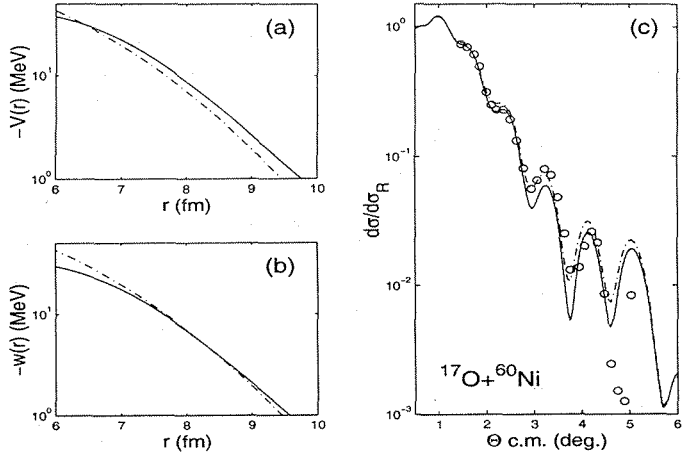


Figure 4: The same as in Fig.1 but for scattering $^{17}\text{O} + ^{60}\text{Ni}$ at 1435 MeV with optical potential U_{opt}^C from Table 1B. Experimental points and the fitted WS-potential are taken from [18]

The comparison between (5) and (7) ensures that the HEA real part V^H of the optical potential corresponds only to the direct part V^D of the full potential while the V^{DF} -real potential consists of two terms, direct and exchange ones, where the latter has a nonlocal nature and arises from the anti-symmetrization between two colliding nuclei, and it accounts for the Pauli-blocking and the so-called knock-on exchange nonlocality. Thus we have two microscopic types of the real potentials V^{DF} and V^H , and one for the imaginary part W^H . The HEA-potentials have slightly different slopes in their asymptotics as compared to the DF-potential. In principle, the real and imaginary parts of optical potentials have different physical nature. The first one, as its origin, has the one-particle densities while the second one can get the additional contributions, coming from excitations of collective states and the nucleons removal reactions. Besides, one should bear in mind that at high energies, the peripheral region of the nucleus-nucleus interaction plays the essential role, while the exchange effects reveal themselves mainly in the internal region. At the same time, we pay attention to the result given in [15] that at high energies the nucleons removal reactions mostly contribute to the absorption part of the optical potential while the excitation channels are suppressed. Therefore, one-particle densities take part in equal footing in the formation of both the real and imaginary potentials. Thus, considering not high but intermediate energies of collisions and at about 100 MeV/nucleon one can utilize both the shapes HEA- and DF-patterns for composing total microscopic potentials. As a result, we shall test three types of optical potentials, each have only two parameters N_r and N_{im} , namely:

$$U_{opt}^A = N_r^A V^H + iN_{im}^A W^H \quad (8)$$

$$U_{opt}^B = N_r^B V^{DF} + iN_{im}^B W^H \quad (9)$$

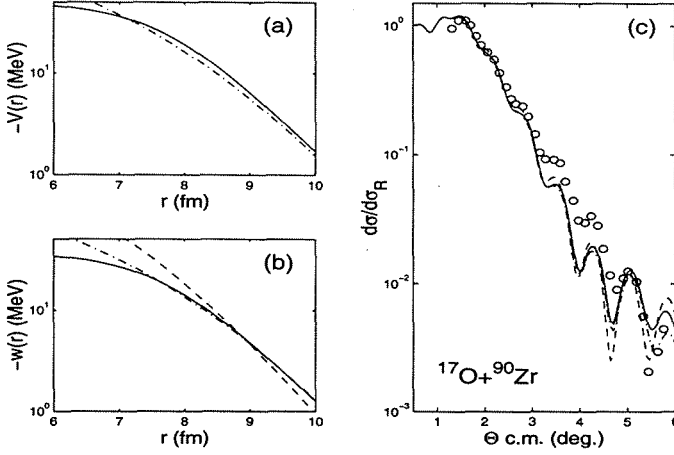


Figure 5: The same as in Fig.4 but for scattering $^{17}\text{O}+^{90}\text{Zr}$ with optical potentials U_{opt}^B and U_{opt}^C

$$U_{opt}^C = N_r^C V^{DF} + iN_{im}^C V^{DF} \quad (10)$$

Usually, in heavy-ion scattering at comparably high energies, the potential tails determine the pattern of the elastic differential cross-sections because of the strong absorption happened at shorter distances. Then, roughly speaking one needs only four parameters to describe the positions and the slope parameters of these tails. In our case we use the microscopic models for both the real and imaginary patterns of the optical potentials given by Eqs.(8)-(10), where by the fitting of only two parameters N_r and N_{im} we can, in fact, change the strength and shift of the potential tails in the surface region. In practice, the fit of phenomenological potentials at $E \sim 100$ Mev/nucleon shows that the range from R_{in} to ∞ determines the main pattern of the differential cross-sections, and R_{in} is the radius where $V(R_{in}) = -50$ Mev. So, below in Figures we show potentials only in this region of their displaying.

3. Results, Discussion, and Conclusions

We calculate the ratio of the elastic differential cross-sections $d\sigma/d\Omega = |f(q)|^2$ to the Rutherford cross-section

$$\frac{d\sigma_R}{d\Omega} = \left(\frac{Z_p Z_t e^2}{\hbar v} \right)^2 \frac{1}{4k^2} \frac{1}{\sin^4(\vartheta/2)} \quad (11)$$

For this purpose we apply the expression for the HEA-scattering amplitude

$$f(q) = ik \int_0^\infty db b J_0(qb) [1 - e^{i\Phi_N(b) + i\Phi_C(b)}]. \quad (12)$$

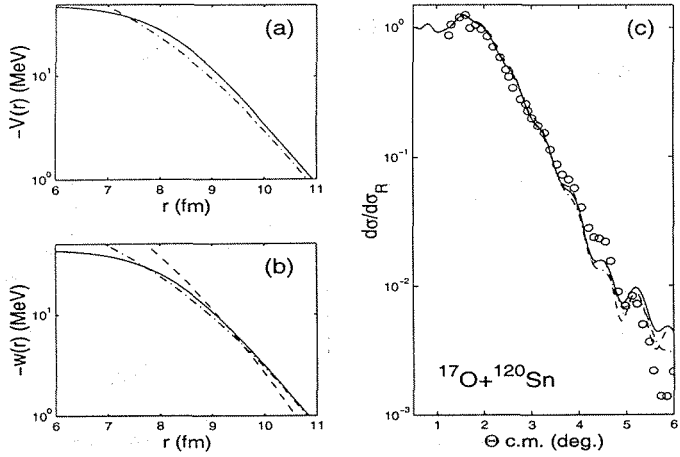


Figure 6: The same as in Fig.4 but for scattering $^{17}\text{O}+^{120}\text{Sn}$ with optical potentials U_{opt}^B and U_{opt}^C

which is valid at $E \gg |U|$ and for small scattering angles $\vartheta < \sqrt{2/kR}$ where R is the nucleus-nucleus interacting radius, say, $R \sim R_p + R_t$. Here $q = 2k \sin(\vartheta/2)$ is the momentum transfer. The Coulomb phase $\Phi_C(b)$ is taken in an analytic form for the uniformly charged spherical density distribution. The nuclear phase $\Phi_N(b)$ is calculated with a help of the optical potentials (8)-(10), using the microscopic HEA- and DF-models. The trajectory distortion in the Coulomb field is taken into account by changing the impact parameter b by $b_c = \bar{a} + \sqrt{\bar{a}^2 + b^2}$ in all functions of the integrand of (12) with the exception of $\Phi_C(b)$; here b_c is the distance of closest approach in a Coulomb field, where $\bar{a} = Z_p Z_t e^2 / 2E_{c.m.}$. Details of calculations of (12) one can find in [16]. In addition, in calculations, we take into account the relativistic kinematics by substituting the respective expressions of velocity v and the c.m. momentum k in (3), (11) and (12) as follows:

$$\hbar v = 197.327 \frac{\sqrt{E_l(E_l + 2A_p m)}}{E_l + A_p m} \quad (\text{in MeV fm}), \quad (13)$$

$$k = \frac{1}{197.327} \frac{A_t \sqrt{E_l(E_l + 2A_p m)}}{\sqrt{(A_p + A_t)^2 + 2A_t E_l/m}} \quad (\text{in fm}^{-1}), \quad (14)$$

where E_l (in MeV) is the kinetic energy of the projectile nucleus in laboratory system, and $m=931.494$ (in MeV) is the unified atomic mass unit.

Below we present our calculations of the cross-section $d\sigma/d\sigma_R$ for scattering of ^{16}O on the targets ^{40}Ca , ^{90}Zr , and ^{208}Pb at incident energy $E_l=1503$ MeV, and ^{17}O on ^{60}Ni , ^{90}Zr , ^{90}Sn , and ^{208}Pb at $E_l=1435$ MeV, and compare these calculations with the corresponding experimental data from Refs. [17] and [18], respectively. The pattern potentials V^H , W^H ,

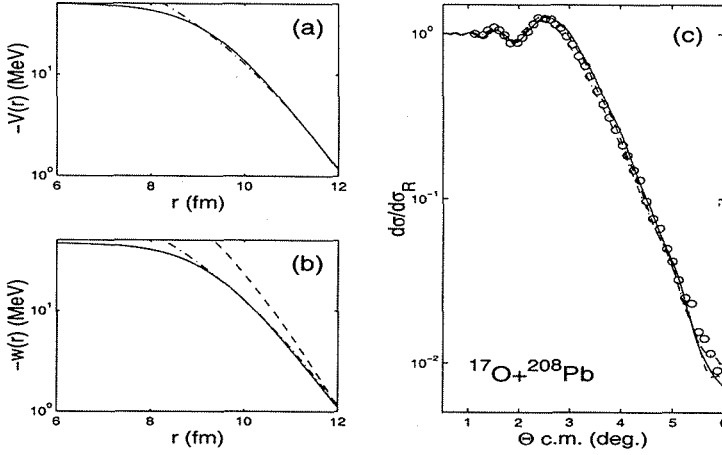


Figure 7: The same as in Fig.4 but for scattering $^{17}\text{O}+^{208}\text{Pb}$ with optical potentials U_{opt}^B and U_{opt}^C

and V^{DF} were computed with the help of (4)-(7) using the point density distribution functions $\rho^o(r)$ for ^{16}O and respective target-nuclei from [14], and for the corresponding nuclei in collisions of ^{17}O - from [19] and [20]. Also, parameterization of $\bar{\sigma}_{NN}$ and $\bar{\alpha}_{NN}$ are taken from [21] and [22] while the effective v_{NN} -forces of the type CDM3Y6 are obtained from [4]. The normalizing coefficients N_r and N_{im} in (8)-(10) were fitted for each couple of colliding nuclei and presented in Tables 1A and 1B.

In Figs.1-7, panels (a) and (b) show the real and imaginary parts of the optical potentials U_{opt}^A , U_{opt}^B , and U_{opt}^C calculated by using the microscopic models HEA and DF as patterns. Dashed curves represent the potentials with patterns V^H and W^H , while those with V^{DF} are shown by dash-dotted curves. The phenomenological Woods-Saxon (WS) potentials, are shown by solid lines. The ratios of the respective elastic to Rutherford differential cross-sections are presented in panels (c) of Figs.1-7, where dashed curves show the HEA-calculations with the potentials U_{opt}^A or U_{opt}^B , dashed-dotted lines - with the potentials U_{opt}^C , and solid curves - with the fitted WS-potentials; open circles are the experimental data.

One can see that the slopes of the calculated and the fitted potentials in the outer region have a coincidence to each others. The differential cross-sections fall down by an exponential law beyond the Coulomb rainbow angle, and have an acceptable agreement with the experimental data. As to applicability of the HEA-calculations, we can refer to the sufficient agreements with the experimental data of the HEA cross-sections for the WS-potentials (solid curves). On the other hand, these potentials were obtained by fitting to the same data given in [17] and [18] not by the HEA-calculations but with the help of numerical solutions of the Schroedinger equation. Indeed, this agreement takes place at angles $\vartheta < 5.5^\circ$ where the HEA is valid by definition. In Tables 1A and 1B the fitted normalizing factors N_r and N_{im} of both the real and imaginary parts of the

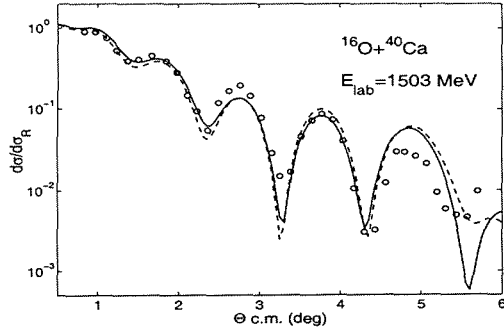


Figure 8: The effect of relativization in case of scattering $^{16}\text{O}+^{40}\text{Ca}$. Solid(dashed) lines show $d\sigma/d\sigma_R$ with(without) relativization. The potential U_{opt}^C is from Table 1A

different microscopic optical potentials are demonstrated. In addition, we demonstrate in Fig.8 the relativistic effect on the differential elastic scattering cross-section of $^{16}\text{O}+^{40}\text{Ca}$ at $E_l=1503$ MeV, when one uses the relativistic formulae (13),(14) for k and v in (3),(11), (12). Although this effect is seen not to be large at this energy, the calculated cross-section $d\sigma/d\sigma_R$ is in favor of its improvement when compared with its experimental counterpart.

Table 1A. Optical potentials for the ^{16}O heavy-ion scattering on different nuclei

U	$^{16}\text{O} + ^{40}\text{Ca}$	$^{16}\text{O} + ^{90}\text{Zr}$	$^{16}\text{O} + ^{208}\text{Pb}$
U_{opt}^A	—	$1.13V^H + iW^H$	—
U_{opt}^B	$V^{DF} + i1.32W^H$	—	$V^{DF} + iW^H$
U_{opt}^C	$V^{DF} + i0.88V^{DF}$	—	$V^{DF} + i0.6V^{DF}$

Table 1B. Optical potentials for the ^{17}O heavy-ion scattering on different nuclei

U	$^{17}\text{O} + ^{60}\text{Ni}$	$^{17}\text{O} + ^{90}\text{Zr}$	$^{17}\text{O} + ^{120}\text{Sn}$	$^{17}\text{O} + ^{208}\text{Pb}$
U_{opt}^A	—	—	—	—
U_{opt}^B	—	$0.6V^{DF} + i0.9W^H$	$0.5V^{DF} + i0.9W^H$	$0.5V^{DF} + i1.3W^H$
U_{opt}^C	$0.6V^{DF} + i0.6V^{DF}$	$0.6V^{DF} + i0.5V^{DF}$	$0.5V^{DF} + i0.5V^{DF}$	$0.5V^{DF} + i0.8V^{DF}$

Our main conclusion, although we did not intend to achieve a perfect fit as usually experimentalists do, is that the presented idea proves itself to utilize the microscopic models as patterns for further fit with the experimental data. In addition, this method introduce only two adjusted normalizing free parameters instead of, at least, twice the number of parameters required in case of use the phenomenological WS-optical potential. Moreover, at high energy interactions, one can be confident to claim that the results of the calculations done by using the microscopic potentials show that in the outer region of the interactions a true prediction and behavior of these potentials can be gained in the very sensitive domain of the heavy-ion scattering.

Acknowledgments

The co-authors V.K.L. and B.S. are grateful to the Infeld-Bogoliubov Program for support of this work. One of us E.V.Z. thanks the Russian Foundation Basic Research (project 03-01-00657) for support. Also deep gratitude from K.M. Hanna to the authorities of AEA-Egypt and JINR for their support.

References

- [1] G.R.Satchler G.R. and W.G.Love, Phys.Rep. **55**, 183 (1979).
- [2] Dao Tien Khoa and O.M.Knyaz'kov, Phys.El.Part.&Nucl. **27**, 1456 (1990).
- [3] D.T.Khoa and G.R.Satchler, Nucl.Phys.A **668**, 3 (2000).
- [4] D.T.Khoa, G.R.Satchler, and W.von Oertsen, Phys.Rev.C **56**, 954 (1997).
- [5] R.J.Glauber, *Lectures in Theoretical Physics* (N.Y.: Interscience, 1959. P.315).
- [6] A.G.Sitenko, Ukr.Fiz.Zhurn.**4**, 152 (1959) (*in Russian*).
- [7] W.Czyz, L.C.Maximon, Ann.of Phys.(N.Y.) **52**, 59 (1969).
- [8] J.Formanek, Nucl.Phys.B **12**, 441 (1969).
- [9] H.Feshbach, Ann.Phys. **5**, 357 (1958);*ibid.* **19**, 287 (1962).
- [10] V.K.Lukyanov, E.V.Zemlyanaya, B.Słowiński, and K.Hanna, Izv.RAN, ser.fiz., **67**, no.1, 55 (2003) (*in Russian*);
K.M.Hanna, V.K.Lukyanov, B.Słowiński, and E.V.Zemlyanaya, Proc.Nucl. Part.Phys.Conf. (NUPPAC'01), Cairo, Egypt (2001) (ed.by M.N.H.Comsan and K.M.Hanna, printed in Cairo by ENPA, 2002, Nasr City 11787), p.121.
- [11] V.K.Lukyanov and E.V.Zemlyanaya, J.Phys.G **26**, 357 (2000).
- [12] P.Shukla, Phys.Rev.C **67**, 054607 (2003).
- [13] V.K.Lukyanov, E.V.Zemlyanaya, and K.V.Lukyanov, Preprint P4-2004-115, JINR, Dubna, 2004.
- [14] V.K.Lukyanov, E.V.Zemlyanaya, and B.Słowiński, Yad.Fiz. **67**, 1306 (2004) (*in Russian*);
V.K.Lukyanov, E.V.Zemlyanaya, and B.Słowiński, Phys.Atom.Nucl. **67**, 1282 (2004).
- [15] J.H.Sørensen and A.Winther, Nucl.Phys.A **550**, 329 (1992).
- [16] V.K.Lukyanov and E.V.Zemlyanaya, Int.J.Mod.Phys.E **10**, 169 (2001).
- [17] P. Roussel-Chomaz, et al, Nucl.Phys.A **477**, 345 (1988).
- [18] R.Liguori Neto, et al, Nucl.Phys.A **560**, 733 (1993).
- [19] J.D.Patterson and R.J.Peterson, Nucl.Phys.A **717**, 235 (2003).
- [20] M.El-Azab Farid and G.R.Satchler, Nucl.Phys.A **438**, 525 (1985).
- [21] S.K.Charagi and S.K.Gupta, Phys.Rev.C. **41**, 1610 (1990).
- [22] P.Shukla, *arXiv:nucl-th/0112039*.

AZIMUTHAL STRUCTURES OF PRODUCED PARTICLES IN HEAVY ION INTERACTIONS

S. Vokál^{1†}, A. Kravčáková², S. Lehocká² and G. I. Orlova³

(1) *VBLHE, JINR, Dubna, Russia*

(2) *University of P. J. Šafárik, Košice, Slovakia*

(3) *Lebedev Physical Institute, Moscow, Russia*

† *E-mail: vokal@sunhe.jinr.ru*

Abstract

The angular substructures of particles produced in ^{208}Pb at 158 A GeV/c and ^{197}Au at 11.6 A GeV/c induced interactions with Ag(Br) nuclei in emulsion detector have been investigated. Nonstatistical ring-like substructures of produced particles in azimuthal plane of a collision have been found and their parameters have been determined.

1. Introduction

An important aim of nucleus collision investigation at high energies is to search for a phenomena connecting with large densities obtained in such collisions. As an example, the transition from the QGP (quark-gluon plasma) back to the normal hadronic phase is predicted to give large fluctuations in the number of produced particles in local regions of phase space [1, 2]. The observed effects of such type are dominated by statistical fluctuations. Significant deviations from them are only observed after removing the statistical part of the fluctuations [3].

In case of angular structures of produced particles investigation two different classes were revealed, which could be referred to as jet-like and ring-like substructures.

The goal of our work was to study the ring-like substructures of produced particles in azimuthal plane. They are occurrences if many particles are produced in a narrow region along the rapidity axis, which at the same time are diluted over the whole azimuth. The jet-like substructures consist of cases where particles are focused in both dimensions [4].

For the first time the individual nucleus-nucleus collisions with a ring-like substructure of produced particles in the azimuthal plane have been observed more than 20 years ago in cosmic ray experiments [5]. Later a lot of the nucleus-nucleus collisions with the ring-like substructure were observed in the accelerator experiments at high energy [3, 6, 7, 8, 9, 10].

A new mechanism of multiparticle production at high energies was proposed in [11, 12, 13]. This mechanism is similar to that of Cherenkov electromagnetic radiation. As a hadronic analogue, one may treat an impinging nucleus as a bunch of confined quarks each of which can emit gluons when traversing a target nucleus [14, 15]. The idea about possible Cherenkov gluons is relying [11] on experimental observation of the positive real part of the elastic forward scattering amplitude of all hadronic processes at high energies. This is a necessary condition for such process because in the commonly used formula for the refractivity index its excess over 1 is proportional to this real part. Later I. M. Dremin [12] noticed that for such thin targets as nuclei the similar effect can appear due to small

confinement length thus giving us a new tool for its estimate. If the number of emitted gluons is large enough and each of them generates a mini-jet, the ring-like substructure will be observed in the target (azimuthal) diagram. If the number of emitted gluons is not large, we will see several jets correlated in their polar, but not in the azimuthal angles. Central collisions of nuclei are preferred for observation of such effects because of a large number of participating partons.

In the present study the ring-like substructures of charged produced particles from ^{208}Pb and ^{197}Au induced interactions with Ag(Br) target nuclei in emulsion detector at 158 A GeV/c and 11.6 A GeV/c, correspondently, have been analyzed. The comparison with the FRITIOF calculations [16] has been made. All used data are obtained in the frames of EMU01 Collaboration.

2. Experiment

The stacks of NIKFI BR-2 nuclear photoemulsions have been irradiated horizontally by ^{208}Pb beam at 158 A GeV/c (the CERN SPS accelerator – experiment EMU12) and by ^{197}Au beam at 11.6 A GeV/c (the BNL AGS accelerator – experiment E863).

The photoemulsion method allows to measure: *multiplicities of any charged particles*: produced particles (N_s) with $\beta > 0.7$, projectile fragments (N_F) with $\beta \approx 0.99$ and target fragments (N_h) with $\beta < 0.7$, *angles of particles* with the resolution of $\Delta\eta = 0.010 - 0.015$ rapidity units in the central region, pseudo-rapidity is given by $\eta = -\ln(\tan(\theta/2))$, and θ is the emission angle with respect to the beam direction, *charges of projectile fragments* Z_F .

Further details on both experiments, measurements and experimental criteria can be found in [17, 18].

In this work we have analyzed:

- 628 Pb+Ag(Br) collisions found by the along-the track scanning. From the collisions we have selected three centrality groups determined by the multiplicity of the produced particles: $350 \leq N_s < 700$, $700 \leq N_s < 1000$ and $N_s \geq 1000$. As it was shown in our previous paper [20] the criterion $N_s \geq 350$ selects the interactions of lead nuclei at 158 A GeV/c with the heavy emulsion targets Ag and Br with $b_{imp} < 8$ fm only. Moreover the group with $N_s \geq 1000$ comprises the central Pb+Ag(Br) interactions with impact parameter $b_{imp} \approx (0 - 2)$ fm.
- 1128 Au+Ag(Br) collisions found by the along-the track scanning. From the collisions we have selected analogous three centrality groups determined by the multiplicity of the produced particles: $100 \leq N_s < 200$, $200 \leq N_s < 300$ and $N_s \geq 300$.

3. Method

A method we use to search for a ring-like substructure and to determine parameters they have been devised in paper [3]. The produced particle multiplicity N_d of analyzed subgroup from an individual event is kept a fixed. Each N_d -tuple of consecutive particles along the η -axis of individual event can then be considered as a subgroup characterized by a *size*: $\Delta\eta = \eta_{max} - \eta_{min}$, where η_{min} and η_{max} are the pseudo-rapidity values of the first and last particles in the subgroup, by a *density*: $\rho_d = \frac{N_d}{\Delta\eta}$ and by a *average pseudo-rapidity* (or

a subgroup position): $\eta_m = \frac{\sum \eta_i}{N_d}$. Another way is to keep a fixed the $\Delta\eta$ interval. This method has been used by G. L. Gogiberidze et al. in papers [9, 10].

To parameterize the azimuthal structure of the subgroup in a suitable way a parameter of the azimuthal structure $S_2 = \sum (\Delta\Phi_i)^2$ have been suggested, where $\Delta\Phi$ is the difference between azimuthal angles of two neighboring particles in the investigated subgroup (starting from the first and second and ending from the last and first). For the sake of simplicity it was counted $\Delta\Phi$ in units of full revolutions $\sum (\Delta\Phi_i) = 1$.

The parameter S_2 is large ($S_2 \rightarrow 1$) for the particle groups with the jet-like structure and is small ($S_2 \rightarrow 1/N_d$) for the particle groups with the ring-like structure. The expectation value for the parameter S_2 , in the case of stochastic scenario with independent particles in the investigated group, can be analytically expressed as $\langle S_2 \rangle = \frac{2}{N_d+1}$. This expectation value can be derived from the distribution of gaps between neighbors.

What can one wait to see in the experimental S_2 - distributions in different scenarios? As it was shown in [20] in case of a pure stochastic scenario the normalized $S_2/\langle S_2 \rangle$ - distribution would have peak position at $S_2/\langle S_2 \rangle = 1$. The existence of the jet-like substructures in collisions results to appearance of additional $S_2/\langle S_2 \rangle$ - distribution from this effect but shifted to the right side in comparison with stochastic distribution. Analogously, the existence of the ring-like substructures results to appearance of additional $S_2/\langle S_2 \rangle$ - distribution from this effect but shifted to the left side. As result, the summary $S_2/\langle S_2 \rangle$ - distribution from this three effects may have different form depends of mutual order and sizes [20].

4. Results

The first detailed study of the average values of the parameter S_2 was performed in [3]. The azimuthal substructures of particles produced within dense and dilute groups along the rapidity axis in the central ^{16}O and ^{32}S induced collisions with Ag(Br) and Au targets at 200 A GeV/c (EMU01 data sets) were analyzed. The results were compared with different FRITIOF calculations including γ -conversion and the HBT effects. It was conclude that jet-like and ring-like events do not exhibit significant deviations from what can be expected from stochastic emission.

The study of the S_2 -parameter distributions for subgroups of the particles produced in ^{197}Au interactions at 11.6 A GeV/c with Ag(Br) targets in emulsion detector has been done in [19]. Nonstatistical ring-like substructures have been found and cone emission angles as well as other parameters they have determined.

In Fig. 1(a - c) the S_2 - distributions for groups with $N_d = 35$ are shown for Au+Ag(Br) collisions with multiplicities of the produced particles $N_s > 300$ (a), $200 \leq N_s < 300$ (b) and $100 \leq N_s < 200$ (c). The analogical S_2 spectra for subgroups with $N_d = 90$ obtained in Pb+Ag(Br) collisions are shown in Fig. 1(d - f) for different centrality groups with $N_s > 1000$ (d), $700 \leq N_s < 1000$ (e) and $350 \leq N_s < 700$ (f). As one can see at all three cases of different centralities the S_2 - distributions have the peak position around the value corresponding to the stochastic scenario ($S_2/\langle S_2 \rangle = 1$) and tails at the right side. In order to study the ring-like substructures the only left part of the S_2 - distribution, where a signal of ring-like substructure may be expected, is essential. As one can see the only central collisions ($N_s > 300$ in Au- and $N_s > 1000$ in Pb-induced collisions with Ag(Br) targets) have a proved additional peak on the left part. This indicates that a certain ring-like substructures are present at these two experiments.

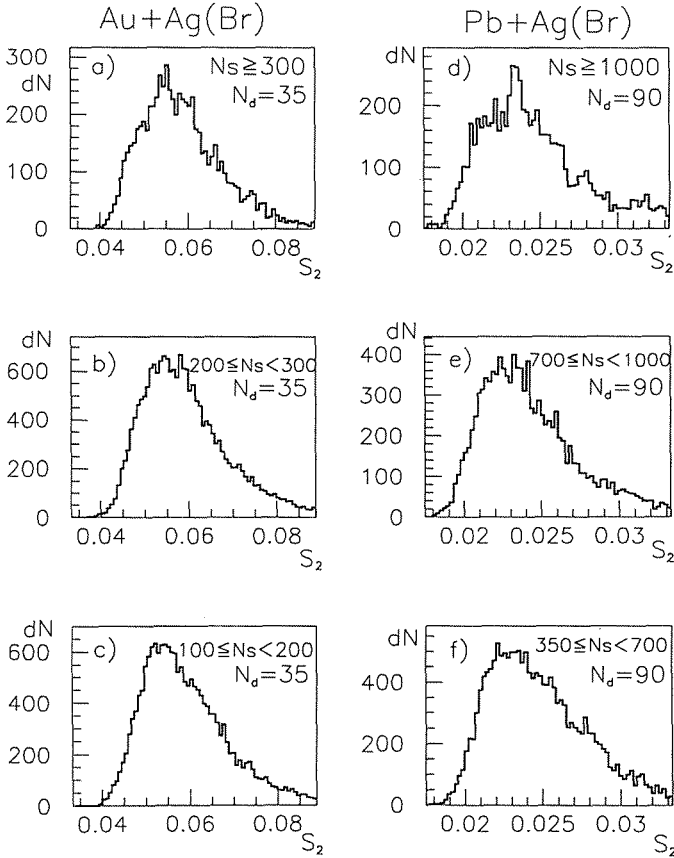


Figure 1: (a, b, c) The S_2 - distributions for subgroups with $N_d = 35$ and different groups of shower particles multiplicity N_s in Au+Ag(Br) collisions at 11.6 A GeV/c; (d, e, f) The S_2 - distributions for subgroups with $N_d = 90$ and different groups of shower particles multiplicity N_s in Pb+Ag(Br) collisions at 158 A GeV/c

The experimental normalized $S_2/\langle S_2 \rangle$ - distributions compared with the calculated ones by the FRITIOF model for the most central groups of events measured in ^{197}Au and ^{208}Pb induced collisions with Ag(Br) nuclei at 11.6 and 158 A GeV/c are presented on the Fig. 2. The model distributions were aligned according to the position of the peak with the expe-

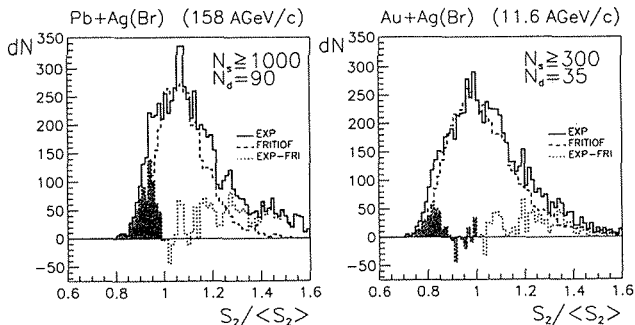


Figure 2: The experimental and FRITIOF model normalized $S_2/\langle S_2 \rangle$ - distributions for central ^{208}Pb and ^{197}Au induced collisions with Ag(Br) targets in the emulsion detector. Here, N_s is the number of produced particles and N_d is the number of particles in the analysed subgroup

rimental one. The FRITIOF model includes neither the ring-like nor the jet-like effects, so the model distributions are used like the statistical background.

One can see that both experimental distributions are shifted to the right, have a tail in the right part and are broader than the spectra calculated by the FRITIOF. The left parts of both experimental distributions are not as smooth as in the model and there are some shoulders that refer to the surplus of the events in this region.

The results obtained from the experimental data after the subtraction of the statistical background are also shown on this figure. The resultant distributions have two very good distinguishable hills, the first in the region $S_2/\langle S_2 \rangle < 1$, where the ring-like effects are expected and the second in the jet-like region $-S_2/\langle S_2 \rangle > 1$. The probability of the formation of the nonstatistical ring-like substructures can be estimated as a rate of the surface of the ring-like part to the full surface of the experimental distribution.

Our preliminary results for $^{208}\text{Pb}+\text{Ag}(\text{Br})$ collisions at 158 A GeV/c are shown that the estimated contribution of the events with nonstatistical ring-like substructures in the emission of produced particles is about 10 – 12% in the most central group of collisions with $N_s \geq 1000$. This value slowly decreases in two other groups of less central events with $350 \leq N_s < 700$ and $700 \leq N_s < 1000$.

To analyze the ring-like subgroup position on the pseudorapidity axis the η_m - distributions for subgroups with $S_2/\langle S_2 \rangle < 1$ from central collisions are presented for experimental data and FRITIOF model in Fig. 3. One can see that the experimental distributions have a downfall in the central region, where the produced particle and FRITIOF distributions have maximum and two symmetrical hills from both sides of the center. For central $^{208}\text{Pb}+\text{Ag}(\text{Br})$ collisions η_m - distribution has two hills – one at $\eta = 1.6 - 3.2$ and other

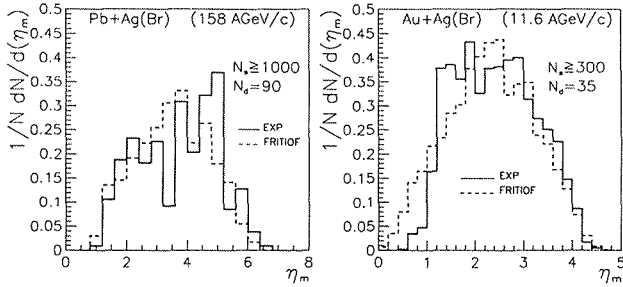


Figure 3: The ring-like subgroup position (η_m) distributions for central experimental (solid histogram) and FRITIOF model (dashed histogram) for $^{208}\text{Pb}+\text{Ag}(\text{Br})$ and $^{197}\text{Au}+\text{Ag}(\text{Br})$ collisions

at $\eta = 3.6 - 5.2$, the center of the distribution for produced particle is at $\eta \approx 3.5$. For central $^{197}\text{Au}+\text{Ag}(\text{Br})$ collisions η_m - distribution has two hills - one at $\eta = 1.2 - 2.0$ and other at $\eta = 2.2 - 3.0$, the center of the distribution is at $\eta \approx 2.2$. The downfall of the η_m - distributions is more visible for $^{208}\text{Pb}+\text{Ag}(\text{Br})$ interactions that are probably connected with larger cross section of the effect for the collisions with bigger multiplicity that realized at higher beam energy and for more central collisions.

To investigate the ring-like subgroups size $\Delta\eta$ in Fig. 4 the $\Delta\eta$ - distributions are shown in the region of the ring-like effects ($S_2/\langle S_2 \rangle < 1$) for the most central ^{208}Pb ($N_s \geq 1000, N_d = 90$) and ^{197}Au ($N_s \geq 300, N_d = 35$) induced collisions with $\text{Ag}(\text{Br})$ targets compared with FRITIOF model. One can see that there are some distinctions in the shapes of the experimental and model distributions for Pb induced collisions. There appeared 3 or 4 peaks in the experimental $\Delta\eta$ - distributions in the ring-like effect region that we don't see in other cases. The difference for ^{197}Au data is not so obvious. Moreover, in our previous paper [20] it was shown that from one side there are some distinctions in the shapes of the experimental distributions for the regions $S_2/\langle S_2 \rangle < 1$ and $S_2/\langle S_2 \rangle > 1$ but from the other side there are no differences in the $\Delta\eta$ - distributions calculated by the model for both classes of events ($S_2/\langle S_2 \rangle < 1$ and $S_2/\langle S_2 \rangle > 1$).

If the ring-like substructures have been appeared due to an effect analogous to Cherenkov light there may be in a collision two such substructures forming two produced particle cones - one in the forward and another in the backward direction in center-of-mass system. In such case the cones must have the equal emission angles, because as well known the Cherenkov emission angel depends on the refractive index of matter only. In our case, in case of nuclear matter, it is a way to measure the refractive index of nuclear matter. It is interesting to note that the refractive index of nuclear matter has to be changed in the case of the changes the nuclear matter properties, for example, in the case of phase transition from a normal hadronic matter to quark-quon plasma.

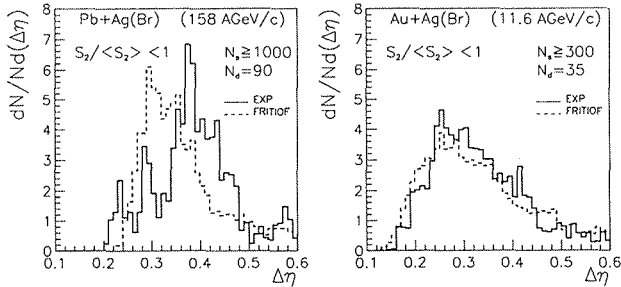


Figure 4: Comparison of the experimental and the FRITIOF model $\Delta\eta$ - distributions for central interactions of ^{208}Pb and ^{197}Au nuclei with $\text{Ag}(\text{Br})$ targets for ring-like region ($S_2/\langle S_2 \rangle < 1$)

5. Conclusion

The azimuthal ring-like substructures of produced particles from collisions induced by the 11.6 A GeV/c ^{197}Au and 158 A GeV/c ^{208}Pb beams with $\text{Ag}(\text{Br})$ targets in the emulsion detector have been investigated.

- The additional subgroups of produced particles in the region of the ring-like substructures ($S_2/\langle S_2 \rangle < 1$) in comparison to the FRITIOF model calculations have been observed.
- The difference with the FRITIOF model calculations in the η_m - distributions in ring-like region $S_2/\langle S_2 \rangle < 1$ indicates to existence of two symmetrical η_m - regions of preferred emission of ring-like substructures - one in the forward and second in the backward direction in center-of-mass system.
- The $\Delta\eta$ - distribution, which gives the information about a ring-like substructure size in pseudorapidity scale, for the experimental data in ring-like region ($S_2/\langle S_2 \rangle < 1$) differs from the FRITIOF model calculations.
- The nonstatistical ring-like substructures formation is more visible for central collisions and for bigger energies.
- The results are in good agreement with an idea that the ring-like substructures have been appeared due to an effect analogous to Cherenkov light.

Acknowledgements

This work was supported by Science and Technology Assistance Agency (Slovak Republic) under the contract No. APVT-51-010002 and by RFBR grants No. 03-02-17079 and No. 04-02-16593.

References

- [1] E. Stenlund *et al.*, Nucl. Phys. **A498** (1989) 541c.
- [2] L. van Hove, Z. Phys. **C21** (1984) 93.
- [3] M. I. Adamovich *et al.*, J. Phys. **G19** (1993) 2035.
- [4] E. Stenlund *et al.*, Talk given at XXII. Multiparticle Dynamics Symposium, Santiago de Compostella, Spain, July 13-17 (1992).
- [5] A. B. Apanasenko, N. A. Dobrotin, I. M. Dremin, K. A. Kotelnikov, Pisma v ZhETF, **30** (1979) 157.
- [6] A. El-Naghy and K. S. Abdel-Khalek, Phys. Lett. **B299** (1993) 370.
- [7] A. El-Naghy *et al.*, J. Phys. Soc. Jpn. **58** (1989) Suppl. 741.
- [8] N. M. Astafyeva, I. M. Dremin, K. A. Kotelnikov, hep-ex/9795003, (1997).
- [9] G. L. Gogiberidze, E. K. Sarkisyan, L. K. Gelovani, Nucl. Phys. Proc. Suppl. **92** (2001) 75.
- [10] G. L. Gogiberidze, L. K. Gelovani, E. K. Sarkisyan, Phys. Atom. Nuclei **64** (2001) 143, Yad. Fizika **64** (2001) 147.
- [11] M. I. Dremin, Pisma v ZhETF **30** (1979) 152.
- [12] M. I. Dremin, Jad. Fiz. **33** (1981) 1357.
- [13] M. I. Dremin, Pisma v ZhETF **34** (1981) 617.
- [14] I. M. Dremin, hep-ph/0011110, (Nov 2000).
- [15] I. M. Dremin *et al.*, Phys. Lett. **B499** (2001) 97.
- [16] B. Nilsson-Almqvist, E. Stenlund, Comp. Phys. Com. **43** (1987) 387.
- [17] A. Sh. Gaitinov *et al.*, Talk given at XVII. Meeting of the EMU01 Collaboration, Dubna, Russia, May 18-20 (1999).
- [18] M. I. Adamovich *et al.*, Eur. Phys. J. **A5** (1999) 429.
- [19] G. I. Orlova, A. Kravčáková, S. Vokál, V. V. Prosin, Proc. of the Hadron Structure 2002, Herľany, Slovakia, 22-27 Sept 2002, edited by P. J. Šafárik University Košice (2003) 155.
- [20] S. Vokál, A. Vokálová, A. Kravčáková, S. Lehocká, G. I. Orlova, Preprint JINR, E1-2004-173, Dubna (2004).

THE EXTRAORDINARY INTERACTION OF ^{14}N - NUCLEUS IN PHOTOEMULSION

G.Orlova^{1†}

(1) *Lebedev Physical Institute, Moscow*

† *E-mail: orlova@sci.lebedev.ru*

Abstract

The extraordinary interaction of ^{14}N -nucleus in photoemulsion at 2.9 A GeV/c has been found. The observed interaction is of coherent dissociation type. It has five target fragments and four projectile fragments, there are no produced particles in the interaction. Four projectile fragments have five secondary interactions in turn on total length 71.3 mm. Three from this interactions, including primary one, have inelastic charge exchange. The probability of a random coincidence for such a chain of interactions is about 10^{-14} .

Introduction

The observed extraordinary interaction has been found during the processing of the data, recorded in the frames of BECQUEREL Project. The project is aimed to study the processes of the relativistic fragmentation of light nuclei at the low energy-momentum transfers, so the interaction of a coherent dissociation type have been recorded only. The coherent dissociation interactions haven't produced particles but projectile and target fragments only. It allows to pick out a interactions with inelastic charge exchange of nucleons: there are interactions in which a sum of projectile fragment charges isn't equal to the projectile charge.

Experiment

The photoemulsion method has been used in the experiment. The stacks of NIKFI BR-2 nuclear photoemulsion have been irradiated horizontally by 2.9 A GeV/c ^{14}N beam at the Dubna Nuclotron. Photoemulsion layers had a thichness about 550 mkm and a size 10cm x 20 cm. The photoemulsion method allows to measure:

multiplicities of any charged particles:

produced particles (N_s) with $\beta > 0.7$,

projectile fragments (N_F) with $\beta \sim 0.99$ and

target fragments (N_h) with $\beta < 0.23$;

angles of particles; θ is emission angle with respect to the beam direction;

charges of projectile fragments Z_f ;

momenta of particles, using multiple coulomb scattering;

length of tracks with the accuracy 1 mkm.

The projectile fragments are separated from produced particles using criteria - projectile

fragment emission angle $\theta_f < \theta_0 = 0.2 \text{ GeV}/c/P_0$, where P_0 is a projectile momentum. For $P_0 = 2.9 \text{ A GeV}/c - \theta_0 = 4.0^\circ$.

The measurements of angles, momenta and charges of particles from the interactions have been made in two laboratories independently and have shown the good agreement of the results.

Results

The observed extraordinary interaction has five target fragments and four projectile fragments. There aren't produced particles in the interaction.

From four projectile fragments there are two with charges equal to two and two with charges equal to one, that results to sum charge equal to six, while projectile charge equal to seven. It means, that the inelastic nucleon charge exchange process takes place in the interaction. The experimental probability of the inelastic nucleon charge exchange process for the coherent dissociation interactions was received in ${}^6\text{Li} + E_m$ experiment [1]. It is less than $5 \cdot 10^{-3}$.

Except this, three from four projectile fragments participate in five secondary interactions on the total path of 49 mm. The nucleon inelastic charge exchanges, similar to that, observed in the primary interaction, take place in two ones of these five secondary interactions, occurring along the same track. Scheme of the interaction is shown in Fig. 1.

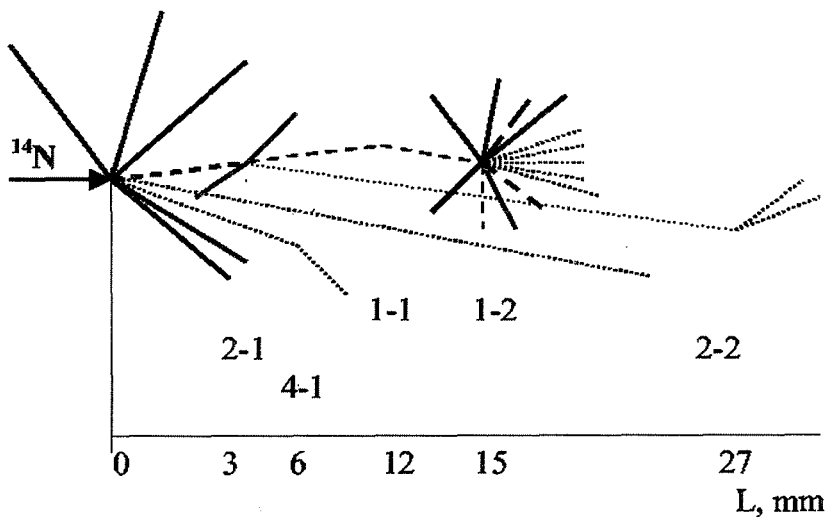


Figure 1: Scheme of the interaction. Fragments N1 and N2 with $Z=2$ have very close emission angles

Below there are results of measurements of projectile and secondary fragments characteristics.

Fragment No 3.1:

$\theta_f = 3.9^\circ$, $Z_f = 1$, $p\beta c = (2.2 \pm 0.3)$ GeV/c, $m_f=1$, $L=22.4$ mm.

Fragment No 4.1:

$\theta_f = 4.1^\circ$, $Z_f = 1$, $p\beta c = (4.2 \pm 1.3$ or $\geq 2.2 \pm 0.3)$ GeV/c, $m_f=2$ (or 1).

After $L=6.5$ mm fragment No 2.2 has a break - interaction No 5.

After the break deep angle is too big to measure its momentum.

The results of the measurements are collected in Fig.2, where the most probable scenarios of the interaction are shown.

The estimation of the probability of a random coincidence of the interactions, imitating the observed event, is about 10^{-14} .

Conclusion

The very small probability of a random coincidence for such a chain of interactions (about 10^{-14}) makes it reasonable to look for another cause except of a random coincidence.

Acknowledgment

This work was supported by the RFBR grant No 04-02-16593.

References

- [1] M.I.Adamovich, V.G.Bogdanov, et al, *Jad.Phys.* **62**, 1461 (1999).

ρ MESON PRODUCTION IN ULTRAPERIPHERAL dAu COLLISION

S.L. Timoshenko[†] (for STAR collaboration)

(1) *Moscow Engineering Physical Institute (State University), Moscow, Russia*

[†] *E-mail: tim@intphys3.mephi.ru*

Abstract

Ultra-peripheral heavy ion collisions involve long range electromagnetic interactions at impact parameters larger than twice the nuclear radius, where no nucleon-nucleon collisions occur. We report on the first observation of rho production in $dAu \rightarrow dAu\rho^0$ and $dAu \rightarrow npAu\rho^0$.

In ultraperipheral heavy-ion collisions, two nuclei geometrically “miss” each other. The impact parameter is larger than twice nuclear radius. In such conditions hadronic interactions do not occur [1]. Relativistic ions are sources of electromagnetic and pomeron fields. The electromagnetic fields have a large radius of interaction, than strong interactions. So, in ultraperipheral collisions, the nuclei interact by two photons or photon-pomeron exchange. The photon flux is proportional to the square of the nuclear charge Z^2 [2], and the forward cross section for elastic $\rho^0 A$ scattering scales as $A^{5/3}$ for surface coupling and A^2 in the bulk. Thus the cross section for photon-pomeron interaction $\sim A^2 Z^2$ for “heavy” states (as like J/ψ) and $Z^2 A^{4/3}$ for lighter mesons (ρ, ω, ϕ).

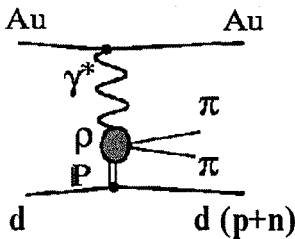


Fig.1(a)

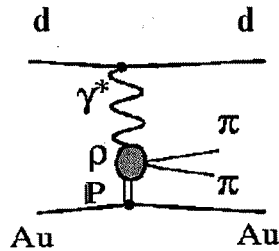


Fig.1(b)

Exclusive vector meson production $dAu \rightarrow d(np)Au\rho^0$ (fig.1(a,b)) can be described by using Weizsacker-Williams approach [2] to photon and pomeron fluxes and vector dominance model. Photon emitted by one nucleus can be consider as a state of virtual photons plus some fluctuations of quark-antiquark pairs. When the nucleus absorbs “photonic” part of wave function, the quark-antiquark pairs contribution becomes dominant. This pair can elastically scatters on the other nucleus and appears as a real vector meson.

In ultraperipheral deuteron gold interactions there are two mechanisms of ρ -meson production. First, a photon emitted by the gold interacts with the deuteron producing

ρ -meson and in this case deuteron can break up ($\gamma d \rightarrow np\rho^0$) or remains in the ground state ($\gamma d \rightarrow d\rho^0$). The cross section of such process is approximately a factor of 16,000 ($Z^2 A^{4/3} \sim 79^2 2^{4/3}$). But there is a process when a photon emitted by the deuteron interacts with the gold. The cross section of such process is approximately a factor of 1,200 ($Z^2 A^{4/3} \sim 1^2 197^{4/3}$). One can see that the cross section first reactions much larger than last. One therefore, at experiment will be dominated production ρ -meson in photon-deuteron interaction.

In the year 2002 RHIC at Brookhaven National Laboratory gold and deuteron nuclei collided at $\sqrt{s_{NN}} = 200$ GeV. In the Solenoidal Tracker at RHIC (STAR) [3], charge particles are reconstructed in a 4.2 meter long, 4 meter diameter cylindrical time projection chamber (TPC). A solenoid magnet surrounds TPC [4]. In 2002 the TPC was operated in a 0.5 T solenoidal magnetic field. Particles were identified by their energy loss in the TPC. The TPC is surrounded by a cylindrical central trigger barrel (CTB). CTB consists of 240 scintillator slats covering $|\eta| < 1$. For registration of neutrons there are two zero degree calorimeters (ZDC) at 18 m from the interaction point [5]. These calorimeters are sensitive to single neutrons and have an efficiency of close to 100 percent.

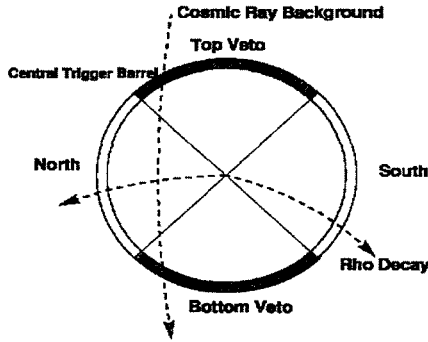


Fig.2

Exclusive ρ^0 production in UPC has a distinctive experimental signature: the $\pi^+\pi^-$ decay products of the ρ^0 meson are observed in an otherwise “empty” spectrometer. Two different triggers were used for this analysis. For $dAu \rightarrow dAu\rho^0$, about 700,000 events were collected using a low-multiplicity “topology” trigger. The topology trigger was designed to detect the products of ρ^0 decay in the CTB system. The CTB was divided into four azimuthal quadrants (fig.2). Selected events were required to have at least one hit in the north and south sectors. The top and bottom quadrants were used as a veto, to reject cosmic rays. To study $dAu \rightarrow npAu\rho^0$ reaction, about 250,000 thousands events are used for the analyses another trigger consists from “topology” trigger and ZDC(West). This trigger (“topology-ZDC”) required the detection of a neutron from the deuteron breakup. The main background for two triggers are cosmic rays, beam gas interaction, pile-up.

For our analysis we selected events with exactly two reconstructed tracks in the TPC. Total charge two tracks must be equal zero. Number of hits in the track can be more than 13. Events were accepted if two tracks were consistent from a single vertex.

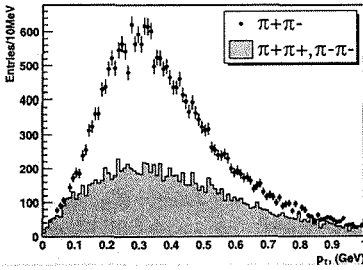


Fig.3

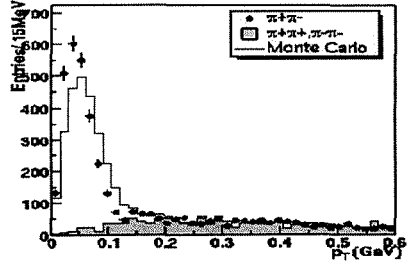


Fig.4

Figure 3 shows the transverse momentum spectrum of oppositely charged pion pairs production in deuteron gold collisions. As one can see, there is a large peak about 300 MeV. It is necessary to remind p_T spectrum of ρ^0 mesons produced in gold-gold collision [6]. Figure 4 shows the transverse momentum spectrum for $\pi^+\pi^-$ pairs. A clear peak, the signature for coherent coupling, can be observed at $p_T < 100$ MeV. This is consistent with coherent ρ^0 meson production. A background model from like-sign combination pairs (shaded histogram), which is normalized to the signal at $p_T > 250$ MeV does not show such a peak. But in dAu collisions a background couldnt normalize to the signal.

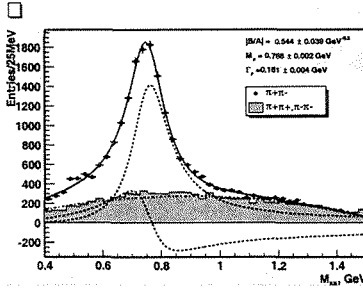


Fig.5(a)

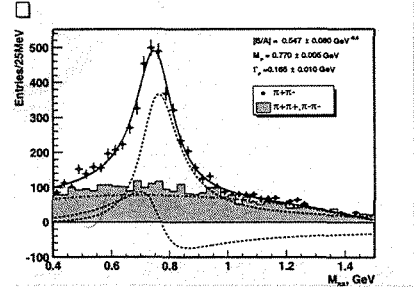


Fig.5(b)

Figure 5(a,b) shows invariant mass of the $\pi^+\pi^-$ pairs for "topology" and "topology-ZDC" triggers. There is a clear ρ^0 peak. About 1,500 and 14,000 events around the ρ^0 mass from the "topology" and "topology-ZDC" triggers respectively were used in the analysis. The fit (solid) is the sum of a relativistic Breit-Wigner for ρ^0 production and a Soding interference term for direct $\pi^+\pi^-$ production (both dashed) [7]. A second order polynomial (dash-dotted) describes the combinatorial background (shaded histogram). The interference shifts the of the distribution to lower masses $M_{\pi^+\pi^-}$. The ρ mass and width are consistent with its values from Particle date book. The direct $\pi\pi$ to ratio agree with ZEUS collaboration in γp interactions [8].

We study the p_T spectra using the variable $t_{\perp} = p_T^2$. At RHIC energies, the longitudinal component of the 4-momentum transfer is small, so $t \approx t_{\perp}$. Figure 6(a,b) shows t spectrum for two different triggers. One can see that t spectrum at fig 6(a) decrease at small t . Our data we have compared with the data from fixed target (fig.7) γd experiment [9]. One can see the incoherent behavior of distribution similar to t distribution at fig.6(a). One can conclude that ρ meson production in reaction when a photon interaction with deuteron and then deuteron break up occur is a incoherent reaction. While t spectrum (fig.6(b)) is similar to coherent behavior. The data were fitted with the function $dN/dt \sim \exp(-bt)$. We obtained $b = 10 \pm 0.13 \text{ GeV}^{-2}$ and $b = 8.42 \pm 0.41 \text{ GeV}^{-2}$ accordingly for “topology” and “topology-ZDC” triggers.

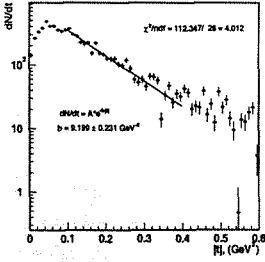


Fig.6(a)

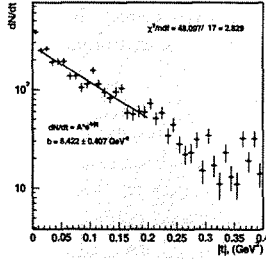


Fig.6(b)

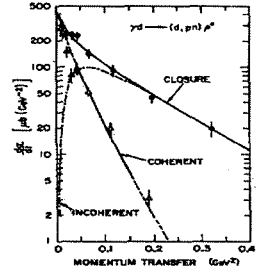


Fig.7

In summary, the first measurements of ρ^0 production in $dAu \rightarrow dAu\rho^0$ and $dAu \rightarrow npAu\rho^0$, confirm the existence of vector meson production in ultra-peripheral heavy ion collisions. It was shown, what in reaction with deuteron break up the ρ -meson production mechanism is incoherent.

References

- [1] G. Baur, K. Hencken and D. Trautmann, J. Phys. **G24**, 1657 (1998).
- [2] C.F. Weizsacker, Z. Phys. **88**, 612 (1934); E.J. Williams, Phys. Rev. **45**, 729 (1934).
- [3] K.H. Ackermann et al., Nucl. Instrum. and Meth. **A499**, 624 (2003).
- [4] M. Anderson et al., Nucl. Instrum. and Meth. **A499**, 659 (2003).
- [5] C. Adler et al., Nucl. Instrum. and Meth. **A470**, 488 (2001).
- [6] C. Adler, Phys. Rep. Lett. **89**, 272302 (2002).
- [7] P. Soding, Phys. Lett. **19**, 702 (1966).
- [8] J. Breitweg et al., Eur. Phys. J. **C2**, 247 (1998).
- [9] Y. Eisenberg et al., Nucl. Phys. **B104**, 61 (1976).

RANDOM MATRIX THEORY AND ANALYSIS OF NUCLEUS-NUCLEUS COLLISION AT HIGH ENERGIES

E. I. Shahaliev ^{1,2†}, R. G. Nazmitdinov ^{3,4}, A. A. Kuznetsov ¹,
M. K. Suleymanov ¹, O. V. Teryaev ⁴

- (1) *High Energy Physics Laboratory, Joint Institute for Nuclear Research, 141980, Dubna, Russia*
- (2) *Institute of Radiation Problems, 370143, Baku, Azerbaijan*
- (3) *Departament de Física, Universitat de les Illes Balears, E-07122 Palma de Mallorca, Spain*
- (4) *Boogoliubov Laboratory of Theoretical Physics, Joint Institute for Nuclear Research, 141980 Dubna, Russia*
† *E-mail: shah@sunhe.jinr.ru*

Abstract

We propose a novel method for analysis of experimental data obtained at relativistic nucleus-nucleus collisions. The method, based on the ideas of Random Matrix Theory, is applied to detect systematic errors that occur at measurements of momentum distributions of emitted particles. The unfolded momentum distribution is well described by the Gaussian orthogonal ensemble of random matrices, when the uncertainty in the momentum distribution is maximal. The method is free from unwanted background contributions.

Relativistic heavy ion collisions are among major experimental tools that allow to get insight into nuclear dynamics at high excitation energies and large baryon densities. It is expected that in central collisions, at energies that are and will be soon available at SPS(CERN), RHIC(BNL) and LHC(CERN), the nuclear density may exceed by tens times the density of stable nuclei. At such extreme conditions one would expect that a final product of heavy ion collisions could present a composite system that consists of free nucleons, quarks and quark-gluon plasma. However, identification of the quark-gluon plasma, for example, is darken due to a multiplicity of secondary particles created at these collisions. There is no a clear evidence of the quark constituent as well. In fact, there are numerous additional mechanisms of a particle creation that mask the presence of the quark-gluon plasma (QGP). It appears that the QGP could be manifested via the observation of indirect phenomena. The natural question arises: how to identify a useful signal that would be unambiguously associated with a certain physical process ?

The most popular methods of analysing data produced at relativistic heavy ion collisions are the correlation analysis [1], the analysis of missing masses [2] and effective mass spectra [3], the interference method of identical particles [4]. We recall that results obtained within those methods are sensitive to assumptions made upon the background of measurements and mechanisms included into a corresponding model consideration. As was mentioned above, the larger is the excitation energy, the larger is a number of various mechanisms of the creation that should be taken into account.

As an alternative approach, one could develop a method that should be independent on the background contribution. For instance, there are attempts to use the maximum entropy principle [5], Fourier transform [6] and even by even analysis [7]. Thus, a formulation of a criteria for a selection of meaningful signals is indeed a topical objective of the relativistic heavy ion collisions physics. The major aim of this paper is to suggest a method that does not depend on the background information and relies only upon the fundamental symmetries of the composite system.

Our approach is based on Random Matrix Theory [8] that was originally introduced to explain the statistical fluctuations of neutron resonances in compound nuclei [9] (see also Ref.[10]). The theory assumes that the Hamiltonian belongs to an ensemble of random matrices that are consistent with the fundamental symmetries of the system. In particular, since the nuclear interaction preserves time-reversal symmetries, the relevant ensemble is the Gaussian Orthogonal Ensemble (GOE). When the time-reversal symmetry is broken we can apply the Gaussian Unitary Ensemble (GUE). The GOE and GUE correspond to ensembles of real symmetric matrices and of Hermitian matrices, respectively. Besides these general symmetry considerations, there is no need in other properties of the system under consideration.

Bohigas *et al* [11] conjectured that RMT describes the statistical fluctuations of a quantum systems whose classical dynamics is chaotic. Quantum spectra of such systems manifest a strong repulsion (anticrossing) between quantum levels, while in non-chaotic (regular) systems crossings are a dominant feature of spectra (see, e.g., [12]). In turn, the crossings are observed when there is no mixing between states that are characterized by different good quantum numbers, while the anticrossings signal about a strong mixing due to a perturbation brought about by either external or internal sources. Nowadays, RMT has become a standard tool for analysing the fluctuations in nuclei, quantum dots and many other systems (see for a review, for example, Ref.[13]). The success of RMT is determined by the study the statistical laws governing fluctuations having very different origins. Regarding the relativistic heavy ion collision data the study of fluctuation properties of the momentum distribution of emitted particles could provide an information about i) possible errors in measurements and ii) kinematical and dynamical correlations of the composite system.

Let us consider the discrete spectrum $\{E_i\}, i = 1, \dots, N$ of a d-dimensional quantum system (d is a number of degrees of freedom). A separation of fluctuations of a quantum spectrum can be based on the analysis of the density of states below some threshold E

$$S(E) = \sum_{i=1}^N \delta(E - E_i). \quad (1)$$

We can define a staircase function

$$N(E) = \int_{-\infty}^E S(E') dE' = \sum_{i=1}^N \theta(E - E_i), \quad (2)$$

giving the number of points on the energy axis which are below or equal to E . Here

$$\theta(x) = \begin{cases} 0 & \text{for } x < 0 \\ 1 & \text{for } x > 0 \end{cases} \quad (3)$$

We separate $N(E)$ in a smooth part $\zeta(E)$ and the remainder that will define the fluctuating part $N_{\text{fl}}(E)$

$$N(E) = \zeta(E) + N_{\text{fl}}(E) \quad (4)$$

The smooth part $\zeta(E)$ can be determined either from semiclassical arguments or using a polynomial or spline interpolation for the staircase function.

To study fluctuations we have to get rid of the smooth part. The usual procedure is to "unfold" the original spectrum $\{E_i\}$ through the mapping $E \rightarrow x$

$$x_i = \zeta(E_i), \quad i = 1, \dots, N \quad (5)$$

Now we can define spacings $s_i = x_{i+1} - x_i$ between two adjacent points and collect them in a histogram. The effect of mapping is that the sequence $\{x_i\}$ has on the average a constant mean spacing (or a constant density), irrespective of the particular form of the function $\zeta(E)$ [14]. To characterize fluctuations one deals with different correlation functions [8]. In this paper we will use only a correlation function related to spacing distribution between adjacent levels. Below, we follow a simple heuristic argument due to Wigner [15] that illustrates the presence or absence of level repulsion in an energy spectrum.

For a random sequence, the probability that the level will be in the small interval $[x_0 + s, x_0 + s + ds]$ is independent of whether or not there is a level at x_0 . Given a level at x_0 , let the probability that the next level be in $[x_0 + s, x_0 + s + ds]$ be $p(s)ds$. Then for $p(s)$, the nearest-neighbor spacing distribution, we have

$$p(s)ds = p(1 \in ds | 0 \in s)p(0 \in s) \quad (6)$$

Here, $p(n \in s)$ is a probability that the interval of length s contains n levels and $p(n \in ds | m \in s)$ is the conditional probability that the interval of length ds contains n levels when that of length s contains m levels. One has $p(0 \in s) = \int_s^\infty p(s')ds'$, the probability that the spacing is larger than s . The term $p(1 \in ds | 0 \in s) = \mu(s)ds$ [$\mu(s)$ is the density of spacings s], depends explicitly on the choices, 1 and 0, of the discrete variables n, m . As a result, one obtains $p(s) = \mu(s) \int_s^\infty p(s')ds'$ which can be solved to give

$$p(s) = \mu(s) \exp\left(-\int_0^s \mu(s')ds'\right) \quad (7)$$

The function $p(s)$ and its first moment are normalized to unity,

$$\int_0^s p(s)ds = 1, \quad \int_0^s sp(s)ds = 1. \quad (8)$$

For a linear repulsion $\mu(s) = \pi s/2$ one obtains the Wigner surmise,

$$p(s) = \frac{\pi}{2}s \exp\left(-\frac{\pi}{4}s^2\right), \quad s \geq 0 \quad (9)$$

For a constant value $\mu(s) = 1$ one obtains the Poisson distribution

$$p(s) = \exp^{-s}, \quad s \geq 0 \quad (10)$$

As discussed above, when quantum numbers of levels are well defined, one should expect for the spacings the Poisson type distribution, while a Wigner type distribution occurs

due to either internal or external perturbations that destroy these quantum numbers. In fact, one of the sources of external perturbations can be attributed to the uncertainty in the determination of the momentum distribution of emitted particles in relativistic heavy ion collisions. We make a conjecture that the above discussed ideas of the RMT are applicable to the momentum distribution as well. We assume that the momentum distribution may be associated with eigenstates (quantum levels) of a composite system. The difference between energy and momentum is inessential for pions (see below), while we assume that the proton mass should not affect significantly the correlation function.

Another possibilities are the association of the momentum distribution to the spectrum of scattering matrix, or density matrix, which can equally be the object of statistical analysis. Note also, that here we are dealing with the momentum distribution in the target rest frame only, postponing its comparison to that in the center of mass frame, which is more natural for description of interaction. Therefore, we simply replace in Eqs.(1)-(5) the variable E by the variable $|p|$ and construct the corresponding correlation function $p(s)$.

To test the utility and the validity of the proposal we use the experimental data that have been obtained from the 2-m propane bubble chamber of LHE, JINR [16, 17]. The chamber, placed in a magnetic field of 1.5 T, was exposed to beams of light relativistic nuclei at the Dubna Synchrophasotron. Practically all secondaries, emitted at a 4π total solid angle, were detected in the chamber. All negative particles, except those identified as electrons, were considered as π^- -mesons. The contaminations by misidentified electrons and negative strange particles do not exceed 5% and 1%, respectively. The average minimum momentum for pion registration is about 70 MeV/c. The protons were selected by a statistical method applied to all positive particles with a momentum of $|p| > 500$ MeV/c (we identified slow protons with $|p| \leq 700$ MeV/c by ionization in the chamber). In this experiment, we had got 20407 ^{12}CC interactions at a momentum of 4.2A GeV/c (for methodical details see [17]) contents 4226 events with more than ten tracks of charged particles. Thus, it was known in advance the accuracy of measurements for available range of the momentum distribution of secondary particles. Consequently, our analysis has been done for different range of values of the momentum distribution to illuminate the degree of the accuracy.

On Fig. 1 the dependence $dN/d|p|$ as a function of the measured momentum (0.15-7.5 GeV/c) of the secondary particles is displayed. The numerical data $N(p)$ were approximated by the polynomial function of the sixth order and we obtain the distribution of various spacings s_i in 2636 events satisfying the condition of χ^2 per degree of freedom less than 1.0. Momenta are well defined in the region 0.15-1.14 GeV/c (region I, Fig. 2a), where the minimal value of the proton momentum is 0.15 GeV/c. The intermediate region (region II, Fig. 2b) covers the values 1.14-4.0 GeV/c. The region 4.0-7.5 GeV/c is the less reliable one (Fig. 2c). The spacing probability nicely reproduces this tendency depending on the region of the momentum distribution. The function $p(s)$ has the Poisson distribution for the region I, where the momentum distribution was defined with a high accuracy. The region II corresponds to the intermediate situation, when the spacing distribution lies between the Poisson and the Wigner distributions. The less reliable region of the values has a Wigner type distribution for the spacing probability (Fig. 2c). Indeed, the distribution reflects a strong deviation from the regular behavior, observed for the measurements with a high degree of the accuracy.

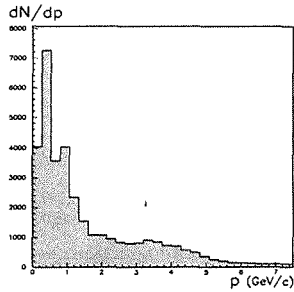


Fig.1 $dN/d|p|$ as a function of the measured momentum of the secondary particles

Summarizing, we propose a method to analyse data obtained at relativistic heavy ion collisions. The method does not depend on the background of the measurements and provides a reliable information about correlations brought about by external or internal perturbations. In particular, we demonstrate that the method manifests the perturbations due to the uncertainty in the determination of the momentum distribution of secondary emitted particles.

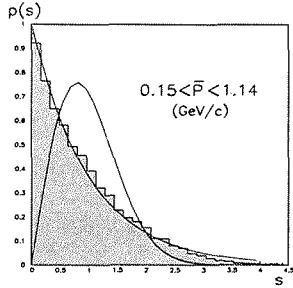


Fig.2 a

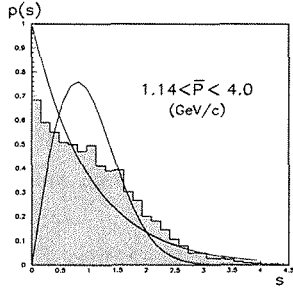


Fig.2 b

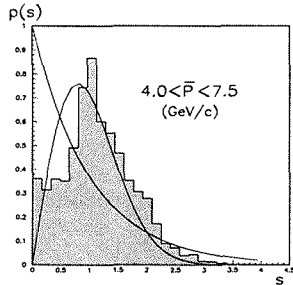


Fig.2 c Nearest-neighbor spacing momentum distribution $p(s)$ for different regions of measured momenta: a) $0.15 < |p| < 1.14$ GeV/c; b) $1.14 < |p| < 4.0$ GeV/c; c) $4.0 < |p| < 7.5$ GeV/c. The solid line is the Wigner-Dyson distribution and the dashed line is the Poisson distribution

Acknowledgments

This work was partly supported by Grant No. BFM2002-03241 from DGI (Spain). R. G. N. gratefully acknowledges support from the Ramón y Cajal programme (Spain).

References

- [1] E. A. De Wolf, I. M. Dremin, and W. Kittel, *Usp. Fiz. Nauk* **163**, 3 (1993).
- [2] E. Byckling, K. Kajantie, *Particle Kinematics* (John Wiley & Sons, London, 1973).
- [3] G. I. Kopylov, *Bases of Resonans Kinematics* (Nauka, Moscow, 1970).
- [4] M. I. Podgoretsky, *Particle and Nuclei*, **22**, 628 (1989).
- [5] B. R. Frieden, *Picture Processing and Digital Filtering*, **6**, 232 (Springer-Verlag, 1975).
- [6] L. M. Soroko, JINR Communication, 1-5030. Dubna (1970).
- [7] Fu Jinghua and Liu Lianshou, *Phys. Rev. C* **68**, 064904 (2003).
- [8] M. L. Mehta, *Random Matrices* Second ed.(Academic, New York, 1991).
- [9] C. E. Porter, *Statistical Theories of Spectra: Fluctuations* (Academic, New York, 1965).
- [10] T. A. Brody, J. Flores, J. B. French, P. A. Mello, A. Pandey, and S. S. M. Wong, *Rev. Mod. Phys.* **53**, 385 (1981).
- [11] O. Bohigas, M. J. Giannoni, and C. Schmit, *Phys. Rev. Lett.* **52**, 1 (1984).
- [12] W. D. Heiss, R. G. Nazmitdinov, and S. Radu, *Phys. Rev. Lett.* **72**, 2351 (1994); *Phys. Rev. C* **52**, R1179 (1995); *ibid.* **52**, 3032 (1995).
- [13] T. Cuhnr, A. Müller-Groeling, and H. Weidenmüller, *Phys. Rep.* **299**, 189 (1998).
- [14] O. Bohigas, *Lecture Notes in Physics* **263**, 18 (Springer-Verlag, 1986).
- [15] E. P. Wigner, Contribution to *Conference on neutron physics by time-of-flight*, Gatlinburg, Tennessee 1956, reprinted in Ref.[9].
- [16] The BBCDHSSTTU-BW Collaboration, A. U. Abdurakhimov *et al.*, *Phys. Lett. B* **39**, 371 (1972).
- [17] N. Akhbabian *et al.*, JINR Report No. 1-12114, 1979.

IV.
MULTIPARTICLE
DYNAMICS

Λ AND K_s^0 PRODUCTION IN pC COLLISIONS AT 10 GeV/c

P.Zh.Aslyan^{1,2†}, V.N.Emelyanenko¹, G.G. Rikhkvitzkaya¹

vskip 5mm (1) *Joint Institute for Nuclear Research*

(2) *Yerevan State University*

† *E-mail: paslanian@jinr.ru*

Abstract

The experimental data from the 2m propane bubble chamber have been analyzed for $pC \rightarrow \Lambda(K_s^0)X$ reactions at 10 GeV/c. The estimation of experimental inclusive cross sections for Λ and K_s^0 production in the $p^{12}C$ collision is equal to $\sigma_\Lambda = 13.3 \pm 1.7$ mb and $\sigma_{K_s^0} = 3.8 \pm 0.6$ mb, respectively.

The measured Λ/π^+ ratio from pC reaction is equal to $(5.3 \pm 0.8) \cdot 10^{-2}$. The experimental Λ/π^+ ratio in the pC reaction is approximately two times larger than the Λ/π^+ ratio from pp reactions or from simulated pC reactions by FRITIOF model for the same energy. The Λ/π^+ ratio in interaction C+C at momentum 10 GeV/c is four times larger than the Λ/π^+ ratio from p+p reactions at the same energy.

The investigation has been performed at the Veksler and Baldin Laboratory of High Energies, JINR.

1. Introduction

Strangeness enhancement has been extensively discussed as a possible signature for the quark-gluon plasma (QGP) [1, 2]. Strange particle production has also been analyzed regarding such reaction mechanisms as the multinucleon effect [3], or the fireball effect [4], or the deconfinement signal, within the context of thermal equilibration models [5]-[8].

In particular, strange particles have been observed extensively on hadron - nucleus and nucleus-nucleus collisions 4-15 GeV regions [9]-[14]. The strange hyperon yields [9]-[11] are therefore of great interest as an indicator of strange quark production. The number of Λ s produced in $\bar{p}+Ta$ reaction at 4 GeV/c was 11.3 times larger than that expected from the geometrical cross section [9]. Experiments with Si+Au and Au+Au collisions at 11.6 [13] and 14.6 A GeV/c [14] measured a K^+/π^+ ratio in heavy-ion reactions that is four to five times larger than the K^+/π^+ ratio from p+p reactions at the same energy. The thermal model [6] gives a good description of K^+/π^+ , Λ/π^+ ratio for data Au+Au, Si+Au interaction at momenta 10-15 A GeV/c and, showing a broad maximum at the same energies.

However, there have not been sufficient experimental data concerning strange-hyperon production over 10-40 GeV/c momentum range. In this paper the new results are presented: the measured inclusive cross sections for $\Lambda(K_s^0)$ production and Λ/π^+ ratio in the reaction $p+^{12}C$.

2. Experimental procedure

2.1. METHOD

Searching for the V^0 on ≈ 700000 (or 345×2 tapes) photographs of the JINR 2m propane bubble chamber exposed to a 10GeV/c proton beam [16]-[21]. The primary proton beams must be to satisfy of conditions: $|tg\alpha| < 0.02$ $1.62 < \beta < 1.69$ rad. The magnetic field ($B=15.2$ kG) measurement error is $\Delta B/B=1\%$. The fit GRIND -based program GEOFIT[18] is used to measure the kinematics track parameter p , α , β . Measurements were repeated three times for events which failed in reconstruction by GEOFIT.

The estimate of ionization, the peculiarities of the end track points of stopping particles permitted one to identify them over the following momentum ranges : protons of $0.150 \leq p \leq 0.900$ GeV/c and $K^\pm of p \leq 0.6$ GeV/c.

2.2. Identification of Λ and K_s^0

The events with V^0 (Λ and K_s^0) were identified using the following criteria [19, 20]:

1) V^0 stars from the photographs were selected according to $\Lambda \rightarrow \pi^- + p$, neutral $K_s \rightarrow \pi^- + \pi^+$ or $\gamma \rightarrow e^+ + e^-$ hypothesis. A momentum limit of K_s^0 and Λ is greater than 0.1 and 0.2 GeV/c, respectively ; 2) V^0 stars should have the effective mass of K_s^0 and of Λ 3) these V^0 stars are directed to some vertices(complanarity); 4) they should have one vertex, a three constraint fit for the M_K or M_Λ hypothesis and after the fit, $\chi_{V^0}^2$ should be selected over range less than 12; 5)The analysis has shown[20] that the events with undivided ΛK_s^0 were assumed to be events as Λ .

Table 1 presents (70%) the number of experimental V^0 events produced from interactions of: a) primary proton beams, b)secondary charged particles and c)secondary neutra particles.

The V^0 s classified into three grades. The first grade comprised V^0 s which could be identified with above cuts and bubble densities of the positive track emitted from the V^0 s. The second grade comprised V^0 s which could be undivided ΛK_s^0 . For correctly identification the undivided V^0 s are used the α (Fig.1a) and the $\cos\theta_{\pi^-}^*$ (Fig.1b) distributions.

$$\alpha = (P_{\parallel}^+ - P_{\parallel}^-)/(P_{\parallel}^+ + P_{\parallel}^-)$$

Where P_{\parallel}^+ and P_{\parallel}^- are the momentum components of positive and negative charged track from the V^0 s relative direction of the V^0 s momentum.The

$\cos\theta_{\pi^-}^*$ is the angular distribution of π^- from K_s^0 decay. The α (Fig.1a) and the $\cos\theta_{\pi^-}^*$ distributions from K_s^0 decay were isotropic in the K_s^0 rest frame after removing undivided ΛK_s^0 . Then these ΛK_s^0 events appropriated events as Λ . After we show in Fig.1c that the $\cos\theta_{\pi^-}^*$ distributions for the $\Lambda + \Lambda K_s^0$ s have been also isotropic in V^0 rest frame. As a result of above procedure have lost of K_s^0 8.5% and admixture of K_s^0 in Λ s events 4.6%. The third grade comprised V^0 s which could be the invisible V^0 s at a large azimuth angle ϕ [20]. The average ϕ weights were $\langle w_\phi \rangle = 1.06 \pm 0.02$ for K_s^0 and $\langle w_\phi \rangle = 1.14 \pm 0.0$ for Λ .

Figures.2a,c and 2b,d show the effective mass distribution of Λ (8657-events), K^0 (4122 events) particles and their χ^2 from kinematics fits, respectively, produced from the bear protons interacting with propane targets. The measured masses of these events have th

following Gaussian distribution parameters $\langle M(K_s) \rangle = 497.7 \pm 3.6$, s.d. = 23.9 MeV/c² and $\langle M(\Lambda) \rangle = 1117.0 \pm 0.6$, s.d. = 10.0 MeV/c². The masses of the observed Λ , K_s^0 are consistent with their PDG values. The expected functional form for χ^2 is depicted with the dotted histogram(Fig.2).

Each V^0 event weighted by a factor w_{geom} ($=1/e_\tau$), where e_τ is the probability for potentially observing the V^0 , it can be expressed as

$$e_\tau = \exp(-L_{min}/L) - \exp(-L_{max}/L),$$

where $L(=c\tau M)$ is the flight length of the V^0 , L_{max} the path length from the reaction point to the boundary of fiducial volume, and L_{min} (0.5 cm) an observable minimum distance between the reaction point and the V^0 vertex. M, τ , and p are the mass, lifetime, and momentum of the V^0 . The average geometrical weights were 1.34 ± 0.02 for Λ and 1.22 ± 0.04 for K^0 .

Now, let us examine a possibility from neutron stars of imitating Λ and K_s^0 the using model FRITIOF[22] for the hypotheses reaction $p+C \rightarrow n+X, n+n \rightarrow \pi^- p$ (or $\pi^- \pi^+ \pi^+$) + X^0 with including fermi motion in carbon. Then, these background events were analyzed by using the same experimental condition for the selection V^0 s. The 2 vertex analysis have shown the background from neutron stars are equal to 0.1% for Λ and 0.001 for K_s^0 events.

2.3. The selection of interactions on carbon nucleus

The criteria for selection of interaction with carbon has shown[19, 25]. The $p+C \rightarrow \Lambda(K_s^0)X$ reaction were selected by the following criteria:

1. $Q = n_+ - n_- > 2$;
2. $n_p + n_\Lambda > 1$;
3. $n_p^b + n_\Lambda^b > 0$;
4. $n_- > 2$;
5. $n_{ch} = \text{odd number}$;
6. $\frac{E_p(\Lambda) - P_{p(\Lambda)} \cos \Theta_{p(\Lambda)}}{E_p(\Lambda) - P_{p(\Lambda)} \cos \Theta_{p(\Lambda)}} > 1$.

n_+ and n_- are the number of positive and negative particles on the star; n_p and n_Λ are the number protons and Λ hyperons with momentum $p < 0.75$ GeV/c on the star. n_p^b and n_Λ^b are the number protons and Λ hyperons to emitted in backward direction. $E_{p(\Lambda)}$, $P_{p(\Lambda)}$ and $\Theta_{p(\Lambda)}$ are a energy, a momentum and a emitted angle of protons(or Λ s) in the Lab. system. m_t is the mass of target. These criteria were separated ≈ 83 % from all inelastic $p+C$ interactions[25]. The $p+C$ events were selected by the above criteria the using FRITIOF model [22]. Results of the simulation have lost 18% and 20% from interactions $pC \rightarrow \Lambda X$ and $pC \rightarrow K_s^0 X$, respectively. The contribution from $pp \rightarrow \Lambda X$ and $pp \rightarrow K_s^0 X$ in pC interactions are equal to 1.0% and 0.3%, respectively.

3. The measured cross sections Λ and K^0

The cross section is defined by the formula:

$$\sigma = \frac{\sigma_0}{e} \prod_i w_i = \frac{\sigma_r * N_r^{V^0} * w_{hyp} * w_{geom} * w_\phi * w_{kin} * w_{int}}{N_{int}^r * e_1 * e_2 * e_3}, \quad (3.1)$$

where e_1 is the efficiency of search for V^0 on the photographs, e_2 the efficiency of measurements. The V^0 s of 75%(preliminary) could be successfully reconstructed and accepted in the analysis. e_3 the probability of decay via the channel of charged particles ($\Lambda \rightarrow p\pi^-, K^0 \rightarrow \pi^+\pi^-$), $\sigma_0 = \sigma_r/N_r$ the total cross section, where σ_r is the total cross section for registered events, N_r is the total number of registered interactions of beam protons over the range of the chamber. $\sigma_t(p + C_3H_8) = 3\sigma_{pC} + 8\sigma_{pp} = (1456 \pm 88)\text{mb}$ [27], where σ_t, σ_{pC} and σ_{pp} are the total cross sections in interactions $p + C_3H_8, p+C$ and $p+p$, respectively. The propane bubble chamber method have been permitted the registration the part of all elastic interactions with the propane [23, 24] therefore the total cross section of registered events is equal to: $\sigma_r(p + C_3H_8) = 3\sigma_{pC}(inelastic) + 8\sigma_{pp}(inelastic) + 8\sigma_{pp}(elastic)0.70 = (1049 \pm 60)\text{mb}$.

w_i are weights for the lost events with V^0 for (Table 2): w_{geom} - the V^0 decay outside the chamber; w_ϕ - the required isotropy for V^0 in the azimuthal (XZ) plane; w_{hyp} - the undivided ΛK_s^0 events; w_{int} - the selected as $p + {}^{12}C$ from the interaction of $p + C_3H_8$; w_{kin} - the kinematic conditions (with FRITIOF); w_{int} - the $V^0 +$ propane interactions.

Table 3 show that the experimental cross sections are calculated by formula 3.1 for inclusive Λ hyperons and K_s^0 mesons productions in the interactions of pp and pC at beam momentum 10 GeV/c.

Ratios of average multiplicities Λ hyperons and K_s^0 mesons to multiplicities π^+ mesons in p+C interaction at beam momenta 4.2 GeV/c and 10 GeV/c show in Table 4. Experimental data on multiplicities π^+ mesons in the interactions of pC at momenta 4.2 GeV/c ($\langle n_{\pi^+} \rangle = 0.71 \pm 0.01$) and 10 GeV/c ($\langle n_{\pi^+} \rangle = 1.0 \pm 0.05$) taken from publications [26] and [25], respectively.

The Λ/π^+ ratio for C+C reaction is shown in Table 5 and on Fig.3. This ratio have been obtained by using the Glauber approach on the experimental cross section for $p+C \rightarrow \Lambda X$ reaction.

4. Conclusion

The experimental data from the 2 m propane bubble chamber have been analyzed for $pC \rightarrow \Lambda(K_s^0)X$ reactions at 10 GeV/c. The estimation of experimental inclusive cross sections for Λ and K_s^0 production in pC collisions is equal to $\sigma_\Lambda = 13.3 \pm 1.7$ mb and $\sigma_{K_s^0} = 3.8 \pm 0.6$ mb, respectively. The measured Λ/π^+ ratio in pC and pp reactions is equal to $(5.3 \text{ } 0.8) \cdot 10^{-2}$ and $(2.7 \text{ } 0.4) \cdot 10^{-2}$, respectively. The experimental Λ/π^+ ratio in the pC reaction is approximately two times larger than the Λ/π^+ ratio from pp reactions or from simulated pC reactions by FRITIOF model for the same energy. The Λ/π^+ ratio in C+C collisions at 10.0 A GeV/c obtained that is four times larger than the Λ/π^+ ratio from p+p reactions at the same energy.

Table 1: The amount (70 %) of V^0 events from interactions of different types which were registered on photographs with propane bubble chambers method.

Chanel	The amount events from interactions.:			Total events
	primary beam protons	sec. charged particles	sec. neutral particles	
$\rightarrow \Lambda(\text{only})x$	5276	2814	1063	9387
$\rightarrow K_s^0(\text{only})x$	4122	1795	481	6543
$\rightarrow (\Lambda \text{ and } K_s^0) x$	3381	1095	376	4608

Table 2: Weight of the lost experimental events with Λ and K_s^0 for pC and pp interactions.

Type of reaction	$1/e_1$	$1/e_2$	w_{geom}	w_ϕ	w_{int}	w_{kin}	$1/e_3$	W_{sum}
pC $\rightarrow \Lambda X$	1.14	1.25	1.34	1.14	1.11	1.18	1.56	4.37 ± 0.37
pp $\rightarrow \Lambda X$	1.14	1.25	1.36	1.14	1.11	1.37	1.56	5.15 ± 0.44
pC $\rightarrow K_s^0 X$	1.14	1.25	1.22	1.06	1.04	1.04	1.47	2.93 ± 0.25
pp $\rightarrow K_s^0 X$	1.14	1.25	1.36	1.06	1.05	1.06	1.47	3.31 ± 0.28

Table 3: Cross sections Λ hyperons and K_s^0 mesons for pp and pC interactions at beam momentum 10 GeV/c.

Type of reaction	$N_{V^0}^{exp.}$	W_{sum}	$N_{V^0}^t$ Total	$n_{V^0} = N_{V^0}^t / N_{in}$	σ mb
pC $\rightarrow \Lambda X$	6126	4.37 ± 0.37	26770	0.053 ± 0.005	13.3 ± 1.6
pp $\rightarrow \Lambda X$	836	5.15 ± 0.44	4303	0.026 ± 0.003	0.80 ± 0.08
pC $\rightarrow K_s^0 X$	3188	2.93 ± 0.25	9341	0.018 ± 0.002	3.8 ± 0.5
pp $\rightarrow K_s^0 X$	699	3.31 ± 0.28	2313	0.015 ± 0.001	0.43 ± 0.04

Table 4: Ratios of average multiplicities Λ hyperons and K_s^0 mesons to multiplicities π^+ mesons for p+C interaction at beam momenta 4.2 GeV/c and 10 GeV/c.

	pC This experiment (10 GeV/c)	pC FRITIOF (10 GeV/c)	Cp Experiment (4.2 GeV/c)	Cp FRITIOF (4.2 GeV/c)
$\langle n_\Lambda \rangle / \langle n_{\pi^+} \rangle \times 10^2$	5.3 ± 0.8	2.6	0.7 ± 0.3	0.9
$\langle n_{K_s^0} \rangle / \langle n_{\pi^+} \rangle \times 10^2$	1.8 ± 0.3	1.8	0.3 ± 0.2	0.3

Table 5: Ratios of average multiplicities Λ hyperons to multiplicities π^+ mesons for C+C interactions at beam momentum 4.2 and 10 GeV/c.

	4.2 Experiment	10 Experiment
$\langle n_\Lambda \rangle / \langle n_{\pi^+} \rangle \times 10^2$	2.0 ± 0.6	10.9 ± 1.7

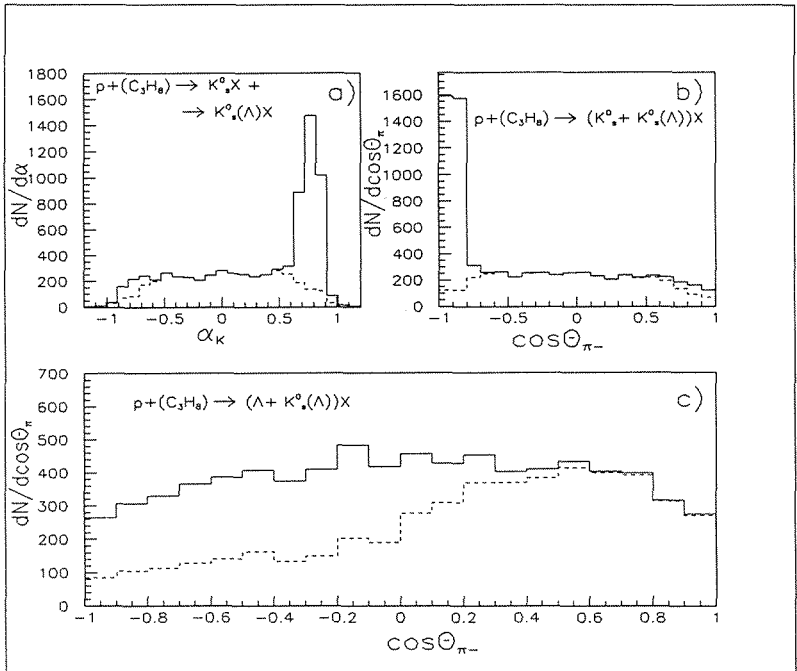


Figure 1: Distributions of α (Armenteros parameter) and $\cos\Theta^*$ are used for correctly identification of the undivided V0s. $\alpha = (P_{\parallel}^+ - P_{\parallel}^-) / ((P_{\parallel}^+ + P_{\parallel}^-))$. Where P_{\parallel}^+ and P_{\parallel}^- are the parallel components of momenta positive and negative charged tracks. $\cos\Theta^*$ is the angular distribution of π^- from K_s^0 decay. Distributions of α and $\cos\theta^-$ were isotropic in the rest frame of K_s^0 when undivided ΛK_s^0 were assumed to be events as Λ

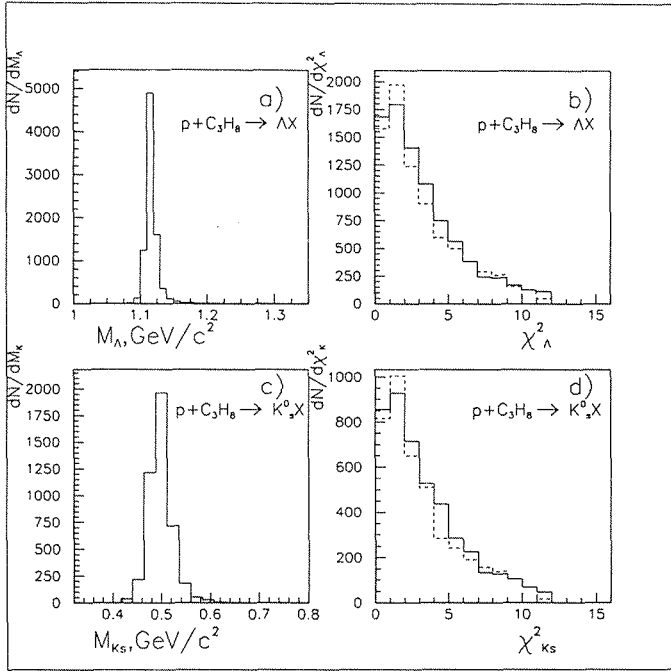


Figure 2: The distribution of experimental V^0 events produced from interactions of beam protons with propane: a) for the effective mass of M_Λ ; b) for $\chi_\Lambda^2(1V - 3C)$ of the fits via the decay mode $\Lambda \rightarrow \pi^- + p$; c) for the effective mass of $M_{K_s^0}$; d) for $\chi_{K_s^0}^2(1V - 3C)$ of the fits via decay mode $K_s^0 \rightarrow \pi^- + \pi^+$. The expected functional form for χ^2 is depicted with the dotted histogram

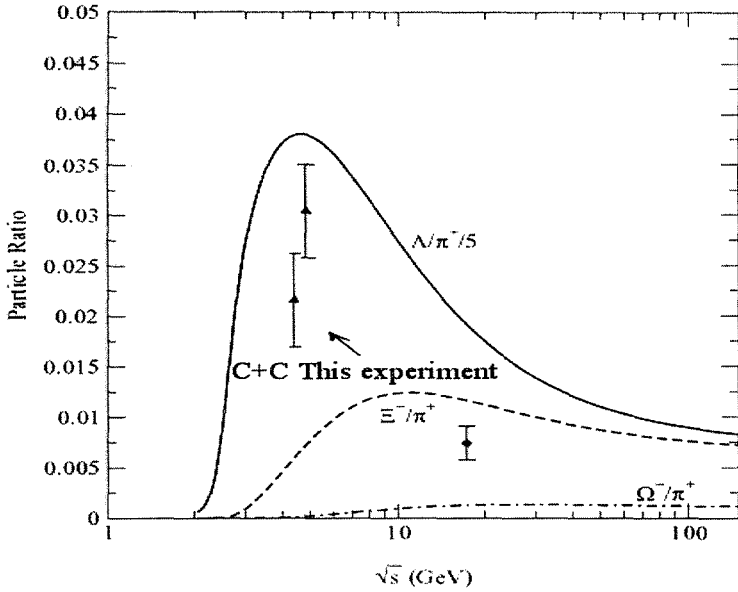


Figure 3: Prediction of the statistical-thermal model[6] for Λ/π^+ (note the factor 5), and Ξ^-/π^+ and Ω^-/π^+ ratios a function of \sqrt{s} . For compilation of AGS data see [7]. The Λ/π^+ ratio in interaction C+C on figure is obtained by using data from this experiment

References

- [1] J.Rafaelski et al., PHYS. Lett. 91B,281,1980; Phys. Rev. Lett. 48, 1066,1982.
- [2] P.Koch, J.Rafaelski and W.Greiner, Phys. Lett. 123B, 151, 1983.
- [3] J.Rundrup and C.M.Ko, Nucl.Phys. A343, 519, 1980.

- [4] F.Asai, H.Sato and M.Sano, Phys. Lett. 98B, 19, 1981.
- [5] J. Cleymans and K.Redlich, Phys.Rev. C60(1999).
- [6] P. Braun-Munzinger et al.,Nucl.Phys.A697:902-912,2002; Phys. Lett. B 344, 43, 1995.
- [7] F. Becattini et al, PHYS. REV. C24,024901,2001;hep-ph/0002267.
- [8] M. Gazdzicki, hep-ph/0305176v2,2003.
- [9] K. Miyano et al., Phys. Rev. C38 (1988).
- [10] M. Anikina et al., Phys. Rev. Lett. 50 (1971).
- [11] S. Albergo,et. al.,Phys. Rev. Lett. 88,v.6, 2002.
- [12] B. Back et al.,E866, E917 Collaborations, nucl-ex/9910008.
- [13] L. Ahle et al., Phys. Rev. C60 (1999), Phys.Lett B476(2000)1.
- [14] T. Abbott et al., Phys. Lett. B 291, 341 (1991); T. Abbott et al., Phys. Rev. C 50, 1024 (1994).
- [15] Compilation of cross-sections, CERN-HERA 79-03,1979;
- [16] M.Balandin et al., Nucl.Instr. and Meth.,20.,p.110,1963.
- [17] A.I. Bondarenko et al., JINR Commun., Dubna,P1-98-292,1998.
- [18] K.P.Vishnevskaya et al., JINR Commun., 1-5978,1971.
- [19] D.A.Armutlijski et. al., Yad. Fiz.,1986,43(2),p.366,37.
- [20] E.N.Kladnitskaya , K.J.Jovchev , P1-86-166 JINR, S.G. Arakelian et al., JINR Commun., 1-82-683, 1982.
- [21] P.Z.Aslyan et al., JINR Commun., E1-2001-265,2002
- [22] FRITIOF, H. Pi, Comput. Phys.Commun. 71(1992)173.
- [23] N.O.Akhababian et al., JINR Commun., 1-82-445, 1982; Yad.Phys.,v.37, p. 124, 1983.
- [24] G.N.Agakshiev et al., JINR Commun, 1-83-662, 1983.
- [25] D.A.Armutlijski et. al.,JINR Commun.,P1-86-459,1986;JINR Commun.,P1-87-423,1987.
- [26] A.S.Galoian et al., JINR Commun., P1-2002-54, 2002:Journal of Nuclear Physics(Russian),v.66,num.5,p.868,2003.
- [27] B.S. Barashenkov, V.D. Toneev,"Interactions of particles and nucleus with nucleus. Atomizdat, 1972.

SEARCH FOR SCALING PROPERTIES IN MANY-PARTICLE STOCHASTIC PROCESSES

B. Słowiński

Institute of Atomic Energy, Otwock-Świerk, Poland

Faculty of Physics, Warsaw University of Technology, Warsaw, Poland

E-mail: slowb@if.pw.edu.pl

Abstract

A brief overview of the scaling properties arising in phenomena of radiation passage through dense media and high energy nuclear reactions is done. A suggestion is put forward that the revealing of scaling in all these processes are mainly a consequence of their multiparticle stochastic nature and, so, the depletion of correlation between elementary constituent acts of interaction.

I. INTRODUCTION

The search for scaling properties arising in various structures and phenomena has become during several last tens of years a convenient tool of investigations, and it is even the main goal of these investigations although the notion itself has not been strictly determined till now. Nevertheless, in a broad sense, usually one keeps in mind some kind of universality of the relation between observables describing the investigated phenomenon and/or structure. But this universality should not result directly from known laws of nature (i.e. laws of conservation or, for example, basic statistic distributions, such as Boltzman, Fermi-Dirac and Bose-Einstein distributions) to simply avoid a trivial substitution of notions.

The quest of the scaling has also a practical meaning as a method of contraction of information about the process under study in a wide range of conditions. Moreover, if the scaling property of a phenomenon is established firmly then any significant deviation may suggest that another effect may appear (for example, a new resonance state on the smooth background of effective mass distribution).

Scaling properties are ubiquitous in several fields of investigation, in particular, in engineering, chemistry, biology, social sciences, astronomy and physics, the most frequently. But so far distinguished unambiguously enough were only two simplest reasons of scaling behavior: geometric similarity and dimensional analysis (for example, [1]). The third reason it seems to be the stochasticity which take place in multi-particle processes such as cascade phenomena arising when high-energy particles penetrate through dense media. In this work briefly discussed are several examples of typical stochastic multi-particle processes of such a kind. The most extensively studied from the viewpoint of scaling properties are till now electron-photon cascades created by high-energy gamma quanta or electrons in dense amorphous materials [2]. Even a cursory examination of these phenomena suggest that we are dealing in this case with some kind of limit regime of their stochastic nature like the central limit theorem of the theory of probability.

II. ELECTROMAGNETIC CASCADES

The electromagnetic cascade (em. cascade or shower) induced by a gamma quantum or electron in a dense amorphous medium consists basically of a sequence and superposition of four dominant elementary electromagnetic processes: pair production as the main breeding process, bremsstrahlung or radiation (also as partly breeding) and ionization of atoms as stopping factors, and Coulomb multiple scattering owing to which the shower acquires a three-dimensional form. Other processes play a considerably smaller part in the energy

balance and space structure formation of the shower, although, for example, Čerenkov radiation is widely used for the detection of photons and electrons. From the practical viewpoint the following shower characteristics are of basic importance: longitudinal and transverse (or lateral) distributions of average ionization loss (or profiles), the relevant fluctuations and correlations (see, for instance, [2] and references quoted herein).

II.1. Shower profiles

As a result of experimental investigations performed using different techniques, as well as computer simulation, it has been found that the longitudinal shower profile can be satisfactorily approximated by the gamma function:

where the parameters a_1 , a_2 and a_3 are to be calculated as the best fit to the concrete experi-

$$F_t(t) = a_1 t^{a_2} \exp(-a_3 t) \quad (1)$$

mental data [2]. These parameters depend on energy of a particle initiating cascade and a cut-off energy E_c of cascade particles (usually E_c for shower electrons is typically taken to be about 1-1.5 MeV). Moreover, if the shower depth t (measured from the shower origin) is expressed by the dimensionless ratio $x=t/\langle t(E) \rangle$, where $\langle t(E) \rangle$ is the average cascade depth depending on the energy E of a cascade initiated particle, then the longitudinal profile displays a clear scaling with the energy at least when $E \geq 500$ MeV up to several hundred of GeV, where other processes gradually start, and at $x \geq 0.15$ [3]. Notice that at E_c lower than 1 MeV the parameter a_3 perceptibly diminishes at larger depths as showed our preliminary results of modeling showers using EGS4 code [4].

Much more complicated is the situation concerning the transverse shower profile [2,3]. But again, if the shower width r is expressed by the similar as above dimensionless ratio $x=r/\langle p(t,E) \rangle$, where $\langle p(t,E) \rangle$ is the average width of a cascade at its depth t , then the transverse profile as well scales with E , at least for primary gamma quanta of energy 500-3500 MeV in liquid xenon [2,3] can be parameterized in the form of the function:

$$F(x) = \int_0^1 [(1/s) + (1/x)] / [s^2 \sqrt{1-s^2}] \exp[-(x/s)] ds.$$

II.2. Shower equations

In the simplest, i.e. one-dimensional approach, the diffusion equations for shower's electrons (and positrons, further also called electrons) and photons have been obtained about 60 years ago [5]. They describe the longitudinal distribution of average numbers of electrons, $n_e(E, E_c, t)$, and photons, $n_\gamma(E, E_c, t)$, along the direction of flight of a particle initiating the shower, as follows [5]:

$$\begin{aligned} \frac{\partial n_e(E, E_c, t)}{\partial t} &= 2 \int_E^\infty n_\gamma(E, E', t) \sum_p(E', E) dE' + \\ &+ \int_E^\infty n_e(E, E', t) \sum_b(E', E' - E) dE' - \int_0^E n_e(E, E', t) \sum_b(E, E') dE' + \epsilon \frac{\partial n_e(E, E_c, t)}{\partial E}; \\ \frac{\partial n_\gamma(E, E_c, t)}{\partial t} &= \int_E^\infty n_e(E, E', t) \sum_b(E', E) dE' - \int_0^E n_\gamma(E, E', t) \sum_p(E, E') dE'. \end{aligned} \quad (2)$$

Here \sum_p and \sum_b are the differential cross-sections of pair creation and bremsstrahlung, correspondingly, ϵ is the average ionization loss of shower's electrons over 1 radiation length (r.l.). But the most often measured quantities are the numbers of electrons $N_e(E, E_c, t)$ with an energy greater than E_c at a shower depth t :

$$N_e(E, E_c, t) = \int_{E_c}^E n_e(E, E', t) dE',$$

or the quantities proportional to $N_e(E, E_c, t)$, such as the differential ionization loss and Čerenkov radiation. They practically correspond to the longitudinal shower's profile [2]. Note also that these equations have very limited practical meaning and apply mainly to very high energies and light media, such as air and water, although surprisingly they reflect correctly the energy dependence of such important shower's characteristics as the position of average shower's depth (also called as the center of gravity) as a function of energy E , $\langle t(E) \rangle$, and the average position of shower's maximum $t(E)_{max}$, both proportional to $\ln E$.

The equations (2) are relatively simple as compared to the analytical description of many other known stochastic processes occurring in nature and having practical and cognitive significance (see, for example, [2,6-8]). However, they are not so transparent to reveal whether the functions $n_e(E, E_c, t)$ and $n_\gamma(E, E_c, t)$, being divided by some energy dependent function, say $\langle t(E) \rangle$, $t(E)_{max}$ or another quantile, become energy independent (and so $N_e(E, E_c, t)$), which is the case actually. The situation is much more complicated when one considers the three-dimensional shower equation (see, for example, [9]).

II.3. Fluctuations

Longitudinal and transverse fluctuations of energy release of shower's electrons also can be described in the roughly universal, i.e. energy independent form when they are expressed as the A-dependence of the rms deviation σ_A from the average fraction A of ionization energy loss deposited along the shower axis and in its transverse direction [2,3]. But these data have been obtained only for gamma quanta of energy 200-3500 MeV producing showers in liquid xenon and are poorly provided by a good statistics.

III. HADRONIC CASCADES

The knowledge of the development of hadronic cascades (also: showers) produced by different high-energy particles in various dense media is indispensable for many purposes, in particular, for hadron calorimetry, radiation protection, spallation reactions and the investigation of radiation hardness of materials. So far a great deal of information concerning as well the longitudinal and transverse distribution of energy release in hadronic showers has been accumulated (see, for instance, [10,11] and references quoted herein). Below we reproduce the results most important from the point of view of scaling description of these important shower characteristics.

III.1. Longitudinal development

The well-known parameterization of the longitudinal development of a hadronic shower consists of the weighted superposition of two distributions, each being of the above indicated form (1) and describing respectively the electromagnetic and hadronic component of

$$dE_s(x) / dx = N \{ w(x / X_0)^{a-1} e^{-b(x / X_0)} + (1-w)(x / \lambda_I)^{a-1} e^{-d(x / \lambda_I)} \}. \quad (3)$$

the shower [11]:

Here X_0 is the r.l. of the material, λ_I is the interaction length, a , b , d , w are parameters, N is the normalization constant, $w=0.4634$ and a and d linearly depend on $\ln E$. Mention also that often it is enough to use simply the one-component distribution, just like (1) only.

III.2. Transverse spread

The typical radial energy density in hadronic showers produced by 100 GeV pions in ion can be parameterized practically by the sum of exponential functions [11]. One can notice its qualitative, at least, resemblance to the relevant distribution describing transverse profiles of em. showers.

IV. NUCLEAR AND HADRONIC REACTIONS AT HIGH ENERGIES

A manifestation of scaling properties is especially common in nuclear and/or hadronic reactions at high enough energies, that is in the field where we have only a set of rules, laws of conservation, various approaches and models, mainly based on Monte-Carlo techniques instead of a comprehensive, practical and predictive theory. At the same time a huge amount of experimental data has been gathered about miscellaneous simple and sophisticated characteristics of these phenomena: multiplicity, energy/momentum, angular distributions of different produced particles, multi-dimensional scatter plots etc. To store and systematize such an information the search for a suitable tool as scaling behavior of these characteristics, previously normalized in an appropriate way, is actively conducted for several years. The most popular are: the Feynman scaling, for inclusive particle production [12], KNO scaling [13], y -scaling in deep inelastic scattering on nuclei [14], z -scaling [15] etc. But the meaning of the scaling laws is not restricted to the problem of compression of information. When established at given conditions (energy or momentum transfer etc) the violation of scaling may indicate that under changed conditions a new phenomenon (e.g. new degrees of freedom) comes into play.

V. CONCLUSIONS

Although information about, in particular, the characteristics of em. and hadronic showers, collected till now is far to be satisfactory one can suggest the following conclusions:

1. The fact that these processes so different in the main, but all being of many-particle nature, admit very similar formal description indicates that the origin of the observed scaling laws is purely stochastic when the physics features of these processes turns out no more important and their purely stochastic character becomes a dominant factor like in the case of the central limit theorem in the theory of probability but for stochastic processes (see also [8]). Moreover, the same suggestion seems to be supported by the fact that em. showers scale with energy in the very similar way as, for example, the well-known KNO scaling (see, for instance, an overview article [12] and references herein), namely, using an average multiplicity of produced particles $\langle n \rangle$ or another central moment as a scaling (normalization) parameter.

2. Usually when saying about scaling in high-energy physics (and not only) one means the possibility of the energy independent representation of some characteristics of the process under consideration. For example, dealing with nuclear reactions one says about nuclear scaling, KNO scaling, z -scaling (see, for example, [15]) etc. But examining a macroscopic process it is also of great importance to investigate whether and to what extent one can describe this process as independent of the properties of the material in which the process takes place. It is evident that to this purpose such quantities as radiation length, Molière unit and interaction length in the case of em. showers, are too rough as scaling parameters. Unfortunately, the attempts to find the relevant scaling parameters for em. cascades propagating in dense amorphous materials showed that this problem is much more complicated [14]. Nevertheless, it seems that the so-called material scaling description of these macroscopic processes is to be achieved and the appropriate representation would be very useful as

well for another processes exclusively important from the practical viewpoint as spallation reactions produced in thick heavy target by relativistic ions and swift ion implantation into materials.

3. The above-discussed scaling properties of many-particle processes have not a strict character since some correlations do always remain on account of, for example, the laws of conservation of energy, momentum, electrical charge, because of the change of regime of the process etc.

References

1. Kurt Wiesenfeld. *Am.J.Phys.* **69**(9), September 2001, p.938-942.
2. B.Śłowiński. *Phys.Part.Nucl.* **25**(2), March-April 1994, 173.
3. B.Śłowiński. *Radiat.Phys.Chem.* V.49, No.3(1997) 327-329.
4. W.R.Nelson, H.Hirayama and D.W.O.Rogers. *The EGS4 Code System.* SLAC-265 (1985).
5. B.Rossi and K.Greisen. *Rev.Mod.Phys.* **13**, 240 (1941).
6. N.G.van Kampen. *Stochastic processes in physics and chemistry.* North-Holland, Tokyo 1987.
7. C.W.Gardiner. *Handbook of stochastic methods for physics, chemistry and the natural sciences.* Sec.ed. Springer-Verlag Berlin, Heidelberg, New York, Tokyo. 1985.
8. J.Jacob and A.N.Shiryayev. *Limits theorems for stochastic processes.* Springer-Verlag, Berlin, Heidelberg, New York, London, Paris, Tokyo, 1987.
9. I.P.Ivanenko. *Electromagnetic cascade processes* [in Russian]. Moscow State University Press, Moscow, 1972.
10. Y.A.Kulchitsky, M.V.Kuzmin, V.B.Vinogradov. *JINR Comm.*, E1-99-326. Dubna, 1999.
11. Y.A.Kulchitsky. *JINR Comm.*, E1-2000-5. Dubna, 2000.
12. R.P.Feynman. *Photon-hadron interaction.* Benjamin, New-York, 1972.
13. A.I.Golokhvastov. *Journ. of Nucl. Phys.*, v.64, N.1 (2001) 88-100.
14. P.Benecke et al., *Phys.Rev.Lett.* **49**, 1380 (1982).
15. I.Zborovsky, M.V.Tokarev, Yu.A.Panebratsev, G.P.Skoro. *Phys.Rev.* **C59** (1999)2227.
14. B.Śłowiński, A.Wojciechowski. *JINR Preprint*, E1-95-537. Dubna, 1995.

STUDY OF MULTIPARTICLE PRODUCTION BY GLUON DOMINANCE MODEL (Part I) ¹

E.S. Kokoulina^{1,2†}, V.A. Nikitin²

(1) *GSTU, Belarus*

(2) *JINR*,

† *E-mail: Elena.Kokoulina@sunse.jinr.ru*

Abstract

The gluon dominance model offers a description of multiparticle production in e^+e^- - annihilation and proton-proton collisions. The multiplicity distributions in e^+e^- annihilation are well described. The energy dependence of model parameters gives the dynamic parton stage and hadronisation picture. It is shown that this model has confirmed oscillations in sign of the ratio of factorial cumulant moments over factorial moments of the increasing order.

The collective behavior of secondary particles in pp -interactions at 70 GeV/c is studied in the project "Thermalization". An active role of gluons is shown in the multiparticle dynamics. This paper gives a simple thermodynamic interpretation of interactions mentioned above.

1. Introduction

At present to investigate and construct a contemporary picture of nuclear matter structure requires to develop new methods and approaches.

Since 80's the Quark-Gluon Plasma conception has undergone a lot of changes after the experiments carried out at CERN (SPS) and BNL (RHIC). Different approaches are used to explain extraordinary phenomena in behavior of the new matter produced at high energy of nuclear collisions [1].

Still there is no single theory nor the model that could explain all the results obtained at RHIC and SPS. We would like to find a solution for this difficult problem by using multiparticle production (MP) in hadron and nucleus interactions. Up to now the nature of "soft" hadronic events has not been fully understood.

A new way to investigate MP at high energy is offered in this work by means of construction a model based on the multiplicity distribution (MD) description using the QCD and phenomenological scheme of hadronisation. The model description of MD in e^+e^- annihilation is given in section 2. The application of this model approach to pp -interaction can be found in section 3.

¹Talk given at the XVII International Baldin Seminar "Relativistic Nuclear Physics and Quantum Chromodynamics". JINR. September 27 to October 2, 2004, Dubna, Russia.

2. MD for e^+e^- -annihilation at high energies

The e^+e^- annihilation is one of the most suitable to study MP. It can be realized through the formation of virtual γ or Z^0 -boson which then decays into two quarks:

$$e^+e^- \rightarrow (Z^0/\gamma) \rightarrow q\bar{q}. \quad (1)$$

The e^+e^- -reaction is simple for analysis, as the produced state is pure $q\bar{q}$. It is usually difficult to determine the quark species on the event-by-event basis. The experimental results are averaged over the quark type. Perturbative QCD (pQCD) may be applied to describe the process of parton fission (quarks and gluons) at big virtuality, because strong coupling α_s is small. This stage can be called as the stage of cascade. When partons get small virtuality, they change into hadrons, which we observe. At this stage we can not apply pQCD. Therefore phenomenological models are used to describe hadronisation in this case.

Parton spectra the quark and gluon fission in QCD were studied by K. Konishi, A. Ukawa and G. Veneciano. The probabilistic nature of the problem has been established [2] while working at the leading logarithm approximation and avoiding IR divergences by considering finite x . Studying MP at high energy we used ideas of A. Giovannini [3] to describe quark-gluon jets as Markov branching processes. Giovannini proposed to interpret the natural QCD evolution parameter $Y = \frac{1}{2\pi b} \ln[1 + \alpha_s b \ln(\frac{Q^2}{\mu^2})]$, where $2\pi b = \frac{1}{6}(11N_C - 2N_f)$ for a theory with N_C colours, N_f flavours and virtuality Q as the thickness of the jets and their development as the Markov process.

Three elementary processes contribute into QCD jets: (1) gluon fission; (2) quark bremsstrahlung and (3) quark pair production. Let $A\Delta Y$ be the probability that gluon will convert into two gluons in the infinitesimal interval ΔY , $\tilde{A}\Delta Y$ be the probability that quark will radiate a gluon, and $B\Delta Y$ be the probability that a quark-antiquark pair will be produced from a gluon. A. Giovannini constructed a system of differential equations for generating functions (GF) of quark $Q^{(q)}$ and gluon $Q^{(g)}$ jets

$$\frac{dQ^{(g)}}{dY} = \tilde{A}Q^{(g)}(Q^{(g)} - 1), \quad \frac{dQ^{(q)}}{dY} = A(Q^{(g)2} - Q^{(g)}) + B(Q^{(q)2} - Q^{(q)})$$

and obtained explicit solutions of MD in the case $B = 0$ (process of quark pair production is absent)

$$P_0^P(Y) = \left(\frac{k_p}{k_p + \bar{m}}\right)^{k_p}, \quad P_m^P(Y) = \frac{k_p(k_p + 1) \dots (k_p + m - 1)}{m!} \left(\frac{\bar{m}}{\bar{m} + k_p}\right)^m \left(\frac{k_p}{k_p + \bar{m}}\right)^{k_p}, \quad (2)$$

where $k_p = \tilde{A}/A$, $\bar{m} = k_p(e^{AY} - 1)$ is the mean gluon multiplicity. These MD are known as negative binomial distribution (NBD). The GF for them is

$$Q^{(g)}(z, Y) = \sum_{m=0}^{\infty} z^m P_m(Y) = [1 + \bar{m}/k_p(1 - z)]^{-k_p}. \quad (3)$$

Two Stage Model (TSM) [4] was taken (2) to describe the cascade stage and added with a sub narrow binomial distribution for the hadronisation stage. We have chosen it basing on the analysis of experimental data in e^+e^- annihilation lower than 9 GeV.

Second correlation moments were negative at this energy. The choice of such distributions was the only one that could describe the experiment. We suppose that the hypothesis of soft decoloration is right. Therefore we add the hadronisation stage to the parton stage for the sake of its factorization. MD in this process can be written as follows:

$$P_n(s) = \sum_m P_m^P P_n^H(m, s), \quad (4)$$

where P_m^P is MD for partons (2), $P_n^H(m, s)$ - MD for hadrons produced from m partons at the stage of hadronisation. Further we substitute variable Y on a center of masses energy \sqrt{s} . MD of hadrons P_n^H formed from one parton and their GF $Q_p^H(z)$ are [4]

$$P_n^H = C_{N_p}^n \left(\frac{\bar{n}_p^h}{N_p} \right)^n \left(1 - \frac{\bar{n}_p^h}{N_p} \right)^{N_p - n}, \quad Q_p^H = \left[1 + \frac{\bar{n}_p^h}{N_p} (z - 1) \right]^{N_p}, \quad (5)$$

where $C_{N_p}^n$ - binomial coefficient, \bar{n}_p^h and N_p ($p = q, g$) have a sense of mean multiplicity and maximum of secondary hadrons are formed from parton at the stage of hadronisation.

MD of hadrons in e^+e^- annihilation are determined by convolution of two stages (cascade and hadronisation)

$$P_n(s) = \sum_{m=0}^{\infty} P_m^P \frac{1}{n!} \frac{\partial^n}{\partial z^n} (Q^H)^{2+m} \Big|_{z=0}, \quad (6)$$

where $2 + m$ is the total number of partons (two quarks and m gluons).

We introduce parameter $\alpha = N_g/N_q$ to distinguish the hadrons, produced from quark or gluon. Also we have carried out simplification for designation $N = N_g, \bar{n}^h = \bar{n}_q^h$. Introducing expressions (2), (5) in (6) and differentiating on z , we obtain MD of hadrons in the process of e^+e^- annihilation in TSM

$$P_n(s) = \sum_{m=0}^{M_g} P_m^P C_{(2+\alpha m)N}^n \left(\frac{\bar{n}^h}{N} \right)^n \left(1 - \frac{\bar{n}^h}{N} \right)^{(2+\alpha m)N - n}. \quad (7)$$

The results of comparison of expression (7) with experimental data [5] are shown in Figs. 1-2. We have obtained that MD in TSM (solid curve) describe well the experimental e^+e^- -data from 14 to 189 GeV [6]. The mean gluon multiplicity \bar{m} has a tendency to rise, but lower than the logarithmic curve. Values k_p remain ~ 10 at almost all energies. One of the most interesting physical senses of this parameter is temperature T [7]: $T \sim k_p^{-1}$.

The next picture of the hadronisation stage is discovered in conformity with parameters of the second stage: N, \bar{n}^h and α . The first parameter N determines the maximum number of hadrons, which can be formed from quark while its passing through this stage. We can imagine that fission is continuous but process (3) (formation $q\bar{q}$ pair) becomes comparable with the other ones (1),(2). We can not reveal a steady energy rise or fall for N .

The second parameter \bar{n}^h has a sense of the mean hadron multiplicity from quark at the second stage. We have found out the tendency to a weak rise with big scattering. The value of \bar{n}^h is about 5 – 6 in the research region. A possible explanation of these rocks for N and \bar{n}^h : only two initial quarks exist among a lot of newly born gluons at the beginning of hadronisation.

The last parameter α was introduced to compare the quark and gluon hadronisation. It is equal to 0.2 with some deviations. If we know α , then we can determine $N_g = \alpha N$ and $\bar{n}_g^h = \alpha \bar{n}^h$ for gluon. It is surprising that gluon parameters remain constant without considerable deviations in spite of the indirect finding: $N_g \sim 3 - 4$ and $\bar{n}_g^h \sim 1$ (Fig. 3-4). Therefore we can confirm the universality of gluon hadronisation. The fact that $\alpha < 1$ shows that hadronisation of gluons is softer than that of quarks.

It was shown [8] that the ratio of factorial cumulative moments K_q over factorial moments F_q changes the sign as a function of the order. We use MD formed in TSM to explain this phenomenon. F_q and K_q are obtained from the relations

$$F_q = \sum_{n=q}^{\infty} n(n-1) \dots (n-q+1) P_n, \quad K_q = F_q - \sum_{i=1}^{q-1} C_{q-i}^i K_{q-i} F_i. \quad (8)$$

The ratio of their quantities is $H_q = K_q/F_q$. The generating function for MD of hadrons (7) in e^+e^- annihilation $Q(z)$ is the convolution

$$Q(z) = \sum_{m=0} P_m^g [Q_g^H(z)]^m Q_q^2(z) = Q^g(Q_g^H(z)) Q_q^2(z). \quad (9)$$

We calculate F_q and K_q in TSM, by using (9) and the sought-for expression for H_q will be [6]

$$H_q = \frac{\sum_{m=1} k_p \alpha m (\alpha m - \frac{1}{N}) \dots (\alpha m - \frac{q-1}{N}) (\frac{\bar{m}}{\bar{m}+k_p})^m \frac{1}{m} - 2(-1)^q \frac{(q-1)!}{N^{q-1}}}{\sum_{m=0} (2 + \alpha m)(2 + \alpha m - \frac{1}{N}) \dots (2 + \alpha m - \frac{q-1}{N}) P_m}. \quad (10)$$

The comparison with experimental data [8] has shown that (10) describes the ratio of factorial moments (Fig. 5). The minimum is seen at $q = 5$. We have obtained that in the region before Z^0 (91.4 GeV), H_q oscillates in the sign only with the period equal to 2 and changes the sign with parity q . At higher energies the period is increased to 4. It can be explained by influence of a more developed cascade of partons with narrow hadronisation.

3. MD in pp -interactions

The study of MD in pp interactions is implemented in the framework of the project "Thermalization". This project is aimed at studying the collective behavior of secondary particles in proton-proton interactions at 70 GeV/c [9]. On the basis of the present understanding of hadron physics, protons consist of quarks and gluons. After the inelastic collision the part of the energy of the initial motive protons are transformed to the inside energy. Several quarks and gluons become free. Our model study has shown that quark branching of initial protons in pp interactions is almost absent from 70 to 800 GeV/c. MP are realized by active gluons. Domination of gluons was first proposed by S. Pokorski and L. Van Hove [10].

Our choice of the MP model is based on comparison with the experimental partial cross section $\sigma(n_{ch})$ in pp interaction at 70 GeV/c on the U-70 accelerator [11] and the present picture of strong interactions.

At the beginning of 90s a successful description of MD at this energy was realized by the quark model (Fig. 6) [12]. This model suggests that one proton quark pair, two

pairs or three can collide and fragment into hadron jets. MD in quark jets were described by Poisson. Second correlation moments of charged particles for MD in this model will be always negative. It is known they are become positive at higher energies. In this model gluons are absent. The calculation by the MC PHYTHIA code has shown that the standard generator predicts a value of the cross section which is in a reasonably good agreement with the experimental data at small multiplicity ($n_{ch} < 10$) but it underestimates the value $\sigma(n_{ch})$ by two orders of the magnitude at $n_{ch} = 18$ (Fig. 6).

We have managed to build a scheme of hadron interactions to describe MD with the quark-gluon language as well as to investigate the high multiplicity region. The mentioned models are very much sensitive in this region.

We consider that at the early stage of pp interactions the initial quarks and gluons take part in the formation of quark-gluon system (QGS). They can give branches. We offer two model schemes. In the first scheme we study hadroproduction with account of the parton fission inside the QGS and build the two stage model with branch (TSMB). If we are not interested in what is going inside QGS, we come to the thermodynamical model (TSTM). Onward we name models involving active gluons into hadroproduction as the gluon dominance models (GDM) [13].

We begin our MD analysis with the scheme of branch. MD for quark and gluon jets may be described NBD and Farry distributions [3], accordingly. On the hadronisation stage we have taken a binomial distribution (5). As in TSM we have used a hypothesis of soft decoloration for quarks and gluons at their while passing of this stage and add the hadronisation stage to the branch one by means of factorization

$$P_n(s) = \sum_m P_m^P(s) P_n^H(m), \quad (11)$$

where $P_n(s)$ - resulting MD of hadrons, P_m^P - MD of partons (quarks and gluons), $P_n^H(m)$ - MD of hadrons (second stage) from m partons. Generating function (GF) for MD in hadron interactions is determined by convolution of two stages:

$$Q(s, z) = \sum_m P_m^P(s) (Q^H(z))^m = Q^P(s, Q^H(z)), \quad (12)$$

where Q^H and Q^P are GF for MD at hadronisation stage and in QGS.

At the beginning of research we took model where some of quarks and gluons from protons participate in the production of hadrons. Parameters of that model had values which differed very much from parameters obtained in e^+e^- annihilation, especially hadronisation parameters. It was one of the main reasons to refuse the scheme with active quarks. After that we chose the model where quarks of protons did not take part in the production of hadrons, but remained inside of the leading particles. All of the newly born hadrons were formed by gluons. We name these gluons active. They could give a branch before hadronisation.

It is important to know how much active gluons are into QGS at the first time after the impact of protons. We can assume that their number may change from zero and higher. It is analogous with the impact parameter for nucleus. Only in the case of elastic scattering the active gluons are absent. The simplest MD to describe the active gluons formed in the moment of impact is the Poisson distribution $P_k = e^{-\bar{k}} \bar{k}^k / k!$, where k and \bar{k} are the number and mean multiplicities of active gluons, correspondingly.

To describe MD in the gluon cascade formed by the branch process of k active gluons, we have used the Farry distribution [3]

$$P_m^B(s) = \frac{1}{\bar{m}^k} \left(1 - \frac{1}{\bar{m}}\right)^{m-k} \cdot \frac{(m-1)(m-2)\dots(m-k+1)}{(k-1)!}, \quad (13)$$

$$P_m^B(s) = \frac{1}{\bar{m}} \left(1 - \frac{1}{\bar{m}}\right)^{m-1}, \quad (14)$$

at $k > 1$ - (13) and at $k = 1$ - (14). m and \bar{m} are the number of secondary gluons and mean multiplicites of them (averaged to all gluons). Expressions (13)-(14) have been obtained from the assumption about the independent branch of gluons

$$Q_k^B = (Q_1^B)^k = \frac{z^k}{\bar{m}^k} \left[1 - z \left(1 - \frac{1}{\bar{m}}\right)\right]^{-k}, \quad Q_1^B = \frac{z}{\bar{m}} \left[1 - z \left(1 - \frac{1}{\bar{m}}\right)\right]^{-1}. \quad (15)$$

In the case $k = 0$ (the impact was elastic and active gluons are absent) MD of hadrons in pp-scattering is equal to $P_2^{el}(s) = e^{-\bar{k}}$.

On the second stage some of active gluons may leave QGS and transform to real hadrons. We can name that gluons "evaporated". Let us introduce parameter δ as the ratio of evaporated gluons, leaving QGS, to all active gluons, which may transform to hadrons. Our binomial distributions for MD of hadrons from the evaporated gluons on the stage of hadronisation are

$$P_n^H(m) = C_{\delta m N}^{n-2} \left(\frac{\bar{n}^h}{N}\right)^{n-2} \left(1 - \frac{\bar{n}^h}{N}\right)^{\delta m N - (n-2)} \quad (16)$$

In this expression the gluon parameters are \bar{n}^h and N (without index "g") which have the same meaning that of the quark parameters. An effect of two leading protons is also taken into account. GF for MD (16) has the following form:

$$Q_m^H = (Q_1^H)^{\delta m} = \left[1 - \frac{\bar{n}^h}{N}(1-z)\right]^{\delta m N}, \quad Q_1^H = \left[1 - \frac{\bar{n}^h}{N}(1-z)\right]^N. \quad (17)$$

MD of hadrons in the process of proton-proton scattering in two stage gluon model with branch (TSMB) is

$$P_n(s) = \sum_{k=1}^{MK} \frac{e^{-\bar{k}} \bar{k}^k}{k!} \sum_{m=k}^{MG} \frac{1}{\bar{m}^k} \frac{(m-1)(m-2)\dots(m-k+1)}{(k-1)!} \cdot \left(1 - \frac{1}{\bar{m}}\right)^{m-k} C_{\delta m N}^{n-2} \left(\frac{\bar{n}^h}{N}\right)^{n-2} \left(1 - \frac{\bar{n}^h}{N}\right)^{\delta m N - (n-2)}. \quad (18)$$

In comparison with experimental data [11] the numbers of gluons in sums on k and m were restricted by values MK and MG as the maximal possible number of gluons on the transition. For comparison we have taken the data at 69 GeV/c because they do not differ from data at 70 GeV/c [11]. χ^2/ndf in are equal to about $\sim 1/3$ at 70 GeV/c and ~ 5 at 69 GeV/c and the parameters are similar. We obtained $N = 40(\text{fix})$, $\bar{m} = 2.61 \pm 0.08$, $\delta = 0.47 \pm 0.01$, $\bar{k} = 2.53 \pm 0.05$, $\bar{n}^h = 2.50 \pm 0.29$ from the comparison with [11]. We can conclude that the branch processes are absent, since parameters \bar{m} and \bar{k} are equal

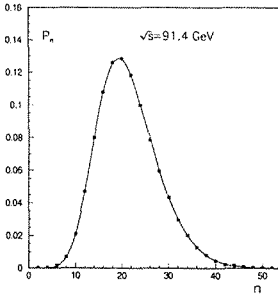


Figure 1: MD at 91.4 GeV

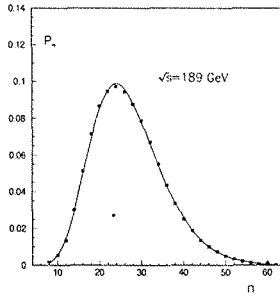


Figure 2: MD at 189 GeV

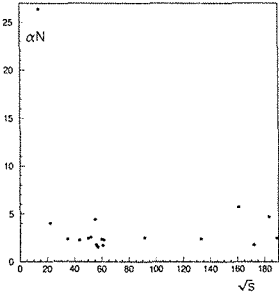


Figure 3: $N_g = \alpha N_q$

to the errors. The fraction of the evaporated gluons is equal to 0.47. A maximal possible number of hadrons from the gluon looks very much like the number of partons in the glob of cold quark-gluon plasma of L.Van Hove [14]. The gluon branch should be very active inside of QGS. At the fixed parameter of hadronisation \bar{n}^h equal to 1.63 (see below the thermodynamic model) the fraction of the evaporated gluons δ is about 0.73. After the evaporation the part of active gluons do not convert into hadrons. They stay in QGS and become sources of soft photons (SP). Further we will analyze the experimental effect of SP excess (it is impossible to describe them by means QED).

In the thermodynamic model without branches the active gluons which appear in the moment of the impact may leave QGS and fragment to hadrons. We consider that active gluons evaporated from QGS have Poisson MD with a mean multiplicity \bar{m} . Using the idea of the convolution of two stages (11) as well as the binomial distribution for hadrons from gluons we obtain MD of hadrons in pp-collisions in framework of the two stage thermodynamic model (TSTM):

$$P_n(s) = \sum_{m=0}^{ME} \frac{e^{-\bar{m}} \bar{m}^m}{m!} C_{mN}^{m-2} \left(\frac{\bar{n}^h}{N} \right)^{n-2} \left(1 - \frac{\bar{n}^h}{N} \right)^{mN-(n-2)} \quad (n > 2), \quad (19)$$

$P_2^{el}(s) = e^{-\bar{m}}$. Our comparison (19) with the experimental data [11] (see Fig. 8) gives values of parameters $N = 4.24 \pm 0.13$, $\bar{m} = 2.48 \pm 0.20$, $\bar{n}^h = 1.63 \pm 0.12$, and the normalized factor $\Omega = 2$ with $\chi^2/\text{ndf} \sim 1/2$. We are restricted in sum (19) $ME = 6$ (the maximal possible number of evaporated gluons from QGS). The found gluon parameters N and \bar{n}^h agree with the values of these parameters obtained at the e^+e^- annihilation [6]. From TSTM the maximal possible number of charged particles is 26. This quantity is the product of maximal multiplicities of active gluons and of the maximal number of hadrons forming from one gluon $ME \cdot N$. In TSMB there are no restrictions of this sort.

Project "Thermalization" is partially supported by RFBR grant 03-02-16869.

References

- [1] RHIC collaboration white paper: <http://www.phenix.bnl.gov/WWW/infor/comment>.
- [2] K. Konishi, A. Ukawa, G. Veneciano, Nucl.Phys. **B157**, 45 (1979).

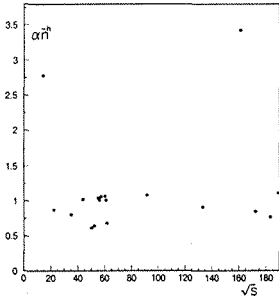


Figure 4: $\bar{n}_q^h = \alpha \bar{n}_q^h$

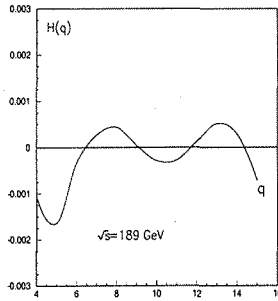


Figure 5: H_q at 189 GeV

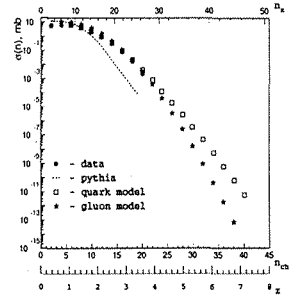


Figure 6: $\sigma(n)$ in pp

- [3] A. Giovannini, Nucl. Phys. **B161**, 429 (1979); A. Giovannini and R. Ugocioni, [hep-ph/0405251].
- [4] V.I. Kuvshinov, E.S. Kokouline, Acta Phys. Pol.**B13**, 533 (1982); E.S. Kokouline, V.I. Kuvshinov, Proc.6 Int.Conf. on HEP Problems; JINR, Dubna, D1, 2-81, 299 (1981).
- [5] TASSO Collab., Braunschweig W. et al. Z. Physik **C45**, 193 (1989); AMY Collab., Zheng H.W. et al. Phys. Rev. **D42**, 737 (1990); DELPHY Collab., Abreu P. et al. Z.Phys. **C52**, 271 (1991); OPAL Collab., Acton P.D. et. al. Z.Physik. **C53**, 539 (1992); OPAL Collab., Alexander G. et al. Z.Physik. **C72**, 191 (1996); OPAL Collab., Acketstaff K. et al. Z.Physik. **C75**, 193 (1997); OPAL Collab., Abbiendi G. et al. CERN-EP/99-178 [hep-ex/0002012].
- [6] E.S. Kokouline, Int.School-seminar, Gomel, 2001 [hep-ph/0111372]; E.S. Kokouline, XI Ann.Sem. NPCS, Minsk, Belarus, 2002 [hep-ph/0209334];, E.S.Kokouline, Report on the XXXII ISMD, Alushta, Crimea, Ukraine. (2002).
- [7] Kokouline E.S., Kuvshinov V.I. Vesti AN BSSR. Ser.Phys.-Math.Sc.**3**, 49 (1988).
- [8] SLD Collab., Abe K. et al. Phys. Lett. **B371**, 149 (1996); I.M. Dremin, Phys.Lett. **B341**, 95(1994);
- [9] P.F.Ermolov et al. Yad. Phys.**67**, 108 (2004).
- [10] P.Pokorski and L. Van Hove, Nucl.Phys. **86**, 243 (1975).
- [11] V.V.Babintsev et al. IHEP preprint M-25, Protvino (1976); V.V. Ammosov et al., Phys. Let. **42B**, 519 (1972).
- [12] O.G. Chikilev and P.V. Chliapnikov, Yad. Phys., **55** , 820 (1992).
- [13] E.S. Kokouline and V.A. Nikitin, International School-Seminar "The Actual Problems of Microworld Physics", Gomel, Belarus, 2003 [hep-ph/0308139]; E.S.Kokouline, ISMDXXXIII, Krakow, Poland, Acta Phys.Polon. **B35** 295 (2004) [hep-ph/0401223].
- [14] P.Lichard and L.Van Hove, Phys. Let. **B245**, 605 (1990).

STUDY OF MULTIPARTICLE PRODUCTION BY GLUON DOMINANCE MODEL (Part II) ¹

P.F. Ermolov¹, E.S. Kokoulina^{2,3†}, E.A. Kuraev³, A.V. Kutov³,
V.A. Nikitin³, A.A. Pankov², I.A. Roufanov³, N.K. Zhidkov³

(1) *SINP MSU*

(2) *GSTU, Belarus*

(3) *JINR*

† *E-mail: Elena.Kokoulina@sunse.jinr.ru*

Abstract

The gluon dominance model presents a description of multiparticle production in proton-proton collisions and proton-antiproton annihilation. The collective behavior of secondary particles in pp -interactions at 70 GeV/c and higher is studied in the project "Thermalization". The obtained neutral and charged multiplicity distribution parameters explain some RHIC-data. The gluon dominance model is modified by the inclusion of intermediate quark topology for the multiplicity distribution description in the pure $p\bar{p}$ -annihilation at few tens GeV/c and explains behavior of the second correlative moment. This article proposes a mechanism of the soft photon production as a sign of hadronization. Excess of soft photons allows one to estimate the emission region size.

1. Introduction

A new model of investigating multiparticle production (MP) at high energy is proposed. It is based on multiplicity distribution (MD) description of different interactions on basis of QCD and a phenomenological hadronization scheme. It is shown that the proposed model agrees with experimental data in a wide energy region and, perhaps, can be used for analysis of jet quenching and other phenomena at RHIC [1].

Application of this model approach to pp -interaction (for the beginning see [2]) is given in Section 2. The additional investigations of MD in the $p\bar{p}$ annihilation channel at a few tens GeV/c are carried out in Section 3. The emission region size for soft photons and the possible mechanisms of their formation are discussed in Section 4. The main results of these studies are given in Section 5.

2. MD in pp -interactions (continuation)

MD of charged particles in proton interactions by means of the gluon dominance model were studied in [2]. It is interesting to get MD for neutral mesons. For this purpose we take experimental mean multiplicity of π^0 in pp -interactions at 69 GeV/c ($\sqrt{s} \simeq 11.6$ GeV). It was found 2.57 ± 0.13 [3]. So the mean multiplicity in this process is

¹Talk given at XVII International Baldin - Seminar "Relativistic Nuclear Physics and Quantum Chromodynamics". JINR. September 27 - October 2, 2004, Dubna, Russia.

calculated as the product of the mean number of evaporated active gluons ($\bar{m} = 2.48$) and hadron parameter \bar{n}^h . We can determine the hadronization parameter for neutral mesons: $\bar{n}_0^h = 1.036 \pm 0.041$ [4]. We expect approximate equality of probabilities of different hadron production at the second (hadronization) stage. MD for neutral mesons have a form as for charged particles [2]:

$$P_n(s) = \sum_{m=0}^{ME} \frac{e^{-\bar{m}} \bar{m}^m}{m!} C_{mN}^{n-2} \left(\frac{\bar{n}^h}{N} \right)^{n-2} \left(1 - \frac{\bar{n}^h}{N} \right)^{mN-(n-2)}, \quad (1)$$

and can be easily obtained if they are normalized to mean multiplicity π^0 's (Fig. 1). From this distribution we see that the maximal possible number of π^0 from TSTM [4] is 16. MD for the total multiplicity are shown in Fig. 2. The maximal total number of particles in this case is equal to 42.

The dependence of the mean multiplicity of neutral mesons \bar{n}_0 versus the number of charged particles n_{ch} can be determined by means of MD $P_{n_{tot}}(s)$:

$$\bar{n}_0(n_{ch}, s) = \frac{\sum_{n_{tot}=n_1}^{n_2} P_{n_{tot}}(s) \cdot (n_{tot} - n_{ch})}{\sum_{n_{tot}=n_1}^{n_2} P_{n_{tot}}(s)}, \quad (2)$$

where n_1 and n_2 are lower and top boundaries for the total multiplicity at the given number of charged particles n_{ch} . The MD of charged and neutral secondaries obtained by TSTM give the maximal number for charged $n_{ch} = 26$, neutral $n_0 = 16$ and total $n_{tot} = 42$. That is why we have the following limits for n_1 and n_2 : $n_1 \geq n_{ch}$, $n_2 \leq 16 + n_{ch}$. These restrictions result in great disagreement with experimental data [3] at small multiplicities. It was shown in [4].

A significant improvement will be reached if we decrease the top limit at low multiplicities ($n_{ch} \leq 10$) to $n_2 = 2n_{ch}$. This corresponds to the case when the maximal number of neutrals is equal to the number of charged particles, and a double excess of neutral mesons over positive (negative) pions is possible. Fig. 3 shows that multiplicity of neutrals versus n_{ch} when n_2 is taken equal to $2n_{ch}$ at small n_{ch} and $n_2 = 16 + n_{ch}$ at $n_{ch} > 10$. This restriction in (2) indicates that AntiCentauro events (a large number of neutrals and very few charged particles) must be absent. Centauro events (a large number of charged particles and practically no accompanying neutrals) may be realized only in the region of high multiplicity.

It is assumed [5] that at the second stage different kinds of quark pairs from the gluon (maximal possible number is equal to N_{tot}) occur with equal probabilities. We will try to consider the formation of neutral and charged mesons as an example of the above assumption. The $u\bar{u}$ and $d\bar{d}$ quark pairs may appear at sufficient energy. At the end of hadronization the formation of two charged mesons (the law of charge conservation of quarks) may take place. Production of an additional neutral particle is not necessary while formation of a neutral meson. So we can claim that the number of charged hadrons will be larger than the number of the neutral ones, or the probability of the charged hadron production is higher than of the neutral ones. We can estimate these probabilities in GDM.

MD of π^0 from one gluon at the second stage may be described by the binomial distribution $P_{n_0} = C_{n_t}^{n_0} p_0^{n_0} p_c^{n_t - n_0}$. Here n_t is the total number of hadrons formed from

gluon, n_0 - the number of neutral mesons among these secondaries (the number of charged hadrons $n_c = n_t - n_0$), $p_c(p_0)$ - the probability of production of charged pair (one π^0). The normalized condition is $p_0 + p_c = 1$. From TSTM we have obtained $\bar{n}_{ch} = 1.63$ and $\bar{n}_0 = 1.036$. The mean multiplicities for binomial distributions will be equal to: $\bar{n}_{ch} = p_c \bar{n}_t$, $\bar{n}_0 = p_0 \bar{n}_t$. The probability of the charge particle production is higher than of the neutral mesons ($\bar{n}_{ch} > \bar{n}_0$). The ratio of these values is $p_c/p_0 \sim 1.46$.

The mean multiplicity of newly born hadrons (charged or neutral) in proton interactions in GDM is equal to the product of the mean multiplicity of gluons obtained at the first stage and the mean multiplicity of hadrons (\bar{n}_{ch}^h or \bar{n}_0^h) produced from one gluon at the second stage. In the case of binomial distribution $\bar{n}_{ch} = \bar{n}_t \cdot p_c$, $\bar{n}_0 = \bar{n}_t \cdot p_0$. Taking into account two leading protons, the mean multiplicity is $\bar{n}_{ch}(s) = 2 + \bar{m}_g(s) \cdot \bar{n}_{ch}^h$ for charged particles in pp-interactions. The mean multiplicity of neutral mesons in this process is $\bar{n}_0(s) = \bar{m}_g(s) \cdot \bar{n}_0^h$. The ratio of the mean charged pairs to the neutral mesons in proton interactions is

$$\frac{\bar{n}_{ch}(s)/2}{\bar{n}_0} = \frac{1}{\bar{m}(s) \cdot \bar{n}_0^h} + \frac{1}{2} \cdot \frac{\bar{n}_{ch}^h}{\bar{n}_0^h}. \quad (3)$$

At 69 GeV/c this ratio (3) is equal to $1.19 \pm .25$. At the higher energy the mean number of active gluons \bar{m} increases and becomes much more than 3. In this case (3) it will be around the ratio of $\bar{n}_{ch}^h/2\bar{n}_0^h$. The experimental data have shown 1.6 for Au-Au peripheral interactions (80 – 92(%) centrality class) at 200 GeV and for pp interactions at 53 GeV [6]. We can compare these results with GDM at higher energies.

The application of GDM to describe MD in the energy region (102, 205, 300, 405 and 800 GeV/c) [7] in both schemes (TSMB and TSTM) [2] leads to good results (Fig. 4-8). Parameters of TSTM in this domain are given in Table 2.

Table 1. Parameters of TSTM

\sqrt{s} GeV	\bar{m}	M_g	N	\bar{n}^h	Ω	χ^2/ndf
102	2.75 ± 0.08	8	3.13 ± 0.56	1.64 ± 0.04	1.92 ± 0.08	2.2/5
205	2.82 ± 0.20	8	4.50 ± 0.10	2.02 ± 0.12	2.00 ± 0.07	2.0/8
300	2.94 ± 0.34	10	4.07 ± 0.86	2.22 ± 0.23	1.97 ± 0.05	9.8/9
405	2.70 ± 0.30	9	4.60 ± 0.24	2.66 ± 0.22	1.98 ± 0.07	16.4/12
800	3.41 ± 2.55	10	20.30 ± 10.40	2.41 ± 1.69	2.01 ± 0.08	10.8/12

We see that the number of active gluons and their mean multiplicity increase, parameters of hadronization N and \bar{n}_{ch}^h vary very slowly. At these energies the charged hadron/pion ratio (3) grows up to 1.6. The parameter of hadronization \bar{n}_{ch}^h has a trend to increase weakly but \bar{n}_0^h does not almost change. This behavior may be related with the production of other charged particles (not only pions): protons, antiprotons, kaons and so on. We consider that parameter \bar{n}_{ch}^h goes to the limit value (like saturation).

On the other side a small growth \bar{n}_g^h in proton interactions also points at a possible change mechanism of hadronization of gluons in comparison with the transition gluons to hadrons in e^+e^- annihilation. It is considered that in the last case partons transform to hadrons by the fragmentation mechanism at the absence of the thermal medium. Our MD analysis gives $\bar{n}_g^h \sim 1$ for this fragmentation [8]. The recombination is specific for the hadron and nucleus processes. In this situation a lot of quark pairs from gluons appear

almost simultaneously and recombine to various hadrons [9]. The value \bar{n}_q^h becomes bigger $\sim 2 - 3$), that indicates to the transition from the fragmentation mechanism to the recombination one. The recombination mechanism provides justification for applying the statistical model to describe ratios of hadron yields (the ratio $Baryon/Meson \approx 1$) [9]. The collective flow of quarks may be explained by the recombination mechanism, too. The rapid local thermalization may be a consequence of this formation of secondary hadrons [9].

In this way we try to compare two kinds of processes which have different values of hadronization parameters. The first one is e^+e^- - annihilation. It is usually supposed that fragmentation dominates in it and newly formed hadrons fragment with a high moment of parton into the surrounding vacuum (such objects can also appear from the hot surface in peripheral events in nucleus and hadron collisions) [9].

The nuclear modification factor R_{CP} and elliptic flow v_2 in Au-Au collisions at RHIC have revealed an apparent quark-number dependence in the p_T region from 1.5 to 5 GeV/c. Moreover, the baryon production increases more rapidly with centrality than the meson production. These observations confirm the picture of hadron formation by quark recombination [9] and point out that the hadronization processes in high energy nucleus interactions are modified to the comparison of $e^+ + e^-$ and partly $p + p$ collisions.

The GDM with a branch gives growth of the part of the evaporated gluons to 0.85-0.98 and a small rise of gluon branch number at higher energies. Besides we have got data about emergence of hard constituent in MP [10]. In GDM it can be explained not only by not only evaporation of a single gluon sources but also of groups with several gluons (formed by branch). A simple MD scheme of this superposition will be analyzed below.

Let us compare MD (1) with the descriptions of experimental data obtained by various approaches. We bring two of them. A fortunate expression for KNO function was obtained by a group from IHEP [11] who combined the elastic and inelastic processes. We can see (Fig. 9) good agreement with data [7] at 800 GeV/c both of MD in MGD (solid line) and KNO-function (dot line).

A wide research of MD in pp-interactions was fulfilled by L. Van Hove, A. Giovannini and R. Ugoccioni [10]. They proposed a two-step mechanisms of MP. The independent (Poisson) production of groups of ancestor particles (named "clan ancestors") were supplemented by their decay, according to a hadron shower process (the logarithmic MD within each clan). Such convolution of two mechanisms gives a negative binomial distribution (NBD) for hadrons

$$P_n(s) = \frac{k_h(k_h + 1) \dots (k_h + n - 1)}{n!} \left(\frac{\bar{n}(s)}{\bar{n}(s) + k_h} \right)^n \left(\frac{k_h}{k_h + \bar{n}(s)} \right)^{k_h}, \quad (4)$$

where k_h - the NBD parameter and $\bar{n}(s)$ - the mean multiplicity of hadrons. The comparison of NBD (dot line) and our MD in GDM (solid line) with data at 800 GeV/c is given in Fig. 10. A. Giovannini emphasizes that the nature of this clan is gluon bremsstrahlung [10]. Our investigations by GDM allows to give a concrete gluon content. Binomial distributions (BD) describe the hadronization stage. The clan model of [10] uses the logarithmic distribution of secondaries in a single clan. Both of MD have the similar behavior.

At the top energy (especially at 900 GeV) the shoulder structure appears in P_n [12]. The comparison of data with one NBD does not describe data well. But the weighted

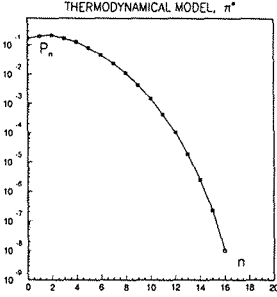


Figure 1: MD for π^0

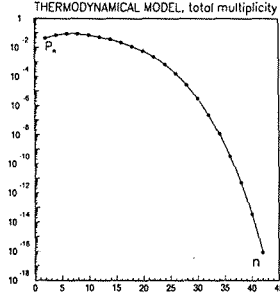


Figure 2: MD for n_{tot}

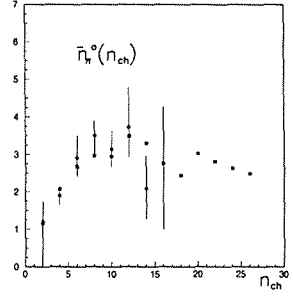


Figure 3: $\bar{n}_\pi^o(n_{ch})$

superposition of two NBD gives a good description of the shoulder structure $P_n(s)$ [10]. At 14 TeV A.Giovannini expects the weighted superposition of the three classes of events.

We can modify our GDM considering that the gluon fission may be realized at higher energies. The independent evaporation of gluons sources of hadrons may be realized by single gluons and also groups from two and more fission gluons. Following A.Giovannini we name such groups of gluons - clans. Their independent emergence and following hadronization content of GDM. MD in GDM with two kinds of clans are:

$$P_n(s) = \alpha_1 \sum_{m_1=0}^{Mg_1} \frac{e^{-\bar{m}_1} \bar{m}_1^{m_1}}{m_1!} C_{m_1, N}^{n-2} \left(\frac{\bar{n}^h}{N} \right)^{n-2} \left(1 - \frac{\bar{n}^h}{N} \right)^{m_1 \cdot N - (n-2)} +$$

$$+ \alpha_2 \sum_{m_2=0}^{Mg_2} \frac{e^{-\bar{m}_2} \bar{m}_2^{m_2}}{m_2!} C_{2 \cdot m_2, N}^{n-2} \left(\frac{\bar{n}^h}{N} \right)^{n-2} \left(1 - \frac{\bar{n}^h}{N} \right)^{2 \cdot m_2 \cdot N - (n-2)}, \quad (5)$$

where α_1 and α_2 are the contribution single and double gluon clans ($\alpha_1 + \alpha_2 = 1$). The comparison (5) with experimental data for proton interactions at $\sqrt{s} = 62.2$ GeV [13] is given in Fig. 8. We have obtained the following values of parameters: $N = 7.06 \pm 3.48$, $\bar{m}_1 = 3.59 \pm 0.03$, $\bar{m}_2 = 1.15 \pm 0.25$, $\bar{n}^h = 3.23 \pm 0.14$, $Mg_1 = 8$, $Mg_2 = 4$, $\alpha_1/\alpha_2 \sim 1.8$ at $\chi^2/\text{ndf} = 9.12/13$. The mean multiplicities of the two kinds of clans are similar.

The specific feature of our GDM approach is the dominance of a lot of active gluons in MP. We can expect the emergence of them in nucleus collisions (experiments at RHIC) and the formation of a new kind of matter (quark-gluon plasma) at high energy. We consider that our gluon system can be a candidate for this. So the mean multiplicity of active gluons approached 10 at RHIC. For Au+Au central collisions their number may be equal to $200 \cdot \bar{m} \approx 2000$ before the branch. This gluon medium facilitates the quenching.

3. MD in $p\bar{p}$ -annihilation

In the midst of interesting and enough inextricable hadron interactions the $p\bar{p}$ annihilation shows up especially [14]. Experimental data at tens GeV/c [14] point out on some maxima in differences between $p\bar{p}$ and pp inelastic topological cross sections what may witness about the contribution of different mechanisms of MP

$$\Delta\sigma_n(p\bar{p} - pp) = \sigma_n(p\bar{p}) - \sigma_n(pp). \quad (6)$$

The important information about the MP mechanism may be picked out from the MD moment analysis of charged particles. The second correlative moment for negative particles f_2^{--} are available to study MP

$$f_2^{--} = \overline{n_-(n_- - 1)} - \bar{n}_-^2. \quad (7)$$

The negative value of second correlative moments is characteristic for a more narrow MD than Poisson, and they indicate the predominance of the hadronization stage in MP. According to MGD, active gluons are a basic source of secondary hadrons.

At the initial stage of annihilation three valent $q\bar{q}$ -pairs (uud and $\bar{u}\bar{u}\bar{d}$) are. They can turn to the "leading" mesons which consist from: a) valent quarks or b) valent and vacuum quarks [5]. In the case a) only three "leading" neutral pions (the "0" topology) or two charged and one neutral "leading" mesons ("2" - topology) may form. In b) case the "4"- and "6"- topology is realized for "leading" mesons. We suggest that the formation neutron and antineutron (exchange) can be realized.

A simple scheme of MP for annihilation may give the negative second correlative moments in GDM. We suggest that the active gluon emergence together with the formation of intermediate topology occurs. The GF for a single active gluon $Q_1(z) = [1 + \bar{n}/N(z-1)]^N$ gives [4]

$$f_2 = Q_1''(z)|_{z=1} - [Q_1(z)|_{z=1}]^2 = -(\bar{n}^h)^2/N < 0. \quad (8)$$

Reciprocally for m gluons GF and f_2 will be

$$Q_m(z) = [1 + \bar{n}^h/N(z-1)]^{mN}, \quad f_2 = -m(\bar{n}^h)^2/N. \quad (9)$$

We consider that m grows while increasing the energy of the colliding particles, and f_2 will decrease almost linearly from m . Such behavior qualitatively agrees with experimental data [14]. If we take concrete MD P_m^G for gluons, then GF for secondary hadrons and f_2 are

$$Q(z) = \sum_m P_m^G [1 + \bar{n}^h/N(z-1)]^{mN} \quad (10)$$

$$f_2 = [f_2^G + 1 - 1/N] \cdot \bar{m} \cdot (\bar{n}^h)^2, \quad f_2^G = \overline{m(m-1)} - \bar{m}^2, \quad (11)$$

where f_2^G - the second correlative moment for gluons. In this scheme f_2 may be negative or positive. We consider that the negative value f_2 in the large energy region in comparison with $p+p$ interactions may be related with the destruction of the initial system on three or more shares and the number of active gluons related with a "leading" pion will be less than in the case of a leading proton in pp -collisions at the same energy. Herewith the total number of such gluons at annihilation may be bigger, their manifestation happens independently but the number of them per one pion grows slowly. The explanation of the negative f_2 was given R.Lednicky [15] at the assumption of the independent MP of charged particles. The second correlative moment has a zero value only in the small energy domain. And so we should restrict the region to apply this explanation.

According to GDM for $p\bar{p}$ annihilation and taking into account three intermediate charged topology and active gluons, GF $Q(z)$ for final MD may be written as the convolution gluon and hadron components:

$$Q(z) = c_0 \sum_m P_m^G [1 + \frac{\bar{n}^h}{N}(z-1)]^{mN} + c_2 \sum_m z^2 P_m^G [1 + \frac{\bar{n}^h}{N}(z-1)]^{mN} + c_4 \sum_m z^4 P_m^G [1 + \frac{\bar{n}^h}{N}(z-1)]^{mN}.$$

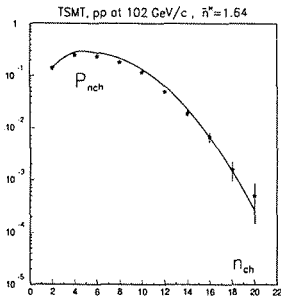


Figure 4: MD at 102 GeV/c

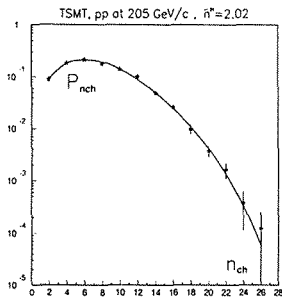


Figure 5: MD at 205 GeV/c

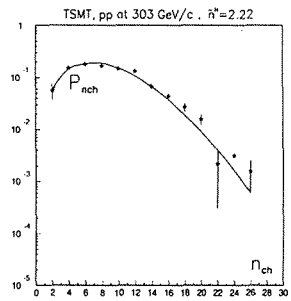


Figure 6: MD at 303 GeV/c

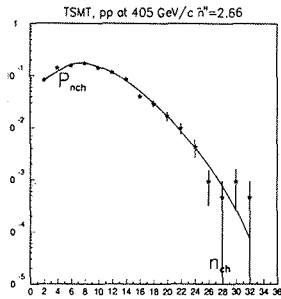


Figure 7: MD at 405 GeV/c

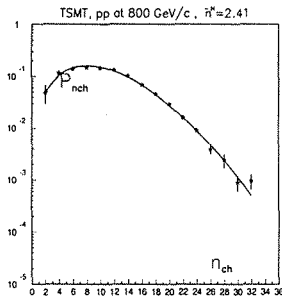


Figure 8: MD at 800 GeV/c

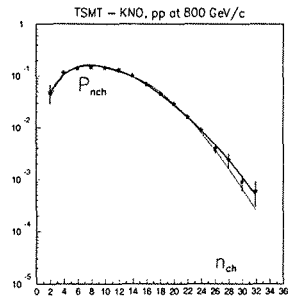


Figure 9: MD in GDM and KNO-function [11]

The parameters of c_0 , c_2 and c_4 are determined as the part of intermediate topology ("0", "2" or "4") to the annihilation cross section ($c_0 + c_2 + c_4 = 1$). For the simplicity we are limited by Poisson distribution with the finite number of gluons for P_m^G .

The comparison of the experimental data (Fig. 12) gives the following values of parameters: $\bar{m} = 3.36 \pm 0.18$, $N = 4.01 \pm 0.61$, $\bar{n}^h = 1.74 \pm 0.26$, the ratio $c_0 : c_2 : c_4 = 15 : 40 : 0.05$ at $\chi^2/ndf = 5.77/4$ and the maximum possible number of gluons $M = 4$ at "4"-topology. The sum begins from $m = 1$ (inelastic events), at $n \geq 2$ - from $m = 0$ and finishes up $m < M$ at small multiplicities ($n \leq 4$). We should to emphasize very complicated events $n_{ch} = 0$ and 2. This research of $p\bar{p}$ annihilation requires to be continued. We will develop MGD to describe MD at energies 200, 500, 900 GeV [16] and higher.

1. Soft photons

The production of photons in particle collisions at high energies was studied in many experiments [17]. In project "Thermalization" it is planned to investigate low energetic photons with $p_t \leq 0.1 \text{ GeV}/c$ and $x \leq 0.01$ [18]. Usually these photons are named soft photons (SP). Experiments shown that measured cross sections of SP are several times larger than the expected ones from QED inner bremsstrahlung. Phenomenological models

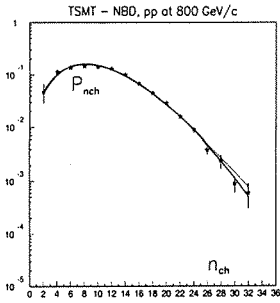


Figure 10: MD in TSTM and NBD

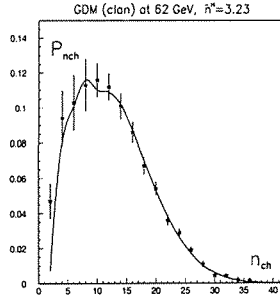


Figure 11: MD in GDM (clan)

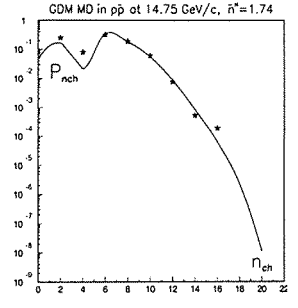


Figure 12: GDM MD in $p\bar{p}$ at 14.75 GeV/c

were proposed to explain the SP excess: the glob model of Lichard and Van Hove and the modified soft annihilation model of Lichard and Thomson [19].

We consider that at a certain moment QGS or excited new hadrons may set in an almost equilibrium state during a short period or finite time. That is why, to describe massless photons, we will try to use the black body emission spectrum [20]. From experimental data [18] the inelastic cross section is equal to approximately $40mb$, the cross section of SP formation is about $4mb$, and since $\sigma_\gamma \simeq n_\gamma(T) \cdot \sigma_{in}$, then the number of SP will be equal to $n_\gamma \simeq 0.1$. For convenience, we may use the well-known density of MVB at $T_r = 2.275K$ and get the number of photons by means of MVB $n_\gamma(T) = n_\gamma(T_r) \cdot \left(\frac{T}{T_r}\right)^3$. The density of SP in the region $1fm^3$ will be equal to

$$\rho(T) = n_\gamma(T)/V = 4.112 \cdot 10^8 \cdot 10^{-6} \cdot 10^{-39} \cdot \left(\frac{T}{T_r}\right)^3 fm^{-3}.$$

The estimates of temperature are implemented by transfer moment: $T = p \approx p_T \sqrt{2}$ ($1MeV = 1.16 \cdot 10^{10}K$). If $T(p_T)$ is known, using n_γ we can estimate the linear size of radiation system ($V \simeq L^3$). Dependencies of the linear size of system (L) from the SP moment (p_T) are given in Table 2.

Table 2. The size of system L (fm) versus p_T (MeV/c) of SP

p_T	10	15	25	30	40	50
L	11	6.9	4.1	3.5	2.6	2.0

It is well-known that the temperature of second hadrons is higher than the temperature of SP. We presume that objects with soft gluon content may not transform into hadrons but turn into SP. The amount of such soft gluons is estimated by N_g in TSMB.

5. Conclusion

In our research we have undertaken an attempt to give MP description in different processes by means of a unified approach based on quark-gluon picture using the phenomeno-

logical hadronization model. The implemented model investigation allows us to understand deeper the picture of MP at various stages. We have obtained qualitative and quantitative agreements of our schemes with experimental data in e^+e^- , $p\bar{p}$ annihilation and pp and nucleus collisions in a very wide energy domain.

The authors appreciate for the support of physicists from JINR, GSTU who encouraged our investigations. *Project "Thermalization" is partially supported by RFBR grant 03-02-16869.*

References

- [1] RHIC collaboration white paper: <http://www.phenix.bnl.gov/WWW/infor/comment>.
- [2] E.S.Kokouлина and V.A.Nikitin. ISHEPP, JINR, Dubna, Russia (2004), [hep-ph/0502224].
- [3] V.S.Murzin and L.I.Sarycheva. Interactions of high energy hadrons. (Russian ed.) 288p. (1983); V.G. Grishin, Phys. El.Part. and At.Yad., **10**, 608 (1979); K.Jager. *et al.*, Phys. Rev. **D11**, 2405 (1975).
- [4] E.S. Kokouлина and V.A. Nikitin, International School-Seminar "The Actual Problems of Microworld Physics", Gomel, Belarus, 2003 [hep-ph/0308139]; E.S.Kokouлина, ISMDXXXIII, Krakow, Poland, Acta Phys.Polon. **B35** 295 (2004) [hep-ph/0401223].
- [5] M.K.Volkov, E.S.Kokouлина and E.A.Kuraev, Ukr.Jour. of Physics **48**, 1252 (2003); M.K.Volkov, E.S.Kokouлина and E.A.Kuraev Particles and Nuclei, Letters, **1**, 16 (2004) [hep-ph/0402163].
- [6] K.Adcox *et. al.* [nucl-ex/0410003]; X. Zhang and G.Fai, [hep-ph/0306227]; B.Alper *et al*, Nucl. Phys. **B100**, 237 (1975).
- [7] C.Bromberg *et al.*, Phys. Rev. Lett. bseries 31, 1563 (1973); W.M.Morse *et al.*, Phys.Rev., **D15**, 66 (1977); S.Barish *et al.*, Phys. Rev., **D9**, 2689 (1974); A.Firestoun *et al.*, Phys. Rev., **D10**, 2080 (1974); P.Slattery, Phys.Rev., **D7**, 2073 (1973).
- [8] E.S.Kokouлина, ISMDXXXII, Alushta, Crimea, Ukraine. (2002).
- [9] R.C. Hwa and C.B. Yang, Phys. Rev., **C67**, 034902 (2003), [nucl-th/0211010]; R.Hwa, ISMD2004 [nucl-th/0410003]; B.Müller, [nucl-th/0404015] (2004); U.Heinz, [nucl-th/0407067] (2004); P.Sorensen, Subm. to J. Phys. G: Nucl. Phys., [nucl-exp/0412003].
- [10] A. Giovannini and R. Ugocioni, [hep-ph/0405251].
- [11] S.V. Semenov *et al.*, Yad.Phys. **22**, 792 (1975).
- [12] R.E. Ansorge *et al.* UA5-collaboration, CERN-EP/88-172 (1988).
- [13] A. Breakstoune *et al.*, Phys.Rev., **D30**, 528 (1984).

- [14] J.G.Rushbrooke and B.R.Webber, Phys. Rep. **C44**, 1 (1978); F.T. Dao et al. Phys. Lett., **51B**, 505 (1974); L.N. Abesalashvili et al. Phys. Lett., **52B**, 236 (1974).
- [15] R.Lednicky, Phys. El. Part. At. Yad., **15**, 617 (1984).
- [16] G.I.Alner et al. Z. Phys., **C33**, 1 (1986).
- [17] P.V.Chliapnikov et al., Phys. Let., **141B**, 276 (1984); S.Banerjee et al., Phys.Let.,**B305**,182 (1983); J.Antos et al., Z.Phys., **C59**, 547 (1993); J.F.Owens., Rev. Mod.Phys., **59**,465 (1987).
- [18] P.F.Ermolov et al. Yad. Phys.**67**, 108 (2004).
- [19] P.Lichard and L.Van Hove, Phys. Let. **B245**, 605 (1990).
- [20] Yu.B.Rumer and M.Sh.Ryvkin. Thermodynamika, statistical physics and kinetics. (Russian ed.) (1977).

THE LOBACHEVSKY SPACE IN RELATIVISTIC NUCLEAR PHYSICS

A.A.Baldin

Anton.Baldin@sunhe.jinr.ru

LHE, JINR, Dubna

Abstract

Relativistic nuclear collisions are considered in terms of relative 4-velocity and rapidity space (the Lobachevsky space). The connection between geometric relations in the Lobachevsky space and measurable (experimentally determined) kinematical characteristics are discussed. General properties of relativistic invariants distributions characterizing geometric position of particles in the Lobachevsky space are discussed. Possible applications of the obtained results for planning of experimental research and analysis of data on multiple particle production are discussed. The analysis is illustrated by processed experimental data.

1. Introduction

A desire to discover simple laws of Nature describing a wide range of phenomena, plays a progressive role of one of the basic principles of fundamental science. An important step in constructing theories is the selection of a set of variables for description of observed phenomena. That is why special attention is paid in this paper to the discussion of the variables used in analysis of relativistic particle collisions.

The theory of nuclear interactions is at present far from completeness. Essentially, it represents a set of phenomenological models and approaches describing the available experimental data. The most complicated from the point of view of theoretical description of nuclear matter is, in our opinion, the transition region between proton-neutron model of a nucleus and the region where excitation of internal quark-gluon degrees of freedom is essential.

One of the most important problems nowadays, as it was formulated by a distinguished scientist S.Nagamia in 1994, is the determination of the conditions in which hadrons lose their identity, and sub-nucleonic degrees of freedom begin to play a dominant role. A.M.Baldin proposed a classification of applicability of the notion "elementary particle"

on the basis of a variable b_{ik} (square relative four-velocity between the considered objects) [1] introduced by him, in answer to the above problem.

Relativistic nuclear physics which originated at the interface between elementary particle physics and nuclear physics needs mathematically adequate space of variables for investigation of the processes of particle interaction and production. The Lobachevsky space is considered as such space in the present paper.

The investigation of the properties of the 4-velocity space allows to formulate general rules of particle distributions, to develop relativistically invariant methods of analysis of multiparticle production, and imposes a number of intrinsic limitations on the relativistic collision models. Long-term investigations (see, for example, [10-13]) are dedicated to the application of the Lobachevsky geometry in physics.

2. The relative 4-velocity space. General characteristics of particle distributions

When studying nuclear reactions the experimentally determined quantities are momentum, angle, type of registered particle, collision energy, reaction cross section, and their derivatives.

The relativistically invariant measurable scalar quantity $\frac{P_i P_j}{m_i m_j}$, where P_i, P_j are 4-momenta of particles i and j , and m_i, m_j are masses of these particles, underlies the determination of invariant mass, rapidity ρ , square relative 4-velocity b_{ik} and invariant cross section.

Rapidity ρ forms a metric space – the Lobachevsky space. Investigation of the properties of this space is necessary for understanding of the relation between the 4-dimensional energy-momentum space and the 3-dimensional Euclidean space of physical experiment.

The invariant variable described through measurable quantities is the particle 4-velocity:

$$U = \{U^0; \mathbf{U}\}, \quad (1)$$

where $U^0 = \frac{E}{m}$, $\mathbf{U} = \frac{\mathbf{p}}{m}$. Here E is the total energy, \mathbf{p} is the 3-dimensional momentum, and m is the mass of particle.

The 3-dimensional Lobachevsky space is connected with the 4-dimensional velocity space by expressing the fourth component of the velocity through the first three:

$$U^0 = \pm \sqrt{1 + U_x^2 + U_y^2 + U_z^2} \quad (2)$$

The Lobachevsky geometry of the 3-dimensional rapidity space is defined on the upper sheet of the two-sheet hyperboloid (3). The relations between the components of the 4-velocity and rapidity are the following:

$$U^0 = \text{ch } \rho ; \quad |U| = \text{sh } \rho . \quad (3)$$

So, the relation between the particle energy, momentum and mass $E^2 - \vec{p}^2 = m^2$ takes the following form in the rapidity space: $(\text{ch } \rho)^2 - (\text{sh } \rho)^2 = 1$.

The particle rapidity in the laboratory system can be expressed through measurable parameters as follows:

$$\rho = \frac{1}{2} \ln \frac{E + |\vec{p}|}{E - |\vec{p}|} \quad (4)$$

The invariant variable b_{ik} is defined as [1]:

$$b_{ik} = -(U_i - U_k)^2 = 2[(U_i U_k) - 1] = 2 \left[\frac{E_i E_k - \vec{p}_i \vec{p}_k}{m_i m_k} - 1 \right] \quad (5)$$

The relation between the variable b_{ik} and rapidity is evident:

$$b_{ik} = 2[(U_i U_k) - 1] = 2[\text{ch } \rho_{ik} - 1] \quad (6)$$

Consider typical particle distributions over the variable b_{ik} for the data obtained using the propane bubble chamber illuminated by 4.2 GeV/c p, d, He, C beams at interaction of relativistic nuclei with matter [2]. The experimental data used hereafter were obtained by the collaboration [3,4] for investigations using the 2m propane chamber [5]. Fig.1 shows the normalized distributions of relative 4-velocities of pairs of particles (protons and π -mesons) registered in the reactions C+Ta, He+Ta, d+Ta, p+Ta. It is seen that the character of the distributions for all four reactions is similar. It is also seen that the number of particles with relative 4-velocities close to zero grows steeper than an exponent – in a pole-like way. The pole approximation in the form

$$\frac{d\sigma}{dN} \approx \frac{C}{(b_{ik} + \alpha)^2}, \text{ where } \alpha \approx 0.002 \quad (7)$$

was proposed for the first time for the cross sections of fragmentation processes in [1].

The experimentally observed change of the character of b_{ik} distributions from the pole-like to the exponent and power-like illustrates the classification of elementary particle interactions proposed by A.M.Baldin [6]:

- the region $0 \leq b_{ik} \leq 10^{-2}$ relates to non-relativistic nuclear physics, where nucleons can be considered as point objects;
- the region $b_{ik} \sim 1$ relates to excitation of internal degrees of freedom of hadrons;
- the region $b_{ik} \gg 1$ should, in principle, be described by quantum chromodynamics.

A large number of publications (see, for example, [6,7]) are dedicated to investigation of particle distributions over b_{ik} and analysis of general properties of these distributions, in particular, the correlation depletion principle.

The analysis of b_{ik} distributions carried out by the authors showed that the shape of these distributions is independent of particle multiplicity in an event. Fig.2 shows the distributions of relative 4-velocities of all combinations of pairs of protons and π -mesons in the reaction C+Ta for the selected events arranged into five groups: for multiplicity in the intervals 16-20 particles, 26-30 particles, 36-40 particles, 46-50 particles, and 56-60 particles.

Independence of inclusive cross sections of meson production of multiplicity was noted by the authors in [8]. Independence of such distributions of experimentally observed particle characteristics of multiplicity indicates that the mechanism of independent nucleon-nucleon collisions prevails in multiple particle production. This general property should be taken into account in theoretical and computer models of nucleon-nucleon collisions and in planning of experiments aimed at investigation of exotic states of nuclear matter (quark-gluon plasma and other collective effects).

Consider particle – target relative 4-velocity distributions for protons, registered using the propane bubble chamber in the reactions C+Ta, p+C (Fig.3). The plots demonstrate the existence of transition to internal degrees of freedom of nucleons for b_{ik} close to unity. Note that this effect is the same for different interacting nuclei and different collision energies.

The transition to internal nucleon degrees of freedom can be demonstrated on the basis of the available data on total cross sections of hadron interactions (Fig.4) [9]. Thus, it is in the region $b_{ik} \sim 1$, both for a pair target-registered proton (Fig.3), and a pair target-projectile (Fig.4), that sub-nucleonic degrees of freedom of nuclear matter are significant, and nucleons are no more point-like.

It should be noted that the variable b_{ik} does not form a metric space, i.e. the relation $b_{12} + b_{13} \geq b_{23}$ is, generally speaking, wrong. It can be illustrated using the experimental data of the collaboration for investigations using the 2m propane chamber. Fig.5 shows the distribution of the value $b_{13} + b_{23} - b_{12}$, where 1, 2 indicate the projectile and target, respectively, and 3 – the registered proton, for the reaction C+Ta. It is seen from Fig.5 that large part of protons tends to be displaced “close” to the projectile and target simultaneously. Rapidity ρ_{ik} has an advantage that, being, along with b_{ik} , the relativistic invariant, it forms, unlike b_{ik} , a metric space – the Lobachevsky space.

Total interaction cross sections of π -mesons, K-mesons, protons as functions of particle-target relative rapidity are shown in Fig.6. The rapidity range between 1 and 4, corresponding to the projectile momentum between 1 and 25 AGeV/c, defines the transition energy region between classical nuclear physics and quantum chromodynamics.

Thus, taking into account non-Euclidean character of the 4-velocity space is important already at relatively low hadron energies (starting from hundreds of MeV), and non-relativistic mechanistic images based on the notions of isotropy, thermalization, etc., have principle limitations related with the selection of a reference system.

3. Geometric characteristics of particle distributions in the rapidity space

Analysis of particle properties in terms of rapidity is more complete than consideration of its longitudinal and transversal components. In literature, however, experimental data are often presented as functions of longitudinal rapidity (projection on the reaction axis) and transversal momentum (or transversal mass). Longitudinal rapidity is defined as follows:

$$y = \frac{1}{2} \ln \frac{E + p_{\parallel}}{E - p_{\parallel}}, \quad (8)$$

and transversal mass as:

$$m_T = \sqrt{m^2 + p_T^2}, \quad (9)$$

where p_T is transversal momentum.

Define transversal rapidity τ :

$$\text{ch } \tau = \frac{m_T}{m}, \quad (10)$$

Total rapidity ρ is related with longitudinal and transversal rapidities by the Pythagorean theorem in the Lobachevsky space:

$$\text{ch } \rho = \text{ch } y \cdot \text{ch } \tau. \quad (11)$$

The properties of the space pose certain limitations on the rapidity range (the consequence of metric characteristics of triangles with the sides - relative rapidities):

$$(\rho_{23})_{\min}^{\max} = |\rho_{12} \pm \rho_{13}|; (\rho_{13})_{\min}^{\max} = |\rho_{12} \pm \rho_{23}|; (\rho_{12})_{\min}^{\max} = |\rho_{23} \pm \rho_{13}| \quad (12)$$

The simplest geometric element is a triangle. Basic relations for a triangle with the vertices - rapidities in the Lobachevsky space (see Fig.7) are given below.

Two theorems can be used to define the relations between sides and angles of the triangle: the law of cosines:

$$\text{ch}(\rho_{12}) = \text{ch}(\rho_{13}) \cdot \text{ch}(\rho_{23}) - \text{sh}(\rho_{13}) \cdot \text{sh}(\rho_{23}) \cdot \cos(\alpha_3) \quad (13)$$

and the law of sines:

$$\frac{\text{sh}(\rho_{12})}{\sin(\alpha_3)} = \frac{\text{sh}(\rho_{13})}{\sin(\alpha_2)} = \frac{\text{sh}(\rho_{23})}{\sin(\alpha_1)} \quad (14)$$

Note, that the height of the triangle h (see Fig.7) is defined as:

$$\text{sh}(h) = \text{sh}(\rho_{23}) \cdot \sin(\alpha_2) = \text{sh}(\rho_{13}) \cdot \sin(\alpha_1)$$

Thus, h coincides with the transversal rapidity of particle 3, i.e. is a dimensionless relativistically invariant characteristic of transversal motion.

Usually, when analyzing experimental data, the registered particles are classified on the basis of the criterion of interaction «hardness». For example, the «evaporating» protons with momenta less than 300 MeV with respect to the target and «stripping» protons with momenta close to the projectile momentum and laboratory angles less than 4° , are attributed to the results of “soft” interactions [2]. The analysis in the rapidity space allows to apply a unified relativistically invariant criterion for such classification using particle-target and particle-projectile relative rapidities. For “soft” interactions the upper limit of relative rapidity is ~ 0.3 .

Note that such relativistically invariant analysis is valid for all and with respect to any registered particles, as well as, generally speaking, to all points of the rapidity space, rather

than only two points corresponding to the colliding objects. Such approach is especially helpful in analysis of multiple particle production for their separation into groups (pair correlations, clusters, jets, etc.).

In any projective geometry, including the Lobachevsky geometry, the principle of duality is valid, according to which statements formulated in terms of distances between points are equivalent to statements formulated in terms of angles between beams.

Thus, the degree of «hardness» of interactions can be analyzed using the values of angles of the triangles in the rapidity space. Fig.8 shows the ρ_{23} distributions of protons for the selected angle α_3 intervals (see Fig. 7). The regions of ρ_{23} in the vicinity of 0 and 3 corresponding to the target and projectile fragmentation, respectively, can be extracted applying a selection criterion to the angle α_3 between the rapidities ρ_{12} and ρ_{13} .

A triangle is characterized by its defect, which is proportional to the area of the triangle (the constant of proportionality equals to square curvature of the space):

$$defect = \pi - \alpha_1 - \alpha_2 - \alpha_3 \quad (15)$$

Angular defect is the scalar characteristic of relative position of trios of particles in the rapidity space. Fig.9 shows the distribution of defects of triangles formed by all combinations of protons and all combinations of π -mesons registered at interaction of 10 GeV/c protons with carbon. The defect distribution for proton trios, as seen from the figure, has an exponential shape, i.e. the probability to observe three protons «far» from each other (in terms of rapidity) drops exponentially. It should be noted that the data on protons from the RQMD simulation [14] agrees very well with the experiment. The defect distribution for π -mesons has another shape – these trios form triangles of larger area in the rapidity space, as compared to protons. Note, that the model adequately reproduces inclusive spectra both of protons and π -mesons. The distribution of trios of π -mesons, however, differs noticeably from the experimental data.

Let us illustrate another general property of particle distributions in the rapidity space. Consider combinations of three particles: point 1 – projectile, point 2 – target and point 3 – any registered particle. Fig.10 shows the defects of such triangles as functions of their perimeters calculated for the experimental data on π -meson production in the reaction $p(10 \text{ GeV/c})+C$. For a certain perimeter particles with maximum allowed defects are produced with higher probability. It is consistent with the known feature that cross sections grow towards the phase space boundary, and agrees with the simulation [14].

Let us consider defects as functions of the position of registered particle with respect to colliding nuclei (difference of rapidities, see Fig. 7). Fig.11 shows the plots of defect vs. $(\rho_{12}-\rho_{13})$ for the experimental and simulated protons produced in the reaction $p(10 \text{ GeV}/c)+C$. It is seen that the model does not reproduce the peculiarities of the transition region, $\rho \sim 1$ (Fig.11 a,b). The target fragmentation region is shown in more detail in Fig.11 c,d. It is seen that the specific fine structure of proton distribution corresponding to symmetric configurations in the rapidity space is not reproduced by the model. In this region the peculiarities in the cross sections of the registered protons correspond to isosceles triangles, when relative target-projectile and projectile-registered particle rapidities are close. Higher probability of particle production is observed also when relative target-particle and projectile-particle rapidities become close (the symmetric position of the registered particle with respect to the colliding nuclei). Fig.12 illustrates the above idea for π -mesons.

Multiple particle production takes place when their relative velocities approach the light velocity. This suggests that the whole problem of particle production (birth) can be considered from the point of view of the fundamental limitation on experimental observation due to three-dimensional character of Euclidean space. The relationship between four-dimensional Minkowsky space in which energy and momentum conservation laws are formulated and three-dimensional Euclidean space of experiment is realized through the Lobachevsky space.

It is important to stress that, unlike the Euclidean space, the area-to-perimeter ratio for triangles in the Lobachevsky space is limited (see Fig.13). This fundamental difference can hardly be imagined on the basis of mechanistic three-dimensional images which, as a rule, underlie models pretending to describe particle interaction dynamics.

One of the most remarkable variables introduced by N.I.Lobachevsky in his geometry is the angle of parallelism

$$\Pi_L(\hbar) = 2 \arctg(e^{-\hbar}) \quad (16)$$

What is the meaning of this parameter and how can it be applied to analysis of experimental data? What rapidity corresponds to the angle of parallelism? Let us consider the height of the triangle 123 (see Fig. 7), where 1 and 2 denote colliding particles and 3 the registered particle. Fig.14 shows the probability to register protons and π -mesons as function of the variable $2\Pi_L - \alpha_3$ (the difference between doubled angle of parallelism and angle at the registered particle in the rapidity space). It is seen from the figure that there exists a strongly pronounced

maximum of proton and π -meson production. It is important to note that this maximum corresponds to the angle of parallelism calculated for the value of relative rapidity of colliding objects.

Conclusion

The unified relativistically invariant criteria for particle classification, for example, selection of “stripping” and “evaporating” protons, can be formulated on the basis of spatial rapidities (angles). It is possible to select particles produced by different mechanisms using such characteristics in the Lobachevsky space as defect and perimeter.

The analysis of the data obtained using the propane bubble chamber showed that the general character of particle distributions in the 4-velocity space is similar for different reactions and does not depend on multiplicity.

The comparison of experimental data and model simulations showed that the model [14], while adequately reproducing integral characteristics of particle distributions – inclusive spectra, filling of phase space, is incapable of correct reproduction of two and three- particle correlations.

Taking into account the properties of the Lobachevsky space, in particular, that there is no geometric similarity (unlike the Euclidean geometry), is very important for analysis of experimental data and construction of models of multiple particle production. It is the author’s opinion that the Lobachevsky space is the most adequate for description of the processes of particle interaction and production.

Calculation of areas and volumes of arbitrary figures in the Lobachevsky space is a complicated mathematical problem. The property of limited surface area – to - volume ratio is a fundamental property of the Lobachevsky space. It is the author’s belief that this property is a key to deeper comprehension of the problem of confinement in strong interactions.

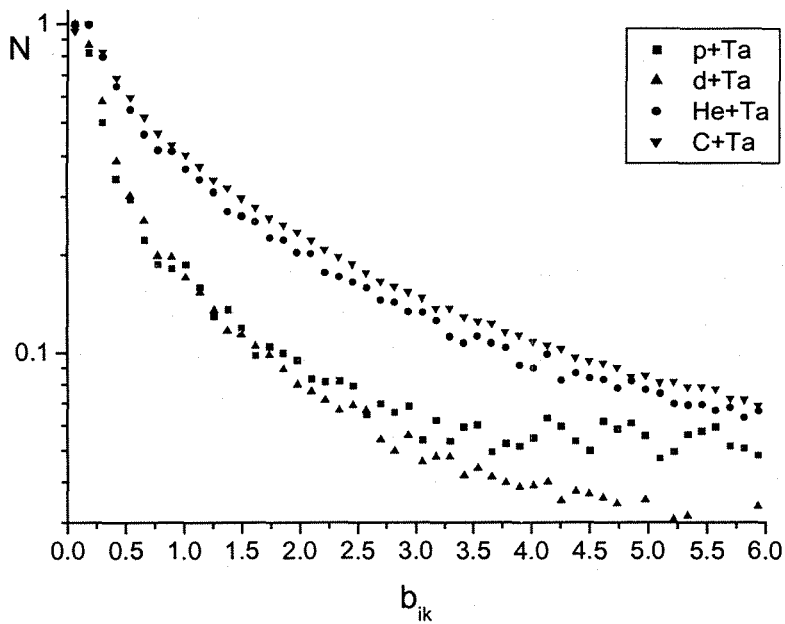


Fig.1. The normalized distributions of relative 4-velocities of the pairs of registered particles (p - p , p - π and π - π) in the reactions C+Ta, He+Ta, d+Ta, p+Ta

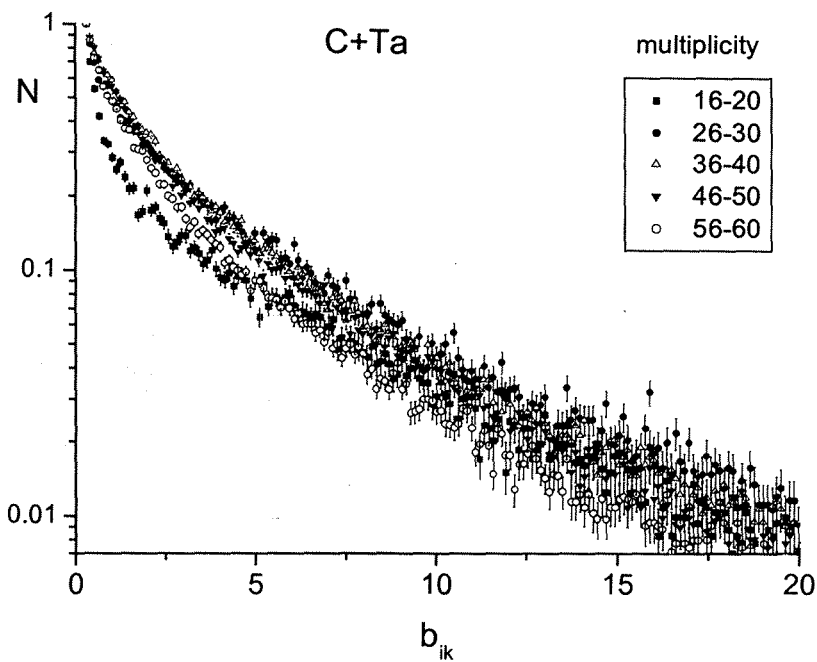


Fig.2. The normalized distributions of relative 4-velocities of the pairs of registered particles (p - p , p - π and π - π) in the reaction C+Ta for five groups of the selected events: with multiplicity in the intervals 16-20 particles, 26-30 particles, 36-40 particles, 46-50 particles, and 56-60 particles

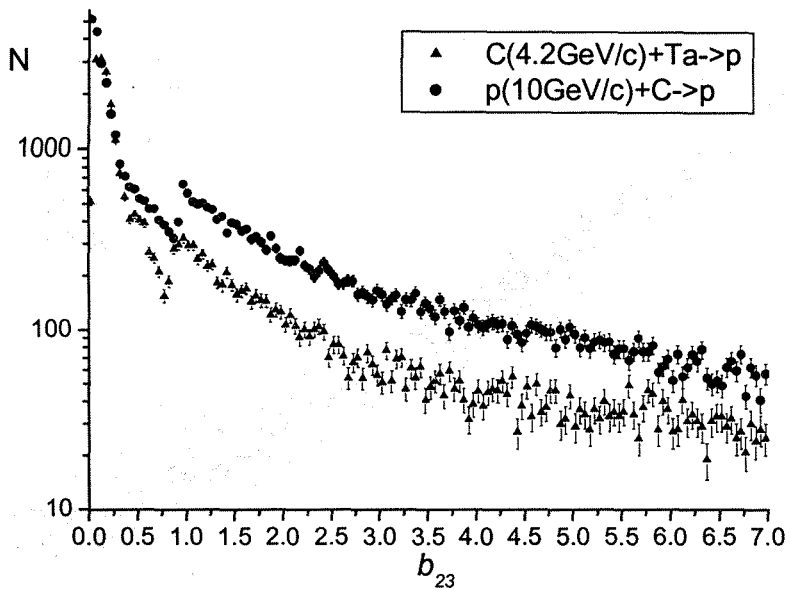


Fig.3. The particle – target relative 4-velocity distributions for the registered protons in the reactions C+Ta, p+C

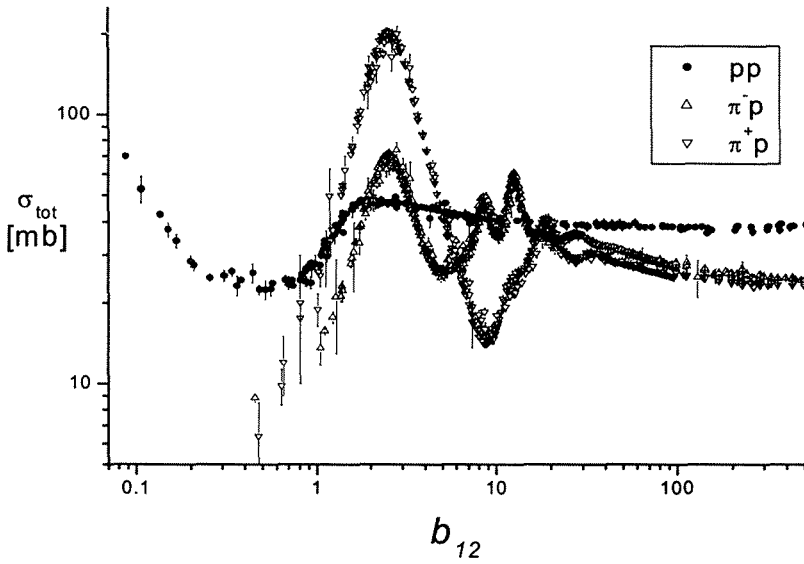


Fig.4. Total cross sections of hadron interactions as functions of relative four-velocity. The data are taken from [9]

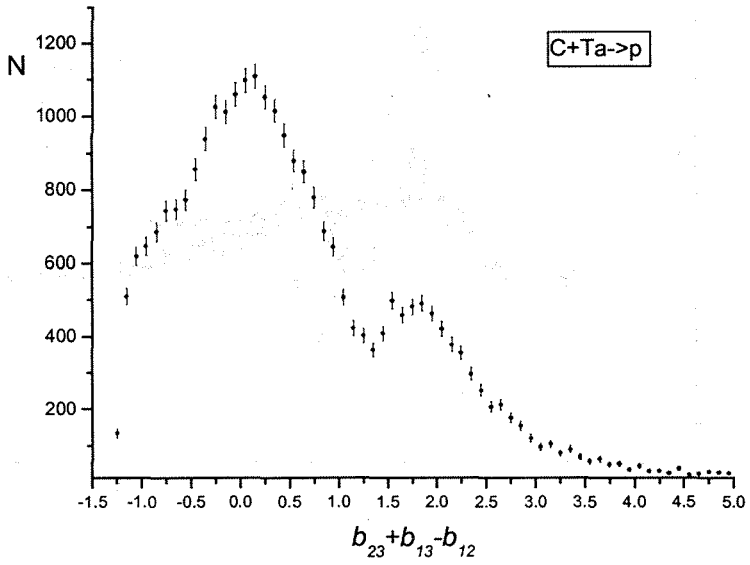


Fig.5. The distribution of relative four-velocities $b_{13} + b_{23} - b_{12}$, where 1, 2 are the projectile and target, respectively, and 3 is the registered proton, for the reaction C+Ta

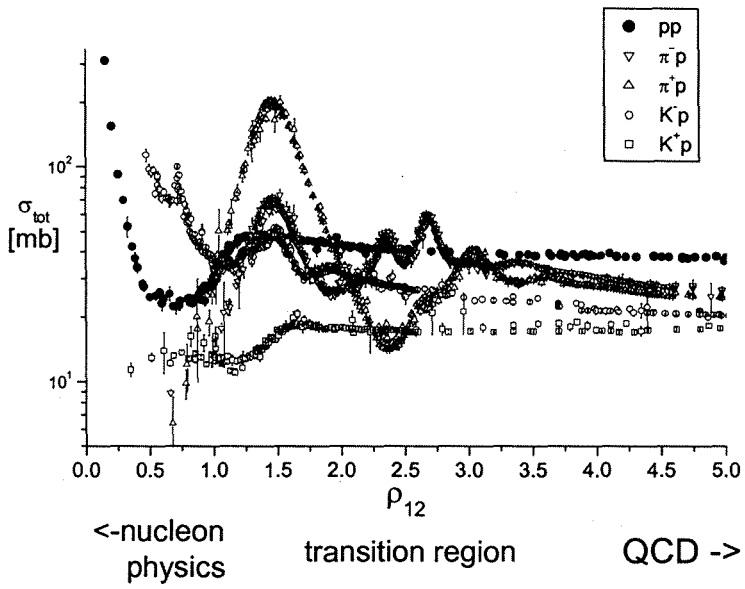


Fig.6. The total interaction cross sections of π -mesons, K-mesons, protons as functions of particle-target relative rapidity. The data are taken from [9]

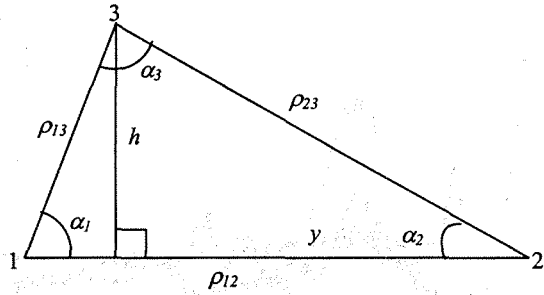


Fig.7. A simplex in the Lobachevsky space. Particles with rapidities ρ_1, ρ_2, ρ_3 correspond to the vertices of the triangle 123. The triangle sides $\rho_{12}, \rho_{13}, \rho_{23}$ are relative rapidities of particles 1, 2, 3.

If 2 is a target at rest in the laboratory system, then the angle α_2 is equal to the laboratory angle of the registered particle

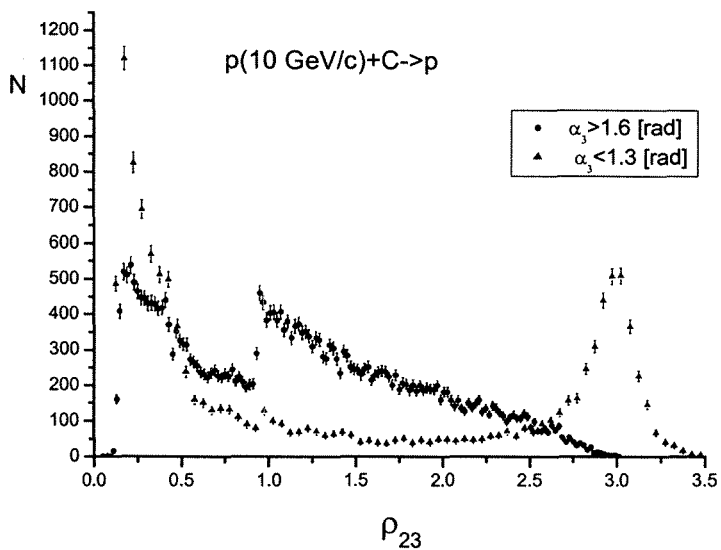


Fig.8. The ρ_{23} distributions of protons for two selected angle α_3 intervals: $\alpha_3 > 1.6$ rad and $\alpha_3 < 1.3$ rad in the reaction $p(10\text{GeV}/c)+C$.

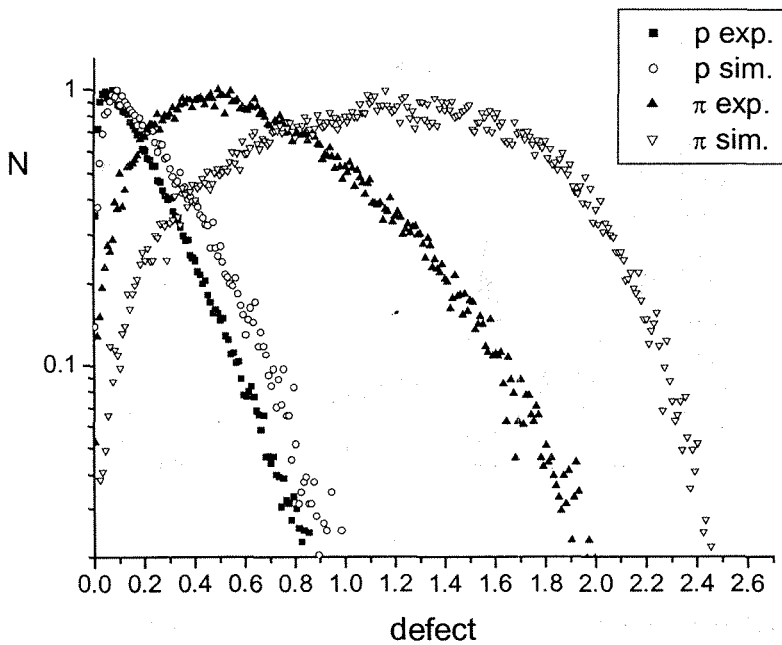


Fig.9. The normalized distributions of defects of triangles formed by all combinations of protons and all combinations of π -mesons registered in the reaction $p(10\text{GeV}/c)+C$

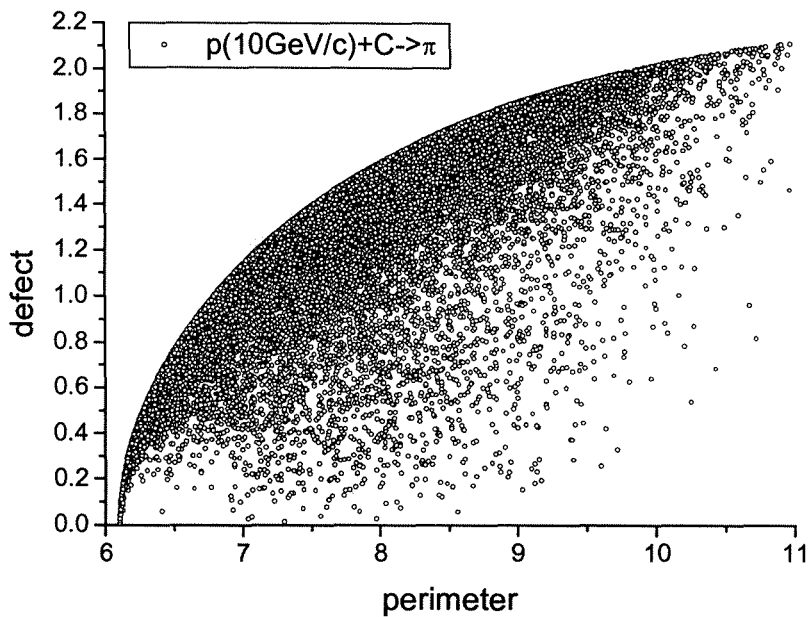
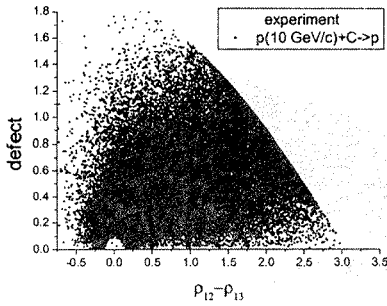
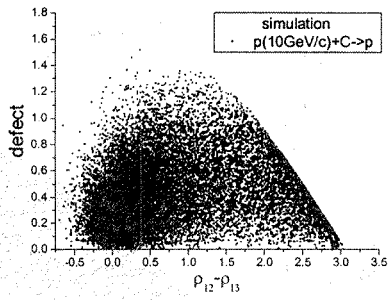


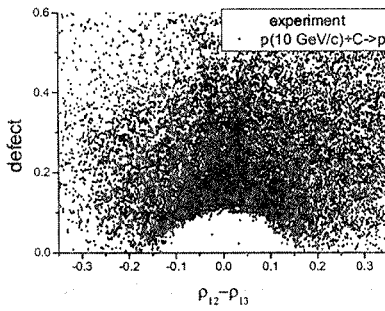
Fig. 10. Defect vs. perimeter for the triangles formed by combinations of three particles: point 1 – projectile, point 2 – target, point 3 – any π -meson registered in the reaction $p(10\text{ GeV}/c)+C$



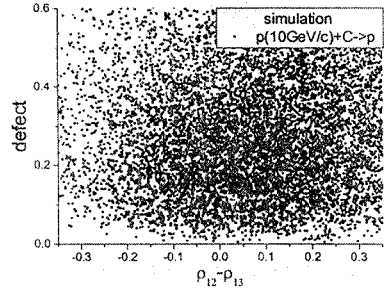
a)



b)



c)



d)

Fig.11. Defect vs. $(\rho_{12}-\rho_{13})$, where ρ_{12} is the projectile-target relative rapidity and ρ_{13} - the projectile-particle relative rapidity for protons produced in the reaction $p(10 \text{ GeV}/c)+C$: the experimental (a) and simulated (b) data; and in more detail the region near zero: the experimental (c) and simulated (d) data.

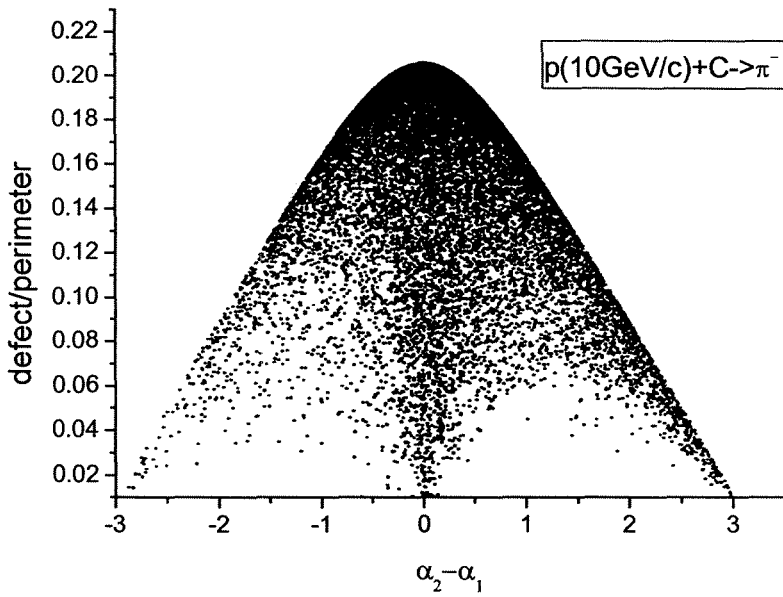


Fig.12. The ratio defect/perimeter vs. the difference of the angles at the target and at the projectile for π -mesons measured in the reaction $p(10\text{GeV}/c)+C \rightarrow \pi^-$. Prevalence of certain symmetric structures is observed

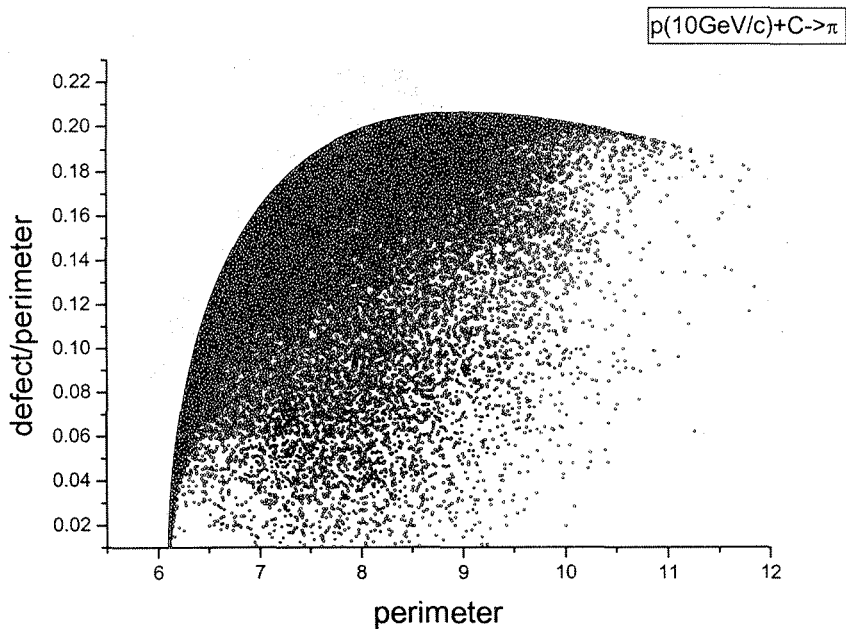


Fig. 13. The defect – to perimeter ratio for triangles 123 (see Fig.7), where $1,2$ are interacting particles, 3 is a π -meson registered in the reaction $p(10\text{GeV}/c) + C$

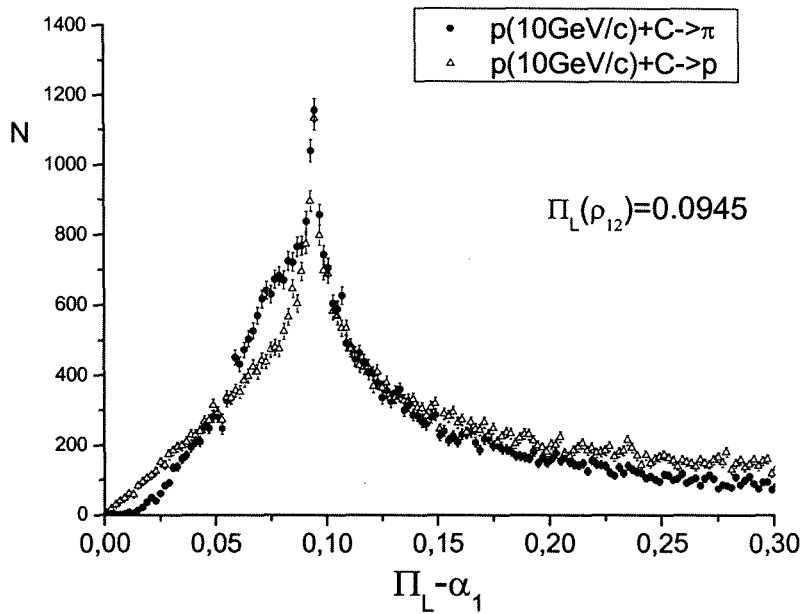


Fig. 14. Probabilities of proton and π -meson production in the reaction $p(10\text{GeV}/c)+C$ as functions of the variable $\Pi_L - \alpha_3$, where Π_L is the angle of parallelism calculated for the height h of the triangle 123 , and α_3 is the angle at the registered particle (see Fig. 7)

References

1. A.M.Baldin. Dokl. Akad. Nauk, V. 222, №5, p.1064 (1975).
2. A.I.Bondarenko, et al., Rus.Nucl. Phys. 65, p.95 (2002).
3. G.N.Agakishiev, et al., Rus. Nucl. Phys. 40, p.1209 (1984) (Zeit Phys. C v. 27, p.177 (1985))
4. D.Armutliysky, et al., Rus. Nucl. Phys. 49, p.182 (1989)
5. M.P.Balandin, et al., NIM 20 p.110 (1963)
6. A.M.Baldin, A.A.Baldin Rus. J. Part. Nucl. v.29, issue 3, p.577 (1998).
7. Baldin A.M., Didenko L.A. Fortsch. Phys., v.38, p.261 (1994).
8. A.A.Baldin, E.N.Kladnitskaya, O.V.Rogachevsky. JINR Rapid Comm. №2 [94]-99.
9. K. Hagiwara *et al.*, Phys. Rev. D **66**, 010001 (2002) (<http://www-pdg.lbl.gov/>)
10. Fok V.A. The theory of space, time and gravity. M., Gostekhizdat, 1955.
11. Kotelnikov A.P. The principle of relativity and the geometry of Lobachevsky. In book: In Memorial N.I.Lobatschevskij. V.2. Kazan, 1927, pp.37-64.
12. N.A.Chernikov. Sov. J. Part. Nucl., v.4, p.773 (1973).
13. A.A.Baldin et al., Part. and Nuclei. Lett., **4 (119)**, 7 (2004).
14. Sorge H. Phys. Rev. C 52, 3291 (1995).

STRANGENESS CONSERVATION AND STRUCTURE OF PAIR CORRELATIONS OF NEUTRAL KAONS WITH LOW RELATIVE MOMENTA IN INCLUSIVE PROCESSES

V.L. Lyuboshitz¹⁾ and V.V. Lyuboshitz²⁾

*Joint Institute for Nuclear Research,
141980, Dubna, Moscow Region, Russia
E-mail: ¹⁾ lyubosh@sunhe.jinr.ru,
²⁾ Valery.Lyuboshitz@jinr.ru*

Abstract

The phenomenological structure of inclusive cross-sections of the production of two neutral K -mesons in collisions of hadrons and nuclei is investigated taking into account the strangeness conservation in strong and electromagnetic interactions. The relations describing the dependence of the correlations of two short-lived and two long-lived neutral kaons $K_S^0 K_S^0$, $K_L^0 K_L^0$ and the correlations of "mixed" pairs $K_S^0 K_L^0$ at small relative momenta upon the space-time parameters of the generation region of K^0 and \bar{K}^0 -mesons, which involve the contributions of Bose-statistics and S -wave strong final-state interaction, have been obtained. It is shown that under the strangeness conservation the correlation functions of the pairs $K_S^0 K_S^0$ and $K_L^0 K_L^0$, produced in the same inclusive process, coincide, and the difference between the correlation functions of the pairs $K_S^0 K_S^0$ and $K_S^0 K_L^0$ is conditioned by the production of the pairs of non-identical neutral kaons $K^0 \bar{K}^0$.

1. Consequences of the strangeness conservation

In the work [1] the properties of the density matrix of two neutral K -mesons, following from the strangeness conservation in strong and electromagnetic interactions, have been investigated. By definition, the diagonal elements of the non-normalized two-particle density matrix coincide with the two-particle structure functions, which are proportional to the double inclusive cross-sections.

Strangeness is the additive quantum number. Taking into account the strangeness conservation, the pairs of neutral kaons $K^0 K^0$ (strangeness $S = +2$), $\bar{K}^0 \bar{K}^0$ (strangeness $S = -2$) and $K^0 \bar{K}^0$ (strangeness $S = 0$) are produced incoherently. This means that in the K^0 - \bar{K}^0 -representation the non-diagonal elements of the density matrix between the states $K^0 K^0$ and $\bar{K}^0 \bar{K}^0$, $K^0 K^0$ and $K^0 \bar{K}^0$, $\bar{K}^0 \bar{K}^0$ and $K^0 \bar{K}^0$ are equal to zero. However, the non-diagonal elements of the two-kaon density matrix between the two states $|K^0\rangle^{(p_1)} |\bar{K}^0\rangle^{(p_2)}$ and $|\bar{K}^0\rangle^{(p_1)} |K^0\rangle^{(p_2)}$ with the zero strangeness are not equal to zero, in general. Here \mathbf{p}_1 and \mathbf{p}_2 are the momenta of the first and second kaons.

The internal states of K^0 -meson ($S = 1$) and \bar{K}^0 -meson ($S = -1$) are the superpositions of the states $|K_S^0\rangle$ and $|K_L^0\rangle$, where K_S^0 is the short-lived neutral kaon and K_L^0 is the long-lived one. Neglecting the small effect of CP non-invariance, the CP -parity of the

state K_S^0 is equal to $(+1)$, and the CP -parity of the state K_L^0 is equal to (-1) ; in doing so,

$$|K^0\rangle = \frac{1}{\sqrt{2}}(|K_S^0\rangle + |K_L^0\rangle), \quad |\bar{K}^0\rangle = \frac{1}{\sqrt{2}}(|K_S^0\rangle - |K_L^0\rangle).$$

It is clear that both the quasistationary states of the neutral kaon have no definite strangeness.

It is easy to show that

$$|K^0\rangle^{(\mathbf{p}_1)} \otimes |K^0\rangle^{(\mathbf{p}_2)} = \frac{1}{2}(|K_S^0\rangle^{(\mathbf{p}_1)} \otimes |K_S^0\rangle^{(\mathbf{p}_2)} + |K_L^0\rangle^{(\mathbf{p}_1)} \otimes |K_L^0\rangle^{(\mathbf{p}_2)} + |K_S^0\rangle^{(\mathbf{p}_1)} \otimes |K_L^0\rangle^{(\mathbf{p}_2)} + |K_L^0\rangle^{(\mathbf{p}_1)} \otimes |K_S^0\rangle^{(\mathbf{p}_2)}), \quad (1)$$

$$|\bar{K}^0\rangle^{(\mathbf{p}_1)} \otimes |\bar{K}^0\rangle^{(\mathbf{p}_2)} = \frac{1}{2}(|K_S^0\rangle^{(\mathbf{p}_1)} \otimes |K_S^0\rangle^{(\mathbf{p}_2)} + |K_L^0\rangle^{(\mathbf{p}_1)} \otimes |K_L^0\rangle^{(\mathbf{p}_2)} - |K_S^0\rangle^{(\mathbf{p}_1)} \otimes |K_L^0\rangle^{(\mathbf{p}_2)} - |K_L^0\rangle^{(\mathbf{p}_1)} \otimes |K_S^0\rangle^{(\mathbf{p}_2)}). \quad (2)$$

It follows from the Bose-symmetry of the wave function of two neutral kaons with respect to the total permutation of internal states and momenta that the CP -parity of the system $K^0\bar{K}^0$ is always positive [2] (the C -parity is $(-1)^L$, the space parity is $P = (-1)^L$, where L is the orbital momentum).

The system of two non-identical neutral kaons $K^0\bar{K}^0$ in the symmetric internal state, corresponding to even orbital momenta, is decomposed into the schemes $|K_S^0\rangle|K_S^0\rangle$ and $|K_L^0\rangle|K_L^0\rangle$ [2]:

$$\begin{aligned} |\psi^+\rangle &= \frac{1}{\sqrt{2}}(|K^0\rangle^{(\mathbf{p}_1)} \otimes |\bar{K}^0\rangle^{(\mathbf{p}_2)} + |\bar{K}^0\rangle^{(\mathbf{p}_1)} \otimes |K^0\rangle^{(\mathbf{p}_2)}) = \\ &= \frac{1}{\sqrt{2}}(|K_S^0\rangle^{(\mathbf{p}_1)} \otimes |K_S^0\rangle^{(\mathbf{p}_2)} - |K_L^0\rangle^{(\mathbf{p}_1)} \otimes |K_L^0\rangle^{(\mathbf{p}_2)}); \end{aligned} \quad (3)$$

meantime, the system $K^0\bar{K}^0$ in the antisymmetric internal state, corresponding to odd orbital momenta, is decomposed into the scheme $|K_S^0\rangle|K_L^0\rangle$ [2]:

$$\begin{aligned} |\psi^-\rangle &= \frac{1}{\sqrt{2}}(|K^0\rangle^{(\mathbf{p}_1)} \otimes |\bar{K}^0\rangle^{(\mathbf{p}_2)} - |\bar{K}^0\rangle^{(\mathbf{p}_1)} \otimes |K^0\rangle^{(\mathbf{p}_2)}) = \\ &= \frac{1}{\sqrt{2}}(|K_S^0\rangle^{(\mathbf{p}_1)} \otimes |K_L^0\rangle^{(\mathbf{p}_2)} - |K_L^0\rangle^{(\mathbf{p}_1)} \otimes |K_S^0\rangle^{(\mathbf{p}_2)}). \end{aligned} \quad (4)$$

The strangeness conservation leads to the fact that all the double inclusive cross-sections of production of pairs $K_S^0 K_S^0$, $K_L^0 K_L^0$ and $K_S^0 K_L^0$ (two-particle structure functions) prove to be symmetric with respect to the permutation of momenta \mathbf{p}_1 and \mathbf{p}_2 :

$$\begin{aligned} f_{SS}(\mathbf{p}_1, \mathbf{p}_2) &= f_{SS}(\mathbf{p}_2, \mathbf{p}_1); \quad f_{LL}(\mathbf{p}_1, \mathbf{p}_2) = f_{LL}(\mathbf{p}_2, \mathbf{p}_1); \\ f_{SL}(\mathbf{p}_1, \mathbf{p}_2) &= f_{SL}(\mathbf{p}_2, \mathbf{p}_1). \end{aligned} \quad (5)$$

Besides, due to the strangeness conservation, the structure functions of neutral K -meson produced in inclusive processes are invariant with respect to the replacement of the short lived state K_S^0 by the long-lived state K_L^0 , and *vice versa* [1]:

$$f_{SS}(\mathbf{p}_1, \mathbf{p}_2) = f_{LL}(\mathbf{p}_1, \mathbf{p}_2) = \frac{1}{4} [f_{K^0 K^0}(\mathbf{p}_1, \mathbf{p}_2) + f_{\bar{K}^0 \bar{K}^0}(\mathbf{p}_1, \mathbf{p}_2) + f_{K^0 \bar{K}^0}(\mathbf{p}_1, \mathbf{p}_2) + f_{\bar{K}^0 K^0}(\mathbf{p}_1, \mathbf{p}_2)] + \frac{1}{2} \text{Re} \rho_{K^0 \bar{K}^0 \rightarrow \bar{K}^0 K^0}(\mathbf{p}_1, \mathbf{p}_2), \quad (6)$$

$$f_{SL}(\mathbf{p}_1, \mathbf{p}_2) = f_{LS}(\mathbf{p}_1, \mathbf{p}_2) = \frac{1}{4} [f_{K^0 K^0}(\mathbf{p}_1, \mathbf{p}_2) + f_{\bar{K}^0 \bar{K}^0}(\mathbf{p}_1, \mathbf{p}_2) + f_{K^0 \bar{K}^0}(\mathbf{p}_1, \mathbf{p}_2) + f_{\bar{K}^0 K^0}(\mathbf{p}_1, \mathbf{p}_2)] - \frac{1}{2} \text{Re} \rho_{K^0 \bar{K}^0 \rightarrow \bar{K}^0 K^0}(\mathbf{p}_1, \mathbf{p}_2), \quad (7)$$

where $\rho_{K^0 \bar{K}^0 \rightarrow \bar{K}^0 K^0}(\mathbf{p}_1, \mathbf{p}_2) = (\rho_{\bar{K}^0 K^0 \rightarrow K^0 \bar{K}^0}(\mathbf{p}_1, \mathbf{p}_2))^*$ are the non-diagonal elements of the two-kaon density matrix. The difference between the two-particle structure functions f_{SS} and f_{SL} is connected just with the contribution of these non-diagonal elements.

It is evident that the one-particle structure functions for the production of K_S^0 and K_L^0 are equal to each other. After integrating the relations (6) over the momentum distribution of neutral kaons one can obtain the mutual equality of the average multiplicities of the K_S^0 and K_L^0 -states, as well as the mutual equality of the average squares of multiplicities:

$$\langle n_S \rangle = \langle n_L \rangle, \quad \langle n_S^2 \rangle = \langle n_L^2 \rangle. \quad (8)$$

2. Structure of pair correlations of identical and non-identical neutral kaons with close momenta

Now let us consider the correlations of pairs of neutral K -mesons with close momenta within the model of one-particle sources [2-7]. In the case of the identical states $K_S^0 K_S^0$ and $K_L^0 K_L^0$ we obtain the following expressions for the correlation functions R_{SS} , R_{LL} (proportional to structure functions), normalized to unity at large relative momenta:

$$R_{SS}(\mathbf{k}) = R_{LL}(\mathbf{k}) = \lambda_{K^0 K^0} [1 + F_{K^0}(2\mathbf{k}) + 2 b_{\text{int}}(\mathbf{k})] + \lambda_{\bar{K}^0 \bar{K}^0} [1 + F_{\bar{K}^0}(2\mathbf{k}) + 2 \bar{b}_{\text{int}}(\mathbf{k})] + \lambda_{K^0 \bar{K}^0} [1 + F_{K^0 \bar{K}^0}(2\mathbf{k}) + 2 B_{\text{int}}(\mathbf{k})]. \quad (9)$$

Here \mathbf{k} is the momentum of one of the kaons in the c.m. frame of the pair, and the quantities $\lambda_{K^0 K^0}$, $\lambda_{\bar{K}^0 \bar{K}^0}$ and $\lambda_{K^0 \bar{K}^0}$ are the relative fractions of the average numbers of produced pairs $K^0 K^0$, $\bar{K}^0 \bar{K}^0$ and $K^0 \bar{K}^0$, respectively ($\lambda_{K^0 K^0} + \lambda_{\bar{K}^0 \bar{K}^0} + \lambda_{K^0 \bar{K}^0} = 1$). The "formfactors" $F_{K^0}(2\mathbf{k})$, $F_{\bar{K}^0}(2\mathbf{k})$ and $F_{K^0 \bar{K}^0}(2\mathbf{k})$ appear due to the contribution of Bose-statistics:

$$F_{K^0}(2\mathbf{k}) = \int W_{K^0}(\mathbf{r}) \cos(2\mathbf{k}\mathbf{r}) d^3\mathbf{r}, \quad F_{\bar{K}^0}(2\mathbf{k}) = \int W_{\bar{K}^0}(\mathbf{r}) \cos(2\mathbf{k}\mathbf{r}) d^3\mathbf{r}, \\ F_{K^0 \bar{K}^0}(2\mathbf{k}) = \int W_{K^0 \bar{K}^0}(\mathbf{r}) \cos(2\mathbf{k}\mathbf{r}) d^3\mathbf{r}. \quad (10)$$

where $W_{K^0}(\mathbf{r})$, $W_{\bar{K}^0}(\mathbf{r})$ and $W_{K^0 \bar{K}^0}(\mathbf{r})$ are the probability distributions of distances between the sources of emission of two K^0 -mesons, between the sources of emission of two

\bar{K}^0 -mesons and between the sources of emission of the K^0 -meson and \bar{K}^0 -meson, respectively, in the c.m. frame of the kaon pair. Meantime, the quantity $b_{\text{int}}(\mathbf{k})$ describes the contribution of the S -wave interaction of two K^0 -mesons, the quantity $\bar{b}_{\text{int}}(\mathbf{k})$ describes the contribution of the S -wave interaction of two \bar{K}^0 -mesons and the quantity $B_{\text{int}}(\mathbf{k})$ describes the contribution of the S -wave interaction of the K^0 -meson with the \bar{K}^0 -meson. Due to the CP -invariance, the quantities $b_{\text{int}}(\mathbf{k})$ and $\bar{b}_{\text{int}}(\mathbf{k})$ can be expressed by means of averaging the same function $b(\mathbf{k}, \mathbf{r})$ over the different distributions:

$$b_{\text{int}}(\mathbf{k}) = \int W_{K^0}(\mathbf{r})b(\mathbf{k}, \mathbf{r})d^3\mathbf{r}, \quad \bar{b}_{\text{int}}(\mathbf{k}) = \int W_{\bar{K}^0}(\mathbf{r})b(\mathbf{k}, \mathbf{r})d^3\mathbf{r}.$$

The quantity $B_{\text{int}}(\mathbf{k})$ has the structure

$$B_{\text{int}}(\mathbf{k}) = \int W_{K^0\bar{K}^0}(\mathbf{r})B(\mathbf{k}, \mathbf{r})d^3\mathbf{r},$$

where $B(\mathbf{k}, \mathbf{r}) \neq b(\mathbf{k}, \mathbf{r})$.

The relations connecting the contribution of the S -wave strong interaction into the pair correlations of particles at small relative momenta with the parameters of low-energy scattering were obtained earlier in the papers [4-7].¹⁾ It is essential that the "formfactors" (10) and the functions $b_{\text{int}}(\mathbf{k})$, $\bar{b}_{\text{int}}(\mathbf{k})$ and $B_{\text{int}}(\mathbf{k})$ depend on the space-time parameters of the generation region of neutral kaons and tend to zero at high values of the relative momentum $q = 2|\mathbf{k}|$ of two neutral kaons.

Let us emphasize that when the pair of non-identical neutral kaons $K^0\bar{K}^0$ is produced but the pair of identical quasistationary states $K_S^0K_S^0$ (or $K_L^0K_L^0$) is registered over decays, the two-particle correlations at small relative momenta have the same character as in the case of usual identical bosons with zero spin [2].

For the pairs of non-identical kaon states $K_S^0K_L^0$ the correlation functions at small relative momenta have the form:

$$\begin{aligned} R_{SL}(\mathbf{k}) = R_{LS}(\mathbf{k}) = & \lambda_{K^0\bar{K}^0} [1 + F_{K^0}(2\mathbf{k}) + 2b_{\text{int}}(\mathbf{k})] + \\ & + \lambda_{\bar{K}^0K^0} [1 + F_{\bar{K}^0}(2\mathbf{k}) + 2\bar{b}_{\text{int}}(\mathbf{k})] + \\ & + \lambda_{K^0\bar{K}^0} [1 - F_{K^0\bar{K}^0}(2\mathbf{k})]. \end{aligned} \quad (11)$$

In accordance with Eq.(11), at the production of the pair of non-identical neutral kaons $K^0\bar{K}^0$ and the registration of the two-particle state $K_S^0K_L^0$ over decays the pair correlations are analogous to the correlations of two identical fermions with the same spin projections. This is connected with the fact that in the considered case the pair $K_S^0K_L^0$ has odd orbital momenta [2].

It follows from Eqs.(9) and (11) that the correlation functions of pairs of neutral K -mesons with close momenta, which are created in inclusive processes, satisfy the relation

¹⁾ In particular, at characteristic distances between sources of K^0 - and \bar{K}^0 -mesons $r_0 \gg d_0$, where d_0 is the radius of action of short-range forces between the K^0 -meson and \bar{K}^0 -meson (really, already at $r_0 > d_0$), we can use the approximation of the superposition of the plane and spherical waves [4]. Then

$$B(\mathbf{k}, \mathbf{r}) \approx |f_{K^0\bar{K}^0}(k)|^2 \frac{1}{r^2} + 2 \operatorname{Re} \left(f_{K^0\bar{K}^0}(k) \frac{\exp(ikr) \cos \mathbf{k}\mathbf{r}}{r} \right),$$

where $f_{K^0\bar{K}^0}(k)$ is the amplitude of the S -wave $K^0\bar{K}^0$ -scattering, $k = |\mathbf{k}|$, $r = |\mathbf{r}|$.

$$\begin{aligned}
R_{SS}(\mathbf{k}) + R_{LL}(\mathbf{k}) - R_{SL}(\mathbf{k}) - R_{LS}(\mathbf{k}) &= 2 [R_{SS}(\mathbf{k}) - R_{SL}(\mathbf{k})] = \\
&= 4\lambda_{K^0\bar{K}^0} [F_{K^0\bar{K}^0}(2\mathbf{k}) + B_{\text{int}}(\mathbf{k})].
\end{aligned}
\tag{12}$$

We see that the difference between the correlation functions of the pairs of identical neutral kaons $K_S^0 K_S^0$ and pairs of non-identical neutral kaons $K_S^0 K_L^0$ is conditioned exclusively by the generation of $K^0 \bar{K}^0$ -pairs.

3. Summary

1. It is shown that, taking into account the strangeness conservation, the double inclusive cross-sections of the production of two short-lived neutral K -mesons and two long-lived neutral K -mesons are equal to each other. This result is the direct consequence of the strangeness conservation.

2. Within the model of one-particle sources the formulae for the correlation functions $R_{SS} = R_{LL}$ and $R_{SL} = R_{LS}$ are obtained, which involve the contributions of Bose-statistics and the S -wave final-state interaction of two K^0 (\bar{K}^0)-mesons as well as of a K^0 -meson with a \bar{K}^0 -meson, and depend upon the relative fractions of produced pairs $K^0 K^0$, $\bar{K}^0 \bar{K}^0$ and $K^0 \bar{K}^0$.

3. It is shown that the production of $K^0 \bar{K}^0$ -pairs with the zero strangeness leads to the difference between the correlation functions R_{SS} and R_{SL} of two neutral kaons.

This work is supported by Russian Foundation for Basic Research (Grant No. 03-02-16210).

References

- [1] V.L. Lyuboshitz, *Yad. Fiz.* **23**, 1266 (1976) [*Sov. J. Nucl. Phys.* **23**, 673 (1976)].
- [2] V.L. Lyuboshitz and M.I. Podgoretsky, *Yad. Fiz.* **30**, 789 (1979) [*Sov. J. Nucl. Phys.* **30**, 407 (1979)].
- [3] M.I. Podgoretsky, *Fiz. Elem. Chast. At. Yadra* **20**, 628 (1989) [*Sov. J. Part. Nucl.* **20**, 266 (1989)].
- [4] R. Lednicky and V.L. Lyuboshitz, *Yad. Fiz.* **35**, 1316 (1982) [*Sov. J. Nucl. Phys.* **35**, 770 (1982)].
- [5] V.L. Lyuboshitz, *Yad. Fiz.* **41**, 820 (1985) [*Sov. J. Nucl. Phys.* **41**, 523 (1985)].
- [6] V.L. Lyuboshitz, *Yad. Fiz.* **48**, 1501 (1988) [*Sov. J. Nucl. Phys.* **48**, 956 (1988)].
- [7] R. Lednicky, V.V. Lyuboshitz and V.L. Lyuboshitz, *Yad. Fiz.* **61**, 2161 (1998) [*Phys. At. Nucl.* **61**, 2050 (1998)].

V.
ACCELERATOR
FACILITIES:
STATUS
AND
PERSPECTIVES

BEAM - BASED MEASUREMENT OF DYNAMICAL CHARACTERISTICS IN NUCLOTRON

N. Blinnikov¹, O. Brovko¹, E. Ivanov¹, A. Tsarenkov¹, and D. Dinev²

¹*Joint Institute for Nuclear Research
141980 Dubna, Moscow Region, Russia*

²*Institute for Nuclear Research and Nuclear Energy of BAS
72 Tzarigradsko Chaussee Blvd., 1784 Sofia, Bulgaria*

E-mail: dinnet@inrne.bas.bg

Abstract

The real values of dynamical characteristics in Nuclotron have been measured by means of both sinusoidal and kick excitations of the beam. For measurement of betatron tunes the method based on the Beam Transfer Function have been used. Beam-based modeling by means of Orbit Response Matrix allowed us to calculate the amplitude beta function and the betatron phase advance with big accuracy. Applying this method one can also calibrate the Beam Position Monitors and to reveal the bad-working units.

1. Introduction

In first approximation an accelerator is described by the linear optical model. To measure the dynamical characteristics of this model is between the major tasks of accelerator commissioning and optimum exploitation. It is often that the real accelerator optics differs from the machine design. Knowing the correct values of the accelerator optical functions – beta function, betatron tune and betatron phase advance is of first importance.

For measurement of the accelerator optical functions a system of Beam Position Monitors (BPM) and orbit corrector magnets (CM) is used. BPMs measure the beam center of charge position with respect to the reference orbit. CMs produce dipole kicks, that listort the closed orbit.

The behavior of any dynamical system is fully described by its response to one of the standard excitations. The response of a dynamical system to unit step function is known as transient function. The response of a dynamical system to a Dirac pulse function is called impulse transient function or sometimes weight function. The response of a dynamical system to sinusoidal excitation is the well-known frequency characteristic or transfer function.

Either of these characteristics describes both the transient and the steady-state modes.

In accelerator practice the transfer function is known as Beam Transfer Function (BTf). The shock beam excitation by means of a fast kicker magnet results in coherent beam oscillations. The response of the center of charge positions to kicks in closed orbit correctors is called Orbit Response Matrix (ORM). A general theorem states that the transfer function is a Fourier transfer of the impulse response.

One of the most important parameters of any cyclic accelerator is the tune of the betatron oscillations – Q . The value of Q determines the position of the so-called working point of the accelerator. The working point must be kept away from any dangerous resonances during the whole accelerator cycle. Many accelerator parameters, such as chromaticity and the dependence of the tune on the amplitude are firmly connected with the Q -value.

One may say that the efficiency of the accelerator and the possibility to reach the maximum beam intensity are determined by the proper choice and maintenance of the betatron tune.

On the other hand the structural beta function describes the beam envelope and the betatron phase advance.

For measurement of the correct values of the structural beta functions and of betatron phase advance in Nuclotron the method based on the Orbit Response Matrix have been used.

2. Betatron tune measurement in Nuclotron

Nowadays all the existing accelerators have electronic systems for on-line tune measurement.

The Nuclotron tune measurement system is based on the exciting of transverse oscillations of the beam applying an external sinusoidal signal and measurement of the corresponding center of charge response. This response is known as Beam Transfer Function (BTF). Transverse BTF is determined by the ratio of the amplitude of the center of charge oscillations to the external sinusoidal excitation – [1].

A simplified block-diagram of the used equipment is shown on Fig.1.

For the excitation of the transverse betatron oscillations in NUCLOTRON we have used a broadband amplifier. It consists of 9 identical blocks with a transformer output. One of these blocks is used as a preamplifier. Its output signal excites in parallel the other 8 blocks. The secondary windings of these blocks are connected in series and this gives 250 V on the load in the frequency range 0.1 – 6.0 MHz. The load represents 100 pF capacity in parallel with a 75 Ω resistor. The maximum output power is 0.6 KW. Input and control signals are transmitted by 0.5 km matched cables to and from the accelerator ring.

The already existing pick-ups used for orbit measurements have been used also for the beam excitation and for the response measurement. These pick-ups are 13 cm long and are situated in special boxes in the vacuum chamber of the accelerator. The minimum voltage on the pick-up which we can still reliably measure is 200 μ V. This corresponds to 1V on the ADC input.

A spectrum of simultaneous measurement of horizontal and vertical betatron oscillations is shown on Fig.2.

From the measurements we conclude that the horizontal betatron tune in Nuclotron is equal to $Q_h = 7.463$, while the vertical is $Q_v = 7.414$.

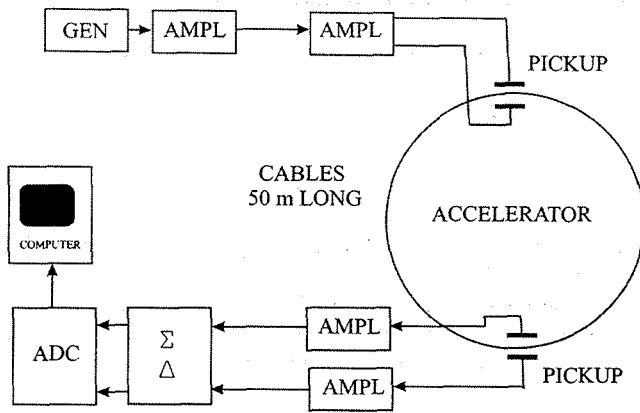


Figure 1: Block-diagram of the tune measurement equipment

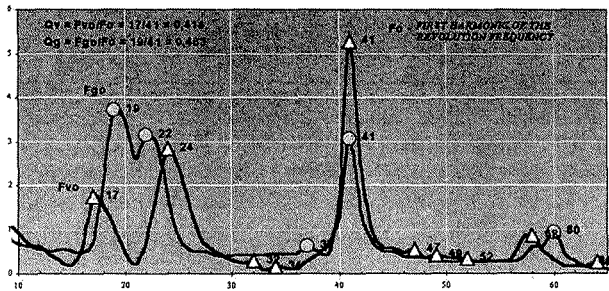


Figure 2: Spectrum of horizontal and vertical BTF

3. Measurement of optical functions in Nuclotron

One powerful method for measurement of optical functions is based on the Orbit Response Matrix (ORM).

The ORM is defined by - [2]:

$$R_{ij} = \frac{\partial x_i}{\partial \epsilon_j} \quad (1)$$

where dx_i is the change of the center of charge position x_i at the i -th BPM due to a change $d\epsilon_j$ in the kick at j -th CM

One should distinguish between theoretical ORM - R^{theor} , which reflects the properties of the accepted linear optical model of the accelerator and measured ORM - R^{meas} .

The theory gives the following expression for the orbit response matrix:

$$R_{ij}^{theor} = \frac{\sqrt{\beta_i \beta_j}}{2 \sin \pi Q} \cos(\pi Q - |\mu_i - \mu_j|) + \frac{D_i D_j}{L \eta} \quad (2)$$

where

$$\eta = (1/\gamma^2 - \alpha) \quad (3)$$

and μ is the phase advance.

There is one more thing that should be taken into account, namely that the different BPMs have different noise level. This can be measured for each BPM by successive orbit measurements under constant corrector strengths. Let σ_i be the rms orbit deviations for the i -th BPM. This rms deviation is a measure for the noise level associated with this BPM. Hence we must introduce the weights $(1/\sigma_i)$ in the fitting.

Summarizing we reach to the following system of equations:

$$R_{ij}^{meas} = \frac{1}{\sigma_i} g_i (R_{ij0} + \sum_l \frac{dR_{ij}}{dk_l} \Delta k_l + \frac{D_i D_j}{L \eta} s_j) \quad (4)$$

where Δk_j are the errors in quadrupole strengths, g_i are the BPMs gain factors and s_j are the correctors scale factors.

As (4) embraces more equations than unknowns it should be solved in LSQ sense. The best way to do this is the singular value decomposition.

The orbit response matrix is a good instrument for studying machine optics due to the very large number of experimental points. This allows for the right individual gradients to be determined. Using the calibrated accelerator model it is possible to compute the right values of the beta functions.

The orbit response matrix gives direct information about the bad operating BPMs and the broken symmetry of the ring. The experimental setup is shown on Fig. 3.

To check the proper work of the BPMs we have realized the following experiment. First of all we measured the closed orbit produced by the random perturbations in the

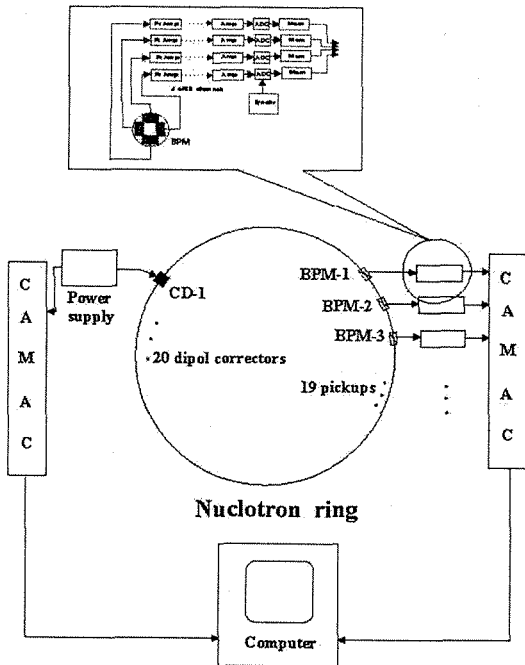


Figure 3: Experimental setup for ORM measurement

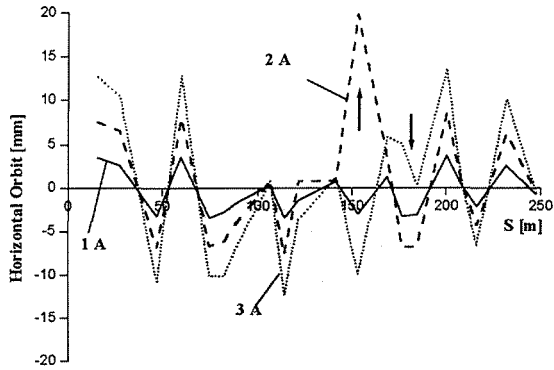


Figure 4: Orbits due to excitement of corrector HK74

magnetic fields and to the random displacement of quadrupoles. After that we fired one of the orbit correctors, increasing the excitation current from 1 to 2 and 3 Amps, and again measured the closed orbit. Subtracting from these latter orbits the initial orbit we received the closed orbit due only to the corrector. The difference orbits in horizontal plane are shown on Fig.4. It is clearly seen that some problems with the BPMs occur around the azimuths 153 m (BPM - #12) and 185 m (BPM - # 15).

References

1. D. Dinev. Betatron Tune Measurement. JINR Preprint, Dubna, 2001.
2. D. Dinev. Measurement of the Dynamical Characteristics of the Betatron Motion in Synchrotrons. In "Problems of Charged Particles Acceleration", Duvna, 2001, pp.

SPIN AS AN ADDITIONAL TOOL FOR QGP INVESTIGATIONS

J. Karachuk, S.S. Shimanskiy[†]

JINR, Dubna

([†] *E-mail: shimansk@sunhe.jinr.ru*)

Abstract

The nearest two years on experiment STAR the upgrade is planned, which will make it possible to identify particles up to momentum ~ 3 GeV/c. This will open possibility to carry out new and more detailed researches of properties of a nuclear matter formed in nucleus-nucleus collision at RHIC. In this work we offer to carrying out of the polarization studies, which can give important additional information about the process of forming the new state of nuclear matter, and also about properties of the formed state.

A unique probe of information about all stages of formation and evolution of nuclear matter are dileptons, due to their electromagnetic interaction with the nuclear matter. In this work we pay main attention to the examination of polarization characteristics of dileptons.

1. Introduction

The first studies on the accelerator RHIC (BNL) have shown that properties of the nuclear matter formed in Au-Au-collisions substantially differ from those of the nuclear matter formed at collisions of nuclei on the accelerator SPS (CERN) [1]. It made it necessary to reconsider theoretical views of the properties of formed quark-gluon plasma [2]. Up to the present time the search of unequivocal signatures of formation of quark-gluon plasma remains active. From our point of view, polarizing studies give us an additional tool allowing to detect the formation of new states of nuclear matter.

The upgrade of STAR setup [3] will allow to identify particles with momenta up to ~ 3 GeV/c. In particular, it will allow us to investigate dilepton production in the range of effective masses $m_{e^+e^-} < 5$ GeV. It is exactly in this range of effective masses where the majority of particles produced by quark-gluon plasma are expected. Dileptons and photons are unique probes because they interact with nuclear matter only via electromagnetic interaction. Due to their weak interaction dileptons and photons carry information about all stages of nuclear-nuclear collisions without noticeable distortion. This is a principal distinction of photons and leptons from hadron probes. Comparison of characteristics received by electromagnetic and hadrons probes will allows us to investigate properties of the forming nuclear matter.

It is expected that in nuclear-nuclear collisions the quark-gluon plasma(QGP) is formed, which is essentially a new source of secondary particles. Characteristic features of this new source are the object of studies which we attempt to find signals of QGP formation. The thermalization may be the main feature of the QGP.

The thermalization means that the information about initial states of nuclear-nuclear collisions has been lost (for example, the information about the initial is lost direction of collisions due to multiple secondary interactions). As a consequence we should see disappearance of all type of polarization connected with the direction of initial state for particles produced by the plasma source. The polarization for particles produced by the plasma can depend only on hadronization characteristics and the plasma collective motion. Therefore there should be no transverse polarization or longitudinal polarization connected with the direction of initial collision. That is why we can use polarization studies as an additional important information to identify the QGP formation.

But it is very important to determine the processes and energy ranges where the absence of polarization can be regarded as a proof of the QGP formation. The first time this type of possibility has been proposed and discussed in detail about ten years ago. In 1994 one of the authors (S.S.S.) proposed to CERES/NA45 collaboration to carry out polarization studies of low mass dileptons ($0.2 < m_{ee} < 0.6 \text{ GeV}/c^2$) to explain the nature of dilepton enhancement in the nucleus-nucleus collisions. However, further analysis showed that CERES/NA45 had a very narrow acceptance [4]. Nowadays there are new setups with possibilities to carry out polarization investigations of dileptons to find formation of the QGP phase in nuclear-nuclear collisions. That is why we think that it is important to analyze the possibility for polarization studies now. Some experiments have been carried out for some years (HADES, NA60, STAR and PHENIX).

2. Polarization and thermalization

CERES/NA45 studies [5] of the dilepton production in nuclear-nuclear collisions with nuclear beams at SPS(CERN) have shown an enhancement of the dilepton production in the mass region $0.2 \text{ GeV} < m_{e^+e^-} < 0.8 \text{ GeV}$. If this enhancement come from the thermalized source we should not see any dilepton anisotropies. That is not so for a secondary $\pi^+\pi^-$ - annihilation process where a strong anisotropy of the electron (positron) emission should occur. Moreover, there must be energy dependence of this anisotropy which is opposite to a thermalized source case which has no the energy dependence. Therefore, we have a real possibility to distinguish these two subprocesses. That time there were no quantitative theoretical estimations of these effects. The author (S.S.S.) had asked theoreticians from JINR for theoretical examination these effects [6]. This work was continued in collaboration with a theoretical group of Giessen [7, 8]. These are the only quantitative theoretical predictions up to now. Theoretical predictions for the anisotropy of leptons in the region of small masses and for energies from SIS(GSI) to SPS(CERN) have been based on the Hadron-String Dynamics(HSD) model [9]. At that time there was no possibility to carry out studies in the region of the dilepton masses $m_{e^+e^-} > 1 \text{ GeV}$ that's why all predictions had been limited to the region of small masses.

Theoretical studies have shown that the dilepton polarization characteristics allow to separate different subprocesses (and models) not only in nuclear-nuclear collisions but in nucleon-nucleon interactions. In 1998 CERES/NA45 has obtained the data for p_T dependences of the dilepton pair production [10]. These data have shown that the dilepton enhancement comes from a low p_T region of pairs. Theoretical description of this enhancement for $p_T \sim 0 \text{ GeV}$ [11] remain difficult, which can be partly explained by a combination of a strong polarization with the narrow CERES/NA45 acceptance. It implies

the domination of the process by the annihilation of non thermalized pions. May be this is the first indirect proof which tells us that the main source that is crucial for the dilepton enhancement is not a thermalized source. If it is so, we have the first direct observation of the annihilation process of secondary pions and its studies have some independent interest.

RHIC have opened essentially new opportunities for polarization studies of dileptons. It is the possibility to carry out investigation of the thermalized source in a wider range of dilepton masses and immediately in the center mass system. Tshe article [12] examines the contribution of the thermalized dilepton source for energies SPS and RHIC. At these energies there are additional interesting region of masses $1 \text{ GeV} < m_{e^+e^-} < 5 \text{ GeV}$ where the thermalized source of dileptons competes with the Drell-Yan annihilation. As well as in a case of small dilepton masses, we have competition of two subprocesses: the thermalized source and the Drell-Yan process. The latter gives a strong alignment of virtual photons and as a consequence of the anisotropy in the lepton angle distribution. Different energies of nuclear-nuclear collisions, the possibility to select events with different impact parameters make a real possibility to unambiguously reveal the appearance of the thermalized source. In our opinion such studies now are unique in the sense that they allow us to detect directly the occurrence of a thermalized source of particle production.

There are independent reasons to study the polarization characteristics of dileptons in nucleon-nucleon collisions on RHIC for small and middle mass regions with polarized proton beams. These investigations will give an additional information about polarized structure of nucleons in the region $x \sim 10^{-2}$.

RHIC setups have possibility to detect hadrons, that is why we can propose to compare hadrons and dileptons polarization characteristics in nuclear-nuclear collisions to investigate influence of formed nuclear matter. For example, the comparison polarization characteristics of dileptons and $\pi^+\pi^-(K^+K^-)$ - pairs gives new information about the QGP formation. There are many other hadron probes where polarization should be used to prove the QGP formation. We can propose to investigate the polarization of Λ which comes from $K^+(\bar{\Lambda}K^-)$ - back to back pairs.

Till now we discuss so-called regions of continuous dilepton mass spectrum. The resonance regions are very interesting too. But we do not have so many quantitative predictions. The ρ -meson alignment can serve as sensitive tool to study mechanisms of formation [13]. Article [14] proposed to investigate J/ψ polarization in nuclear-nuclear collisions. The QGP formation should give a huge value of the alignment for J/ψ in contrast to nucleon-nucleon collisions where the alignment must be zero. It is very useful to compare characteristics of resonance polarizations from dileptons(photons) and hadrons decay modes.

2. Conclusion

In this report we have discussed some ideas which allow to receive the new additional experimental information which can help to proof the QGP formation. Polarization characteristics are the thin tool and these experimental data will give possibility unequivocally to speak about the detection of the thermalized state. The authors are grateful for L. Bratkovskay and O.V. Teryayeva for interest and support.

References

- [1] U. Heinz, M. Jacob, Evidence for a New State of Matter: An Assessment of the Results from the CERN Lead Beam Programme, **nucl-th/0002042**, (2000).
J. Adams et al, Experimental and Theoretical Challenges in the Search for the Quark Gluon Plasma: The STAR Collaborations Critical Assessment of the Evidence from RHIC Collisions, **nucl-ex/0501009**, (2005).
- [2] E. Shuryak, A strong coupled quark-gluon plasma, *J.Phys. G*: **30**, S1221 (1901).
M. Gyulassy, L. McLerran, New form of QCD matter discovered at RHIC, *Nucl. Phys.A* **750**, 30 (2005).
- [3] T. Hallman, The STAR Decadal Plan, RHIC Open Planning Meeting, December 3-4, 2003.
- [4] Guy Tel-Zur, Ph.D. thesis, pp.70,71,73 (1996). <http://www.physi.uni-heidelberg.de/physi/ceres/theses.html>
- [5] G. Agakichiev et al., Enhanced Production of Low-Mass Electron Pairs in 200 GeV/Nucleon S-Au at the CERN Super Proton Synchrotron, *Phys.Rev.Lett.*,**75**, 1272 (1995).
- [6] E.L. Bratkovskaya, O.V. Teryaev, V.D. Toneev, Anisotropy of dilepton emission from nuclear collisions, *Phys.Lett. B* **348**, 283 (1995).
- [7] E.L. Bratkovskaya et al., Anisotropy of dilepton emission from nucleon-nucleon interactions, *Phys.Lett. B* **348**, 325 (1995).
- [8] E.L. Bratkovskaya, W. Cassing, U. Mosel, Probing hadronic polarizations with dilepton anisotropies, *Z.Phys. C* **75**, 119 (1997).
- [9] The Hadron-String Dynamics (HSD) Model, <http://www.th.physik.uni-frankfurt.de/brat/hsd.html>
- [10] G. Agakichiev et al., Low-mass e^+e^- pair production in 158 A GeV Pb-Au collisions at the CERN SPS, its dependence on multiplicity and transverse momentum, *Phys.Lett.B* **422**, 405 (1998).
- [11] W. Cassing, E.L. Bratkovskaya, Hadronic and electromagnetic probes of hot and dense nuclear matter, *Phys.Report* **308**, 65 (1999).
- [12] R. Rapp, Dilepton in high-energy heavy-ion collisions, *PRAMANA*, vol.**60**, No.**4**, 675 (2003)
- [13] A.V. Efremov, O.V. Teryaev, On Vector Meson Spin Alignment in Fusion Model, **P2-82-832**, Preprint of JINR, Dubna 1982.
- [14] B.L. Ioffe, Charmonium polarization in e^+e^- and heavy ion collisions, X Advanced Research Workshop on High Energy Spin Physics (NATO ARW DUBNA-SPIN-03), p.79, Dubna 2004. (**hep-ph/0310343**)

TRANSMUTATION EXPERIMENTS USING THE NUCLOTRON

W. Westmeier^{1,7}, R. Brandt¹, E.-J. Langrock², H. Robotham⁷, K. Siemon⁷, R. Odoj³,
D. Chultem⁴, V.M. Golovatyuk⁴, M.I. Krivopustov⁴, S.R. Hashemi-Nezhad⁵, A.N. Sosnin⁴,
M. Zamani⁶

¹ Institut für Chemie (Kernchemie), Philipps-Universität, D-35032 Marburg (Germany)

² Forschungsbüro Langrock, D-02977 Hoyerswerda (Germany)

³ ISF, Forschungszentrum Jülich GmbH, D-52425 Jülich (Germany)

⁴ Joint Institute for Nuclear Research, 141980 Dubna (Russian Federation)

⁵ Dept. of High Energy Physics, University of Sydney, Sydney, NSW 2006 (Australia)

⁶ Physics Department, Aristotle University, GR-52124 Thessaloniki (Greece)

⁷ Dr. Westmeier GmbH, D-35085 Ebsdorfergrund, (Germany), eMail: Westmeier@Westmeier.com

Transmutation was proposed [1] as a hypothetical means to reduce the amount of very long-lived radioactive waste from technological applications of nuclear fission. With the advent of new technologies this idea came closer to reality and high-precision experimental data are now required to check the feasibility of the concept.

Experiments were carried out with the GAMMA-2 target setup [2] at the NUCLOTRON accelerator using protons in the energy range from 0.53 GeV to 4.15 GeV. Fig.1 gives a schematic view of the GAMMA-2 experimental setup together with its beam monitoring system.

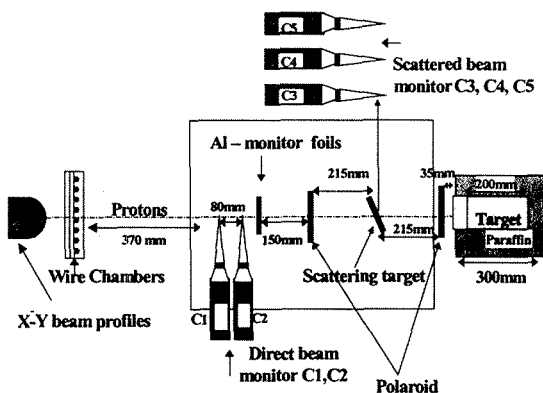


Figure 1: Schematic view of the GAMMA-2 setup. The target is composed of 20 lead disks with 8 cm diameter and 1 cm thickness, the paraffin moderator shell has 20 cm outer diameter, 6 cm thickness and 31 cm length. The Al-monitor contains a stack of three thin aluminium foils where the center foil is used. Polaroid films were used for beam alignment before each irradiation

Five scintillation detectors C1 to C5 and a 1 g/cm² PE target were used to monitor the beam. Aluminium activation foils were used to determine the integral proton fluence on the target. The Al monitor foil stack was placed approx. 60 cm upstream the Pb target in order to avoid activation from backwards emitted particles. In each experiment a stack of three Al foils with

a thickness of 31 μm (1.883×10^{20} atoms $\cdot\text{cm}^{-2}$) was mounted in an aligned position with the target and perpendicular to the beam axis as shown in Fig. 1, and irradiated during the whole run. The beam intensity was determined via the $^{27}\text{Al}(p,3\text{pn})^{24}\text{Na}$ reaction in the center foil. Samples containing 1 gram of lanthanum each were placed on top of the target assembly at distances of 5 cm, 10 cm, 15 cm, 20 cm, and 25 cm from the front side of the paraffin block, i.e. the first sample sits just above the location where the proton beam hits the Pb. B-values for each of the five samples (corrected for neutron anisotropy) were measured in every experiment. The B-value is an absolute cross section which is specific for each experimental setup and defined for the example nuclide ^{140}La as :

$B(^{140}\text{La}) = \text{Atoms of } ^{140}\text{La} \text{ produced in 1 gram of } ^{139}\text{La} \text{ sample by 1 primary proton}$

In order to compare neutron densities from various experiments we have calculated the integrated $B(^{140}\text{La})$ for ^{140}La on the GAMMA-2 setup by fitting the five data points with a modified (skewed) Gaussian function. The function is used because it has a suitable shape and not because of any physical significance.

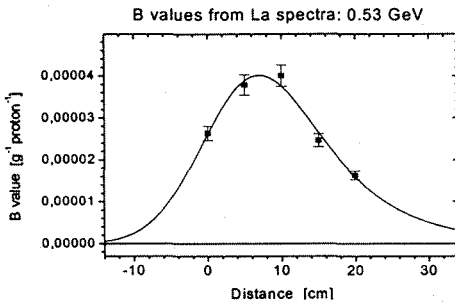


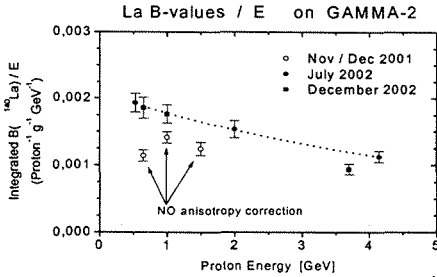
Figure 2:

B-values for ^{140}La along the top of the paraffin moderator in the irradiation with 0.53 GeV protons on the GAMMA-2 target. The distance $d=0$ cm corresponds to the upstream end of the 20 cm long Pb target, i.e. the point of proton impact

The fitted distributions quantify findings from earlier experiments [3,4] that the shapes of B-value distributions (i.e. the neutron densities over the target) are almost identical over the entire proton energy range studied. The maximum of the B-values is always found at about 10 cm downstream the beginning of the lead target and the widths of the distributions are essentially the same for each energy in the $0.53 \text{ GeV} \leq E_p \leq 4.15 \text{ GeV}$ range.

The integrated $B(^{140}\text{La})$ -values divided by the proton beam energy E_p are plotted in Fig. 3 as a function of proton energy E_p . This picture shows the effectiveness of the GAMMA-2 setup for transmutation of ^{139}La via neutron capture reactions. Thus, it also displays the effectiveness of the GAMMA-2 setup for the production of low-energy neutrons. It is interesting to note that the effectiveness of GAMMA-2, which has only 20 cm Pb target length, for low-energy neutron production is best at low proton energies.

Figure 3:



Normalized B-values for ^{140}La on the GAMMA-2 setup. The dotted line serves to guide the eye. Uncorrected data points at 0.65 GeV, 1 GeV and 1.5 GeV proton energy show the necessity of the anisotropy correction of measured B-values.

In Figures 4 and 5 the corresponding functions of B-values/ E_p are shown for the transmutation of ^{129}I and ^{237}Np . In these experiments samples of approx. 1g of radioactive target material, which was weld sealed into Al-containers, were exposed to the secondary neutron fluence on top of the paraffin moderator on the GAMMA-2 target setup.

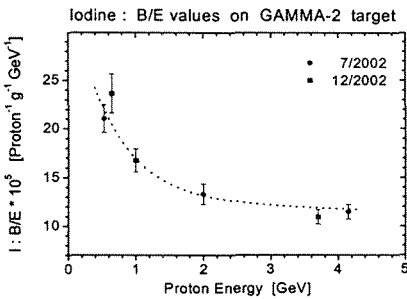


Figure 4: Normalized $B(^{130}\text{I})/E_p$ measured on the GAMMA-2 setup

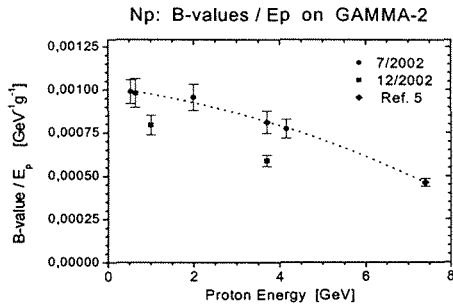


Figure 5: Normalized $B(^{238}\text{Np})/E_p$ measured on the GAMMA-2 setup

The lines in Figs. 4 and 5 serve to guide the eye. Considering results from Figures 3 to 5 it is clear that the transmutation effectiveness B/E_p (also called „neutron economy“ [5]) on the GAMMA-2 target is always highest at low proton energy and gradually falls off with rising bombarding energy. This may favour the use of proton beam energies that are lower than it has been assumed in other design studies. Operating at lower energy would of course be commercially attractive. However, the gradual fall may be a consequence of the size of the target where the small diameter and short length do not allow the intra- and inter-nuclear

cascades originating from incident protons to be completed. Further experiments shall answer that question very soon.

References :

[1] K.D. Tolstov, JINR preprint 18-89-778, Dubna, Russia (1989) and C.D. Bowman et al., Nuclear Instruments and Methods in Physics Research A320 (1992) 336

[2] Adam J. et al., „First nuclear activation experiments using the new accelerator NUCLOTRON in Dubna“, Kerntechnik **68** (2003) 214

[3] Wan J.-S. et al., „Transmutation of ^{129}I and ^{237}Np using spallation neutrons produced by 1.5, 3.7 and 7.4 GeV protons“, Nuclear Instruments and Methods in Physics Research **A463** (2001) 634

[4] Adam J. et al., „Transmutation of ^{239}Pu and other nuclides using spallation neutrons produced by relativistic protons reacting with massive U- and Pb-targets“, Radiochimica Acta **90** (2002) 431

[5] A. Letourneau et al., „Neutron production in bombardments of thin and thick W, Hg, Pb targets by 0.4, 0.8, 1.2, 1.8 and 2.5 GeV protons“, Nuclear Instruments and Methods in Physics Research **B170** (2000) 299

ELECTRON - POSITRON PAIR CREATION IN THE FIELDS OF HIGH-INTENSITY OPTICAL LASERS

D.B. Blaschke^{1,2†}, A.V. Prozorkevich³ and S.A. Smolyansky³

(1) *Fakultät für Physik, Universität Bielefeld, D-33615 Bielefeld, Germany*

(2) *Joint Institute for Nuclear Research, 141980, Dubna, Russia*

(3) *Saratov State University, 410026, Saratov, Russia*

† *E-mail: blaschke@physik.uni-bielefeld.de*

Abstract

We investigate the vacuum creation of electron-positron pairs (EPP) in periodic homogeneous electrical fields within a quantum kinetic approach with non-markovian source term. For a weak field $E \ll E_{cr} = m^2/|e|$, the EPP density changes periodically with twice the field frequency ν . Under these conditions, the residual density n_r taken over an integer number of field periods is negligibly small in comparison to the mean value $\langle n \rangle$ for the density per period. The value $\langle n \rangle$ is proportional to the squared field intensity and does not depend on the frequency in the range of $\nu \ll m$. The possibility to observe vacuum EPP creation using high-intensity optical lasers is discussed.

1. Introduction

QED is considered as the most advanced physical theory, many of its predictions have been proven experimentally with highest available precision. Nevertheless, some questions are discussed till now, e.g., the vacuum pair creation effect by a classical electric field [1]. A complete theoretical description of this effect has been obtained [2, 3, 4, 5, 6], but there is still no experimental proof. The main problem is the high value of the critical electric field strength, necessary to be reached for the pair creation, namely $E_{cr} = 1.3 \times 10^{16}$ V/cm for EPP. According to the Schwinger formula, the pair creation rate in a constant electric field is

$$\frac{dN}{d^3xdt} = \frac{(eE)^2}{4\pi^3} \sum_{n=1}^{\infty} \frac{1}{n^2} \exp\left(-n\pi \frac{E_{cr}}{E}\right) \quad (1)$$

and therefore exponentially suppressed when $E \ll E_{cr}$. Fortunately, the situation changes qualitatively if the field acts a finite time only [3, 7, 8, 9]. In this case, the Schwinger formula as well as its analog for a monochromatic field (Brezin-Itzykson formula [10]) become inapplicable.

There are a few examples for physical situations where the Schwinger effect can be observed, e.g. relativistic heavy ion collisions [11], neutron stars [12, 13] and focussed laser pulses [14]. It is well known [1] that no pairs are produced when both invariants of the field vanish

$$\mathbf{E}^2 - \mathbf{B}^2 = 0, \quad \mathbf{E}\mathbf{B} = 0. \quad (2)$$

The fields produced by focusing laser beams are very close to such configuration [2] and the pair creation must be essentially suppressed. But the pair creation is possible in the

focus of a standing wave of counter-propagating coherent laser beams [15]. The structure of a real laser field is too complicated for the analysis, because the Schwinger effect is non-perturbative and it requires the exact solution of the dynamical equations. That is why the approximation of the homogeneous electric field is used in most cases. According to different estimates [9, 10, 15, 16] the effect of vacuum creation can not be observed with the presently achieved level of laser power, see also [17].

The recent development of laser technology, in particular the invention of the chirped pulse amplification method, has resulted in a huge increase of the light intensity in a laser focal spot [18, 19]. The most advanced lasers produce pulses with intensities reaching 10^{22} W/cm² and the pulse duration decreasing down to few oscillation periods. As the construction of X-ray free electron lasers XFELs [20] is now planned, the possibility of the experimental proof of the Schwinger effect attracts attention again. The non-stationary effects become important under conditions of short pulses. We use in our work the kinetic equation approach, which allows us to consider the dynamics of the creation process taking into account the initial conditions [7]. Compared to the other treatments, the approach within the framework of a transport equation contains some new dynamical aspects, such as longitudinal momentum dependence of the distribution functions and non-markovian character of the time evolution. It takes into account the effects of the field switching and statistics, as well [21]. This approach has been applied already to the periodical field case [8] with near-critical values of the field strength and X-ray frequencies. In particular, it was shown that there is an "accumulation" effect when the intensity of the field is about half critical: the average density of pairs grows steadily with the increase of the field period numbers.

In the present work, we consider the other region of field parameters really achievable nowadays in the optical lasers: $E \ll E_{cr}$ and $\nu \ll m$, where ν is the laser field frequency. We suggest to use in the criterion for the creation efficiency the mean value $\langle n \rangle$ for the density per period is a more appropriate characteristic quantity than the residual density n_r . The latter is taken over an integer number of field periods and calculated using the imaginary time method. The main result is that optical lasers can generate a greater number of pairs per volume λ^3 than X-ray ones [22, 23].

The work is organized as follows. Section 2 contains the statement of the problem and the necessary information about the kinetic equation which is used for the description of vacuum pair creation. We solve this equation numerically for the conditions of the SLAC experiment [24] and study some features of pair production dynamics. We compare here our results obtained on the non-perturbative basis with the predictions of another approach [9] and show that optical lasers can be effective generators of electron-positron pairs during the action of a laser pulse. In Section 3, the low density approximation is considered. It allows to get some analytical results and to make simple estimates. Finally, in Section 4, we discuss some possibilities of direct experimental verification of pair production by high power optical lasers.

2. The kinetic approach

In the kinetic approach [7], the basic quantity is the distribution function $f(\mathbf{p}, t)$ of electrons and positrons which are considered as quasiparticles in a time-dependent external field. The kinetic equation for this function is derived from the Dirac equation in an

external time-dependent field by the canonical Bogoliubov transformation method [3], or by the help of the oscillator representation [25]. This procedure is exact but valid only for the simplest field configurations, e.g., the homogeneous time dependent electric field with the fixed direction

$$\mathbf{E}(t) = (0, 0, E(t)), \quad E(t) = -\dot{A}(t), \quad (3)$$

where the vector potential is given in the Hamiltonian gauge $A^\mu = (0, 0, 0, A(t))$ and the overdot denotes the time derivative. Such a field is not appropriate for a quantitative description of the laser pulse, but can probably be used as qualitative model to estimate results. The corresponding kinetic equation in the collisionless limit has the form [7]

$$\frac{df(\mathbf{p}, t)}{dt} = \frac{1}{2} \Delta(\mathbf{p}, t) \int_{t_0}^t dt' \Delta(\mathbf{p}, t') [1 - 2f(\mathbf{p}, t')] \cos \theta(\mathbf{p}, t', t), \quad (4)$$

where

$$\Delta(\mathbf{p}, t) = eE(t) \frac{\sqrt{m^2 + p_\perp^2}}{\omega^2(\mathbf{p}, t)}, \quad (5)$$

$$\omega(\mathbf{p}, t) = \sqrt{m^2 + p_\perp^2 + [p_\parallel - eA(t)]^2}, \quad (6)$$

$$\theta(\mathbf{p}, t', t) = 2 \int_{t'}^t dt_1 \omega(\mathbf{p}, t_1), \quad (7)$$

and m is the electron mass. Eq. (4) can be transformed to a system of ordinary differential equations, which is convenient for a numerical analysis

$$\begin{aligned} \dot{f} &= \frac{1}{2} \Delta v_1, \\ \dot{v}_1 &= \Delta(1 - 2f) - 2\omega v_2, \\ \dot{v}_2 &= 2\omega v_1, \end{aligned} \quad (8)$$

where v_1, v_2 are real auxiliary functions. The system (8) is integrated via the Runge-Kutta method with the initial conditions $f(\mathbf{p}, t_0) = v_1(\mathbf{p}, t_0) = v_2(\mathbf{p}, t_0) = 0$. The momentum dependence of the distribution function is defined by means of a discretization of the momentum space in a 2-dimensional grid, where the system (8) is solved in each of its nodes. The concrete grid parameters depend on the field strength, where typical values are $\Delta p \approx 0.05 m$ (grid step) and $p_{max} \approx (5-10) m$ (grid boundary). The particle number density can be found after that as a moment of the distribution function

$$n(t) = 2 \int \frac{d^3 p}{(2\pi)^3} f(\mathbf{p}, t). \quad (9)$$

Let us consider a harmonic field which acts during N periods (laser pulse):

$$E(t) = E_m \sin \nu t, \quad A = \frac{E_m}{\nu} \cos \nu t, \quad 0 \leq t \leq N \frac{2\pi}{\nu}. \quad (10)$$

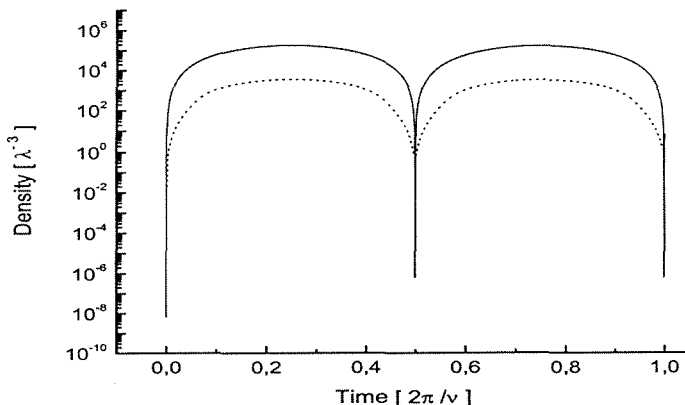


Figure 1: Time dependence of the density $n(t)$ in the volume λ^3 in the weak periodic field $E/E_{cr} = 1.5 \cdot 10^{-5}$ of an optical laser (solid line) compared to the near-critical field case of an X-ray laser [20] with $E/E_{cr} = 0.24$ (dashed line)

The time dependence of density for the field (10) with the parameters $E_m/E_{cr} = 1.5 \cdot 10^{-6}$ and $\nu/m = 2.84 \cdot 10^{-6}$ is shown in Fig. 1 in comparison to the planned X-ray laser [20] with $E/E_{cr} = 0.24$ and $\nu/m = 0.015$. The pair density oscillates with twice the frequency of the laser field. The density value n_r , which is evaluated in the imaginary time method [9, 15], corresponds to an integer number N of field periods, $n_r = n(2\pi N/\nu)$, and it is negligible in comparison with the density value n_m corresponding to the electric field maximum, $n_m = n[\pi(2N - 1)/2\nu]$. The mean density per period $\langle n \rangle$ is of the same order as n_m hence for the considered conditions the ratio of $\langle n \rangle / n_r$ is approximately $3 \cdot 10^{11}$. As a consequence, in spite of the fact that the residual density for the X-ray laser exceeds the one for the optical laser by a large factor, the situation is different regarding the mean density: the optical laser can produce more pairs per volume lambda cubed than the X-ray one.

3. Low density approximation

The low density approximation $f \ll 1$ can be used in the weak field limit $E \ll E_{cr}$. In that case it is possible to obtain analytic estimate for the particle density by means of the Eq. (4). The particle density in this approximation is

$$n(t) = \frac{e^2}{(2\pi)^3} \int d^3 p \varepsilon_{\perp}^2 \int_{t_0}^t dt_1 \frac{E(t_1)}{\omega^2(t_1)} \int_{t_0}^{t_1} dt_2 \frac{E(t_2)}{\omega^2(t_2)} \cos \left(2 \int_{t_2}^{t_1} dt_3 \omega(t_3) \right), \quad (11)$$

and it can be transformed to [22]

$$n(t) = \frac{1}{2(2\pi)^3} \int d^3 p \varepsilon_{\perp}^2 \left| \int_{t_0}^t dt_1 \frac{eE(t_1)}{\omega^2(t_1)} \exp \left(2i \int_{t_1}^t dt_3 \omega(t_3) \right) \right|^2. \quad (12)$$

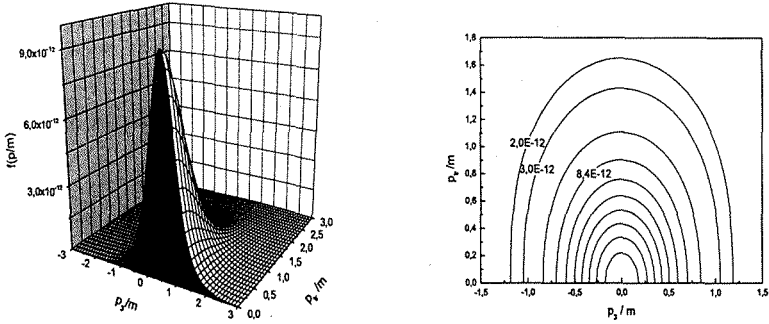


Figure 2: The momentum distribution of the created pairs (left panel) and its $f = \text{const}$ sections (right panel) at $t = \pi/2\nu$ (maximum of the field) for the field strength $E_m = 1.5 \cdot 10^{-5} E_{cr}$ and $\lambda = 100\text{nm}$

Let us assume additionally that the condition

$$\gamma = \frac{m\nu}{|e|E_m} \gg 1, \quad (13)$$

is satisfied, where γ is the adiabaticity parameter [9]. This relation can be treated as the condition for quasi-classical charge transport in an external field on the time scale $\sim 1/\nu$, if only the pairs are created with vanishing momenta. The latter condition was often used in relation to the longitudinal momentum [26] but the real momentum distribution of the EPP has a width of the order of the inverse mass for both transverse and longitudinal momenta, see Fig. 2. The momentum distribution shape varies essentially at the moments of time corresponding to the field minima: a complex quasi-periodic structure with a mean period of about the inverse laser frequency is formed. The mean period value of such a structure decreases proportionally to the number of field periods.

By means of the inequality (13) Eq. (12) is reduced to

$$n(t) = \frac{1}{2(2\pi)^3} \int d^3p \frac{\varepsilon_1^2}{\omega^4} \left| \int_{t_0}^t dt_1 eE(t_1) \exp(2i\omega t_1) \right|^2. \quad (14)$$

The time integral is calculated analytically for the field (10) and $t_0 = 0$ with the result

$$n(t) = \frac{1}{2(2\pi)^3} \int d^3p \frac{\varepsilon_1^2}{\omega^4} \left(\frac{eE_m}{\nu^2 - 4\omega^2} \right)^2 \left\{ \nu^2(1 + \cos^2 \nu t) + 4\omega^2 \sin^2 \nu t - 2\nu[\nu \cos \nu t \cos 2\omega t + 2\omega \sin \nu t \sin 2\omega t] \right\}. \quad (15)$$

According to Eq. (15) the residual pair density after N periods is $n_r = n(2\pi N/\nu)$ and

mean pair density per period $\langle n \rangle$ are estimated as

$$n_r = \frac{(eE_m\nu)^2}{4\pi^3} \int d^3p \left[\frac{\varepsilon_{\perp}}{\omega^2(\nu^2 - 4\omega^2)} \right]^2 \sin^2 \left(2\pi N \frac{\omega}{\nu} \right), \quad (16)$$

$$\begin{aligned} \langle n \rangle = & \frac{(eE_m)^2}{4(2\pi)^3} \int d^3p \left[\frac{\varepsilon_{\perp}}{\omega^2(\nu^2 - 4\omega^2)} \right]^2 \left\{ 3\nu^2 + 4\omega^2 \right. \\ & \left. + \frac{\omega\nu^3}{\pi(\nu^2 - 4\omega^2)} \sin \left(2\pi \frac{\omega}{\nu} \right) \cos \left[2\pi(2N + 1) \frac{\omega}{\nu} \right] \right\}. \end{aligned} \quad (17)$$

Now we shall be limited to the frequency range

$$\nu \ll m, \quad (18)$$

where the dependence of the densities (16), (17) on the number of periods N is negligible and we get

$$n_r = 5.2 \times 10^{-4} \frac{(eE\nu)^2}{m^3}, \quad \langle n \rangle = 1.6 \times 10^{-3} \frac{(eE)^2}{m}. \quad (19)$$

This conclusion differs from the one obtained using the imaginary time method [9] where $n(2\pi N/\nu) \sim N$. The latter approach allows to calculate n_r but not $\langle n \rangle$.

According to (19), a very simple relation connects in our case the residual and the mean densities,

$$\frac{\langle n \rangle}{n_r} \sim \left(\frac{m}{\nu} \right)^2. \quad (20)$$

The mean density of electron-positron pairs is defined in this case only by the field amplitude and does not depend on the frequency within a range of parameters (13),(18). After the integer period number (when the electric field vanishes) the overwhelming part of pairs is absorbed and the residual density, which is estimated within the usual approach [15], is negligible in comparison with the mean one used above. For example, for the Terawatt Nd-glass laser with the wavelength 527nm and the field strength $E_m = 6 \cdot 10^{10}$ V/cm [24] we have $m/\nu \approx 2 \cdot 10^5$, so that the mean density exceeds the residual one by more than 10 orders of magnitude. According to Fig. 1, there are $\approx 3 \cdot 10^6$ pairs in a volume of wavelength cubed on the average for one period of the laser field. Similar pair densities have been estimated for the conditions of an X-ray laser [8]. Let us notice, that the formula from Ref. [10] for the pair creation probability with the condition (13)

$$w \simeq \frac{(eE)^2}{8} \left(\frac{eE}{2m\nu} \right)^{4m/\nu} \quad (21)$$

gives only a negligible creation probability $\approx 10^{-10^5}$ in this case. This is not surprising because the formula (21) is not applicable for field pulses of finite duration.

4. Discussion

The simplest model of the laser field (10) predicts the existence of a dense electron-positron plasma during a laser pulse, which is absorbed almost completely after switching off the field. The mean density is defined by the field strength and does not depend

on frequency. The plasma density reaches 10^{18} cm^{-3} for field strengths in the range of $10^{10} - 10^{11} \text{ V/cm}$. The question arises: Can this effect be accessible to an experimental verification? Below, we discuss two such possibilities. The first (passive) method suggests that the two-photon annihilation of the e^+e^- quasiparticle pairs in the volume of the laser-created EPP may result in an observable signal. The corresponding pair of γ -quanta with a total energy of about 1 MeV should be registered as coincident signals in gamma counters placed on opposite sides of the laser focus. This effect is a possible manifestation of the new non-perturbative e^+e^- pair production effect in the laser field. The second (active) method suggests to use a weak diagnostic laser beam with a tunable frequency directed perpendicularly to the laser beam on the EPP region. The observation of a modulation of the probe laser signal with the time-dependent EPP density will not only prove the existence of the EPP but also allow to measure its properties. Apparently the intensities of these processes are small and therefore they will require a sufficiently long exposure time. We plan to give detailed numerical estimates for these processes in a subsequent work [27].

Acknowledgments. This work was supported partly by Russian Federations State Committee for Higher Education under grant E02-3.3-210 and Russian Fund of Basic Research (RFBR) under grant 03-02-16877. S.A.S. acknowledges support by DFG grant No. 436 RUS 117/78/04. We are grateful to Profs. A.A. Baldin (Dubna) and R. Sauerbrey (Jena) for their discussion of the possible experimental verification of the considered effects.

References

- [1] F. Sauter, Z. Phys. **69**, 742 (1931); W. Heisenberg and H. Euler, Z. Phys. **98**, 714 (1936); J. Schwinger, Phys. Rev. **82**, 664, (1951).
- [2] C.J. Troup and H.S. Perlman, Phys. Rev. D **6**, 2299 (1972).
- [3] A.A. Grib, S.G. Mamaev, and V.M. Mostepanenko, *Vacuum Quantum Effects in Strong External Fields* (Friedmann Lab. Publ., St.-Petersburg, 1994).
- [4] A.I. Nikishov, Tr. Fiz. Inst. Akad. Nauk SSSR, **111**, 152 (1979).
- [5] W. Greiner, B. Müller, and J. Rafelski, *Quantum Electrodynamics of Strong Fields*, (Springer, Berlin, 1985).
- [6] E.S. Fradkin, D.M. Gitman, and S.M. Shvartsman, *Quantum Electrodynamics with Unstable Vacuum*, (Springer-Verlag, Berlin, 1991).
- [7] S.M. Schmidt, D. Blaschke, G. Röpke, S.A. Smolyansky, A.V. Prozorkevich, and V.D. Toneev, Int. J. Mod. Phys. E, **7**, 709 (1998).
- [8] R. Alkofer, M.B. Hecht, C.D. Roberts, S.M. Schmidt, and D.V. Vinnik, Phys. Rev. Lett. **87**, 193902, (2001); C.D. Roberts, S.M. Schmidt, and D.V. Vinnik, *ibid*, **89**, 153901, (2002).
- [9] S.V. Popov, JETP Lett. **74**, 133, (2001); Phys. Lett. A **298**, 83 (2002).

- [10] E. Brezin and C. Itzykson, *Phys. Rev. D* **2**, 1191, (1970).
- [11] A. Casher, H. Neuberger, and A. Nussinov, *Phys. Rev. D* **20**, 179 (1979).
- [12] V.S. Beskin, A.V. Gurevich, and Ya.N. Istomin, *Physics of the Pulsar Magnetosphere* (Cambridge: Cambridge Univ. Press, 1993).
- [13] R. Ruffini, L. Vitagliano, and S.-S. Xue, *Phys. Lett. B* **559**, 12 (2003).
- [14] B. Richards and E. Wolf, *Proc. Roy. Soc. A (London)* **253**, 358 (1959).
- [15] M.S. Marinov and V.S. Popov, *Fortschr. Phys.* **25**, 373 (1977).
- [16] F.V. Bunkin and I.I. Tugov, *Dokl. Akad. Nauk. SSSR* **187**, 541 (1964) [*Sov. Phys. Dokl.* **14**, 678 (1969)].
- [17] S.S. Bulanov, *Phys. Rev. E* **69**, 0326408 (2004); S.S. Bulanov, N.B. Narozhny, and V.D. Mur, V.S. Popov, hep-ph/0403163; S.S. Bulanov, A.M. Fedotov, and F. Pedoraro, hep-ph/0409301.
- [18] G.A. Mourou, C.P.J. Barty, and M.D. Perry, *Phys. Today* **51**, No.1, 22 (1998).
- [19] S.V. Bulanov, T. Esirkepov, and T. Tajima, *Phys. Rev. Lett.* **91**, 085001 (2003), *ibid.* **92**, 159901 (2004)(E).
- [20] A. Ringwald, *Phys. Lett. B* **510**, 107 (2001).
- [21] S.M. Schmidt, D. Blaschke, G. Röpke, A.V. Prozorkevich, S.A. Smolyansky, and V.D. Toneev, *Phys. Rev. D*, **59**, 094005 (1999); J. C. Bloch, V. A. Mizerny, A.V. Prozorkevich, C. D. Roberts, S.M. Schmidt, S.A. Smolyansky, and D. V. Vinnik, *Phys. Rev. D*, **60**, 1160011 (1999).
- [22] A. V. Prozorkevich, A. Reichel, S. A. Smolyansky, A. V. Tarakanov, *Proceedings of SPIE*, **5476**, 68 (2004)
- [23] D. B. Blaschke, A. V. Prozorkevich, S. A. Smolyansky and A. V. Tarakanov, arXiv:physics/0410114.
- [24] C. Bula et al., *Phys. Rev. Lett.* **76**, 3116 (1996); D.L. Burke et al., *Phys. Rev. Lett.* **79**, 1626 (1997).
- [25] V.N. Pervushin, V.V. Skokov, A.V. Reichel, S.A. Smolyansky, and A.V. Prozorkevich, hep-th/0307200.
- [26] A. Casher, H. Neuberger, and S. Nussinov, *Phys. Rev. D*, **20**, 179 (1979).
- [27] D. Blaschke, A.V. Prozorkevich, S.A. Smolyansky, R. Sauerbrey, in preparation.

Научное издание

Relativistic Nuclear Physics and Quantum Chromodynamics

*Proceedings of the XVII International Baldin Seminar
on High Energy Physics Problems*

V. 1

Релятивистская ядерная физика и квантовая хромодинамика

*Труды XVII Международного Балдинского семинара
по проблемам физики высоких энергий*

Т. 1

E1,2-2005-103

Сборник отпечатан методом прямого репродуцирования
с оригиналов, предоставленных оргкомитетом.

Ответственные за подготовку сборника к печати *С. Г. Бондаренко, Е. Б. Плеханов.*

Фотографии *Ю. А. Туманова, Е. Б. Плеханова, И. Г. Зарубиной.*

Подписано в печать 14.09.2005.

Формат 60 × 90/16. Бумага офсетная. Печать офсетная.

Усл. печ. л. 24,38. Уч.-изд. л. 42,16. Тираж 300. Заказ 55006.

Издательский отдел Объединенного института ядерных исследований

141980, г. Дубна, Московская обл., ул. Жолио-Кюри, 6.

E-mail: publish@pds.jinr.ru

www.jinr.ru/publish/